

**Analysis report coarse sand  
barrier**

**Analysis of small scale configuration (phase 2a)**

preliminary

An aerial photograph of a river delta system, showing a complex network of channels and distributaries. A prominent, wide, light-colored sand barrier runs across the middle of the delta, separating the main river channel from the smaller distributaries. The water is a deep blue, and the surrounding land is a lighter, sandy color. The overall scene is a vast, intricate landscape of water and sand.

# **Analysis report coarse sand barrier**

**Analysis of small scale configuration (phase 2a)**

E. Rosenbrand  
V.M. van Beek

11200952-006

**Title**  
Analysis report coarse sand barrier

<b>Client</b>	<b>Project</b>	<b>Reference</b>	<b>Pages</b>
Water Board Rivierenland	11200952-006	11200952-006-GEO-0006- ydh	126

**Keywords**  
Piping, preventive measure, water level independent, coarse sand barrier, innovation,

**Summary**  
Piping is one of the most important threats for the safety of Dutch levees, especially for the sections that are located along the main rivers. Based on research conducted in the past years several preventive measures have been developed that prevent the pipe from progressing towards the river. One of these measures is the coarse sand barrier. The coarse sand barrier is a trench of coarse sand that hinders the pipe from progressing upstream below the dike, and if properly designed, prevents fine sand from upstream of the barrier from being eroded. Due to increased resistance against erosion of coarser grains the barrier will only fail at relatively larger head drops. The coarse sand barrier seems to be a promising measure based on preliminary experiments, but further research is required to assess the feasibility of this measure in practice. The report at hand describes the research conducted in the second phase (2a) of a larger research programme in which the feasibility of this method is assessed: the analysis of small-scale experiments. The small-scale experiments illustrate the potential of the measure, but also show that the method requires investigation at a larger scale for a better assessment of the quantitative potential of the method. The small-scale experiments indicate the existence of a criterion for damage of the barrier.

Version	Date	Author	Initials	Review	Initials	Approval	Initials
	nov. 2017	Dr.ir. E. Rosenbrand		Prof.dr.ir. A. Bezuijen		Ir. L. Voogt	
		Dr.ir. V.M. van Beek					

**State**  
preliminary  
This is a preliminary report, intended for discussion purposes only. No part of this report may be relied upon by either principal or third parties.

## Contents

<b>1</b>	<b>Introduction</b>	<b>1</b>
<b>2</b>	<b>Background</b>	<b>3</b>
<b>3</b>	<b>Experiments</b>	<b>9</b>
3.1	Sand selection	11
3.2	Experimental programme	15
<b>4</b>	<b>Analysis of experimental results</b>	<b>17</b>
4.1	Observations	17
4.1.1	Pipe progression	17
4.1.2	Pipe depth at the barrier interface	18
4.1.3	Sand boil and erosion lens	18
4.1.4	Sand transport	18
4.2	Head drop	19
4.2.1	Head drop in all capillaries	21
4.2.2	Upstream head loss	21
4.2.3	Exit head loss	23
4.2.4	Head drop across sand bed	24
4.2.5	Head drop parallel to the barrier	27
4.3	Gradients	28
4.3.1	Vertical gradients	28
4.3.2	Horizontal gradient in barrier	31
4.3.3	Horizontal gradient over upstream interface fine sand and barrier- filter cake formation	33
4.4	Flow rate	38
4.5	Flow regimes	41
4.5.1	In sand and barrier	41
4.5.2	In pipe	42
4.6	Apparent hydraulic conductivity	42
4.6.1	Fine sand upstream	42
4.7	Damage condition	45
4.8	Residual strength	53
4.9	Comparison to reference test	58
<b>5</b>	<b>Numerical simulations</b>	<b>61</b>
5.1	Software	62
5.2	Schematisation and mesh	62
5.2.1	Pipe depth	62
5.2.2	Flow regime	62
5.2.3	Boundary conditions	62
5.2.4	Mesh	63
5.3	Benchmarking DgFlow	66
5.3.1	Comparison to analytical solutions	66
5.3.2	Comparison to Plaxis	66
5.3.3	Comparison to Abaqus	67
5.4	Programme sensitivity analyses	68

5.4.1	Effect of hydraulic conductivity contrast in 2D and 3D models	69
5.4.2	Sensitivity analysis transverse extension of pipe	73
5.4.3	Sensitivity analysis of pipe depth	75
5.4.4	Sensitivity analysis of barrier depth	81
5.5.1	Fitting for postdictions	83
5.5.2	Postdiction procedure and assumptions	83
5.5.3	Schematisations	84
5.5.4	Results	88
5.5.5	Evaluation of the damage criterion	95
5.6	100	
5.7	Predictions	100
5.7.1	Medium-scale tests	101
5.7.2	Delta Flume tests	106
5.8	Small-scale tests with the Sellmeijer model	109
5.8.1	Summary of Results	109
5.8.2	Analysis	111
<b>6</b>	<b>Conceptual models</b>	<b>113</b>
6.1	Pipe development in the fine sand	113
6.2	Refinement	114
6.3	Piping into the barrier	114
6.4	Pipe progression through the barrier	116
6.5	Effect of particle size, grading, relative density, permeability contrast, barrier dimensions and scale on damage and critical head	117
<b>7</b>	<b>Conclusions and recommendations</b>	<b>119</b>
7.1	Conclusion damage criterion	119
7.1.1	Limitations of small-scale tests	120
7.1.2	Predictions	121
7.2	Recommendations	123
<b>8</b>	<b>References</b>	<b>125</b>
<b>Appendices</b>		
<b>A</b>	<b>Mesh analysis small-scale mesh</b>	<b>A-1</b>
<b>B</b>	<b>Comparison to analytical solution for uniform hydraulic conductivity</b>	<b>B-1</b>
<b>C</b>	<b>Comparison DgFlow and Plaxis</b>	<b>C-1</b>
<b>D</b>	<b>Report XI.17.11 Deltares Coarse sand barrier (numerical simulations)</b>	<b>D-1</b>
<b>E</b>	<b>Comparison DgFlow and Abaqus</b>	<b>E-1</b>
<b>F</b>	<b>Effect of hydraulic conductivity contrast in 2D and 3D models</b>	<b>F-1</b>
<b>G</b>	<b>Sensitivity analysis transverse extension of pipe</b>	<b>G-1</b>
<b>H</b>	<b>Sensitivity analysis of pipe depth</b>	<b>H-1</b>

<b>I Sensitivity analysis of barrier depth</b>	<b>I-1</b>
<b>J Postdictions</b>	<b>J-1</b>
<b>K Analysis of effect pipe depth on postdiction 191</b>	<b>K-1</b>
<b>L Analysis of effect of downstream hydraulic conductivity on postdiction 191</b>	<b>L-1</b>
<b>M Technical drawing of medium-scale set-up</b>	<b>M-1</b>
<b>N Schematisation of Delta Flume tests</b>	<b>N-1</b>
<b>O Small-scale tests with the Sellmeijer model</b>	<b>O-2</b>

# 1 Introduction

The current safety assessment method for piping, applied in the Netherlands, results in large sections to be reinforced. One of the sections that failed the safety assessment criteria is located within dike ring 16, nearby the village of Gameren. A dike stretch of 0.3 km failed the safety assessment criteria in the third safety assessment round, that was conducted in the period 2006-2011 and will need to be reinforced within short term. However, this is not the only dike section that will need to be reinforced. Indicative studies show that approximately half of the levees that are operated by Dutch Water Authority Rivierenland will not pass the current safety assessment criteria for piping.

Traditional reinforcement methods, like berms to increase seepage length, become less and less attractive due to the large required seepage length and the dense population and building development in this area. Several alternative (and innovative) methods are available that require less space. A new alternative method is the coarse sand barrier. This method entails the replacement of existing sand with coarse sand in a trench on the landside of the levee directly below the blanket layer. The blanket layer is restored after trenching.

The Dutch Water Authority Rivierenland intends to apply the coarse sand barrier at the pilot location Gameren as an innovative measure. Although experiments in the laboratory and at the IJkdijk (a former full-scale test facility in the North-Eastern part of the Netherlands) indicate the potential of the method, it is required to conduct a feasibility study to investigate whether the method offers sufficient resistance against piping in the field, both for the intended pilot location and for other, comparable locations. Based on the result of this feasibility study and the exploration of alternative measures, a preferential measure will be selected for the pilot location.

The purpose of the study is to assess the feasibility of the application of a coarse sand barrier as a piping measure for the location of Gameren, and for other locations along the main rivers in a more generic sense. To quantify the strength of the barrier, a criterion needs to be identified that predicts pipe formation into the barrier. Damage to the barrier – i.e. initial pipe formation into the barrier, caused by primary erosion – could be considered as failure of the barrier, since the thickness of the barrier (i.e. the dimension of the barrier in the flow direction) is small in practice and the initiation of a pipe into the barrier is relatively easy to predict. When the pipe has breached through the barrier, failure of the levee is likely a matter of time. The hypothesis is that the local horizontal gradient in the barrier near the pipe characterises the strength of a given barrier material at a given relative density, i.e. different tests with the same material are expected to show the same local damage gradient in the barrier at the moment the pipe damages the barrier, regardless of the configuration or dimensions of the barrier. To validate this hypothesis, other damage criteria are considered as well, such as the local velocity and (combined horizontal and) vertical gradient.

The approach to the feasibility study is described in (Koelewijn and Van Beek, 2017) and consists of the following phases:

- Phase 1: Literature study filter requirements and selection of barrier material.
- Phase 2a: Small-scale experiments and numerical simulation.
- Phase 2b: Medium-scale experiments and numerical simulation.
- Phase 2c: Large-scale experiments and numerical simulation.

The feasibility study is oriented towards one pilot location, but much of the knowledge developed in this study will be applicable in a more generic sense (at other locations). The study focusses explicitly on the technical feasibility of the measure and will not address the practical aspects of installing the coarse sand barrier in the field. Phase 1 was reported in Deltares note Literatuurstudie “Filtercriteria ten behoeve van grofzandbarrière” Deltares memo11200952-003-GEO-0001 (Rosenbrand, 2017)) and has led to the selection of barrier materials used for the small-scale experiments reported in “Sand selection Coarse sand barrier experiments”. Deltares memo 11200952-004-GEO-0001-m (Van Beek, 2017). The report at hand presents the analysis of the experiments conducted for phase 2a of the feasibility study. The research questions for phase 2, which contains: the small-scale tests in phase 2a (this report), and the medium-scale tests in phase 2b, and the Delta Flume tests in phase 2c, are:

- How much additional resistance to erosion will the barrier material provide, given the characteristics of the original sand body at the pilot location?
- What is the local damage gradient upstream of the pipe, at which the pipe progresses into the barrier, in small-, medium- and large-scale experiments? How does this local damage gradient affect the average damage gradient for the pilot location?
- What is the influence of the hydraulic conductivity contrast and grain size contrast of the chosen barrier material and original material on the resistance to piping?
- What are the effects of trench thickness and penetration depth?
- How can we monitor pipe formation through the barrier (failure of the barrier)?

The purpose of the small-scale experiments is to determine the resistance to piping of the three selected barrier materials for the pilot location in combination with different sands that are prevalent at the pilot location. For the three barrier materials, the local damage gradient was investigated; this is defined as the local gradient upstream of the pipe in the coarse sand barrier once the pipe progresses into the barrier. The hypothesis is that this local damage gradient is independent of the circumstances (surrounding sand, barrier penetration depth etc.). This hypothesis is tested using the experiments described in this report. The results of phase 2a are used to make predictions for phases 2b and 2c.

Following a Chapter on the background of the coarse sand barrier, the experimental set-up, sand selection and experimental programme are discussed in Chapter 3. The experiments are described in the Factual Report (Rosenbrand and Van Beek, 2017), and their analysis is given in Chapter 4. The numerical simulations are described in Chapter 5, including the comparison to the experiments. A conceptual model explaining the coarse sand barrier is presented in Chapter 6. The comparison of experiments and numerical simulation leads to the establishment of a criterion for damage of the barrier and to the conclusions and recommendations in Chapter 7. Finally, the appendices provide more details on the numerical simulations.

## 2 Background

The coarse sand barrier is a method that prevents the backward erosion (progression) of a pipe, and by doing so prevents failure of the levee due to backward erosion piping. Backward erosion piping is an internal erosion mechanism that can occur below levees with an unfiltered exit (e.g. by heave and cracking of the blanket layer) when sand particles are transported by seepage water towards the surface. Shallow hollow spaces are formed in the top of the aquifer below the blanket layer that progressively grow (progress) towards the river.

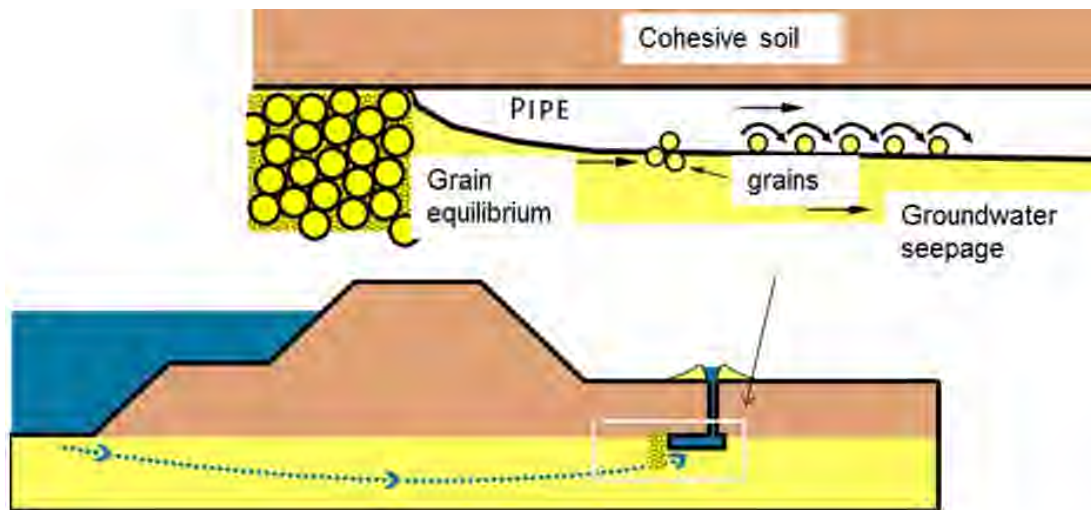


Figure 2.1 Schematic illustration of a coarse sand barrier preventing progressive backward erosion piping. Arrows indicate direction of seepage and of sand transport. The pipe grows in the direction opposite to sand transport (backwards) towards the river

The coarse sand barrier was applied in 2012 for the first time as a piping measure in one of the backward erosion piping experiments at the IJkdijk test facility. Financial resources were lacking for an initially planned other piping measure; therefore the coarse sand barrier was applied as a low-budget alternative. The seepage length was 15 meter in these experiments. Similar tests conducted in 2009 without piping measures indicated a critical head of approximately 2.2 m could be withstood by the levee. In the test with the barrier, the water level was raised to 3.3 m, before failure occurred by micro-instability of the sand core of the levee. The coarse sand barrier was found to be effective at least to this level (Koelewijn et al., 2013).



Figure 2.2 Schematic cross section of the IJkdijk experiment in 2012 (Koelewijn et al., 2013)

The concept of the coarse sand barrier was tested previously at small-scale (Van Beek et al., 2008) with a seepage length of approximately 0.30 m. In contrast to the IJkdijk experiment, where the levee failed due to a different failure mechanism than piping, these experiments were pursued until failure by piping. In a 2D-configuration (which can be compared to a levee without blanket layer) the critical head was found to be 3.2 to 3.5 times higher compared to a similar experiment without barrier. A 3D-configuration (representing an aquifer with a locally punctured blanket layer) was tested in 2015 (Van Beek et al., 2015b). With this configuration an increase of the critical head with a factor of 4.5 to 4.8 was found.

Due to scale effects that are inherent to the piping phenomenon, with different physical mechanisms that are expected to result in different scaling laws, it is necessary to conduct experiments at large scale before this method can be safely applied in practice. It is expected that at a larger scale the expected ratio of critical head with and without barrier will be lower than in the laboratory, but nonetheless a significant safety gain is expected at relatively low costs. This expectation was also endorsed by the working group 'Innovatie uit de markt', part of the POV Piping<sup>1</sup> (Senhorst, 2016).

<sup>1</sup> Project boundary transcending exploration, a programme that is part of the Hoogwaterbeschermingsprogramma, a programme aimed at flood protection in the Netherlands

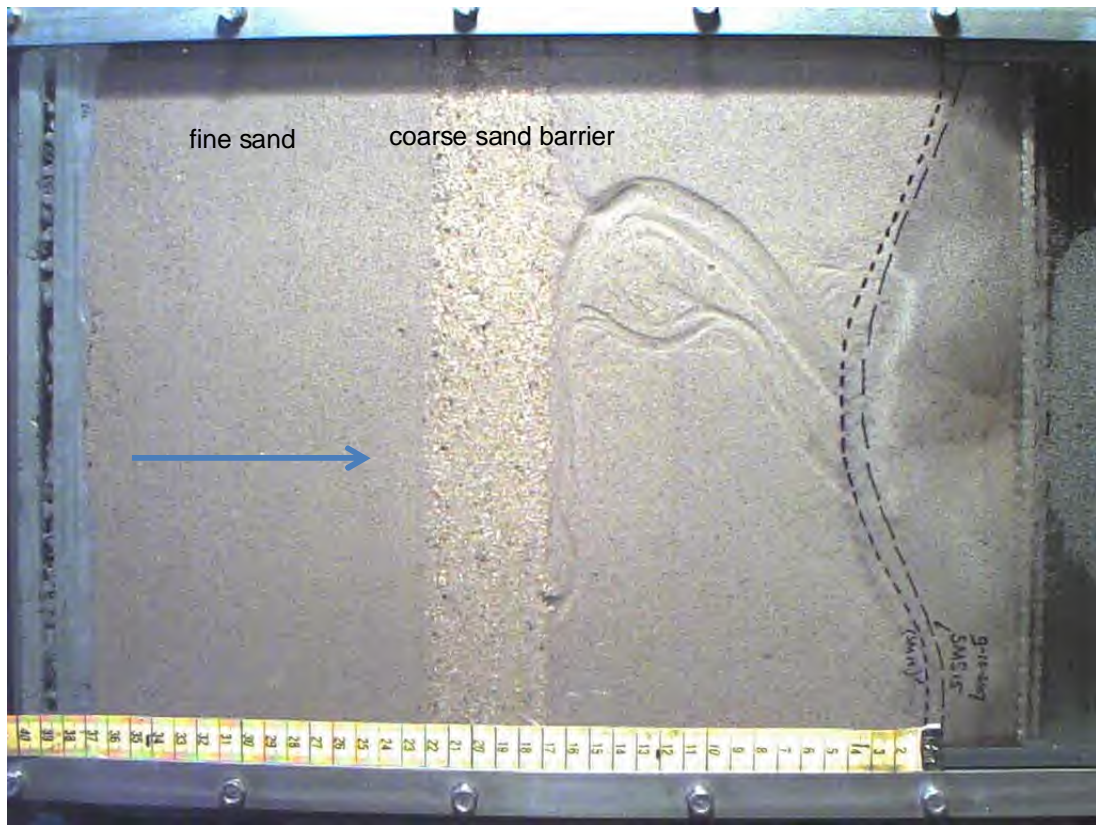


Figure 2.3 Laboratory experiments at small-scale: the pipe seeks a path along the coarse sand barrier (Van Beek et al., 2008)

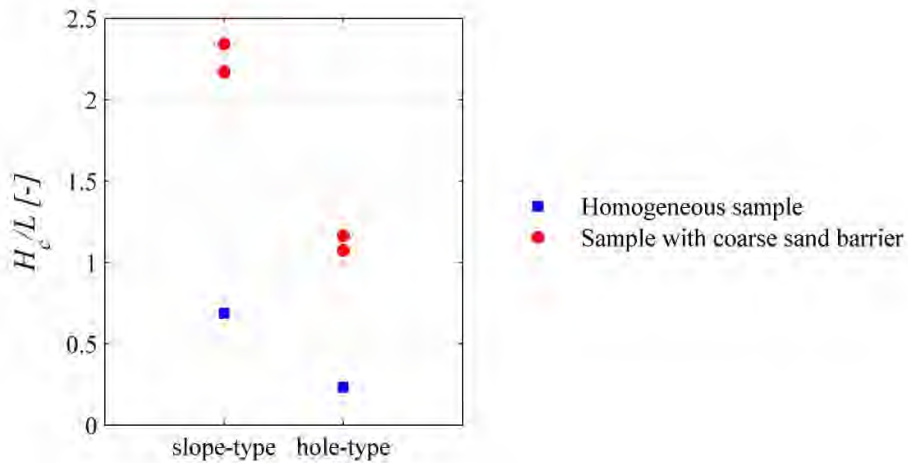


Figure 2.4 Critical gradients in samples with and without coarse sand barrier for different configurations (Van Beek et al., 2015a)

The effectiveness of the barrier relies on the relatively large resistance of the barrier material to pipe formation. The Sellmeijer model reflects the influence of particle size on the critical head, but shows that a homogeneous layer of coarse sand will not be effective to prevent

pipng. This is due to the counteracting effect of a higher hydraulic conductivity, which increases with grain size, on the critical head. In case of a coarse sand barrier, a trench of limited dimensions will be applied, such that the flow under the levee will hardly increase, whereas the resistance to erosion does increase.

Although a combination of a large particle size and relatively low hydraulic conductivity will give an increase of critical head according to the Sellmeijer model, the model will most likely not be suitable for prediction of the effectiveness of the coarse sand barrier. The resistance to pipe formation in sands with variable properties is likely to be determined by the *local hydraulic gradient* upstream of the pipe, which is not included in the Sellmeijer model, which relies solely on the equilibrium of particles at the pipe bottom. The local gradient depends on the location and increases significantly near exits, such as the pipe tip. Erosion at the pipe tip is denoted as *primary erosion*. Water flow through the pipe causes erosion of the pipe walls and bottom, resulting in increased pipe dimensions and less resistance to flow. This type of erosion is denoted by *secondary erosion*. The Sellmeijer model fully relies on secondary erosion, combined with empirical findings in the adapted calculation rule (Sellmeijer et al., 2011; Sellmeijer, 1988).

When we would like to know the strength of a barrier, the local damage gradient at the pipe tip at which a pipe grows into the barrier needs to be determined. Experiments illustrate that the pipe develops parallel to the barrier, perpendicular to the flow direction, upon encountering the barrier (Figure 2.3) and before breaking through the barrier. This means that the local gradient near the pipe tip is sufficient to erode the fine sand parallel to the barrier, but not sufficient for pipe formation in the coarse sand. The pipe formation parallel to the barrier is important for two reasons.

Firstly, the transverse pipe development causes a risk of horizontal seepage flow bypassing the structure. This can occur when the preventive measure has finite dimensions, causing the pipe to develop in transverse direction up to the end of the structure and subsequently towards the river. Secondly, the transverse pipe development causes a decrease in local gradient in the barrier upstream of the pipe. Figure 2.5 and Figure 2.6 illustrate this effect: the flow lines in the coarse sand barrier upstream of the pipe are less severely concentrated once the pipe has developed in transverse direction.

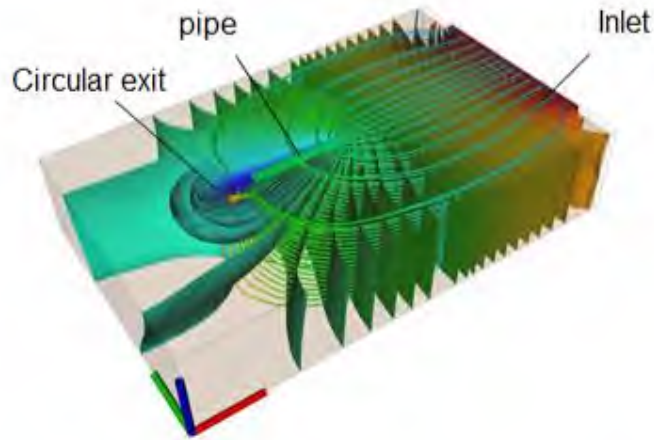


Figure 2.5 Simulation of a small-scale experiment: the pipe is modelled without transverse development (Negrinelli et al., 2016): the flow lines strongly concentrate towards the pipe tip

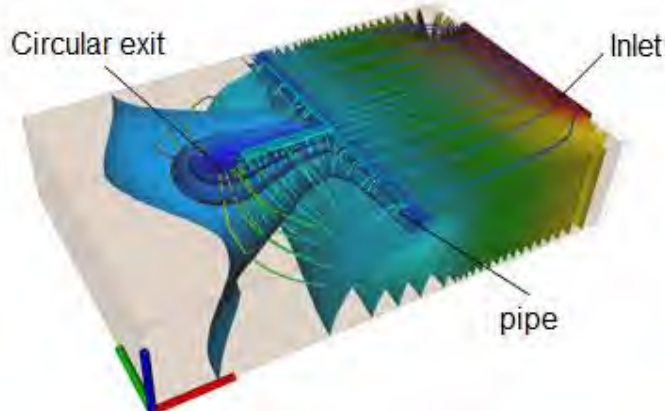


Figure 2.6 Simulation of a small-scale experiment: the pipe is modelled with full transverse development (Negrinelli et al., 2016): the flow lines are distributed over the full length of the barrier and are less concentrated.

The gradient at the tip of the pipe has been investigated for uniform sands using a specialised set-up in (Robbins et al., n.d.). This set-up consists of a horizontal tube with the sand body and pressure transducers closely spaced along the centreline at the top and the bottom of the tube. Due to the shape of the tube, the pipe will progress directly below the transducers allowing for accurate measurement of the head conditions just upstream of the progressing pipe. The experiments found: a) a local horizontal gradient causing pipe progression that depends on the sand type; b) they measured a drop in the head measurements up to a distance of ca. 130 grains upstream of the pipe tip of the progressing pipe.

The available experiments and numerical simulations provide understanding of the qualitative potential of the method, but are not sufficient to quantify the strength of the barrier in practice. In the small-scale experiments, the barrier material was not optimized for field conditions and failure was not achieved in the IJkdijk experiments. Therefore, additional experiments with

optimized barrier material and numerical simulations are required for extrapolation to field conditions.

The measure is intended for the pilot location at Gameren along the river Waal. In the first stage of the project, the sand characteristics at this location are important as the combination of the local sand and the barrier material has to fulfil the filter criteria, as discussed in (Rosenbrand, 2017). The hydrogeology of the site will also play a role in the effectiveness of the barrier. This is investigated in later phases of the project.

### 3 Experiments

Two set-ups have been used for investigation of the coarse sand barrier at small-scale: a flat box (internal dimensions  $L \times W \times D = 483 \times 300 \times 101$  mm) for which a sketch of the set-up is shown in Figure 3.2 and a set-up where the box is rotated by  $90^\circ$  ( $L \times W \times D = 483 \times 101 \times 300$  mm), referred to as the rotated set-up, which is shown in Figure 3.3. The general concept and seepage length are the same for both set-ups.

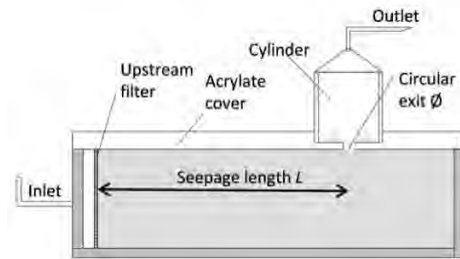


Figure 3.1 Small-scale experiment set-up with circular exit

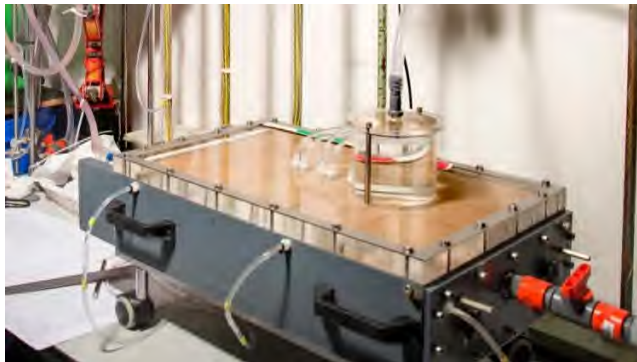


Figure 3.2. Set-up with horizontal container

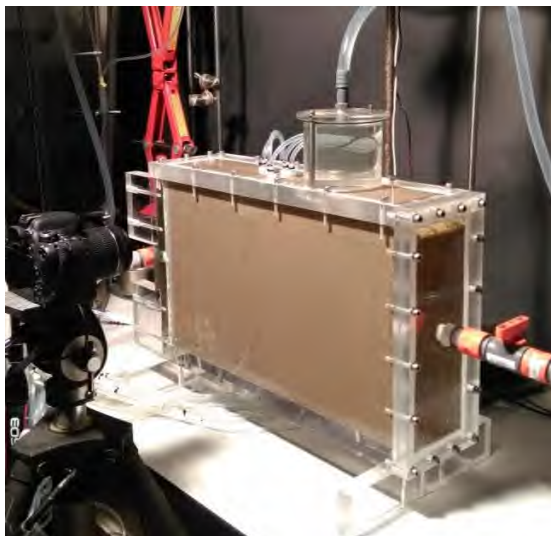


Figure 3.3. Set-up with the rotated container

The sand layer is covered with an acrylate plate, coated with silicone gel on the inside. The acrylate plate simulates the levee and the cohesive blanket layer. Both types have the conservative configuration of a punctured blanket layer (circular exit). Recent research (Van Beek et al., 2015b) has indicated that this configuration, which is common in practice, results in considerably lower critical gradients in comparison with a similar 2D-configuration (ditch, absence of blanket layer). It is expected that the pipe formation parallel to the pipe will change the initially 3D flow configuration to 2D flow. The acrylate lid has an outlet hole of 24 mm diameter with a cylinder to collect the sand that is removed from the container by erosion. A sand body with a seepage length of approximately 0.35 m and a depth of 0.10 m can be prepared in the flat small-scale box. The set-up of the rotated box is quite comparable to the normal set-up, although the depth of the sand layer is increased from 101 mm to 300 mm and the width is decreased from 300 to 101 mm. The water enters through a permeable plastic grid, covered with a nylon filter. The water exits through a circular hole of again 24 mm in the acrylate plate and is directed towards the water storage vessel through a cylinder that allows for sand boil development around the exit hole.

The hydraulic head was measured in several locations. The hydraulic heads are important for the postdiction of the experiments and for the analysis of the local damage gradient at which the pipe grows into the barrier. Figure 3.4 and Figure 3.5 show the locations of the capillaries in the flat box. The locations of the capillaries are similar for the rotated set-up (Figure 3.6). A more detailed description of the set-up, as well as a description of the preparation of the sample is given in the Factual Report (Rosenbrand and Van Beek, 2017).

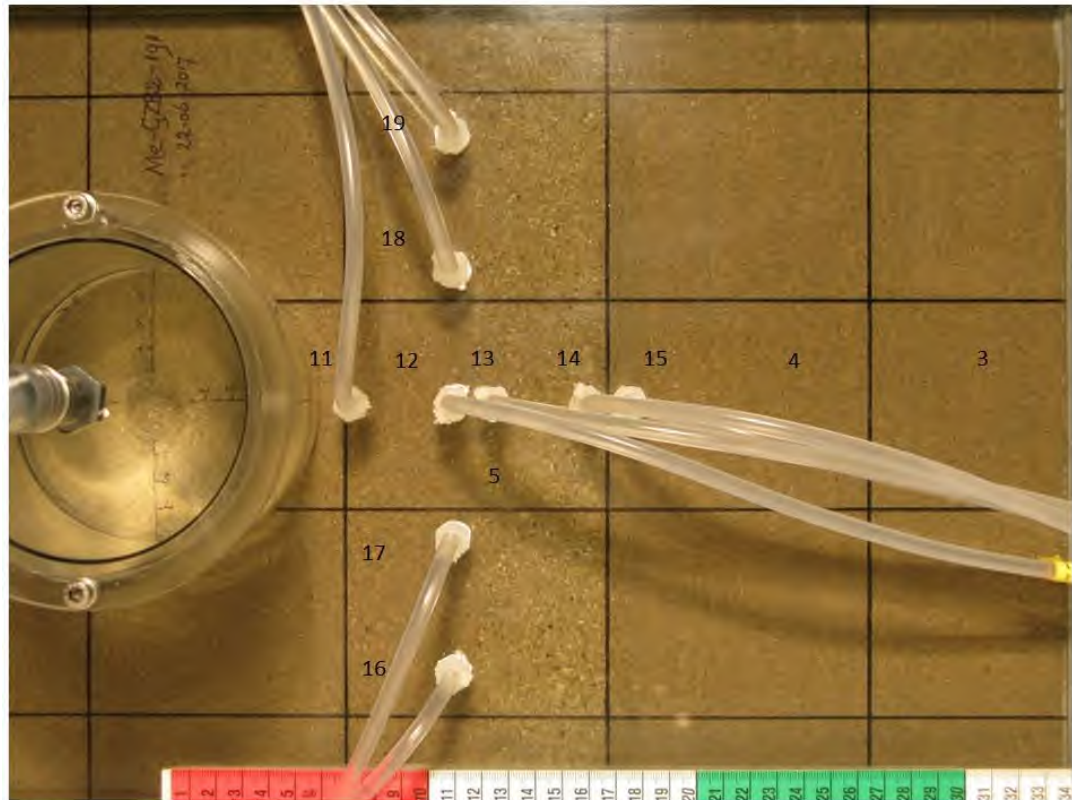


Figure 3.4 Locations of capillaries in the piping box

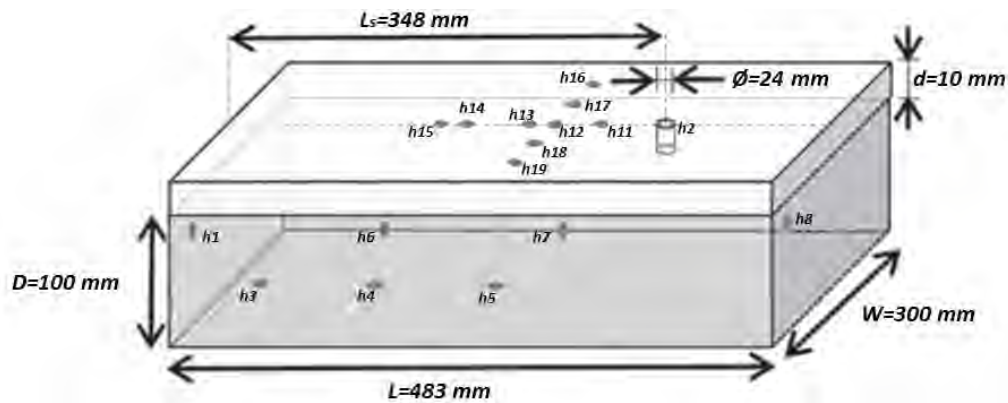


Figure 3.5 Locations of capillaries in the flat piping box

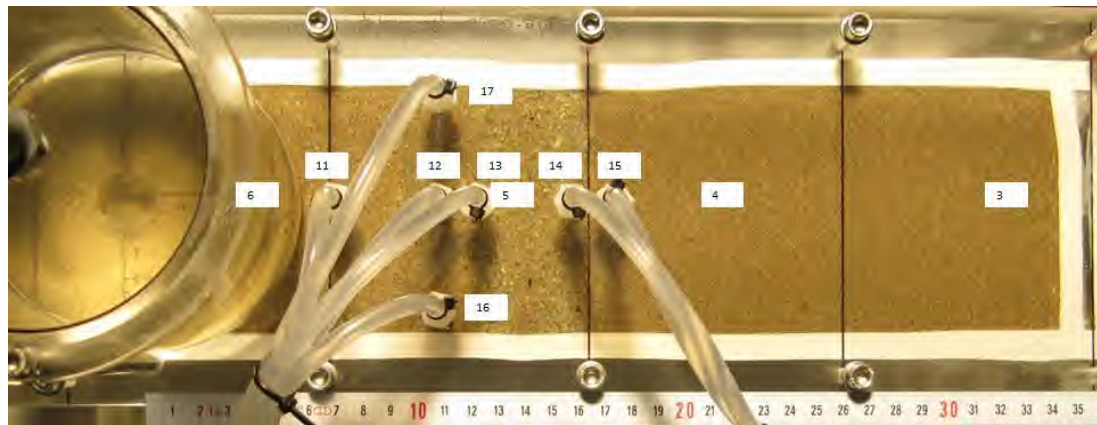


Figure 3.6 Photograph of test Me-GZB2-198, with the rotated set-up, with the location of the capillaries to measure head indicated. Image is only included to indicate locations numbers of capillaries. Capillaries 3, 4 and 5 are in the bottom of the box

### 3.1 Sand selection

The barrier material should be chosen carefully to retain particles from the sand layer upstream of the barrier, yet provide optimal resistance against backward erosion piping. When carefully selected, washout of particles from the upstream side of the barrier is not expected regardless of the head drop across the water retaining structure. Literature on filtration and suffusion (washout of fine particles from a gap graded soil) provides several rules that give guidance to whether particles can be transported through or out of the barrier. A more extensive description of literature related to particle transport is provided in (Rosenbrand, 2017). When the combination of original sand upstream of the barrier and the barrier material fulfils the filtration rules, failure of the barrier can only occur when the pipe forms through the barrier, provided that the barrier is deep enough and clogging of the barrier does not occur.

For the selection of the barrier material, the following requirements have been applied:

1.  $d_{15, \text{barrier}}/d_{85, \text{base material}} < 5$ ;
2.  $d_{50, \text{barrier}}/d_{50, \text{base material}} < 25$ ;
3. Kenney & Lau (1986, 1985) criterion for internal stability of the barrier material.

The first and the second requirement are filter rules as derived by Terzaghi, as given by Lambe and Whitman (1969). The third requirement is given by Kenney & Lau (1986, 1985) and implies that for the whole sieve curve, the value of the percentage of grains (by mass) with a diameter between  $d$  and  $4*d$ , divided by the percentage of grains with a diameter smaller than  $d$  should be smaller than 1.3 for loosely packed soil, and larger than 1.0 for densely packed soils, provided  $d_5 < 0.075$  mm. The criterion is meant to determine whether finer fractions are sufficiently prevented from washing out by the coarser fraction. This implies that the coarsest particles will never satisfy this criterion which is meant for the finer parts only.

The barrier material should match the material available at the pilot location. Although field investigation at the pilot location of Gameren was still on-going at the time the sand types for the barrier were selected, the available borings and grain size distribution allowed for a first assessment of the materials to be encountered. The available grain size distributions from the field, along with the selected materials representative for the background materials are shown below.

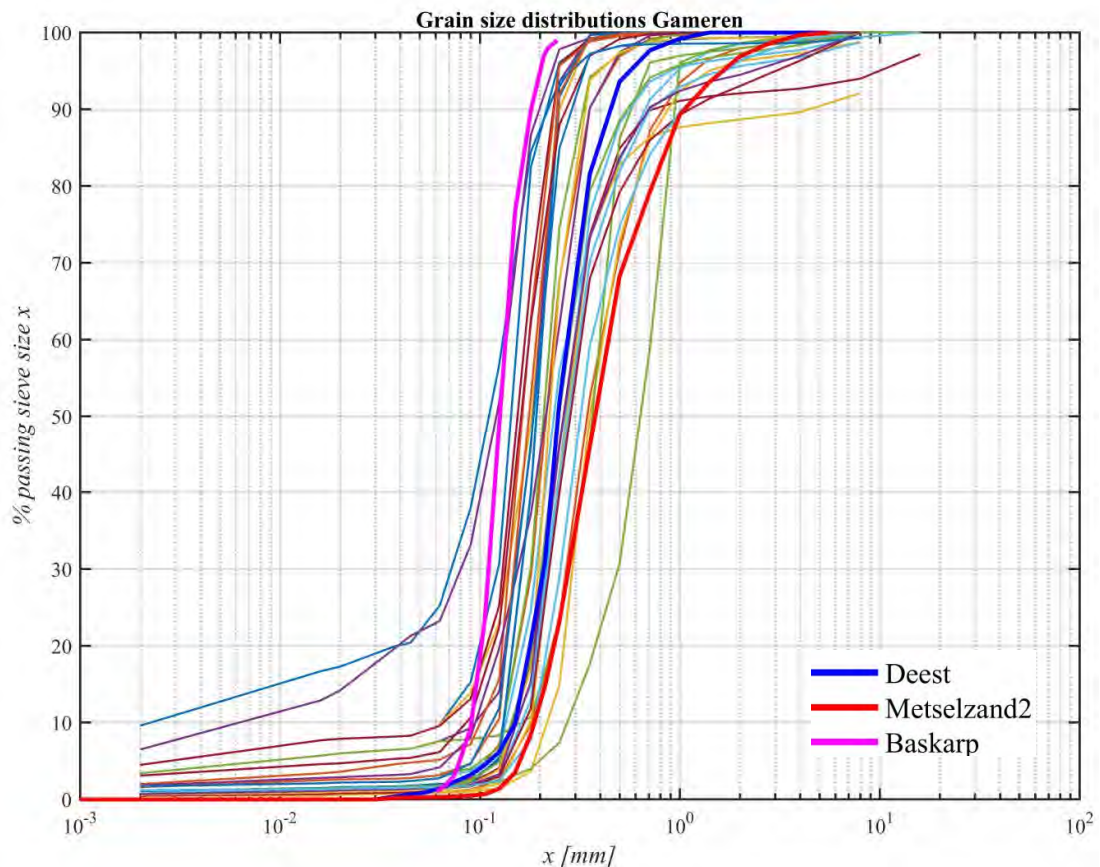


Figure 3.7 Grain size distributions of sand samples obtained from the field (thin lines) and selected materials for laboratory experiments (thick lines – see legend)

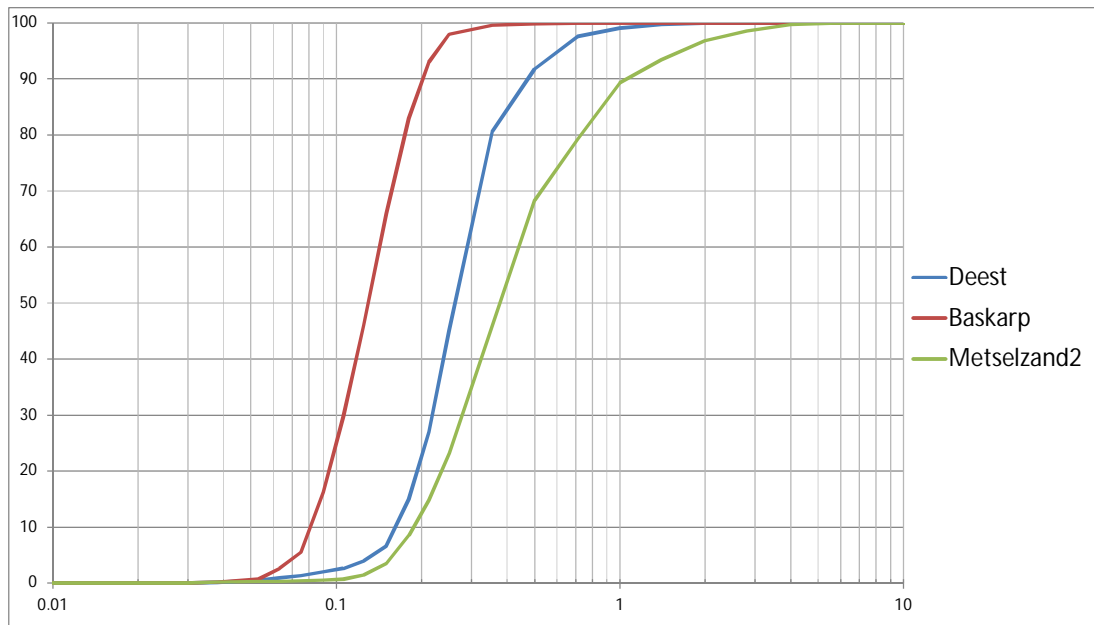


Figure 3.8 Sieve curves of base materials

With available sands, three suitable barrier materials have been constructed for application in the tests:

- GZB1, a mixture of 50% coarse filter sand, 30% fine filter sand and 20% Iitterbeck 431 sand.
- GZB2, a mixture of 80% fine filter sand and 20% Metselzand2 sand.
- GZB3, consisting of fine filter sand only.

These sands were selected based on the background sands, the available criteria, on the available reviews and on the experiences in the first experiments. The first barrier material GZB1 was based on optimized performance balancing coarse grains that fulfil the filter criteria and using commercially available sands. The second and third barrier materials were based on the experiences with GZB1, the reviews, as described in “Sand selection Coarse sand barrier experiments”. Deltares memo 11200952-004-GEO-0001-m (Van Beek, 2017)

The relevant characteristics of the barrier materials and the background materials are summarized in Table 3.1. The last column indicates to which fraction the material satisfies the Kenney & Lau criteria for internal stability. As mentioned above, the criterion is fulfilled for retaining the fine fraction. The next tables provide the ratios checked by the first two criteria as stated above. For all materials and combinations the criteria are met, except for the first criterion for the combination of GZB3 and Baskarp sand.

*Table 3.1 Sand characteristics with Kenney & Lau criterion*

Material	d <sub>5</sub> (mm)	d <sub>15</sub> (mm)	d <sub>50</sub> (mm)	d <sub>85</sub> (mm)	Internal stability satisfied until fraction (%)
GZB1	0.222	0.581	1.356	2.289	1.4 mm (56.7%)
GZB2	0.255	0.602	1.053	1.311	1.4 mm (97.5%)
GZB3	0.755	0.843	1.105	1.322	1.4 mm (98.5%)
Deest	0.112	0.164	0.246	0.378	0.25 mm (51.9%)
Baskarp	0.077	0.096	0.123	0.160	0.125 mm (52.5%)
Metselzand2	0.159	0.213	0.378	0.875	Loosely packed: 0.355 mm (46.0%) Densely packed: 0.5 mm (68.3%)

*Table 3.2 Criterion 1 for all possible combinations*

	Deest	Baskarp	Metselzand2
GZB1	1.5	3.6	0.7
GZB2	1.6	3.8	0.7
GZB3	2.2	5.3	1.0

*Table 3.3 Criterion 2 for all possible combinations*

	Deest	Baskarp	Metselzand2
GZB1	5.5	11.0	3.6
GZB2	4.3	8.6	2.8
GZB3	4.5	9.0	2.9

The sieve curves of all these materials are shown in Figure 3.9 and Figure 3.10.

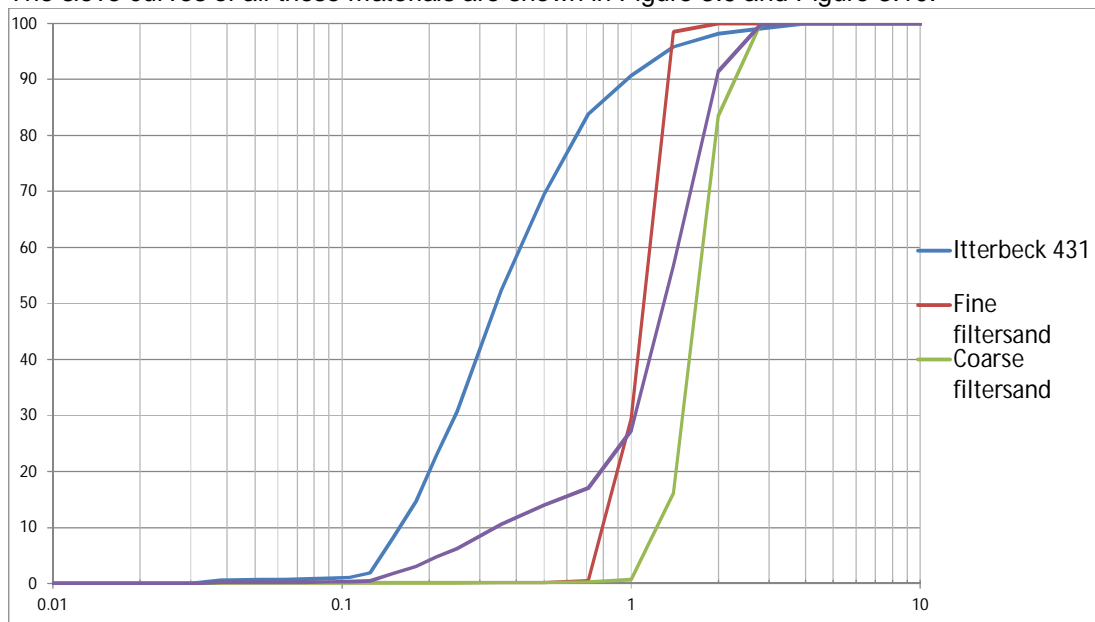


*Figure 3.9 Sieve curves of GZB1 barrier material and constituting materials*

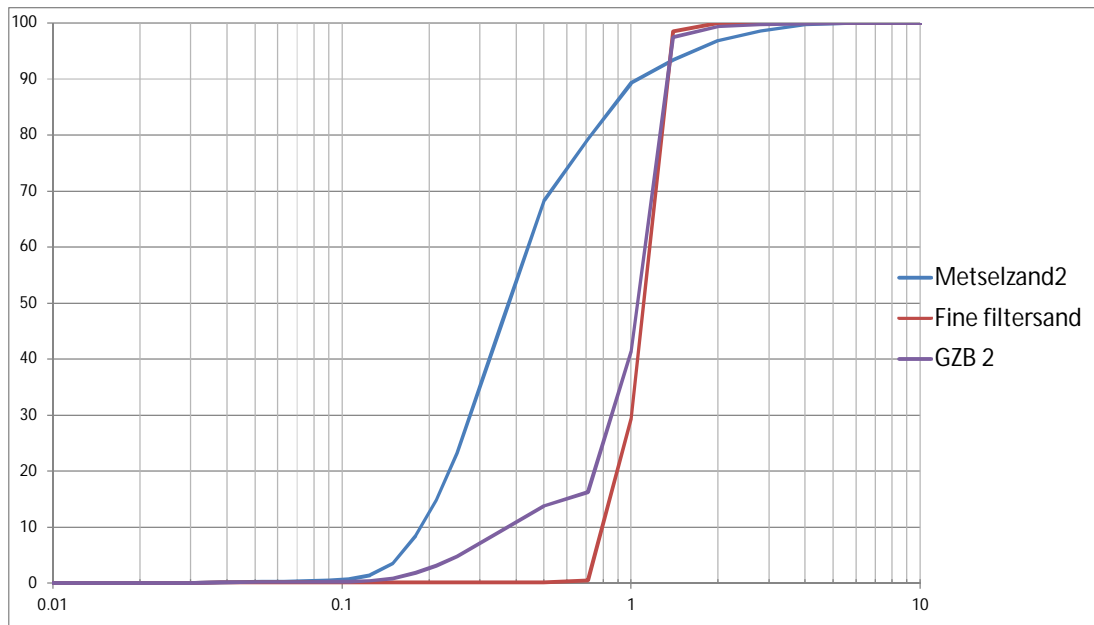


Figure 3.10 Sieve curves of GZB2 barrier materials and constituting materials

### 3.2 Experimental programme

The initial experimental programme, described in the approach of the feasibility study, was adapted after the second experiment, since the barrier provided so much additional strength, that it could not be breached within the range of heads possible in the laboratory set-up. In addition the comments of reviewers were taken into account. The adaptation is described in (Van Beek, 2017).

The final experimental programme is presented in Table 3.4.

Table 3.4 Final experimental programme

No.	Piping box	Barrier material	Depth barrier cm	Thickness barrier cm	Surrounding material	Relative density barrier and upstream sand
De-GZB1-188	Regular	GZB1 – alt1	Full	5	Deest - lower b.	High
Me-GZB1-189	Regular	GZB1 – alt1	Full	5	Metselzand – upper b.	High
Me-GZB1-190	Regular	GZB1 – alt1	Full	until filter	Metselzand – upper b.	High
Me-GZB2-191	Regular	GZB2 - pref	Full	5	Metselzand – upper b.	High
Me-GZB-192	Regular	GZB2 – pref	3 cm	5	Metselzand – upper b.	High
Me-GZB2-193	Regular	GZB2 - pref	Full	5	Metselzand – upper b.	Low
Me-194	Regular	No barrier	n.a.	n.a.	Metselzand – upper b.	n.a.
B-GZB2-195	Regular	GZB2 - pref	Full	until filter	Baskarp - lower b.	High
Me-GZB3-196	Regular	GZB3 – alt2	Full	5	Metselzand – upper b.	High
B-GZB3-197	Regular	GZB3 – alt2	Full	until filter	Baskarp - lower b.	High
Me-GZB2-198	Rotated	GZB2 – pref	3	5	Metselzand – upper b.	High
Me-GZB2-199	Rotated	GZB2 – pref	10	5	Metselzand – upper b.	High
Me-GZB2-200	Rotated	GZB2 – pref	10	5	Metselzand – upper b.	Low

In total three different barrier materials have been tested (GZB1, GZB2, GZB3), with three background materials (Deest sand, Metselzand (masonry sand) and Baskarp sand). GZB2 is the preferential material with which most variations have been conducted. The barrier depth has been varied for this barrier material to investigate the possibility of piping underneath the barrier. Three experiments have been conducted with the rotated box, to investigate scale effects. In the experiments in which the damage head drop was expected to be too high for the laboratory set-up (both experiments with Baskarp sand and the last one of the experiments with GZB1), the barrier was expanded towards the upstream side, to reduce the total head at which the barrier would breach within the maximum applicable head range. A more detailed description of each of the experiments is presented in the Factual Report (Rosenbrand and Van Beek, 2017).

## 4 Analysis of experimental results

This Chapter analyses the experimental results which are reported in the Factual Report (Rosenbrand and Van Beek, 2017). First, an overview of observations and measurements is presented and commented on in Section 4.1 through Section 4.6. Then, in order to establish a damage criterion for the barrier strength, the values of possible indicators of barrier strength at the damage condition are analysed in Section 4.7. The same is done for those parameters at the point the barrier fails in Section 4.8. In Section 4.9 a comparison is made to the reference test without a coarse sand barrier.

### 4.1 Observations

#### 4.1.1 Pipe progression

Progression of the pipe could be seen by visual observations during the experiments. The progress of a pipe in the fine sand has been described in for instance (Van Beek, 2015) and similar events are seen here. In the fine sand, the pipe progresses by detachment of groups (clouds) of fine grains rather than by erosion of individual grains.

In all experiments except test for 200 (where the pipe started upstream of the barrier) the following sequence of events was observed:

- The pipe develops from the outlet hole to the barrier, initially the pipe may develop in all directions, as the head drop is increased the pipe grows upstream.
- The pipe progresses in the direction perpendicular to the flow along the width of the barrier (as also observed in earlier tests with a barrier by (Negrinelli et al., 2016)).
- There is some crumbling of the barrier at the interface between the barrier and the pipe.
- The pipe damages the barrier, i.e. a pipe progresses a short distance into the barrier, this was noted as the critical condition.
- Several more pipes progress into the barrier, at different locations along the width of the barrier as the head drop is increased.
- One or more of the pipes lengthen inside the barrier (with increasing head drop over the model).
- One pipe causes failure of the barrier, by breaching the upstream interface of the barrier and progresses upstream.

In no case did the pipe deepen or grow downwards and progress below the barrier as could happen for a sheet pile wall or an impermeable geotextile. Even when the barrier was only three centimetres deep the failure was caused by the pipe growing through the barrier.

When the pipe progresses into the barrier at the damage condition, a pipe with a length between 1 and 4 cm forms in the barrier in one head increment. With further increases of the head drop, the pipe lengthens discontinuously, by erosion of a group of barrier grains. However, intermittent transport of individual barrier grains through the pipe was also observed, typically this did not result in lengthening of the pipe.

In the first three tests (188, 189 and 190 with GZB1) no failure took place. Therefore, those tests are not analysed in detail here, however they are included in the Factual Report (Rosenbrand and Van Beek, 2017). Barrier material GZB1 is stronger than GZB2, and for the

current analyses of the strength of the barrier, it is required to reach failure during the experiments.

#### 4.1.2 Pipe depth at the barrier interface

In the laboratory experiments the pipe depth increased as a result of head increase. For one test (189 Metselzand with barrier material GZB1) there was no failure and the depth of the pipe at the end of the test could be measured, which showed a maximum depth of ca. 1 cm (Rosenbrand and Van Beek, 2017). However, observations indicated that generally this maximum pipe depth was achieved at a location in between the barrier and the outlet hole, and not directly at the barrier interface. Furthermore, the depth of the pipe parallel to the barrier at the interface between the barrier and the pipe was much less than the depth of the central pipe shape leading to the exit hole.

The depth of the pipe parallel to the barrier at the damage condition (when the pipe first progresses into the barrier) was estimated to be in the order of 1 to 3 mm.

#### 4.1.3 Sand boil and erosion lens

When the pipe grows, the material that is transported out of the model forms a sand boil (crater) above the exit hole, and some fine suspended material is being deposited around the crater. Previous research (Van Beek, 2015) has shown that an erosion lens forms below the exit hole, which is a deeper circular zone where the sand has been eroded due to converging flow towards the exit, and where flow may well be non-laminar. Although this erosion lens is not visible during most of the experiments, in some experiments this zone can be observed to extend beyond the limits of the sand that is deposited on the cover.

Both the sand boil and the erosion lens contribute to a head loss in the experiment, which may not be present in a field situation. The head loss due to the sand boil and the erosion lens are quantified in Section 4.2.3.

In previous experiments with a smaller exit hole, there was a more or less uniform vertical flow through the exit hole. In some of these experiments with a larger exit hole, it was observed that the outflow was only present in a part of the hole. From the horizontal pipe there is a 'water jet' flowing nearly horizontal.

#### 4.1.4 Sand transport

##### 4.1.4.1 *Inside the barrier*

Two barriers are analysed here, GZB2 and GZB3. The barrier material of GZB2 was a mixture of coarse grains (80%) and Metselzand (20%), this barrier is considered internally stable and able to retain the fine sand upstream according to the filter rules as described in Section 3.1.

In the tests with a barrier with a high relative density, there were no observations of fine sand being transported into the barrier from upstream, or of fine sand that was already present in the barrier being transported out of the barrier before the pipe first progresses into the barrier. This does not prove that the barrier was internally stable, as it is not possible to ascertain that indeed no transport took place, however it appears that the majority of the fine sand that was present in the barrier remained so during the tests.

GZB3 did not contain a finer fraction. However, it is possible that some fine sand was transported from upstream of the barrier through the barrier in the only test done with this barrier material and fine sand on the upstream side of the barrier (test 196). This was not observed, however as discussed in Section 4.3.3, it appears that visual observation is insufficient to rule out entirely the possibility of transport of the background sand. The

possibility of transport of the finest grains through the barrier is indicated by the lack of filter cake formation in this test, as discussed in Section 4.3.3.

#### 4.1.4.2 *At the upstream interface of the barrier*

In some tests the head measurements over the upstream interface of the barrier indicated the formation of a filter cake on the upstream interface of the barrier. This was difficult to observe visually, and images do not conclusively show whether or not sand accumulated at the upstream interface. This implies that visual observations in the current set of tests are not a sufficient indicator of processes such as filtration during the experiments.

In test 200 it was observed that pipe formation started on the upstream side of the barrier and the eroded fine sand was deposited in the barrier. This was a test with a low density barrier and apparently there was sufficient space inside the barrier for fine grains to be transported into the barrier to some extent. The fine sand did not pass immediately through the barrier, and a significant amount of it got filtered creating 'inverse' pipes in the barrier. The pipes on the upstream side of the barrier did not progress to the inlet. Instead they stopped progressing, possibly because the eroded fine sand was filtered and thereby further erosion upstream was prevented. This self-healing process thus creates additional strength.

#### 4.1.4.3 *At the barrier edge*

When the pipe has reached the barrier and widened along the barrier often some crumbling of the barrier is reported. This implies that some individual barrier grains rolled into the pipe. In some tests also some particle movements which can better be described as slope instability of the barrier is observed, where a very shallow (max 0.5 mm into the barrier) wider (ca. 1 cm wide) section is eroded. These shallow erosion phenomena are distinguished from the progression of the pipe into the barrier and are not considered as damage to the barrier. The actual progression of the pipe into the barrier involves erosion of an area that reached at least as far into the barrier as the width of the area. Typically this creates shapes with a width of 0.5 to 1 cm and reaching between 1 and 4 cm upstream in the barrier. These differences are illustrated in Figure 4.1.



Figure 4.1 *Illustration of processes occurring before and at damage condition. Left individual grains from the barrier roll into the pipe. Middle slope instability a group of grains from the barrier slides into the pipe leaving. Right pipe entering the barrier*

## 4.2 **Head drop**

During the experiments, the head was measured in several locations in the barrier and, upstream, and downstream of the barrier and in the inlet and outlet tubing. Head measurements were used in order to calculate the local hydraulic gradients in the model and to fit the postdictions of the experiments. The locations of the capillaries used to compute the

different head drops and gradients are shown in Figure 4.2, the locations of the capillaries in the model are shown in Table 4.1

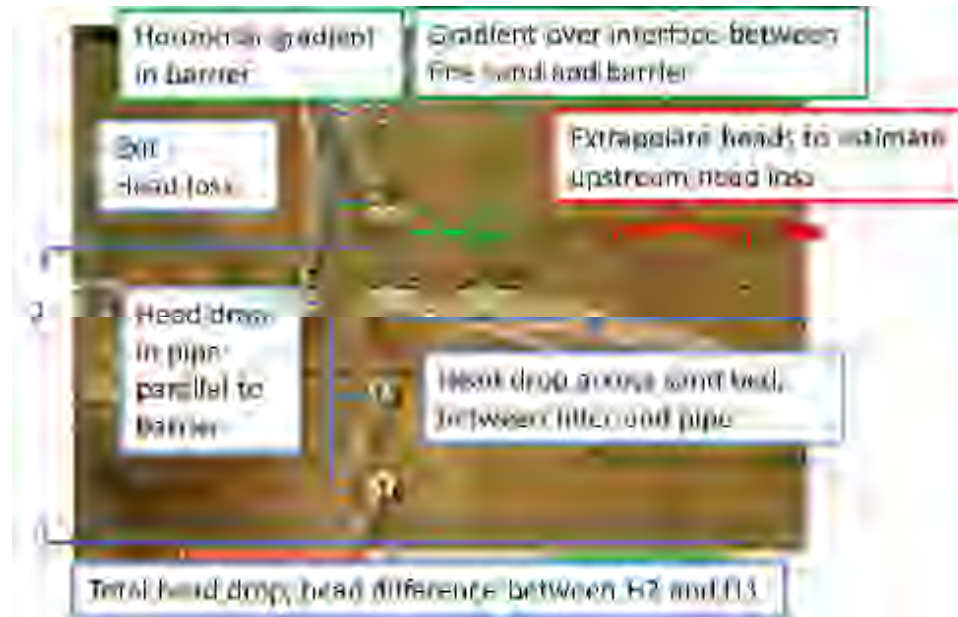


Figure 4.2 Picture of the setup, numbers indicate the numbers of the capillaries where the head measurements are made. Numbers in italics, 3,4 and 5, are capillaries in the bottom of the setup. Blue brackets indicate between which capillaries the head drops are calculated. Green brackets indicate capillaries between which gradients are calculated. Red bracket indicate capillaries used to calculate upstream head loss, red dot indicates the location of the head extrapolated head, at the upstream end of the set-up in the sand body. Vertical gradients are computed based on the value of capillary H5 in the bottom centre of the barrier and the average of capillaries H13 and H14 in the top of the barrier

Table 4.1 Locations of capillaries relative to centre of outlet hole

	Location relative to centre of the outlet hole, mm*												
Model set-up	H2	H3	H4	H5	H11	H12	H13	H14	H15	H16	H17	H18	H19
Flat model	Tubing	330	240	140	70	107.5	122.5	157.5	172.5	107.5	107.5	107.5	107.5
Rotated model	Tubing	339	249	159	70	107.5	122.5	157.5	172.5	107.5	107.5	Not present	Not present

\* the upstream end of the set-up is the start of the sand body beyond the filter

The head drop between the capillary that is furthest upstream in the sand bed (H3) and the outlet is referred to as the total head drop<sup>2</sup>.

The estimated error in the head measurements is ca. 1 mm water head, note that this is only a rough first estimate. Error bars are not shown in the figures below but are accounted for in the analysis of the damage condition and the failure conditions, in Section 4.7 and Section 4.8 respectively, and in the fitting of the numerical analyses in Section 5.5.4.

<sup>2</sup> This head drop therefore excludes the resistance in the upstream tubing and in the filter on the upstream side of the experiments, but includes head loss in the pipe and the sand boil.

#### 4.2.1 Head drop in all capillaries

The capillaries give insight into the flow pattern in the sand sample, changing over time due to the head increase and the pipe formation. In the Factual Report (Rosenbrand and Van Beek, 2017) graphs of the head drop in all capillaries are shown for all of the experiments. An example of the heads in one test is shown below for illustration (test 191). In this test the pipe progressed into the barrier at a head drop of 41 cm: this is considered the critical condition. There is a small jump in H4, but no noticeable change in the other capillaries. The response of the head to pipe formation was similar in all experiments, which makes it difficult to detect the damage condition based on the head measurements.

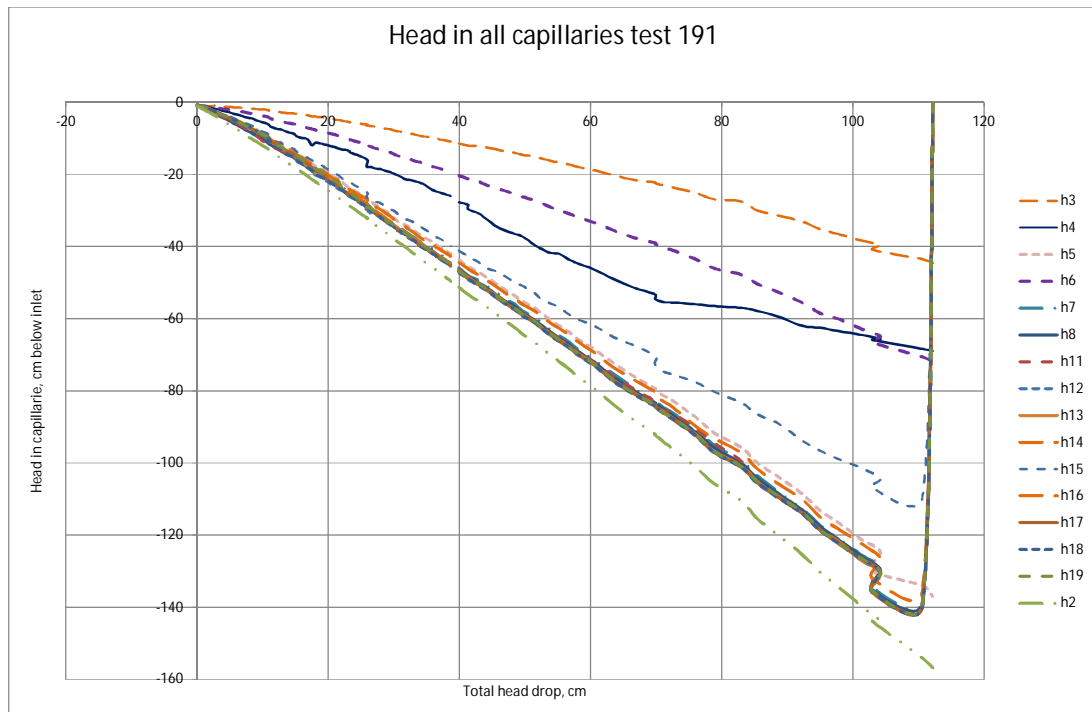


Figure 4.3 Head in all capillaries during test 191. The x axis shows the head drop between capillary H3 in the sand body on the upstream side of the set-up just beyond the filter, and H2 in the outlet tubing ('total head drop'). The pipe enters the barrier at a head drop of 41 cm, this does not produce a significant change in the readings in the capillaries

#### 4.2.2 Upstream head loss

The head loss over the part of the set-up upstream of the sand body, i.e. in the tubing and the filter at the inlet of the box, is estimated by extrapolating the line of best fit through the heads measured in the bottom of the model in H3 and H4 for tests with a fine sand upstream, and H3, H4 and H5 for tests where the barrier is present all the way to the upstream side (as H5 is always in the barrier). This head loss over the filter is a function of the flux, as shown below.

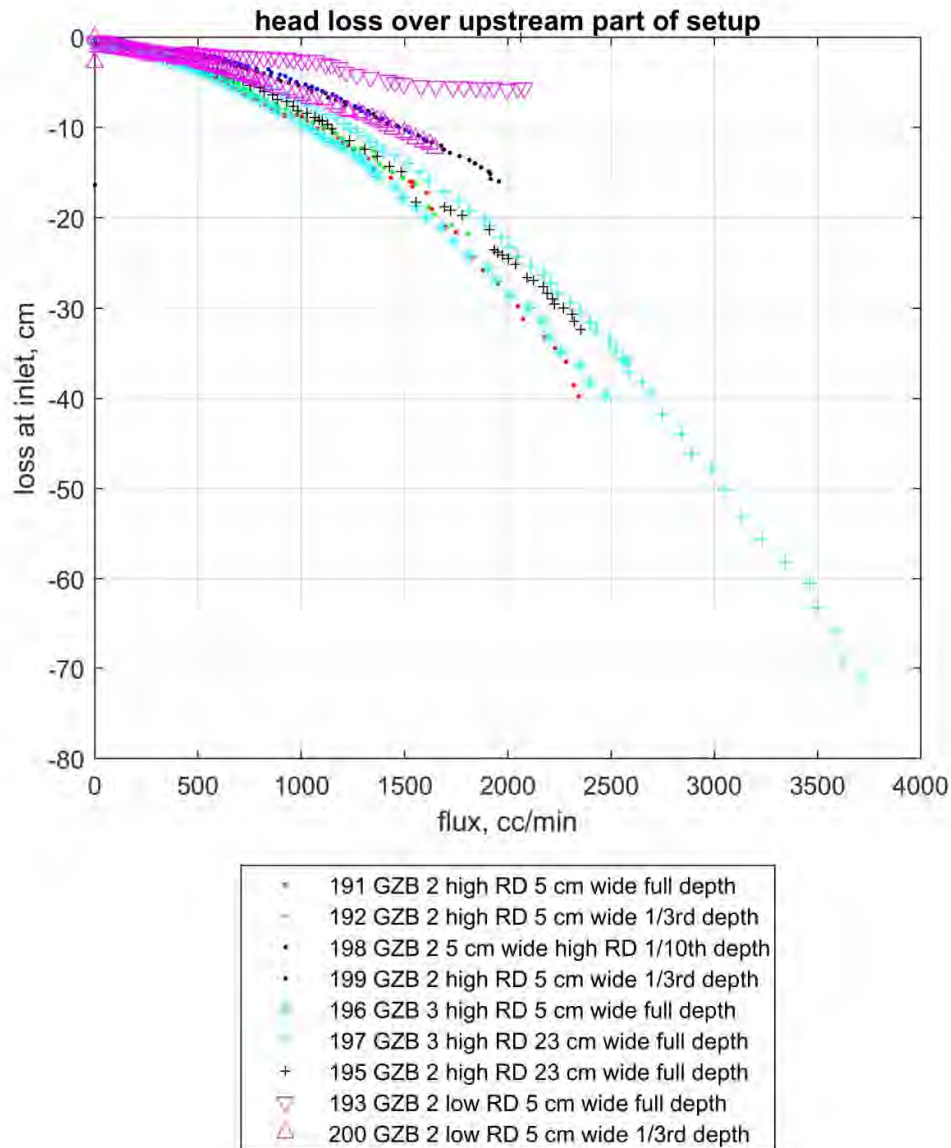


Figure 4.4 Head loss over the upstream tubing and filter as a function of flux during the test

In all experiments there is an increase in the loss at the inlet with increasing flux. Test 193 shows a much smaller head loss than the other tests. This is the test with the largest head drop over the interface between the barrier and the fine sand upstream, possibly due to the formation of a filter cake (as discussed in Section 4.3.3). The resistance of the filter at the inlet is determined by the combination of the properties of the filter and the sand touching the filter as shown in (Van Beek et al., 2015b). Possibly, in test 193 with a low relative density of the barrier more of the finer sand grains were washed from the filter reducing the filter's resistance to flow.

#### 4.2.3 Exit head loss

The exit head loss is calculated as the head loss between the capillaries in the location of the pipe just downstream of the barrier (the average of the heads measured in H16-H19 and H12) and the outlet. After the pipe has widened along the barrier, this is the head loss in the pipe, the erosion lens and the sand boil described in Section 4.1.3.

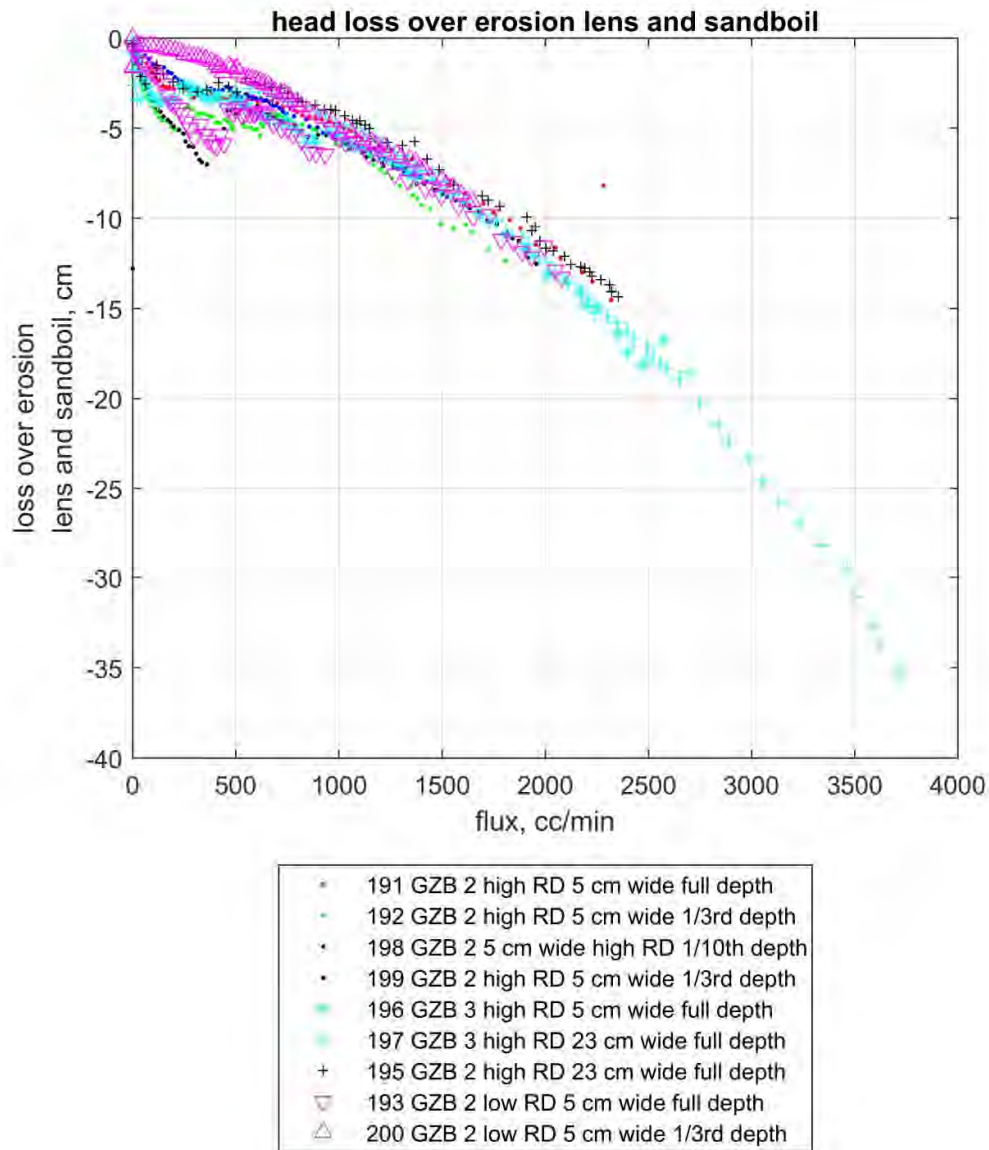


Figure 4.5 Head loss over the pipe, the sand boil and the erosion lens a function of flux during the tests

Most experiments show an increase in the resistance (i.e. the head drop gets more negative) up to approximately 400 or 500 cc/min followed by a levelling off or even a reduction in the magnitude of the head drop as a function of the flux (the head drop gets more positive). This is because the pipe is not present below the capillaries in the initial phase, so this initially steeply increasing head drop reflects the resistance of the fine sand. After the pipe has reached below the capillaries the head loss in the pipe and sand boil decreases, as there is

less resistance in the pipe. Then as the sand boil and the erosion lens grow, the head drop further increases as a function of flux. The head drop increase is not linear with the flux, this suggests that there is also a turbulent component in the flow near the exit. It was observed in some tests that grains were whirling around in the erosion lens, this is evidence of non-laminar flow, and this contributes to the head drop.

In test 200 the head loss is initially much smaller than the head loss in the other experiments. In this test pipes formed first on the upstream interface of the barrier, and later there was no pipe formation on the downstream end but a general washout of fines to the exit. This, in combination with the low head loss suggests that there may have been some space between the sample and the top of the model. This does not appear to have been the case in the other test with a low relative density barrier, test 193, as there is the initial steeper gradient in the head loss which reflects more resistance of the fine sand. The different set-up of test 200, the rotated box, may have contributed to this.

#### 4.2.4 Head drop across sand bed

The head drop over the sand bed, i.e. excluding the head loss in the upstream tubing and in the sand boil and erosion lens, is shown as a function of flux in Figure 4.6. This is the head drop calculated from the upstream end of the set-up, in the fine sand just beyond the filter, to the capillaries on the downstream interface between the barrier and the fine sand that are in the fine sand (i.e. capillaries H12 and H16-H19) as in (Rosenbrand and Van Beek, 2017).

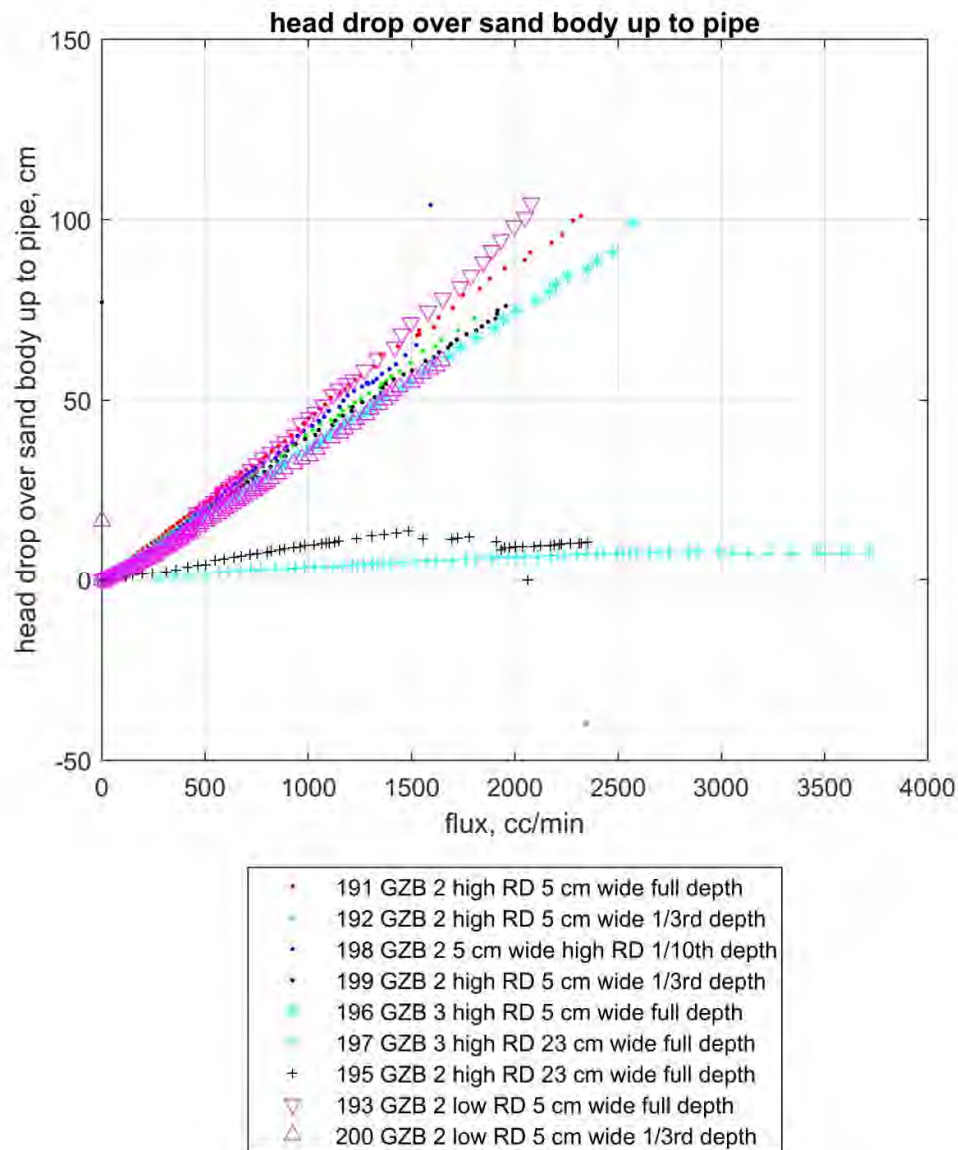


Figure 4.6 Head drop over the sand body up to the pipe as a function of flux

The head drop over the sand body increases with increasing flux. A constant gradient implies a constant hydraulic conductivity. Test 193 shows an increase in the gradient in the course of the test, implying a reduction of hydraulic conductivity. This is probably due to the formation of a filter cake, as elaborated on in Section 4.3.3.

There is a clear distinction in the head drop over the sand body for tests 195 and 197 and the other tests. Those two tests are conducted with the barrier reaching all the way upstream in the model, and with Baskarp sand downstream. Therefore there is much less resistance to flow in the sand bed. Test 195 shows a higher resistance initially, but the head drop falls to a similar level as in test 197, when the pipe lengthens in the barrier between fluxes 1500 and 2000 cc/min. The hydraulic conductivity of the barrier is higher in test 197 which could

account for the higher head loss in test 195. Progression of the pipe increases the hydraulic conductivity of the barrier and thus reduces the head drop.

The figures below show the head drop at damage condition, when the pipe first progresses into the barrier. It is clear that beyond this point both the flux and the head drop can increase significantly before the pipe reaches the upstream side of the box. In Section 4.7 an overview of all tests is given of the head drop when the pipe first progresses into the barrier, and in Section 4.8 this overview is given for the head drop where the pipe breaches through the upstream interface between the barrier and the fine sand upstream and progresses upstream.

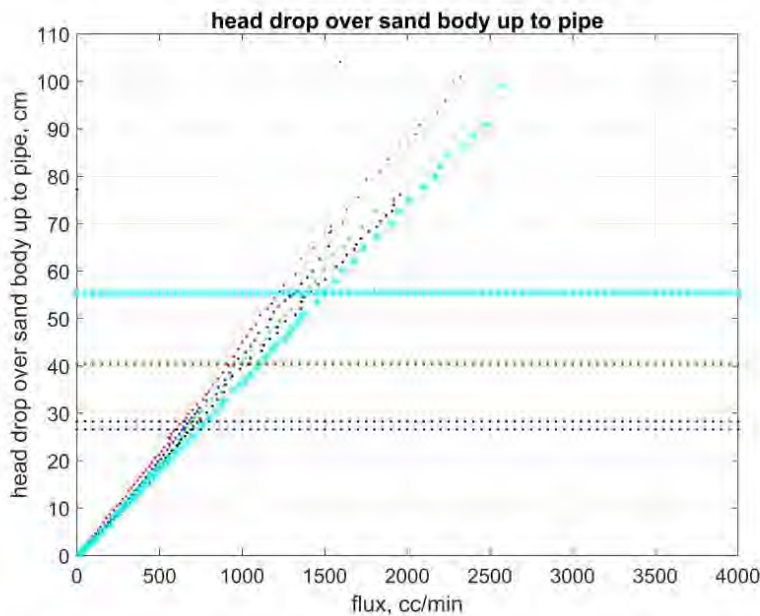


Figure 4.7 Head drop over the sand body up to the pipe as a function of flux. Legend is the same as in Figure 4.6. Horizontal lines indicate the head drop at the damage condition when the pipe first grows into the barrier

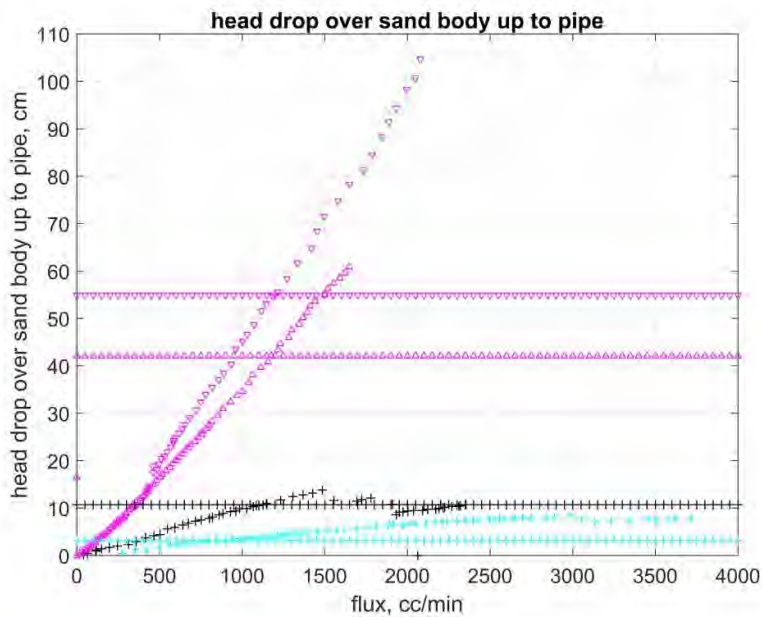


Figure 4.8 Head drop over the sand body up to the pipe as a function of flux. Legend is the same as in Figure 4.6.  
Horizontal lines indicate the head drop at the damage condition when the pipe first grows into the barrier

#### 4.2.5 Head drop parallel to the barrier

The head was measured at several locations along the barrier, to investigate the head loss in the pipe. The head drop in the capillaries parallel to the barrier therefore indicates the extension of the pipe parallel to the barrier. The head drop between neighbouring capillaries initially increases as the overall head over the set-up is increased, due to pipe formation. When the pipe reaches the barrier below one of a pair of capillaries the gradient becomes very high, as there is a low head in the capillary above the pipe and a higher head in the capillary above the sand bed. When the pipe grows below the next capillary, the head there will also fall and the head drop becomes very low, indicating the low resistance to flow in the pipe. Subsequently there may be some fluctuations as material is eroded from the barrier and passes below one of the capillaries, temporarily increasing the head locally. A sample of the head drop among capillaries is shown below, along with the interpretation for that test.

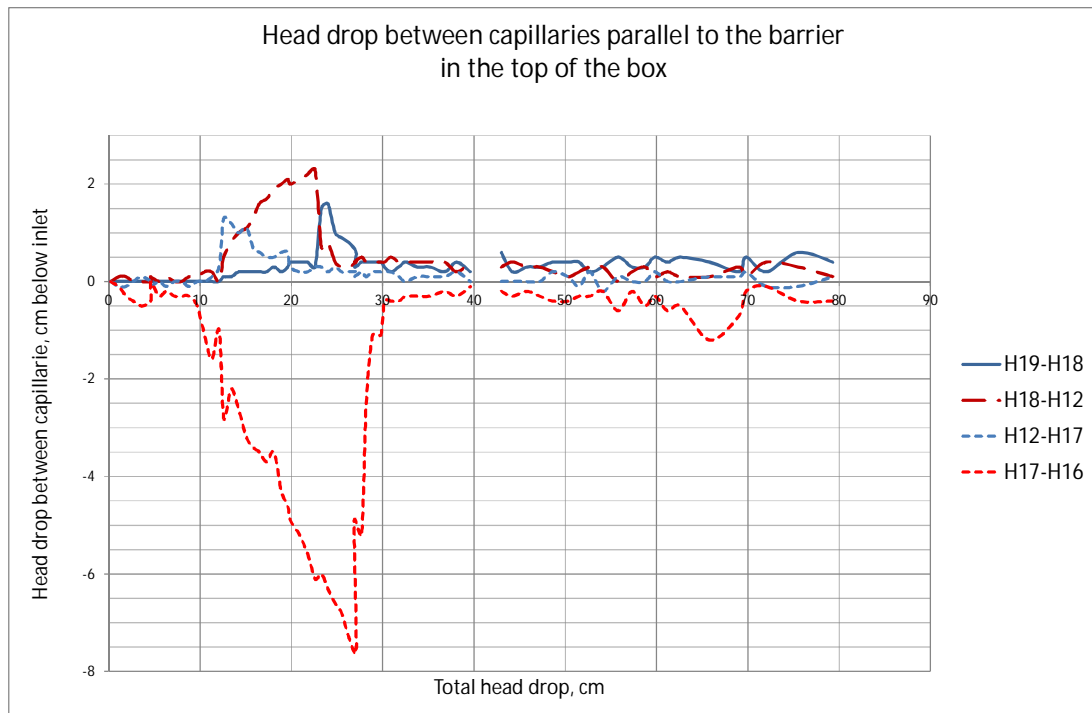


Figure 4.9 Head drop between two neighbouring capillaries at the location where the pipe forms parallel to the barrier is shown for test 192. The x axis shows the head drop between capillary H3 in the sand body on the upstream side of the set-up just beyond the filter, and H2 in the outlet tubing

The head drop between pairs of capillaries is initially highest during the phase when the pipe still has to develop all the way to the North (H16) and to the South between H12 and H18 and subsequently between H18 and H19 along the barrier. Once the pipe has fully developed the head loss between the pairs of capillaries (separated by 5 cm) is less than 0.5 cm, i.e. the gradient in the pipe is less than 0.1. This is similar to test 191. The difference between H17 and H16 is very large, possibly because the pipe reaches the barrier at H17 and deepens most there whilst progressing mainly to the South, whereas it takes much longer to progress to the North (H16) (text from Factual Report (Rosenbrand and Van Beek, 2017)).

In the experiments the barrier runs from North to South, in flow direction is from West to East.

### 4.3 Gradients

Head measurements are used to calculate the local gradients within the model. The local gradients are important as the hypothesis is that the local gradient will determine whether the pipe progresses or not. Furthermore, the local gradient relates to the local hydraulic conductivity, and changes in the local hydraulic gradient can therefore reflect changes in the hydraulic conductivity.

Local gradients are shown as a function of the head drop over the set-up, estimated as the head drop between capillary H3 in the upstream end of the set-up just beyond the filter, and H2 in the outlet tubing. This head drop therefore includes head losses in the sand boil and the erosion lens.

#### 4.3.1 Vertical gradients

The average vertical gradient in the barrier is computed using the average measured head between H13 and H14 at the top of the model in the barrier and the head measured in H5 in

the middle in the bottom of the barrier. The figures below show the development of the vertical gradient over the course of the experiments. The experiments are grouped into those where the barrier is present over the entire depth of the set-up in Figure 4.10 and those where this is not the case in Figure 4.11. In the latter case the actual vertical gradient in the barrier cannot be derived from the measurements, since the vertical head loss is partly caused by the fine sand.

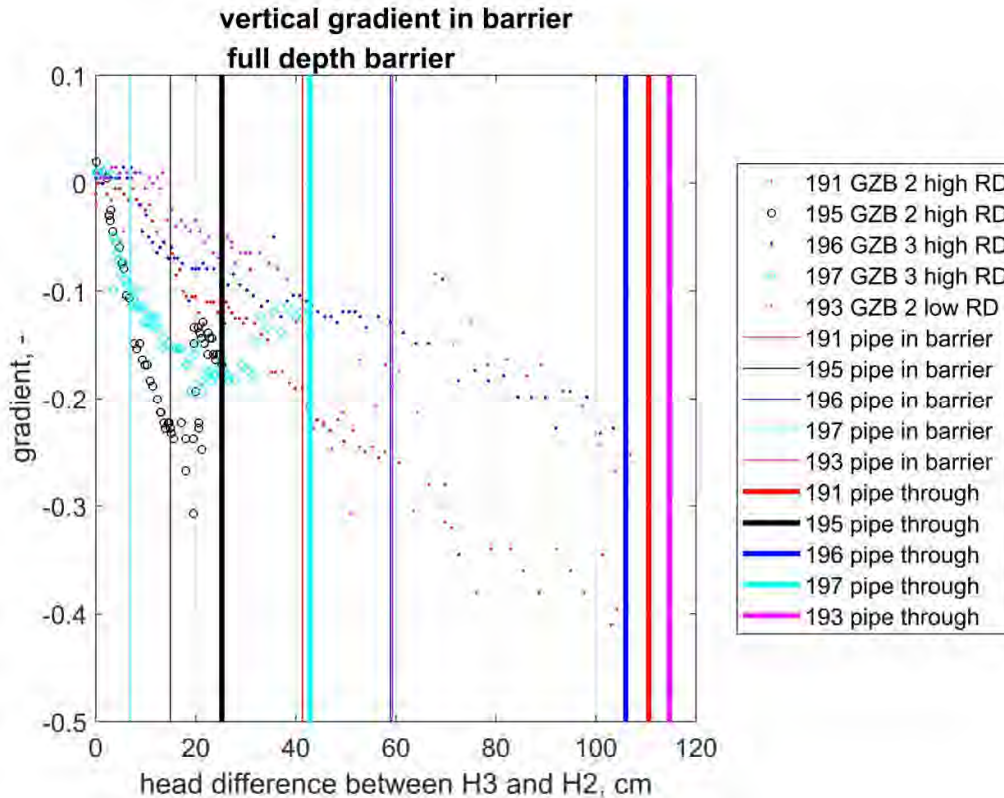


Figure 4.10 Vertical gradients in the tests with a barrier over the full depth of the model. Symbols indicate measurements throughout the test. Straight thin lines indicate the damage condition when the pipe enters the barrier; straight thick lines indicate the point where the pipe breaks through the barrier. The x axis shows the head drop between capillary H3 in the sand body on the upstream side of the set-up just beyond the filter, and H2 in the outlet tubing

Tests with Baskarp sand downstream where the barrier extends to the upstream interface (195 with GZB2 high RD and 197 with GZB3 high RD) show a more negative vertical gradient in the first portion of the test than tests with the same barrier materials at high relative density with Metselzand where the barrier does not extend upstream. In the tests with Baskarp sand, however, the gradient increases again after the pipe has breached the barrier. In these tests there is a higher hydraulic conductivity contrast between the barrier and the fine sand so there is more convergence of flow to the top of the model. When the pipe breaches the barrier, i.e., when the pipe grows through the entire barrier, there is a larger outflow area and flow will converge to the pipe, reducing the head in the bottom of the model at the location of H5, and thereby making the vertical gradient less negative. This convergence is less pronounced in the tests with the 5 cm barrier, where the hydraulic conductivity contrast is also

less. The effect of the hydraulic conductivity contrast on convergence of flow in the barrier is shown in Section 5.4.1 and Appendix F.

Vertical gradients shown for tests 198, 199 and 200 in the Factual Report (Rosenbrand and Van Beek, 2017) were a factor 3 too high, the correct values are shown in the current report.

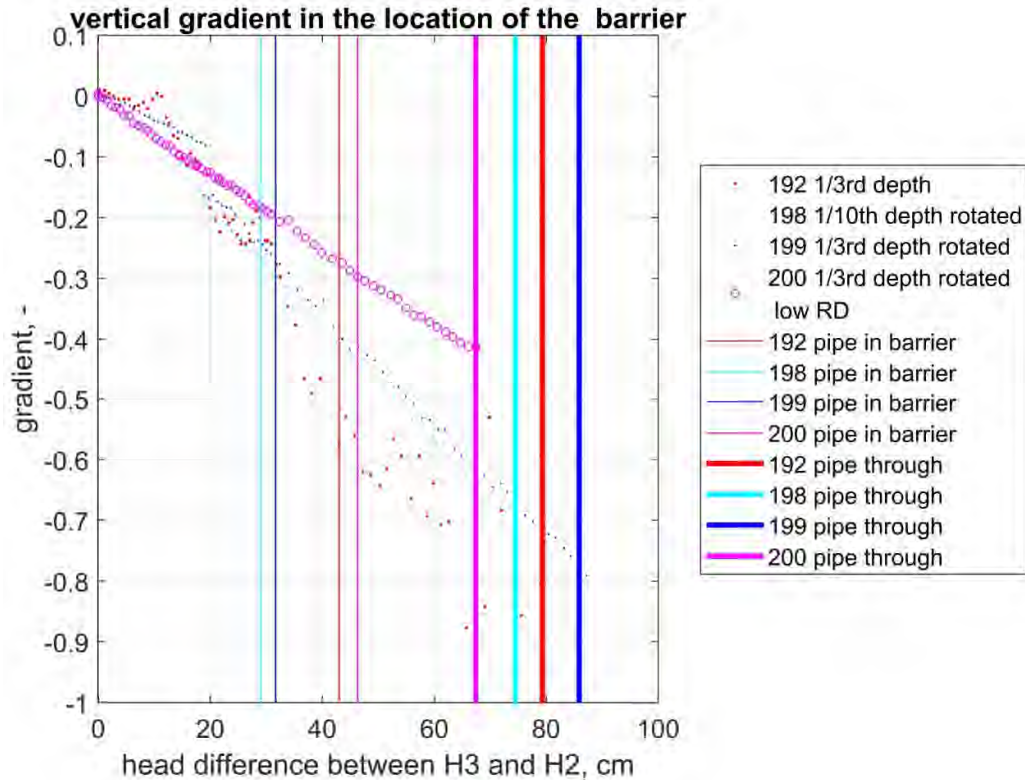


Figure 4.11 Vertical gradients in the tests with a barrier over part of the depth of the model. Symbols indicate measurements throughout the test. Straight thin lines indicate the damage condition when the pipe enters the barrier; straight thick lines indicate the point where the pipe breaks through the barrier. The y axis shows the vertical gradient. The x axis shows the head drop between capillary H3 in the sand body on the upstream side of the set-up just beyond the filter, and H2 in the outlet tubing

The vertical gradient in the tests where the barrier is only present over part of the depth of the model show a more negative vertical gradient than tests with a barrier over the full depth, as can be expected due to the greater resistance of the fine sand to flow. The gradient for the two tests in the rotated set-up with the same relative density (tests 198 and 199), where there is 27 cm (198) and 20 cm (199) of fine sand below the barrier show a very similar value of vertical gradient. This suggests that the vertical gradient is determined mainly by the fine sand below the barrier, and that the difference between 27 cm of fine sand and 20 cm of fine sand below the barrier is small.

The experiment 200 with the lower relative density barrier also has lower relative density sand below the barrier. This accordingly shows a lower vertical gradient, than the test with the same set-up and a higher relative density, due to the higher hydraulic conductivity of the sand. The upstream sand in this test does have a high relative density.

#### 4.3.2 Horizontal gradient in barrier

The horizontal gradient in the barrier is measured between H13 and H14 and is an indicator for the local gradient causing damage to the barrier (pipe formation). The figures below show the horizontal gradient as a function of the head drop between H3 and H2 as well as the head drop between H3 and H2 at the damage condition when the pipe first progresses into the barrier, and at failure when the pipe passes through the barrier. The data are sorted into the tests with GZB2 with a high relative density in Figure 4.12, which are all expected to have a similar horizontal gradient in the barrier at the damage condition, and the tests on the other barrier materials in Figure 4.13.

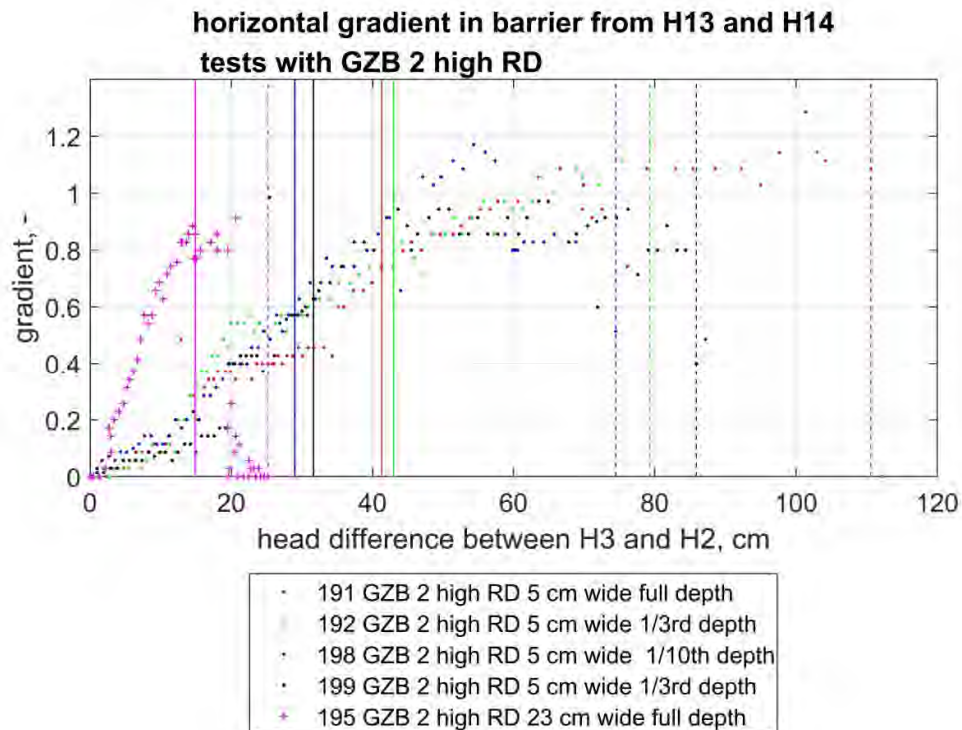


Figure 4.12 Horizontal gradient in the barrier measured between H13 and H14. The x axis shows the head drop between capillary H3 in the sand body on the upstream side of the set-up just beyond the filter, and H2 in the outlet tubing. The vertical solid lines indicate the damage condition, when the pipe first enters the barrier. The vertical dashed lines indicate failure of the barrier

It can be seen that the horizontal gradient in the barrier increases much steeper with overall head drop in test 195 than in the other tests; this is because the barrier extends all the way upstream, so the total resistance to flow is less than in the tests where there is fine material upstream of the barrier, and the gradient in the barrier can increase relatively faster.

The intersection of the vertical solid lines, which indicate the damage condition, with the horizontal gradient curves indicates the value of the horizontal gradient in the barrier at damage condition. Although the head difference at damage condition varies significantly among tests, the variation in the local horizontal gradient in the barrier proves to vary less (this is shown in more detail in Section 4.7). The local horizontal gradients in the barrier do increase even after the pipe first enters the barrier. This might possibly be in part explained by the reduction in the head in the downstream capillary in the barrier due to pipe formation. However, when the pipe enters the barrier, no significant reduction in the head at H13 (or in

other capillaries) was typically noticed during the tests, as noted in Section 4.2.1. This can be due to the fact that the pipe did not penetrate the barrier directly below the capillaries in most tests. The increase of gradient is therefore explained by the continuous increase of overall head drop.

The vertical dashed lines indicate the head drop when the pipe passes through the barrier and progresses upstream, or for tests with a barrier that is present all the way to the upstream end of the set-up this is the head drop where the pipe progresses upstream in the barrier. Clearly there is a significantly higher head drop required to cause the progression of the pipe through the barrier than to cause pipe formation in the barrier. For several tests, and most notably for test 195 the local horizontal gradient in the barrier falls before this point, caused by the lengthening of the pipe in the barrier, reducing the head in H14 as well as in H13. Note however that in most tests the pipe was not present directly below these capillaries, so that the gradient measured there is not equal to the gradient in the pipe, but the gradient measured will be influenced by the presence of the pipe.

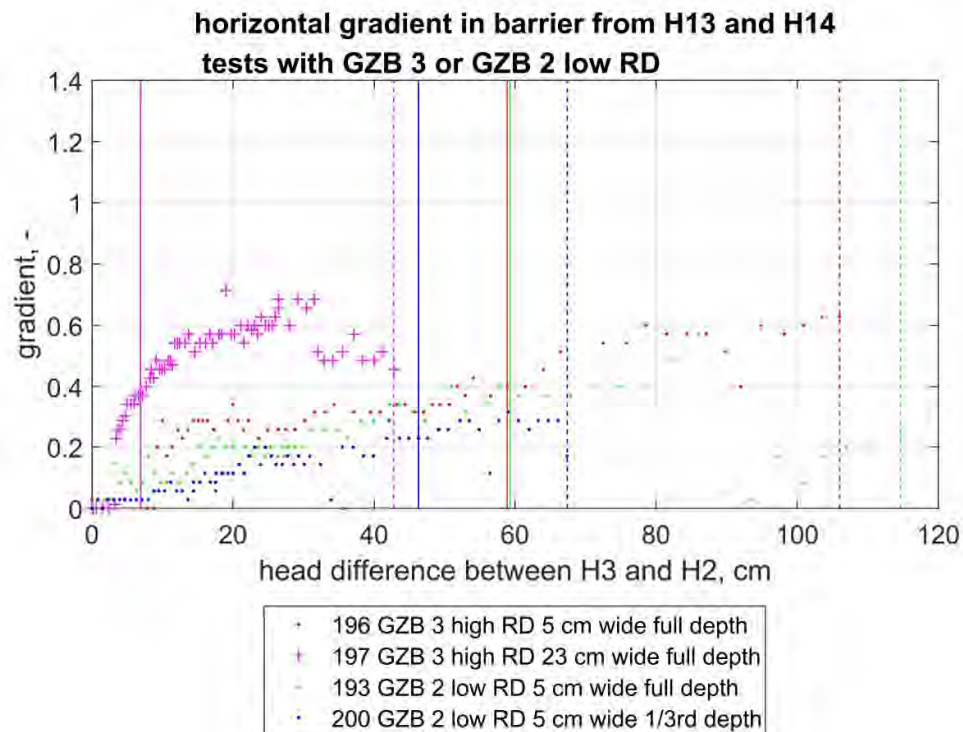


Figure 4.13 Horizontal gradient in the barrier measured between H13 and H14. The x axis shows the head drop between capillary H3 in the sand body on the upstream side of the set-up just beyond the filter, and H2 in the outlet tubing. The vertical solid lines indicate the damage condition, when the pipe first enters the barrier. The vertical dashed lines indicate failure of the barrier

Test 197, like test 195 in Figure 4.12 shows a steeper increase in the local horizontal gradient between H13 and H14 due to the barrier being present all the way upstream. The horizontal gradients in the tests with GZB3 are lower than in the GZB2 (high relative density tests), although the mean grain size is similar for both tests. The lower strength of

GZB3 might be related to the higher hydraulic conductivity of the barrier or to the decreased number of particle-particle contacts in comparison with GZB2. Also the gradients in the tests with GZB2 with a low relative density are lower than the gradients in tests with GZB2 with a higher relative density. A lower relative density results in a higher hydraulic conductivity and lower strength, which might have affected the local damage gradient. A decrease of local damage gradient with decrease of relative density was observed in previous experiments (Robbins and Van Beek, 2017). The values of the horizontal gradient at damage condition are analysed for all tests in Section 4.7 and at failure conditions in Section 4.8.

- 4.3.3 Horizontal gradient over upstream interface fine sand and barrier- filter cake formation  
In the sand selection in Section 3.1, filter rules were applied to ensure that the fine background sand does not pass through the barrier; the pores of the barrier are small enough to retain eroded grains. However, it appears that there has been some movement of material from the fine sand just into the barrier, where it indeed gets filtered. This zone of filtered material, the so-called filter cake, can have a lower hydraulic conductivity than the fine sand. Evidence of the filter cake comes from the local measurements of hydraulic head.

Capillary H15 is present just upstream of the interface between the barrier and the fine sand in the tests where the barrier is only 5 cm wide. H14 is present just inside the barrier; the distance between these capillaries is only 1.5 cm. During some tests it was observed that the head drop between these two capillaries became very large relative to the increase of overall head drop.

The horizontal gradient between H14 and H15 is shown in Figure 4.14.

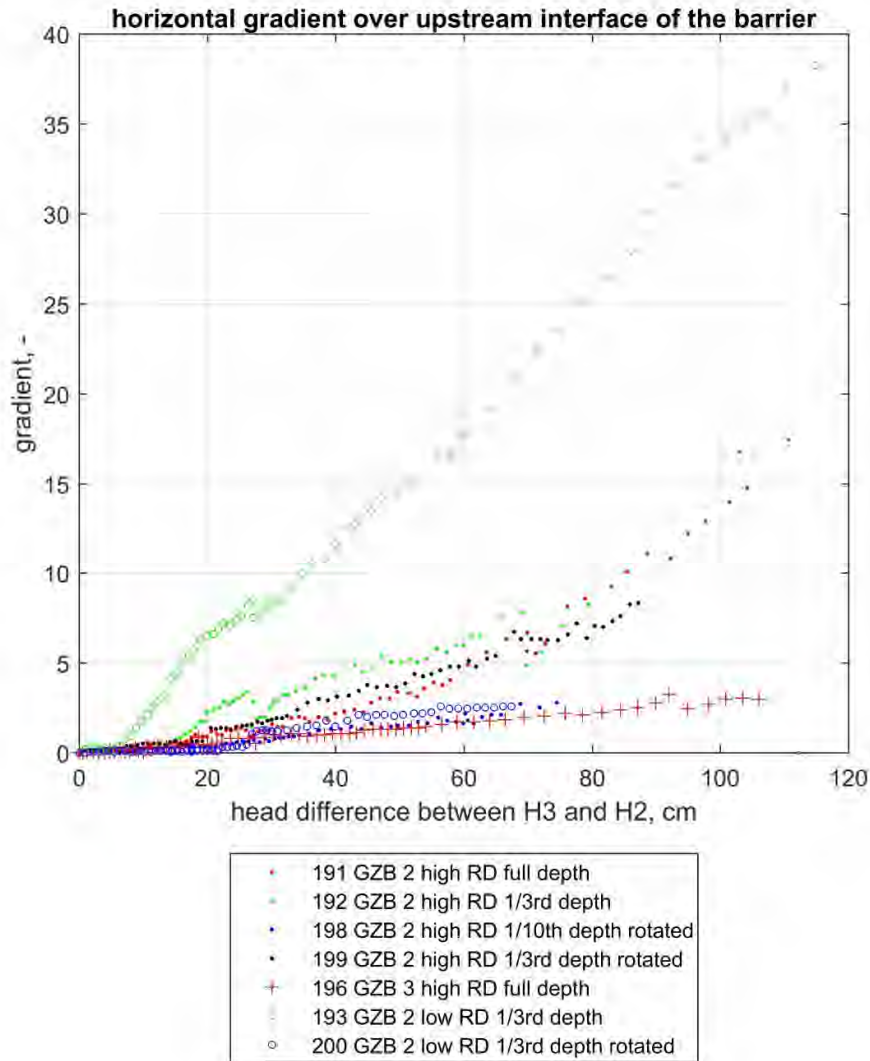


Figure 4.14 Horizontal gradient between H14 and H15 over the interface between the fine sand and the upstream side of the barrier. The x axis shows the head drop between capillary H3 in the sand body on the upstream side of the set-up just beyond the filter, and H2 in the outlet tubing. All tests with a barrier thickness of 5 cm

In order to analyse differences between the other tests in terms of sand characteristics (Section 4.3.3.1) and in terms of relative density (Section 4.3.3.2), Figure 4.15 zooms in on the results for gradients between 0 and 10.

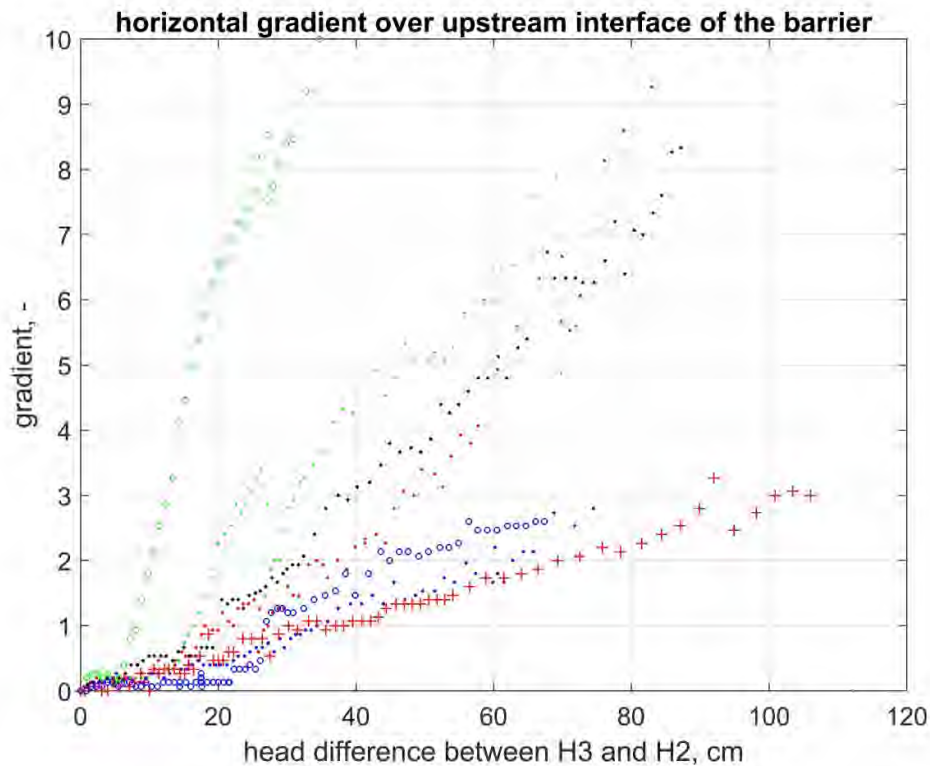


Figure 4.15 Horizontal gradient between H14 and H15 over the interface between the fine sand and the upstream side of the barrier. The x axis shows the head drop between capillary H3 in the sand body on the upstream side of the set-up just beyond the filter, and H2 in the outlet tubing. All tests with a barrier thickness of 5 cm. Refer to Figure 4.14 for legend

#### 4.3.3.1 Effect of sand characteristics on formation of a filter cake

It can be observed that the gradient over the interface of the fine sand and the barrier is initially low in all tests. The gradient gradually increases during the test. This would suggest the building up of a filter cake during the course of the test as opposed to a filter cake being present as a consequence of the test preparation.

As noted in Section 3.1 the combination of the barrier and the Metselzand should fulfil the filter criteria, and visual inspection did not indicate transport of fine grains into or through the barrier except during test 200.

It appears likely that at the interface of the coarse sand barrier and the fine sand, some of the Metselzand grains are pushed into the barrier, and these are filtered in the barrier, creating locally smaller pores. If there is some suffusion of the finest fraction of the Metselzand in the region near the barrier, these fines may accumulate in these locally smaller pores, further reducing the hydraulic conductivity and forming a filter cake.

Considering the period of the test when the filter cake seems to be most dominant, for head drops exceeding 30 cm, it can be seen that the gradient is lower in test 196 with GZB3 than in the other tests which all have GZB2. This suggests that more material is filtered by GZB2. However if similar amounts of grains or fines are mobilised, this would suggest that more material passes through GZB3 rather than being filtered.

There is no clear distinction between the tests with a barrier over the full length of the model and those tests where the barrier is only present in the top of the model. However, the measurements in H14 and H15 will predominantly reflect the properties of the sands at the top of the model.

#### 4.3.3.2 *Effect of relative density on formation of a filter cake*

The process of filter cake formation appears to have been most significant in test 193 with a low relative density barrier that is present over the full depth of the model. The gradient here becomes almost 40. That may be due to the effect of relative density on the constriction size in the barrier. The figures below illustrate the effect of relative density on the constriction size, using ping pong balls to represent the  $d_{50}$  of the barrier grains and glass marbles to represent the  $d_{50}$  of the Metselzand. With a looser packing the fine grains can just enter into the barrier material and they are filtered there creating smaller pores that might filter even smaller grains.

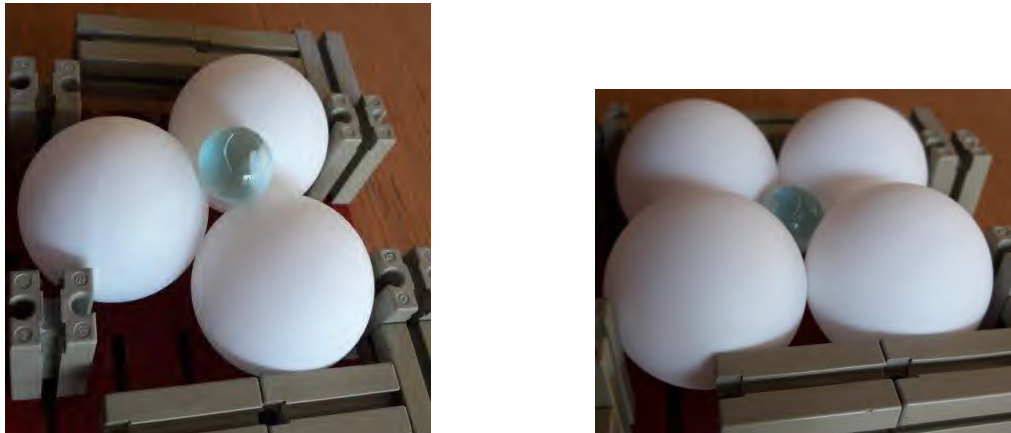


Figure 4.16 Simulation of the  $d_{50}$  of sand grains of the coarse sand barrier by ping pong balls and  $d_{50}$  of sand grains of the Metselzand by marbles. Left densest packing of barrier grains, retaining the Metselzand grains, right loosest packing of barrier grains allowing Metselzand grains to enter the packing

#### 4.3.3.3 *Effect of flow rate on formation of a filter cake*

In order to estimate at which flow rates the filter cake starts to form, the results for the gradient over the upstream interface are plotted below as a function of flow rate. Here the flow rate is estimated from the flux divided by the cross sectional area of the model, i.e. the convergence of flow which can lead to locally higher flow rates is not accounted for. Therefore, this figure only gives an impression of the average flow rates at which the filter cakes start to develop.

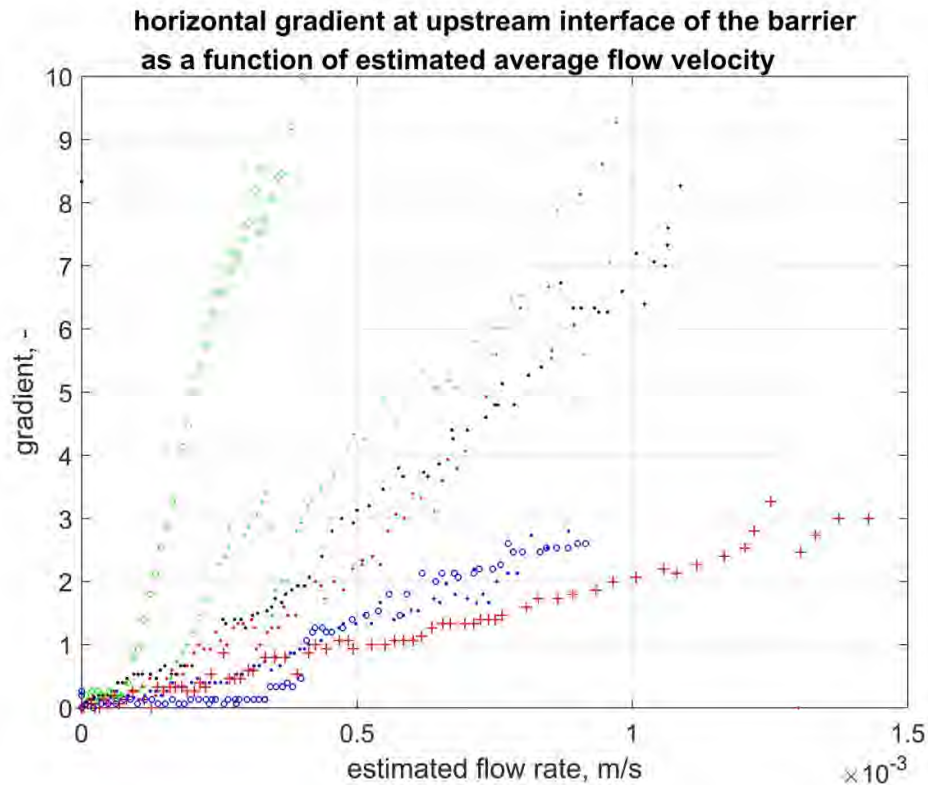


Figure 4.17 Horizontal gradient between H14 and H15 at the interface between the fine sand and the upstream side of the barrier as a function of the estimated average flow velocity. All tests with a barrier thickness of 5 cm. Refer to Figure 4.14 for legend

To put this in perspective of the conditions that a coarse sand barrier in the field operates in we can look at day to day flow rates or flow rates at critical conditions (high water levels). Typical flow rates during day to day situations are difficult to estimate and indeed these can be positive (seepage from the river to the polder) or negative (when the polder water level is higher than the river water level).

An estimate of the flow rates during a high water level can be made for the IJkdijk experiments without a coarse sand barrier by considering the critical head drop and the hydraulic conductivity of the sand. Table 4.4 suggests flow rates would be in the order of  $0.2 \times 10^{-3}$  to  $0.3 \times 10^{-3}$  m/s. During this phase of the tests, the effect of the filter cake is still relatively small in Figure 4.17.

Table 4.2 Results from IJkdijk experiments without a coarse sand barrier. Critical head drop is the head drop beyond which the pipe developed upstream (Van Beek et al., 2011)

Experiment description	Critical head drop, m	Hydraulic conductivity sand, m/s	Estimated flow velocity m/s
IJkfs01 Fine IJkdijk	2.30	8.0e-5	1.8e-4
IJkfs02 Coarse IJkdijk	1.75	1.4e-4	2.5e-4
IJkfs03 Fine IJkdijk	2.10	8.0e-5	1.7e-4
IJkfs04 Coarse IJkdijk	2.00	1.2e-4	2.4e-4

#### 4.4 Flow rate

The flow rate is recorded during the experiments at a time interval of 5 minutes. The estimated error margin on the flux is ca. 1.5% of the measured flux. Figure 4.18 shows the development of the flux as a function of the difference between H2 and H3.

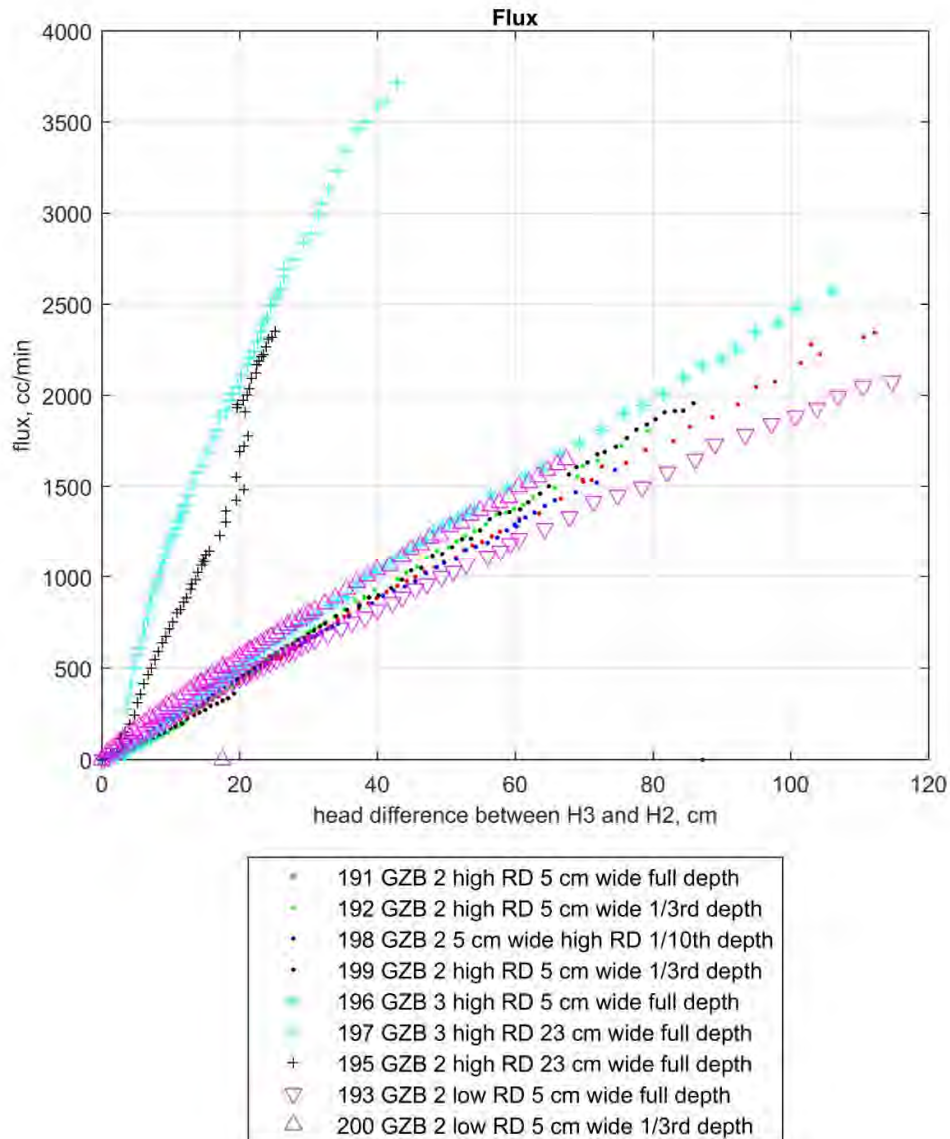


Figure 4.18 Flux as a function of the head drop. The x axis shows the head drop between capillary H3 in the sand body on the upstream side of the set-up just beyond the filter, and H2 in the outlet tubing

As expected for each of the experiments an increase of flux is observed as a result of increase in overall head drop. The higher flux in tests 197 and 195 is caused by the barrier being present to the upstream end. In the other tests, Metselzand is present upstream of the barrier and this controls the flux to a large extent, which is reflected in the similar values for those tests.

In test 195 there is an increase in the flux during a period where the head drop between H2 and H3 does not significantly increase. At this point the pipe grows up to 12 cm into the barrier. This increased the hydraulic conductivity of the system significantly causing the steep increase in the flux for a negligible increase in head drop.

Test 195 shows clearly that laminar flow is dominant in the system (there is a linear increase in the flux with the increase in hydraulic head. The pipe formation increases the hydraulic conductivity of the system in two steps as shown in Figure 4.19. However, if the pipe stops growing, there is again a linear relation between flux and hydraulic head but with a steeper slope. This is also observed in previous piping experiments. This is not seen by the tests with a localized barrier, because there the relation between flux and conductivity is determined by the Metselzand upstream.

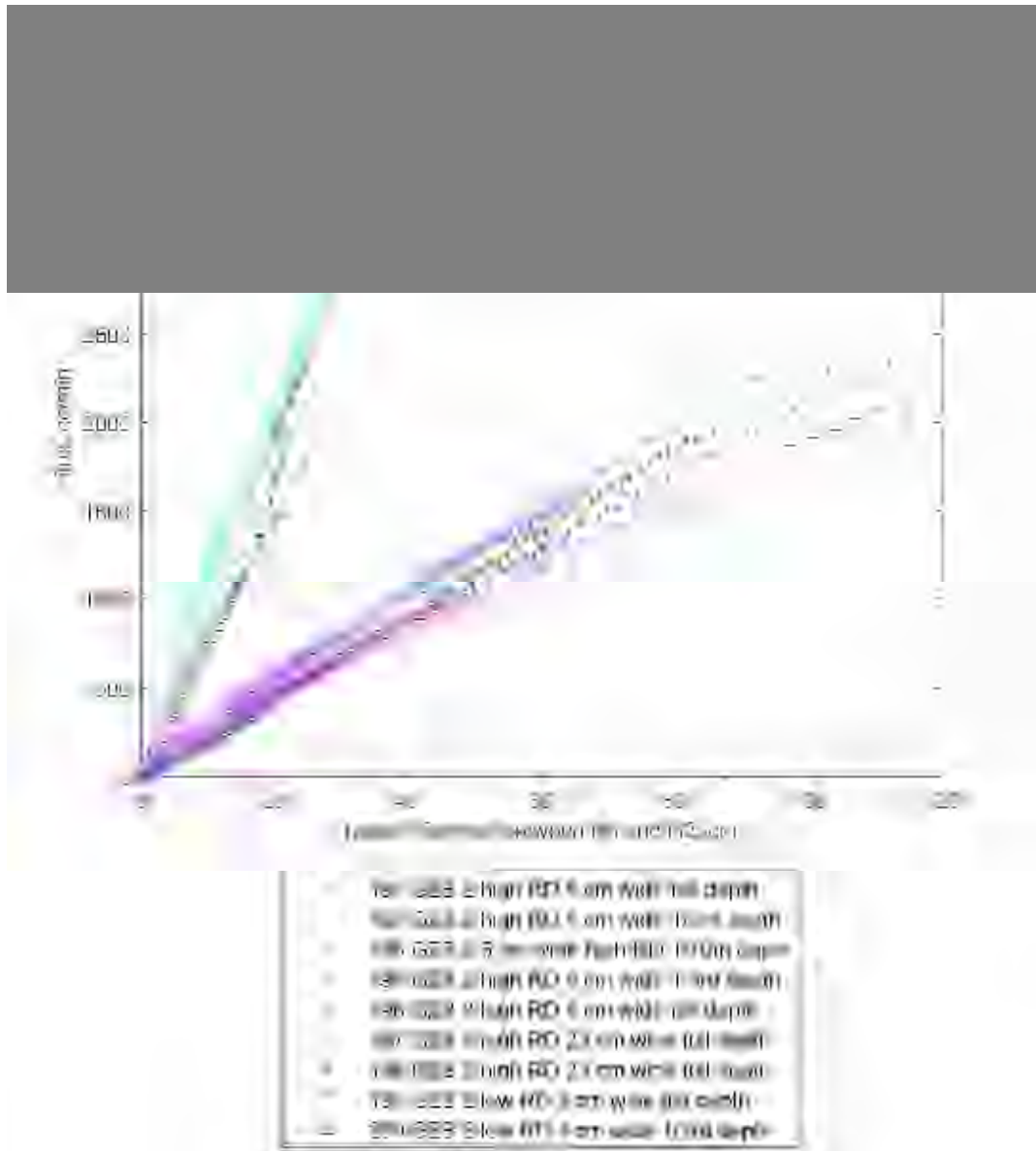


Figure 4.19 Flux as a function of the head drop. The x axis shows the head drop between capillary H3 in the sand body on the upstream side of the set-up just beyond the filter, and H2 in the outlet tubing. Blue lines in test 195 indicate periods of relatively constant hydraulic conductivity

The tests with a low relative density barrier, and thus also a low relative density fine sand downstream show a higher flux initially, probably also due to the higher hydraulic conductivity downstream. However, for test 193 the flux falls relative to the other tests. This is probably due to the higher resistance of the developing filter cake. Figure 4.20 zooms in on the data in the initial phase of the test.

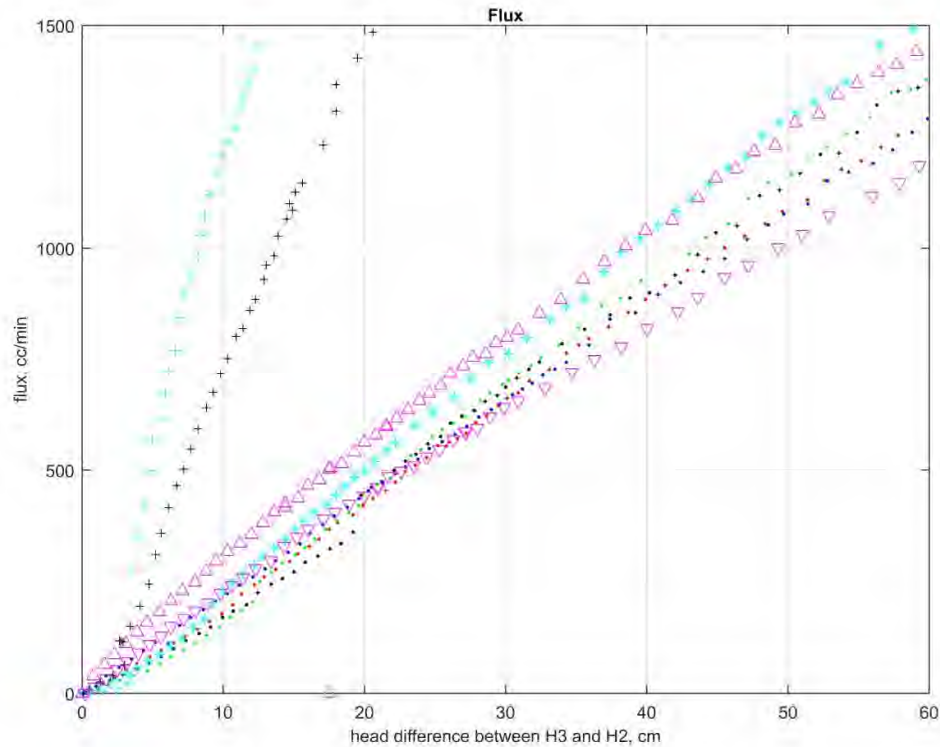


Figure 4.20 Flux as a function of the head drop. The x axis shows the head drop between capillary H3 in the sand body on the upstream side of the set-up just beyond the filter, and H2 in the outlet tubing. See Figure 4.18 for legend

There is no significant difference in the flux for tests with GZB2 with a high relative density, the tests with a normal and a rotated box, and with a barrier with partial and full depth barrier give comparable results. This indicates that the overall hydraulic conductivity is dominated by the hydraulic conductivity of the Metselzand upstream of the barrier.

#### 4.5 Flow regimes

The flow regime is estimated for the pipe, and for the fine sand and for the barrier. For the fine sand and for the barrier, this is done by assuming that all flow is plane flow through the cross section of the model, i.e. the situation before flow converges due to pipe formation.

##### 4.5.1 In sand and barrier

The grain Reynolds number was calculated as in Bear (1972) by

$$Re = \frac{qd}{\eta}$$

Where  $d = d_{50}$ ,  $q$  is (average) flow velocity (here volumetric flow/width model/length model),  $\eta$  is dynamic viscosity. Bear notes that Darcy's law can be assumed to be valid for grain  $Re$

less than 1 to 10. Beyond this he distinguishes a transition zone up to  $Re$  ca. 100, and only beyond this point, flow would be turbulent.

The  $Re$  at the point that the pipe damages the barrier is calculated for all experiments in the Factual Report (Rosenbrand and Van Beek, 2017). Based on those values of  $Re$ , Darcy's law could be considered valid for all experiments. This was also seen in the linear trend between head loss and discharge in Section 0.

#### 4.5.2 In pipe

Estimates of the flow regime in the pipe are made in the Factual Report (Rosenbrand and Van Beek, 2017), using the Reynolds numbers for laminar flow in a pipe accounting for roughness after (Kandlikar et al., 2006). However, as the grain size of the coarse sand grains exceeds the limit where this expression is valid, it is questionable to what extent these estimates are valid. Nonetheless, these suggest that flow in the pipe may not be laminar for a significant part of the experiment, including the damage condition in all tests. This is also supported by the non-linear relation between flux and head drop over the pipe and exit in Section 4.2.3.

The flow regime in the pipe is currently not considered of great significance for determining the damage criterion in the barrier, since the head loss in the pipe is negligible, but it may affect the extent to which the pipe deepens and the head loss in the pipe, which may be important for progression of the pipe.

### 4.6 Apparent hydraulic conductivity

The apparent hydraulic conductivity of the sands is measured in column tests (Rosenbrand and Van Beek, 2017) and estimated from the experiments based on measurements in the bottom of the model on the upstream side of the barrier. In the following sections these measurements are analysed.

#### 4.6.1 Fine sand upstream

Figure 4.21 shows the estimated hydraulic conductivity of the fine sand as a function of the head drop over the set-up between H2 and H3 for all of the seven experiments analysed here. This was estimated by using the capillaries H3 and H4 on the bottom of the set-up in the fine sand. As the formation of pipes in the downstream end of the model, and particularly in the barrier are expected to cause convergence of flow in the upstream sand, the hydraulic conductivity is expected to be best estimated by data from the early phases of the test. However, those values often show more scatter and only stabilise later during the tests.

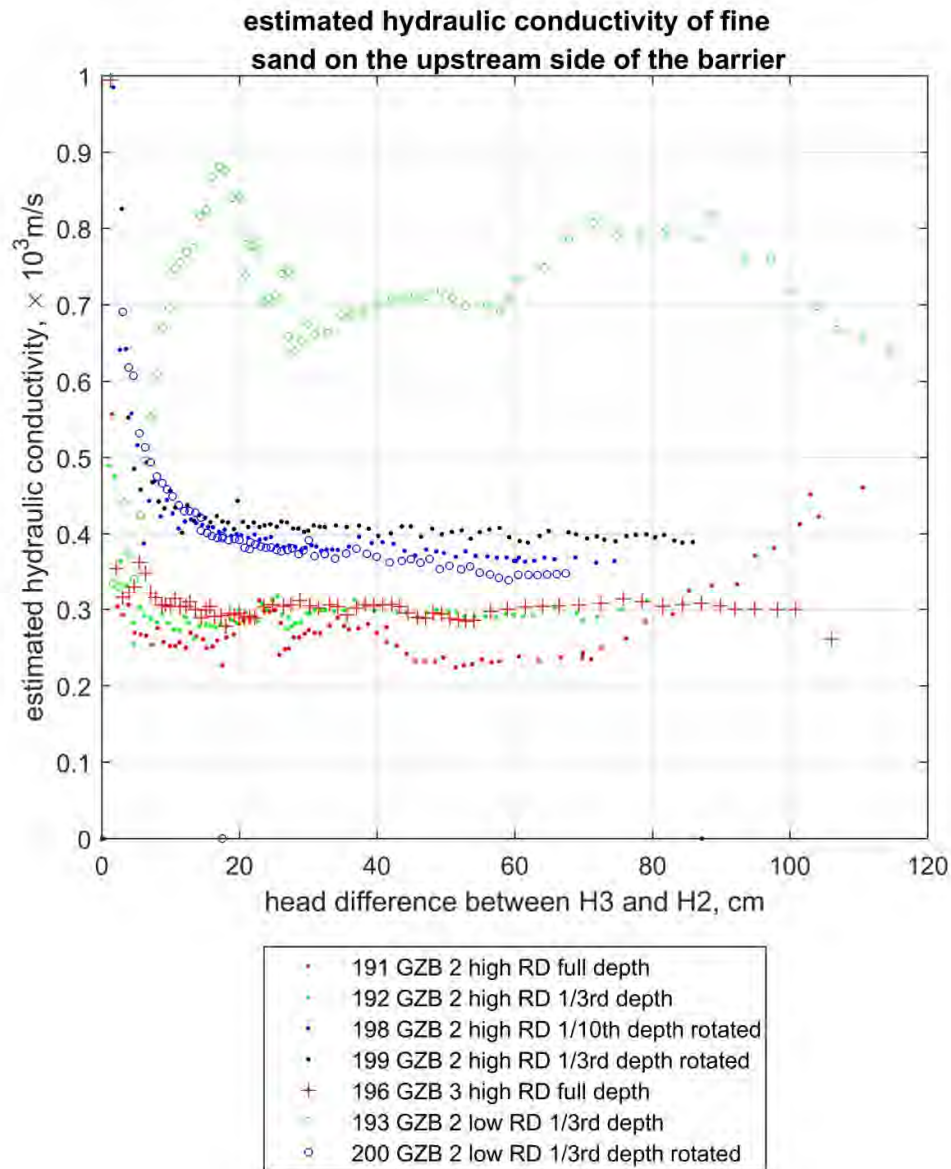


Figure 4.21 Estimated hydraulic conductivity of the fine sand based on measurements in the bottom of the box upstream of the barrier. The x axis shows the head drop between capillary H3 in the sand body on the upstream side of the set-up just beyond the filter, and H2 in the outlet tubing

The hydraulic conductivity of the fine sand in test 193 is significantly higher than in the other tests. This is the test in which it appears that a filter cake had formed. The higher hydraulic conductivity estimated here could possibly be due to loss of material, possibly the finer fraction, of the Metselzand.

The estimates for tests 198, 199 and 200 with a rotated set-up yield a higher value than the estimates for the normal set-up. The relative density estimated for those latter tests was in the order of 90%, whereas this was about 95% for the tests 191, 192 and 193, however, test 196 also had a relative density of about 90% and the estimated hydraulic conductivity for that test is also lower in Figure 4.21. As relative density is estimated with an accuracy of 5% it is

difficult to say to what extent these small differences affect the hydraulic conductivity difference.

It is more likely that the difference in the flow pattern for the normal and the rotated set-up causes this difference. The extent to which flow converges to the top of the model is different, and this results in a different head distribution in the bottom of the model. In the hydraulic conductivity estimates linear (1D) flow is assumed, so the effect of converging flow is not incorporated in the estimates. The flow patterns are modelled in the postdictions in Appendix J.

Table 4.3 summarizes the hydraulic conductivity measurements from the column tests as a function of relative density for the range of relative density of the fine sand in the upstream part of the set-up (refer to the Factual Report (Rosenbrand and Van Beek, 2017) for the full set of hydraulic conductivity data).

*Table 4.3 Summary of hydraulic conductivity measured in column tests for Metselzand*

Relative density	Hydraulic conductivity, m/s
85	3.35E-04
90	2.90E-04
95	2.45E-04
100	2.00E-04

The estimated hydraulic conductivity from the experiments is higher than from the column experiments. This could possibly be an indication that the flow converges towards the top of the model, as the heads used to estimate the hydraulic conductivity are measured in the bottom of the set-up. Therefore these estimates based on the experimental data have a limited accuracy and the difference among results for the normal and the rotated box may not be significant. For future tests it is recommended to have more closely spaced head measurements nearby to the upstream filter.

#### 4.6.2 Barrier

The hydraulic conductivity of the barrier could be in principle estimated using the two capillaries in the top of the barrier. As the formation of pipes in the downstream end and particularly in the barrier are expected to cause convergence of flow, the hydraulic conductivity is expected to be best estimated by data from the early phases of the test. This effect will be stronger than for the hydraulic conductivity estimates in the fine sand, as those are made further upstream, away from the interface between the barrier and the pipe. Therefore, although estimates based on the experiments are made in the Factual Report (Rosenbrand and Van Beek, 2017), these are not considered accurate or reliable and are therefore not reproduced here.

Hydraulic conductivity from column tests is generally significantly higher than hydraulic conductivity estimated from the experiments. This would be expected when the flow converges towards the top of the model, as the heads used to estimate the hydraulic conductivity are measured in the top of the set-up. In the two experiments where the barrier is present until the upstream end, tests 195 and 197, the hydraulic conductivity can be estimated from head measurements both in the top and in the bottom of the model. The hydraulic conductivity measured in the bottom shows a better agreement match with the hydraulic conductivity measured in the column test. This is shown below for test 197, to the results of test 195 can be found in the Factual Report (Rosenbrand and Van Beek, 2017).

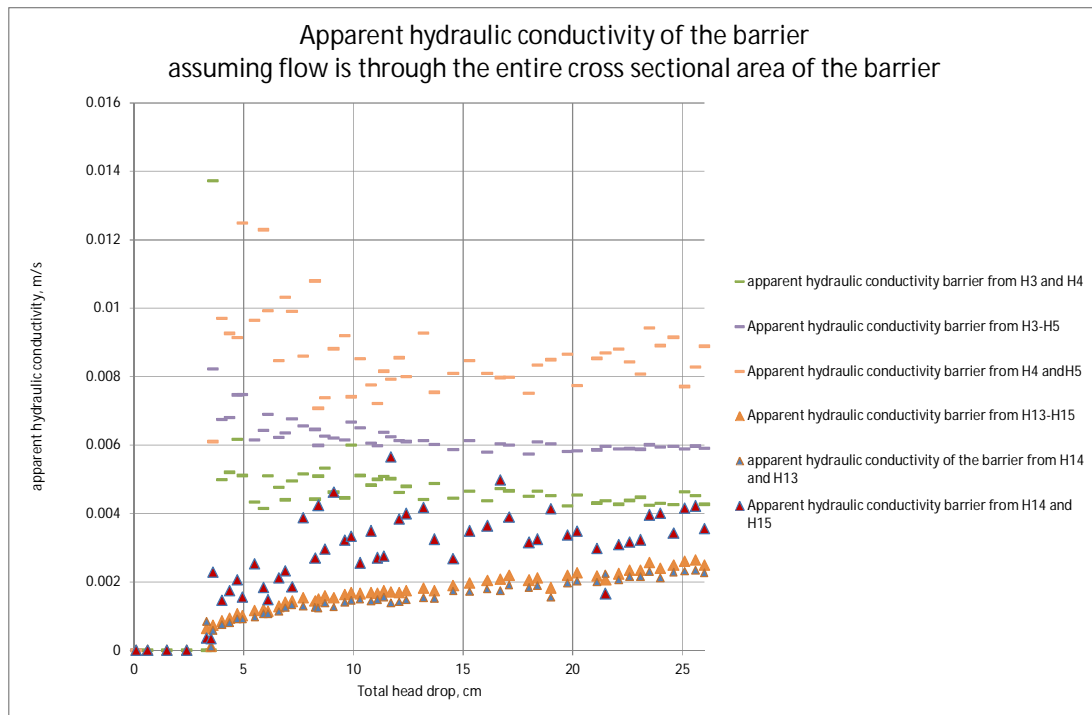


Figure 4.22 Estimated (apparent) hydraulic conductivity estimates for GZB3 in test 197 based on measured head drops and flux through the model. The x axis shows the head drop between capillary H3 in the sand body on the upstream side of the set-up just beyond the filter, and H2 in the outlet tubing. It is an apparent hydraulic conductivity as it is assumed all flow is linear whereas convergence of flow will affect the results. Estimates based on capillaries in the bottom of the model, (H3, H4 and H5) are therefore higher than estimates based on capillaries in the top of the model (H13, H14 and H15). Dashes indicate estimates based on capillaries in the bottom, triangles indicate estimates based on capillaries in the top

#### 4.7 Damage condition

The damage condition is considered to be the point where the pipe first progresses into the barrier, i.e. breaching of the downstream barrier interface. It is observed in all tests that after this point the overall head drop can be increased further before the pipe actually breaches the upstream barrier interface and progresses upstream. During the interval between damage and failure of the barrier, several more pipes form into the barrier and several of these pipes progress inside the barrier.

Often there is not a significant change in the head measurements in the capillaries at the point that the pipe enters the barrier. Possibly this is because the barrier is already very permeable, so an increase of the hydraulic conductivity of the barrier due to breaching by the pipe does not have a significant effect on the flow or on the head distribution.

The hypothesis is that the local horizontal gradient in the barrier determines the strength of a given barrier material at a given relative density, i.e. that different tests with the same material have the same value of the local horizontal gradient at the damage condition, provided that the relative density is the same. However, other possible criteria, which can be obtained from the measurements during the test, that reflect the strength of the barrier could be the overall head drop over the model between the filter and the pipe, the flux in the model, and the

vertical gradient in the barrier. Numerical modelling is used in Chapter 5 to investigate other criteria that cannot be directly estimated from the measurements, such as the local gradient or the velocity over a selected region of the barrier. For the progression of the pipe through the entire barrier, the gradient over the upstream interface of the barrier could be considered.

In order to assess which of the possible damage criteria best characterises the barrier strength, the table below summarises the value of these possible damage criteria at the damage condition for the small-scale tests. The value which is most constant for different tests with the same barrier type is most likely to characterise the barrier strength.

Vertical gradients shown for tests 198, 199 and 200 in the Factual Report (Rosenbrand and Van Beek, 2017) were a factor 3 too high, the correct values are shown in the table below.

*Table 4.4 Summary of the values of possible damage criteria at the point where the pipe first breaches the downstream end of the barrier*

test	barrier type	background sand type	test specification	head drop between filter and pipe	flux in test	horizontal gradient at location of H13 and H14 in the barrier	vertical gradient in barrier at location of H5	gradient over upstream interface of the barrier at the location of H15 and H14
				cm	cc/min	-		
191	GZB2	Metselzand	basis	40.2	918	0.74	0.19	2.33
192	GZB2	Metselzand	barrier depth 3 cm	40.8	987	0.74	0.58	4.93
193	GZB2	Metselzand	low relative density barrier	55.0	1186	0.34	0.19	17.67
196	GZB3	Metselzand	basis	55.4	1493	0.40	0.13	1.73
198	GZB2	Metselzand	rotated model barrier depth 3 cm	26.4	635	0.57	0.27	0.80
199	GZB2	Metselzand	rotated model barrier depth 10 cm	28.2	728	0.63	0.27	1.93
200	GZB2	Metselzand	rotated model barrier depth 10 cm low RD barrier	42.1	1178	0.23	0.30	2.13
Tests where the barrier is present to the upstream end of the set-up								
195	GZB2	Baskarp	Baskarp sand, barrier to upstream side of model	10.7	1085	0.86	0.23	0.47
197	GZB3	Baskarp	Baskarp sand, barrier 3 to upstream side of model	3.2	844	0.37	0.11	0.20

To better characterise the variation in the results, Table 4.5 summarises 5 tests with the same barrier at the same relative density (GZB2 high relative density) along with the statistics for the different possible damage criteria.

Table 4.5 Summary of experimental measurements and statistics at the point where the pipe first breaches the downstream end of the barrier for tests done with coarse sand barrier GZB2 at a high relative density

test	background sand type	test specification	head drop between filter and pipe	flux in test	horizontal gradient in barrier	vertical gradient in barrier	gradient over upstream interface barrier
			cm	cc/min	-		
191	Metselzand	basis	40.2	918	0.74	0.19	2.33
192	Metselzand	barrier depth 3 cm	40.8	987	0.74	0.58	4.93
195	Baskarp	Baskarp sand, barrier to upstream side of model	10.7	1085	0.86	0.23	0.47
198	Metselzand	rotated model barrier depth 3 cm	26.4	635	0.57	0.27	0.80
199	Metselzand	rotated model barrier depth 10 cm	28.2	728	0.63	0.27	1.93
average			29.3	871	0.71	0.31	2.09
standard deviation			11.0	166	0.10	0.14	1.58
CoV*			-0.38	0.19	0.14	0.45	0.75

\* Coefficient of variation, (standard deviation/average)

For GZB2 with high relative density it is clear that the variation of the horizontal gradient in the barrier (with a coefficient of variation (COV) of 0.14) is smaller than the COV of the other parameters. This supports the hypothesis that the local horizontal gradient is an appropriate damage criterion for the barrier.

Following the hypothesis that the horizontal gradient can be used as a damage criterion, this means that this gradient causes the loosening of the barrier grains. Primary erosion is then the important failure mechanism. This is to be expected, since there is hardly a pipe present when the first damage on the barrier occurs. Yet this is an important finding, since it means that when the horizontal gradient is known in the neighbourhood of the outflow of the barrier to the pipe, we can use a small-scale model test to see if the barrier material is stable for that flow condition. The horizontal gradient can be determined by means of a numerical calculation.

The larger variation in the other possible criteria at the damage condition can be accounted for by consideration of the physical processes occurring during the test. The head drop between the filter and the pipe and the flux in the test are strongly affected by the hydraulic conductivity of the background sand and not as much by properties of the barrier. The vertical gradient in the barrier cannot be well enough assessed from the experimental data, as this is measured over the entire depth of the barrier in tests with a full depth barrier, and the local gradient at the top near the pipe interface would be higher than the local gradient in the lower part of the barrier due to converging flow. Furthermore in tests 192, 198 and 199 the barrier does not reach to the bottom of the model, so that the vertical gradient is due to both the fine sand and the barrier, and as shown in Section 4.3.1 this is mainly controlled by the fine sand

below the barrier. The gradient over the upstream interface of the barrier can also be considered an unlikely predictor of the damage point when the pipe grows into the downstream interface of the barrier.

For GZB2 with a low relative density there are only two tests (193 and 200) so no meaningful statistics can be computed, the same holds for GZB3 (196 and 197). However, the bar graphs below illustrate the variation of the possible criteria at the damage condition for all tests. In these graphs the error bars represent the estimated error margin that is due to the measurements.

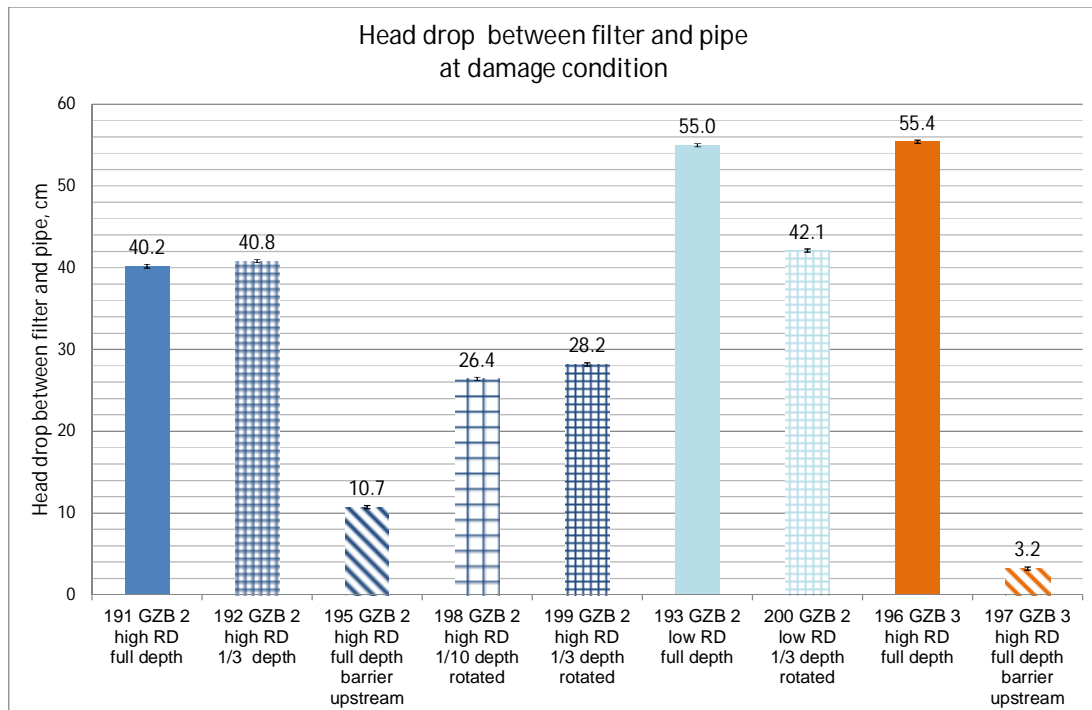


Figure 4.23 Head drop between filter and pipe at damage condition. Colours indicate type of barrier: GZB2 high relative density = dark blue, GZB2 at low relative density = light blue, GZB3 at high relative density = orange. Texture indicates test specifics: slope = barrier to upstream end of model, large squares = barrier 1/10<sup>th</sup> depth of model, small squares = barrier 1/3<sup>rd</sup> depth of model. Error bars represent the estimated error margin in the measurements

The head drop is strongly dependent on the upstream sand, therefore the head drop is smallest for the two tests where the barrier goes all the way upstream. Figure 4.23 shows no indication that the given head drop between the filter and the pipe is constant for a given barrier material. Therefore this property does not seem applicable to characterise the strength of the barrier.

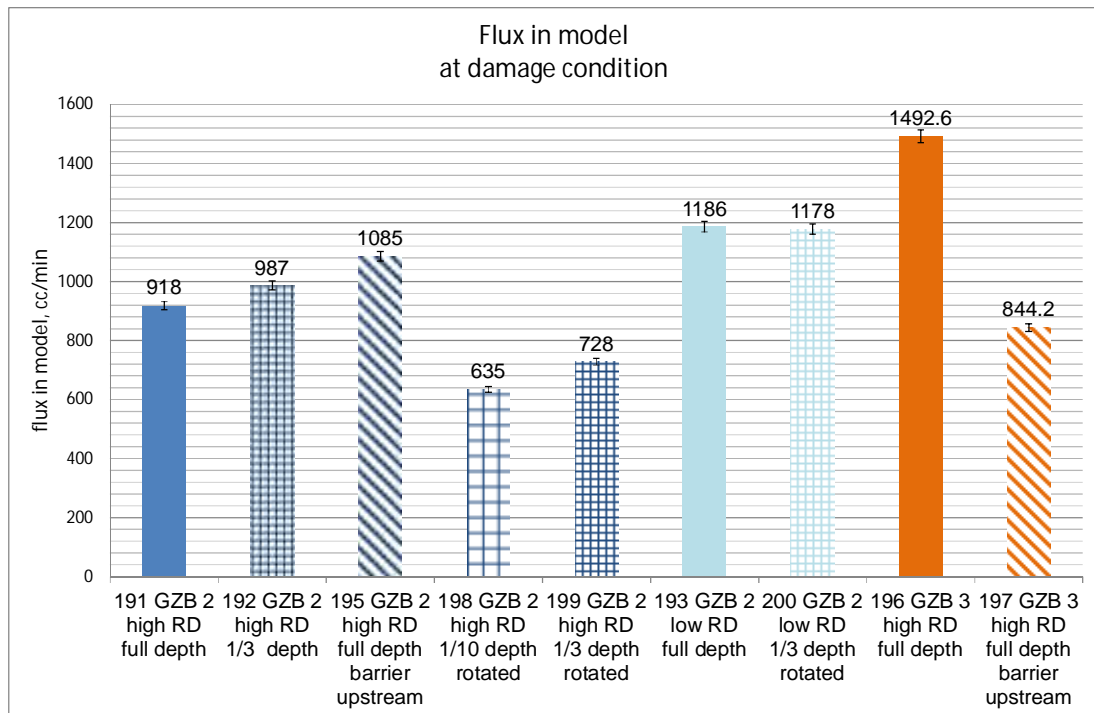


Figure 4.24 Flux at damage condition. Colours indicate type of barrier: GZB2 high relative density = dark blue, GZB2 at low relative density = light blue, GZB3 at high relative density = orange. Texture indicates test specifics: slope = barrier to upstream end of model, large squares = barrier 1/10<sup>th</sup> depth of model, small squares = barrier 1/3<sup>rd</sup> depth of model. Error bars represent the estimated error margin in the measurements

The flux is strongly dependent on the hydraulic conductivity; this gives a relatively high flux for the cases with a low relative density and with a barrier all the way upstream. The large scatter in the flux for tests with the same barrier material indicates that this is not a suitable damage criterion. This scatter is mainly the result of the two tests with a rotated set-up where the depth of the sand layer below the barrier is larger so there is more concentration of flow to the pipe. The flux criterion is sensitive to the overall geometry and not an intrinsic parameter of the barrier, and therefore this is not a suitable damage criterion.

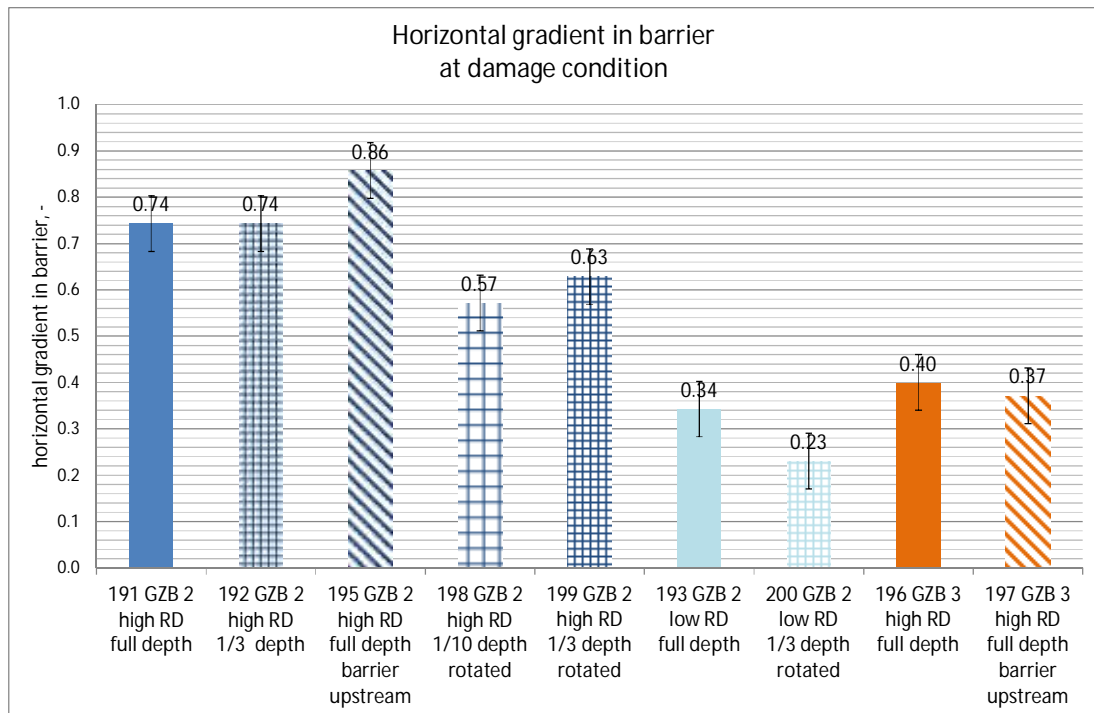


Figure 4.25 Local horizontal gradient at damage condition. Colours indicate type of barrier: GZB2 high relative density = dark blue, GZB2 at low relative density = light blue, GZB3 at high relative density = orange. Texture indicates test specifics: slope = barrier to upstream end of model, large squares = barrier 1/10<sup>th</sup> depth of model, small squares = barrier 1/3<sup>rd</sup> depth of model. Error bars represent the estimated error margin in the measurements

The local horizontal gradient shows variation, but for a given barrier material deviations among the local horizontal gradients are within, or close to, the error margin estimated for the measurements. Additional uncertainty and scatter might possibly be due to small differences in the relative density of the sample (in the order of 5 % RD), and due to slight differences in the location of the barrier, and thus the range over which the local horizontal gradient is measured. Thus this figure does not disprove the hypothesis that a local horizontal gradient characterises barrier strength.

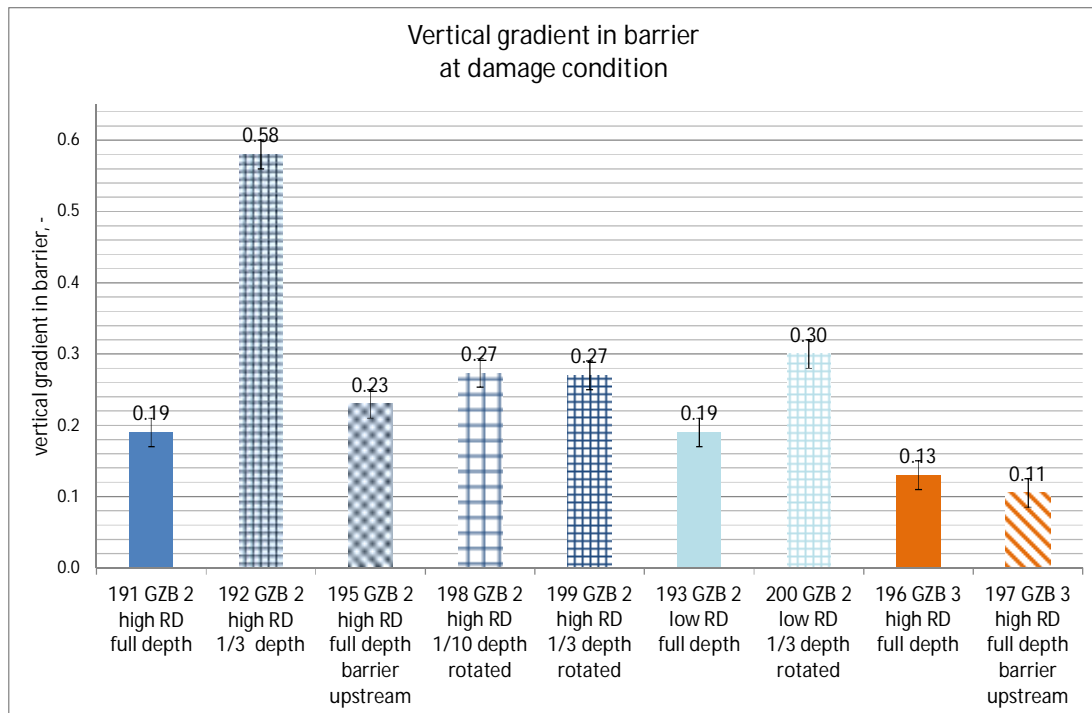


Figure 4.26 Vertical gradient at damage condition. Colours indicate type of barrier: GZB2 high relative density = dark blue, GZB2 at low relative density = light blue, GZB3 at high relative density = orange. Texture indicates test specifics: slope = barrier to upstream end of model, large squares = barrier 1/10<sup>th</sup> depth of model, small squares = barrier 1/3<sup>rd</sup> depth of model. Error bars represent the estimated error margin in the measurements

There is a large difference in the vertical gradients in the barrier at damage condition but this is also due to the fact that the barrier does not penetrate all the way to the bottom of the model. This means that in some tests the gradient is now averaged over the barrier and the fine sand below the barrier, whereas the gradient in the barrier is of interest for failure. The gradient in tests 198 and 199 and 200 with a rotated model also measure the gradient over 30 cm whereas this is measured over 10 cm in the other tests. In order to better assess the vertical gradient, numerical modelling is used in Section 5.5.

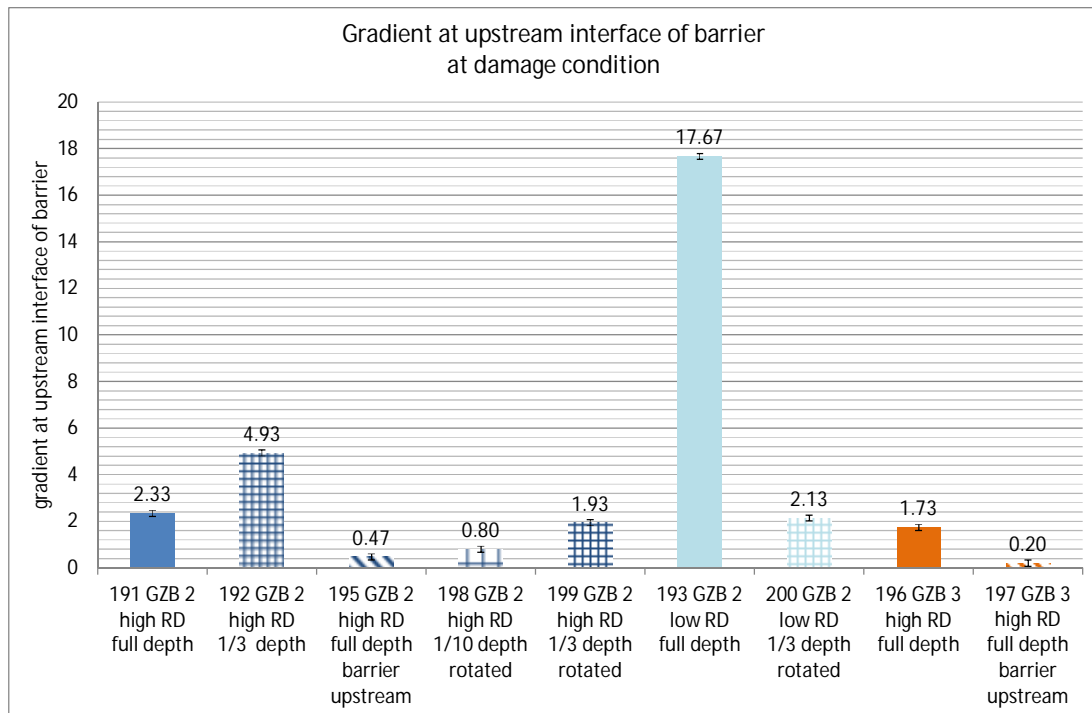


Figure 4.27 Gradient over the upstream interface of the barrier at damage condition. Colours indicate type of barrier: GZB2 high relative density = dark blue, GZB2 at low relative density = light blue, GZB3 at high relative density = orange. Texture indicates test specifics: slope = barrier to upstream end of model, large squares = barrier 1/10<sup>th</sup> depth of model, small squares = barrier 1/3<sup>rd</sup> depth of model. Error bars represent the estimated error margin in the measurements

The gradient at the upstream interface of the barrier at damage condition is not a criterion for the strength of the barrier, as pipe development occurs downstream in the barrier. However, it is an indicator of the extent to which there is a reduction of the local hydraulic conductivity over the upstream interface possibly due to the formation of a filter cake whereby fine grains get filtered on the upstream interface of the barrier. This is discussed in detail in Section 4.3.3. The gradient over the upstream interface would be more likely to be a criterion for the failure of the barrier, as analysed in Section 4.8.

These figures lend further support to the hypothesis that at damage condition a local horizontal gradient is exceeded inside the barrier, i.e. that the local horizontal gradient can be considered as the damage criterion for the barrier. However, there is still a relatively large scatter among values of local horizontal gradient for a given barrier type. Possible reasons for this are:

- Small differences between the experiments in terms of the relative density of the barrier.
- The exact position of the barrier location relative to the capillaries may vary slightly, and this may be affected also by crumbling of the barrier during the test. Due to the steep local gradient near the pipe tip this can have a significant impact on the results.
- The gradient in the barrier is currently only measured between H13 and H14, over a distance of 3.5 cm, the damage condition may need to be exceeded over a larger or smaller distance.
- The thickness of the barrier in the experiments might be too small to mobilise the full strength that can possibly be achieved in the barrier material, i.e. if the barrier were

wider it is possible that a higher damage gradient would be obtained. This should be investigated in phase 2b.

The second point can be partially accounted for by using numerical modelling to postdict the tests, as the gradient can be analysed over a fixed distance from the barrier downstream interface. The numerical analysis of the experiments is addressed in Chapter 5. Postdiction of the tests also allows for the evaluation of different failure criteria, i.e. the flux locally at the pipe tip in the barrier, and the local vertical gradients in the barrier near the pipe tip. To address whether the full strength that can be mobilised in the barrier (by arching) requires a wider barrier. Tests with a wider barrier can be performed as part of the foreseen medium-scale tests.

#### 4.8 Residual strength

A significant additional increase in the hydraulic head is required before the barrier is actually breached. The table below shows the head drop between the inlet and the pipe at the damage condition and at the moment the pipe breaks through the barrier.

Table 4.6 Overview of damage head drop and head drop at failure when the pipe passes through the barrier. The head drop over the sand body (i.e. excluding upstream head loss in the filter and tubing and head loss in the sand boil) is shown

experiment number	barrier type and extent	head drop over sand body at damage condition m	head drop over sand body when pipe breaks through barrier, m	difference between head drop at damage condition and breakthrough, m	ratio head drop breakthrough/ damage head drop
191	GZB 2; 5 cm wide	0.40	1.01	0.61	2.5
192	GZB 2; 5 cm wide	0.41	0.74	0.33	1.8
193	GZB 2 low RD 5 cm wide	0.55	1.05	0.50	1.9
196	GZB 3 5 cm wide	0.55	1.0	0.45	1.8
198	GZB 2; 5 cm wide	0.26	1.05	0.79	4.0
199	GZB 2; 5 cm wide	0.28	0.76	0.48	2.7
200	GZB 2 low RD; 5 cm wide	0.42	0.61	0.19	1.5
Tests where the barrier is present to the upstream end of the set-up					
195	GZB 2; 22.8 cm wide	0.11	0.11	0.00	1.1
197	GZB3 22.8 cm wide	0.03	0.08	0.05	2.3

As noted in Section 4.2.4 in test 195 the progression of the pipe inside the barrier increased the flux but reduced the head drop over set-up by increasing the hydraulic conductivity. The

overall head drop over the system was increased however due to the higher hydraulic conductivity of the sand body with the pipe, this mainly resulted in a higher inlet head loss. Tests 195 and 197 cannot be compared well to the tests in which the barrier is only 5 cm wide as in those tests the barrier continues to the upstream end of the set-up.

For the other tests there is a large scatter in the difference between, or in the ratio of the head drop at failure and at damage condition. Ratios are in the range of 1.5 to 4.

Although currently beyond the scope of this study, it is desirable to also know a criterion for breach through the barrier. A first analysis could consider the same damage criteria as for the damage condition when the pipe enters the barrier. The table below shows the value of the possible failure criteria just prior to breaching of the barrier. For the tests where the barrier is present all the way to the upstream end, the head drop just before the pipe progresses all the way upstream in the test are shown.

Table 4.7 Summary of experimental measurements at the point where the pipe breaches the upstream end of the barrier and progresses upstream

test	barrier type	background sand type	test specification	head drop between filter and pipe	flux in test	horizontal gradient at location of H13 and H14 in the barrier	vertical gradient in barrier at location of H5	gradient over upstream interface of the barrier at the location of H15 and H14
				cm	cc/min	-		
191	GZB2	Metselzand	basis	101.2	2320	1.09	0.36	17.47
192	GZB2	Metselzand	barrier depth 3 cm	74.4	1806	1.17	1.02	8.27
193	GZB2 low RD	Metselzand	low relative density barrier	105.2	2079	0.23	0.32	38.27
196	GZB3	Metselzand	Barrier 3 basis	99.7	2572	0.63	0.24	3.00
198	GZB2	Metselzand	rotated model barrier depth 3 cm	104.5	1592	0.51	1.95	2.80
199	GZB2	Metselzand	rotated model barrier depth 10 cm	76.2	1957	0.40	0.78	8.27
200	GZB2 Low RD	Metselzand	rotated model barrier depth 10 cm low RD barrier	61.0	1647	0.17	0.41	2.60
Tests where the barrier is present to the upstream end of the set-up								
195	GZB2	Baskarp	Baskarp sand, barrier to upstream side of model	11.0	2353	0.00	0.17	0.07
197	GZB3	Baskarp	Baskarp sand, barrier 3 to upstream side of model	7.7	3717	0.46	0.14	0.40

As in Section 4.7 statistics can be computed for the tests on GZB2 with a high relative density, these are shown in Table 4.8.

Table 4.8 Summary of experimental measurements and statistics at the point where the pipe breaches the upstream end of the barrier and progresses upstream

test	background sand type	test specification	head drop between filter and pipe	flux in test	horizontal gradient in barrier	vertical gradient in barrier	gradient over upstream interface barrier
			cm	cc/min	-		
191	Metselzand	basis	101.2	2320	1.09	0.36	17.47
192	Metselzand	barrier depth 3 cm	74.4	1806	1.17	1.02	8.27
195	Baskarp	Baskarp sand, barrier to upstream side of model	11.0	2353	0.00	0.17	0.07
198	Metselzand	rotated model barrier depth 3 cm	104.5	1592	0.51	1.95	2.80
199	Metselzand	rotated model barrier depth 10 cm	76.2	1957	0.40	0.78	8.27
average			73.4	2006	0.63	0.86	7.37
standard deviation			33.6	294	0.44	0.62	5.96
CoV			0.46	0.15	0.69	0.73	0.81

For the breakthrough the CoV for the flux is lowest, rather than the CoV for the horizontal gradient. It would be expected that the horizontal gradient in the barrier does not characterise the breakthrough, as the pipe has already passed through most of the barrier, i.e. the gradient between H13 and H14 has little effect on the processes at the tip of the pipe. The CoV of the flux remains high, comparable to the CoV of the flux at the point the pipe grows into the barrier. As discussed in Section 4.7 the flux depends on the configuration and is not an intrinsic property of the barrier, therefore this is not considered suitable as a failure criterion.

The figures below show the variation in the values of these possible failure criteria. None of these seem appropriate to determine the residual strength. It is remarkable that the gradient on the upstream interface of the barrier can reach such high values, up to 38. The presence of a filter cake on this interface is discussed in Section 4.3.3. This may lend considerable strength to the barrier in the tests. The extent to which filter cakes form depends on the combination of the background sand, the barrier and the relative density of the barrier as this determines the ratio of the size of the fine particles that form the filter cake to the size of the voids in the barrier in which they get trapped.

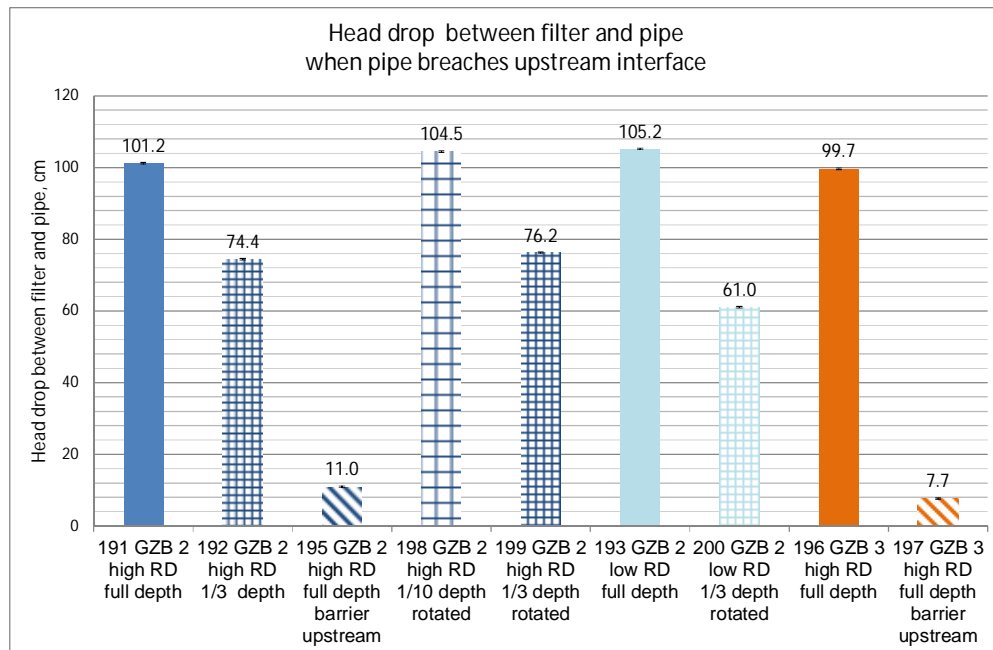


Figure 4.28 Head drop between filter and pipe when the pipe breaches the barrier and progresses upstream. Colours indicate type of barrier: GZB2 high relative density = dark blue, GZB2 at low relative density = light blue, GZB3 at high relative density = orange. Texture indicates test specifics: slope = barrier to upstream end of model, large squares = barrier 1/10<sup>th</sup> depth of model, small squares = barrier 1/3<sup>rd</sup> depth of model. Error bars represent the estimated error margin in the measurements

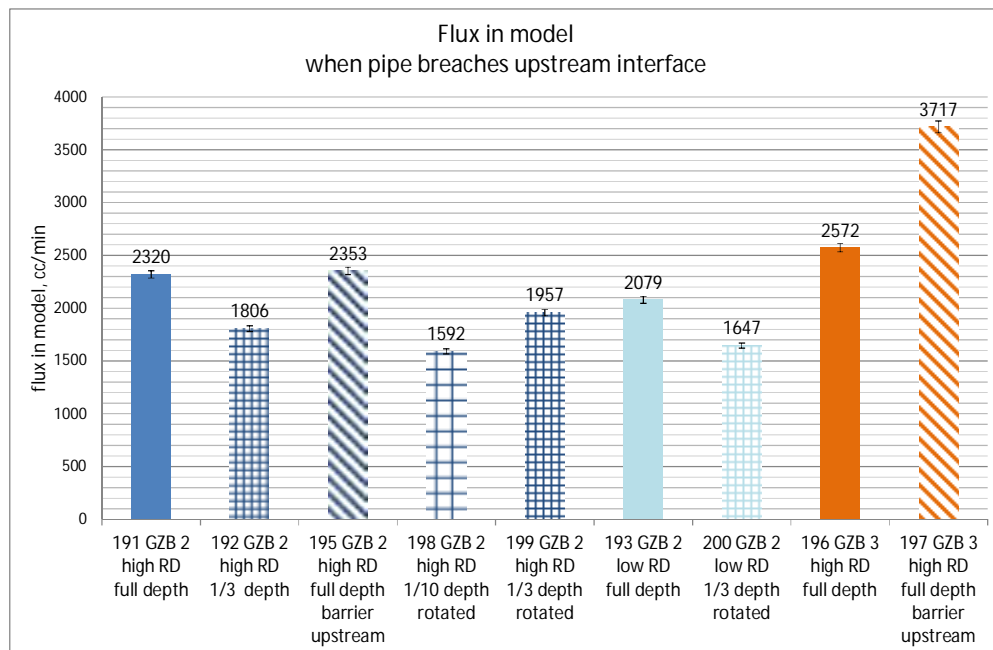


Figure 4.29 Flux when the pipe breaches the barrier and progresses upstream. Colours indicate type of barrier: GZB2 high relative density = dark blue, GZB2 at low relative density = light blue, GZB3 at high relative density = orange. Texture indicates test specifics: slope = barrier to upstream end of model, large squares = barrier 1/10<sup>th</sup> depth of model, small squares = barrier 1/3<sup>rd</sup> depth of model. Error bars represent the estimated error margin in the measurements

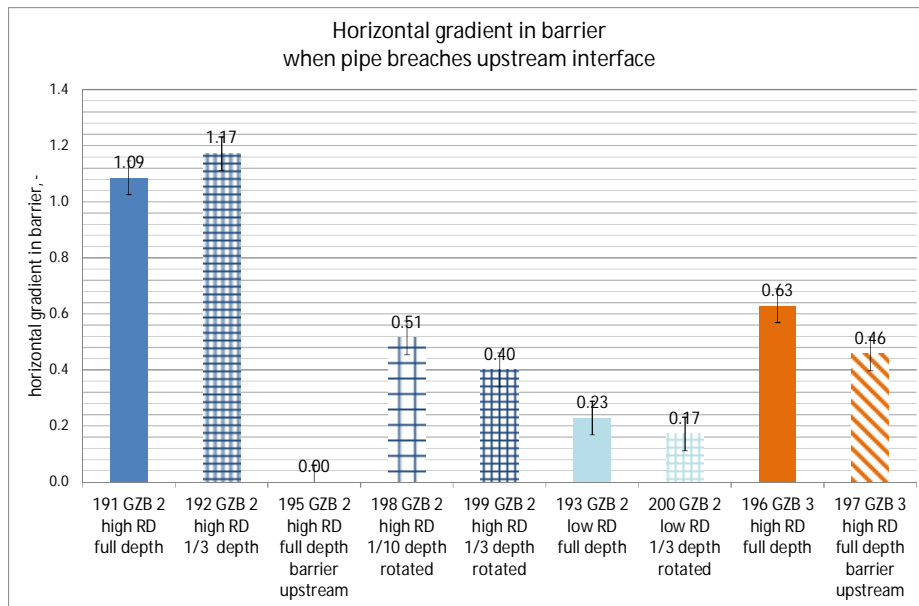


Figure 4.30 Local horizontal gradient in barrier when the pipe breaches the barrier and progresses upstream. Colours indicate type of barrier: GZB2 high relative density = dark blue, GZB2 at low relative density = light blue, GZB3 at high relative density = orange. Texture indicates test specifics: slope = barrier to upstream end of model, large squares = barrier 1/10<sup>th</sup> depth of model, small squares = barrier 1/3<sup>rd</sup> depth of model. Error bars represent the estimated error margin in the measurements

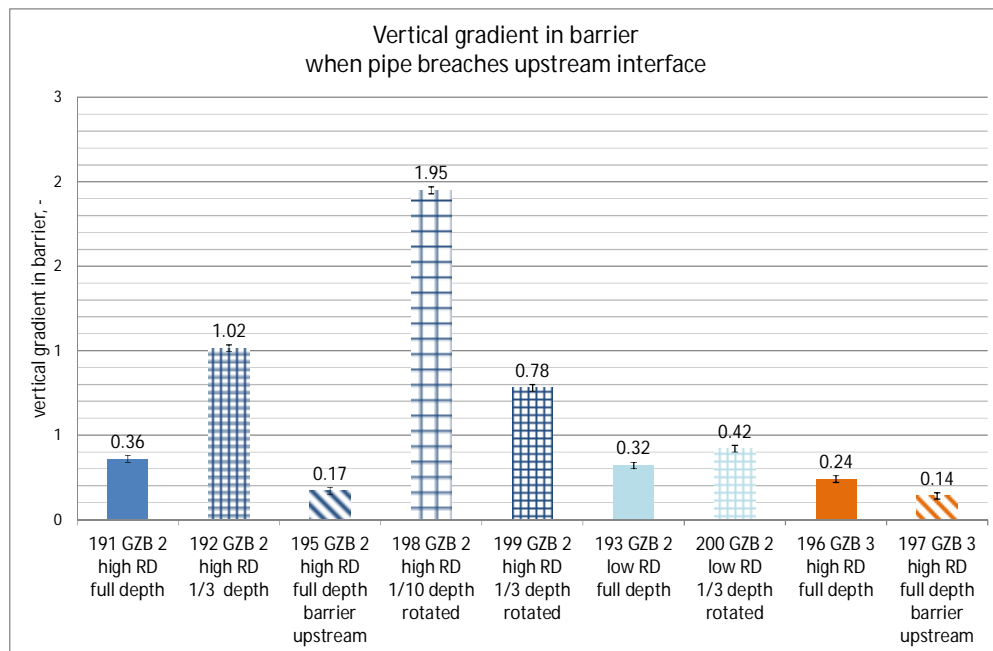


Figure 4.31 Vertical gradient in barrier when the pipe breaches the barrier and progresses upstream. Colours indicate type of barrier: GZB2 high relative density = dark blue, GZB2 at low relative density = light blue, GZB3 at high relative density = orange. Texture indicates test specifics: slope = barrier to upstream end of model, large squares = barrier 1/10<sup>th</sup> depth of model, small squares = barrier 1/3<sup>rd</sup> depth of model. Error bars represent the estimated error margin in the measurements

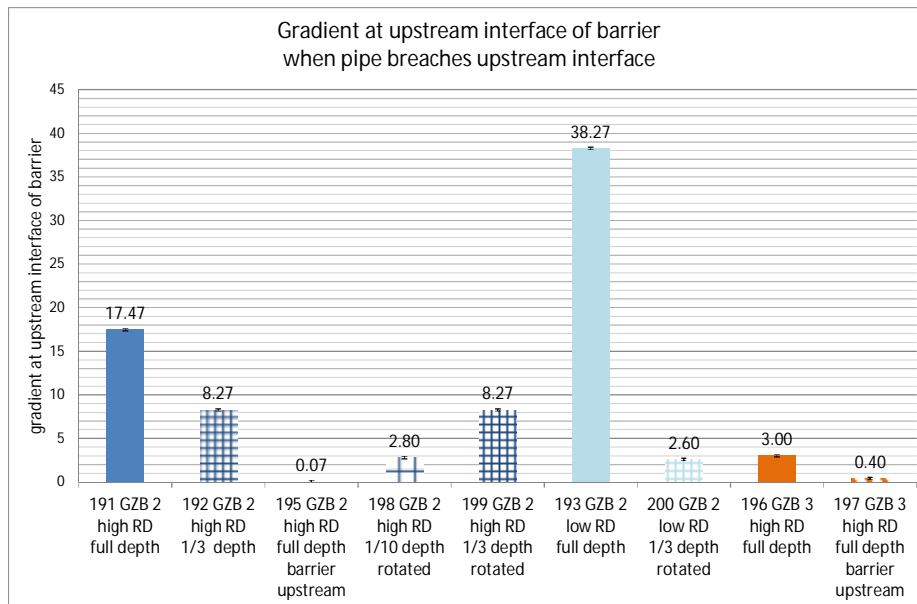


Figure 4.32 Gradient at upstream interface of barrier when the pipe breaches the barrier and progresses upstream. Colours indicate type of barrier: GZB2 high relative density = dark blue, GZB2 at low relative density = light blue, GZB3 at high relative density = orange. Texture indicates test specifics: slope = barrier to upstream end of model, large squares = barrier 1/10<sup>th</sup> depth of model, small squares = barrier 1/3<sup>rd</sup> depth of model. Error bars represent the estimated error margin in the measurements

#### 4.9 Comparison to reference test

In order to compare the effect of the coarse sand barrier to a case without a barrier, test 194 was done, this test is described in (Rosenbrand and Van Beek, 2017). The flat set-up is used and the sand used is Metselzand with a relative density of 65% (i.e. approximately the same relative density as the fine sand downstream of the barrier in the tests with a high relative density barrier).

As the pipe grew below capillaries H11, H12 and H13 in test 194, it is possible to compute the critical head drop over the sand body up to the pipe using the same measurements that were used to compute the damage head drop for the experiments with a coarse sand barrier.

For tests with a barrier the damage head drop is calculated as the head drop between the upstream end of the set-up (i.e. in the sand body just beyond the inlet filter determined by extrapolation from H3 and H4) and the lowest head measured in the capillaries that are in the pipe (H12 in the centre of the model, and H16-H19 when the pipe extends along the width of the barrier), as discussed in Chapter 4 and shown in Figure 4.2. Thereby the head loss over the upstream tubing and the filter and over the sand boil and erosion lens are excluded. In the reference test, the pipe does not widen as there is no barrier so only the head drop up to H12 is considered (as the other capillaries are not in the pipe). The critical condition is the head drop just before the pipe grows all the way upstream in the experiment for test 194. At this point the pipe has progressed beyond H12, however in order to make a meaningful comparison to the tests with a barrier, the head drop between upstream and H12 is used.

Figure 4.33 shows the head drop during test 194. The critical head drop in this reference test without a barrier is 7.6 cm. The critical head drop over the sand body in the reference test is compared to the head drop where the pipe damages the barrier, and to the head drop when

the pipe breaches the upstream interface between the barrier and the fine sand upstream for the tests with a background of Metselzand and the flat box in Table 4.9.

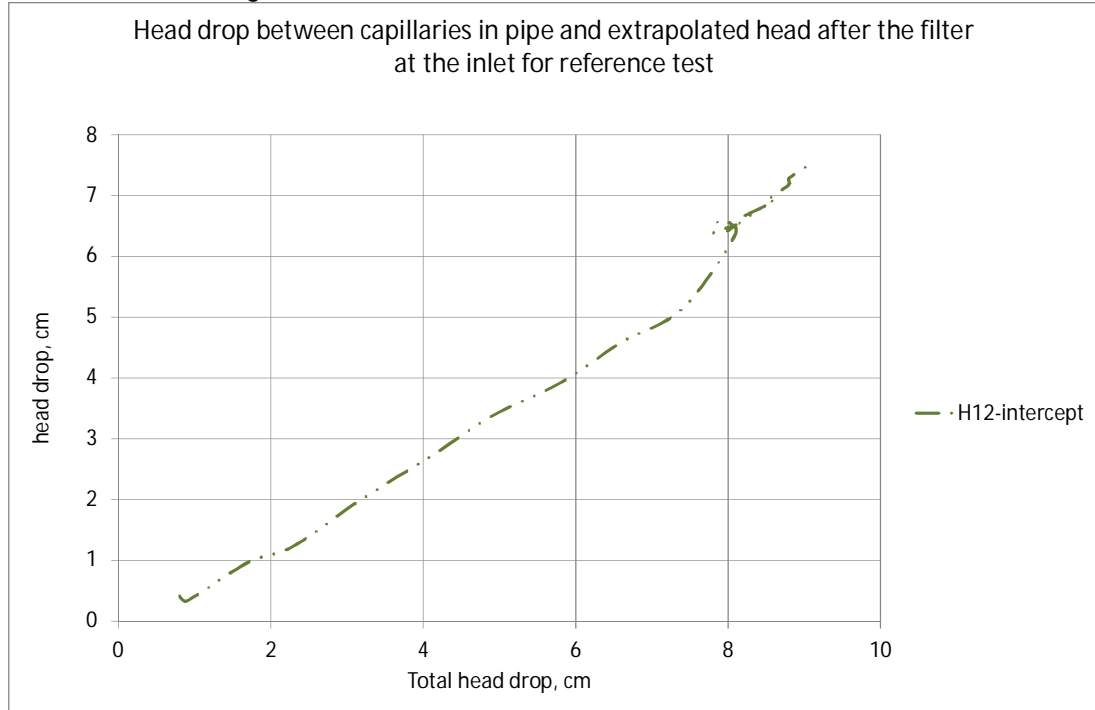


Figure 4.33 Head drop over sand body for reference test (test 194). Head drop on the y axis is the head drop between the upstream end of the set-up (i.e. just beyond the filter in the fine sand) and the head measured in capillary H12 which is in the pipe. This head drop corresponds to the head drop. The x axis shows the head drop between capillary H3 in the sand body on the upstream side of the set-up just beyond the filter, and H2 in the outlet tubing

Table 4.9 Comparison between tests with barrier and reference test 194 without barrier

Experiment number	Head drop over sand body at critical conditions reference case, m	Head drop over sand body at damage condition with barrier, m	Head drop over sand body when pipe breaks through barrier, m	Ratio head drop with barrier to reference case at for damage condition in barrier	Ratio head drop with barrier to reference case when pipe breaks through barrier
191	0.076	0.40	1.02	5.3	13.4
192	0.076	0.41	0.74	5.4	9.7
193*	0.076	0.55	1.05	7.2	13.8
196**	0.076	0.55	1.00	7.2	13.2

\*test with low relative density barrier GZB2, it appears that filter cake formation contributed to additional strength

\*\*test with barrier GZB3

The increase in the head drop that is achieved with a barrier GZB2 at a high relative density is a factor ca. 5, considering the damage criterion when the pipe first enters the barrier. Considering the point that the pipe breaks through the barrier the increase in head drop is in the order of a factor 10.

The higher factors for test 193 with a low relative density barrier are probably due to the formation of a filter cake on the upstream interface between the barrier and the fine sand. This retains a high head drop and thus provides additional strength.

There is only one test with GZB3 and Metselzand in the small box (test 196). This shows a bit higher strength than the tests with GZB2 at damage condition and a comparable strength when the pipe breaches the barrier.

The flux in the reference case at critical conditions is 359 cc/min, this is a factor 2.5 to 4 less than the flux with a barrier at damage condition, and a factor 5 to 7.2 less than the flux when the pipe breaches the barrier in tests 191, 192, 193 and 196 (values for the flux in those tests are shown in Table 4.5 and in Table 4.8).

## 5 Numerical simulations

There are three main reasons for the numerical simulations in this phase 2a of the coarse sand barrier project:

1. To identify a damage criterion for the coarse sand barrier based on the outcome of the small-scale laboratory experiments.
2. To analyse the effect of parameters on the damage head drop.
3. To predict the damage head drop for the medium-scale and Delta Flume tests.

*To identify a damage criterion for the coarse sand barrier based on the outcome of the laboratory experiments*

Postdictions of the experiments at the damage condition are described in Section 5.5. From these postdictions, the horizontal gradient at the top of the model is selected as the damage criterion. This selection is made by comparing several potential damage criteria in order to determine which one shows the least variation among tests with the same barrier at damage condition. That is considered the most likely criterion to characterise the strength of the barrier. This procedure is similar to the analysis of the damage criterion based on experimental results only in Section 4.7.

The horizontal gradient for the damage criterion is evaluated over the distance between the point 1 cm upstream of the interface between the pipe and the barrier and 4.5 cm upstream of this interface. This is a logical choice as, due to the strong convergence of flow at the interface between the barrier and the pipe, the question arises to which extent this is well captured in a continuum approach. Furthermore, as observed in the tests, there is some crumbling at the edge of the barrier which would have a strong effect on the results for the failure criterion that starts directly from the edge of the barrier. Also the most upstream end of the barrier may be affected by the formation of a filter cake. This limits the upstream distance over which the horizontal gradient can be determined.

*To analyse the effect of parameters on the damage head drop*

A range of sensitivity analyses is done to address the effects of parameters on the horizontal gradient in the barrier:

- The hydraulic conductivity contrast between the barrier and the fine sand.
- The transverse extension of the pipe along the barrier.
- The depth of the pipe.
- The depth of the barrier.

These analyses are done using the small-scale models.

*To predict the damage head drop for the medium-scale and Delta Flume tests*

Based on the damage criterion a model for the geometry of the medium-scale and Delta Flume tests is used to predict the upstream head that leads to damage.

The software used is described in Section 5.1. The schematisations used for the sensitivity analyses and predictions are shown in Section 5.2. DgFlow is bench-marked using comparisons to Abaqus and Plaxis in Section 5.3. Section 5.4 contains the sensitivity analyses, which are reported in appendices and only summarised here. Section 5.5 contains the postdictions of the tests and Section 5.6 the predictions for the medium-scale and Delta Flume tests.

## 5.1 Software

The finite element groundwater simulation code DgFlow (Van Esch, 2015, 2014, 2013) is used.

Models are set-up and meshed using the pre-processor GiD (version 13.0), results are visualised using ParaView (version 5.2.0).

## 5.2 Schematisation and mesh

Calculations mainly done using 2D models as the groundwater flow is essentially two dimensional when the pipe has widened along the barrier. To benchmark DgFlow with other software (Section 5.3), to verify the 2D flow profile (Section 5.4.1), and to assess the effect of pipe widening along the barrier (Section 5.4.2), 3D models are used.

### 5.2.1 Pipe depth

The depth of the pipe is initially neglected in the models, and the head drop in the pipe is assumed negligible compared to the head drop in the sand due to the much higher hydraulic conductivity of the pipe. The simplification of a zero depth pipe where flow in the pipe is not explicitly modelled: a) entails no additional assumptions are made about the depth and hydraulic conductivity of the pipe, which are unknowns; b) simplifies the model geometry and thus improves computational efficiency.

However, it should be realised that water cannot flow to a pipe of zero depth. This is true in the real world but also in the 'numerical world'. The 'depth' of a pipe of zero depth in a numerical model will be determined by the dimensions of the elements close to the pipe and the shape functions of those elements. Consequently, the calculated gradient at the front of the pipe tip will be unreliable.

The effect of the pipe depth is analysed in a sensitivity analysis for pipe depth (Section 5.4.3) and also in the bench-marking of DgFlow results by comparison with Abaqus results in which the pipe is explicitly modelled with a finite depth and hydraulic conductivity (Section 5.3). These show that the effect of pipe depth on the head profile can be significant. Based on these results and on estimates of pipe depth during the experiments (Section 4.1.2) postdictions are conducted with a pipe of 2 mm depth where the pipe is still modelled as a boundary condition i.e. flow inside the pipe is not modelled.

### 5.2.2 Flow regime

Based on the Reynolds numbers estimated from the test data at the damage condition and the relation between head loss and discharge in the experiments, the flow in the barrier and in the fine sand is expected to be in the region where Darcy's law is valid. In the model it is assumed that flow is fully saturated, and the compressibility of the water and the soil is neglected. The flow regime in the pipe is irrelevant, since the head drop is negligible.

### 5.2.3 Boundary conditions

The 2D model used in DgFlow for the small-scale tests (not rotated) is shown below. The barrier is present between x-coordinates -170 mm and -120 mm (blue region). The upper boundary of the model is closed between -348 mm and -120 mm and open with a constant head condition from -120 mm to +12 mm. This is the region where the pipe is present.

In simulations where the effect of a deeper pipe is modelled (Section 5.4.3), or in postdictions where the pipe has 2 mm depth (Section 5.5) the sides of the pipe, at the interface between the barrier and the pipe and at the interface between the pipe and the fine sand at the exit hole, are straight and these have a constant head boundary. In those models the elements at

the location of the pipe are not meshed, i.e. the bottom of the pipe is the outflow boundary of the model.

The inflow is through the left vertical boundary at x coordinate -348 mm, and inflow occurs along the entire depth of the model (between z coordinates 0 mm and -101 mm). The bottom and right hand side boundaries are closed.

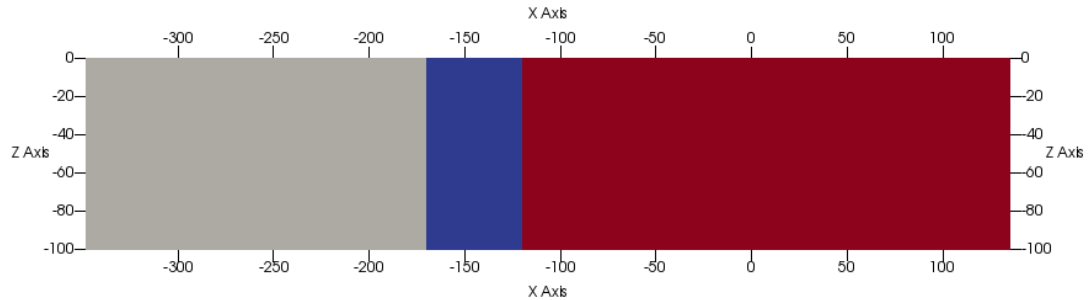


Figure 5.1 Model of the set-up, the barrier is the blue region, fine sand upstream is the grey region, fine sand downstream is the red region

#### 5.2.4 Mesh

For the 2D small-scale models a structured mesh is used with local refinement in the barrier. The optimal mesh size is determined in a mesh analysis as reported in (Appendix A) and this is used for all simulations. This mesh has elements of 1 mm by 1 mm in the top of the model as shown in Figure 5.2, which is the region of most interest for computing the damage criterion.

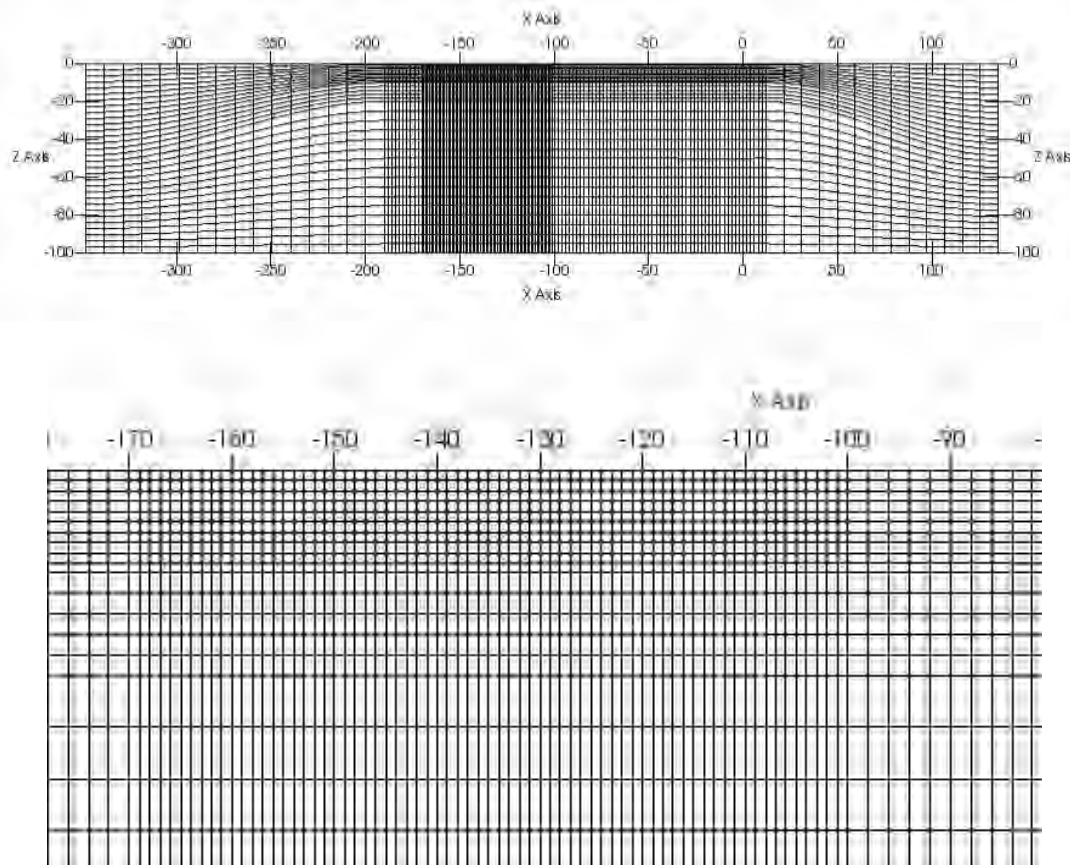


Figure 5.2 The mesh of the 2D model (top) and a close up of the mesh in the barrier (bottom)

For the 3D models in Sections 5.3, 5.4.2 and 5.4.1 an unstructured mesh is used with local refinement of elements of 1 mm at the top of the barrier. The local refinement and the mesh in the 3D model is shown in the figures below.

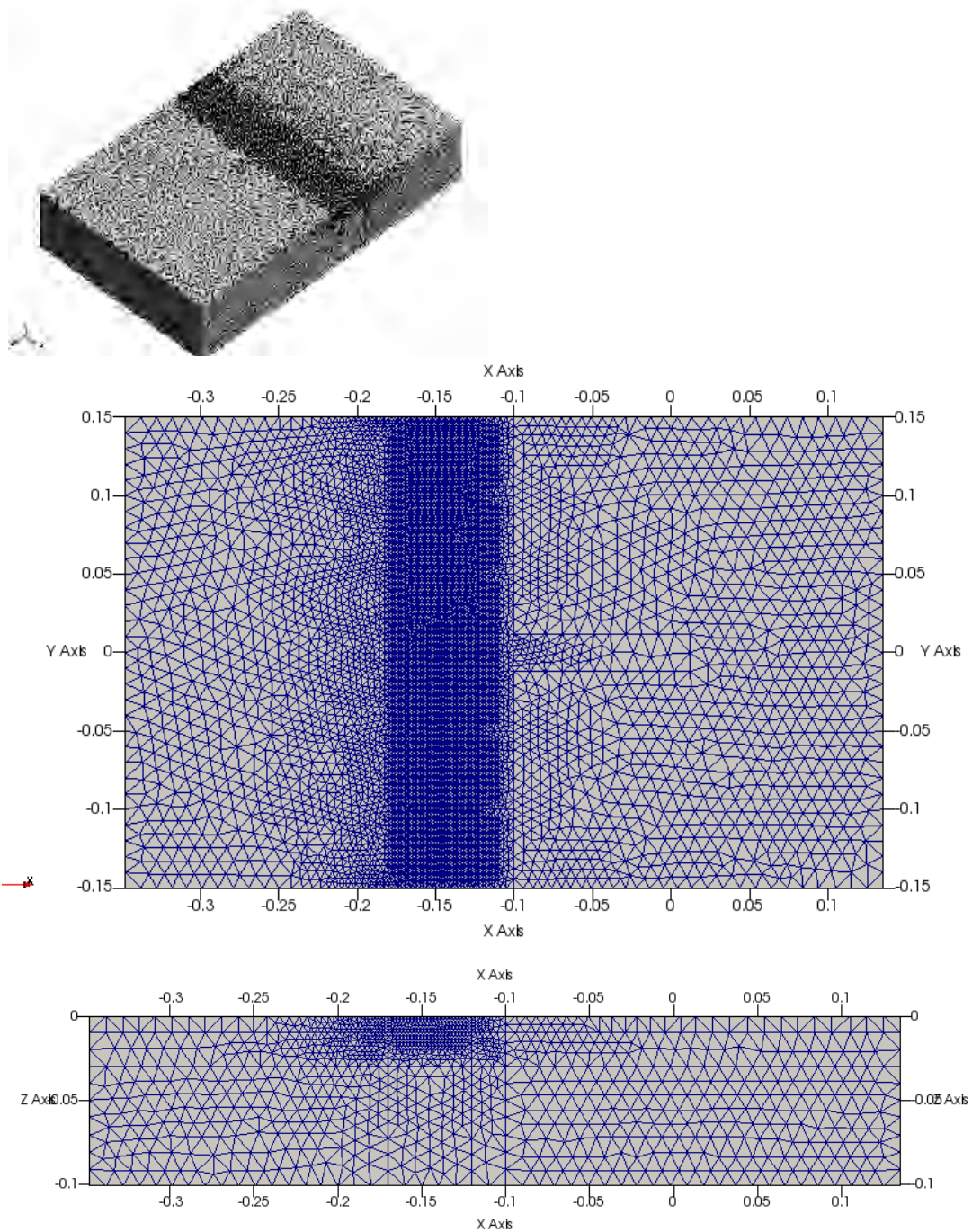


Figure 5.3 The mesh of the 3D model. Top 3D view; middle top view of the model; bottom side view of the model

The 2D and 3D models produce similar results, provided that the pipe extends along the entire length of the barrier (see Sections 5.4.1 and 5.4.2). As the 2D model was benchmarked using the analytical solution (in Appendix B), the mesh refinement of the 3D model is also considered adequate.

Furthermore, as the pipe has been observed to widen along the entire length of the barrier at damage condition, 2D models can adequately be used for postdictions, sensitivity analyses and predictions. The effect of the pipe partially widening along the length of the barrier is analysed in 3D models in Section 5.4.2.

### 5.3 Benchmarking DgFlow

Three methods are used to evaluate the results of DgFlow:

- Comparison to analytical solutions.
- Comparison to identical models in Plaxis.
- Comparison to a model with a pipe with a physical depth in Abaqus.

#### 5.3.1 Comparison to analytical solutions

The comparison to the 2D analytical solution is reported in Appendix B. The analytical Polubarinova-Kochina (PK) solution (Polubarinova-Kochina, 1962) is only valid in cases with a uniform hydraulic conductivity where flow converges to a constant head boundary. This would be comparable to the coarse sand barrier model for the situation where the barrier has the same hydraulic conductivity as the soil (i.e. no barrier).

The DgFlow results for the modelled gradient are calculated by means of the head in the nodes along the top line of the model, and also by means of the velocity in the elements. These values correspond well with the analytical solution. This indicates that the model gives good results, and that the applied mesh refinement is sufficient.

#### 5.3.2 Comparison to Plaxis

The small-scale tests were modelled in Plaxis 3D (version 2016.01) and Plaxis 2D (version 2017) and in DgFlow for a range of hydraulic conductivity contrasts between the barrier and the fine sand. In both models the pipe is a boundary condition with zero depth. The results are reported in Appendix C.

The head profiles along the top of the models are compared. Where there are differences, Plaxis gives a higher head than DgFlow. The 2D results from DgFlow and Plaxis overlie exactly when there is no hydraulic conductivity contrast between the sand and the barrier, and show very little difference for a hydraulic conductivity contrast of 3. The 3D heads modelled by DgFlow and Plaxis are slightly higher than the 2D heads, with a smaller difference between 2D and 3D for DgFlow than for Plaxis. This is probably due to different meshes used in the two models. As the 2D DgFlow model with no hydraulic conductivity contrast was found to fit the analytical solution well in Appendix B, of the two 3D models DgFlow approximates the analytical solution best for this model with no hydraulic conductivity contrast.

For a very high hydraulic conductivity contrast of 100 (larger than in the current test series) the differences between Plaxis and DgFlow, and between 2D and 3D become relatively larger; however, it must be noted that in this case the differences are in the order of 1-2 mm, so in absolute terms these are very small.

The local gradients are evaluated over the barrier and over a distance of 3.5 cm at two locations in the barrier, namely between the interface between the barrier and the pipe and 3.5 cm upstream of this interface, and between the point 1 cm upstream of the interface to 4.5 cm upstream of this interface, which is the distance over which the local damage criterion is defined in this phase of the project. The highest value of the ratio of the damage criterion from DgFlow over the damage criterion from Plaxis is 1.03.

The small differences between the Plaxis and DgFlow results support the conclusion that both models can be used to analyse this situation.

### 5.3.3 Comparison to Abaqus

To address the effect of modelling the pipe as a boundary condition rather than as a volume with a hydraulic conductivity an analysis using the programme Abaqus (CAE 613 Academic) was performed at Ghent University, for which the results are reported in Appendix D. A comparison of results from Abaqus and DgFlow focussing on the differences between the head profiles and the gradients is reported in Appendix E.

In the Abaqus analysis the pipe consists of a T-shape with a main pipe that has a depth of 5 mm in the centre of the model (hydraulic conductivity 20 m/s) and two laterally branched pipes along the barrier with a depth of 5 mm at the centre of the model that declines to 2.5 mm at the edges of the model (hydraulic conductivity 5 m/s). These hydraulic conductivity values are selected in such a way that there is hardly any head loss in the pipe.

The branched pipes have sloping walls so that the pipe also slopes 5 mm into the barrier at the centre of the model (and 2.5 mm at the edges) as shown below. This has a significant effect on the local horizontal gradients at the top of the model. The Abaqus model is therefore compared both to DgFlow models with a depth of 0 mm, and to models with a pipe of a finite depth (but still modelled as a boundary condition as detailed in Section 5.4.3).

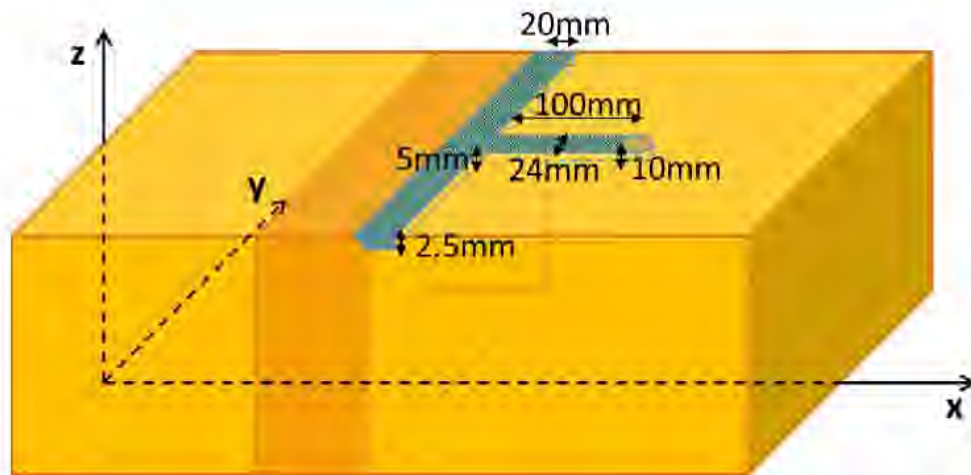


Figure 5.4 Image of the Abaqus model, note the pipe has a sloping edge that extends into the barrier (source Appendix D)

Comparison of the head profiles shows that with a finite depth pipe in DgFlow, the results from Abaqus and DgFlow are more comparable than for a DgFlow model where the pipe has zero depth. The gradient computed over the entire barrier (from -0.120 m to -0.170 m) is also quite similar for both models when these have the same pipe depth. The ratio of the gradients from DgFlow/Abaqus is only 1.03 for a barrier-fine sand hydraulic conductivity contrast of 3, and 0.95 for a contrast of 100. However, considering the local damage criterion, which is computed over a shorter distance, (between -0.130 m and -0.165 m i.e. 1 cm upstream of the interface between the barrier and the pipe and 4.5 cm upstream of this interface), the differences between the models are larger, the ratio is only 0.74 for a hydraulic conductivity contrast of 100.

In summary:

- a) The head profile in the barrier from Abaqus matches better with the head profile from DgFlow when the DgFlow model also uses a pipe with finite depth, of course differences remain due to the use of a sloping wall of the pipe in Abaqus and a straight wall in DgFlow.
- b) The gradient over the entire barrier is comparable for Abaqus and DgFlow simulations when these have a similar pipe depth.
- c) The differences between local gradients within the barrier, such as the gradient over the distance for the damage criterion, are larger.

The good match between the head profiles over the entire model and over the entire barrier from Abaqus and DgFlow, when the two have a similar depth pipe, indicates that modelling the pipe as a boundary condition as opposed to modelling the pipe as a physical volume does not introduce a significant error for the overall head profile at the top of the model.

The good match between the gradients over the entire barrier, as compared to the less good match over a shorter distance, indicates that the modelled gradients over shorter distances are more sensitive to differences between models, such as location of the interface between the barrier and the pipe, which is straight in DgFlow and slanting into the barrier in Abaqus.

Due to the limited size of the barrier in the experiments, it is not possible to define a damage criterion over a larger distance based on these tests. Furthermore, inevitable differences between the exact location of the interface between the barrier and the pipe in tests and in the models will lead to uncertainties, regardless of which model is used to model the results. As assumptions regarding the pipe depth would be required for both models, and additionally for the Abaqus model a hydraulic conductivity has to be assumed for the pipe and also because this model is computationally more expensive, the approach of modelling the pipe as a boundary condition in DgFlow is considered adequate for this project.

The effect of pipe depth on the results is analysed in more detail in Section 5.4.3, and incorporated in the postdiction procedure in Section 5.5.

#### 5.4 Programme sensitivity analyses

The purpose of the sensitivity analyses is to provide insight into the relative effect of different parameters on the results. This enables a better understanding of the process, but is also important for future analyses to determine the optimal dimensions and hydraulic conductivity contrasts in the design of a coarse sand barrier.

The effects of different parameters are compared by considering their effect on the head profile and on the horizontal gradient in the barrier at the top of the model. As the damage criterion for this phase of the project is best characterised by the horizontal gradient from -0.130 m to -0.165 m i.e. 1 cm upstream of the interface between the barrier and the pipe and 4.5 cm upstream of this interface (as shown by the postdictions in Section 5.5), the effect of variations on this gradient is of interest.

In this section, sensitivity analyses are reported concerning:

- Effect of hydraulic conductivity contrast in 2D and 3D models.
- Effect of transverse extension of the pipe (i.e. pipe extension parallel to the barrier).
- Effect of depth of the pipe (a pipe depth of 0 is the default that is used in this section).
- Effect of the depth of the barrier.

For all sensitivity analyses the effect of the hydraulic conductivity contrast between the barrier and the fine sand affects the results and therefore this is analysed for several hydraulic conductivity contrasts (i.e. 3 to 100), spanning a wider range than the range of contrasts present in the current test series.

For all analyses an upstream head of 0.4 m is used, the downstream head in the pipe is 0 m, and the hydraulic conductivity of the fine sand is  $6.0e-4$  m/s. The hydraulic conductivity of the barrier is varied in order to achieve the desired hydraulic conductivity contrast. All sensitivity analyses are done using the small-scale model.

#### 5.4.1 Effect of hydraulic conductivity contrast in 2D and 3D models

The sensitivity analysis is done for the small-scale 2D and 3D models which were described in Section 5.2, the analysis is reported in Appendix F. The hydraulic conductivity contrast used are:

- 1
- 3
- 10
- 33
- 100

The hydraulic conductivity contrast has a strong effect on the convergence of flow in the barrier, as illustrated below for hydraulic conductivity contrasts 1 and 100. With a contrast of 100, the flow direction at the downstream end of the barrier converges upwards towards the pipe rather than entering the fine sand downstream as shown below.

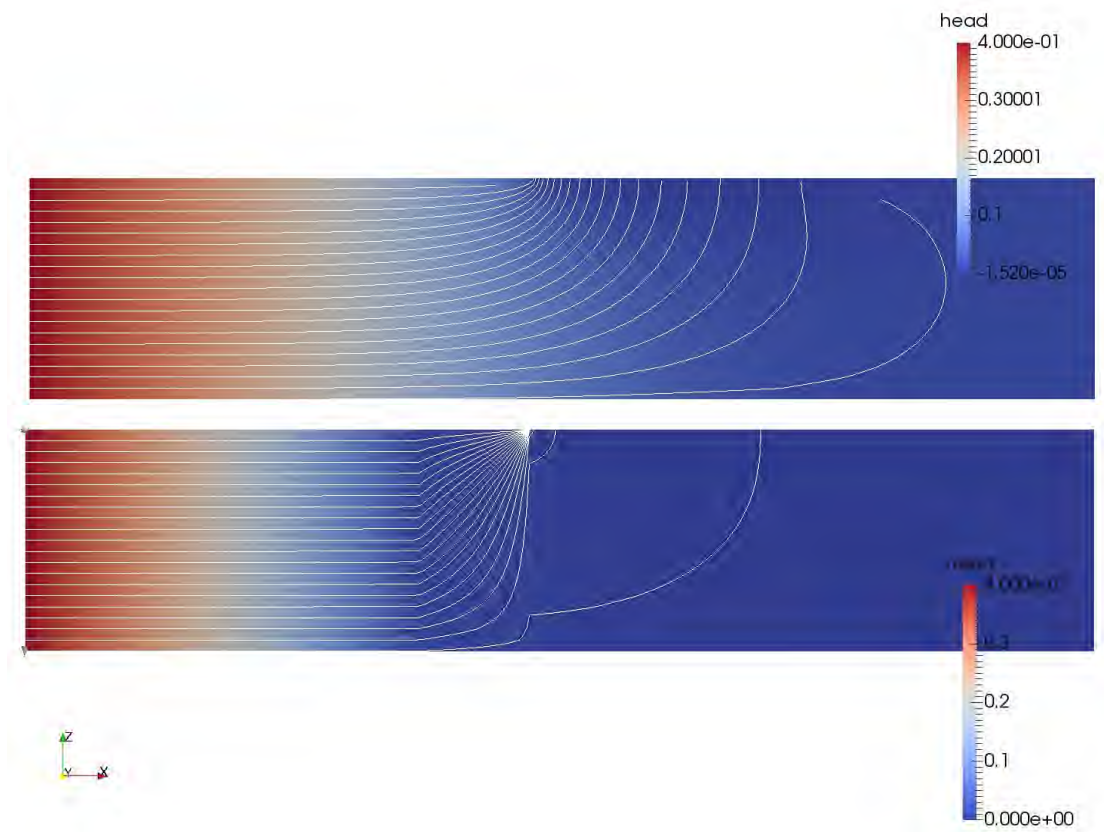


Figure 5.5 The streamlines indicate the flow paths in the 2D models. The background colour is the head distribution. For a higher hydraulic conductivity contrast the flow converges more strongly in the barrier. Top hydraulic conductivity contrast 1, bottom hydraulic conductivity contrast 100. The upstream boundary is on the left side of the model.

Despite the converging flow, the head at the top of the barrier is lower in the case of a high hydraulic conductivity contrast, due to the small resistance to flow. As a consequence the gradient over the barrier is also lower for a greater contrast as shown in Figure 5.6.

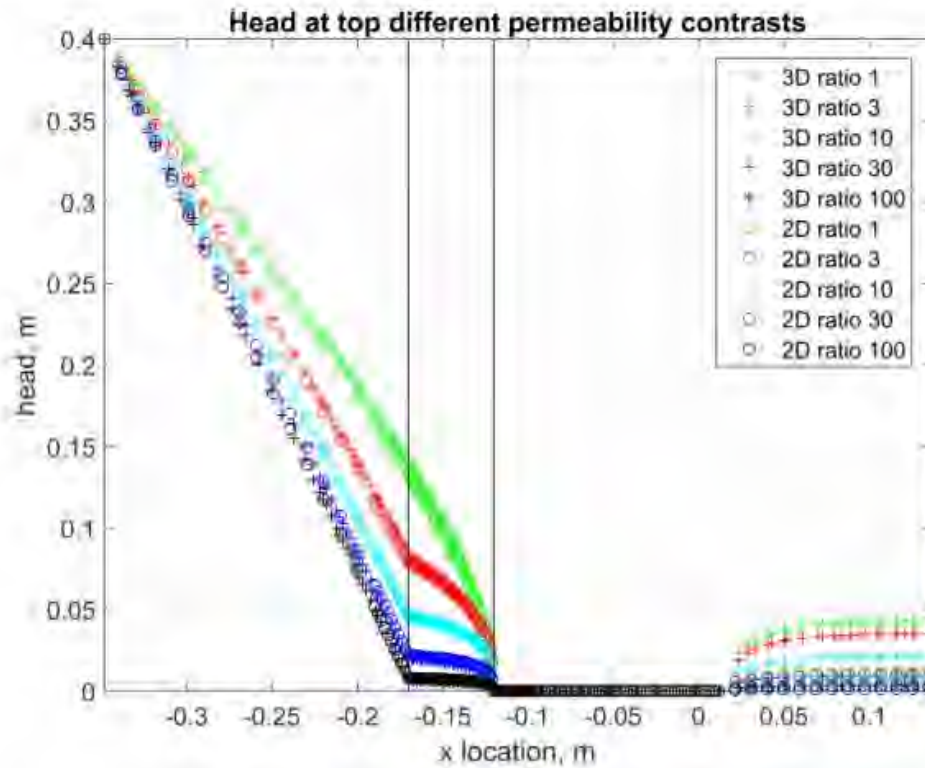


Figure 5.6 Head profiles along top boundary of entire model for different hydraulic conductivity contrasts in 2D models (circles) and 3D models (crosses)

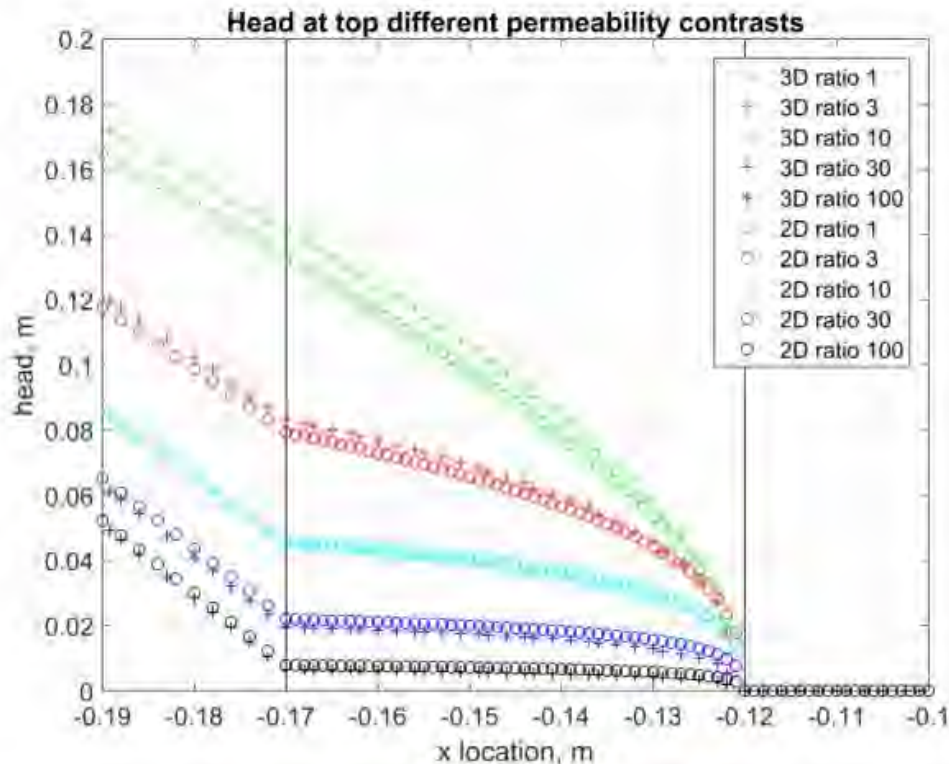


Figure 5.7 Head profiles along top boundary zoomed in on the barrier for different hydraulic conductivity contrasts in 2D models (circles) and 3D models (crosses)

Differences between the gradients in the barrier obtained with 2D and 3D models are dependent on the hydraulic conductivity contrast; for lower contrasts the 2D model gives lower values than the 3D model, whereas this is the opposite for contrasts higher than 10. The maximum difference is a ratio of 2D gradient/3D gradient of 1.21, for a hydraulic conductivity contrast of 100 for the gradient between -0.130 m and -0.165 m. For contrasts between 1 and 30 this ratio is only between 0.95 and 1.14.

Note that although the relative difference between gradients may seem large, the absolute difference between the gradients is very small for the high hydraulic conductivity contrasts. This is due to the very low gradient in the barrier. When inspecting the head profile in the barrier in Figure 5.6 it is also apparent that the differences between the heads in the 2D and 3D models are small.

Increasing the hydraulic conductivity of the barrier leads to a lower horizontal gradient in that barrier (Figure 5.6), but is also leads to more concentration of streamlines at the outflow point (Figure 5.5), which increases flow and thus the horizontal gradient. Consequently, a 3 times higher hydraulic conductivity in the barrier does not lead to a 3 times lower hydraulic gradient.

Considering the uncertainties introduced in the head measurements during the tests, and the preliminary estimated error margin for the fitting of the postdictions as analysed in Section 5.5.4.5, 2D models are considered to be appropriate in this phase of the project.

#### 5.4.2 Sensitivity analysis transverse extension of pipe

In the experiments, the pipe was found to widen along the entire barrier prior to proceeding into the barrier at the damage condition, as also noted by (Negrinelli et al., 2016). Therefore, for modelling the damage situation, when the pipe enters the barrier, the model with a pipe transverse length of 30 cm is used. The effect of a pipe that has not widened parallel to the entire barrier is analysed in a sensitivity analysis, which is reported in Appendix G. This effect is not directly relevant for the current phase of the project but may occur on a larger scale or at the field scale when the pipe does not widen along the entire barrier.

Three geometries are analysed in 3D models, with a pipe width of 10 cm, 20 cm and 30 cm (entire model). Results for the head distribution along the centreline of the model are compared to results from the 2D model. Also the heads along lines at 4 cm from the centreline, and 9 cm from the centreline are analysed. The calculations are done with 2 hydraulic conductivity contrasts, 3 and 100. The head distribution along the central axis of the model for different pipe widths is shown below.

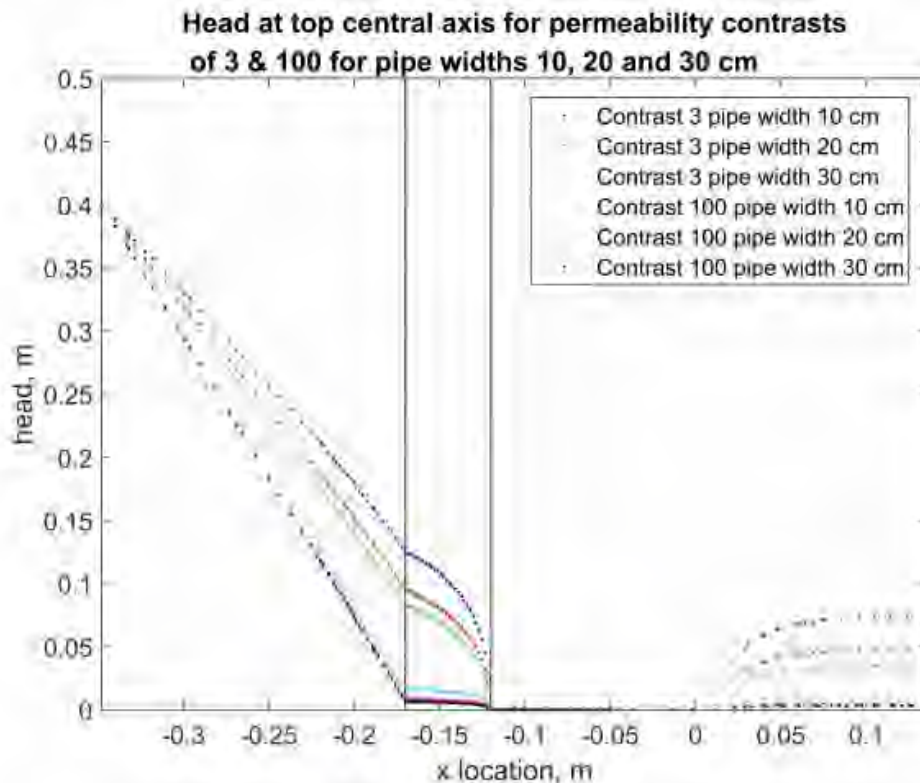


Figure 5.8 Head profiles along top boundary for the entire model

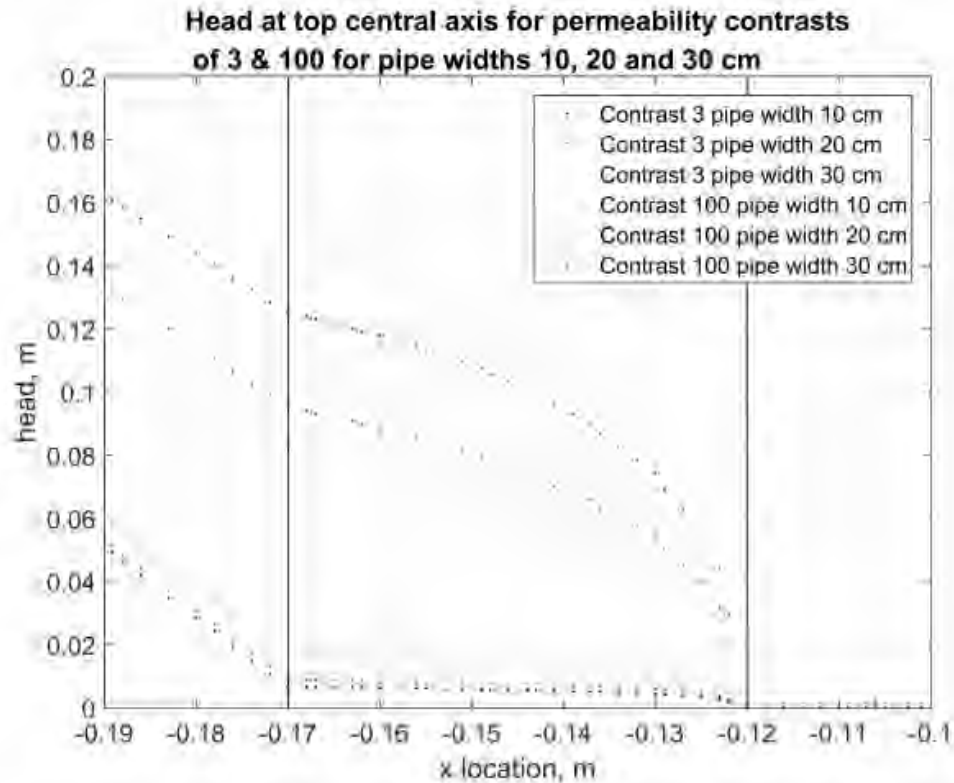


Figure 5.9 Head profiles along top boundary zoomed in on the barrier

As expected, a pipe that has not progressed parallel to the entire barrier results in a higher head in the barrier due to convergence of flow. However, the difference in gradients between a pipe that has a width of 10 cm and a pipe of 20 cm width is much larger than between a pipe of 20 cm width and 30 cm width. This is also shown below for the effect of the pipe width on the gradient between -0.130 and -0.165 m (the damage criterion).

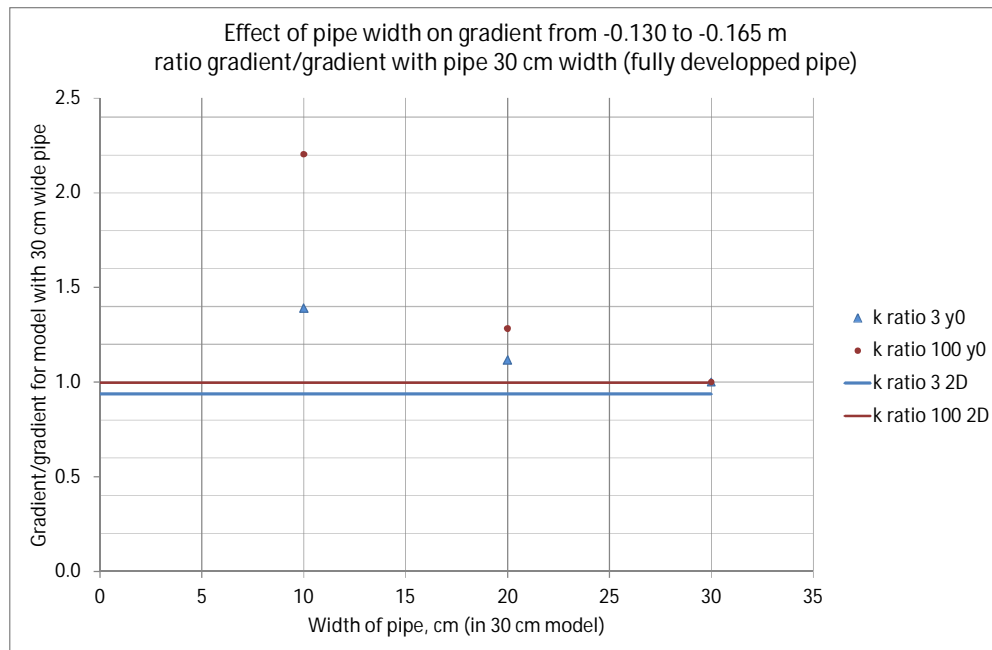


Figure 5.10 Ratio of the gradient over the distance -0.130 to -0.165 m (over which the barrier strength is determined) for a pipe of different widths normalised by the gradient over this distance for a pipe width of 30 cm (i.e. the transversal length of the branched pipe along the barrier = the entire width of the model). Results are shown for a hydraulic conductivity contrast of 3 (blue) and 100 (red). The solid lines indicate the ratio of the 2D results over the 3D results with a full pipe width

This suggests that even if the pipe has not extended along the entire length of the model, but only 28 or 29 cm, results are still well modelled with a width of 30 cm in the model, and thereby by a 2D model (as these were shown to give similar results in Section 5.4.2).

It was also observed that when the pipe is not extended over the full width, the gradient in the barrier near the tip of the pipe is higher than in the centre of the T-shaped pipe. This would favour the widening of the pipe in the fine sand, as fine grains are significantly easier to erode than the barrier grains. This would also favour pipe development in the barrier away from the centre axis, in situations where the pipe cannot fully widen to the edges of the set-up. This also explains why the pipe quickly extends along the full width in the experiments, where there are no obstacles that prevent the pipe from doing so.

A lower gradient inside the barrier for the same head drop means that a higher overall head drop can be withstood when the pipe has widened along the entire barrier. This means that the widening of the pipe along the barrier reduces the load on the barrier, such that a larger outside water level can be withstood.

#### 5.4.3 Sensitivity analysis of pipe depth

The comparison to the results of Abaqus in Section 5.3.3 and Appendix E already indicated that the depth of the pipe has an effect on the head distribution and the gradients in the barrier. The effect of pipe depth on the head distribution, gradients in the barrier and on the flow rate is analysed in Appendix H. The analysis is done in 2D models, thus the pipe is assumed to have developed along the entire width of the barrier, and having the same depth along this width.

The effect of the pipe depth is analysed for hydraulic conductivity contrasts of 3 and 100 for pipe depths of:

- 0 mm
- 2 mm
- 4 mm
- 6 mm
- 10 mm

When the pipe has a fixed depth, the boundary condition is applied to all sides of the pipe, as shown below

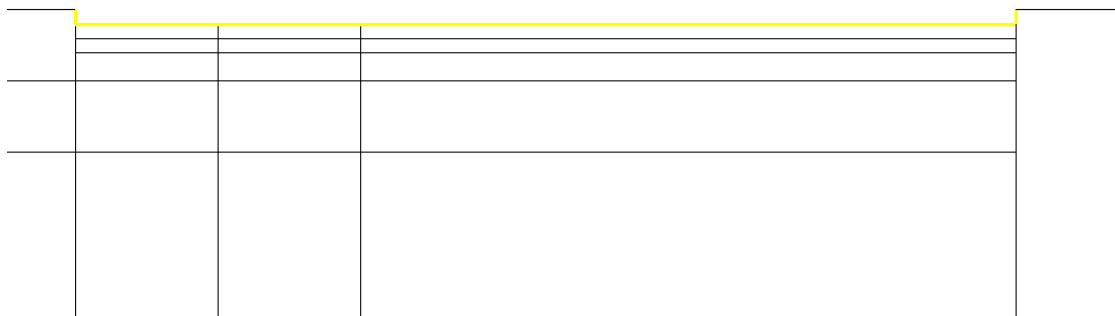


Figure 5.11 Schematisation of the pipe with a finite depth as a boundary condition. Note that the constant head is applied to the bottom and the sides of the pipe

The head profiles in the barrier are strongly affected by the pipe depth as shown in the figures below.

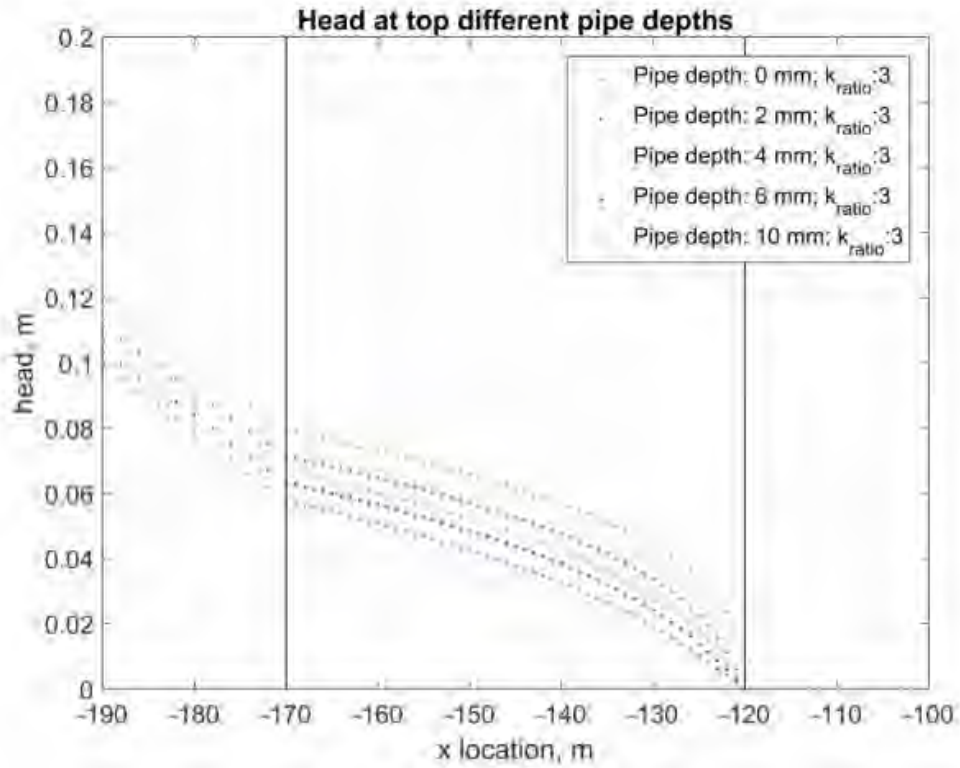


Figure 5.12 Head profile in model zoomed in on the barrier for a hydraulic conductivity contrast of 3

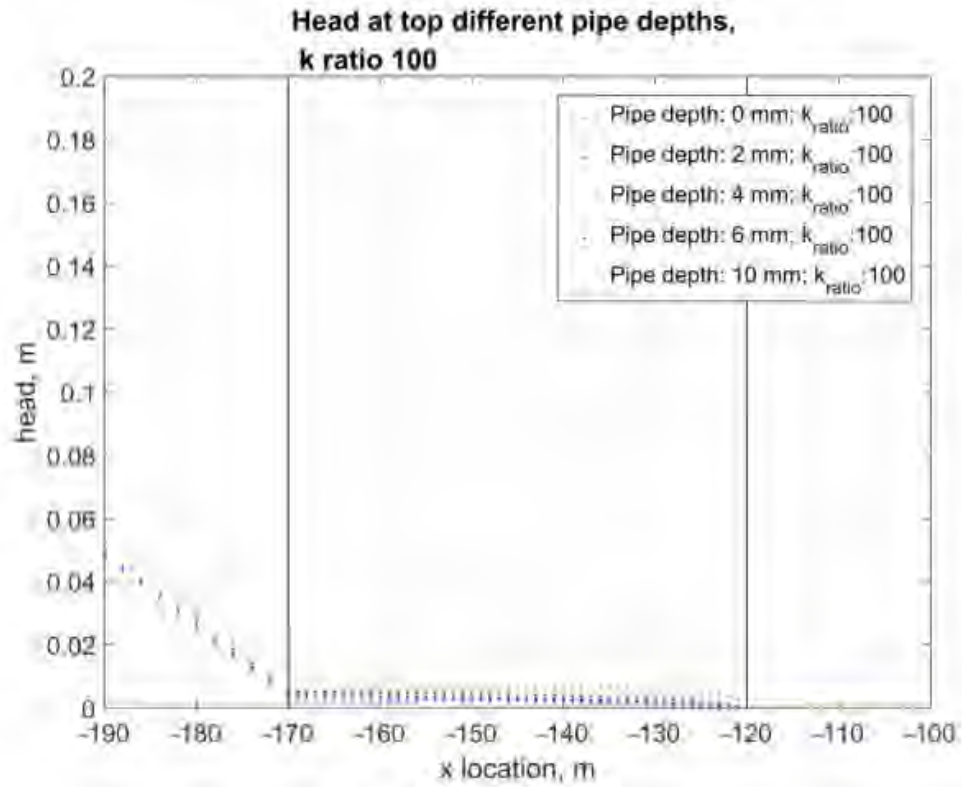


Figure 5.13 Head profile in model zoomed in on the barrier for a hydraulic conductivity contrast of 100

Figure 5.14 shows the effect of pipe depth on the gradient over the entire barrier, but also on the gradient over the distance of the damage criterion (-0.130 m to 0.165 m).

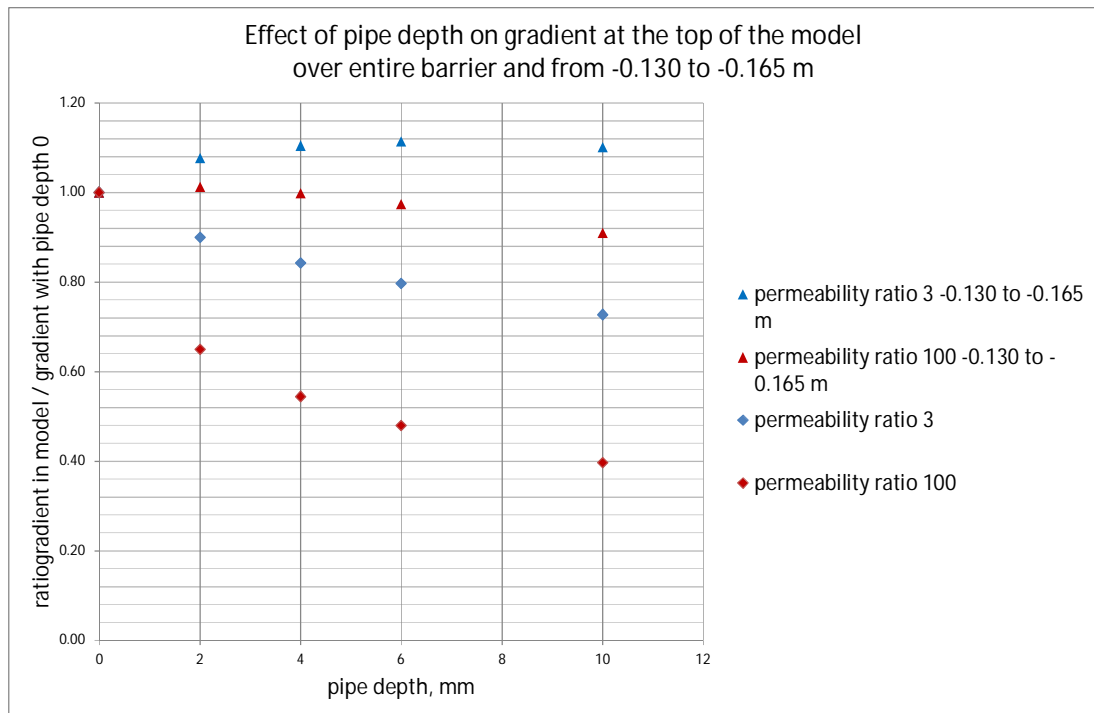


Figure 5.14 Effect of pipe depth on the gradient in the barrier for two hydraulic conductivity contrasts. Shown is the gradient at a given pipe depth normalised by the gradient with 0 mm pipe depth

Note that the effect of depth on the local gradient over the distance of the damage criterion (between -0.130 m and -0.165 m) is much smaller than the effect on the gradient over the entire barrier. Modelling a finite pipe depth gives a smaller gradient over the entire barrier. However looking locally between -0.130 m and -0.165 m, with a hydraulic conductivity ratio of 3 the gradient actually increases slightly with increasing pipe depth.

Increasing the depth of the pipe increases the length of the interface between the pipe and the barrier, which means that water can flow more easily out of the barrier and into the pipe. This reduces the head throughout the barrier and thus the gradient over the entire barrier. However, with a deeper pipe the gradient in the first centimetre from the interface between the pipe and the barrier also becomes less steep, again as there is a larger outflow area. This can be clearly seen in Figure 5.12 and Figure 5.13. This very local reduction of the gradient offsets the reduction of the gradient in the entire barrier, giving a slightly higher gradient over the area of the failure criterion (-0.130 m to -0.165 m) for a hydraulic conductivity contrast of 3. This can be observed comparing the head distributions in Figure 5.15.

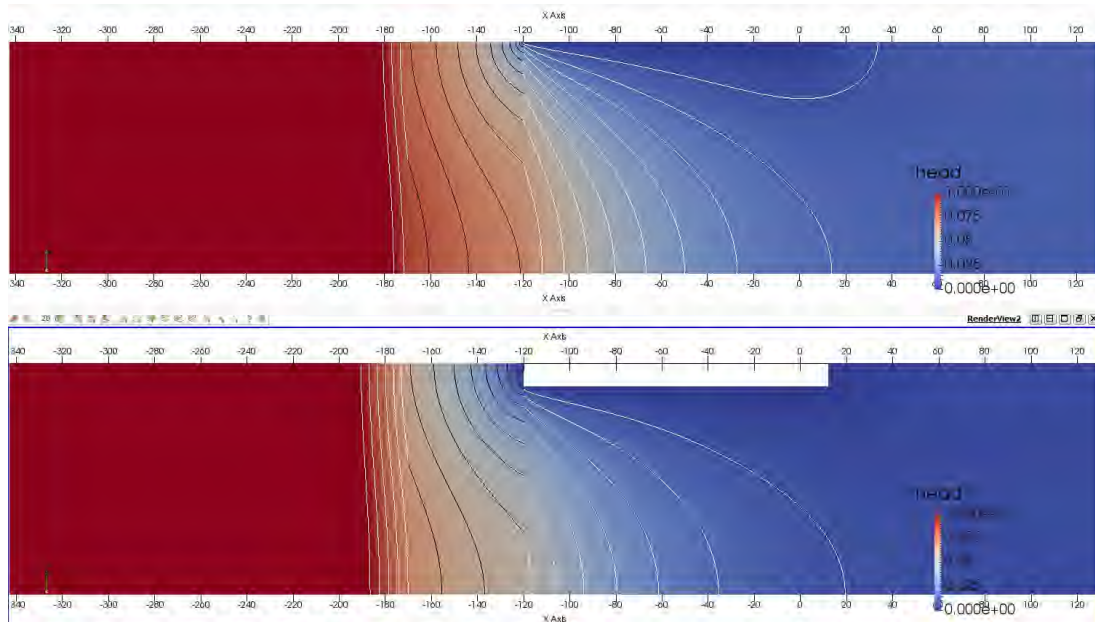


Figure 5.15 Head distribution in models with hydraulic conductivity contrast 3 and pipe depth 0 mm (top) and 10 mm (bottom). The lines are head contours, the colour of these indicates if they are in the fine sand (white) or in the barrier (black). With a pipe depth of 0 mm the head at the upstream interface of the barrier is higher, giving a higher gradient over the entire barrier. However, the gradient is particularly highest in the downstream first centimetre of the barrier, so that the gradient between -0.130 m and -0.165 m is lower than in the model with a pipe depth of 10 mm

For a hydraulic conductivity contrast of 100, there is more convergence of flow in the barrier, therefore the relative effects in the first centimetre from the interface between the barrier and the pipe and over the entire barrier are different. Because there is such a strong convergence of flow in the barrier to the pipe, the increase of the pipe depth, by increasing the area through which flow leaves the barrier, reduces pore pressures and gradient strongly throughout the barrier. This is shown in Figure 5.16.

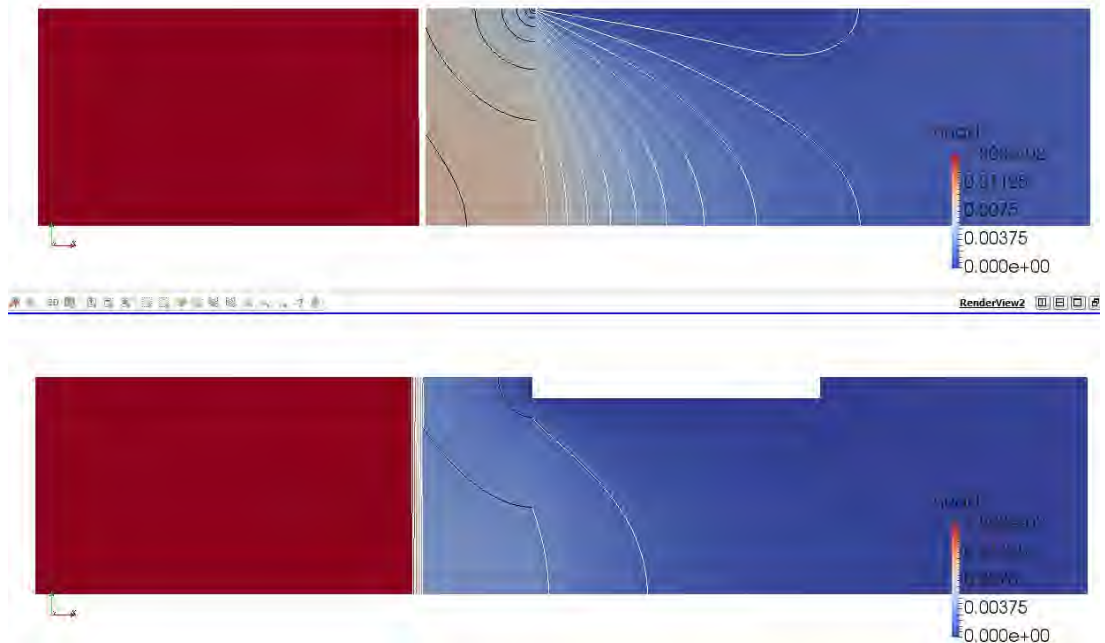


Figure 5.16 Head distribution in models with hydraulic conductivity contrast of 100 and pipe depth of 0 mm (top) and 10 mm (bottom). The lines are head contours, the colour of these lines indicates if they are in the fine sand (white) or in the barrier (black). With a pipe depth of 0 mm the head at the upstream interface of the barrier is higher, giving a higher gradient over the entire barrier. Because of the large hydraulic conductivity contrast there is a strong convergence of flow to the pipe in the barrier, the larger outflow area with a 10 mm deep pipe therefore also results in a lower local gradient in the barrier

The effect of the pipe depth on the flux in the model is very small.

To conclude: for the small-scale model, the pipe depth has a significant effect on the calculated head profile in the barrier; increasing depth reduces the head throughout the barrier and thereby reduces the gradient over the entire barrier. However, the effect of pipe depth causes the strongest reduction in the head within the first cm from the interface between the barrier and the pipe, therefore the gradient over the distance of the failure criterion (from -0.130 to -0.165 m) is less severely affected by the pipe depth (although the overall head profile in this area is significantly reduced).

#### 5.4.4 Sensitivity analysis of barrier depth

The analysis of the effect of the depth of the barrier is done in the 2D model for the rotated set-up, as this allows for a greater variation of the depth of the model. The dimensions of the rotated set-up are shown below, the length of the model is equal to the standard set-up, the depth is a factor 3 greater and the width is a factor 3 smaller. The analysis is reported in Appendix I.

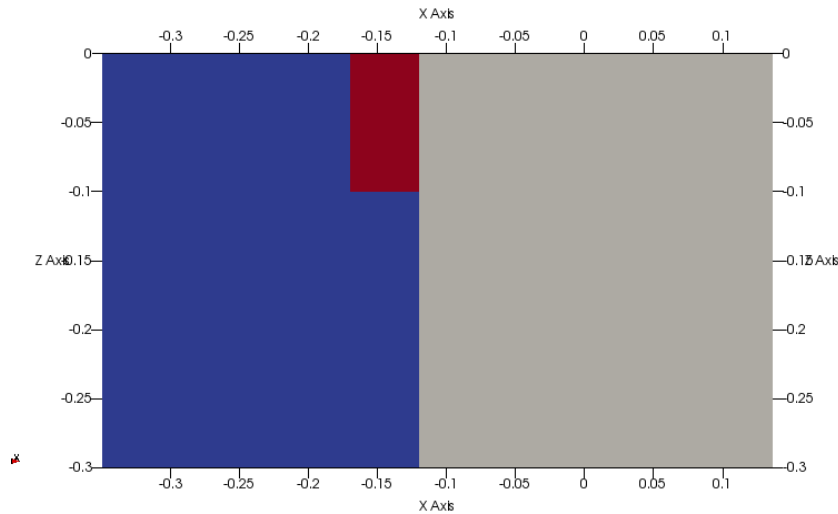


Figure 5.17 Schematisation of the model with a 10 cm deep barrier (red). Blue is upstream fine sand, grey is downstream fine sand

Increasing the barrier depth increases the gradient in the barrier and also increases the flux through the model. The relative increase in the gradient in the barrier is greater for a higher hydraulic conductivity contrast. This means that when a barrier is applied in a field situation, increasing the depth of the barrier will reduce the total head drop that the barrier can withstand. Therefore, it will be necessary to determine the minimum depth for the barrier that is necessary in the field (to avoid, for instance, that pipes can grow below the barrier), since increasing the depth will make the barrier less effective in withstanding a high outside water level. This should be investigated further in this project.

## 5.5 Postdictions

Postdictions are made for the tests in which there was failure of the barrier and where there was piping starting from the downstream end of the model. Thus there are no postdictions for tests 189, 190 and 200. Test 194 is without a barrier and is therefore also not modelled.

The aim of the postdictions is to reproduce the head distribution throughout the entire model in order to be able to compute the damage criterion in the barrier. This Section will show that the horizontal gradient between locations -0.130 m and -0.165 m, i.e. between 1 cm upstream of the downstream interface between the barrier and the pipe and 4.5 cm upstream of this interface, is an appropriate damage criterion in this phase of the project.

Postdictions of the tests are made, and 6 possible damage criteria are computed from the postdictions. From these, the criterion with the smallest variation is considered as the best criterion to define the strength of the barrier material. The 6 possible criteria are:

- Horizontal gradient between -0.130 m and -0.165 m at the surface of the model.
- Vertical gradient at -0.130 m from the surface of the model to a depth of -0.03 m.
- Diagonal gradient from -0.130 at 0 m depth to -0.165 m at -0.03 m depth.
- Horizontal flow velocity between -0.130 m and -0.165 m at the surface of the model.
- Vertical flow velocity at -0.130 m from the surface of the model to a depth of -0.03 m.
- Diagonal flow velocity from -0.130 at 0 m depth to -0.165 m at -0.03 m depth.

This range of distances is selected as the first centimetre from the interface between the barrier and the pipe is sensitive to some crumbling of individual barrier grains into the pipe, therefore it is questionable whether the continuum flow model used here will accurately reproduce the gradients in this zone. Furthermore as shown in Section 5.4.3 this section is less sensitive to assumptions regarding the depth of the pipe.

#### 5.5.1 Fitting for postdictions

Three criteria are considered to evaluate the closeness of fit of the postdiction; these are in descending order of importance:

- Head distribution in the model, as compared to head distribution measured.
- Flow rate in the model, as compared to flow rate measured. Flow rate in the 2D models is computed by taking the flow velocity along the upstream border and multiplying this by the width of the box (300 mm for normal tests, 101 mm for rotated set-up) (i.e. multiplying by inflow area).
- Gradient between capillaries H13 and H14.

This order is used because the head distribution is determined by 3 points in the bottom of the model (H3, H4 and H5) and 3 points in the top of the model (H13, H14 and H15). Thus there is more information over the domain of the model than given by flow or local gradient between H13 and H14 alone.

#### 5.5.2 Postdiction procedure and assumptions

Initially it was considered that the postdictions would only regard the models with 3 fitting parameters: the hydraulic conductivity of the fine sand upstream of the barrier, downstream of the barrier, and the hydraulic conductivity of the barrier itself (except for experiments where there was also fine sand below the barrier where this would have a hydraulic conductivity as well). The depth of the pipe was assumed to be 0 mm (i.e. at the surface).

However, as observed in Section 4.5, filter cakes appear to have formed during the tests. The exact hydraulic conductivity and extent of the filter cake could not be visually evaluated from the tests. Based on the measured heads the filter cakes were present between H15 (in the fine sand upstream of the barrier) and H14 (in the barrier). Therefore it is assumed that the filter cake forms in the upstream section of the barrier. A region of 5 mm is therefore modelled with a lower hydraulic conductivity in the barrier. The conductivity of this region is highly uncertain as its extent in reality is not known. This cannot be measured or derived from the head drop, as in the experiments there is a section of fine sand, filter cake, and barrier, between H15 and H14. Thus in the postdictions the role of the modelled filter cake is purely to better fit the head profile and flux in order to be able to reproduce the head profile in the model. This is sufficient for the current study where the mechanics of the filter cake are not the objective.

Furthermore, it proved difficult to obtain a good fit for the head distribution inside the barrier, in particular for H13 close to the downstream end of the barrier. The head is overestimated in the models. As the analyses in Section 5.4.3 and Section 5.3.3 with a pipe with a depth showed that a deeper pipe, both as a boundary condition in DgFlow, and a physical pipe depth in Abaqus lead to a lower head in the barrier, and particularly at the location of H13, postdictions were also done with a pipe with a fixed pipe depth of 2 mm based on observations during the tests (Section 4.1.2).

Overview of fitting parameters:

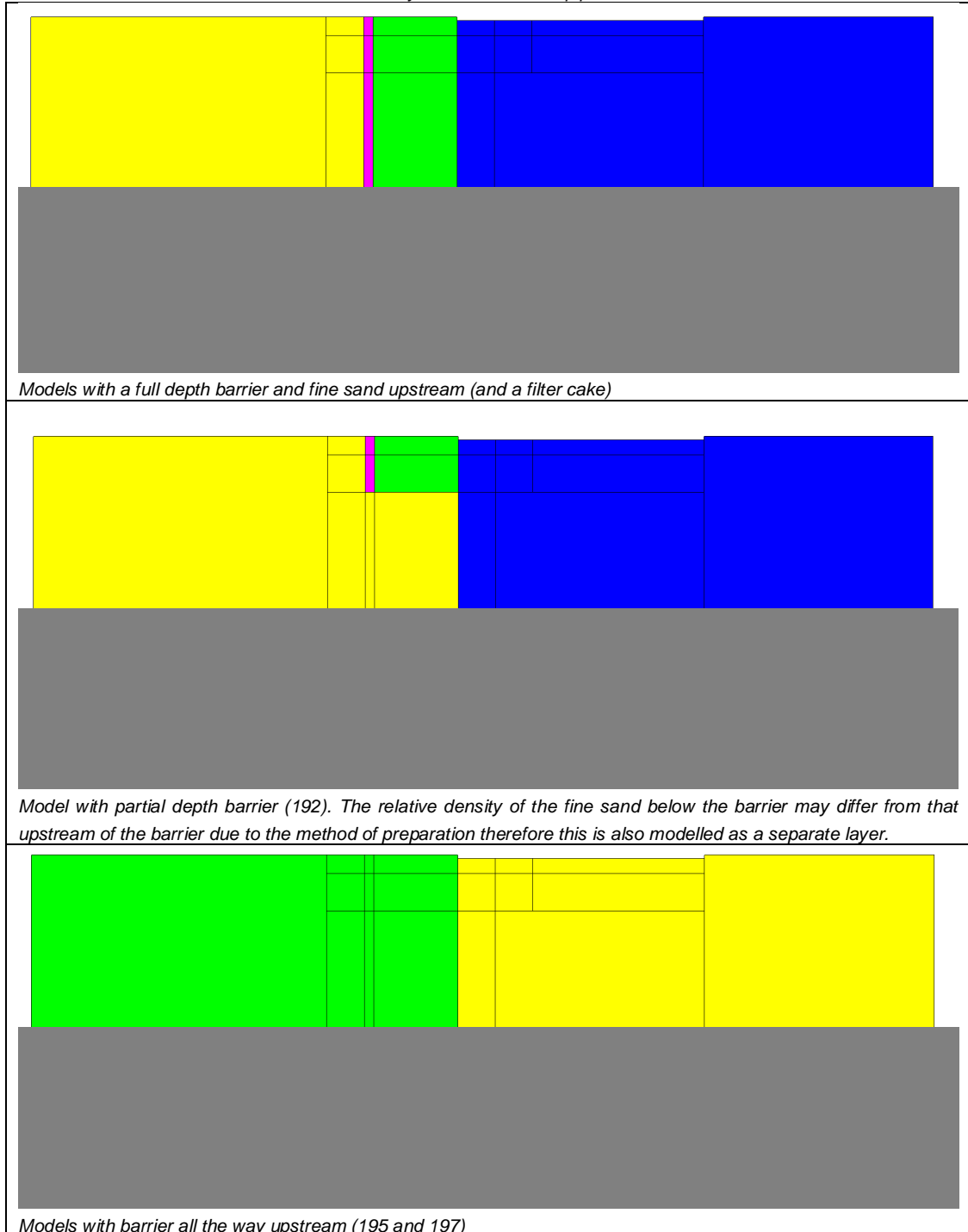
- The hydraulic conductivity of the fine sand upstream is estimated from the experiments and the column tests (Rosenbrand and Van Beek, 2017). If necessary this is adapted to better fit the model to the test results.
- The hydraulic conductivity of the barrier is estimated from the experiments however this value is typically very unstable. Therefore the column tests are used as the basis for the first estimate of this (Rosenbrand and Van Beek, 2017). If necessary this is adapted to better fit the model to the test results.
- The hydraulic conductivity of the sand downstream is taken from the results of the column tests for most postdictions. The exception are those where the barrier goes all the way upstream (with Baskarp fine sand downstream), and the models where the barrier only occupies part of the depth of the model. For those models, adaptation of this value can be needed to be able to fit the model to the results.
- The presence of a low hydraulic conductivity zone on the upstream end of the barrier, a filter cake, as this was the only manner in which to account for the measured head drop over the upstream interface of the barrier. Therefore the hydraulic conductivity of this filter cake was a fitting parameter (Rosenbrand and Van Beek, 2017).

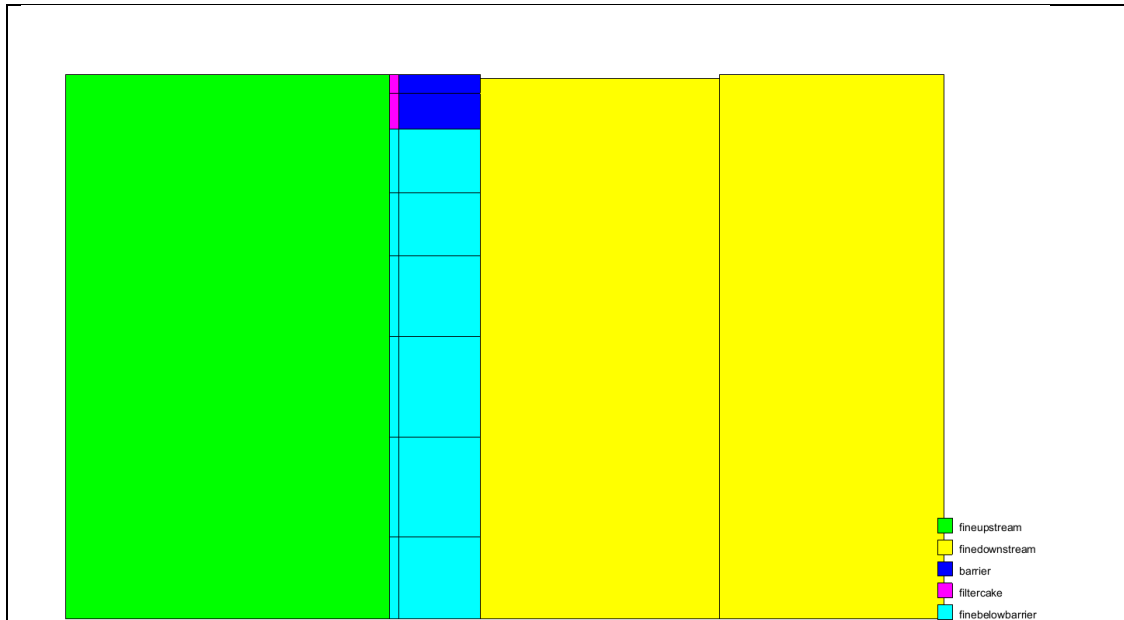
It is assumed that the hydraulic conductivity does not vary in the vertical direction in the models and that the hydraulic conductivity in the horizontal and vertical directions is equal. Also the gradual change of hydraulic conductivity in the horizontal direction within a soil block is not considered. These assumptions may not be valid. The development of filter cakes already indicates there is transport of fine grains which is likely to produce a gradually changing hydraulic conductivity profile, both in the fine sand and in the barrier (development of the filter cake). Furthermore, the development of a filter cake for instance may be more pronounced in the upper part of the model. However, it is not considered desirable to introduce further fitting parameters. Considering the preparation procedure of the sample the hydraulic conductivity is assumed to be isotropic.

### 5.5.3 Schematisations

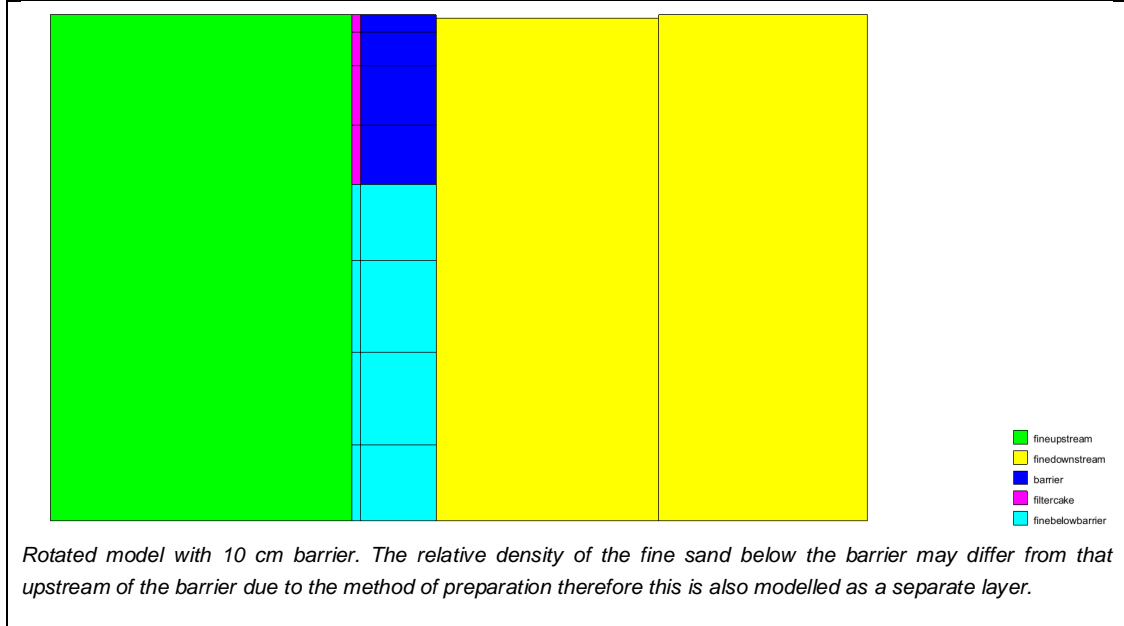
The schematisations (layering, boundary conditions and mesh) for the postdictions are shown in Table 5.1, Table 5.2 and Table 5.3.

Table 5.1 Schematisation of the model with the soil types for final postdictions. Note that the pipe has a finite depth of 2 mm and is modelled as a boundary condition, i.e. the pipe itself is not meshed





Rotated model with 3 cm barrier. The relative density of the fine sand below the barrier may differ from that upstream of the barrier due to the method of preparation therefore this is also modelled as a separate layer



Rotated model with 10 cm barrier. The relative density of the fine sand below the barrier may differ from that upstream of the barrier due to the method of preparation therefore this is also modelled as a separate layer.

Table 5.2 Schematisation of the model with the boundary conditions for final postdictions

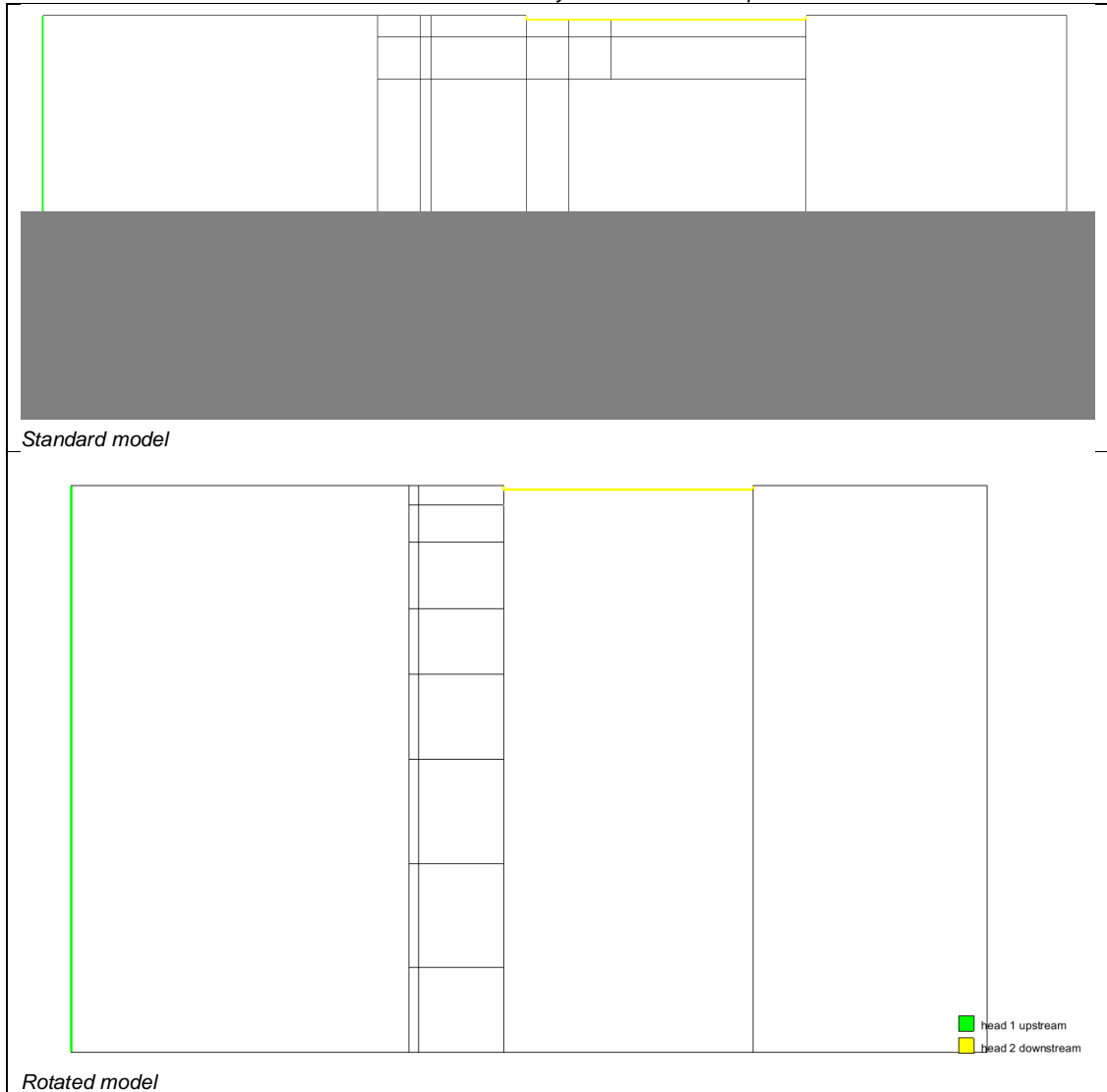
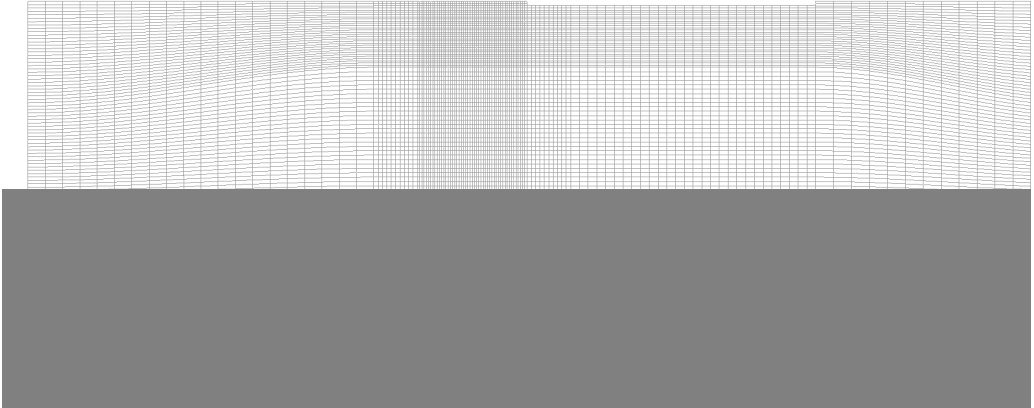
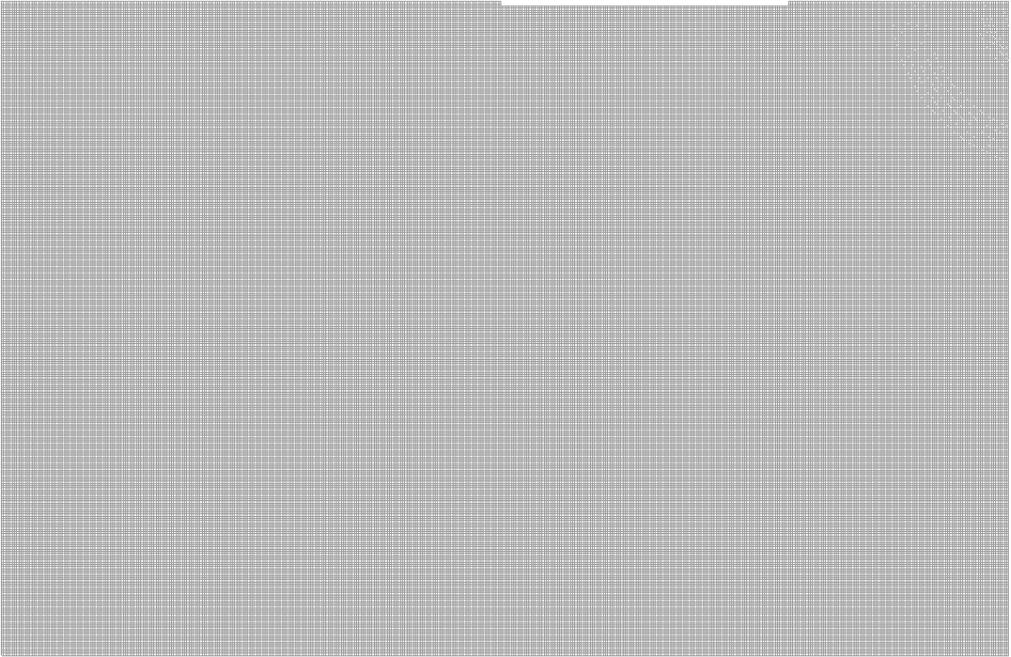


Table 5.3 Schematisation of the model with the mesh for final postdictions


<ul style="list-style-type: none"><li>• Mesh used for postdictions standard model, inside top 3 cm of the barrier elements are 1 mm by 1 mm.</li><li>•</li></ul>

<ul style="list-style-type: none"><li>• Mesh used for postdictions rotated model, uniform mesh with 1 mm by 1 mm elements.</li><li>•</li></ul>

#### 5.5.4 Results

Appendix J shows the results for the postdictions. The tables below give a summary of the fitted model inputs and how they compare to the measured data, and summarize the values of the different possible damage criteria for the different models.

Table 5.4 Overview of the hydraulic conductivity in the model relative to the hydraulic conductivity in the column tests for the sand at the same estimated relative density as the estimated relative density in the experiment

test number	barrier type	background sand type	test specification	Ratio of hydraulic conductivity in model to hydraulic conductivity from column test			
				upstream	downstream	below barrier	barrier
191	GZB 2	Metselzand	basis	1.0	1.0		1.0
192	GZB 2	Metselzand	barrier depth 3 cm	1.2	1.0	1.2	1.0
193	GZB 2	Metselzand	low relative density barrier	2.0	1.0		2.4
195	GZB 2	Baskarp	Baskarp		3.1		0.8
196	GZB 3	Metselzand	Barrier 3 basis	1.0	1.1		1.0
197	GZB 3	Baskarp	Barrier 3 Baskarp		1.4		0.8
198	GZB 2	Metselzand	rotated model barrier depth 3 cm	1.2	1.4	1.4	1.9
199	GZB 2	Metselzand	rotated model barrier depth 10 cm	1.4	0.6	1.4	2.3

Due to uncertainties in both relative density and hydraulic conductivity determination in the column tests, and determination of relative density in the experiments, ratios in the order of 0.8 to 1.2 indicate that the value in the postdiction corresponds well with the value determined in column tests. In particular the hydraulic conductivity of the Metselzand appears to be sensitive to changes in relative density, thus a difference between the relative density in the column test and in the piping test would lead to different hydraulic conductivities. Larger differences may indicate that other processes, such as migration of fines from the barrier or the fine sand, played a role. This is discussed in the evaluation of the postdictions in Section 5.5.4.3.

Table 5.5 Overview of the test and the postdiction results for flux and gradient between H13 and H14

Experiment	upstream head	Flux in test	Gradient H13 to H14 in test	Flux from model	Gradient H13 to H14 from model
	m	cc/min	-	cc/min	-
191	0.404	918	0.74	908	0.65
192	0.408	987	0.74	962	0.61
193	0.550	1186	0.34	1215	0.20
195	0.107	1085	0.85	1120	0.87
196	0.554	1493	0.4	1547	0.42
197	0.032	844	0.38	858	0.34
198	0.266	635	0.57	620	0.48
199	0.283	728	0.63	722	0.47

Table 5.6 Overview of the comparison of test results to postdiction results for flux and gradient between H13 and H14

Experiment	Ratio flux model/ flux test	Ratio gradient model/ gradient test	Ratio gradient model/ gradient test shifted 2 mm closer*	Ratio gradient model/ gradient test shifted 2 mm further*
	-	-	-	-
191	0.99	0.87	1.03	0.77
192	0.97	0.83	0.92	0.76
193	1.03	0.59	0.66	**
195	1.03	1.02	1.20	0.91
196	1.04	1.05	1.29	0.89
197	1.02	0.91	1.13	0.76
198	0.98	0.84	0.97	0.75
199	0.99	0.74	0.86	0.66

\*The location of the barrier is estimated to have an error margin of ca. 2 mm (ca.  $2 \cdot D_{50}$ ) along the length of the barrier. Therefore the gradient between H13 and H14 is calculated for a location shifted 2 mm further upstream from the barrier pipe interface and for a location shifted 2 mm further downstream towards the barrier pipe interface to estimate the error margin resulting from this.

\*\* In this test the barrier was shifted relative to such an extent that H14 would be in the filter cake for this shift, and therefore this would not give an appropriate estimate for the gradient between H14 and H13.

The postdiction results give a relatively good match for the flux of all models, deviations are less than 10%. However the ratio of the gradient in the postdiction to the gradient measured during the test shows larger deviations. Reasons for this are analysed in Section 5.5.4.1 through Section 5.5.4.4. and taken into consideration for the evaluation of the damage criterion in Section 5.5.5.

#### 5.5.4.1 Head in the barrier

In many postdictions the head in H13 close to the downstream interface of the barrier is overpredicted, even with a pipe that has a finite depth. This is probably due to local crumbling of the barrier and due to the fact that continuum modelling is not applicable in this range. Generally, H14 is quite well approximated, as a result of these effects, the gradient between H13 and H14 is typically underestimated in the models. As the different possible damage criteria are all defined starting from 1 cm upstream of the downstream interface of the barrier, this deviation between model and test is considered acceptable provided that the flux, and the head profile at H3, H4, H5 and H15 fit the test data better.

#### 5.5.4.2 Effect of the depth of the pipe on the damage criterion

As discussed in Section 5.5.2, for the postdictions a pipe with a finite depth of 2 mm was modelled. To assess the influence of this on the computed damage criterion, a computation with 0 mm and the same hydraulic conductivities that follow from the postdiction is done for tests 191 in Appendix K.

This analysis shows that the effect of the pipe depth on the flux through the model is negligible. The gradient in the barrier is slightly higher for the model with a 2 mm deep pipe, the difference is in the order of 5-6 % at the locations where the head is fit (H13 and H14) and 4% at the location of the horizontal gradient for the failure criterion, -0.130 to -0.165 mm.

This is in accordance with the results from the sensitivity analysis for the effect of pipe depth in Section 5.4.3 that show a relative difference of 8% between results with 0 mm depth and 2 mm depth at the location of the damage criterion for a hydraulic conductivity contrast of 3% and 1% difference for a hydraulic conductivity contrast of 100.

#### 5.5.4.3 *Effect of the hydraulic conductivity of downstream fine sand*

In the tests where the barrier is present until the bottom of the model and the barrier is not present all the way upstream, the hydraulic conductivity of the fine sand downstream is not altered in the postdiction, as there are no capillaries that would give information to guide this estimate.

In the tests with the Baskarp sand where the barrier goes all the way upstream, only the hydraulic conductivity of the barrier and the downstream sand are fitting parameters, and it was necessary to increase the hydraulic conductivity of the downstream sand in order to model the head distribution. For those experiments the hydraulic conductivity was increased relative to the measurements from the column tests.

For the tests with the rotated model where the barrier has a limited depth, it was also necessary to adapt the hydraulic conductivity of the downstream sand, again raising this above what was measured in the column tests (see Table 5.4). This suggests that possibly in the other models the hydraulic conductivity of the downstream sand may also have been higher. Therefore, for test 191 a check was done what the effect of multiplying the hydraulic conductivity downstream by a factor 0.6 and by a factor 1.4. This is shown in Appendix L. This showed that this has a negligible effect on the flow rate (i.e. this cannot be used to determine the best value for the postdiction), but it can have a significant effect on the gradient in the barrier. In this case the gradient between H13 and H14 was 14% higher for a lower downstream hydraulic conductivity and 6% lower for a higher downstream hydraulic conductivity.

It was also observed that the horizontal failure criterion between -0.130 m and -0.165 m is less sensitive to changes in the value of the downstream hydraulic conductivity than the vertical or the diagonal failure criteria.

#### 5.5.4.4 *Evaluation of the postdictions*

Postdictions in which the hydraulic conductivity had to be adjusted significantly compared to the measured values in column tests suggest that there is some difference between the modelled situation and the experiment.

The formation of the filter cake during the test is one example where a physical process during the experiment altered the hydraulic conductivity in the experiment relative to the situation in the model. This indicates the transport of fine grains due to flow as discussed in Section 4.3.3.

The transport of the finest particles from the fine sand to the barrier, or from the barrier to the pipe, could also locally alter the hydraulic conductivity of the fine sand or the barrier in the experiments, increasing this hydraulic conductivity. Where there are larger deviations between the modelled and measured hydraulic conductivity, the modelled hydraulic conductivity is indeed larger than in the column tests.

Such changes do not necessarily occur uniformly through the model: indeed they are expected to occur more concentrated at the interface of the fine sand and the barrier, and at the interface between the barrier to the pipe. Furthermore, the effect may differ along the vertical dimension of the model, due to convergence of flow and different flow velocities.

Visual observations during the experiments cannot conclusively confirm to what extent these processes did or did not occur during the tests as discussed in Chapter 4.

Table 5.4 in Section 5.5.4 shows that for some tests more adjustment of the hydraulic conductivity in the postdiction was required than for other tests. These postdictions can be

considered less reliable, as the physical processes altering the hydraulic conductivity are uncertain, and we can only check the goodness of fit of the postdiction at a few measured points. Thus, the postdictions of the following tests are considered less reliable:

- 193: this test has a low relative density barrier which is considered to have led to the formation of a filter cake, and possibly depletion of fine particles from the fine sand upstream of the barrier and fine sand from the barrier. Indeed the hydraulic conductivity of the fine sand upstream estimated from the test measurements in Section 4.6.1 is higher than in the column tests and higher than in the other tests with the same upstream sand.
- 195: in this test the downstream hydraulic conductivity of the Baskarp sand had to be increased significantly in order to match the head profile, even after reducing the hydraulic conductivity of the barrier, refer to the factsheet for postdiction 195 in Appendix J for a detailed discussion.
- 198 and 199: in these tests with a partial barrier it was particularly difficult to match the results using hydraulic conductivity values comparable to those in the column tests. The presence of three blocks of fine sand, the barrier and the filter cake, gave five fitting parameters which implies that different combinations (i.e. increasing one and decreasing another) could give similar results. However, in order to reproduce the flux and the head pattern for test 198 all hydraulic conductivities had to be significantly increased. This was also the case for test 199, with the exception of the hydraulic conductivity of the barrier material.

Test 197 with Baskarp sand downstream also required to increase the downstream hydraulic conductivity of the Baskarp sand by a factor 1.4 relative to the column test. However, this modification is smaller than those in the tests above.

Most confidence is therefore placed on the postdictions of tests 191, 192, and 196.

#### 5.5.4.5 Preliminary estimation of error margin

A first attempt is made to estimate the error margin of the fit between the model and the experiment, and thus the error margin for the failure criterion. This is done by estimating values for what are considered to be the main sources of error in the measurements and estimating values for the errors involved in the representation of the test in the model. As the different errors are likely to be independent, these are combined by taking the square root of the sum of squares of the errors. It is emphasised that this is only a first cautious estimate in order to obtain an impression of whether variations between results are significant or within the estimated error margin, i.e. to evaluate the fit between the postdictions and the experiments, and to estimate the bandwidth of the results for the predictions. As not all sources of uncertainty can be quantified, this preliminary estimate is likely to be a lower margin of the actual error margin.

#### Error margin in the measurements

A first estimate of the error in the experimental measurements regards the head that is measured, as reported in Section 4.2.

#### Error margin due to differences between the barrier location in the experiments and in the model

One source of error concerning the representation of the tests in the model regards the extent to which the location of the barrier relative to the capillaries is captured in the model. The

gradient close to the downstream interface of the barrier is steep; therefore results are very sensitive to small shifts of the location of downstream interface of the barrier.

For each test, the location of the barrier at the start of the test is noted, and if the location of the interface between the barrier and the fine sand differs from the location assumed in the model (i.e. -0.120 mm) the locations of capillaries H13, H14 (in the top of the model in the barrier) and H5 (in the bottom of the model in the barrier) are compensated for in the model. However the location of the interface between the barrier and the fine sand may fluctuate slightly along the width of the model due to the preparation. Furthermore, once the pipe has formed, the interface between the barrier and the pipe may change slightly due to crumbling of the edge of the barrier during the experiment. Additionally, the distinction line between barrier and fine sand is not exact. Uncertainty in the location of the barrier in the postdictions relative to the model due to these causes is estimated to be in the order of 2 mm.

Therefore to estimate an error margin for the results of the postdiction due to the uncertainty of the location of the interface between the barrier and the pipe, the gradient between capillaries H13 and H14 is computed from the modelled head distribution as well as the gradients over the same distance shifted 2 mm upstream and downstream in the model. The difference between the gradient between H13 and H14 and the gradient shifted 2 mm upstream or downstream respectively is computed and the average of these is normalised by the gradient between H13 and H14 to give the relative estimated error margin due to barrier location.

#### Error margin due to fitting of hydraulic conductivity

Another source of error concerning the fit between the model and the experiment is the consequence from the assumptions on the hydraulic conductivity in the model. It is assumed that hydraulic conductivity is equal in the horizontal and vertical direction, and that this does not change gradually within the soil layers as discussed in Section 5.5.4.4. This may not be the case, however, the effect of this is difficult to quantify. Therefore that error is currently not included in the error estimation.

However, the effect of varying the downstream hydraulic conductivity is evaluated for one test in Section 5.5.4.3 (Appendix L). Relatively small changes in this value does not appear to have a significant effect on the fit to the flux, which is dominated by the hydraulic conductivity of the upstream sand. The effect on the fit of the overall head profile throughout the models is also small, as there are no measurements downstream to fit the downstream head profile to. However, the effect on the modelled gradient between H13 and H14 is in the order of 10%. Although this was not analysed for all tests, and the effect may be different for the different geometries, as a first approximation of the error margin due to error in the downstream hydraulic conductivity fitting a value of 10% is used at this stage in the analysis. This is likely to underestimate the bandwidth, as the effect of the assumptions on the isotropy and homogeneity of the hydraulic conductivity within the sand layers is not included here.

#### Error margin due to pipe depth

The sensitivity of the computed gradient to the assumption of a pipe depth of 2 mm is addressed in Section 5.5.4.2 and Section 5.4.3. The estimated pipe depth during tests is in the order of 2-3 mm (Section 4.1.2). To account for the error margin due to a pipe depth of 2 mm in the model a margin of 20% on the gradient between H13 and H14 is used based on the difference between the gradient in a model with 2 mm pipe depth and on the one hand 0 mm pipe depth, and on the other hand 4 mm pipe depth.

The table below summarises the error margins which are explicitly considered in this report and the resulting error margin in the fit for the gradient between H13 and H14. This is the

square root of the sum of the errors squared, as the different errors are assumed to be independent. Also shown is the difference between the gradient H13-H14 in the experiment and the modelled gradient between H13 and H14.

Table 5.7 Overview of the estimated error margins for the uncertainty sources and the preliminary estimated total error margin which is considered to apply to the fit of the model in the postdictions. Also shown is the difference between the modelled and measured gradient between H13 and H14. Refer to the text above for the explanation of the uncertainty sources

Test	Estimated error for gradient H13 - H14 due to measurement accuracy in the experiments	Estimated error margin for gradient H13 - H14 due to barrier location	Estimated error margin for gradient H13 - H14 due to hydraulic conductivity of downstream sand	Estimated error margin for gradient H13 - H14 due pipe depth assumption	Preliminary estimated error margin in fit of gradient H13 - H14		Difference between modelled gradient and measured gradient from H13 - H14	
	relative	relative	relative	relative	absolute	relative	absolute	relative
191	9%	15%	10%	20%	0.18	28%	0.09	14%
192	9%	10%	10%	20%	0.16	26%	0.13	20%
193	28%	15%	10%	20%	0.08	39%	0.14	68%
195	7%	14%	10%	20%	0.24	27%	0.02	2%
196	14%	19%	10%	20%	0.14	33%	0.02	4%
197	17%	21%	10%	20%	0.12	35%	0.04	10%
198	12%	13%	10%	20%	0.14	28%	0.09	19%
199	12%	13%	10%	20%	0.13	29%	0.16	34%

The difference between the modelled gradient and the experimentally measured gradient is within the estimated error margin for tests 191, 192, 195, 196, 197, and 198. Experiments 193 and 199 fall beyond the range. However, as noted before the estimated error margin does not include uncertainties which could not be quantified and may therefore underestimate the actual error margin. Furthermore, as noted in Section 5.5.4.4, postdictions in which the hydraulic conductivity differs significantly from that measured in column tests are already considered less reliable. This is the case for postdictions of tests 193 and 199, but also for tests 195, 198 and 197 which do fall within the error margin.

In the evaluation of the damage criterion and for the postdictions is it more practical to use one error margin. The average estimated error margin for the postdictions above is 31%, and the standard deviation is 4%, thus in the subsequent paragraphs a preliminary estimated error margin of 35% is used as an estimate of the error margin in the failure criterion. This preliminary estimate is only for the purpose of indicating a bandwidth of the current results and postdictions, and should be improved on in further stages of the project.

The error sources that cannot be explicitly quantified or estimated are not dealt with in this estimate. The main source of this may be the uncertainty in the definition of the damage condition. As described in Section 4.7 the observation of a pipe entering the barrier is used as a failure criterion. This is to some extent dependent on the observer. As the same observer was present in all tests the error due to this could be considered to be limited, however, it was noted that the distinction between failure and crumbling of the barrier was more difficult to

make in some tests than in others. Another error source that is difficult to quantify is the variation in relative density among experiments, as noted in Section 4.7.

#### 5.5.5 Evaluation of the damage criterion

To characterise the variation of different damage criteria in the postdictions, Table 5.8 summarises the 5 tests with the same barrier at the same relative density (GZB2 high relative density).

Table 5.8 Summary of postdictions and statistics for postdictions of tests with coarse sand barrier GZB2 at a high relative density

test	background sand type	test description	horizontal gradient from -0.13 to -0.165 m at surface	vertical gradient from surface to -0.03 m at -0.130 m	diagonal gradient between (-0.13,0) m and (-0.165,-0.03) m	average horizontal velocity between -0.130 and -0.165 m at surface	average vertical velocity between surface and -0.03 m at 0.130m	average diagonal velocity between (-0.13,0) and (-0.165,-0.03)
						cm/min	cm/min	cm/min
191	Metselzand	basis	0.46	0.29	0.40	5.3	3.4	4.6
192	Metselzand	barrier depth 3 cm	0.52	0.24	0.62	6.1	2.8	7.2
195	Baskarp	Baskarp sand, barrier to upstream side of model	0.63	0.24	0.45	6.7	2.6	4.8
198	Metselzand	rotated model barrier depth 3 cm	0.36	0.18	0.34	8.58	4.34	8.10
199	Metselzand	rotated model barrier depth 10 cm	0.41	0.42	0.40	12.18	12.35	11.63
average			0.48	0.28	0.44	7.77	5.09	7.25
standard deviation			0.09	0.08	0.09	2.46	3.68	2.58
CoV*			0.20	0.29	0.22	0.32	0.72	0.36

\* Coefficient of variation, (standard deviation/average)

The horizontal gradient has the smallest CoV, and therefore appears to be the most suitable damage criterion. The standard deviation in the horizontal gradient is substantially lower than the preliminary estimated error margin, which is estimated in Section 5.5.4.5.

It is noted in Section 5.5.4.4 that the postdictions for tests 193, 198 and 199 are less reliable as these required considerably different hydraulic conductivities for one or more of the soils than would be expected. This is also the case for tests 195 and 197. The bar charts below are used in order to give an overview of the variation in the different criteria for all tests. The preliminary estimated error margin is also shown, although this was estimated only for the horizontal gradient (Section 5.5.4.5), the same relative error margin is used as a first assumption for the other criteria. The expectation is that the error margin for diagonal and horizontal gradients will be larger as there is less data to fit the model to, however, due to this lack of data the size of this error margin is difficult to quantify.

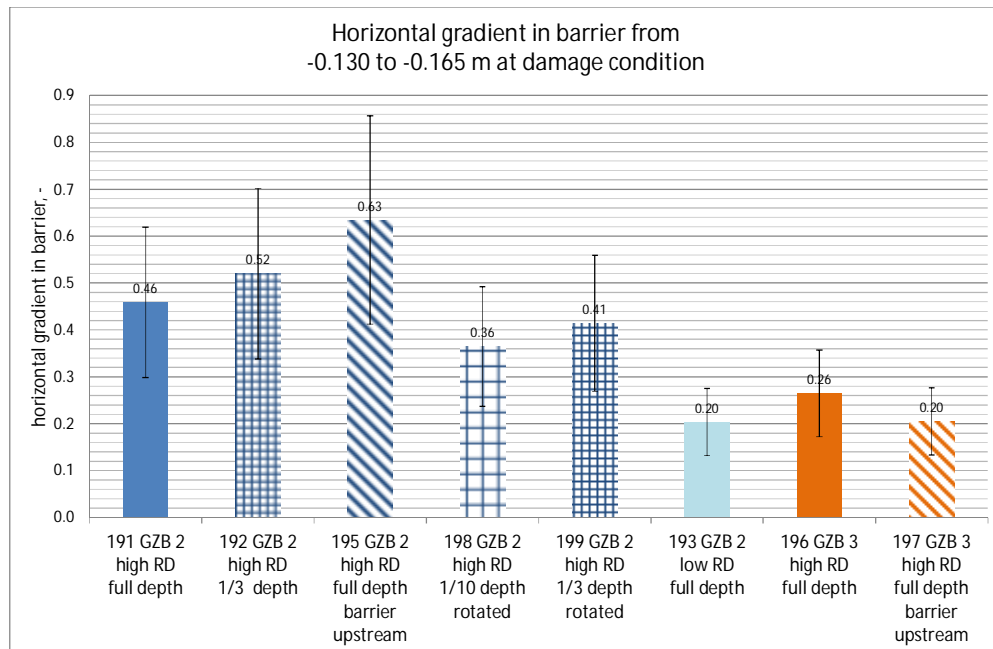


Figure 5.18 Horizontal gradient between -0.130 m and -0.165 m at depth 0 m in the model. Colours indicate type of barrier: GZB2 high relative density = dark blue, GZB2 at low relative density = light blue, GZB3 at high relative density=orange. Texture indicates test specifics: slope = barrier to upstream end of model, large squares = barrier 1/10<sup>th</sup> depth of model, small squares = barrier 1/3<sup>rd</sup> depth of model. Error bars represent the estimated error margin for the horizontal gradient

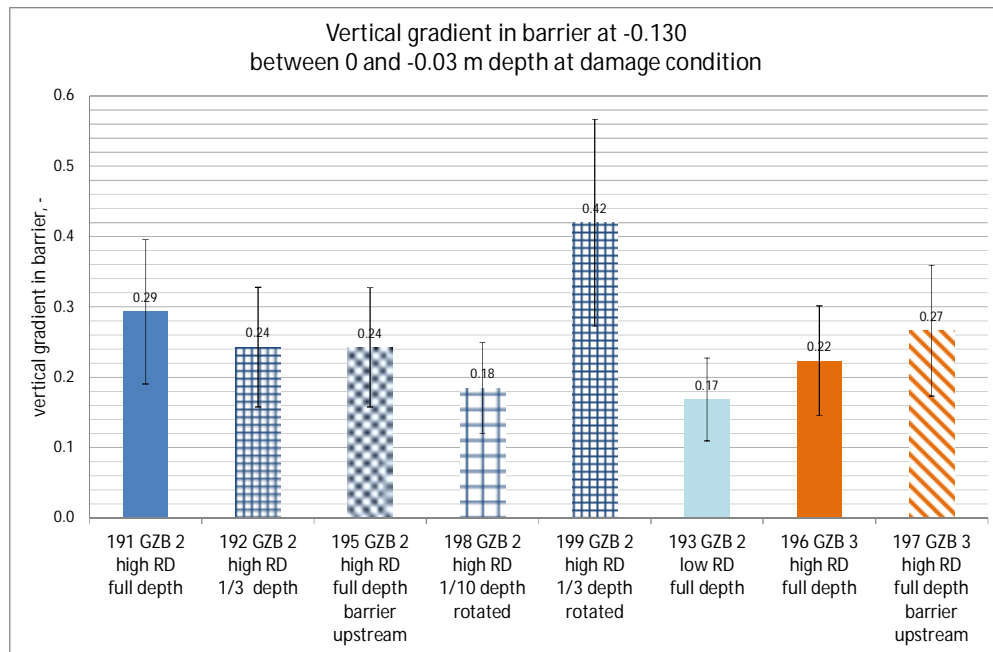


Figure 5.19 Vertical gradient between depth 0 m and depth 0.03 m at horizontal location -0.130 m in the model. Colours indicate type of barrier: GZB2 high relative density = dark blue, GZB2 at low relative density = light blue, GZB3 at high relative density=orange. Texture indicates test specifics: slope = barrier to upstream end of model, large squares = barrier 1/10<sup>th</sup> depth of model, small squares = barrier 1/3<sup>rd</sup> depth of model. Error bars represent the estimated error margin for the horizontal gradient

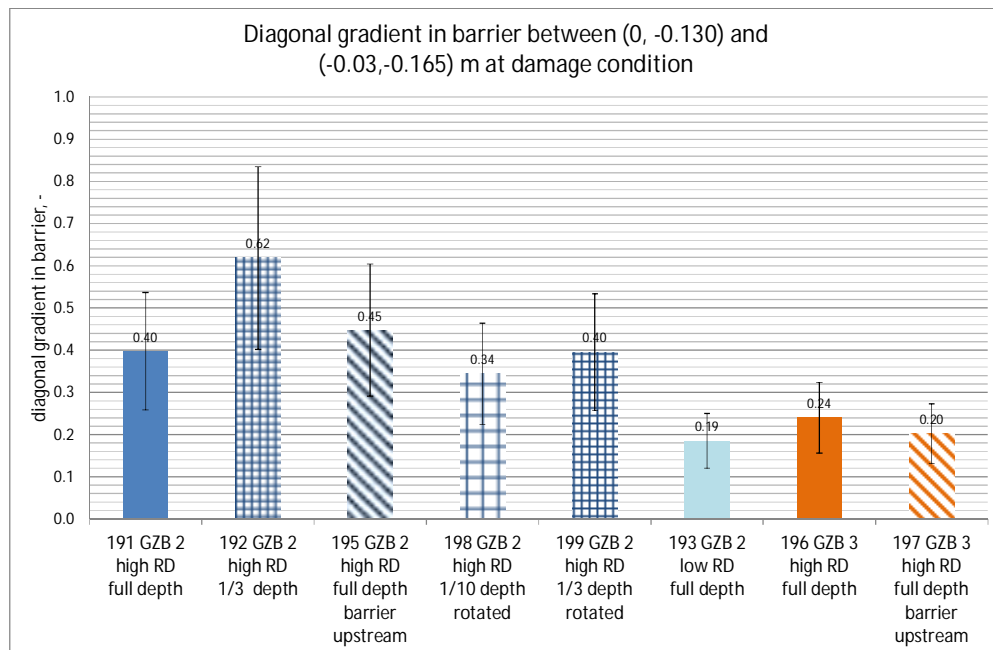


Figure 5.20 Diagonal gradient barrier between (0, -0.130) and (-0.03,-0.165) m in the model. Colours indicate type of barrier: GZB2 high relative density = dark blue, GZB2 at low relative density = light blue, GZB3 at high relative density=orange. Texture indicates test specifics: slope = barrier to upstream end of model, large squares = barrier 1/10<sup>th</sup> depth of model, small squares = barrier 1/3<sup>rd</sup> depth of model. Error bars represent the estimated error margin for the horizontal gradient

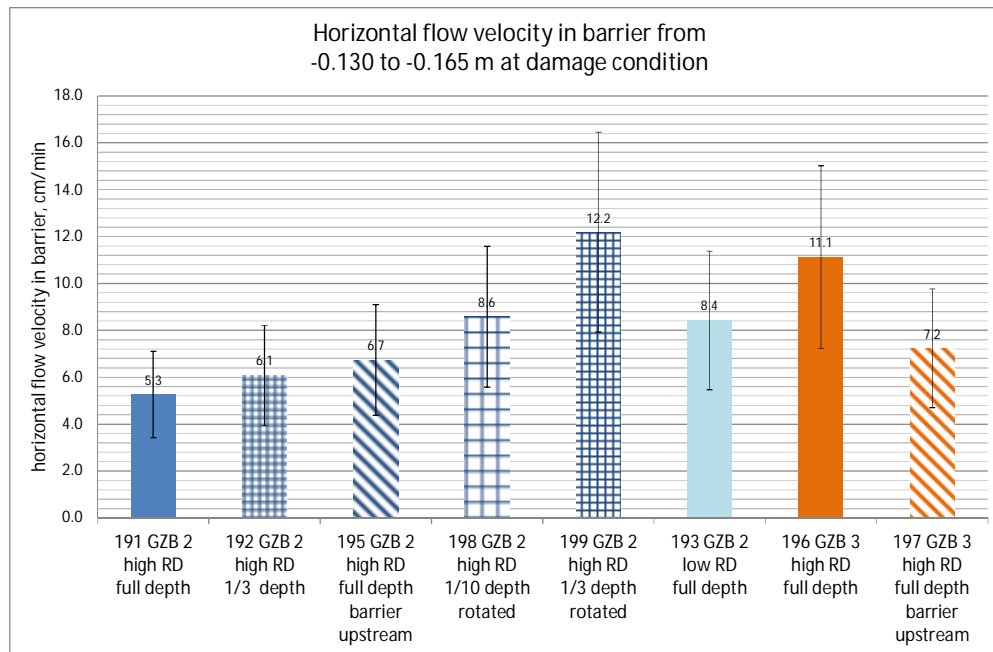


Figure 5.21 Horizontal flow velocity between -0.130 m and -0.165 m at depth 0 m in the model. Colours indicate type of barrier: GZB2 high relative density = dark blue, GZB2 at low relative density = light blue, GZB3 at high relative density=orange. Texture indicates test specifics: slope = barrier to upstream end of model, large squares = barrier 1/10<sup>th</sup> depth of model, small squares = barrier 1/3<sup>rd</sup> depth of model. Error bars represent the estimated error margin for the horizontal gradient

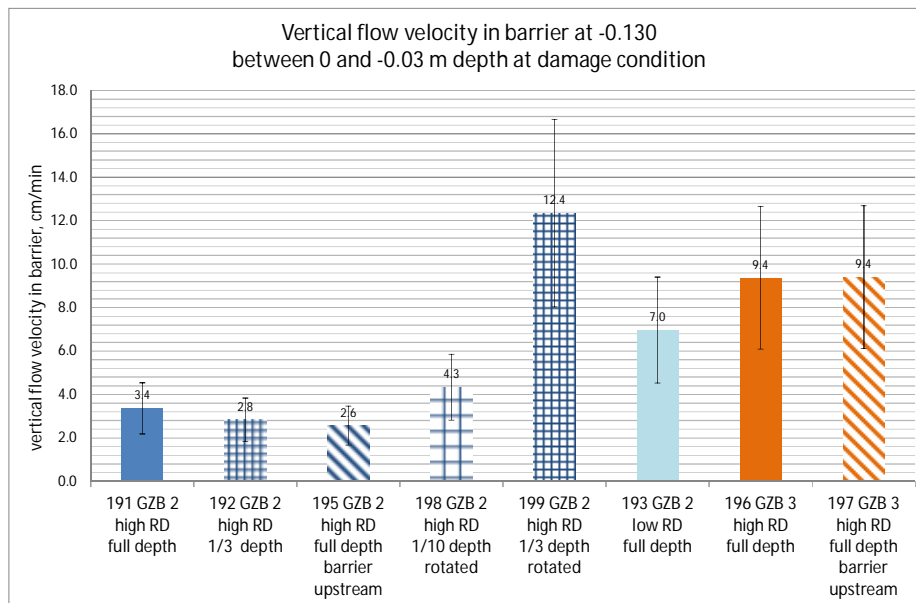


Figure 5.22 Vertical flow velocity between depth 0 m and depth 0.03 m at horizontal location -0.130 m in the model. Colours indicate type of barrier: GZB2 high relative density = dark blue, GZB2 at low relative density = light blue, GZB3 at high relative density=orange. Texture indicates test specifics: slope = barrier to upstream end of model, large squares = barrier 1/10<sup>th</sup> depth of model, small squares = barrier 1/3<sup>rd</sup> depth of model. Error bars represent the estimated error margin for the horizontal gradient

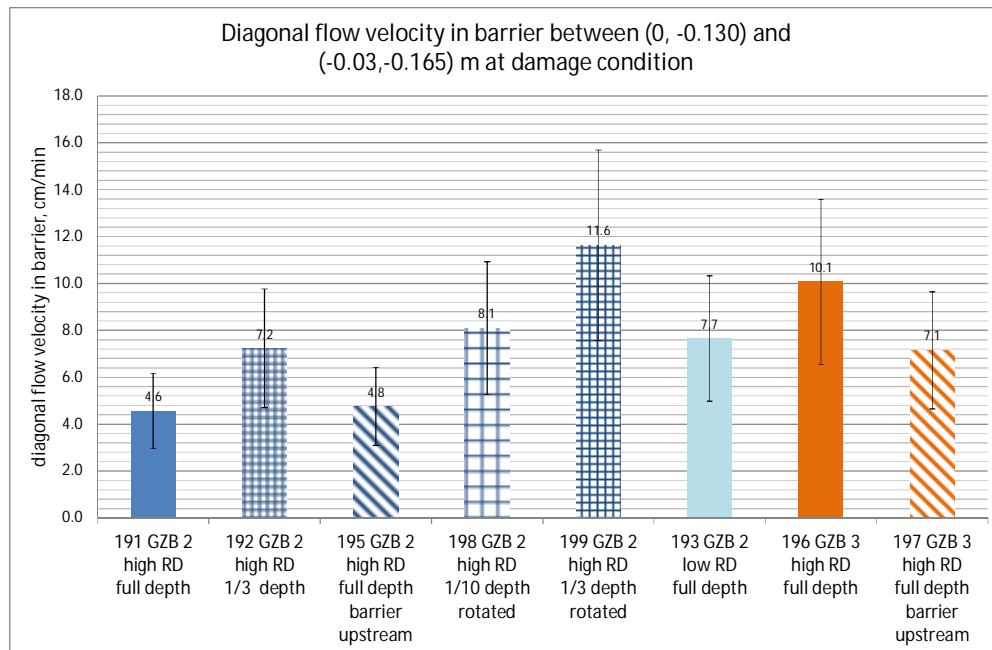


Figure 5.23 Diagonal flow velocity barrier between (0, -0.130) and (-0.03,-0.165) m in the model. Colours indicate type of barrier: GZB2 high relative density = dark blue, GZB2 at low relative density = light blue, GZB3 at high relative density=orange. Texture indicates test specifics: slope = barrier to upstream end of model, large squares = barrier 1/10<sup>th</sup> depth of model, small squares = barrier 1/3<sup>rd</sup> depth of model. Error bars represent the estimated error margin for the horizontal gradient

These figures support the selection of the horizontal gradient as the damage criterion for the barrier materials. This also has the practical advantage that gradients at the top of the model can be easily measured in the small-scale or medium-scale tests, whereas results for gradients over depth (vertical or diagonal) are not directly accessible for verification. Thus, the error margin for the latter can be considered higher than for the horizontal gradients.

Computationally it is also preferable to select the horizontal gradient, as opposed to the vertical or the diagonal gradient as a damage criterion. For predictions of the Delta Flume tests, and for future field scale predictions, models with an unstructured mesh are used. In these models there is limited control over the exact location of nodes within the mesh. As the surface of the model is always defined, there will always be nodes exactly at the surface, whereas this is not the case for locations at depth in the model.

Thus based on the results from experiments, postdictions and based on practical considerations, the gradient between -0.130 m and -0.165 m is considered the optimal damage criterion in this phase of the project. This is referred to as the preliminary damage criterion as this may be altered based on new insights into the effect of scale in later tests. Indeed as shown in Section 5.6 it is to be expected that a damage criterion should be defined over a larger distance to be suitable for larger scale tests and the field situation.

For the three groups of barrier material the failure criterion is shown in the table below. The preliminary estimated error margin on the fit between the model and the test is also used as the preliminary estimated margin for the failure criterion in this phase of the project.

Table 5.9 Preliminary damage criteria for barrier based on postdiction of experiments

Barrier type	Preliminary damage criterion, horizontal gradient between -0.130 and -0.165 m	Preliminary estimated error margin*	Comments
	-	%	
GZB 2 high relative density	0.48	35	Based on 5 tests (of which 3 are considered less reliable). Damage criterion based on the 2 more reliable tests would be 0.49)
GZB 2 low relative density	0.20	35	Based on 1 test with unreliable postdiction model
GZB 3 high relative density	0.23	35	Based on 2 tests (of which 1 is considered less reliable)

\* preliminary estimated error in the fit of the postdictions based on estimated: measurement error, error margin due to barrier location, error margin due to hydraulic conductivity of the downstream fine sand; and error margin due to pipe depth assumption. This estimate does not include all sources of uncertainty and is only based on an estimate of the error margins for underlying uncertainties and therefore considered as a preliminary estimate which is likely to be a lower limit for the actual uncertainty.

Applying these criteria to the postdictions of the experiments we can calculate the predicted damage head for these tests. **Error! Reference source not found.** shows that the experimental tests are always within the range of the modelled values. These all fall within the range of the preliminary estimated error margin.

Table 5.10 Predicted damage head using damage criteria

Test	Preliminary damage criterion	Damage head predicted in test with preliminary damage criterion	Damage head predicted with preliminary damage criterion (estimated upper limit/estimated lower limit)
		m	m
191	0.48	0.40	0.42 (0.57 – 0.27)
192	0.48	0.41	0.38 (0.51 – 0.24)
193	0.20	0.55	0.54 (0.73 - 0.35)
195	0.48	0.11	0.08 (0.11 – 0.05)
196	0.23	0.55	0.48 (0.65 – 0.31)
197	0.23	0.03	0.04 (0.05 – 0.02)
198	0.48	0.27	0.35 (0.47 – 0.23)
199	0.48	0.28	0.33 (0.44 – 0.21)

## 5.6

### 5.7 Predictions

Predictions for the medium-scale and for the Delta Flume tests are described in this Chapter. The failure criterion for the small-scale tests is defined as the gradient between -0.130 to -0.165 m, where the barrier pipe interface is at -0.120 m.

The preliminary estimated error margin on the fit of the predictions is currently used as the preliminary estimated error margin on the failure criterion. Note that this is only a first estimate in order to obtain an impression of the expected error margin in the fit of the predictions. The actual error margin for the damage criterion may be larger as sources of uncertainty which could not readily be quantified are not included in the preliminary estimated error margin, as discussed in Section 5.5.4.5.

It is shown in Section 5.4.3 that the depth of the pipe in the model has a significant effect on the gradient in the barrier in the small-scale model. The effect, however, is much larger on the gradient between H13-H14 than on the location where the damage criterion is defined (-0.130 to -0.165 m). For the situation of the medium-scale or Delta Flume tests, the depth that the pipe will have in the model is uncertain. Furthermore, it is computationally more expensive to give the pipe a finite depth and therefore refine the mesh in the area where the pipe is present. Therefore, a model with 0 mm pipe depth is used, and the computed damage criterion gradient in the barrier is reduced or increased compensate for the depth effect of the pipe. This is done by applying the effect of pipe depth that was found in the sensitivity analyses of the small-scale model in Section 5.4.3. The implicit assumption is that the effect will be the same in the predictions as it was in the small-scale model, however, this is likely to be affected by configuration and thus this is considered a preliminary estimate of the effect of pipe depth on the predictions. This is only intended to give an impression of the band width of the results, and can be improved on in subsequent phases of the project.

The configurations of the barrier and the hydraulic conductivity combinations are not finalised yet, and in the next phases these will be decided on. These predictions are for the configurations which are foreseen at this phase in the project.

#### 5.7.1 Medium-scale tests

The objective of the predictions of the medium-scale tests is to predict the upstream head value that will result in damage of the barrier. In order to do this, the experiments are modelled with a given head drop. For this head drop the gradient in the barrier at the location of the failure criterion is determined.

This gradient is compared to the damage criterion for the barrier as derived in Section 5.5.5 to determine the upstream head at the damage condition, i.e. the head drop that will yield a gradient that is equal to the damage criterion.

##### 5.7.1.1 Model

The set-up for the medium-scale tests is approximately 4 times as large as for the small-scale tests, a top view is shown in Appendix M. The depth of the model is 0.403 m.

Predictions are conducted using 2D models, assuming that the pipe has widened along the entire barrier. In the model the centre of the outflow hole is at coordinates (0,0) and the barrier is located from -0.387 m to -0.687 m (i.e. 30 cm wide). This is shown below in Figure 5.24. The barrier is 30 cm wide in order to be able to also study the progression of the pipe through the barrier and thereby investigate the remaining strength after the pipe damages the barrier.

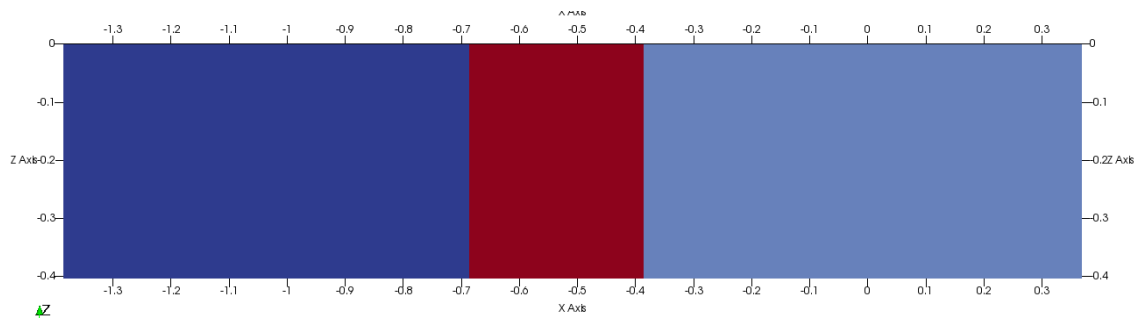


Figure 5.24 Medium-scale model with 30 cm wide barrier (red). Upstream fine sand (dark blue) has a higher relative density, and thus a lower hydraulic conductivity than downstream fine sand

The pipe is modelled with 0 mm depth as a boundary condition as described in Section 5.2.1. The other boundary conditions are as in the models for the small-scale tests. It is shown in Section 5.4.3 that using a model with a deeper pipe in the small-scale models, can yield a higher or a lower value of the local horizontal gradient in the barrier depending on the depth and hydraulic conductivity contrast. The actual depth that the pipe will have in the medium-scale tests is not known, but this is expected to be in the range between 1 and 10 mm. To estimate the effect of this uncertainty on the gradient in the barrier at the location of the damage criterion, the gradient that is obtained from the medium-scale model over that distance is scaled by 1.1 and 0.91 (the maximum and minimum difference between a pipe with 0 mm depth and 10 mm depth for hydraulic conductivity contrasts of 3 and 100 for the small-scale models analysed in Section 5.4.3).

The structured mesh for the medium-scale tests is locally refined at the top of the barrier. There elements are 1 mm by 1 mm as in the models for the small-scale tests. The model and the mesh are shown in Figure 5.25.

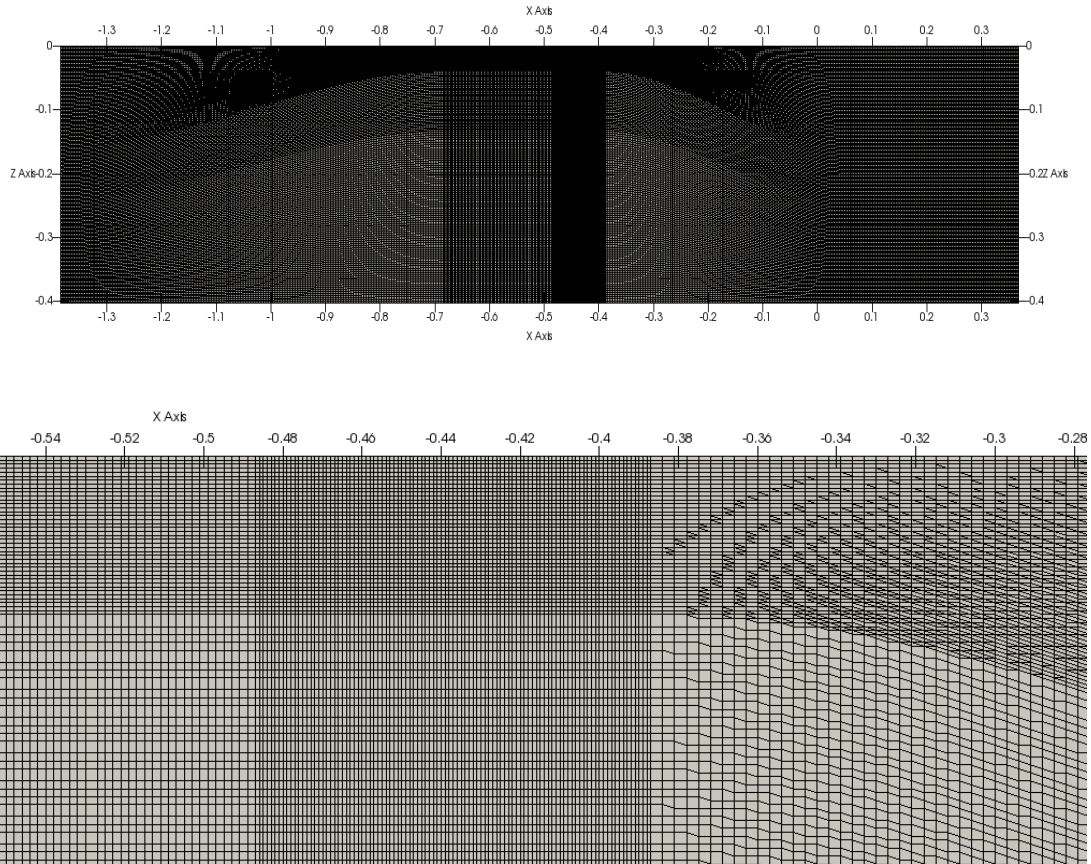


Figure 5.25 Medium-scale model with mesh, local refinement in the barrier. Top total model, bottom close up in barrier at downstream end

### 5.7.1.2 Test programme

The test programme for the medium-scale tests (MSPs) is currently being decided on. Predictions are made for some experiments which are foreseen, however, the actual programme may differ from the cases computed here. The table below shows the test set-up and the hydraulic conductivities for the 6 MSP tests as they are currently foreseen.

Table 5.11 Overview of models for predictions of medium-scale tests. Note this is a preliminary programme the final programme is still being decided on

Test nr	Fine sand upstream hydraulic conductivity m/s	Barrier Name/ hydraulic conductivity m/s	Fine sand downstream hydraulic conductivity m/s	Width barrier m	Depth barrier m	Variation
MSP 1	2.9e-4	GZB2 2.1e-3	5.6e-4	0.3	0.403	Basis
MSP 2	1.15e-4	GZB2 2.1e-3	2.2e-4	0.3	0.403	Lower hydraulic conductivity fine sand
MSP 3	2.9e-4	GZB2 2.1e-3	5.6e-4	0.2	0.403	Less wide barrier
MSP 4	2.9e-4	GZB2 low relative density 2.9e-3	6.5e-4	0.3	0.403	Low relative density barrier
MSP 5	2.9e-4	GZB1 2.1e-3	5.6e-4	0.3	0.403	Barrier stronger
MSP 6	1.15e-4	GZB1 2.1e-3	5.6e-4	0.3	0.403	Barrier stronger and lower hydraulic conductivity fine sand

5.7.1.3 *Damage criterion and damage head drop*

The models yield the head distribution in the barrier, and thus the gradient in the barrier. An example for MSP 1 and MSP 3 with different barrier widths is shown below in Figure 5.26.

.

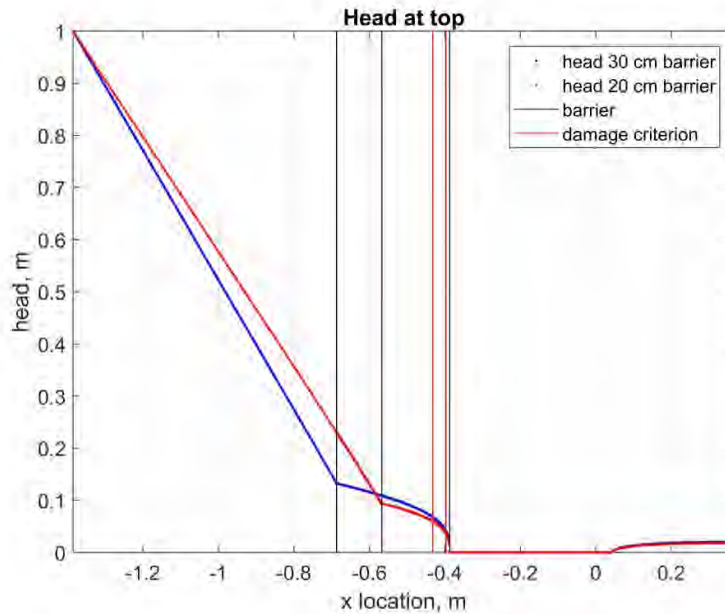


Figure 5.26 Head distribution in medium-scale prediction for barrier of 30 cm wide (MSP 1) and 20 cm wide (MSP 3). The gradient at the location of the damage criterion (indicated by red lines) is highest in the model with the 30 cm wide barrier. This therefore gives the lowest strength

The gradient in the model at the location of the damage criterion (i.e. between 1 cm upstream of the downstream barrier interface and 4.5 cm upstream of this interface) is compared to the damage criterion derived in Section 5.5.5 in order to find the head drop where the damage criterion is fulfilled. This is the predicted head drop.

As it is shown that the assumption of a 0 mm deep pipe can give an underestimation or an overestimation of the damage criterion, depending on the actual pipe depth and the hydraulic conductivity contrast, the damage head drop is adjusted to show the maximal effects of this as described in Section 5.7.1.1. That analysis was done for the small-scale model, and in the current phase it is assumed that the effects are representative for the medium-scale model, i.e. that the relative effect of pipe depth on the gradient is the same in the small-scale and the medium-scale models that may be different. This is another source of uncertainty which is not readily quantified and therefore the actual uncertainty can be higher and this should be investigated further in the next phases of the project.

Due to the size of the preliminary estimated error margin of 35% on the damage criterion there will also be a large error margin on the predicted head drop. This error margin is further increased to account for the uncertainty in the depth of the pipe in the experiment. As both the preliminary estimated error of the damage criterion, and the error margin for the effect of pipe depth on the medium-scale tests is an estimate that does not include quantified sources of error, this error margin is probably a lower estimate of the actual uncertainty margin.

The table below shows the predicted head drop for the models, and the estimated error margin range due to the estimated error margin in the damage criterion, as well as the damage head drops that would correspond to a pipe with depth 10 mm for hydraulic conductivity contrasts of 3 and 100 based on the results in appendix H. For the stronger barrier GZB1, a damage criterion of 0.68 is used, with the same preliminary estimated error of

35%. Note that the value of this damage criterion is not based on the current small-scale tests, as there was no failure of the barrier during those tests. The damage criterion used is only intended to give an indication of the effect of a stronger barrier on the damage head drop. It remains to be investigated what the strength of a stronger barrier is.

Table 5.12 Results for damage head drop from predictions for medium-scale tests

Model	Damage head drop for 0 mm pipe depth in model, m	Maximum damage head drop compensating for estimated error margin due to pipe depth*, m	Minimum damage head drop compensating for estimated error margin due to pipe depth **, m	Upper limit damage head drop based on preliminary estimated 35% error margin***, m	Lower limit damage head drop based on preliminary estimated 35% error margin***, m
MSP 1	0.63	0.69	0.56	0.93	0.37
MSP 2	1.03	1.13	0.93	1.52	0.60
MSP 3	0.71	0.78	0.64	1.05	0.42
MSP 4	0.78	0.86	0.70	1.15	0.46
MSP 5	0.89	0.97	0.80	1.31	0.52
MSP 6	1.45	1.60	1.31	2.16	0.85

\* For a hydraulic conductivity contrast of 100 the local gradient at the damage criterion location is 0.91 times as high in a model with pipe depth 10 mm compared to a model with pipe depth 0 mm.

\*\* For a hydraulic conductivity contrast of 3 the local gradient at the damage criterion location is 1.11 times as high in a model with pipe depth 6 mm compared to a model with pipe depth 0 mm.

\*\*\* includes uncertainty due to pipe depth, the 35% preliminary estimated error margin is estimated for the fit of the postdictions to the experiments, this used as a preliminary estimate of the error margin for the damage criterion and therefore these results are only intended to provide an estimated bandwidth for the results of the predictions.

This gives the estimated band width for the damage head drops based on preliminary estimates of error margins on the postdictions and the effect of pipe depth. As noted these are only first estimates in order to give an indication and are subject to further refinement in the subsequent phases of the project. Note furthermore, that this is the head drop where the pipe enters the barrier, thus failure will require a higher head drop. Furthermore, any losses over the upstream filter or sand boil are not included here. Thus, the experimental facilities will have to enable a significantly higher head drop over the sample.

5.7.2 Delta Flume tests

The objective of the predictions for the Delta Flume tests is to predict the upstream head that will result in damage of the barrier, in the same way as this is done in the predictions for the medium-scale tests in Section 5.7.1.

5.7.2.1 Model

The set-up for the Delta Flume tests is shown in Appendix N. There is a seepage length of approximately 15 m.

Predictions are conducted using a 2D model, assuming that the pipe has widened along the entire length of the barrier. In the model the centre of the outflow opening is at coordinates (0,0) and the barrier is located from -3.75 m to -4.05 m (30 cm wide). The barrier is 0.5 m deep, and the hydraulic conductivity contrast is a factor 5. The model is shown below.



Figure 5.27 Model of the Delta Flume tests used for the prediction of the damage head

The pipe is modelled with 0 depth as a constant head boundary condition. A constant head is applied to the upstream horizontal interface between -15 and -22.5 m as shown. Other boundaries are closed as shown in Figure 5.28.



Figure 5.28 Boundary conditions used in the model of the Delta Flume tests

The unstructured mesh has base elements of 3 cm size and in the barrier elements are refined to 0.3 cm. An unstructured mesh is chosen due to the geometry of the experiments. A mesh analysis was done in which the following combinations of base element size and element size in the mesh were used:

Table 5.13 Overview of meshes used in mesh analysis for Delta Flume model

Model name	Base element size mm	Barrier element size mm
Deltagoot	100	10
Deltagoot 2	50	5
Deltagoot 2e	30	5
Deltagoot 2f	30	3

Figure 5.29 shows that a finer mesh leads to a higher computed gradient in the barrier, and in particular on the downstream interface between the barrier and the pipe.

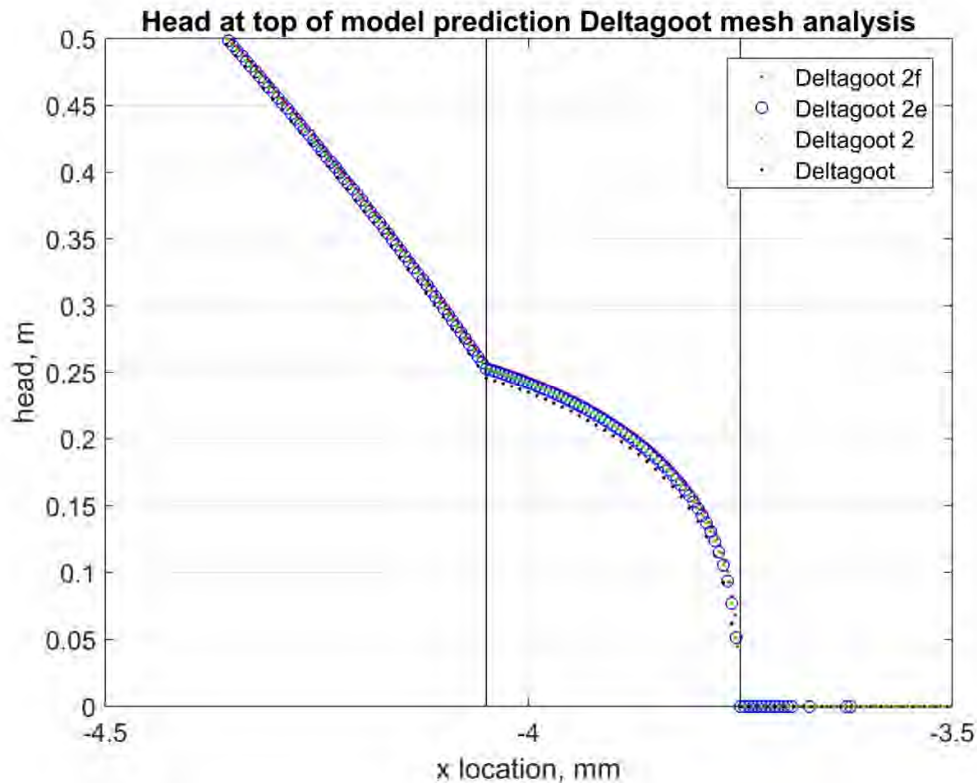


Figure 5.29 Results from mesh refinement analysis for Delta Flume

#### 5.7.2.2 Test programme

Two identical tests will be done. The hydraulic conductivity of the fine sand is  $5.6e-4$  m/s and the hydraulic conductivity of the barrier is  $2.75 e-3$  m/s.

#### 5.7.2.3 Damage criterion and damage head drop

The damage criterion is defined from 1 cm upstream of the interface between the barrier and the pipe to 4.5 cm upstream of this interface. This would be from -3.76 to -3.795 m in the model. However, the mesh does not have nodes at exactly these locations. Therefore the gradient between -3.759 and -3.795 is taken as well as the gradient between -3.762 and -3.798 m. The average value of these two is used.

As for the medium-scale models, the local gradient is adjusted for the effect of pipe depth as analysed for the small-scale models, this can increase or reduce the local gradient (as explained in Section 5.7.1.3). The effect of the preliminary estimated error margin of the fit of the postdictions is used as a preliminary estimate of the error margin of the preliminary damage criterion in order to provide a first estimate of the range of damage head drops. This is therefore only a preliminary estimate. The results are shown below using the damage criterion of GZB2.

Table 5.14 Results for damage head drop from predictions for Delta Flume tests

Damage head drop for 0 mm pipe depth in model, m	Maximum damage head drop compensating for estimated error margin due to pipe depth*, m	Minimum damage head drop compensating for estimated error margin due to pipe depth **, m	Upper limit damage head drop based on preliminary estimated 35% error margin***, m	Lower limit damage head drop based on preliminary estimated 35% error margin***, m
1.7	1.8	1.5	2.5	1.0

\* For a hydraulic conductivity contrast of 100 the local gradient at the damage criterion location is 0.91 times as high in a model with pipe depth 10 mm compared to a model with pipe depth 0 mm.

\*\* For a hydraulic conductivity contrast of 3 the local gradient at the damage criterion location is 1.11 times as high in a model with pipe depth 6 mm compared to a model with pipe depth 0 mm.

\*\*\* includes uncertainty due to pipe depth, the 35% preliminary estimated error margin is estimated for the fit of the postdictions to the experiments, this used as a preliminary estimate of the error margin for the damage criterion and therefore these results are only intended to provide an estimated bandwidth for the results of the predictions.

The maximum head drop that can be applied is 6 m. The estimate of the damage head drop is 1.7 m with a preliminary estimated range of 1.0 m to 2.5 m. The results therefore indicate that the facilities are sufficient to cause the pipe to enter the barrier. However the predicted damage head drop is relatively low.

When the Sellmeijer rule (Förster et al., 2012) is used for this configuration, this yields a critical head drop of 1.86 m. The low predicted strength is due to the significant scale effects, and possibly also due to limitations in the small-scale tests as discussed in Chapter 7. However it is also important to consider that the damage criterion reflects the point at which the pipe first enters the barrier. The tests show that there is a significant remaining strength after the pipe has progressed through the barrier.

## 5.8 Small-scale tests with the Sellmeijer model

Predictions were made for the small-scale experiments using the Sellmeijer model in DgFlow. The kernel was adapted in order to be able to compute the progression of the pipe for the configuration of the coarse sand barrier, with horizontal variation in the sand types. These computations are reported in detail Appendix O. In the current Section a selection of the results is shown in Section 5.7.1 and analysed in Section 5.7.2.

### 5.8.1 Summary of Results

In this section a comparison is made between the results from the computations using the Sellmeijer model and the experiments. Also the effect of the  $D_{70}$  and hydraulic conductivity of the barrier on the results is analysed. These computations with the Sellmeijer model were made with preliminary estimates of the hydraulic conductivities and  $D_{70}$  values of the sands. Therefore these values can differ from the values found in the actual experiments and from the values used in the postdictions of the tests.

The preliminary estimate of the  $D_{70}$  of GZB3 is significantly larger than the  $D_{70}$  of the actual GZB3 used in the experiments (1.85 mm in the computation versus 1.24 mm in the experiment), therefore this computations are not compared to the experiment, they are used to analyse the combined effect of  $D_{70}$  and hydraulic conductivity on the predictions of the Sellmeijer model. The  $D_{70}$  of GZB2 in the computation is similar to that of the barrier used in the experiments (1.29 mm versus 1.20 mm).

Therefore this section shows the results from the Sellmeijer model for tests with GZB2 (tests 191, 192, 193, and 195) as compared to experimental results in Table 5.15. The results from computations for tests with GZB3 (196 and 197) are compared to results from computations

with the same set-up with GZB2 (191 and 195) in Table 5.16. Tests 198 and 199 were not simulated since these tests have a different geometry and this would require a different mesh.

Table 5.15 Comparison of results from DgFlow computation with the Sellmeijer model and experimental results

Experiment number	Experimental measurements		Sellmeijer model				Head drop in experiment/head drop in model	
	Head drop over sand body at damage condition, m	Head drop over sand body when pipe breaks through barrier, m	Head drop over sand body at damage condition, m	Height of the pipe at the interface between the barrier and the pipe at damage condition, m	Head drop over sand body when pipe breaks through barrier, m	Height of the pipe at the interface between the barrier and the pipe when the pipe breaks through the barrier, m	At damage condition	When pipe breaks through barrier
191	0.40	1.02	0.13	0.41	0.50	1.16	3.1	2.0
192	0.41	0.74	0.13	0.41	0.50	1.16	3.2	1.5
193	0.55	1.05	0.13	0.52	0.37	1.31	4.2	2.8
195*	0.11	0.12	0.10	0.26	0.14	1.09	1.1	0.9

Table 5.16 Sellmeijer computations showing the combined effect of  $D_{70}$  and hydraulic conductivity on the results from the Sellmeijer model

Experiment number	$D_{70}$ in model*	Hydraulic conductivity of the barrier	Head drop over sand body at damage condition,	Height of the pipe at the interface between the barrier and the pipe at damage condition,	Head drop over sand body when pipe breaks through barrier,	Height of the pipe at the interface between the barrier and the pipe when the pipe breaks through the barrier,
	mm	m/s	m	m	m	m
191	1.29	2.0E-03	0.13	0.41	0.50	1.16
196	1.85	6.7E-03	0.13	0.52	1.78	2.26
195	1.29	2.0E-03	0.10	0.26	0.14	1.09
197	1.85	6.7E-03	0.09	0.48	0.14	2.41

\*Note this was a preliminary estimate of  $D_{70}$  for the barrier materials, the  $D_{70}$  for the barrier materials used in the experiments are 1.20 mm for GZB2 and 1.24 mm for GZB3

The computation for test 194, the reference test, uses the preliminary estimate of the hydraulic conductivity of the fine sand in the location of the barrier. However the  $D_{70}$  at the location of the barrier used in that computation, is the preliminary estimate of the  $D_{70}$  of the coarse sand. Therefore this is not comparable to the reference test without a barrier (test194). As the hydraulic conductivity is uniform throughout the computational model for test 194, the results are also not directly comparable to the computational model for test 191 to analyse the effect of hydraulic conductivity of the barrier with a constant grain size, as in that model the hydraulic conductivity of the fine sand and the coarse sand are different. Therefore this simulation is not further analysed here.

## 5.8.2 Analysis

The height of the pipe at the location of the interface between the barrier and the pipe at the damage condition (shown in Table 5.15) is smaller than the  $D_{70}$  of the barrier material, i.e. the largest grains would not physically be able to be transported through the pipe. This criterion is not included in the Sellmeijer model. However, as flow in the pipe might be turbulent, this could also lead to a deeper pipe, and turbulent flow is also not included in the current implementation of the Sellmeijer model in DgFlow.

### 5.8.2.1 Comparison to experiments

For tests with Metselzand as a background material (tests 191, 192 and 193) the damage head drop in the experiments is a factor 3 to 4 higher than in the prediction with the Sellmeijer model. The head drop when the pipe breaches the barrier is a factor 1.5 to 2.8 higher.

One reason for this difference could be that the Sellmeijer model is only based on secondary erosion, and does not include primary erosion at the tip of the pipe. However for the test with Baskarp sand as a background material (test 195), where the barrier is present all the way to the upstream end of the set-up, the damage head and the head at which the pipe breaks through the barrier and progresses upstream is well predicted, accounting only for secondary erosion.

Another reason for the higher head drop in the experiments with Metselzand than predicted in the computations could be the additional resistance that is caused by the filter cake on the upstream end of the barrier. This provides an extra strength in the experiment that is not

included in the model. The effect of the filter cake is strongest in test 193 (as discussed in Section 4.3.3) and this is also the test where the under prediction is greatest.

#### 5.8.2.2 *Combined effect of $D_{70}$ and hydraulic conductivity on predictions*

The predictions for tests 191 and 196 (with Metselzand), and test 195 and 197 (with Baskarp sand) show that the combined effect of a larger  $D_{70}$  and a higher hydraulic conductivity on the predicted damage head drop is negligible. A higher hydraulic conductivity of the barrier causes more convergence of flow to the tip of the pipe, and this offsets to a large extent the additional strength due to a larger grain size. The net effect would depend on the combination of grain size and hydraulic conductivity.

In the experiments a slightly higher damage head was found with GZB3 than with GZB2 for the tests with Metselzand (test 191 and 196), for the test with Baskarp sand (195 and 197) the damage head was lower with GZB3. The effect of convergence of flow would have been higher in the test with Baskarp sand, as the total flow is governed by the hydraulic conductivity of the Metselsand and the filter cake, but also because the hydraulic conductivity contrast between the barrier and the downstream sand is smaller for Metselzand. That might contribute to a different effect on the damage head drop in the tests with different background materials. A more detailed analysis of the combined effects of grain size and hydraulic conductivity would be required to establish more definite conclusions.

The head drop at breakthrough of the pipe through the barrier is relevant for predictions 191 and 196 (as the barrier is present all the way upstream in predictions 195 and 197). At breakthrough, the flow at the tip of the pipe is governed by the flow in the fine sand upstream of the barrier, so the hydraulic conductivity of the barrier has little effect on the convergence of flow. Therefore, the larger barrier grain size in prediction 196 leads to a significantly higher head drop in the Sellmeijer model for prediction 196 than for simulation 191. This was not observed to such an extent in the experiments, however, in the experiments the formation of the filter cake might have contributed to additional strength in the test with GZB2 to a greater extent than in the test with GZB3.

## 6 Conceptual models

To get a better understanding of the measurement results and to be able to predict what happens for different geometries, it is useful to have a conceptual model of pipe formation in a sand layer with a coarse sand barrier. This model can be used for understanding the processes. It can be developed further in later stages of the project, if that is necessary based on further insight.

### 6.1 Pipe development in the fine sand

Upon creating a head difference in the intact sand sample with a barrier, the flow will concentrate radially towards the exit hole, resulting in local fluidization of the fine sand near the exit (Figure 6.1). An erosion lens is formed, with pipes forming in all directions. The eroded sand is deposited around the exit and the exit hole becomes filled with fluidized sand in constant motion.

Upon further increasing the head difference, one or more pipes start to develop upstream towards the barrier. When a pipe reaches the barrier, the flow towards the pipe in the barrier is insufficient to cause pipe formation in the barrier. Flow converges from the sides of the model towards the pipe. The combination of high flow rates and low erosion resistance in the fine sand next to the pipe causes pipe formation parallel to the barrier (Figure 6.2).

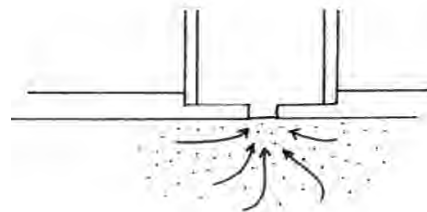


Figure 6.1 High flow velocities near the exit

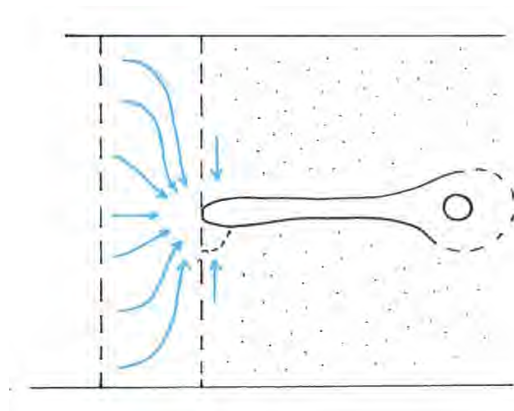


Figure 6.2 High hydraulic gradient transverse to the barrier

The pipe will lengthen in transverse direction (parallel to the barrier) until the side of the box is reached. The transverse development of the pipe causes the flow to be redistributed (Figure 6.3), reducing the load on the barrier.

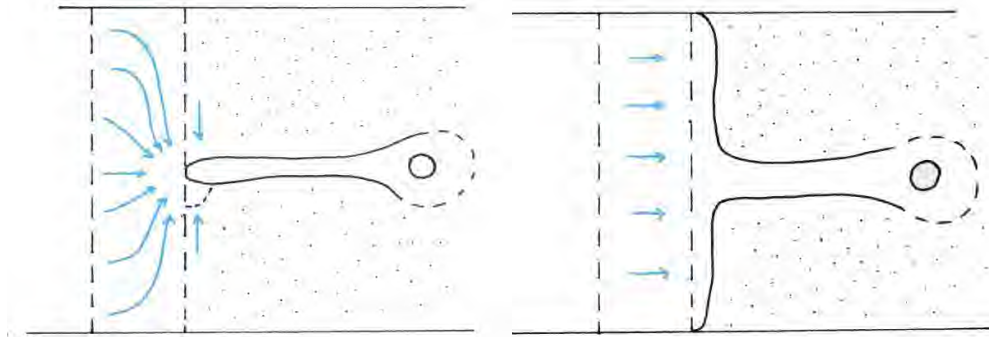


Figure 6.3 Transition from a 3D to a 2D flow configuration

## 6.2 Refinement

The flow through the pipe causes a shear stress on the grains at the pipe walls and bottom, causing the pipe to deepen and widen, until the particles are in limit-state equilibrium with the water passing them. As the pipe deepens the head drop in the pipe decreases: it becomes nearly zero. The flow regime in the pipe will become turbulent with increasing flow rate in the pipe. Although the head drop is insufficient to cause pipe formation in the barrier, the slope of the barrier along the pipe cannot be maintained and the flow from the barrier to the pipe will cause a slope angle less than the angle of a natural slope, causing crumbling of the barrier (Figure 6.4). The barrier particles can be deposited on the pipe bottom, or can be conveyed with the flow towards the exit. The depth of the pipe and the relative density and friction angle of the barrier material, as well as the force exerted by the seepage water will determine the degree of crumbling.

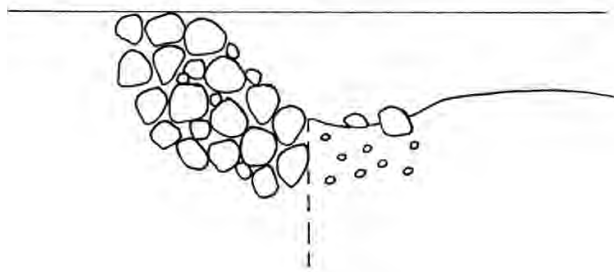


Figure 6.4 Crumbling of the barrier

## 6.3 Piping into the barrier

Due to the contrast in permeability between the barrier and the fine sand downstream, the flow is concentrated towards the exit point of the barrier (Figure 6.6). At some point a group of particles from the barrier is mobilised, forming a pipe in the barrier. In the analysis at hand the gradient computed between 1 cm and 4.5 cm upstream of the interface between the barrier and the pipe in the barrier at the point that the pipe grows into the barrier was selected as the

representative damage criterion for the barrier. However, when looking closely at the particle level, a mechanics-based approach may be more suitable for prediction of loosening the particles, describing the arching effects through particle-particle interactions.

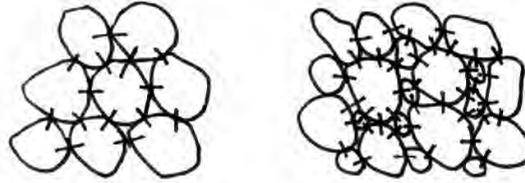


Figure 6.5 The number of particle contacts increases with grading

When specified in terms of the damage gradient, the different barrier materials provide different strengths. The highest strength was found for the GZB1 material, although no qualitative value for the strength could be determined for this material as there was no failure in these experiments, followed by the GZB2 material and the lowest strength was found for GZB3. As expected the presence of a coarse material increases the strength significantly, which explains the high resistance of GZB1, compared to the other materials. The addition of Metselzand to the fine filter sand causes an increase of local damage gradient, which may be explained by the larger number of particle contacts. A lower relative density also results in a decrease of local damage gradient, which might be related to the lower number of grain contacts.

The flow pattern in the barrier and the sand surrounding the barrier dictates the average head across the sample at which the barrier is damaged by pipe formation: this is determined mainly by the contrast in permeability of the barrier and the surrounding sand. A high permeability contrast will result in a large head loss in the upstream sand, and relatively low head loss in the barrier. However, the flow will concentrate towards the pipe, increasing the local gradient (Figure 6.6). A low permeability contrast will result in a lower head loss in the upstream sand causing an increased head loss in the barrier, but the flow will be conveyed through the downstream sand as well, reducing the head loss near the pipe tip. Consequently a barrier that exists out of coarse material (to prevent erosion) but has a low permeability (to avoid contraction of the flow lines to the pile), seems to be ideal. Therefore, the barrier material should be well graded.

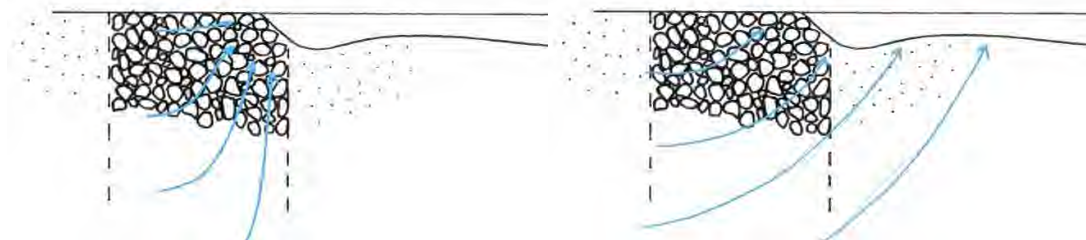


Figure 6.6 Flow patterns for high and low permeability contrasts of barrier and fine sand

When the hydraulic gradient in the barrier close to the pipe reaches a threshold value, the pipe can grow into the barrier. The value can be affected by to arching, and a further

requirement is that the pipe in the fine sand has reached the depth of a few barrier grains, so that the grains can be transported through the pipe.

#### 6.4 Pipe progression through the barrier

Once a pipe has formed in the barrier, the flow pattern changes:

- from 2D distributed flow along the barrier to a 3D concentrated flow near the pipe tip.
- for large permeability contrasts, the flow can exit through a larger area, reducing the concentration of flow, whereas for small permeability contrasts the progression of the pipe will not change the flow pattern that much (Figure 6.7).

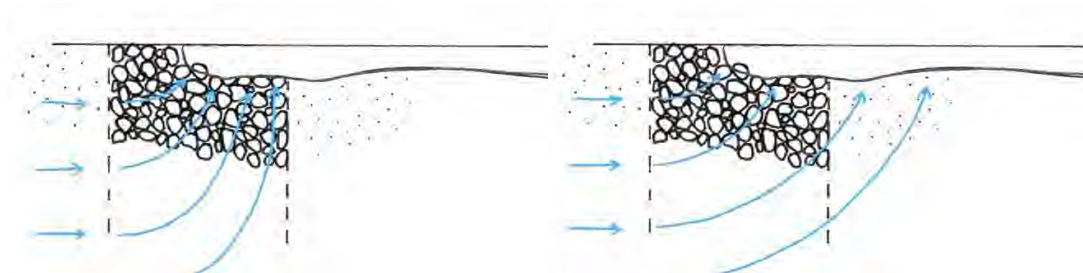


Figure 6.7 Change of flow pattern due to pipe progression for different permeability contrasts

In the tests with fine sand upstream and downstream of the barrier (i.e. all tests except tests 195 and 197 where the barrier continues upstream), the difference in head to fulfil the damage criterion (pipe progresses into barrier) was considerably smaller than the head difference at which the pipe breaks through the barrier. The reason is that the total flow in these tests does not increase significantly when the pipe enters the barrier, as this is determined by the flow resistance in the fine sand upstream, but the outflow area increases (compare Figure 6.6 and 6.7) and the tests had a significant permeability contrast. Consequently, the outflow gradient at the pipe tip will be less and a higher head difference is necessary to cause the pipe to progress. In a situation without a barrier, a longer pipe will reduce the overall flow resistance of the setup and the flow will increase as the pipe grows at the same head difference.

When the pipe has reached the upstream end of the barrier, the permeability contrast and the potential filter cake affect the further pipe progression. Both a large permeability contrast and a filter cake will result in a limited inflow of water at the pipe tip, causing additional resistance for pipe progression (Figure 6.8). The filter cake may also cause additional resistance from a mechanical perspective, due to the zone with mixture of fine and coarse particles, with a high relative density and a large number of grain to grain contacts. On the other hand, such a filter cake will also cause locally high gradients (see Section 4.3.3). It has to be studied more in detail what will be the result of these combined mechanisms.

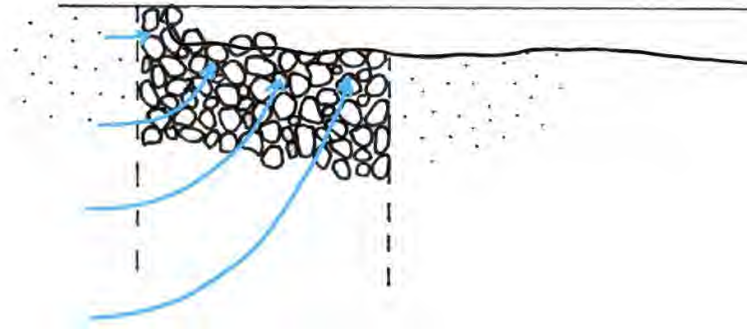


Figure 6.8 limited inflow due to low permeability contrast (and filter cake)

### 6.5 Effect of particle size, grading, relative density, permeability contrast, barrier dimensions and scale on damage and critical head

The conceptual model described above gives insight into the pipe development in different situations with a barrier. The experiments illustrate that a larger particle size, higher uniformity coefficient and higher relative density will provide a larger resistance to pipe formation. This effect holds for both the damage criterion and for the failure criterion, when the pipe passes through the upstream interface of the barrier.

With respect to the damage criterion, it is not clear beforehand whether a low or high permeability contrast will be more advantageous for the selection of a coarse sand barrier:

- A low permeability contrast will lead to a smaller head loss in the upstream sand, but will result in limited concentration of flow near the pipe tip, just before growing into the barrier.
- A high permeability contrast will lead to more head loss in the upstream sand, but will result in more concentration of flow near the pipe tip, just before growing into the barrier.

For the progression of the pipe a large permeability contrast is expected to provide more strength due to the combined effects of large head loss in the upstream sand and the reduction of local gradient upon approach of the end of the barrier. The formation of a filter cake is also advantageous due to the head loss in the filter cake and consequent reduction of local gradient upstream of the pipe when it is approaching the barrier, as well as possibly a higher resistance against erosion in the filter cake.

With respect to barrier dimensions, a larger depth will induce more flow towards the barrier, thereby increasing the local gradient. A smaller depth is therefore more advantageous. However, it is noted that in the current experiments a very small relative depth has not yet been tested. Numerical calculations can provide more insight into the possibility of fluidization of the downstream fine sand, in case of small barrier depth. Based on the current findings, the influence of the thickness of the barrier on the damage and critical head remains questionable and will require more research in the next phase. The currently applied thickness of 3-5 cm provides sufficient (residual) strength at small scale.

Based on the concepts described above, the scale has a large influence on the damage and critical head. A deep aquifer supplies more water to the barrier than a sand sample in a laboratory set up. The larger the depth and hydraulic conductivity of the sand layers below the barrier, the smaller the damage and critical head will be. It is noted here that the scale effects may not be same as those found in the Sellmeijer rule, since these depend on the secondary erosion and pipe flow, whereas breaching of the barrier relies on the erosion at the pipe tip.

## 7 Conclusions and recommendations

This report presents the analysis of the small-scale laboratory experiments and the numerical modelling. Based on this analysis it is attempted to establish a damage criterion that characterises the strength of a given barrier material. This damage criterion was then used to predict damage heads for tests at larger scales. This section presents the conclusions and discusses the limitations of the tests in the current phase. Recommendations for the next test phases are then presented.

Conclusions with respect to observed process:

- The pipe migrates horizontally through barrier, even with a 3 cm shallow barrier no vertical failure mechanism was observed.
- Pipe growth into the barrier occurs at a head five to seven times larger than critical head for reference material. The damage head depends highly on the chosen combination of background sand and barrier sand.
- There is a large difference in damage head and failure head. Failure occurs at a head ten to thirteen times larger than the critical head for reference material.
- At small-scale the coarse sand barrier appears to be promising method for piping prevention.

During the tests there was no significant change in the head measurements at the time at which the pipe first progressed into the barrier, i.e. the damage condition. This condition is currently based only on visual observation which has two drawbacks. There is a degree of subjectivity, which makes establishing them uncertain as discussed in Section 4.7 and in Section 5.5.4.5, but also these cannot be established unless there is a visual observation of the pipe and the barrier. Whereas this will be possible in the medium-scale tests, this is not the case for the Delta Flume tests or the field.

### 7.1 Conclusion damage criterion

Based on the data that can be directly obtained from the experiments, i.e. measured hydraulic head and flux, the local horizontal gradient in the barrier appears to be the best damage criterion to characterise the strength of the barrier. Other possible criteria, the flux, the overall head drop, the vertical gradient over the barrier, and the gradient over the upstream interface of the barrier show a larger scatter for tests with the same barrier material that would be expected to have the same strength.

Postdictions of the experiments using groundwater flow models allow for the assessment of a wider range of possible damage criteria. In addition to the local horizontal gradient, the local vertical gradient, the local diagonal gradient, and the corresponding local flow velocities are compared; these also indicate that the local horizontal gradient is the most constant factor among tests with the same barrier material.

The preliminary damage criterion is therefore considered as the gradient over the distance from 1 cm upstream of the downstream interface between the pipe and the barrier to 4.5 cm upstream of this interface. This range is selected as a compromise between the desire to have a criterion over a large distance, and the desire to limit the effect of crumbling of the barrier on the downstream end (as discussed further in Section 7.1.1). Table 7.1 shows the damage criterion for the barriers tested.

Table 7.1 Preliminary damage criterion for barrier based on postdiction of experiments

Barrier type	Preliminary damage criterion, horizontal gradient *	Preliminary estimated error margin** %	Comments
GZB 2 high relative density	0.48	35	Based on 5 tests (of which 3 are considered less reliable). Damage criterion based on the 2 more reliable tests would be 0.49)
GZB 2 low relative density	0.20	35	Based on 1 test with unreliable postdiction model
GZB 3 high relative density	0.23	35	Based on 2 tests (of which 1 is considered less reliable)

\* in undisturbed part of barrier gradient between 10 mm upstream of the interface between the barrier and the pipe to 45 mm upstream of this interface.

\*\* preliminary estimated error in the fit of the postdictions based on estimated: measurement error, error margin due to barrier location, error margin due to hydraulic conductivity of the downstream fine sand; and error margin due to pipe depth assumption. This estimate does not include all sources of uncertainty and is only an estimate and therefore considered as a preliminary estimate.

The preliminary estimated error margin is only based on the estimated error margins due to several sources that affect the fit of the postdiction. However, some sources of uncertainty could not be quantified, namely the degree of subjectivity in determining the damage condition, the effect of small variations in relative density, and the question whether in the small-scale tests the full strength of the barrier is mobilised. Including these is expected to increase the error margin in the fit of the postdictions; therefore the preliminary estimated error margin is likely to be a lower estimate of the actual error margin. Therefore the estimated damage criterion and the estimated error margin are best referred to as the preliminary damage criterion and the preliminary estimated error margin; these may be subject to modification based on insights from tests at a larger scale.

In the current test series it was observed that there was remaining strength after the pipe grew into the barrier. Failure occurred for much higher head drops. However, this strength was not characterised in this phase of the project. Analysis of this is hampered by the limited size of the barrier, and by the formation of a filter cake on the upstream interface of the barrier that yields additional strength, which does not reflect the strength of the barrier alone.

#### 7.1.1 Limitations of small-scale tests

The limited thickness of the barrier may prevent mobilisation of full strength in the small-scale tests. The data in (Robbins et al., n.d.) does suggest that a larger area of the sand at the tip of the pipe may be affected during the piping process, which might possibly result in a different strength in the medium-scale and Delta Flume tests.

The limited size of the barrier constrains the area over which a preliminary damage criterion can be determined, as this should not be in the filter cake or too close to the downstream end of the barrier as crumbling of the barrier has a stronger effect there. The smaller the distance over which a gradient is determined the greater the uncertainty due to limited measurement accuracy and due to possible small shifts of the location of the barrier.

If rather than a damage criterion, a failure criterion is to be determined, this will depend on the thickness of the barrier, as it is observed that the pipe grows through the barrier in steps rather than at once as soon as the damage criterion is exceeded. In order to study the progression of the pipe in the coarse sand barrier experiments with a wider barrier are required. This might require numerical modelling of a 3D situation with the pipe in the barrier; however, it is probable that flow is still approximately 2D due to the pipe that has widened along the barrier.

The failure strength that is obtained from the current small-scale experiments, the strength where the pipe breaks through the barrier, is not representative for the strength that may be present in a field situation, in part due to the presence of the filter cake. This may yield a significant additional strength that may or may not be present in the field, depending on the grain size distribution of the fine sand and the relation of this to the constriction sizes in the barrier.

#### 7.1.2 Predictions

Predicted head drops for the medium-scale and the Delta Flume tests show a significant effect of scale. The overall damage gradients become significantly lower as scale increases, which could suggest that the strength gain due to the barrier is limited at larger scale. However, at a larger scale the critical gradient without a barrier is also lower which means that the ratio of the damage gradient in the situation with a barrier to the critical gradient without a barrier may still be significant. It is expected that the gain on a larger scale will be less than on a smaller scale, and this will be investigated in phases 2b and 2c.

Furthermore, in the current predictions, the preliminary damage criterion is defined over the same distance for all scales. This is necessary at this stage of the project as the damage criterion has only been determined in small-scale tests so far. Based on the medium-scale tests and the Delta Flume tests a criterion may be determined over a larger scale. The actual criterion should not depend on scale; however, if the actual criterion is over a distance larger than the current barrier, the small-scale tests would not yield this criterion yet. For this reason a criterion over a larger scale may be determined in the next phases of the project.

Due to the geometry of the situation there is a steep gradient on the downstream side of the barrier at the interface between the barrier and the pipe, and this levels off in the barrier. In the small-scale tests the damage criterion is defined over an area where the gradient has already levelled off. This yields a relatively low gradient for the damage criterion in the predictions. However, the same distance from the downstream interface of the barrier in the medium-scale and in the Delta Flume tests is at the location of the steepest gradient, as the levelling off occurs further upstream as shown in Figure 7.1. Thus, in the prediction, a high gradient is computed at the location of the damage criterion, which means that a relatively low overall damage head drop is predicted.

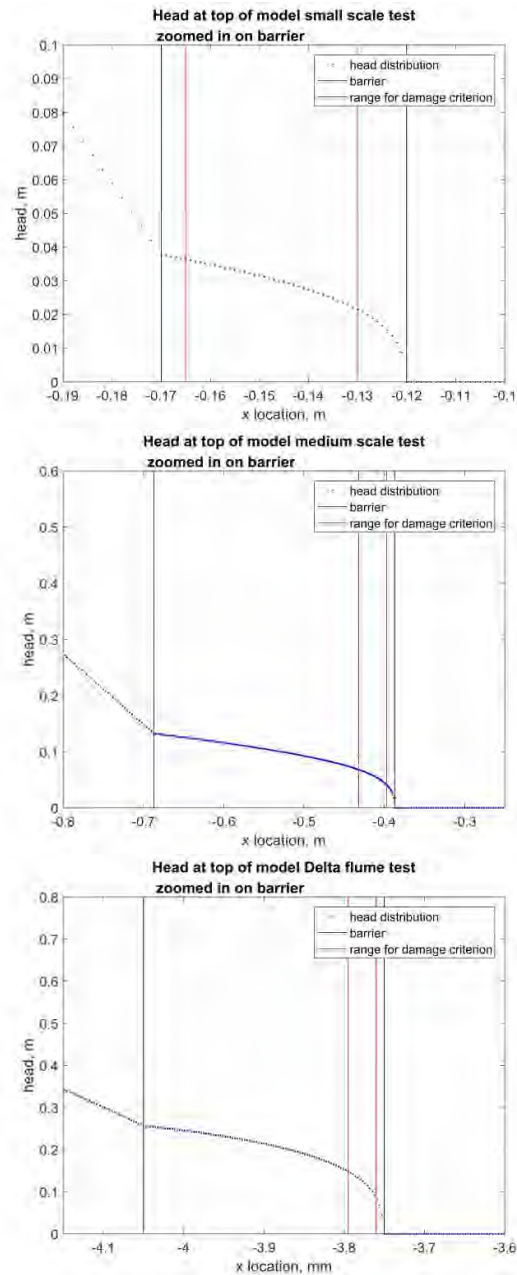


Figure 7.1 Head profile at the top of the barrier (blue dots), the barrier (black lines), and the location over which the damage criterion is determined. For the small-scale tests this is where the head profile had levelled off, whereas the same distance is in the extreme tip of the head profile for the small-scale and medium-scale tests

Figure 7.1 illustrates the importance of addressing to what extent the distance for the damage criterion in the small-scale tests is appropriate for the larger scale tests. If the damage criterion is defined over a larger area, so that the curves for the medium-scale and Delta Flume tests are also levelling off within this area this will lead to a significant improvement of the predicted strength.

The reliability of the predictions is affected by the same limitations of the small-scale tests that affect the reliability of the damage criterion as listed in Section 7.1.1.

## 7.2 Recommendations

In this project the aim is to be able to design a coarse sand barrier for the pilot location and to predict the strength of this barrier. In order to do this, a damage criterion for a given barrier material needs to be determined based on experiments at different scales and numerical modelling. However, tests in the first phase of the project show that after the barrier is damaged there is still a significant amount of strength left. Therefore, depending on whether the strength based on the damage criterion satisfies the required strength or not, it may be necessary to investigate the failure strength of the barrier. This will require significant additional effort in particularly concerning the numerical modelling of the pipe inside the barrier. The additional strength between damage and breach of the barrier may also be considered in the design of the barrier.

However, the current barrier material GZB2 was selected because it was weaker than GZB1 and it was necessary to achieve failure during the tests. If scale effects are large, GZB1 can be further investigated as a means to create a stronger barrier.

Predictions for the larger scale tests show significant scale effects, reducing the expected gain in strength with a coarse sand barrier. Therefore the damage criterion has to be investigated at larger scales in the medium-scale and Delta Flume tests in order to check the effect of scaling, and to overcome the limitations of a limited thickness barrier on the results.

For the medium-scale laboratory tests it is recommended to:

- Have a barrier with a thickness of at least 20 cm or maybe 30 cm in order to be able to mobilise the full strength of the barrier and to be able to analyse the progression of the pipe through the barrier.
- Measure the hydraulic head at more locations in the model, both inside the barrier to determine local gradients and upstream and downstream of the barrier in the bottom of the model in order to better be able to fit the numerical simulations to the results.
- Use a filtered background sand material that does not contain a fine fraction, to limit the formation of a filter cake.
- Expand on the analysis of the error margin.
- Further investigate the effect of the barrier depth.

In order to analyse what distance in front of the pipe is affected by the presence of the pipe and which may be expected relevant to characterise the damage criterion it is necessary to have a high density of head measurements in the path of the pipe tip. With the current set-up the location in the barrier where the pipe penetrates is uncertain and it is not possible to place a dense network of head transducers throughout the entire barrier. Therefore, it is recommended to test the barrier materials in the 1D set-up as described in (Robbins et al., n.d.) in order to be able to assess the damage criterion, and progression, for the failure criterion, more accurately. In this way the results for a damage gradient are also internationally reviewed, resulting in a broader level of support. Furthermore, the damage gradients found in the current phase of the project are lower than the local gradients at the moment of pipe progression that would be expected based on results from such a 1D set-up by (Robbins et al., n.d.). This difference could be investigated further with these tests.

Currently, the damage condition is established based on visual observations alone and these contain a degree of subjectivity. In order to reduce this degree of subjectivity it is recommended to investigate the possibility of image analysis for determination of pipe progression. If it becomes necessary to establish a failure criterion in addition to a damage criterion, image analysis may also be used to characterise the dimensions of the pipe in the barrier, as these will be required for the numerical model.

It is necessary to investigate how the damage criterion can be established in the Delta Flume tests. Head measurements appear insufficient to characterise this.

As the formation of a filter cake is observed during the tests, and this may or may not occur in the field depending on in situ grain size distributions, flow velocities in the field, and barrier material and relative density of the barrier in the field it is recommended to further investigate filter cake formation. The filter rules, which characterise whether or not fine material passes through the filter do not seem sufficient to characterise whether fine material is filtered on the upstream interface of the filter, and thus affect hydraulic conductivity. For practical application, it is therefore recommended to perform some gradient ratio tests with the available sand and the proposed barrier material.

In this phase of the project only a preliminary estimate of some of the errors that affect the determination of the failure criterion by postdiction of the experiments was made. These errors were combined to make a preliminary estimate of the error margin in the fit of the postdiction. That margin was then used as the preliminary estimate of the error margin for the damage criterion, in order to have an indication of the error margin in the predictions. As sources of uncertainty that could not readily be quantified are not included in this analysis this is currently only a preliminary estimate of the minimum error margin. Furthermore effects of pipe depth were analysed in small-scale models, and these effects were assumed to be similar for medium-scale models and for the Delta Flume test. These effects are dependent to some extent on the configuration, and that uncertainty is also not quantified at this stage. However, this preliminary estimate of the error margin may also be reduced if it is possible to reduce the estimated error margin of some of the individual sources of uncertainty that are quantified. It is recommended to further analyse the sources of error in order to obtain a better approximation of the error margin for the damage criterion. For modelling the field situation, uncertainties regarding the hydraulic conductivity of the in situ sand layers will be larger and this effect will have to be considered in order to establish a failure criterion. For the pilot location at Gameren this can be addressed when the results of the ground investigation are available.

## 8 References

- Bear, J., 1972. Dynamics of Fluids in Porous Media. Courier Corporation.
- Förster, U., van den Ham, G., Calle, E., Kruse, G., 2012. Onderzoeksrapport Zandmeevoerende Wellen. doi:1202123-003
- Kandlikar, S.G., Garimella, S., Li, D., Colin, S., King, M.R., 2006. Heat Transfer and Fluid Flow in Minichannels and Microchannels. Elsevier.
- Kenney, T.C., Lau, D., 1986. Internal stability of granular filters: Reply. Can. Geotech. J. 23, 420–423. doi:10.1139/t86-068
- Kenney, T.C., Lau, D., 1985. Internal stability of granular filters. Can. Geotech. J. 22, 215–225. doi:10.1139/t85-029
- Koelewijn, A.R., Peters, D., de Vries, G., van Loon, J., Bersan, S., 2013. All in One-Sensor Validatie Test, Factual report Estdijk – proefverloop en referentiemonitoring. Deltares report 1206252-006-GEO-0002-v2.
- Koelewijn, A.R., Van Beek, V.M., 2017. Feasibility study on the effectiveness of a coarse sand barrier as a piping measure. Deltares report 1220240-004-GEO-0003.
- Lambe, T.W., Whitman, R.V., 1969. Soil Mechanics. John Wiley and Sons Inc.
- Negrinelli, G., Van Beek, V.M., Ranzi, R., 2016. Experimental and numerical investigation of backward erosion piping in heterogeneous sands, in: International Conference on Scour and Erosion. Oxford, pp. 473–482.
- Polubarinova-Kochina, P.Y., 1962. Theory of Filtration of Liquids in Porous Media. Princet. Univ. Press.
- Robbins, B.A., Van Beek, V.M., Lopez, J.F., Montalvo Bartolomei, A.M., Murphy, J., n.d. A novel laboratory test for backward erosion piping. under Rev.
- Rosenbrand, E., 2017. Literatuurstudie Filtercriteria ten behoeve van grofzandbarriere. Deltares memo 11200952-003-GEO-0001.
- Rosenbrand, E., Van Beek, V.M., 2017. Factual report small-scale experiments coarse sand barrier. Deltares report 11200952-004-GEO-0003-v1-r.
- Sellmeijer, H., López de la Cruz, J., Beek, V.M. van, 2011. Fine-tuning of the backward erosion piping model through small-scale, medium-scale and IJkdijk experiments, in: Erosion in Geomaterials. pp. 1139–1154. doi:10.3166/EJECE.15.1139-1154
- Sellmeijer, J.B., 1988. On the mechanism of piping under impervious structures. TU Delft.
- Senhorst, H., 2016. Innovatie uit de markt, fase 2. Eindrapportage werkgroep innovatie uit de markt. Rapportage werkgroep Innovatie uit de markt, POV Piping. RWS Bedrijfsinformatie.
- Van Beek, V.M., 2017. Sand selection Coarse sand barrier experiments. Deltares memo 11200952-004-GEO-0001-m.
- Van Beek, V.M., 2015. Backward Erosion Piping Initiation and Progression. TU Delft, Delft.
- Van Beek, V.M., Knoeff, H., Sellmeijer, H., 2011. Observations on the process of backward erosion piping in small-, medium- and full- scale experiments, in: Erosion in Geomaterials. pp. 1115–1137. doi:10.3166/EJECE.15.1115-1137
- Van Beek, V.M., Koelewijn, A., Kruse, G., 2008. Piping phenomena in heterogeneous sands - experiments and simulations, in: Fourth International Conference on Scour and Erosion. pp. 453–459.
- Van Beek, V.M., Koelewijn, A.R., Negrinelli, G., Förster, U., 2015a. A coarse sand barrier as an effective piping measure. Geotechniek 4–7.
- Van Beek, V.M., Van Essen, H.M., Vandenboer, K., Bezuijen, A., 2015b. Developments in modelling of backward erosion piping. Géotechnique 65, 740–754. doi:10.1680/geot.14.P.119
- Van Esch, J.M., 2015. WTI 2017 : Toetsregel piping Validation piping module DgFlow (report including primary erosion). Deltares report 122084-004-GEO-0002-ydh. Delft.
- Van Esch, J.M., 2014. Flood Defense Assessment Tools for Piping in WTI 2017 - Report 9b. Groundwater Flow Simulator DgFlow 3D Validation piping module. Deltares report 1209435-006-GEO-0001. Delft.
- Van Esch, J.M., 2013. Modeling Groundwater Flow and Piping under Dikes and Dams Model validation and verification. Deltares report 1207809-005-GEO-0001-jvm. Delft.

## **A Mesh analysis small-scale mesh**

## Memo

**To**  
Vera van Beek, Adam Bezuijen

**Date**  
8 November 2017

**Number of pages**  
10

**From**  
Esther Rosenbrand

**Direct line**  
+31(0)88335 7852

**E-mail**  
esther.rosenbrand@deltares.nl

**Subject**  
Mesh analysis small-scale mesh

---

This analysis shows the effect of mesh refinement.

Because the effects will be dependent on the permeability contrast, 3 permeability contrasts are considered which span the range of contrasts that are expected to be realistic for a situation of a coarse sand barrier. These are:

- 3
- 33
- 100

The upstream head is 0.4 m for all cases. The permeability of the fine material is  $6 \text{ e-}4 \text{ m/s}$  for all cases.

## 1 Mesh sizes

The mesh sizes used are uniform meshes with elements of 1 mm, 2 mm, and 4 mm. To obtain a higher precision with less computation time a locally refined mesh is also used. This will be referred to as the final mesh, as this mesh was selected for further computations. The local refinements are shown in the figures below.

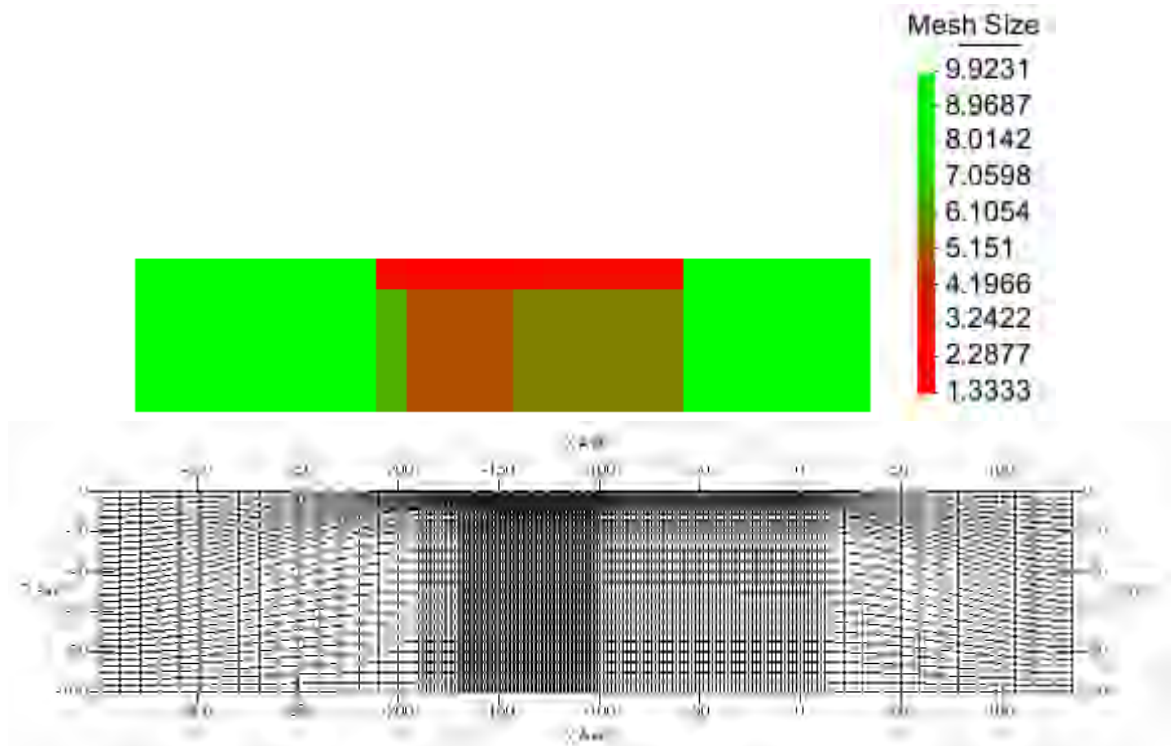
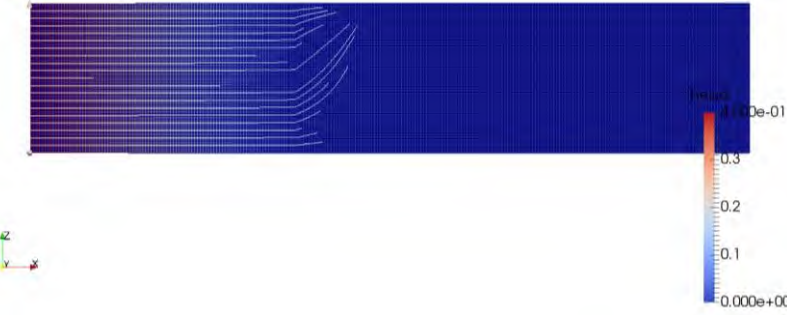
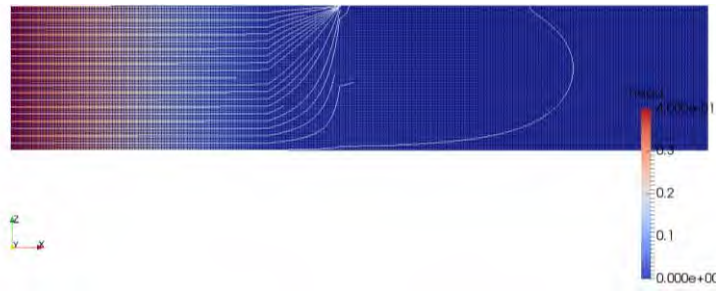


Figure 1.1 Locally refined mesh. Top figure zones of mesh refinement with red being high refinement and green less refinement. Bottom the final mesh.

## 2 Head profiles

The flow in the four models is shown for the permeability contrast of 33 with stream lines sourced from the left boundary (inflow) of the model.

Figure 2.1 Background colour shows the head distribution. White streamlines are shown indicating the flow paths followed from the upstream end of the model. The mesh is shown in dark blue lines. Permeability contrast is 33.

Mesh size, mm	Permeability contrast: 33
1	 <p>*note figure appears darker due to dense mesh, upstream head is the same as in other figures</p>
2	
4	
Final mesh	

### 3 Effect of mesh on head distributions

The calculations are done with permeability contrasts, 3, 33 and 100. In the full scale figures the differences between the different meshes are difficult to distinguish as the results are very similar.

In the close up views below, the heads for the final mesh are shown as crosses as these are too close to the results from the 1 mm mesh to be able to distinguish otherwise.

#### 3.1.1 Effect with permeability contrast 3

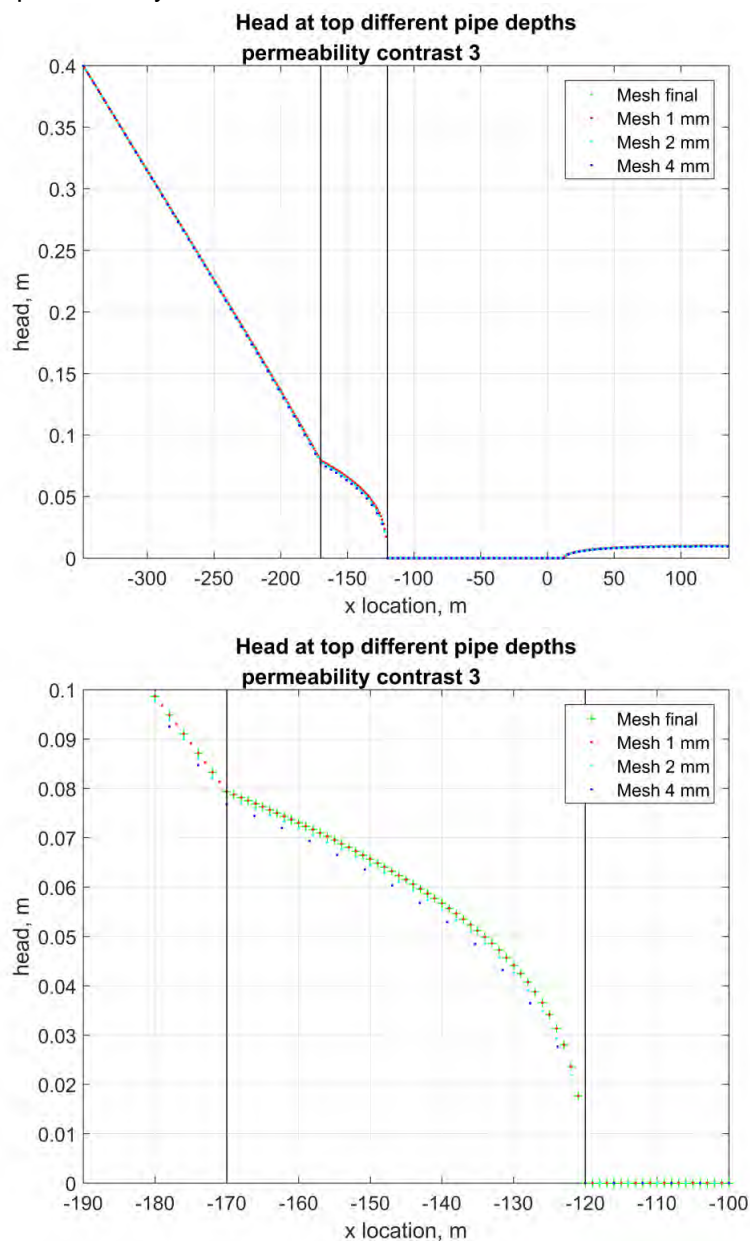


Figure 3.1 Head distribution in the model

### 3.1.2 Effect with permeability contrast 33

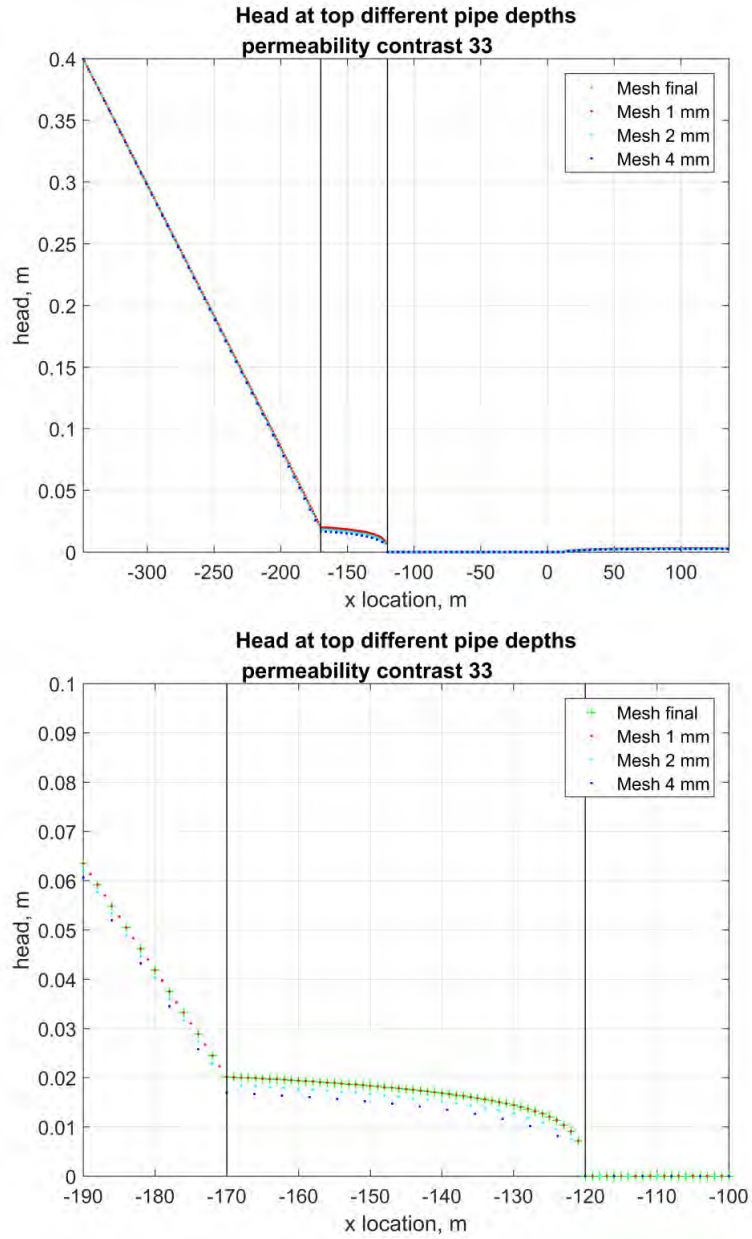


Figure 3.2 Head distribution in the model

### 3.1.3 Effect with permeability contrast 100

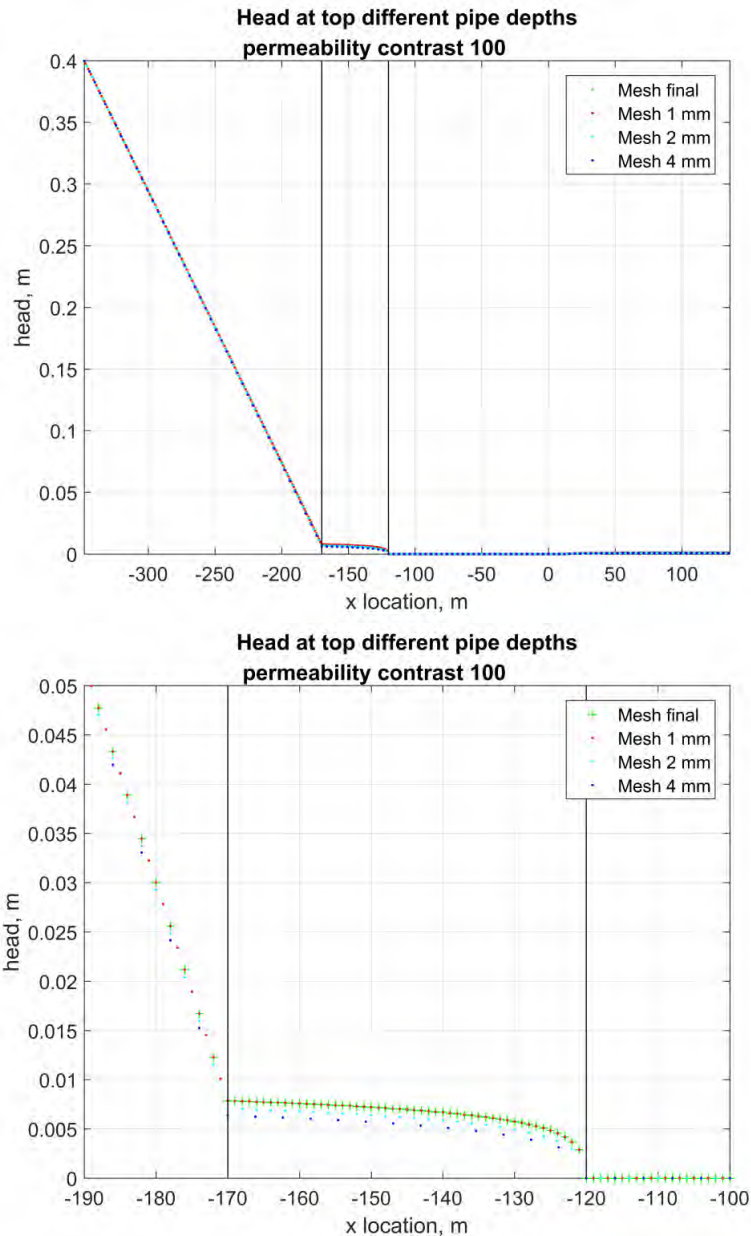


Figure 3.3 Head distribution in the model

## 4 Mesh effect on gradient over barrier

When the gradients are calculated for the mesh with 4 mm elements, there is not always a node at the location that the head is required for. Therefore a linear interpolation is done between the neighbouring nodes.

The effect of barrier depth on the gradient over the barrier for different permeability contrasts is shown below where the gradient is determined from the head difference between -0.130 m and -0.165 m (i.e. 1 cm upstream of the interface between the barrier and the pipe and 4.5 cm

upstream of this interface, the distance for which the damage criterion is defined in the current phase of the project).

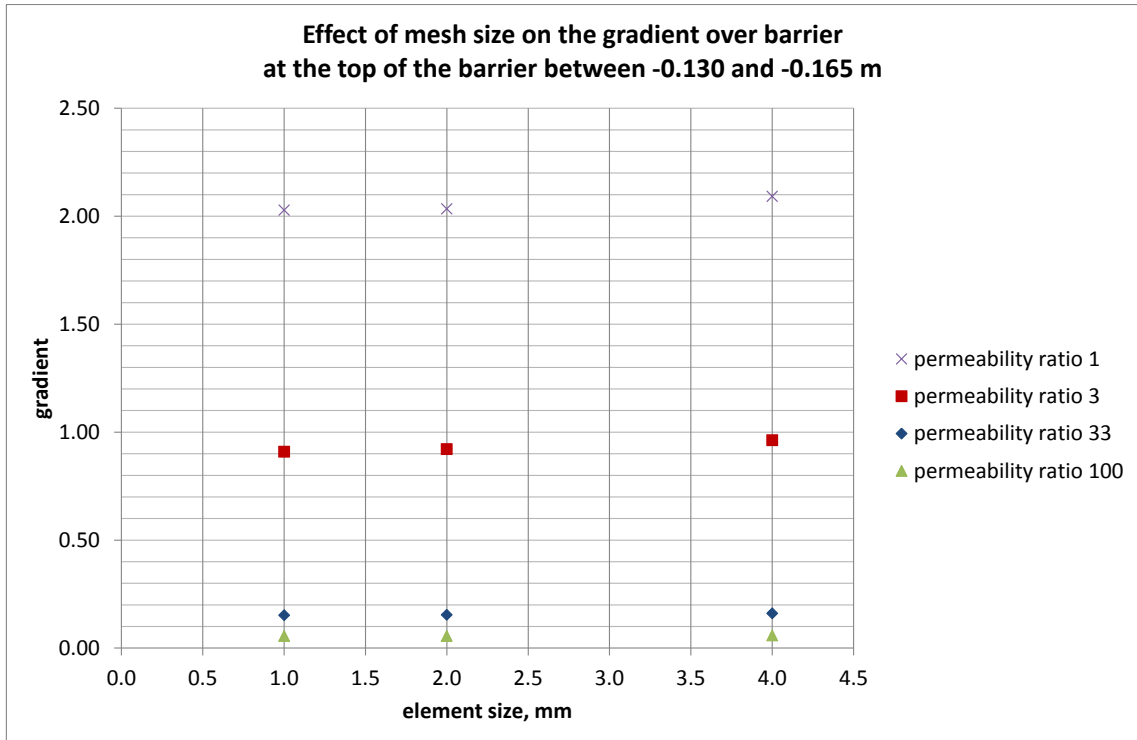


Figure 4.1 Gradients over the barrier show the absolute effect of mesh size on the gradient for different permeability contrasts

This is also shown when looking at the ratio between the gradient in the models with different mesh sizes to the gradient in the model with a mesh size of 1 mm, i.e. the relative effect.

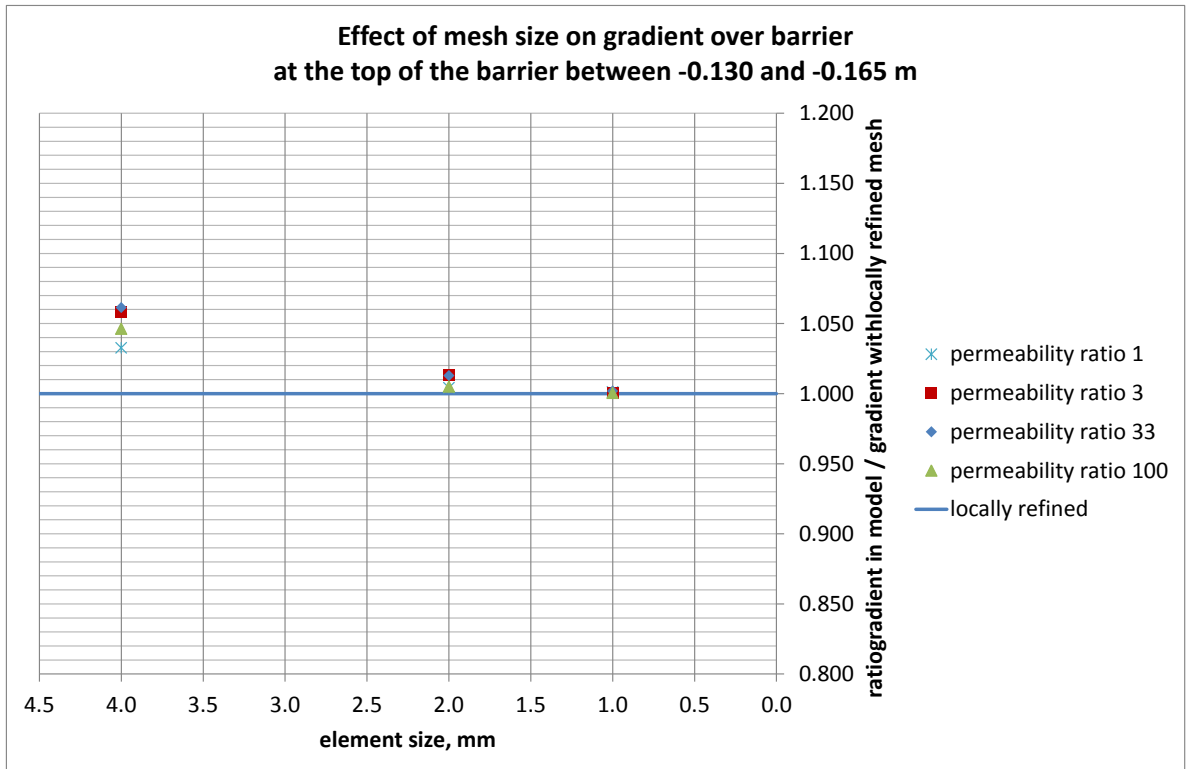


Figure 4.2 The ratio of the gradient over the barrier with element size 1 mm over the gradient over the barrier with a variable element size, for distance between -0.130 and -0.165 m

## 5 Mesh effect on total flux

The effect of element size on the flux is shown below. For a higher permeability contrast the effect of the mesh on the total flux is larger.

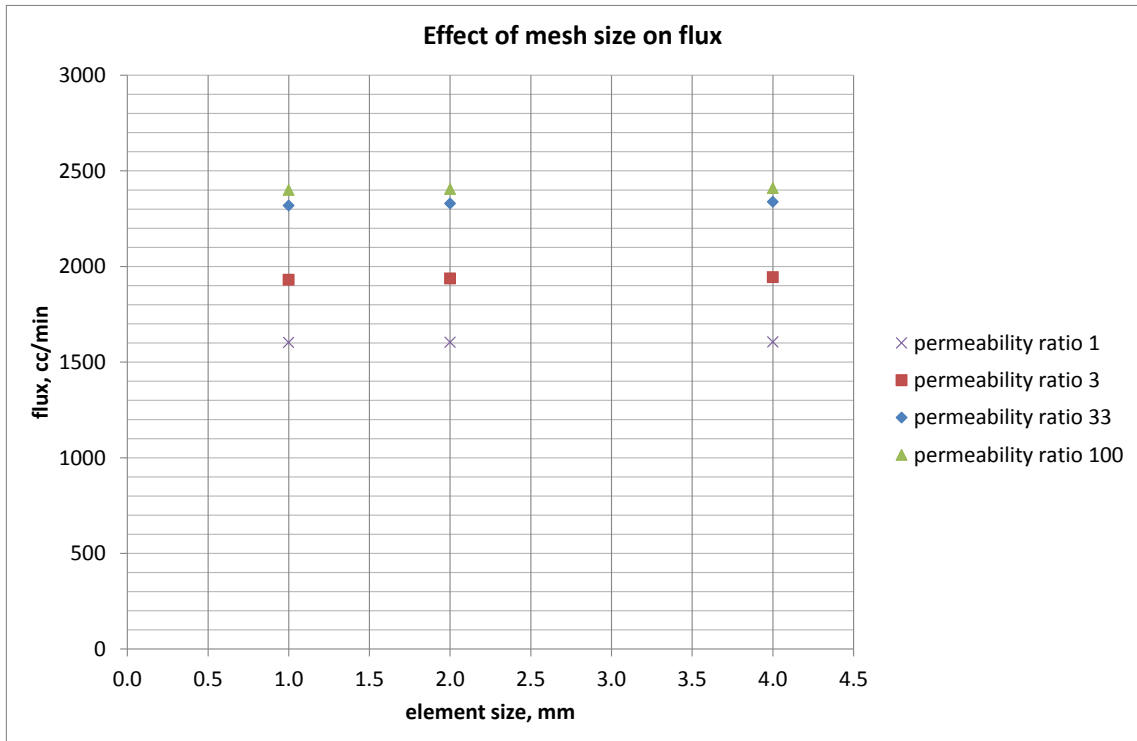


Figure 5.1 Fluxes show the absolute effect of mesh size on the flux

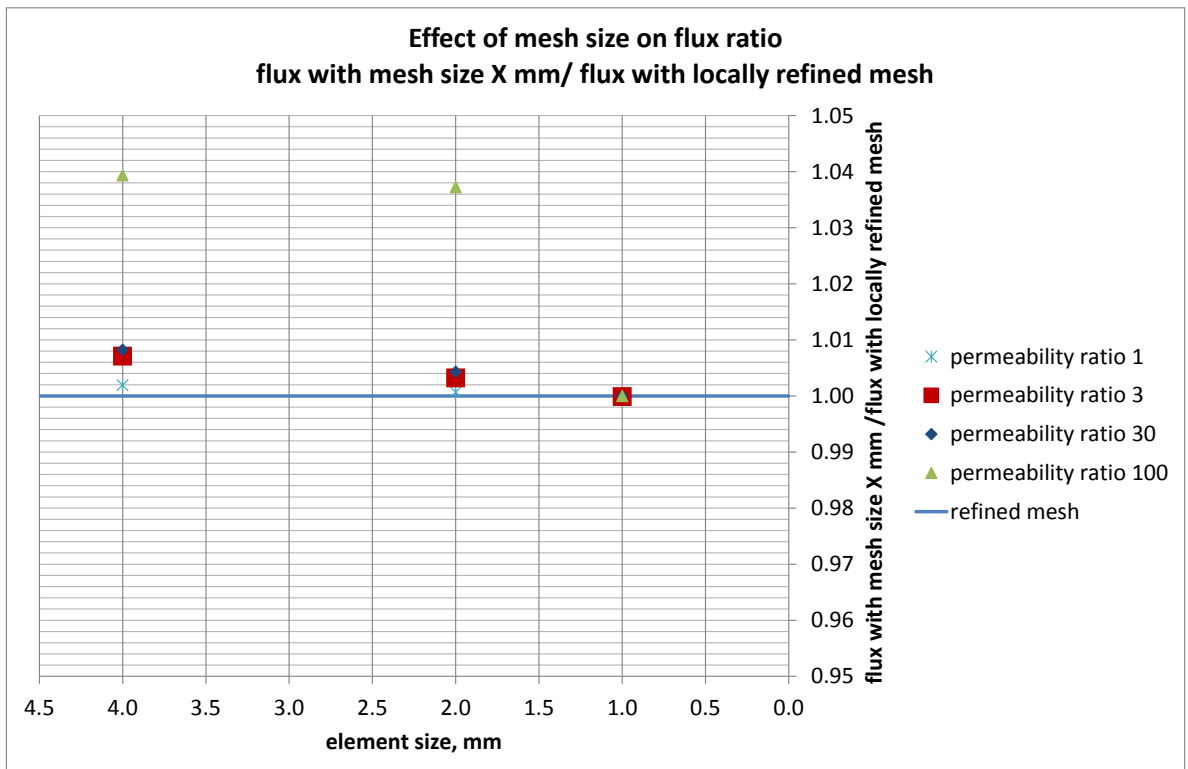


Figure 5.2 The ratio of the flux with a locally refined mesh with element size 1 mm in the barrier over the flux with a variable mesh size

## 6 Conclusions

- The flux is overestimated with a coarser mesh, the local gradient is underestimated;
  - These difference reduce with reducing mesh size;
  - These differences are larger for greater permeability contrasts;
- The locally refined mesh gives results that are the same as the uniform mesh with element size 1 mm. As this is more computationally efficient this mesh is used for subsequent calculations;
- A mesh size smaller than 1 mm is deemed unnecessary considering the physical size of the particles (in the order of 1 mm).

## **B Comparison to analytical solution for uniform hydraulic conductivity**

# Memo

**To**  
Vera van Beek, Adam Bezuijen

**Date**  
3 November 2017

**Number of pages**  
3

**From**  
Esther Rosenbrand

**Direct line**  
+31(0)88335 7852

**E-mail**  
esther.rosenbrand@deltares.nl

**Subject**  
Comparison to analytical solution for uniform permeability

## 1 Comparison to analytical solution for uniform permeability

In this section the results of a simulation using DgFlow are compared to the Polubarinova-Kochina (P-K) (Polubarinova-Kochina, 1962) solution for the exit gradient at the surface downstream of the toe of a confined aquifer (below a dam).

The 2D model used in DgFlow is shown below. The barrier is present between x coordinates -170 mm and -120 mm. As the solution is for an aquifer with a uniform permeability, the permeability of the barrier and the sand are equal in this model.

The upper boundary of the model is closed between -352 mm and -120 mm and open with a zero head condition from -120 to 140 mm.

The inflow is through the left vertical boundary at x coordinate -352 mm, and inflow occurs along the entire depth of the model (between z coordinates 0 mm and -101mm). The bottom and right hand side boundaries are closed.

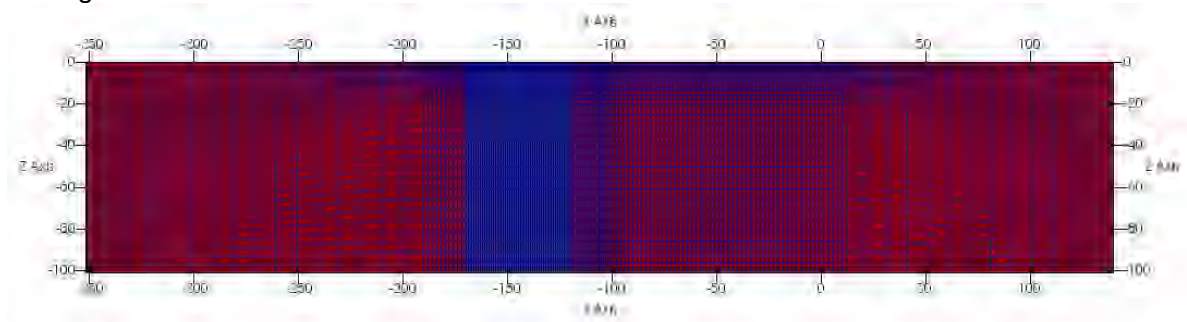


Figure 1.1 Figure of the model and the mesh, the barrier is the blue region

The grid refinement is shown below, the grid size of the elements in the top of the barrier in DgFlow are 1 mm (length and width). This grid refinement is based on the mesh analysis reported in Appendix A of the main report.

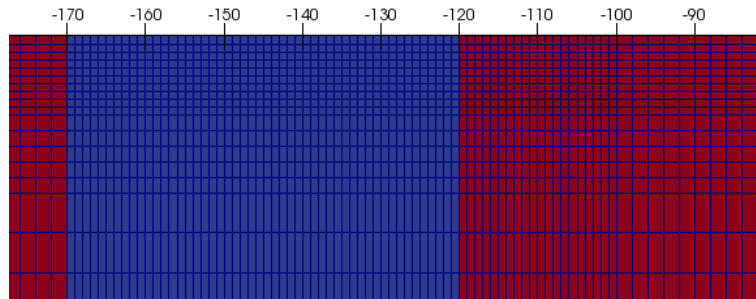


Figure 1.2 Close up of mesh used in the model, blocks at the top of the barrier are 1 mm by 1 mm

The P-K solution is evaluated using a step size of 1 mm and with a step size of 0.5 mm. The P-K solution directly provides the gradient. The DgFlow model provides the head in the elements at the nodes, or the velocity in the x and y directions in the elements. The gradient is calculated from this data in 3 manners:

- Gradient in the x direction is computed by subtracting the head in adjacent nodes. This head is assigned to the position between the nodes;
- The velocity in the x direction is divided by the permeability in the x direction to obtain the gradient in the x direction. This gradient is assigned to the midpoint of the nodes;
- The magnitude of the velocity is calculated from the root of the sum of the velocity in the x and y directions squared. From this magnitude divided by the (isotropic) permeability the gradient is computed.

The figure below shows the results these overly very closely with the exception of the first node upstream of the interface between the barrier and the pipe.

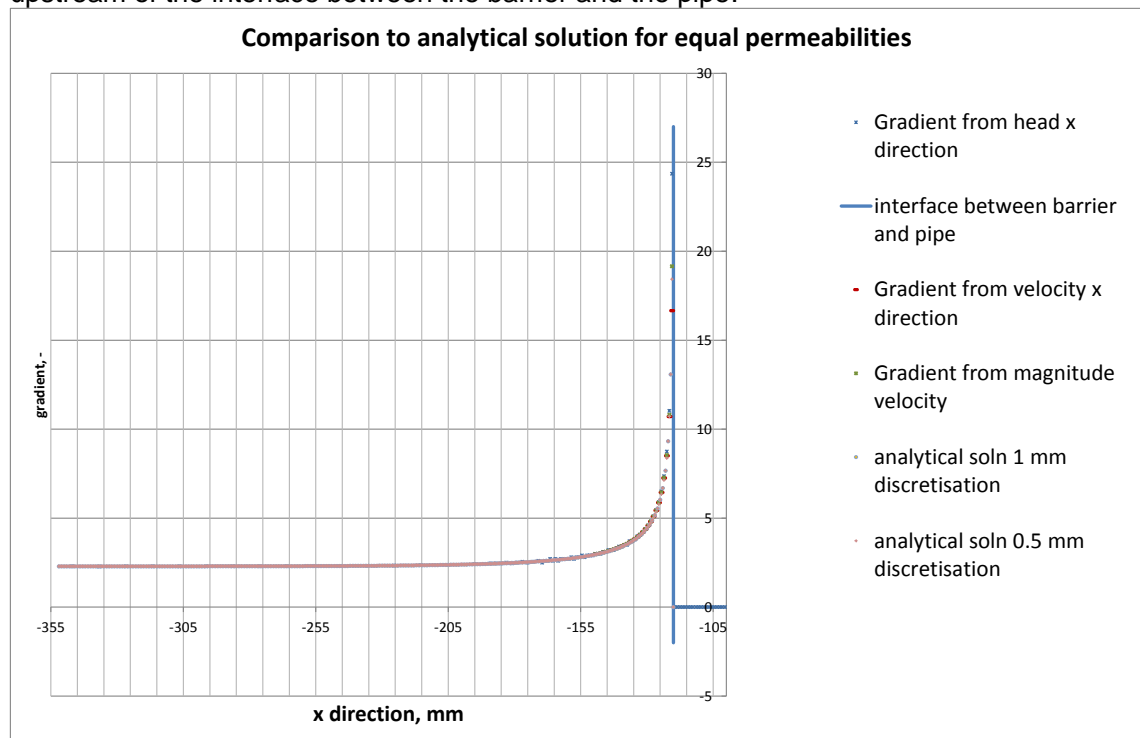


Figure 1.3 Gradient from DgFlow compared to analytical solution. Mesh refinement in the barrier 1 mm blocks

In order to evaluate the fit between the model and the analytical solution and place this in context in relation to uncertainties in head measurements during the experiments, the effect of an estimated error margin of 0.5 mm in the head value on the computed gradient is considered. The black lines in the figure below indicate the gradient that would be found if the head difference were increased or reduced by 0.5 mm.

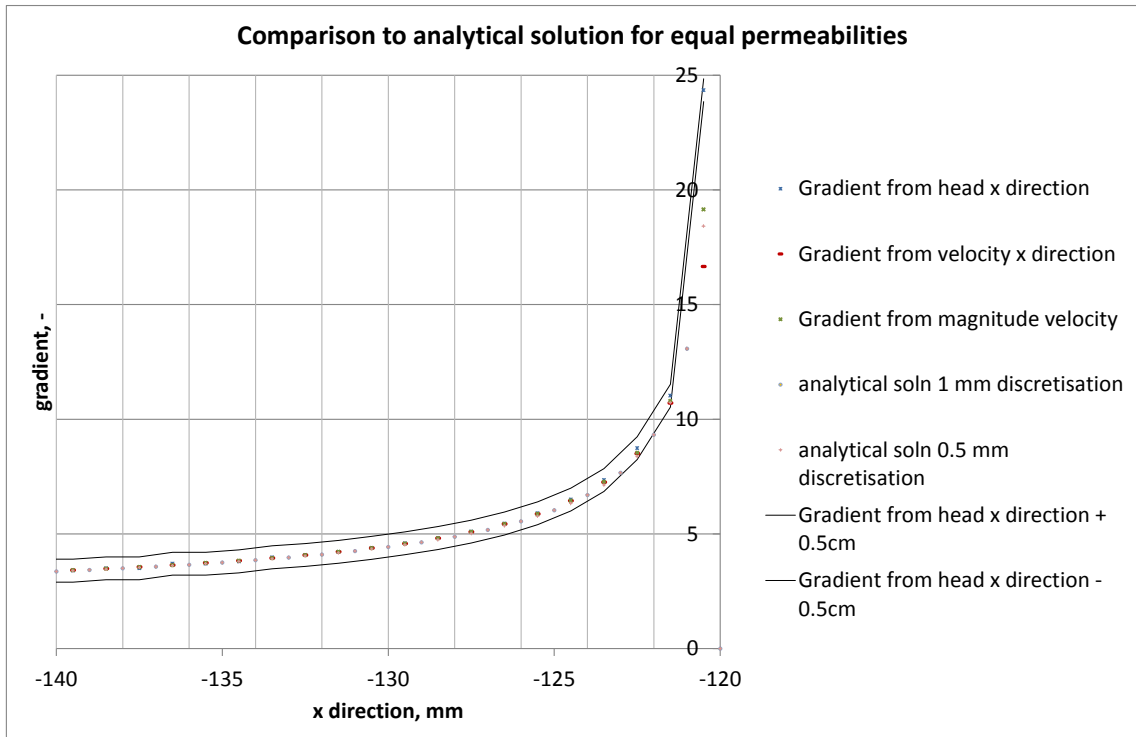


Figure 1.4 Close up of gradient from DgFlow compared to analytical solution and estimated error margin which would result from inaccuracy of the head measurement of 0.5 mm

Figure 1.4 shows that numerical results from DgFlow are within the estimated uncertainty band all the way up to the first millimetre upstream of the interface between the barrier and the pipe. Although the 0.5 mm used here is only a first estimate of the uncertainty in the head measurements, this suggests that at larger distances from the outlet the numerical solution approximates the analytical solution well.

Considering furthermore that the estimated error margin in the exact location of the barrier in experiments is already in the order of 2 mm, and that the damage criterion between 10 mm from the interface between the barrier and the pipe and 45 mm from that interface, the accuracy of the numerical model is sufficient for simulating the laboratory experiments.

## **C Comparison DgFlow and Plaxis**

## Memo

**To**  
Vera van Beek, Adam Bezuijen

**Date**  
3 November 2017

**Number of pages**  
8

**From**  
Esther Rosenbrand

**Direct line**  
+31(0)88335 7852

**E-mail**  
esther.rosenbrand@deltares.nl

**Subject**  
Comparison DgFlow and Plaxis

---

This analysis compares the results from DgFlow to those from Plaxis for 2D and 3D small scale models.

3 permeability contrasts are considered:

- 3
- 100
- 1

The upstream head is 0.4 for all cases. The permeability of the fine material is  $6e-4$  m/s for all cases.

## 1 Models

For the DgFlow simulations, the same small scale model and mesh that are described in the main report are used.

For Plaxis both 2D and 3D models have an unstructured mesh, for DgFlow the 3D model has an unstructured mesh and the 2D model has a structured mesh.

The models are shown below:

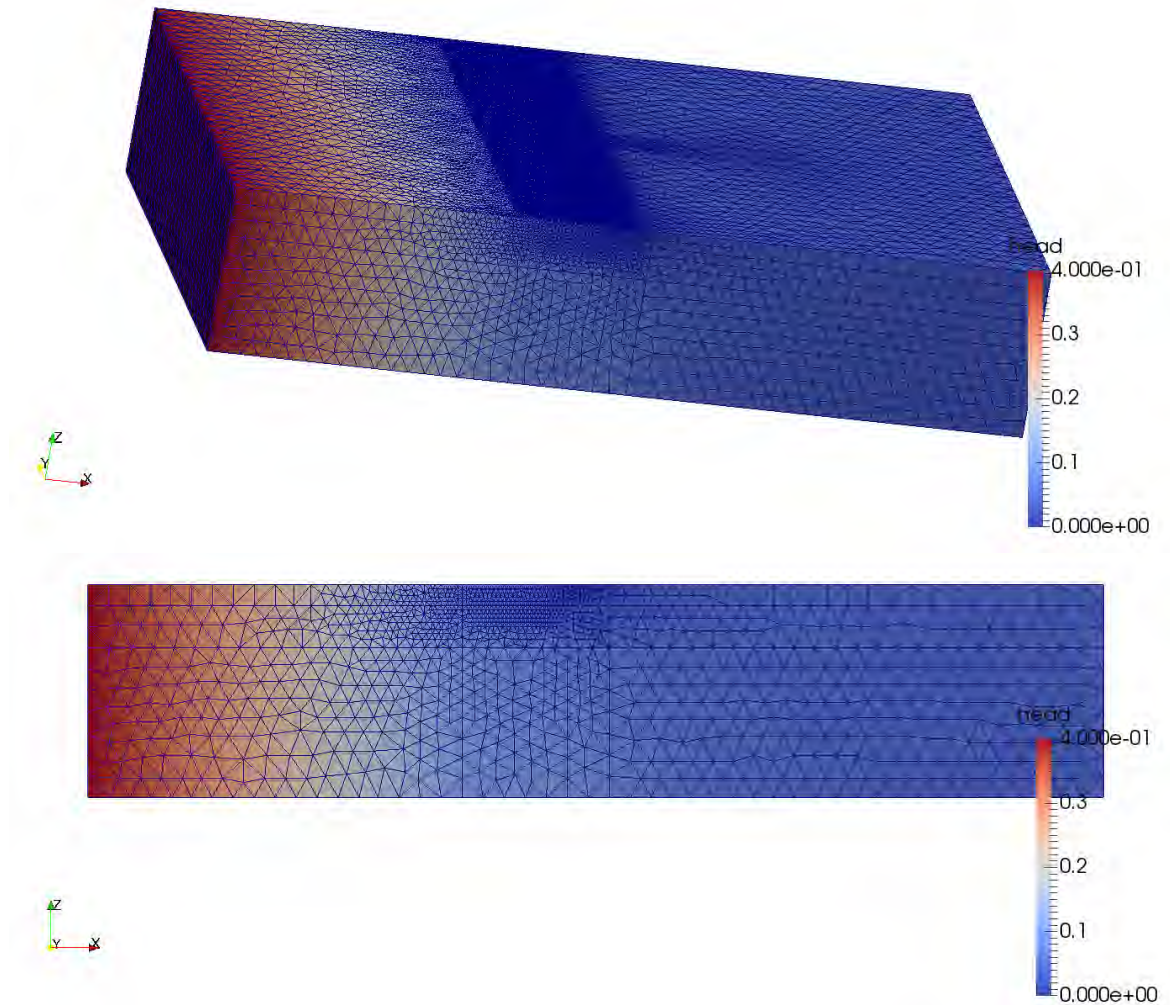


Figure 1.1 DgFlow 3D Head distribution for permeability contrast 3, the model has an unstructured mesh

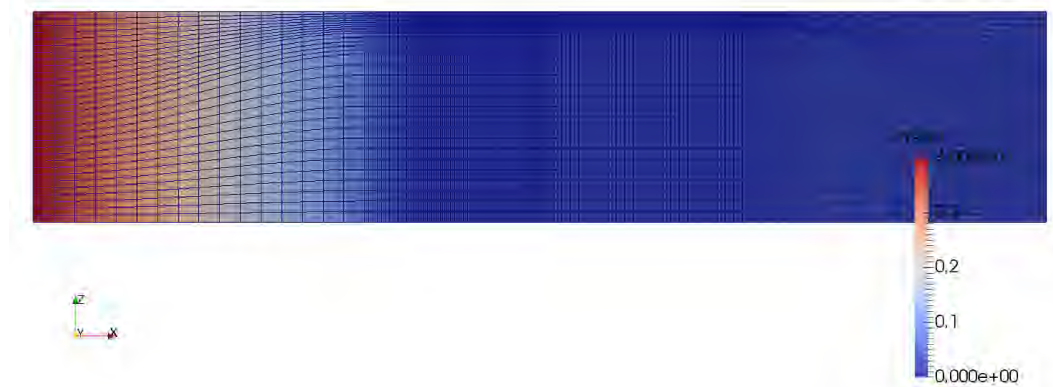


Figure 1.2 DgFlow 3D Head distribution for permeability contrast 3, the model has a structured mesh

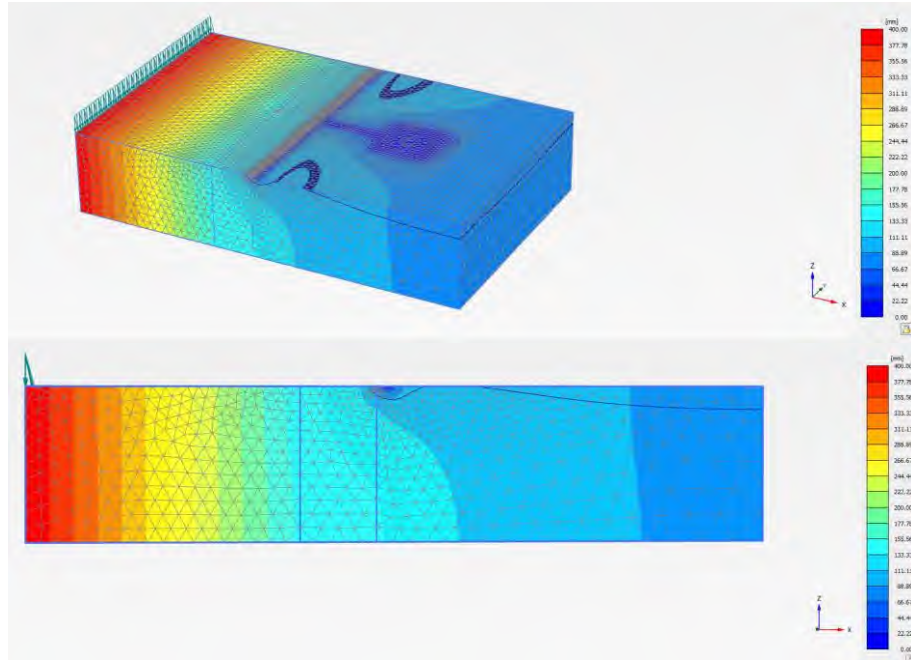


Figure 1.3 Plaxis 3D Head distribution for permeability contrast 3, the model has an unstructured mesh

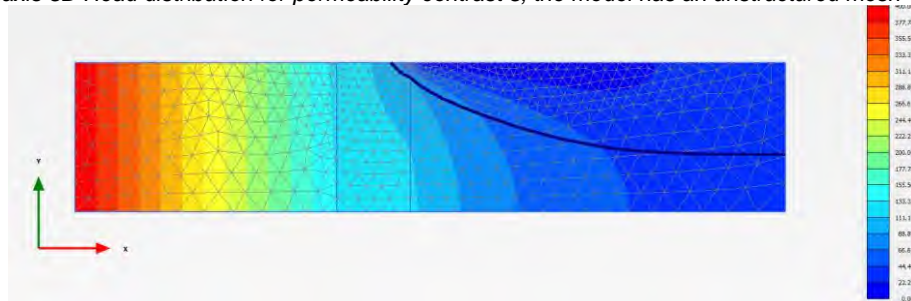


Figure 1.4 Plaxis 2D Head distribution for permeability contrast 3, the model has an unstructured mesh

## 2 Head profiles

The head profiles in the two models are shown below. The differences between the two models are largest for the case with a high permeability contrast. This would be expected as there is most concentration of flow in this case so small differences will have a relatively stronger effect.

For contrasts of 1 and 3, Plaxis 2D and DgFlow 2D give the same results, DgFlow 3D gives a slightly higher head than these two and Plaxis 3D gives a higher head than DgFlow 3D. For a contrast of 100, Plaxis 3D and 2D give a similar head, which is higher than the head in DgFlow for both 2D and 3D. The 3D head in DgFlow is higher than the 2D head in DgFlow.

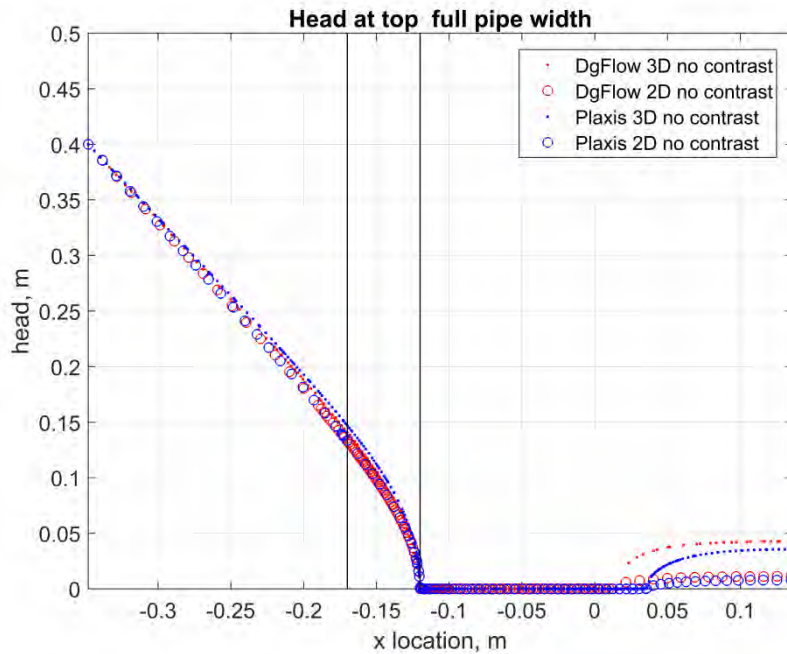


Figure 2.1 Head in the central axis of the model. Barrier is between -0.12 and -0.17 m

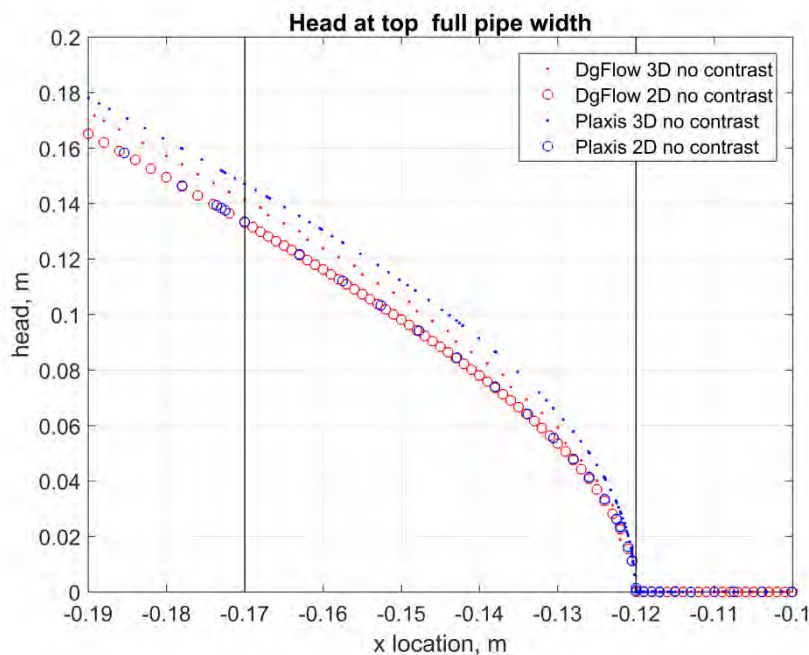


Figure 2.2 Head in the central axis of the model. Barrier is between -0.12 and -0.17 m

For the case with no permeability contrast, the two 2D models, Plaxis and DgFlow give the same head values. The 3D models give slightly higher head values, where the Plaxis 3D model gives higher values than the DgFlow 3D model.

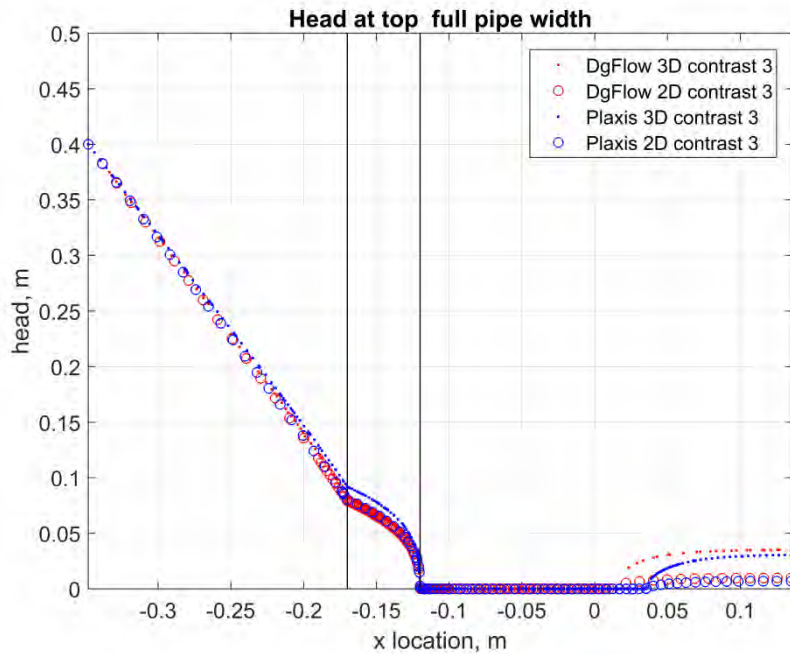


Figure 2.3 Head in the central axis of the model. Barrier is between -0.12 and -0.17 m

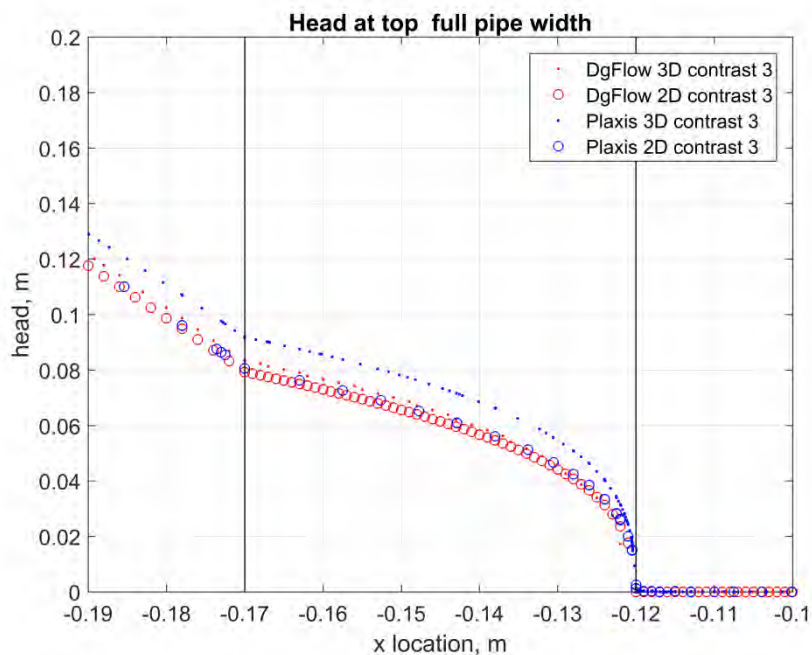


Figure 2.4 Head in the central axis of the model. Barrier is between -0.12 and -0.17 m

For contrast 3 the DgFlow 2D and 3D models give a similar result which is comparable to the Plaxis 2D result. The Plaxis 3D result gives a significant higher gradient especially close to the outflow point.

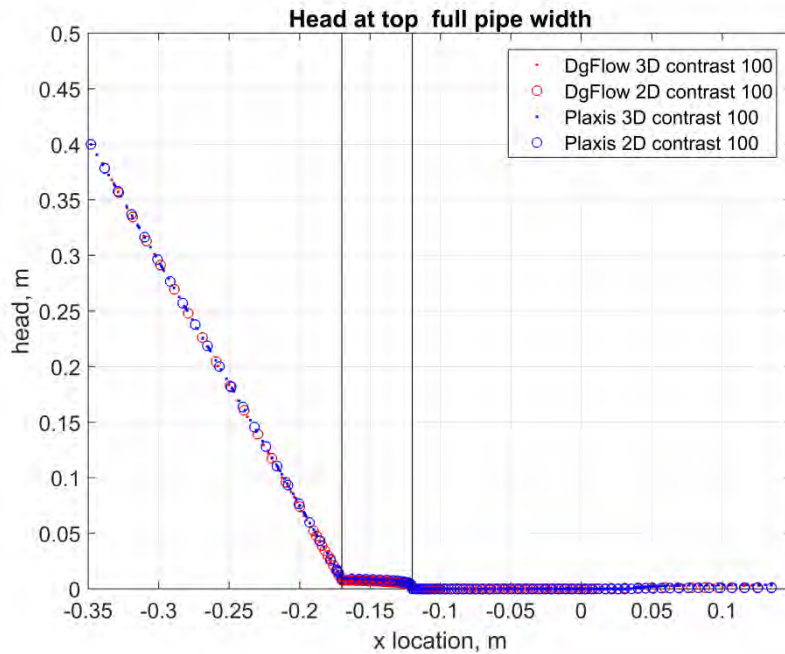


Figure 2.5 Head in the central axis of the model. Barrier is between -0.12 and -0.17 m

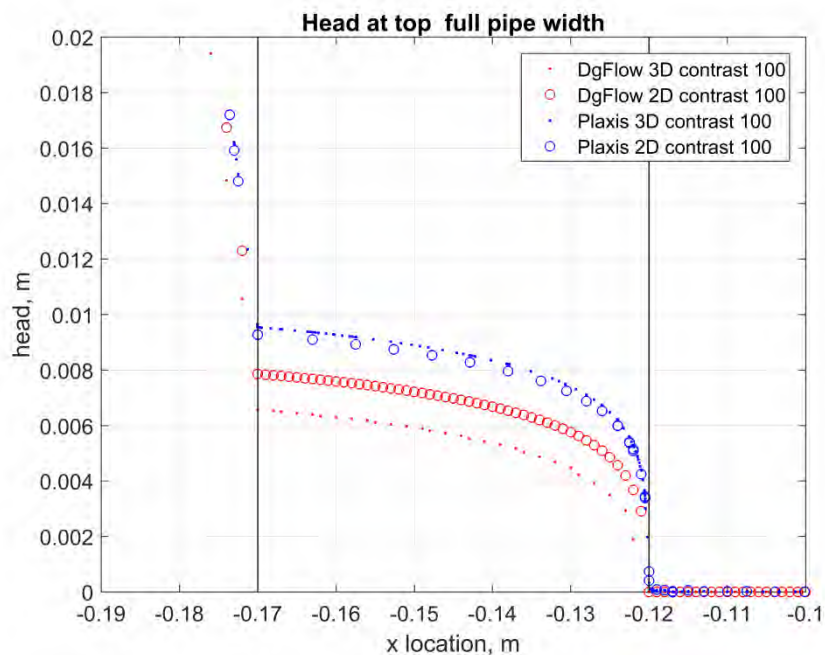


Figure 2.6 Head in the central axis of the model. Barrier is between -0.12 and -0.17 m

For the contrast 100 the head values are very low in the barrier. In this case there is more difference between the DgFlow 3D and 2D simulations; the 2D simulation gives a higher head in the barrier than the 3D model. Both DgFlow simulations give a lower head than the two Plaxis simulations.

### 3 Local gradients

The gradient is computed over the entire barrier and also over a 3.5 cm stretch between the interface between the barrier and the pipe and 3.5 cm upstream of this (-120 mm to -155 mm from the centre of the model) and between 1 cm upstream of the interface between the barrier and the pipe and 4.5 cm upstream of this (-0.130 mm to -165 mm from the centre of the model). This latter gradient is the damage criterion that is used in this phase of the analyses.

The tables below show the gradients from the different models and the ratio of the gradient in the DgFlow model, to the gradient in the Plaxis model.

As expected from the head profiles, difference between the gradients is largest for the models with a high permeability contrast and then it is larger for the 3D model than for the 2D model.

Table 3.1 Gradients from the models

Model name	2D/3D	Permeability barrier	Permeability fine	Permeability contrast	Gradient from model at y=0		
					m/s	m/s	
					from -120 to -170 mm	from -120 to -155 mm	From-130mm to -165 mm
S_2D_k1_w1	2	2.0E-03	6.0E-04	3	1.59	1.93	0.89
S_2D_k2_w1	2	6.0E-02	6.0E-04	100	0.16	0.21	0.05
S_2D_k3_w1	2	6.0E-04	6.0E-04	1	2.66	2.98	1.98
S_3D_k1_w1	3	2.0E-03	6.0E-04	3	1.67	2.03	0.95
S_3D_k2_w1	3	6.0E-02	6.0E-04	100	0.13	0.17	0.06
S_3D_k3_w1	3	6.0E-04	6.0E-04	1	2.83	3.18	2.04
Plaxis_2D_k1	2	2.0E-03	6.0E-04	3	1.56	1.90	0.88
Plaxis_2D_k2	2	6.0E-02	6.0E-04	100	0.17	0.23	0.05
Plaxis_2D_k3	2	6.0E-04	6.0E-04	1	2.64	2.95	2.00
Plaxis_3D_k1	3	2.0E-03	6.0E-04	3	1.78	2.21	0.93
Plaxis_3D_k2	3	6.0E-02	6.0E-04	100	0.18	0.24	0.05
Plaxis_3D_k3	3	6.0E-04	6.0E-04	1	2.92	3.35	2.01

Table 3.2 Comparison of gradients from DgFlow and Plaxis

Permeability contrast/ dimensions	DgFlow/Plaxis		
	from -120 to -170 mm	from -120 to -155 mm	From-130mm to -165 mm
contrast 3: 2D	1.02	1.02	1.01
contrast 100: 2D	0.92	0.92	1.02
contrast 1: 2D	1.01	1.01	0.99
contrast 3: 3D	0.94	0.92	1.02
contrast 100: 3D	0.73	0.72	1.03
contrast 1: 3D	0.97	0.95	1.02

## 4 Conclusion

- DgFlow and Plaxis produce similar results for the head distributions and this results in similar gradients over the barrier.
  - If there is a difference, Plaxis gives a higher head than DgFlow in the barrier.
  - The gradient is sometimes higher and sometimes lower in DgFlow than in Plaxis.
  - The largest difference is for the 3D models with a large permeability contrast. For the permeability contrast of 100 the ratio of the DgFlow result over the Plaxis result is 1.03. This is for the gradient between -130 mm (1 cm upstream of the interface between the barrier and the pipe) and -165 mm (i.e. the distance of the damage criterion to be used in this phase of the project).
- For large permeability contrasts the gradients in the barrier are so low that these are very sensitive to small differences in head. This suggests a limited accuracy of the modelled gradients.
- For equal permeabilities, i.e. no barrier, the 3D DgFlow model approximates the 2D models better than the Plaxis 3D model. As the 2D DgFlow model was found to model the analytical solution for this configuration well (refer to Appendix B of the main report) this shows that the 3D DgFlow model also better fits the analytical solution for that configuration.

**D Report XI.17.11 Deltares Coarse sand barrier (numerical simulations)**

**REPORT XI.17.11**  
**DELTARES**  
**Coarse sand barrier (numerical simulations)**

## Content

1. Introduction.....	3
2. Numerical model.....	4
2.1 Dimensions experimental setup.....	4
2.2 Pipe dimensions .....	5
2.3 Soil characteristics.....	6
2.4 Boundary conditions .....	7
3. Meshing.....	8
4. Results.....	15
4.1. Contrast: 1.....	16
4.1.1. Flow velocity distributions.....	16
4.1.2. Pore pressure distributions .....	21
4.2. Contrast:3.....	23
4.2.1. Flow velocity distributions.....	23
4.2.2. Pore pressure distributions .....	27
4.3. Contrast:10.....	29
4.3.1. Flow velocity distributions.....	29
4.3.2. Pore pressure distributions .....	33
4.4. Contrast:100 .....	35
4.4.1. Flow velocity distributions.....	35
4.4.2. Pore pressure distributions .....	39
5. Overview .....	42

## 1. Introduction

The present project was requested by Deltares and it was classified under the internal code number XI.17.11.

This project concerns numerical simulations of small-scale backward erosion piping experiments including a coarse sand barrier with the numerical software Abaqus. The numerical calculations analyze the groundwater flow at the moment the pipe forms a T-shape between the downstream exit and the barrier. Four calculations are performed and analyzed, in which the permeability of the barrier varies from equal to the permeability of the sand to 100 times larger.

First, a numerical model is to be set up, taking into account the setup dimensions, barrier dimensions, pipe dimensions, boundary conditions and soil characteristics.

The mesh refinement needs to be optimized in the different parts of the model.

In the end, the flow velocity at the pipe tip, and the hydraulic gradient at several locations in the model are extracted from the results and analyzed.

The exact dimensions, boundary conditions and desired results are provided by Deltares.

## 2. Numerical model

### 2.1 Dimensions experimental setup

The setup dimensions are: length = 483 mm, width = 300 mm, height = 101 mm, distance between upstream filter and center of exit hole = 348 mm, diameter of exit hole = 24 mm.

A coarse sand barrier with a width of 50 mm is present over the entire height of the setup from a distance of 178 mm from upstream until 228 mm, see Figure 1 and Figure 2.

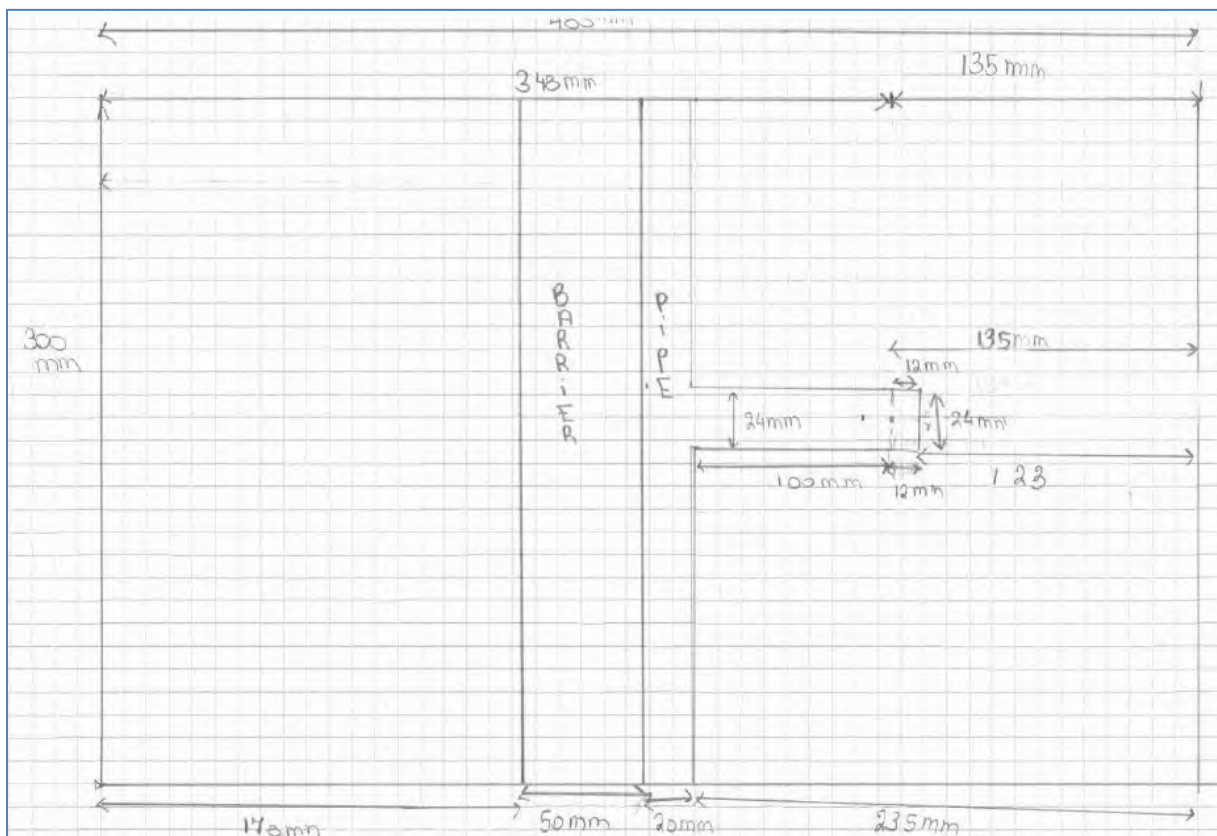


Figure 1 Model dimensions (provided by Deltares)

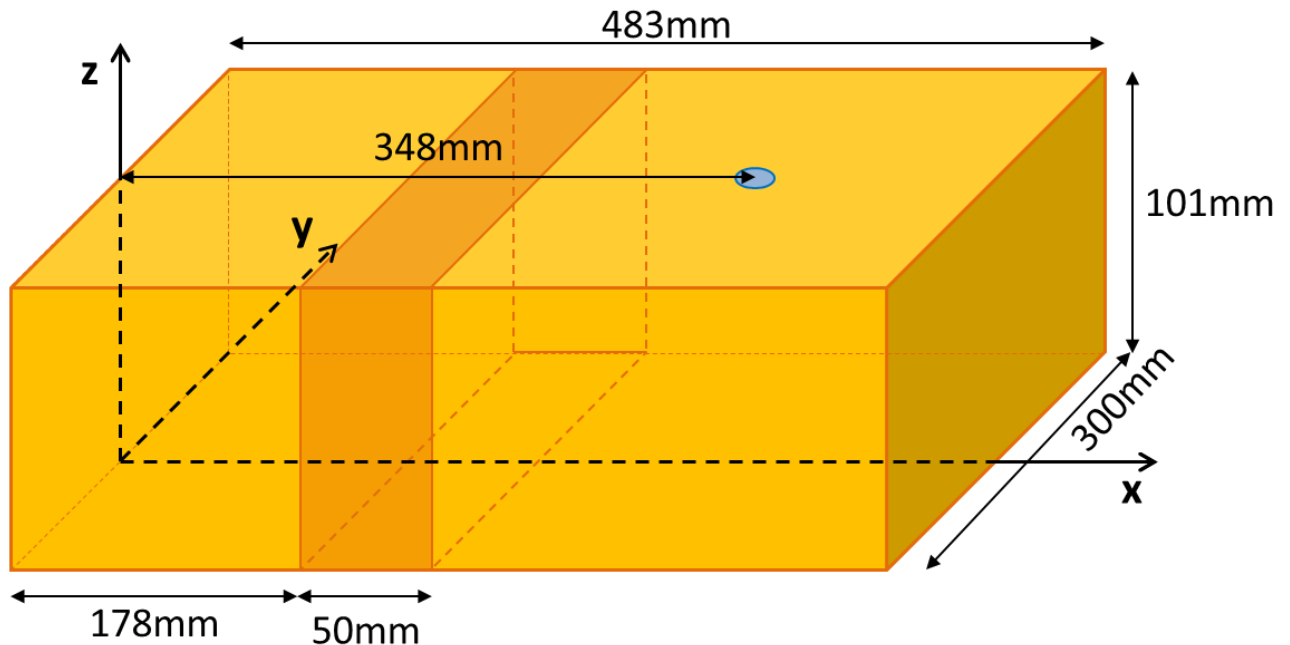


Figure 2 Model dimensions

## 2.2 Pipe dimensions

The numerical model is made for the situation that application of a hydraulic gradient has caused backward erosion piping. We are examining the situation in which the pipe has grown from the downstream exit towards the coarse sand barrier where it widened to the left and right forming a T-shape, see Figure 3. For the analysis, the T-shaped pipe is subdivided in the 'main pipe', i.e. the pipe connecting the downstream exit to the barrier and the 'side pipe' which is along the barrier.

The main pipe has a constant width of 24 mm and a depth decreasing linearly from the exit hole (10 mm) to the side pipe (5 mm). The sides of the pipe are vertical. For numerical simplicity, the downstream side of the pipe is assumed half circular, following to the shape of the exit hole (unlike the angular shape as drawn in Figure 3), see Figure 4.

The side pipe has a constant width at the bottom of 20 mm and its depth varies linearly from 5 mm at the center to 2.5 mm at the outer left and right of the setup. The downstream sides of the side pipe are vertical, while the upstream sides at the barrier are at 45°. The bottom of the side pipe touches the barrier and because of the inclined sides, the top of the pipe is located in the barrier. Because of the linearly decreasing depth of the pipe, the top of the pipe lies within the barrier for 5 mm at the center and only 2.5 mm at the sides of the setup.

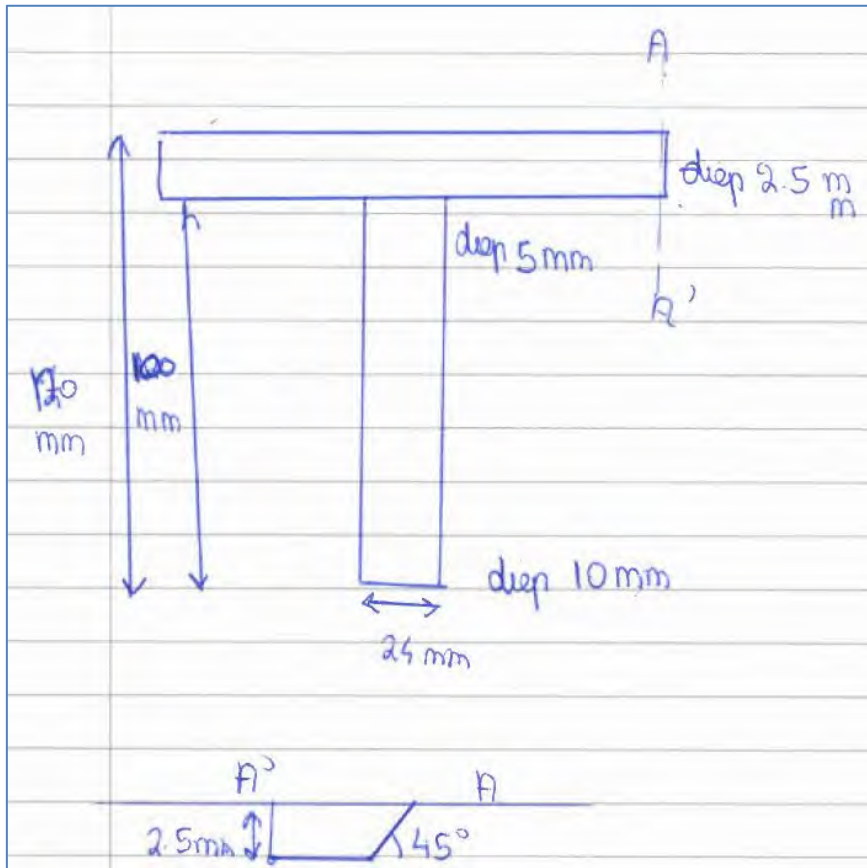


Figure 3 Pipe dimensions (provided by Deltares)

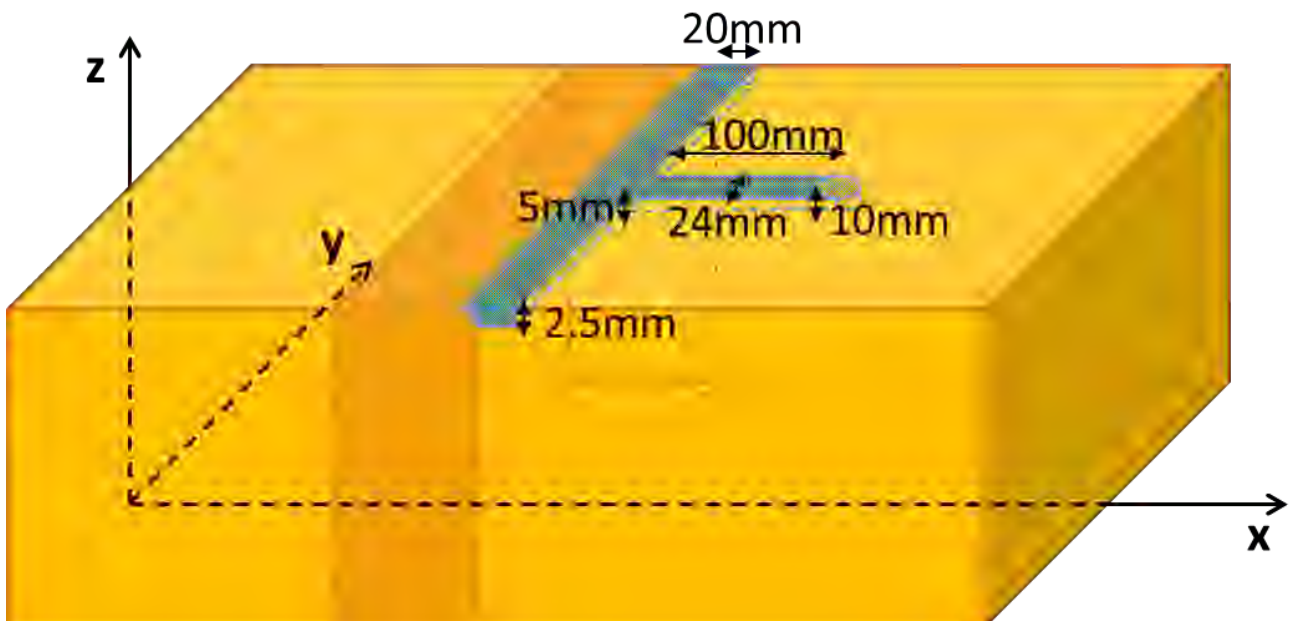


Figure 4 Pipe dimensions

### 2.3 Soil characteristics

The model considers water flow only, so the elastic properties are of no importance and all deformations are blocked in the model.

The permeability of the sand is constant for the four cases and equal to  $6 \cdot 10^{-4}$  m/s, while the permeability of the coarse sand barrier varies from  $6 \cdot 10^{-4}$  m/s to  $6 \cdot 10^{-2}$  m/s, see Table 1.

Table 1 Permeability sand and barrier for the four cases

	Case 1	Case 2	Case 3	Case 4
Contrast:	1	3	10	100
Fine sand:	6.00E-04	6.00E-04	6.00E-04	6.00E-04
Barrier:	6.00E-04	2.00E-03	6.00E-03	6.00E-02

The permeability of the pipes were analytically determined and provided by Deltares as 20 m/s for the main pipe and 5 m/s for the side pipe.

## 2.4 Boundary conditions

Because of the symmetry of the model, it is possible to model only half of the model and apply symmetry conditions.

As mentioned before, all deformations and displacements are blocked.

A hydraulic head difference of 0.4 m or 4 kPa is applied in all cases. This means that the difference in hydraulic head between the top of the upstream filter and the outflow opening is 4 kPa. The pore pressure distribution along the upstream filter increases linearly from top to bottom according to the hydraulic pressure. It is chosen to apply a pore pressure of 10 kPa at the bottom, corresponding to a pore pressure of 8.99 kPa at the top. Therefore, the pore pressure that needs to be applied at the downstream exit is 4.99 kPa (constant in the entire exit), see Figure 5.

All other boundaries are impermeable.

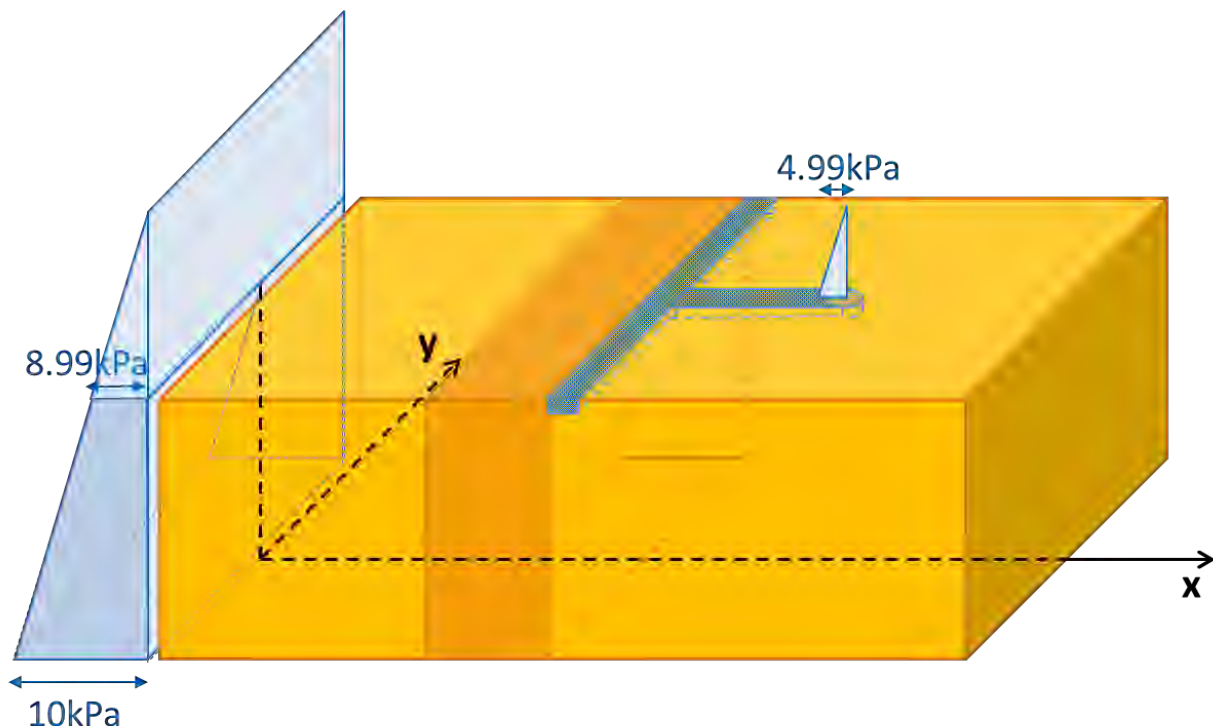


Figure 5 Pore pressure boundaries

### 3. Meshing

In order to enable meshing of the complex geometry, the numerical model is divided into several parts, which are connected to each other by means of 'ties' for the analysis to ensure continuity of the water flow. Figure 6 shows the model geometry divided into the various parts. Some partitions are added in order to enable further mesh refinement within a part.

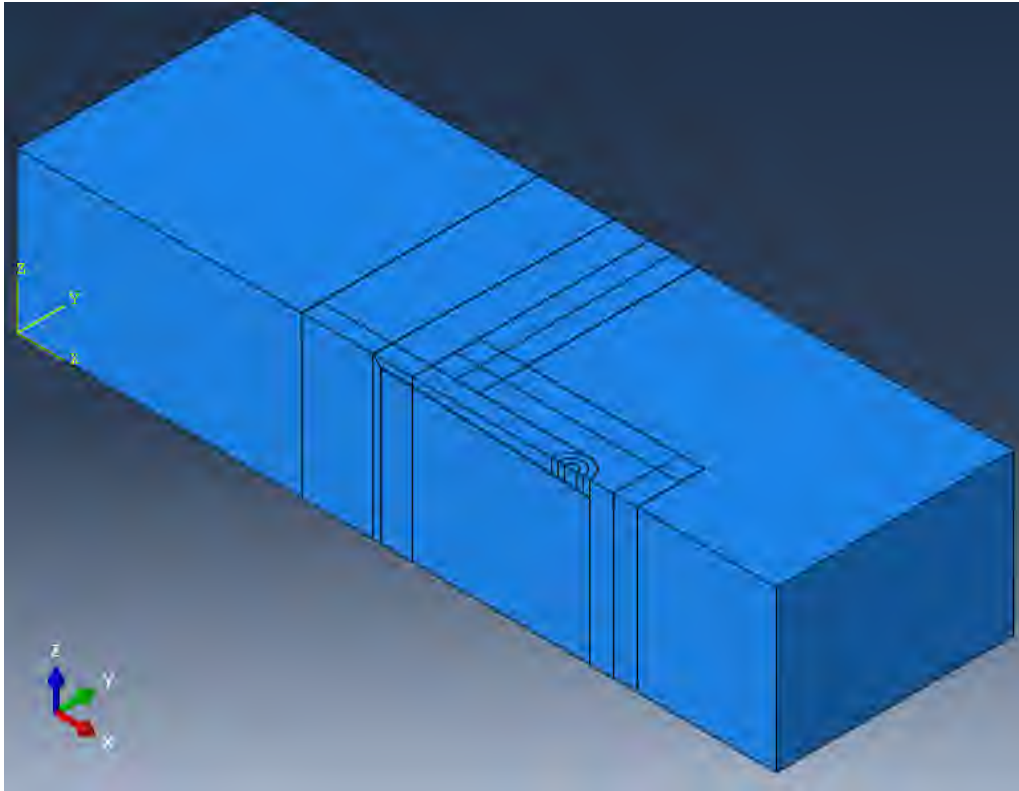


Figure 6 Numerical model geometry divided in parts

The necessary mesh refinement in every part is determined by analyzing the influence of mesh refinement in every part. For this purpose, the flow velocity, the flow velocity in x-direction and the pore pressure at the center line and the total flow through the exit hole are compared for different mesh refinements. For each part, the mesh is refined until the results do not change anymore.

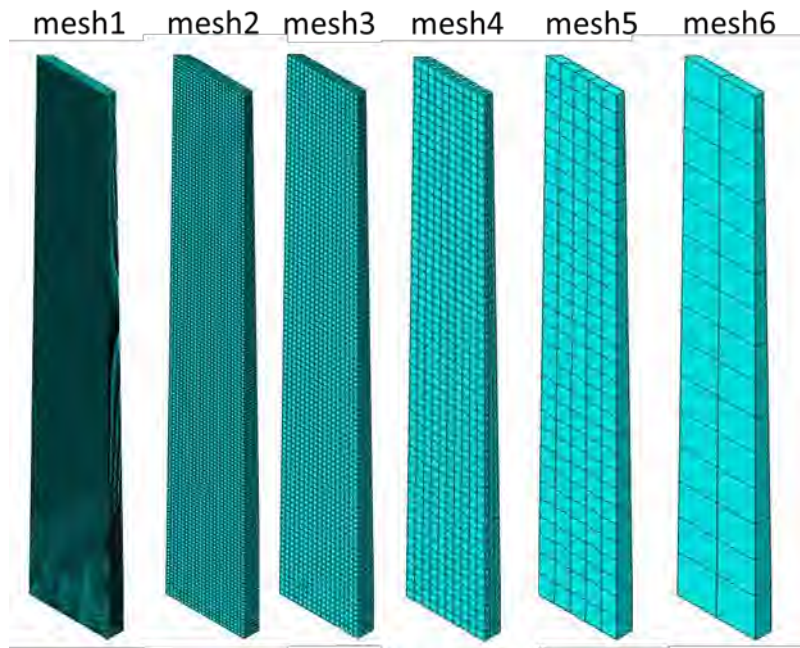


Figure 7 mesh refinement of the side pipe

The mesh refinement of the side pipe for the simulation with contrast 3 is used as an example here. To start, all parts are meshed according to a mesh refinement which seems reasonable based on previous experience. Then, the mesh refinement of each part is assessed separately. Figure 7 shows the various meshes which were used, going from very fine (mesh dimensions mesh 1: 0.5 mm\*0.5 mm\*0.5 mm) to very coarse (mesh dimensions mesh 6: 10 mm\*10 mm\*10 mm).

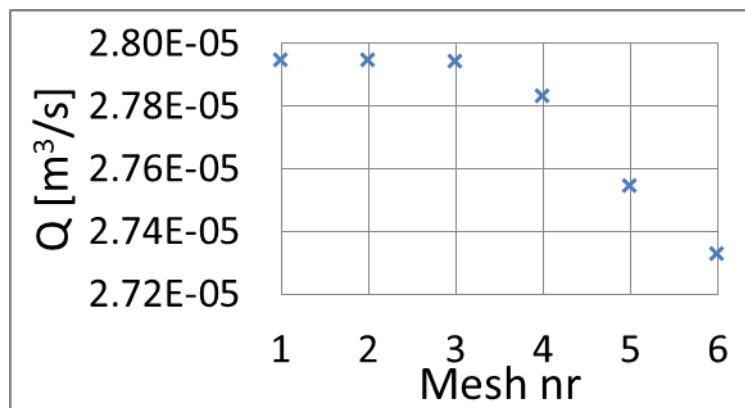


Figure 8 Numerical flow rate through hole-type exit for various mesh refinements of the side pipe

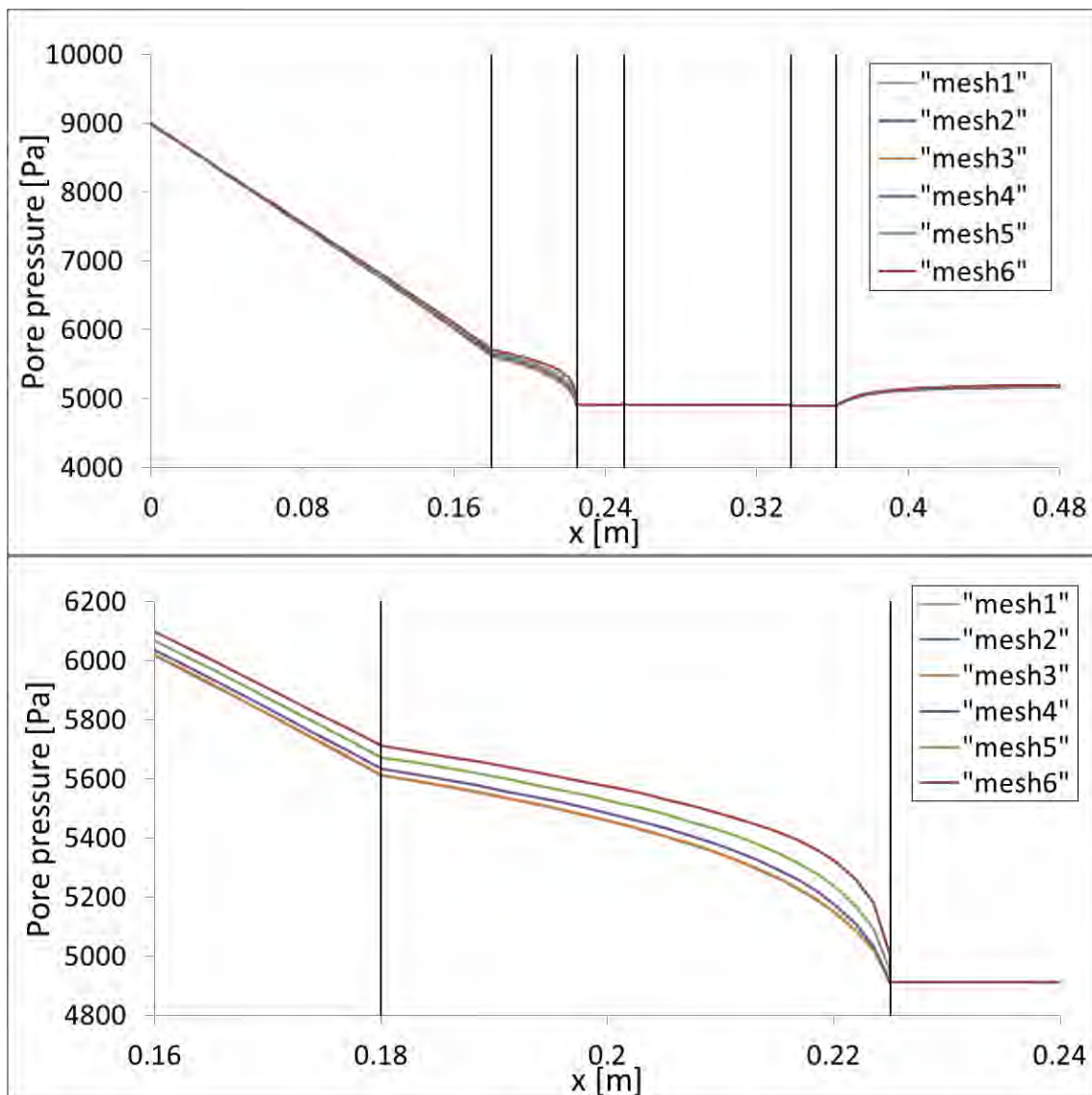


Figure 9 Pore pressure distribution along the center line for various mesh refinements of the side pipe

Figure 8 shows the obtained flow rate through the hole-type exit. The flow rate is slightly lower for mesh 4, 5 and 6, but despite the difference in mesh refinement, the difference in flow rate is limited. Figure 9 shows the pore pressure distribution along the center line of the setup. For mesh 1, 2 and 3, the obtained pore pressure distribution is the same (the curves overlap each other) while it deviates for coarser meshes. The black vertical lines indicate the position of the transition from sand to barrier, side pipe, main pipe, hole and sand. The flow velocity at the center line of the setup is shown in Figure 10 while the x-component (in the direction from upstream to downstream) is shown in Figure 11. It is found that the value of the peak at the transition from the main pipe to the hole-type exit is larger for finer meshes (singularity). Again it is found that for mesh 1, 2 and 3 the curves overlap, while the curves for coarser meshes deviate. In this case it was decided that mesh refinement 3 is sufficient to decently model the pore pressure and flow velocity distribution throughout the setup. Then, this mesh of the side pipe was used to continue the mesh refinement of a next part.

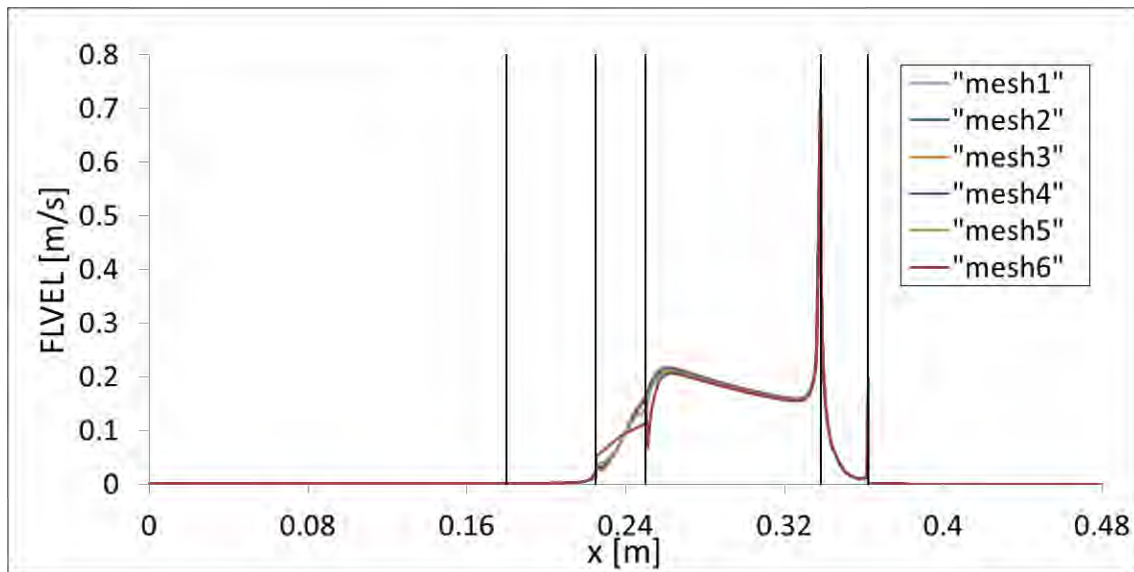


Figure 10 Flow velocity at the center line for various mesh refinements of the side pipe

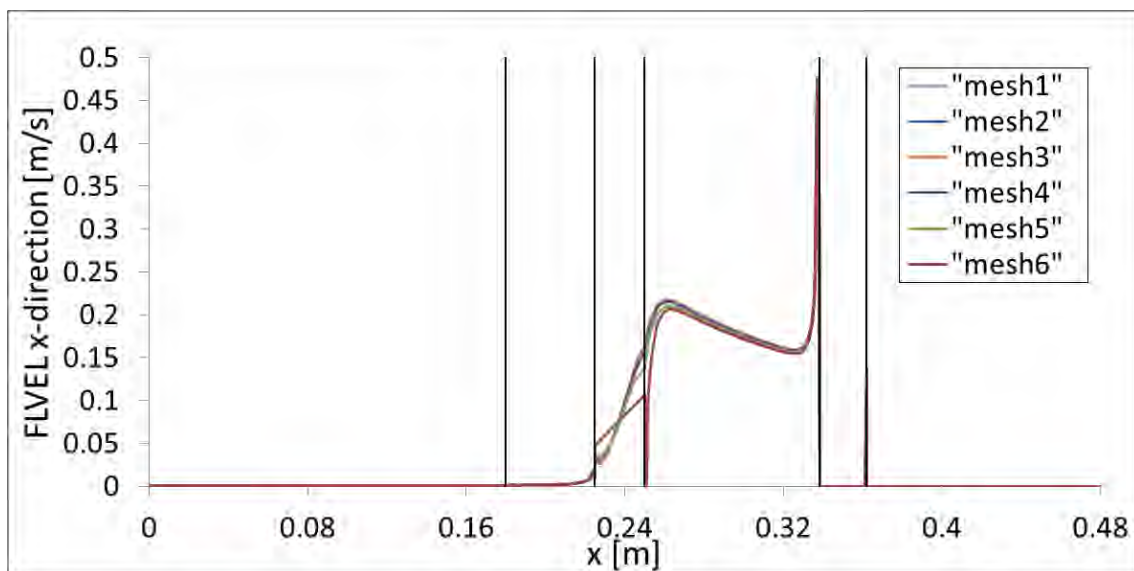


Figure 11 Flow velocity in x-direction at the center line for various mesh refinements of the side pipe

The final mesh refinement obtained for the simulations with contrast 3 is shown in Figure 12. The mesh elements are very fine within the pipes and close to the pipes, and are relatively coarse at the bottom of the model and downstream of the exit hole.

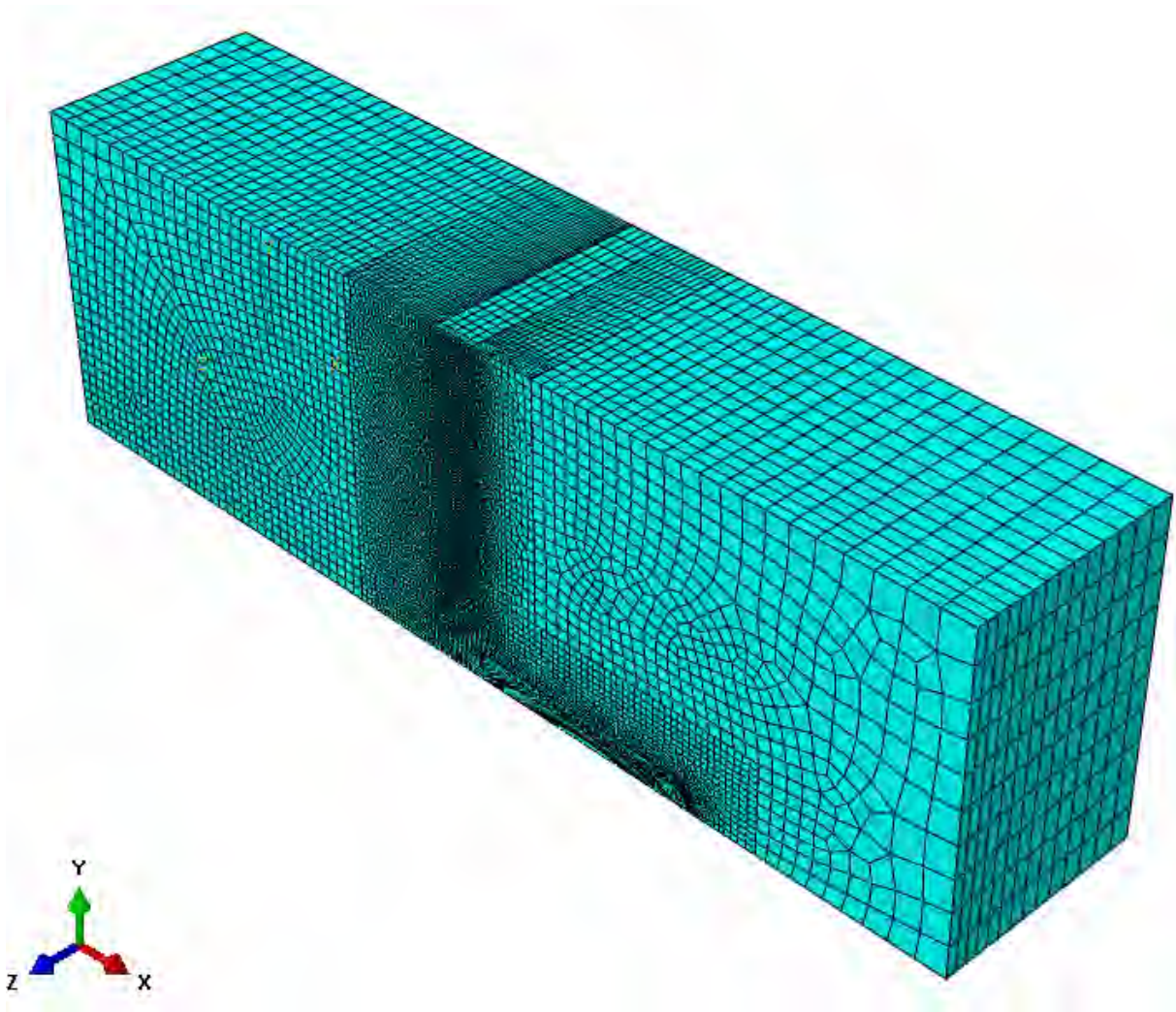


Figure 12 Mesh refinement for model with contrast 3

During the mesh refinement analysis, it was found that the used dimensions in the numerical model slightly deviate from the actual dimensions: the length of the sand package upstream of the barrier was 0.18 m instead of 0.178 m and the length of the sand package downstream of the hole-type exit was 0.118 m instead of 0.123 m. Also, the applied pore pressure at the downstream exit was 4900 Pa instead of 4990 Pa and there was a problem with the connection between the barrier and the side pipe over a small length, due to the complicated geometry. Because of the limited time frame given to finish the project, it was impossible to redo the mesh refinement analysis. Since the deviations are small anyhow, it is expected that they won't have any influence on the mesh refinement. Therefore, the obtained mesh refinement is maintained, and the deviations are corrected to analyze the final results. The mesh refinement in case of the correct dimensions is shown in Figure 13, it is clear that the difference with Figure 12 is minimal.

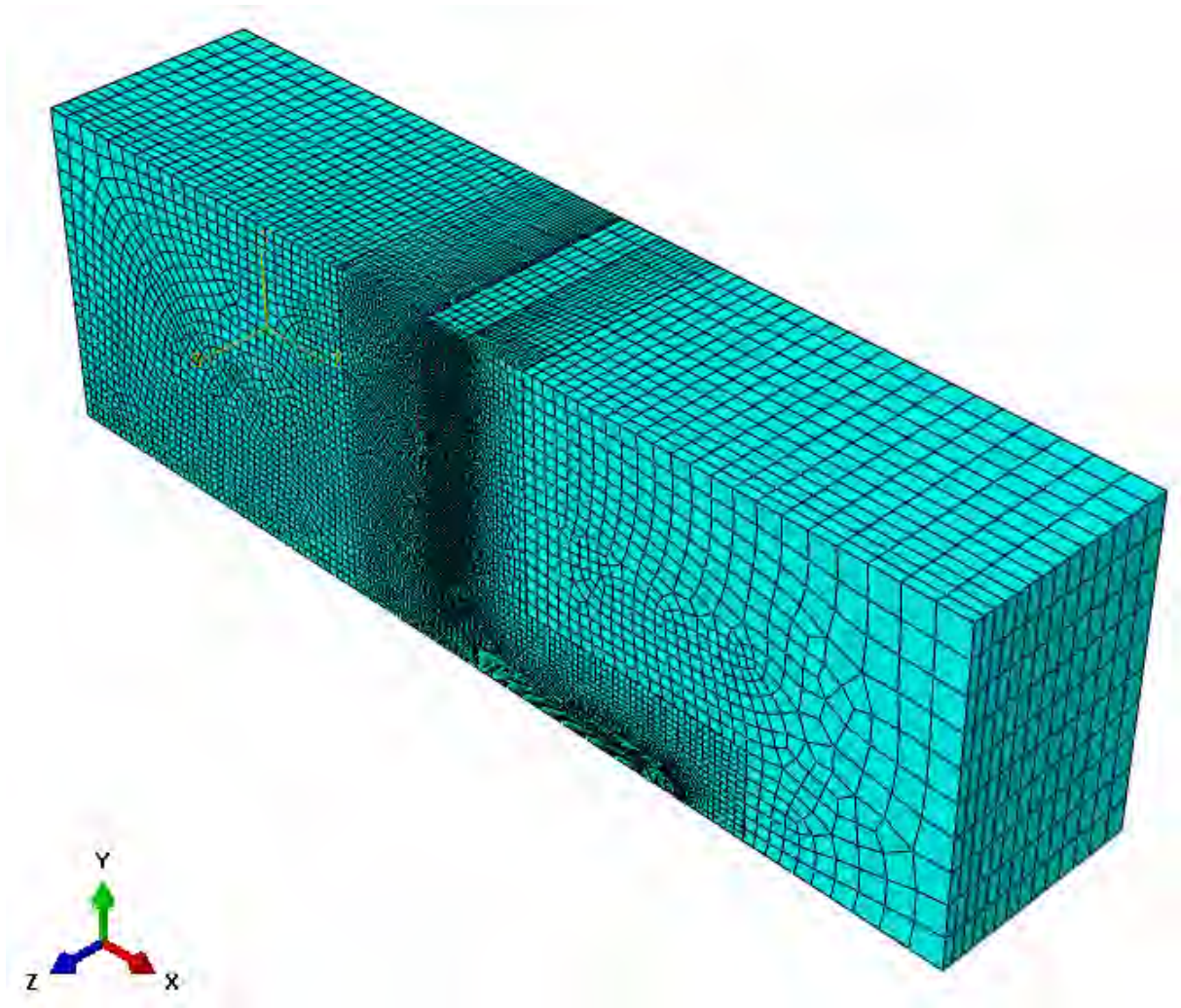


Figure 13 Mesh refinement for model with contrast 3 with correct dimensions

For the models with contrast 1, 10 and 100, the optimal mesh refinement may deviate from the one obtained for the model with contrast 3. Because of the limited time frame for this project however, it was impossible to overdo the mesh refinement three more times. Therefore, the mesh refinement for the model with contrast 3 is used as a basis, for which the mesh size in the barrier and at the transition from barrier to other parts (upstream, pipe, soil below pipe) is refined a little more to be sure, see Figure 14.

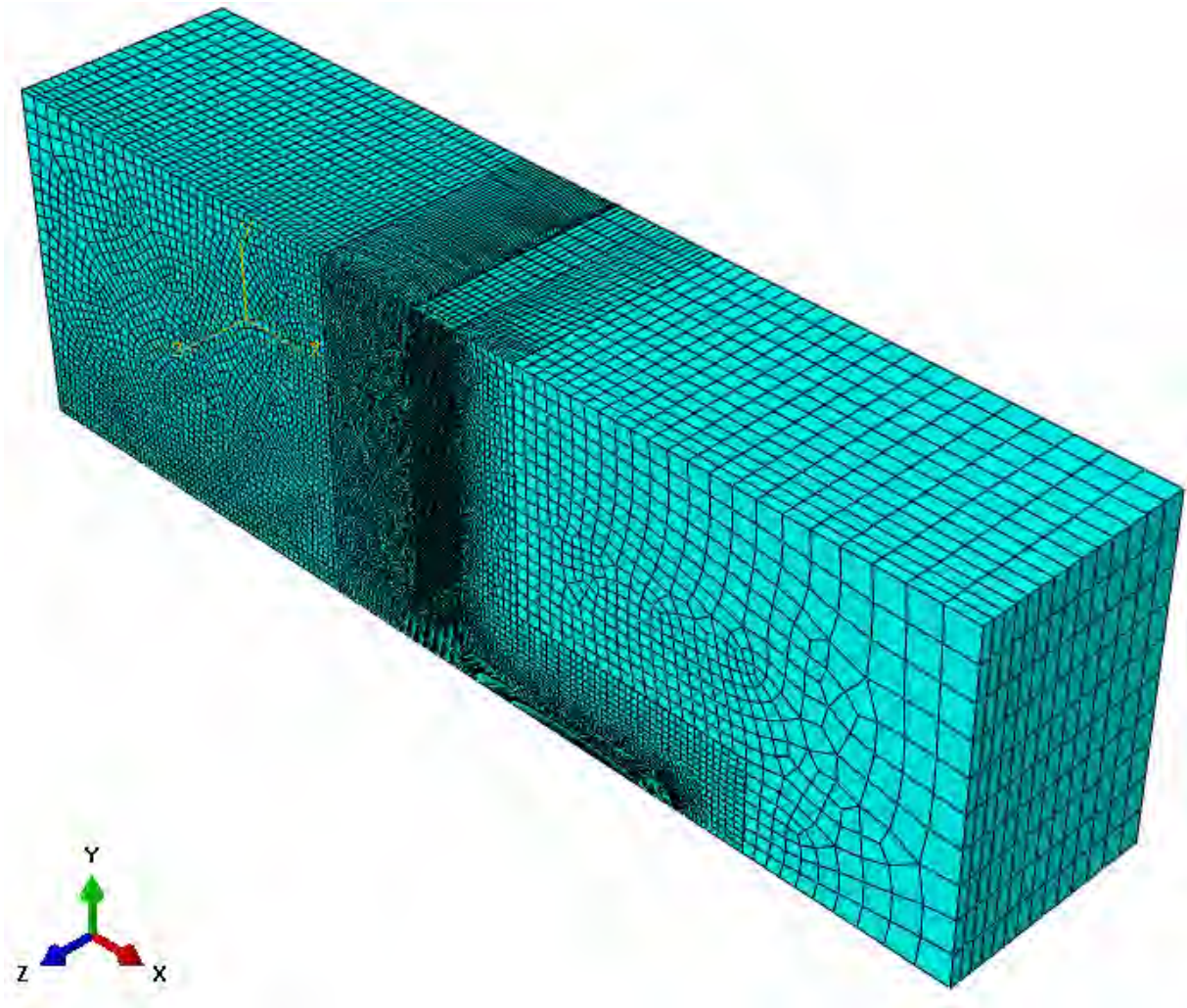


Figure 14 Mesh refinement for model with contrast 1, 10 and 100

## 4. Results

It was asked to present following results:

- Flow velocity at pipe tip
- Pore pressure distribution throughout the setup
- Pore pressure at center line
- Pore pressure in barrier at a distance of 0.0375 m ( $1/4 \cdot 0.15$  m) and at a distance of 0.1125 m ( $3/4 \cdot 0.15$  m) from the center line but parallel to the center line

(see also Figure 15)

In the following sections, these results are presented for the different 'permeability contrasts'. All results (except contour plots and vector plots) are also collected in an excel file.

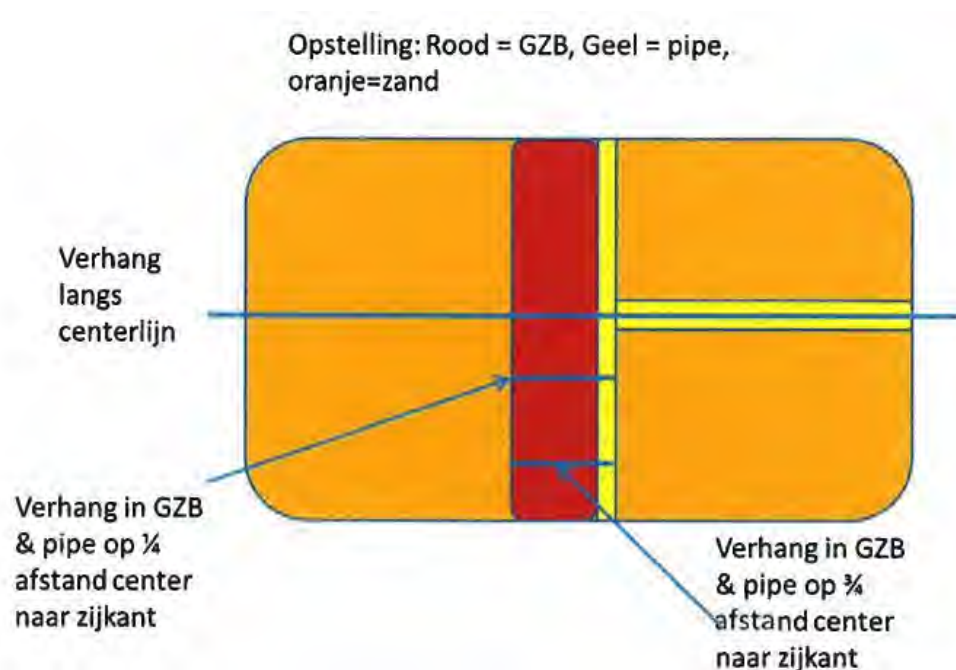


Figure 15 Asked results

4.1. Contrast: 1

4.1.1. Flow velocity distributions

Figure 16 to Figure 18 show the contour plots of the flow velocity in the setup. The highest flow velocities are obtained near the exit hole and within the pipes.

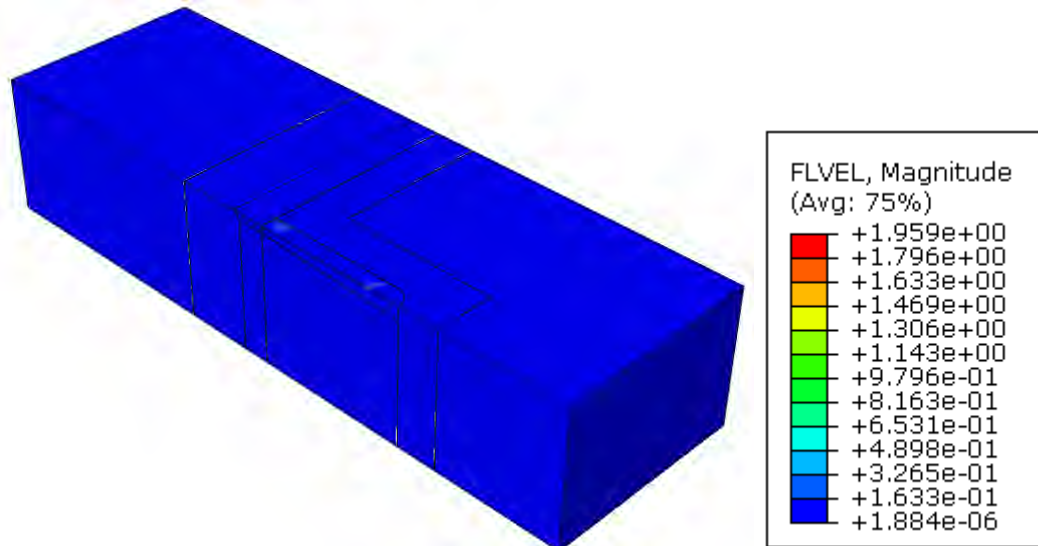


Figure 16 Contour plot of flow velocity for model with contrast 1

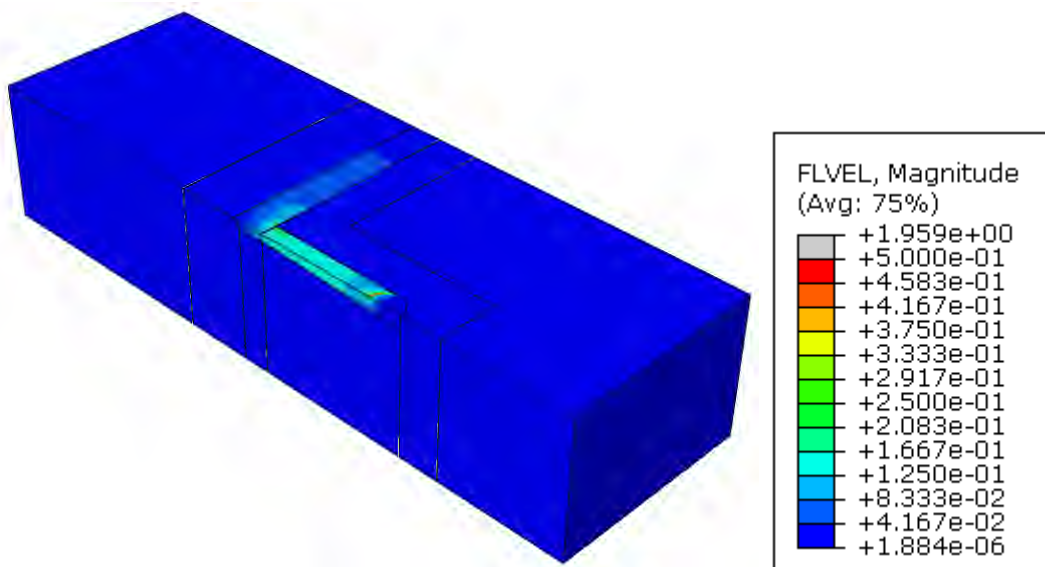


Figure 17 Contour plot of flow velocity for model with contrast 1 with maximum flow velocity 0.5 m/s

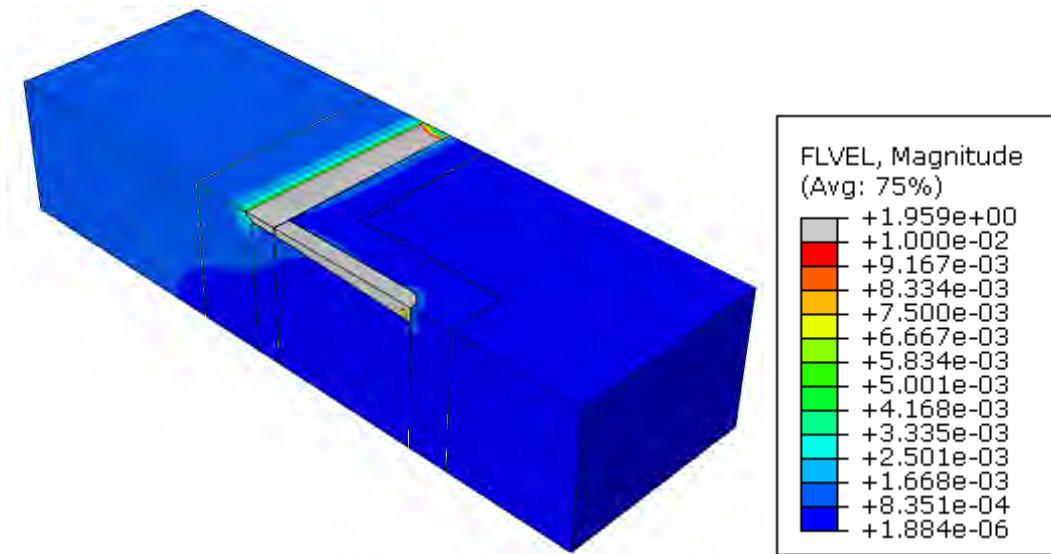


Figure 18 Contour plot of flow velocity for model with contrast 1 with maximum flow velocity 0.01 m/s

Figure 19 to Figure 21 show vector plots of the same results. Figure 22 shows a detail of the flow lines in the side pipe and main pipe.

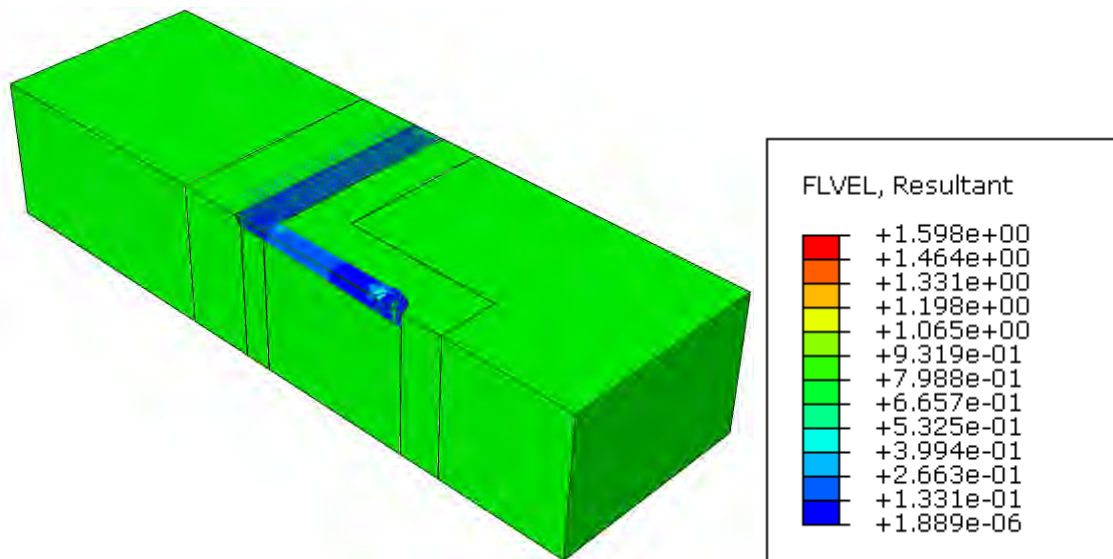


Figure 19 Vector plot of flow velocity for model with contrast 1

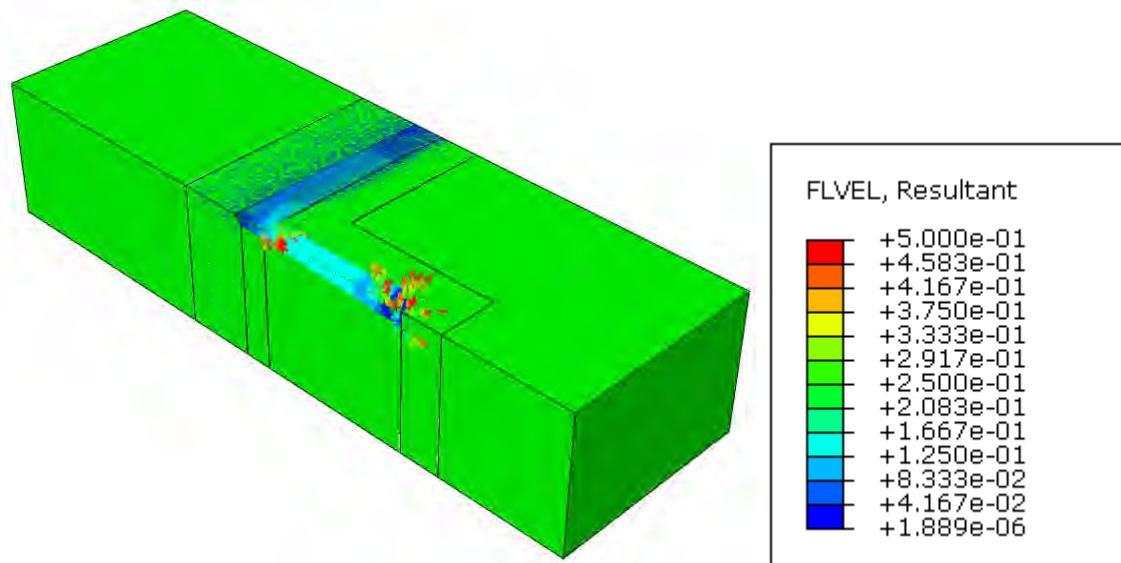


Figure 20 Vector plot of flow velocity for model with contrast 1 with maximum flow velocity 0.5 m/s

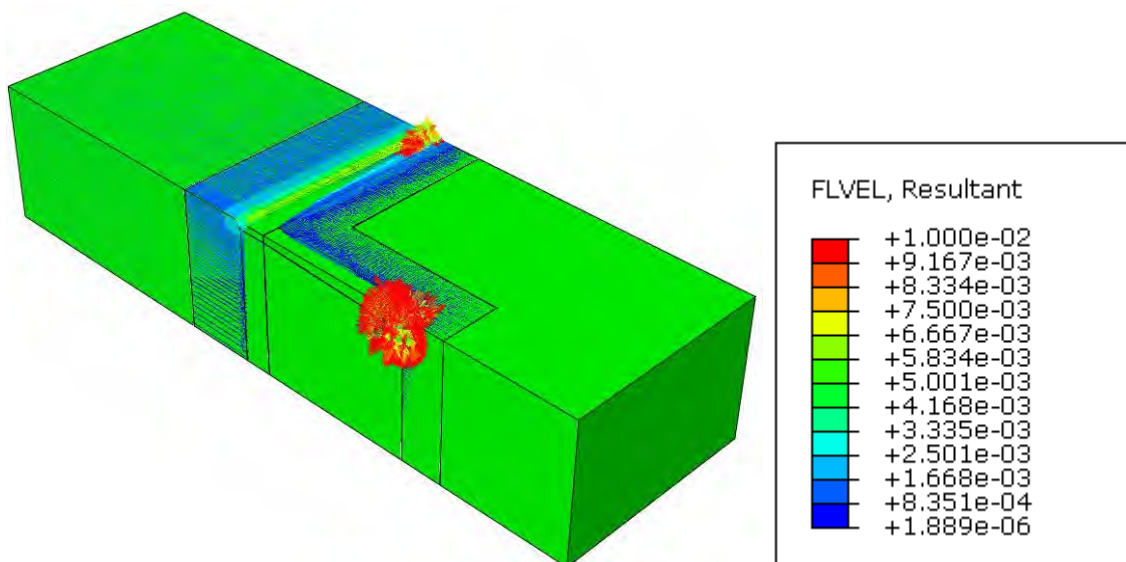


Figure 21 Vector plot of flow velocity for model with contrast 1 with maximum flow velocity 0.01 m/s

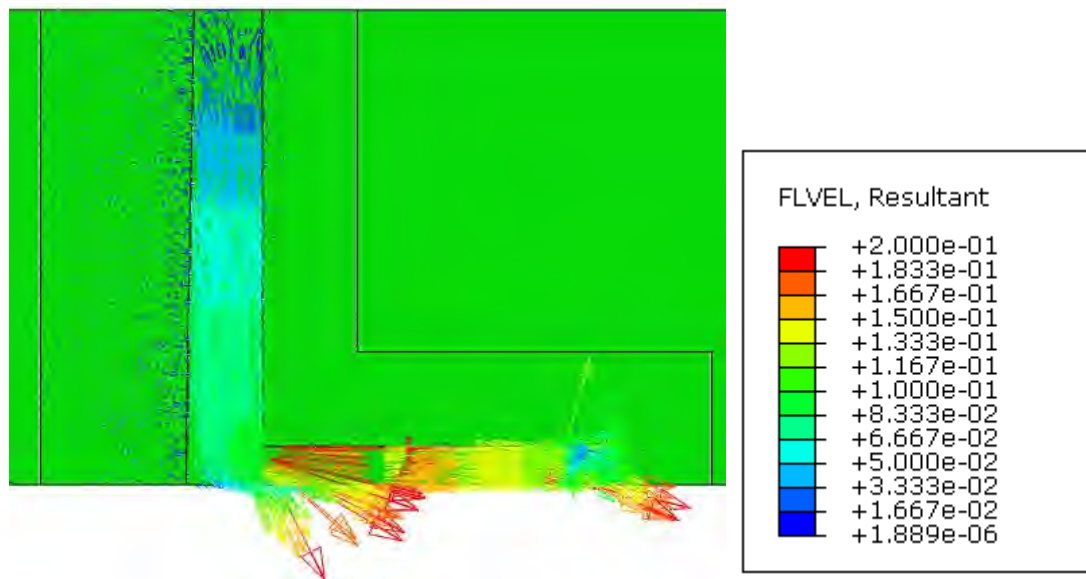


Figure 22 Bended flow lines at transition from side pipe to main pipe (top view) for the model with contrast 1

Figure 23 and Figure 24 show the flow velocity and the x-component of the flow velocity respectively at the center line of the geometry, at a distance of 0.0375 m ( $1/4 \cdot 0.15$  m) and at a distance of 0.1125 m ( $3/4 \cdot 0.15$  m) from the center line but parallel to the center line as a function of x. The vertical black lines represent the transition from one part to another.

It is clear that both the flow velocity and the x-component of the flow velocity at the center line (green lines) are very small in the sand and in the barrier, are high in the pipes and reach a maximum at the singularity at the transition from pipe to exit hole. At a distance of  $1/4$  and  $3/4$  from the center line, the main pipe and exit hole are not passed, and thus only an increased velocity is obtained within the side pipe. The flow velocity is larger close to the center line (close to the main pipe) and thus larger at a distance of  $1/4$  than at a distance of  $3/4$ . The x-component of the flow velocity is rather small at a distance of  $1/4$  and  $3/4$  from the center line, because flow lines are mainly going in y-direction to transport the water which entered the side pipe to the main pipe (see Figure 22), resulting in a high general flow velocity because of the y-component and a limited x-component.

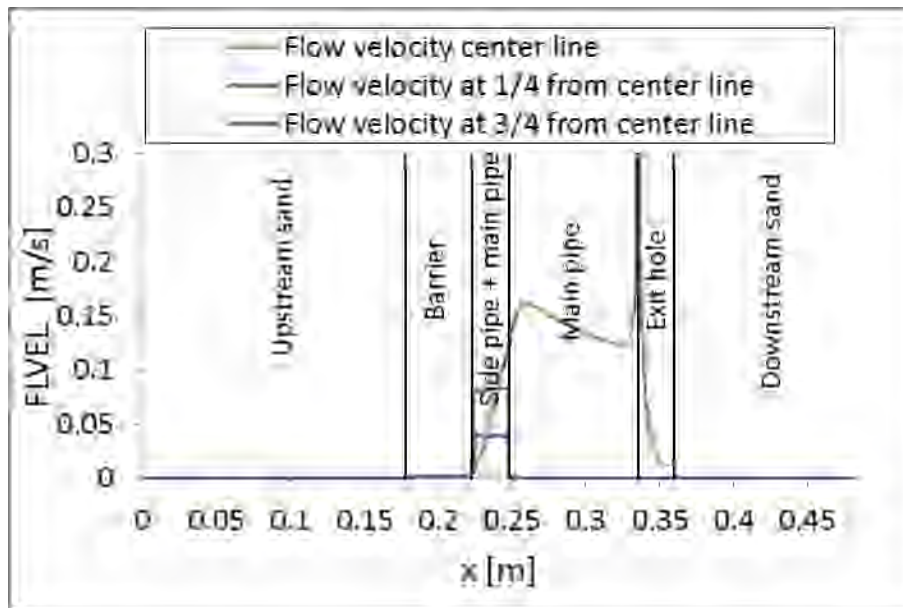


Figure 23 Flow velocity at the center line, at 1/4 from center line and at 3/4 from center line for the model with contrast 1

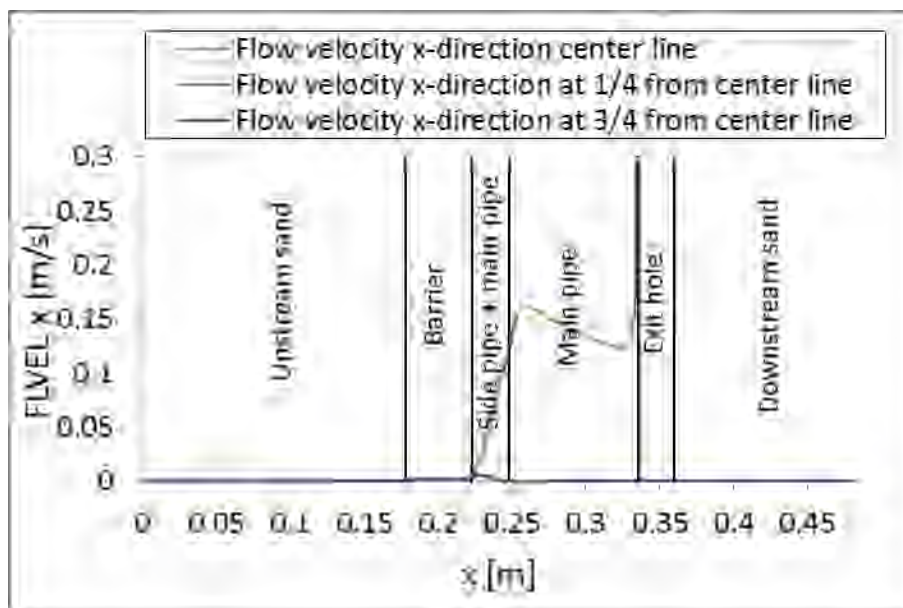


Figure 24 Flow velocity in x-direction at the center line, at 1/4 from center line and at 3/4 from center line for the model with contrast 1

Figure 25 shows both the flow velocity and the x-component of the flow velocity at the transition from the barrier to the pipe at  $x = 0.223$  m as a function of  $y$ , at the top, center and bottom of the side pipe. The vertical black line is placed at the level where, for larger  $x$ -values, the confluence of the main pipe and side pipe is located.

At small  $y$ -values, the flow in  $x$ -direction dominates to directly transport the water from upstream to the main pipe, while at larger  $y$ -values the  $y$ -component becomes more dominant.

The undulations at the top and center are probably caused by the sudden transition from barrier to pipe. With a further mesh refinement at this location, they would probably disappear; although the results at this line were not taken into account for the

mesh refinement, mesh refinement of this line was included and chosen fine enough to have no influence on the total flow velocity and on the results on the center line, as was found in section 3.

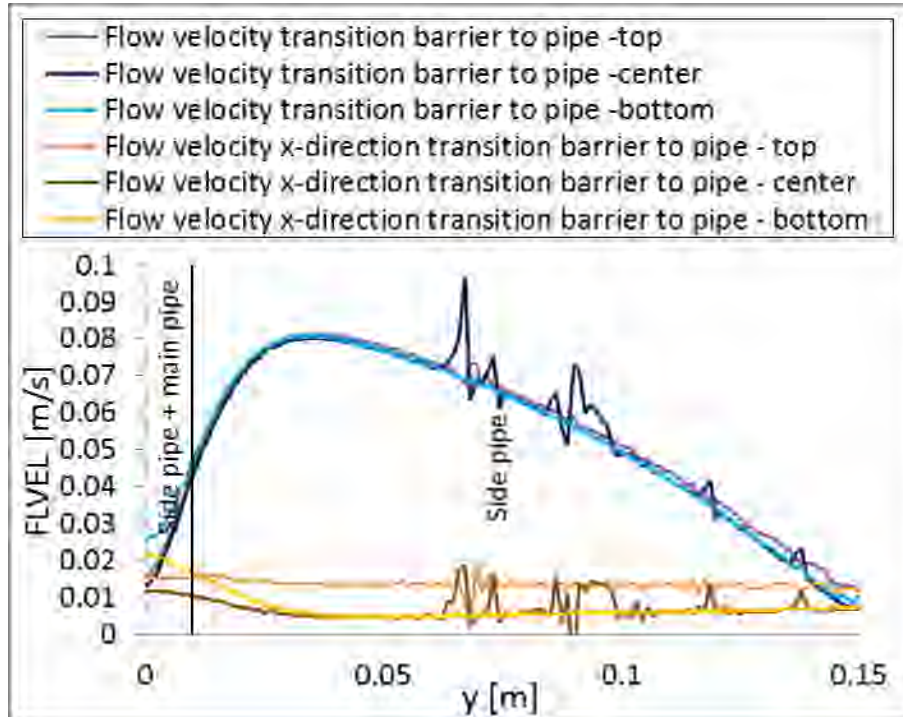


Figure 25 Flow velocity and flow velocity in x-direction at the transition from barrier to pipe line for the model with contrast 1

#### 4.1.2. Pore pressure distributions

Figure 26 shows the contour plot of the pore pressure throughout the model. Again, the distribution is as applied: a hydraulically varying pore pressure at the upstream side with a value of 8990 Pa at the top and a constant value of 4990 Pa at the downstream exit.

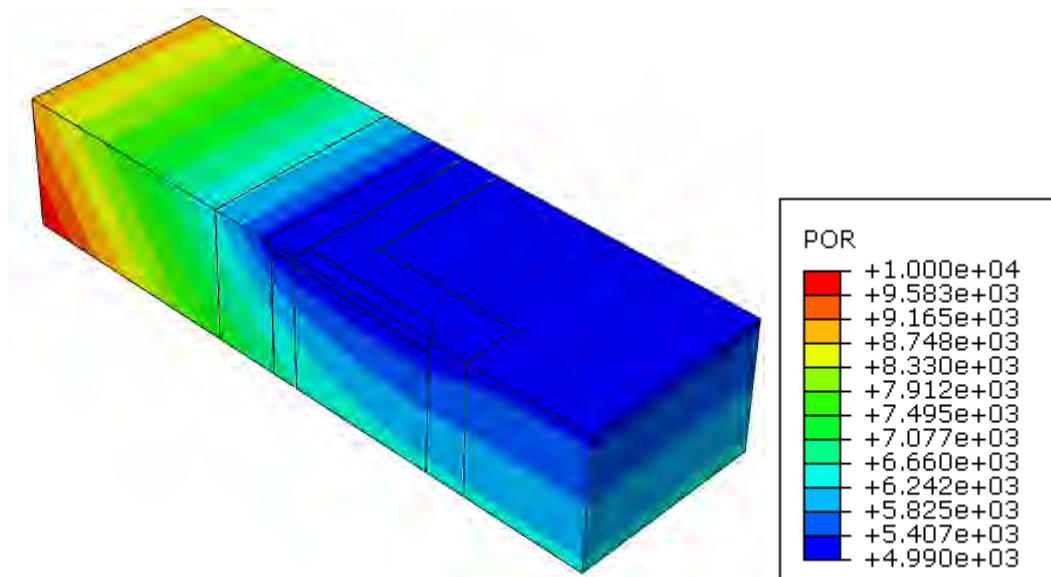


Figure 26 Contour plot of pore pressure for model with contrast 1

Figure 27 shows the variation of the pore pressure at the center line of the geometry, at a distance of 0.0375 m ( $1/4 \cdot 0.15$  m) and at a distance of 0.1125 m ( $3/4 \cdot 0.15$  m) from the center line but parallel to the center line as a function of  $x$ . It is clear that the pore pressure in the pipes is more or less equal to the pore pressure at the exit hole, which is caused by the high permeability of the pipes (20 m/s and 5 m/s).

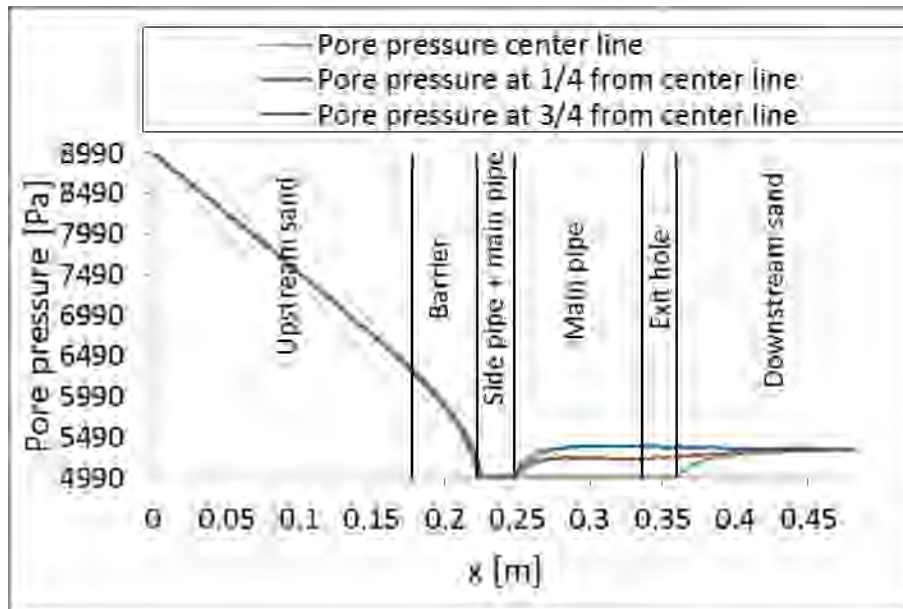


Figure 27 Pore pressure in x-direction at the center line, at 1/4 from center line and at 3/4 from center line for the model with contrast 1

## 4.2. Contrast:3

### 4.2.1. Flow velocity distributions

Figure 28 to Figure 30 show the contour plots of the flow velocity in the setup.

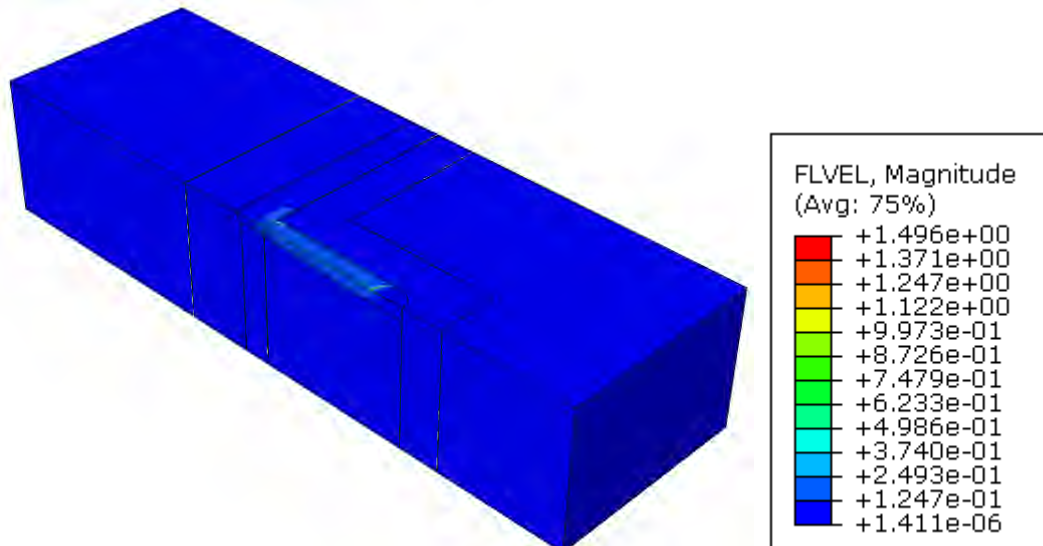


Figure 28 Contour plot of flow velocity for model with contrast 3

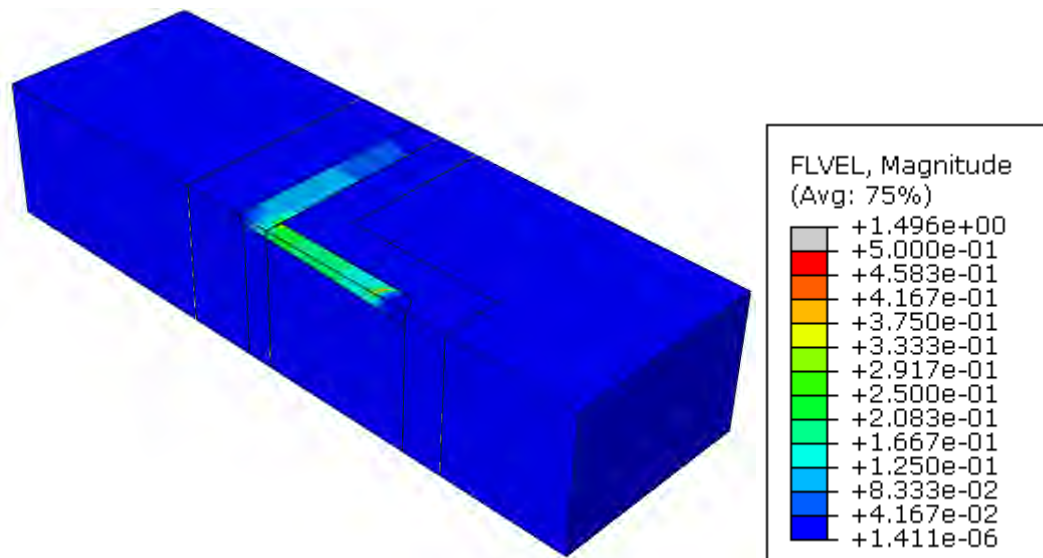


Figure 29 Contour plot of flow velocity for model with contrast 3 with maximum flow velocity 0.5 m/s

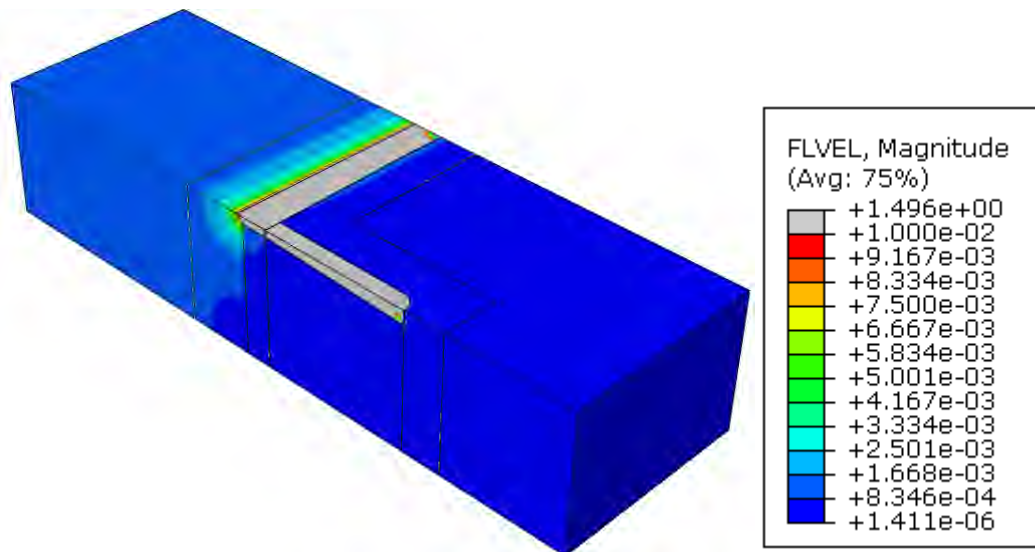


Figure 30 Contour plot of flow velocity for model with contrast 3 with maximum flow velocity 0.01 m/s

Figure 31 to Figure 33 show vector plots of the same results. Figure 34 shows a more detailed view of the flow lines in the main pipe and side pipe.

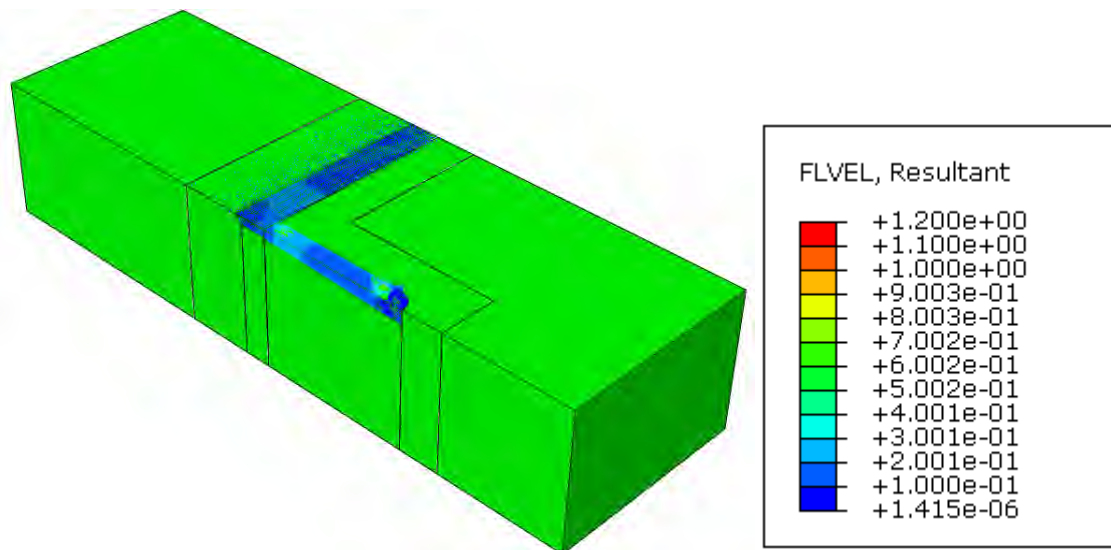


Figure 31 Vector plot of flow velocity for model with contrast 3

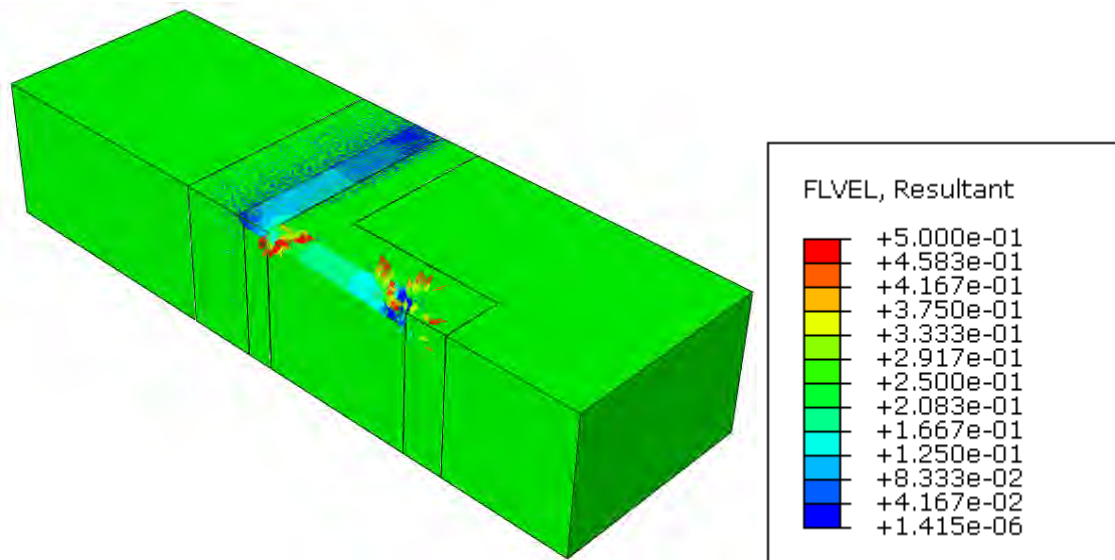


Figure 32 Vector plot of flow velocity for model with contrast 3 with maximum flow velocity 0.5 m/s

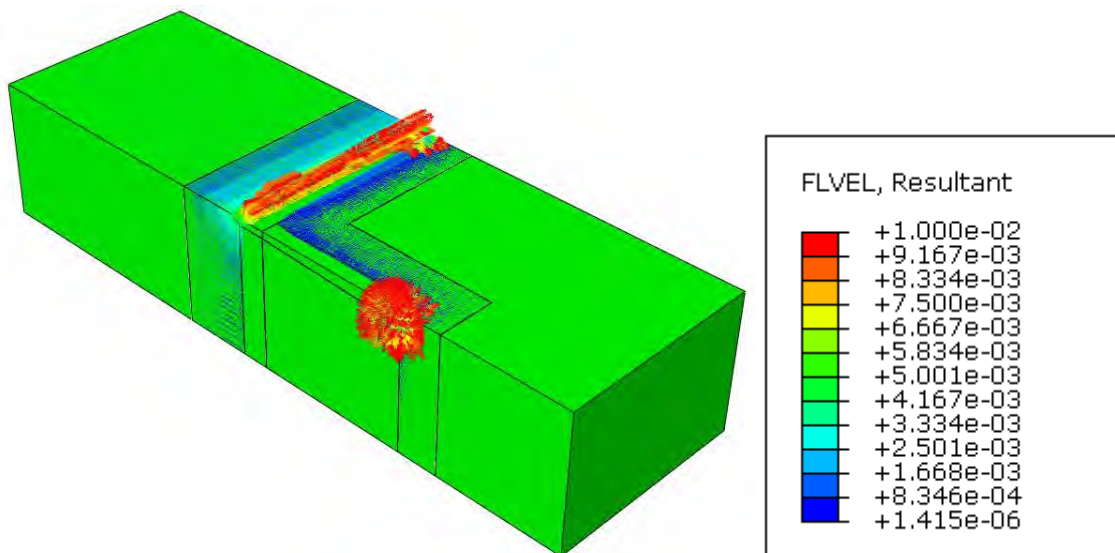


Figure 33 Vector plot of flow velocity for model with contrast 3 with maximum flow velocity 0.01 m/s

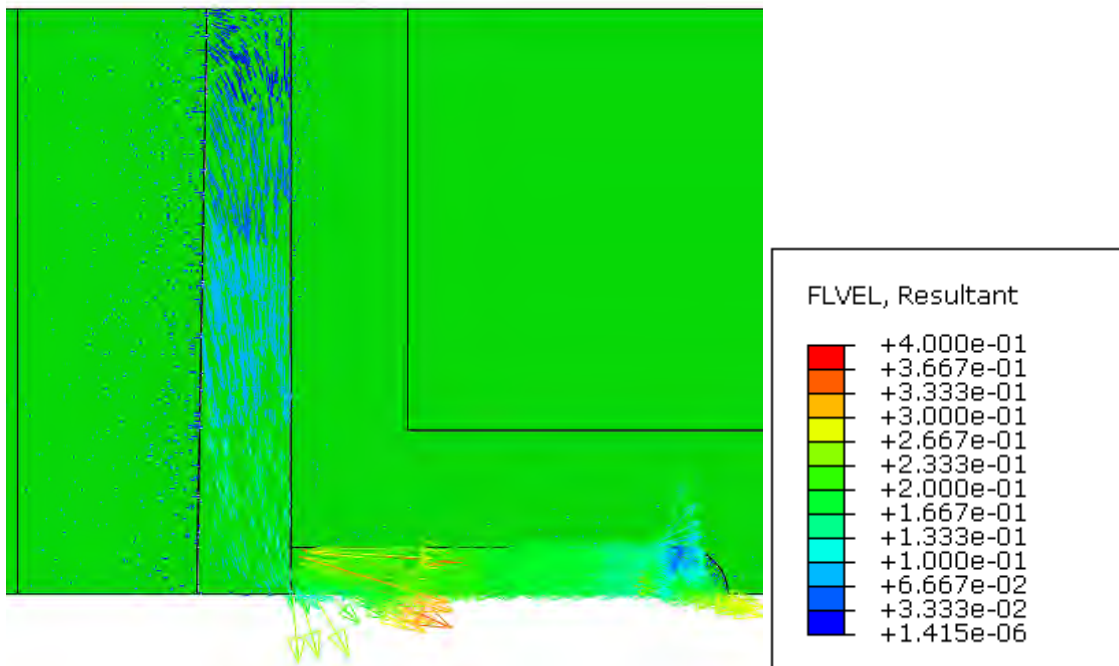


Figure 34 Bended flow lines at transition from side pipe to main pipe (top view) for the model with contrast 3

Figure 35 and Figure 36 show the flow velocity and the x-component of the flow velocity respectively at the center line of the geometry, at a distance of 0.0375 m ( $1/4 \cdot 0.15$  m) and at a distance of 0.1125 m ( $3/4 \cdot 0.15$  m) from the center line but parallel to the center line as a function of  $x$ . The results are very similar to the results found for the permeability contrast of one, except the velocities are slightly higher for contrast 3 due to the higher permeability of the barrier.

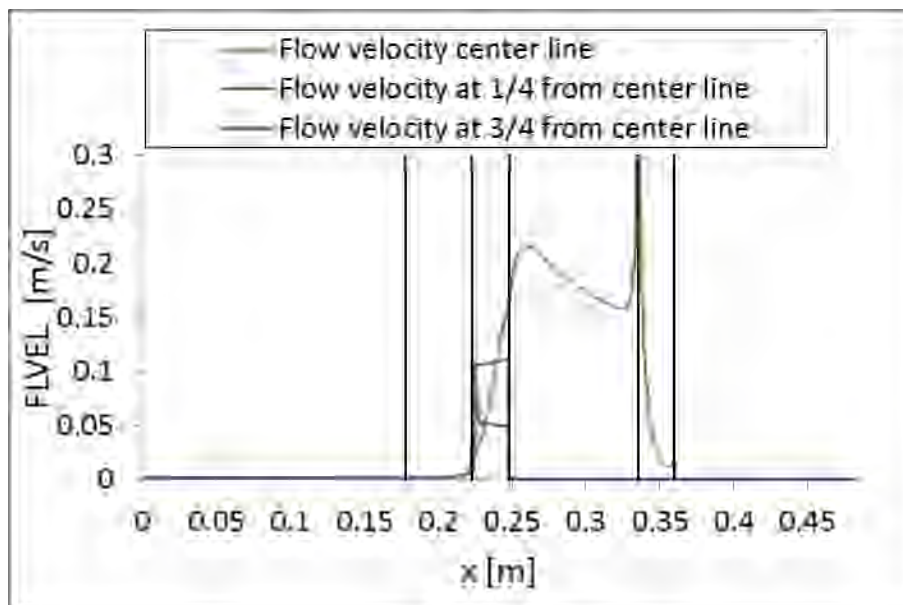


Figure 35 Flow velocity at the center line, at 1/4 from center line and at 3/4 from center line for the model with contrast 3

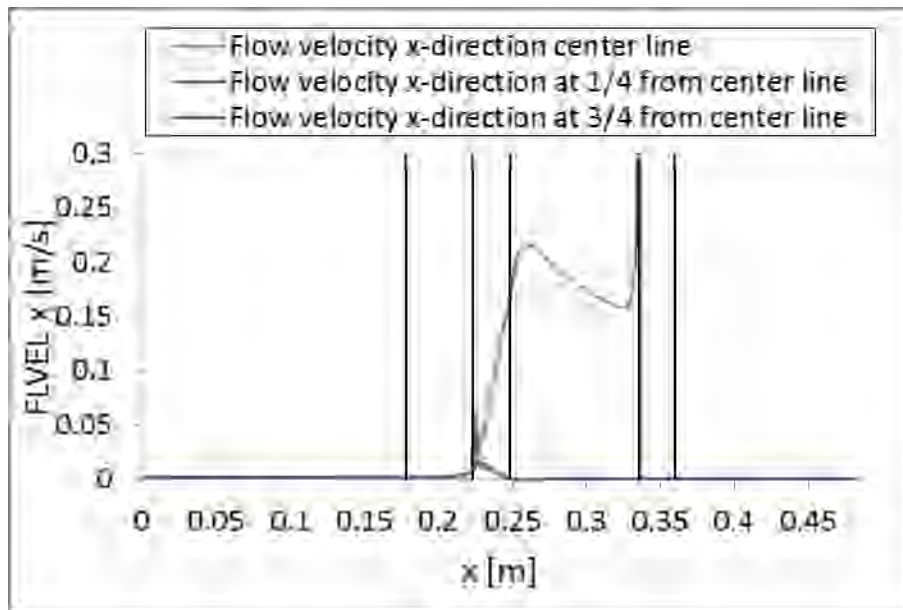


Figure 36 Flow velocity in x-direction at the center line, at 1/4 from center line and at 3/4 from center line for the model with contrast 3

Figure 37 shows both the flow velocity and the x-component of the flow velocity at the transition from the barrier to the pipe at  $x = 0.223$  m as a function of  $y$  at the top, the center and the bottom of the side pipe. The results are again similar but slightly higher than the results for contrast 1.

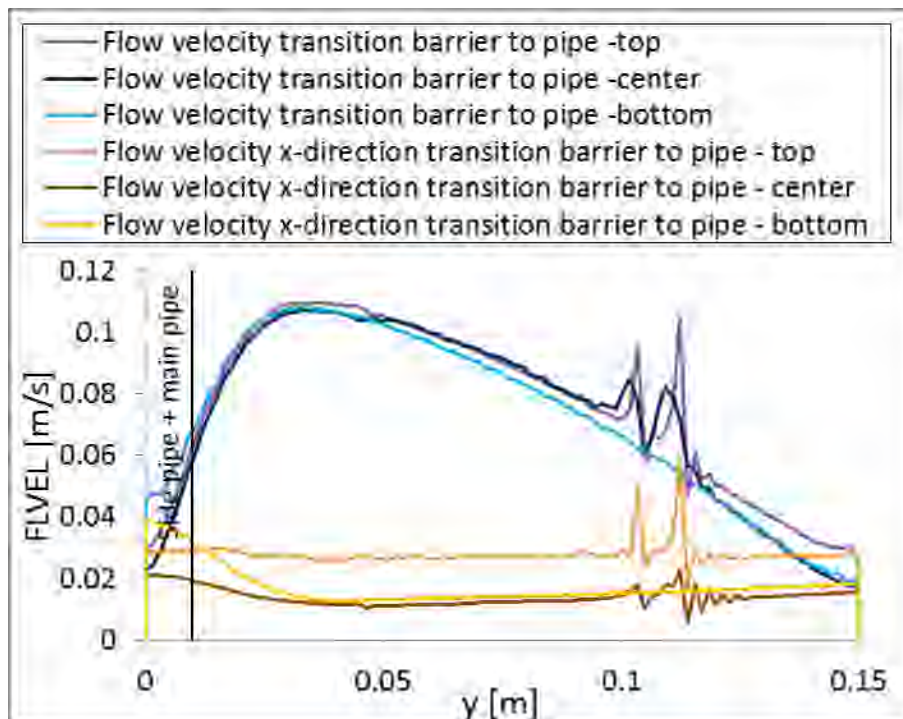


Figure 37 Flow velocity and flow velocity in x-direction at the transition from barrier to pipe line for the model with contrast 3

#### 4.2.2. Pore pressure distributions

Figure 38 shows the contour plot of the pore pressure throughout the model.

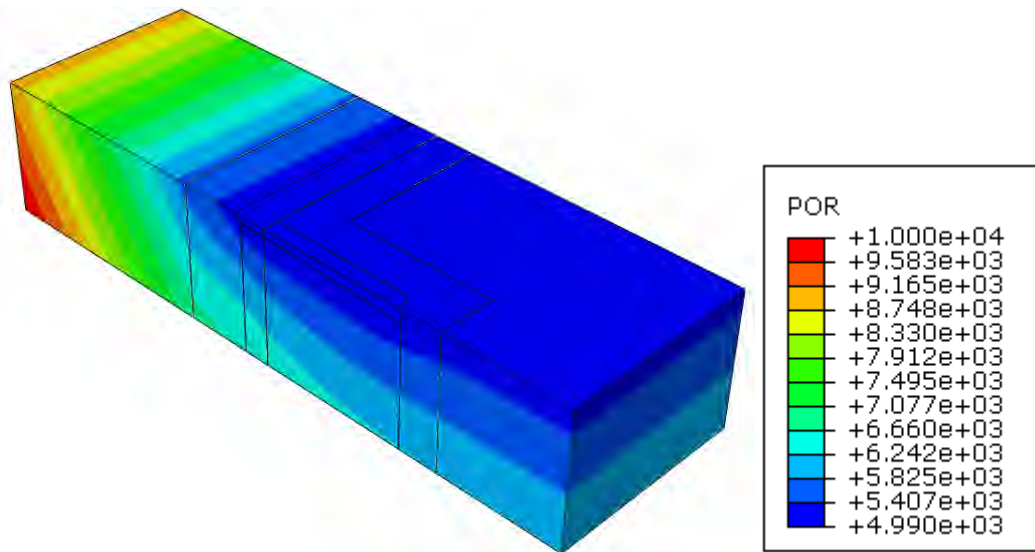


Figure 38 Contour plot of pore pressure for model with contrast 3

Figure 39 shows the variation of the pore pressure at the center line of the geometry, at a distance of 0.0375 m ( $1/4 \cdot 0.15$  m) and at a distance of 0.1125 m ( $3/4 \cdot 0.15$  m) from the center line but parallel to the center line as a function of x.

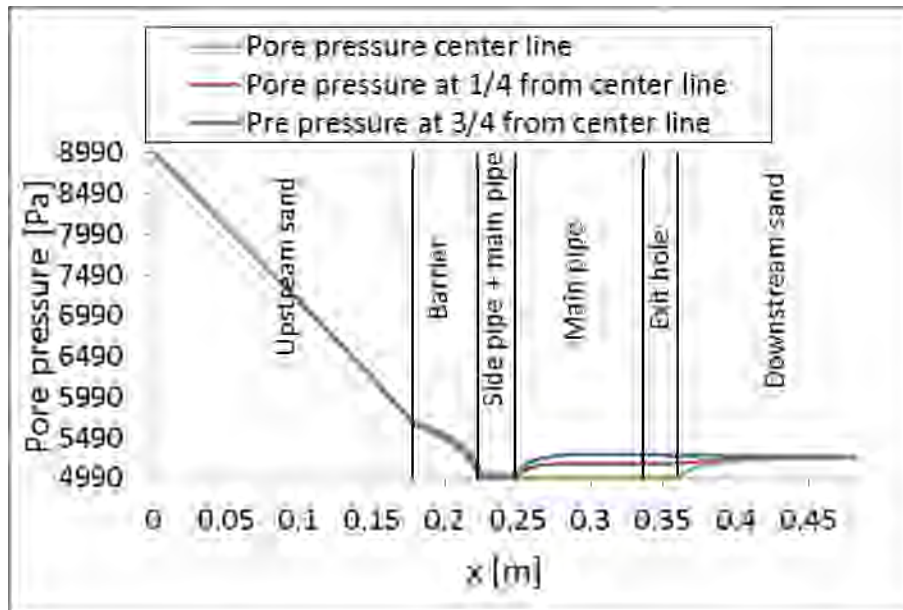


Figure 39 Pore pressure in x-direction at the center line, at 1/4 from center line and at 3/4 from center line for the model with contrast 3

### 4.3. Contrast:10

#### 4.3.1. Flow velocity distributions

Figure 40 to Figure 42 show the contour plots of the flow velocity in the setup.

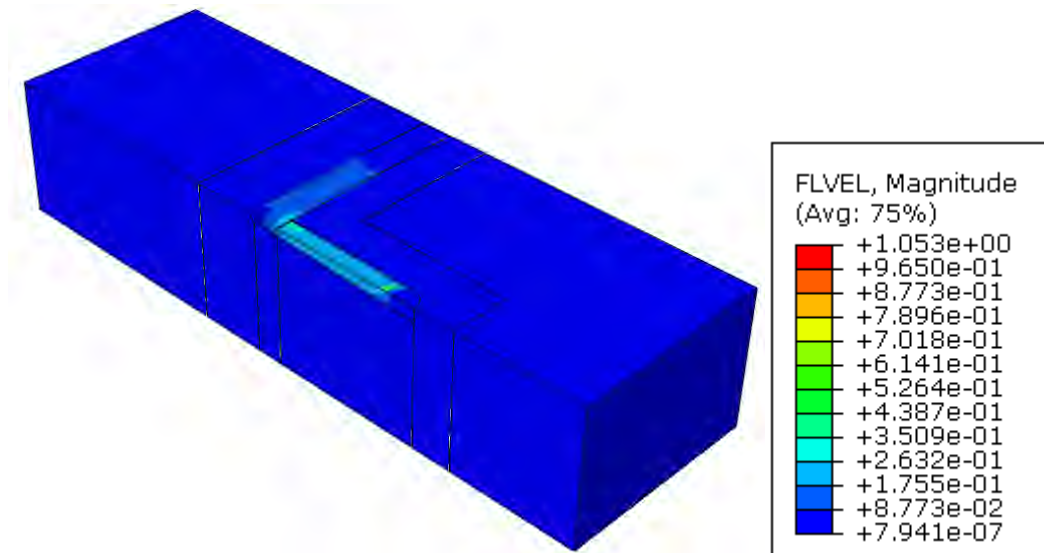


Figure 40 Contour plot of flow velocity for model with contrast 10

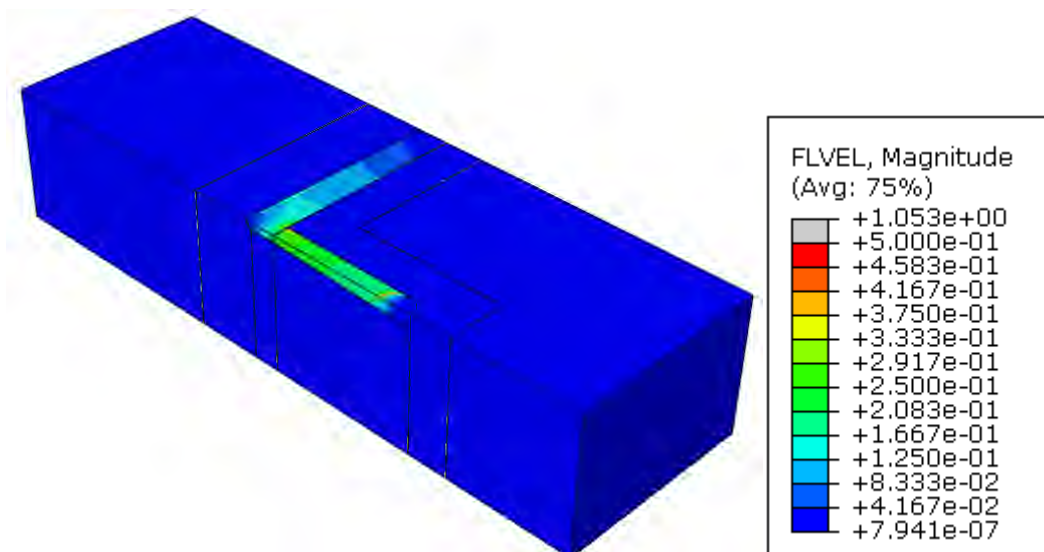


Figure 41 Contour plot of flow velocity for model with contrast 10 with maximum flow velocity 0.5 m/s

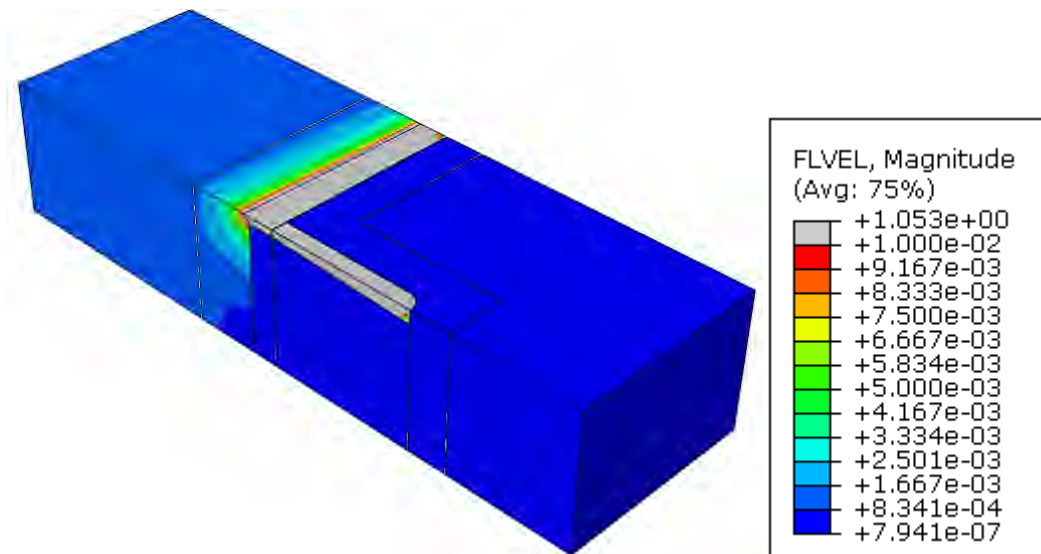


Figure 42 Contour plot of flow velocity for model with contrast 10 with maximum flow velocity 0.01 m/s

Figure 43 to Figure 45 show vector plots of the same results. Figure 46 shows a detail of the flow lines in the main pipe and side pipe.

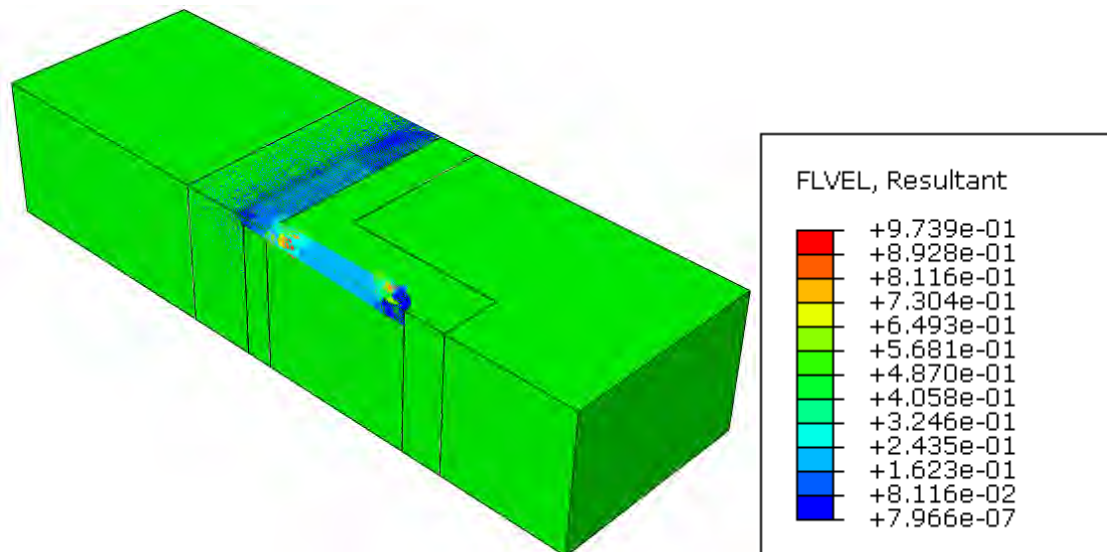


Figure 43 Vector plot of flow velocity for model with contrast 10

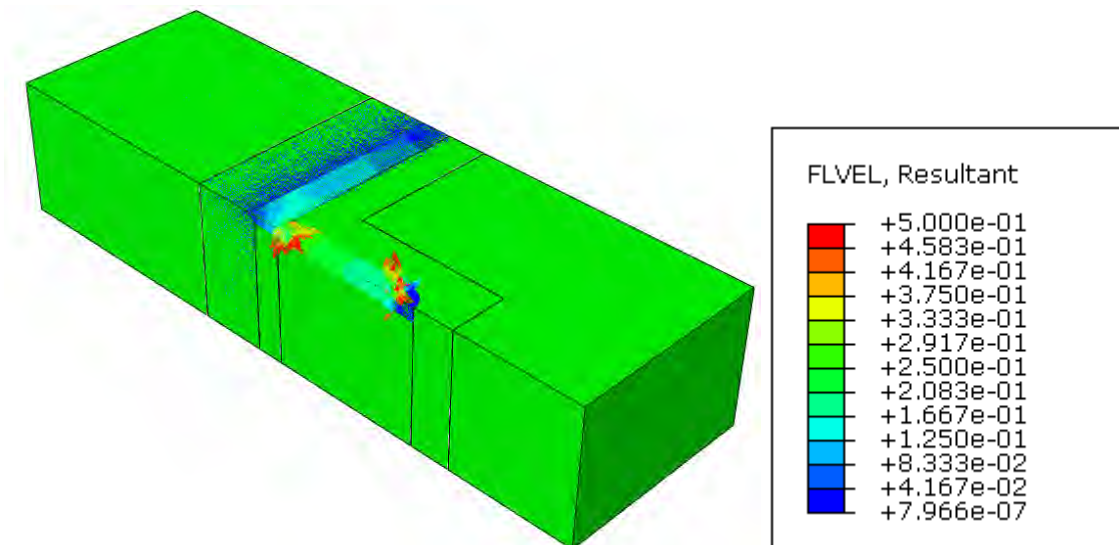


Figure 44 Vector plot of flow velocity for model with contrast 10 with maximum flow velocity 0.5 m/s

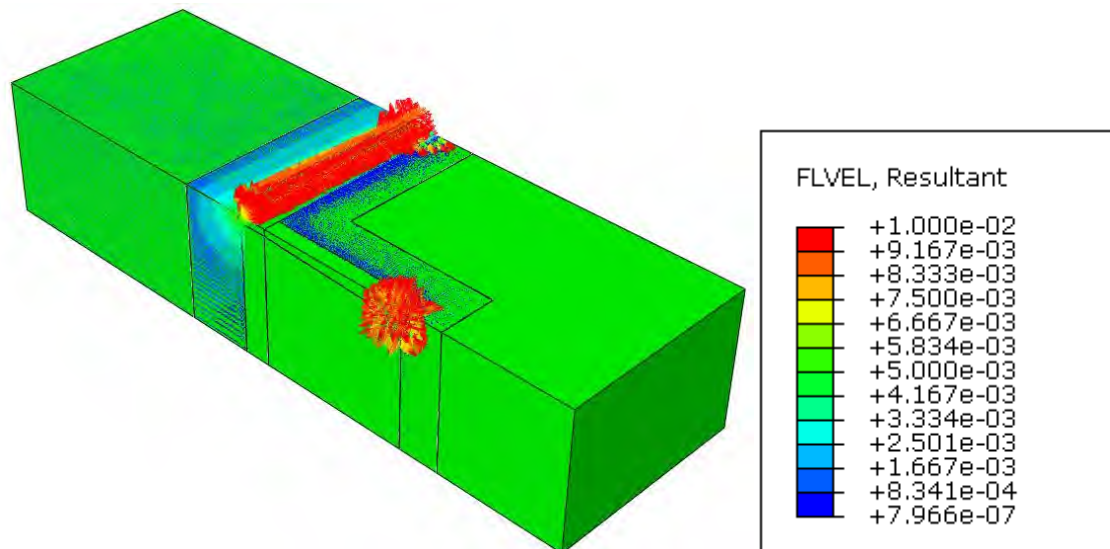


Figure 45 Vector plot of flow velocity for model with contrast 10 with maximum flow velocity 0.01 m/s

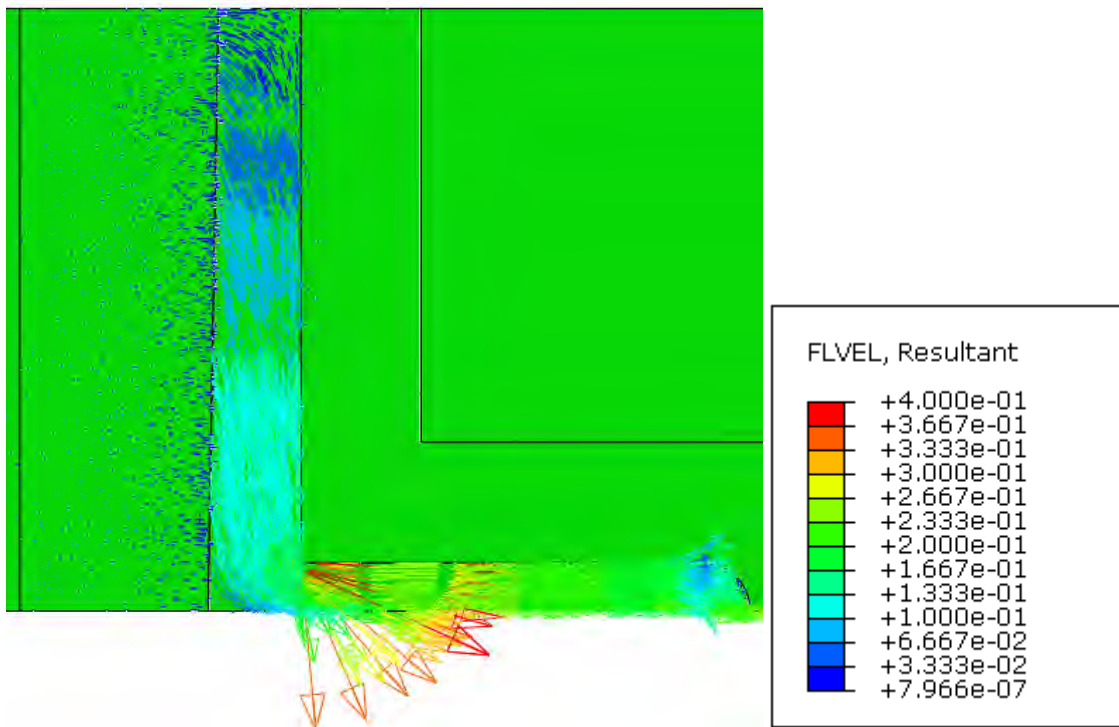


Figure 46 Bended flow lines at transition from side pipe to main pipe (top view) for the model with contrast 10

Figure 47 and Figure 48 show the flow velocity and the x-component of the flow velocity respectively at the center line of the geometry, at a distance of 0.0375 m ( $1/4 \cdot 0.15$  m) and at a distance of 0.1125 m ( $3/4 \cdot 0.15$  m) from the center line but parallel to the center line as a function of x. The obtained velocities are again similar but slightly higher than the velocities obtained for contrast 3 due to the increased permeability of the barrier.

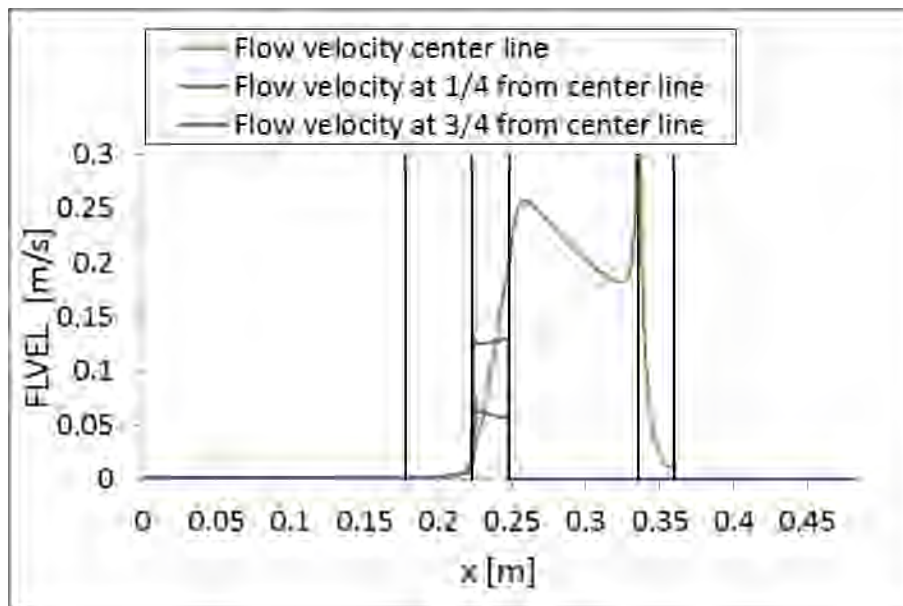


Figure 47 Flow velocity at the center line, at 1/4 from center line and at 3/4 from center line for the model with contrast 10

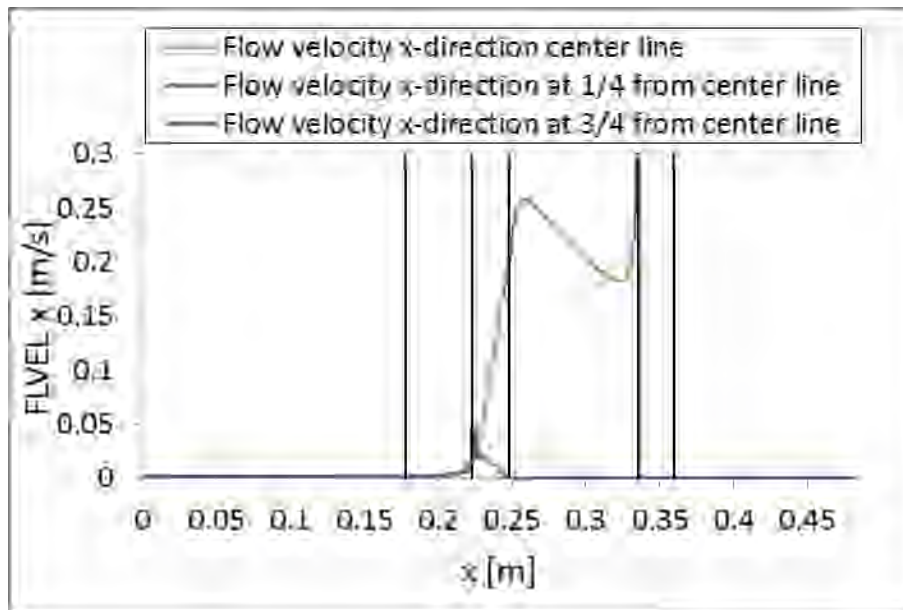


Figure 48 Flow velocity in x-direction at the center line, at 1/4 from center line and at 3/4 from center line for the model with contrast 10

Figure 49 shows both the flow velocity and the x-component of the flow velocity at the transition from the barrier to the pipe at  $x = 0.223$  m as a function of  $y$ . The flow velocities are again similar but slightly higher than for the simulation with contrast 3.

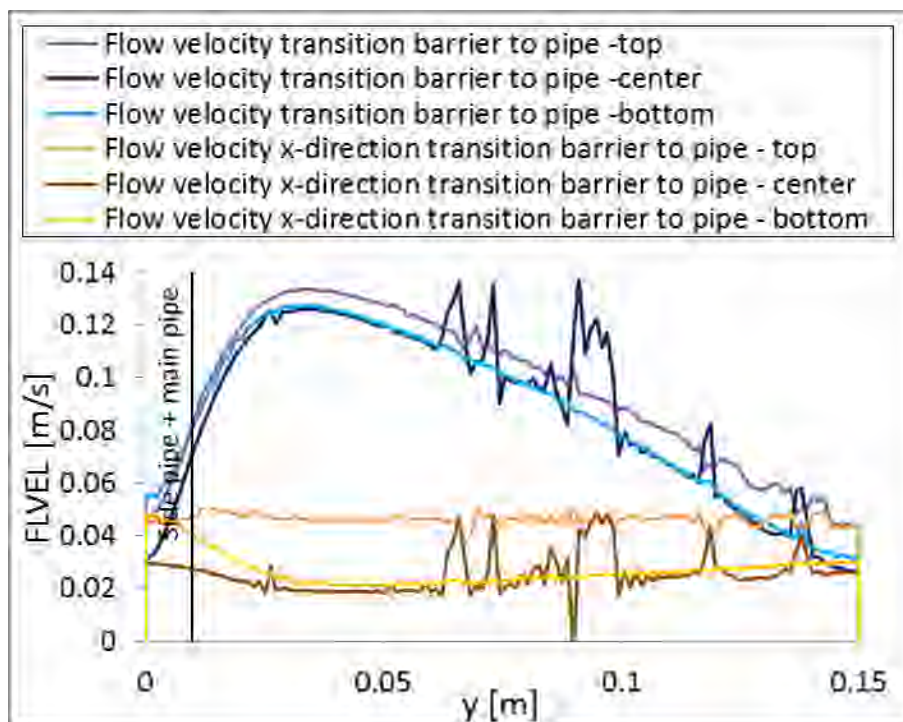


Figure 49 Flow velocity and flow velocity in x-direction at the transition from barrier to pipe line for the model with contrast 10

#### 4.3.2. Pore pressure distributions

Figure 50 shows the contour plot of the pore pressure throughout the model.

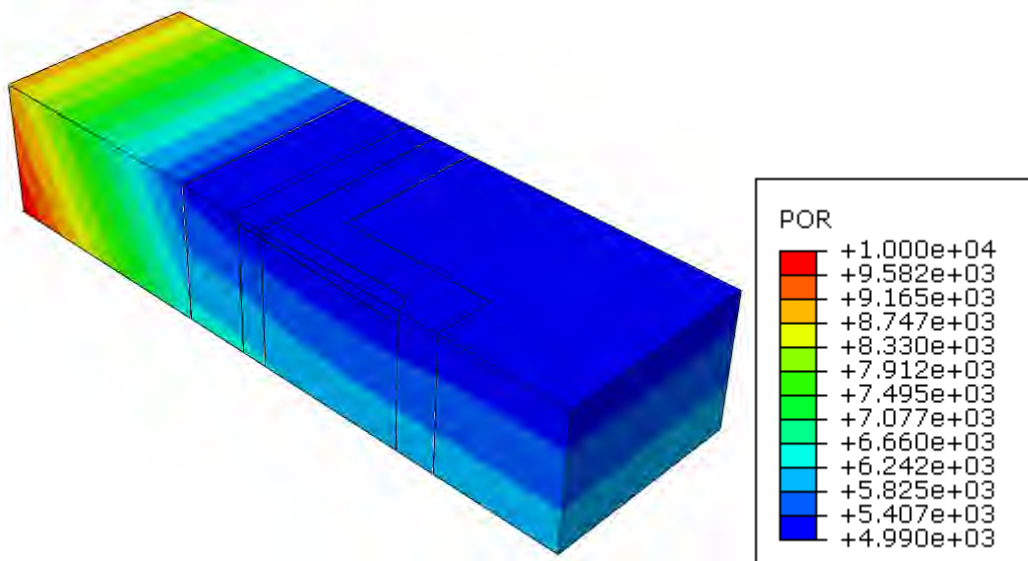


Figure 50 Contour plot of pore pressure for model with contrast 10

Figure 51 shows the variation of the pore pressure at the center line of the geometry, at a distance of 0.0375 m ( $1/4 \cdot 0.15$  m) and at a distance of 0.1125 m ( $3/4 \cdot 0.15$  m) from the center line but parallel to the center line as a function of x.

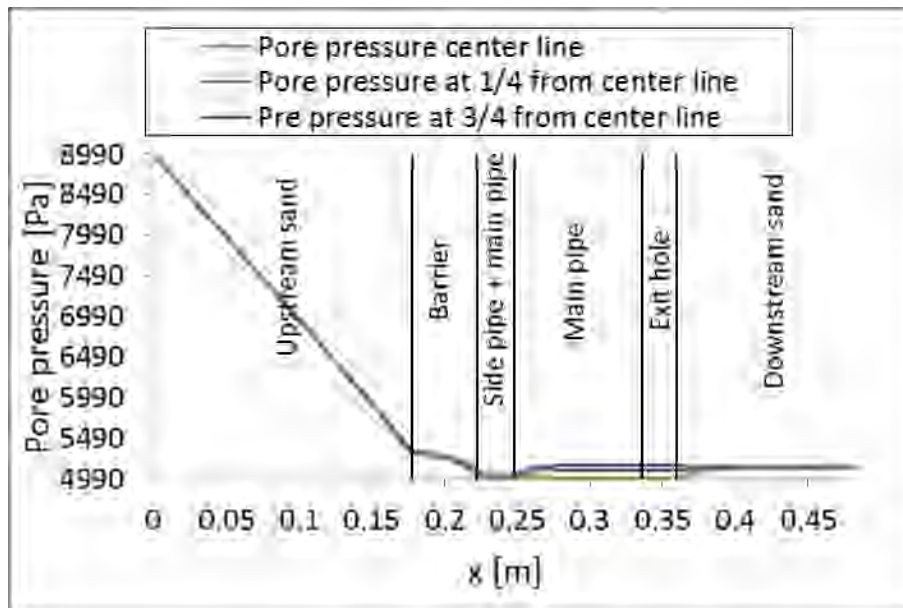


Figure 51 Pore pressure in x-direction at the center line, at 1/4 from center line and at 3/4 from center line for the model with contrast 10

#### 4.4. Contrast:100

##### 4.4.1. Flow velocity distributions

Figure 52 to Figure 54 show the contour plots of the flow velocity in the setup.

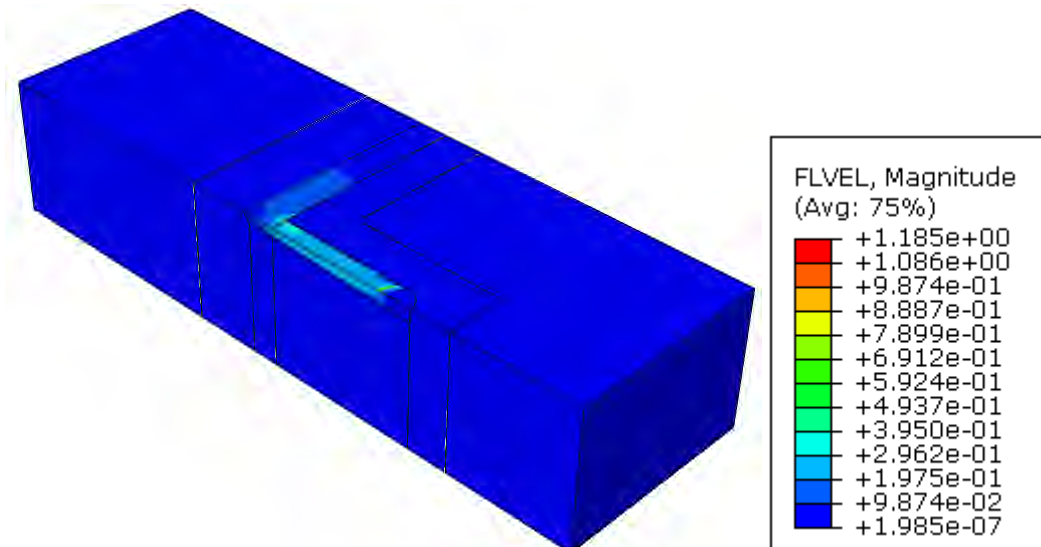


Figure 52 Contour plot of flow velocity for model with contrast 100

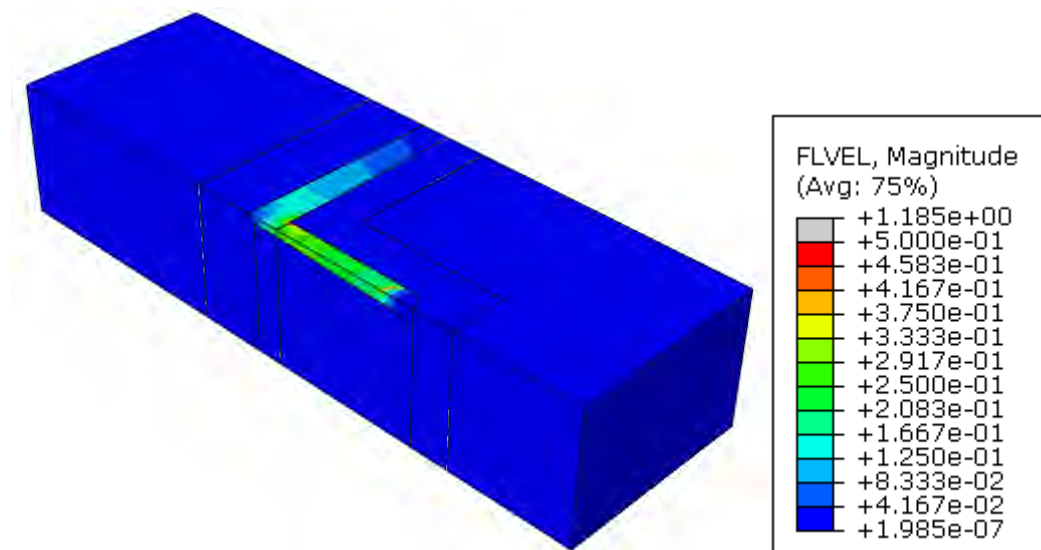


Figure 53 Contour plot of flow velocity for model with contrast 100 with maximum flow velocity 0.5 m/s

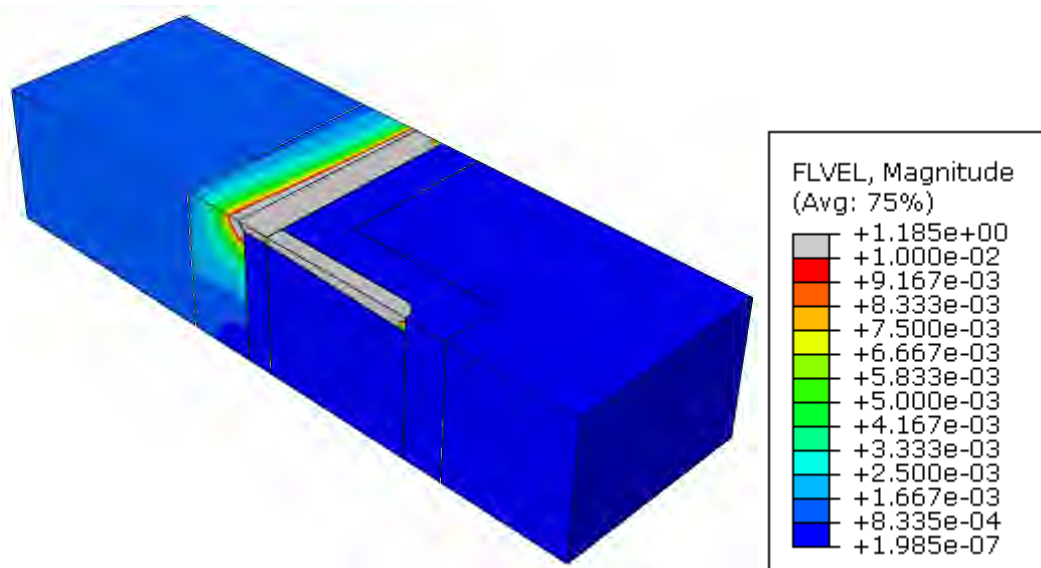


Figure 54 Contour plot of flow velocity for model with contrast 100 with maximum flow velocity 0.01 m/s

Figure 55 to Figure 57 show vector plots of the same results. Figure 58 shows a detail of the flow lines in the main pipe and side pipe.

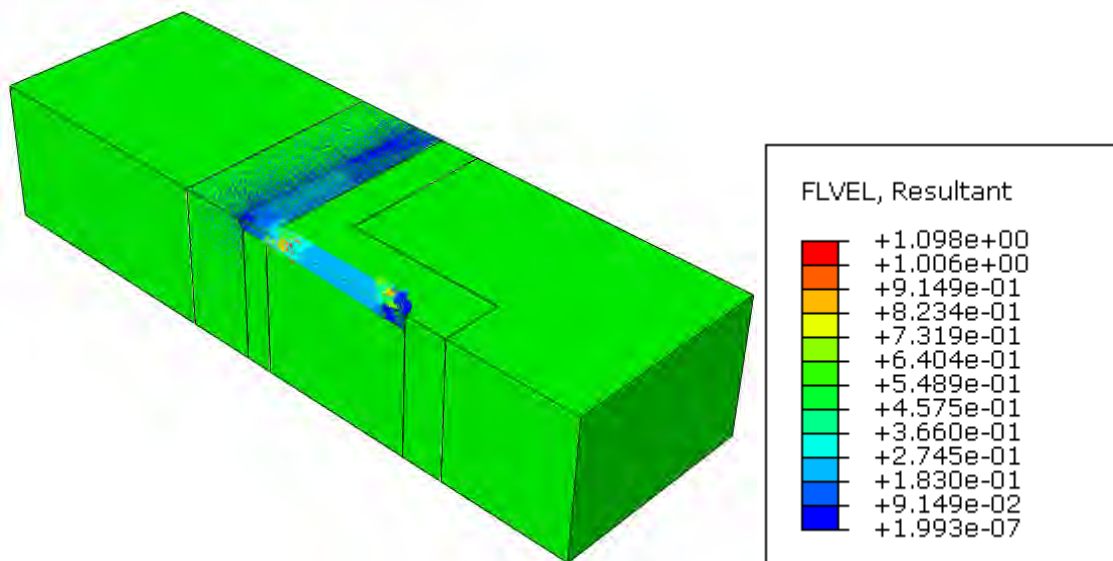


Figure 55 Vector plot of flow velocity for model with contrast 100

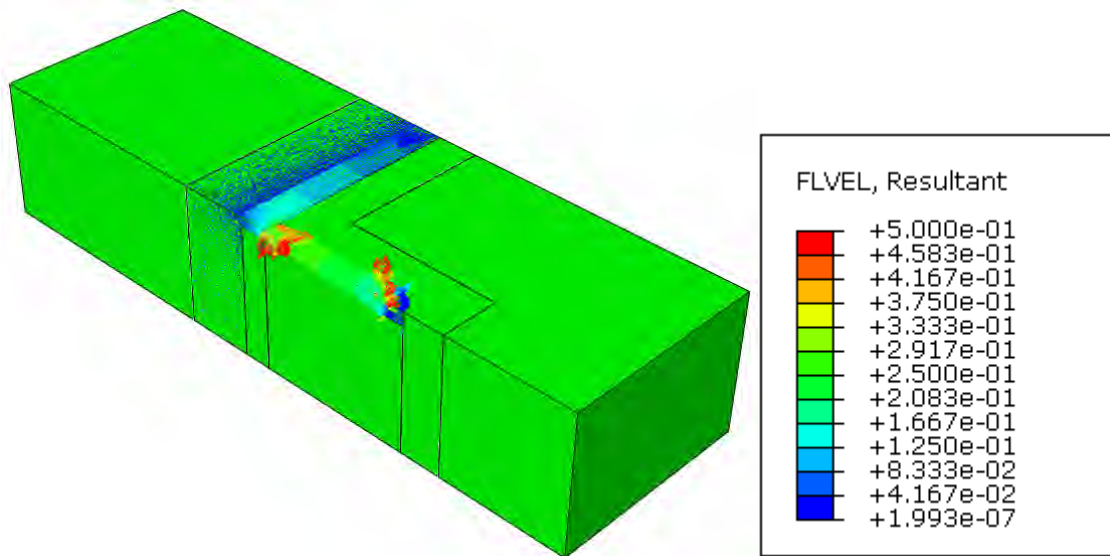


Figure 56 Vector plot of flow velocity for model with contrast 100 with maximum flow velocity 0.5 m/s

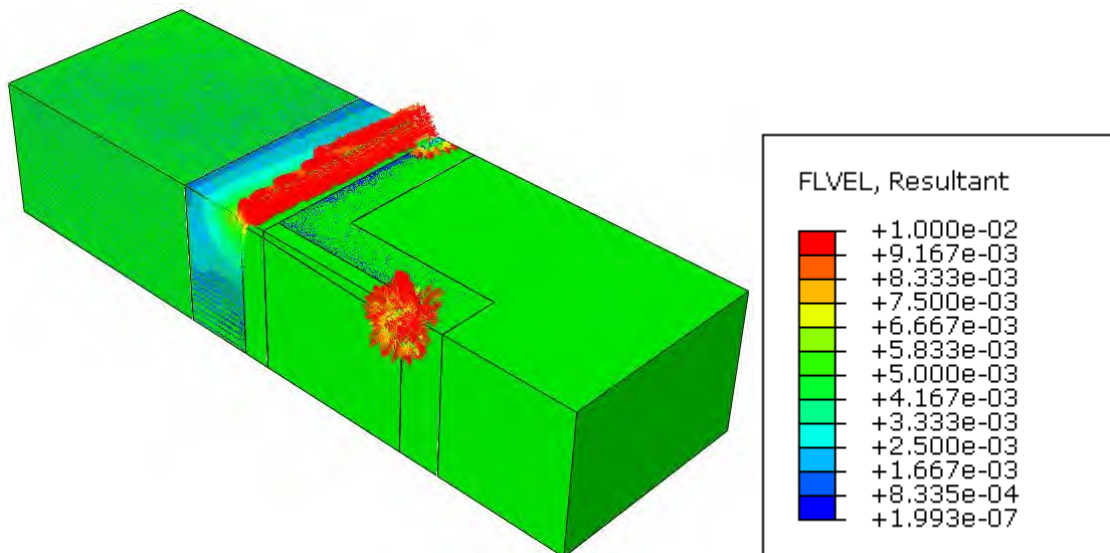


Figure 57 Vector plot of flow velocity for model with contrast 100 with maximum flow velocity 0.01 m/s

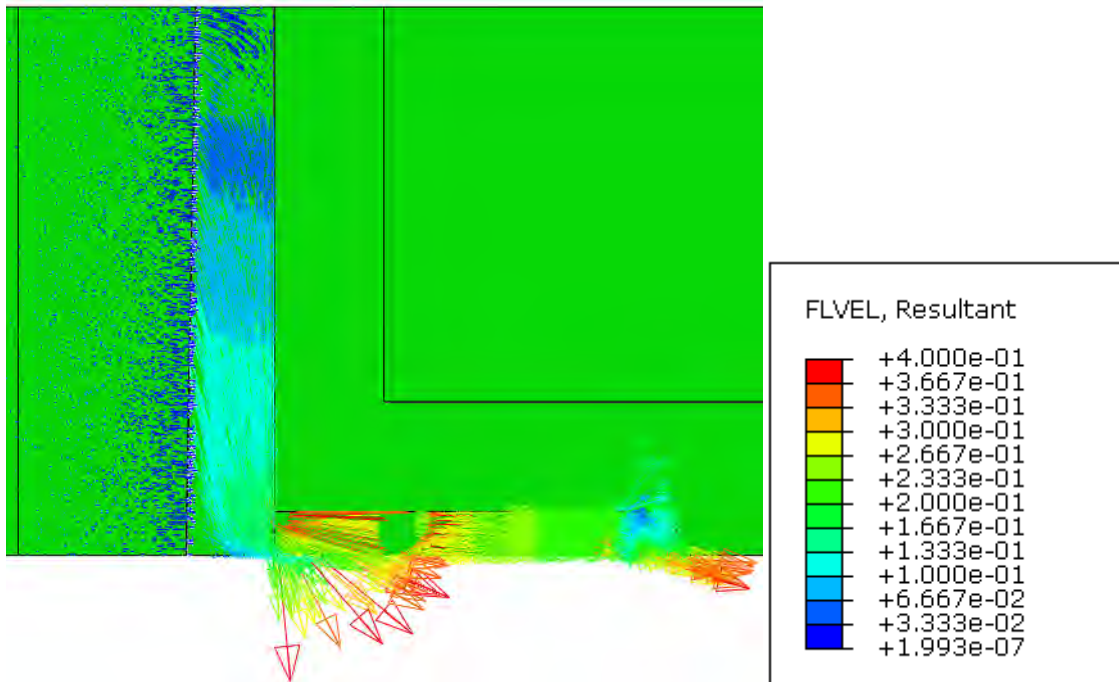


Figure 58 Bended flow lines at transition from side pipe to main pipe (top view) for the model with contrast 100

Figure 59 and Figure 60 show the flow velocity and the x-component of the flow velocity respectively at the center line of the geometry, at a distance of 0.0375 m ( $1/4 \cdot 0.15$  m) and at a distance of 0.1125 m ( $3/4 \cdot 0.15$  m) from the center line but parallel to the center line as a function of x.

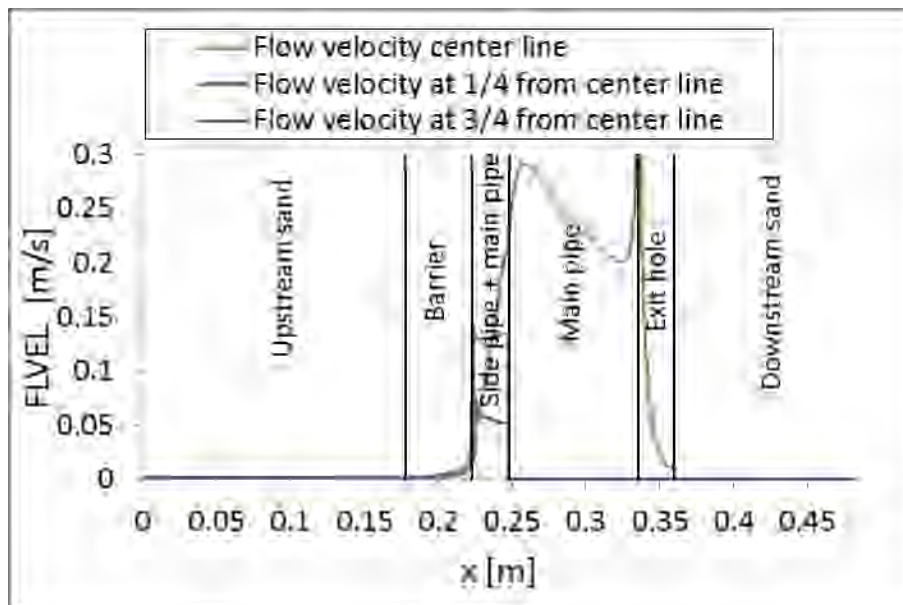


Figure 59 Flow velocity at the center line, at 1/4 from center line and at 3/4 from center line for the model with contrast 100

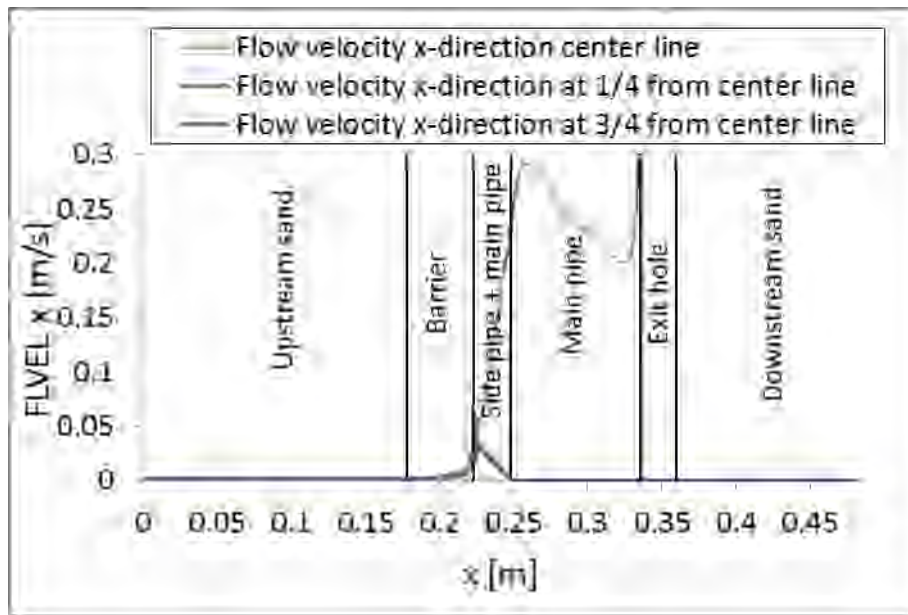


Figure 60 Flow velocity in x-direction at the center line, at 1/4 from center line and at 3/4 from center line for the model with contrast 100

Figure 61 shows both the flow velocity and the x-component of the flow velocity at the transition from the barrier to the pipe at  $x = 0.223$  m as a function of  $y$ .

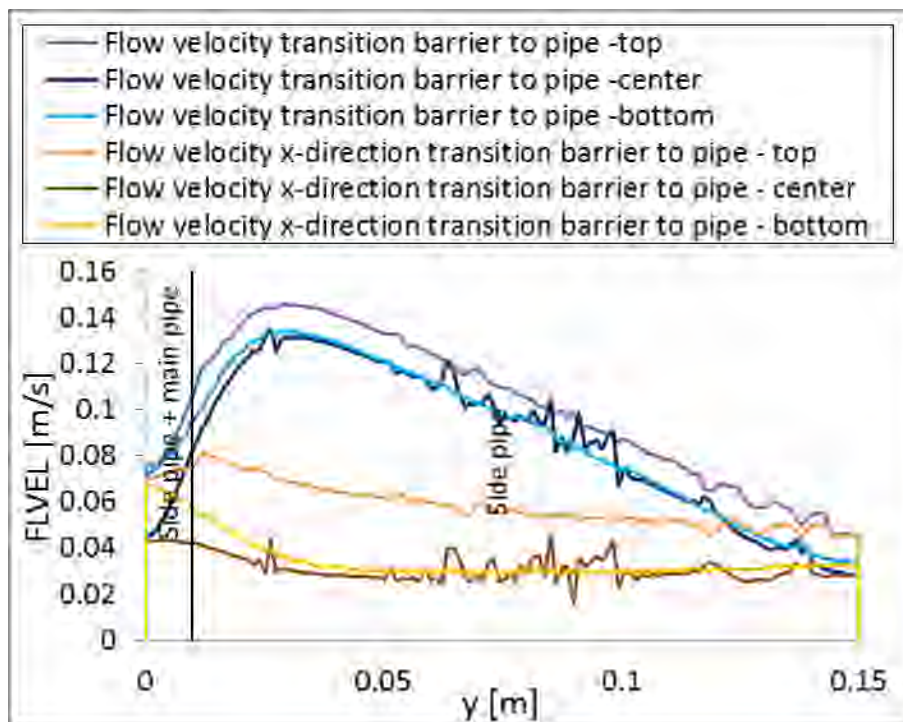


Figure 61 Flow velocity and flow velocity in x-direction at the transition from barrier to pipe line for the model with contrast 100

#### 4.4.2. Pore pressure distributions

Figure 62 shows the contour plot of the pore pressure throughout the model.

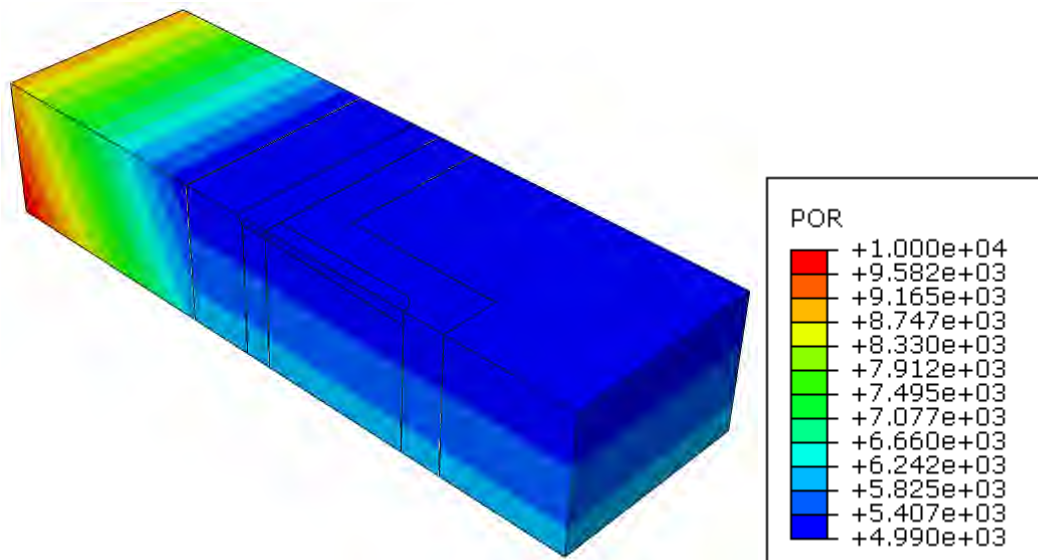


Figure 62 Contour plot of pore pressure for model with contrast 100

Figure 63 shows the variation of the pore pressure at the center line of the geometry, at a distance of 0.0375 m ( $1/4 \cdot 0.15$  m) and at a distance of 0.1125 m ( $3/4 \cdot 0.15$  m) from the center line but parallel to the center line as a function of x.

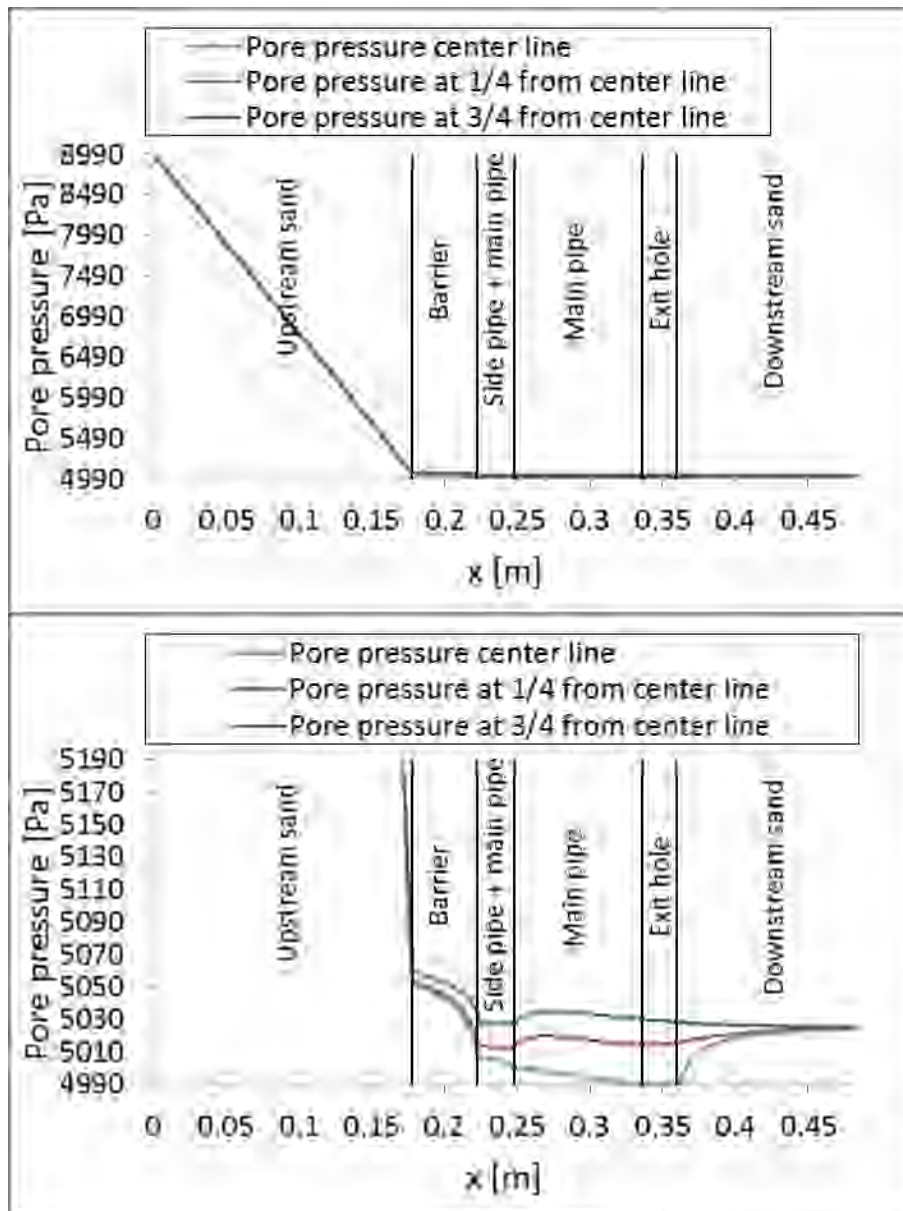


Figure 63 Pore pressure in x-direction at the center line, at 1/4 from center line and at 3/4 from center line for the model with contrast 100

## 5. Overview

Figure 64 - Figure 75 give an overview of the obtained results, compared for the various permeability contrasts.

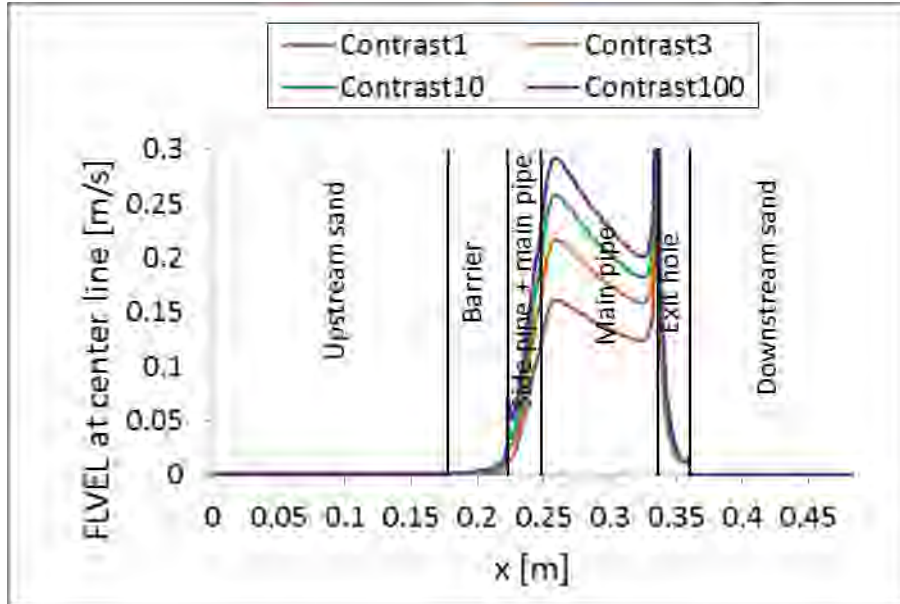


Figure 64 Flow velocity at center line

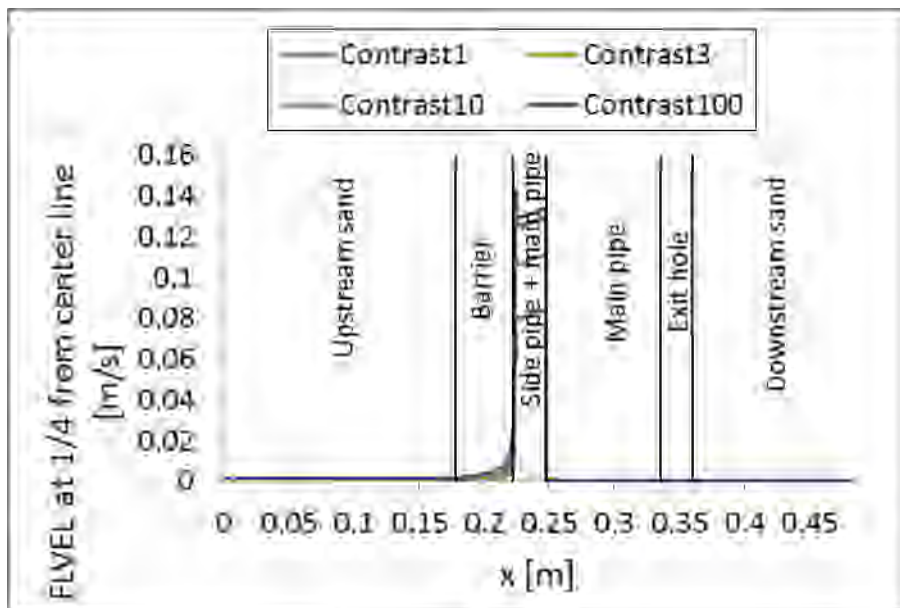


Figure 65 Flow velocity at 1/4 from center line

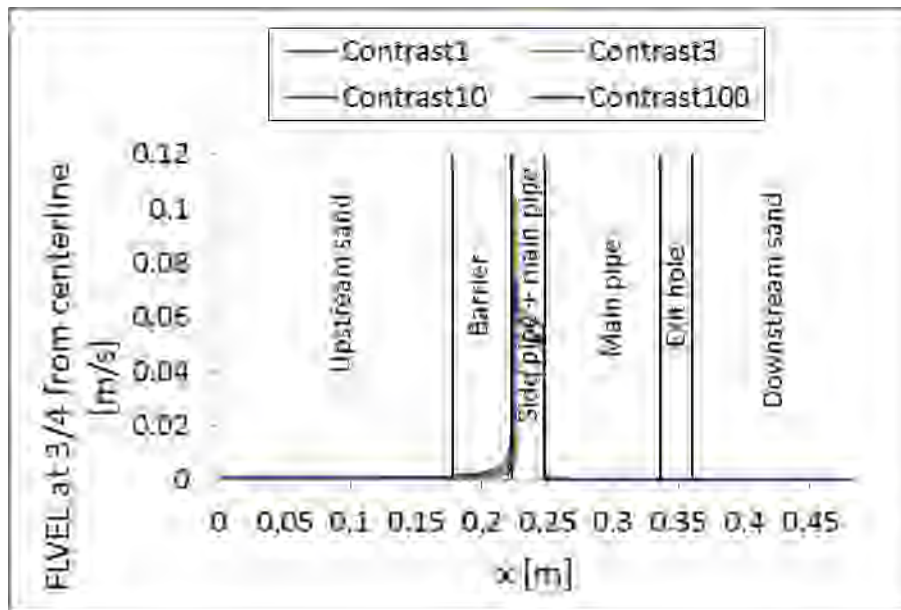


Figure 66 Flow velocity at 3/4 from center line

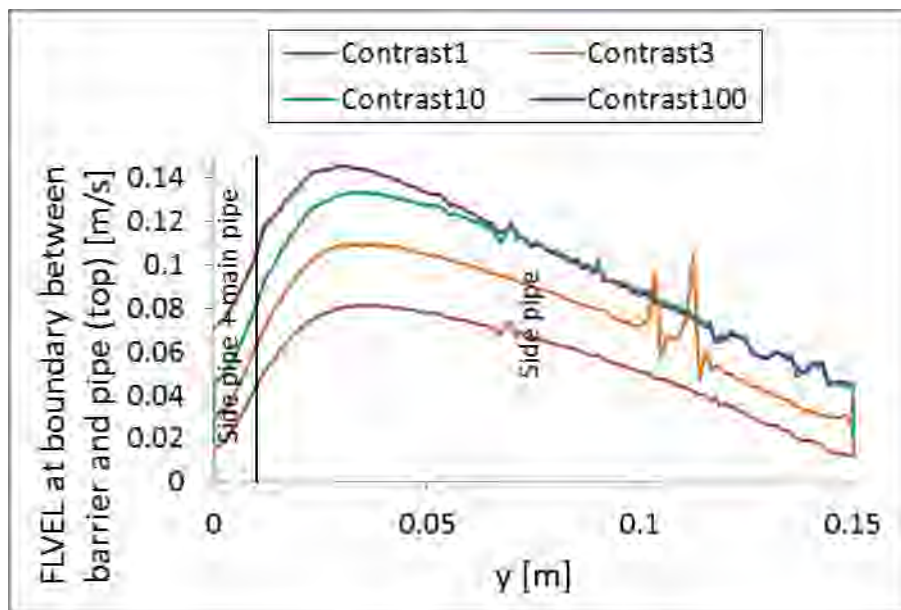


Figure 67 Flow velocity at boundary between barrier and pipe (top)

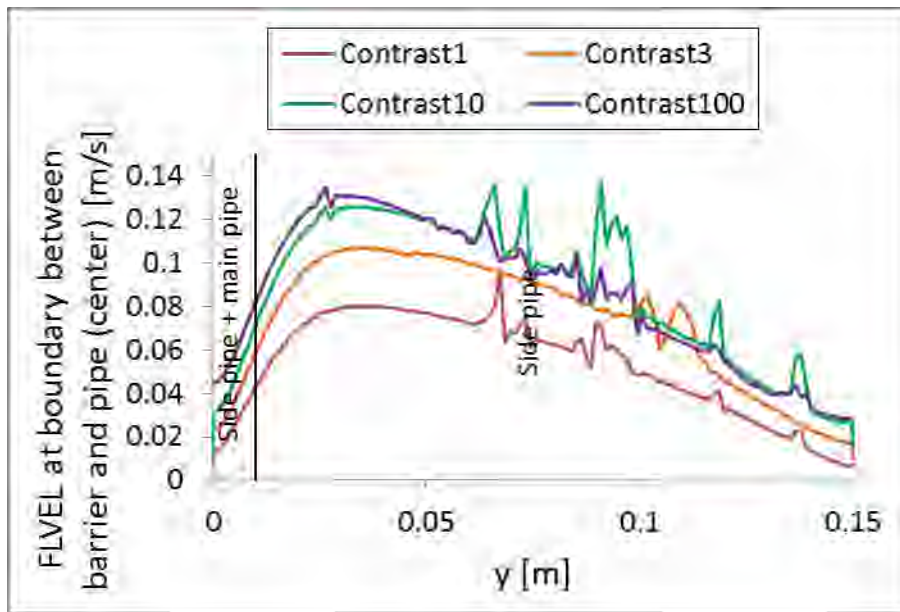


Figure 68 Flow velocity at boundary between barrier and pipe (center)

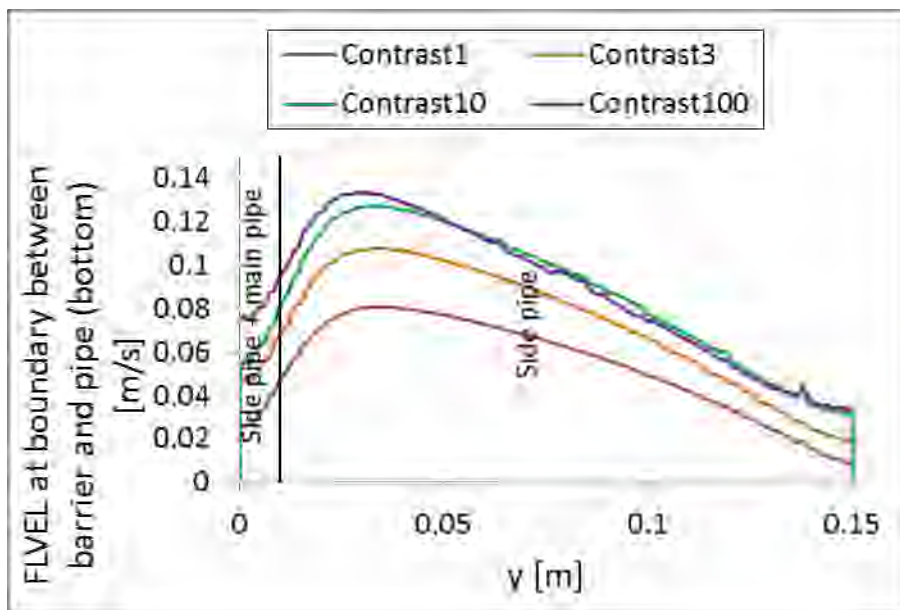


Figure 69 Flow velocity at boundary between barrier and pipe (bottom)

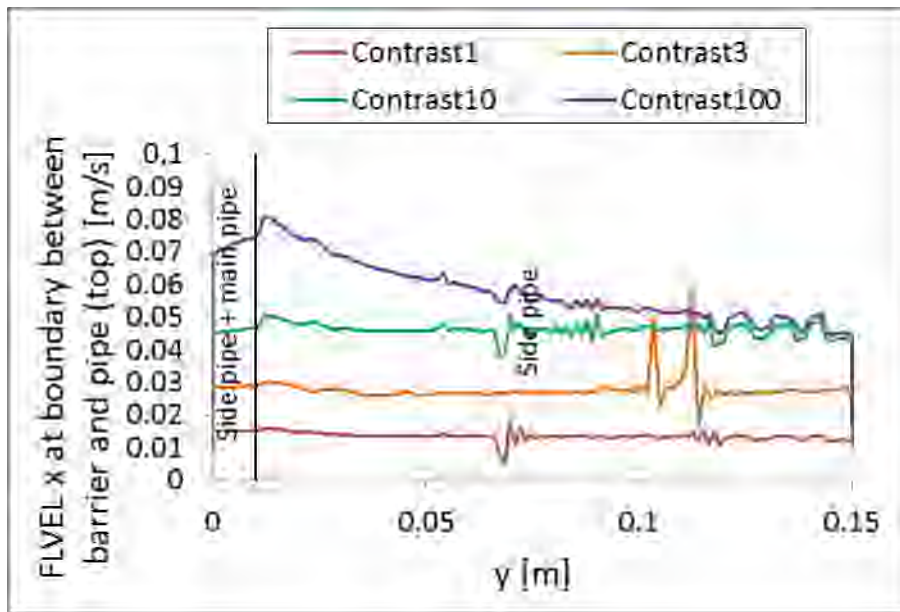


Figure 70 Flow velocity in x-direction at boundary between barrier and pipe (top)

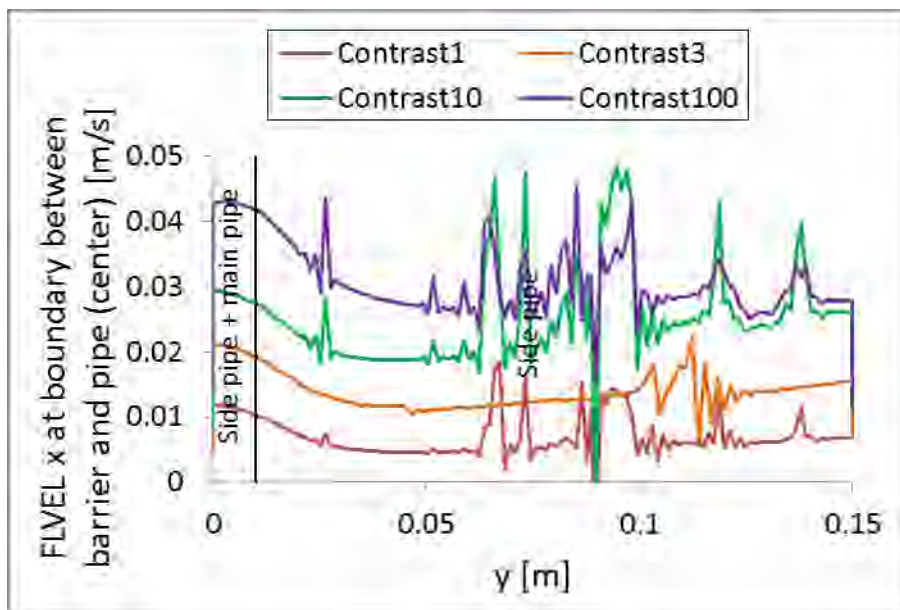


Figure 71 Flow velocity in x-direction at boundary between barrier and pipe (center)

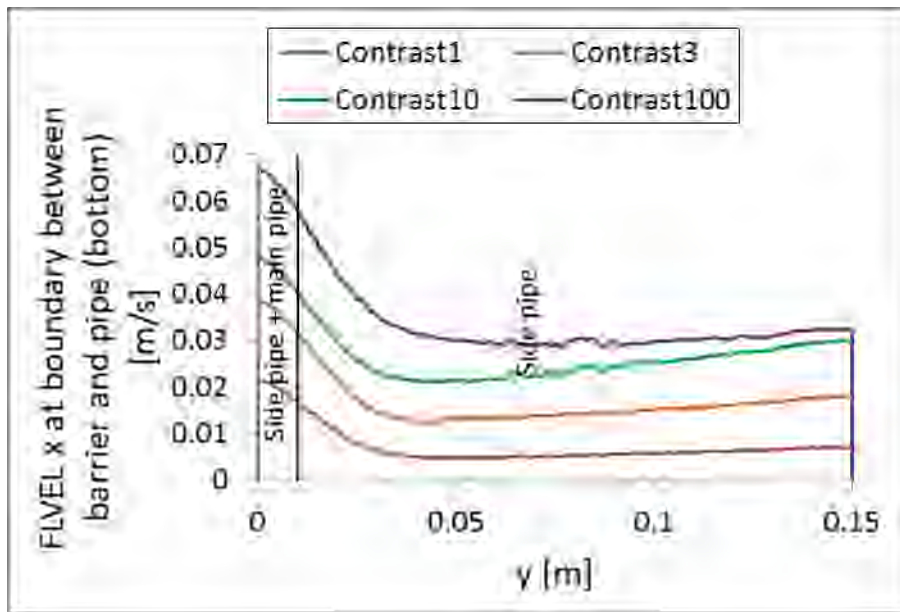


Figure 72 Flow velocity in x-direction at boundary between barrier and pipe (bottom)

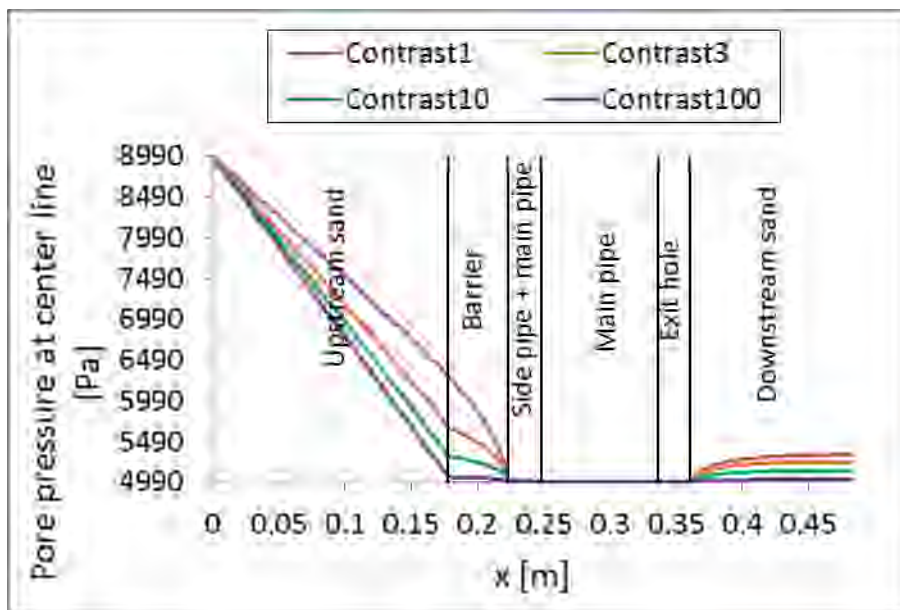


Figure 73 Pore pressure at center line

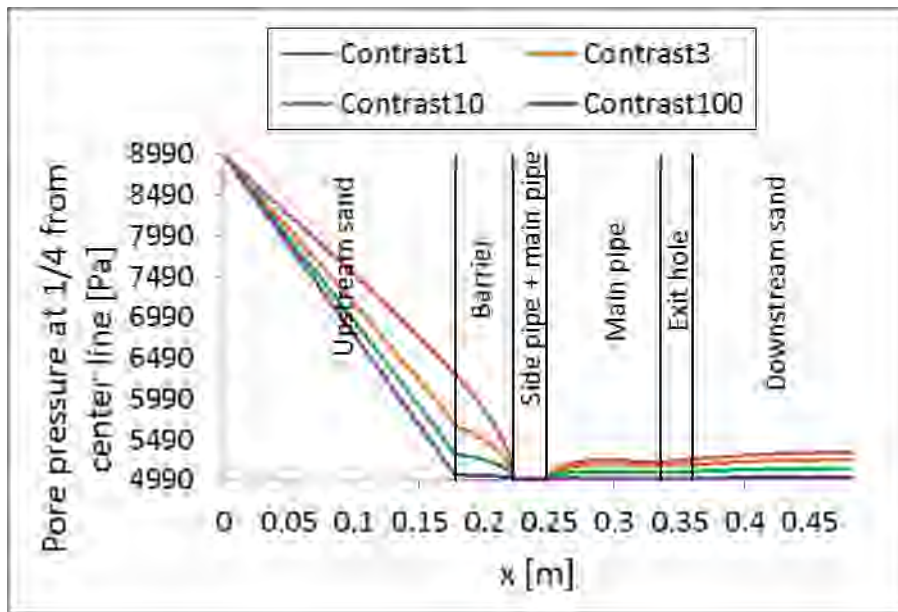


Figure 74 Pore pressure at 1/4 from center line

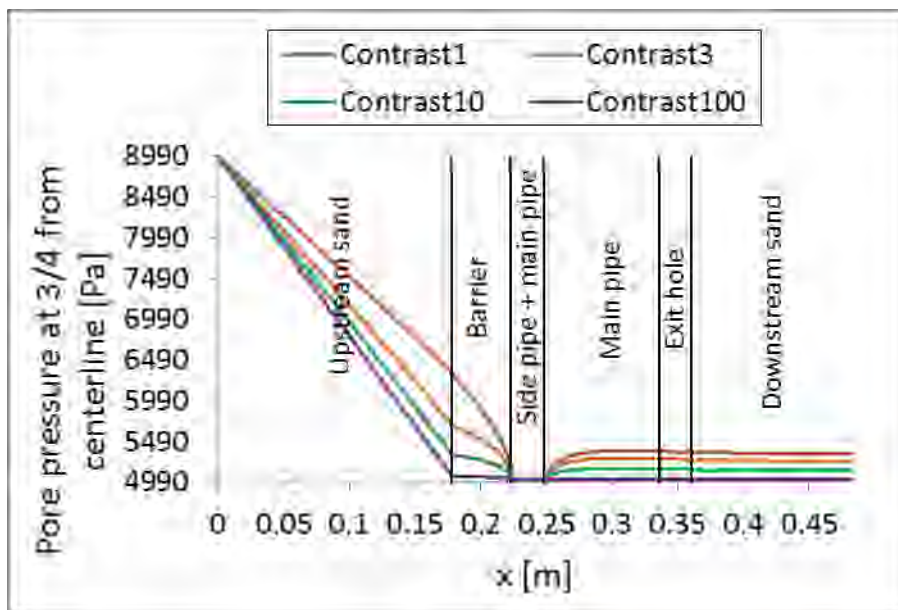


Figure 75 Pore pressure at 3/4 from center line

Ghent, 25/09/2016

Ir. Kristine Vandenkoer

prof. Adam Bezuijen  
Directeur

## **E Comparison DgFlow and Abaqus**

## Memo

**To**  
Vera van Beek, Adam Bezuijen

**Date**  
3 November 2017

**Number of pages**  
12

**From**  
Esther Rosenbrand

**Direct line**  
+31(0)88335 7852

**E-mail**  
esther.rosenbrand@deltares.nl

**Subject**  
Comparison Abaqus and DgFlow

---

This analysis compares the results from DgFlow to those from simulations done in the numerical software Abaqus for the small scale models. The Abaqus study was performed at the Ghent University and is reported in Appendix D as 'Report XI.17.11 Deltares Coarse sand barrier (numerical simulations)'.

4 permeability contrasts are considered:

- 1
- 3
- 10
- 100

The upstream head is 0.4 for all cases. The permeability of the fine material is  $6e-4$  m/s for all cases.

As opposed to the DgFlow simulations, in Abaqus the pipe is modelled as a more permeable zone with a higher permeability.

The comparison in the current analysis is focussed on the head distribution as predicted in both models and on the local gradient in the barrier.

## 1 Models

### 1.1 DgFlow

For the DgFlow simulations, the same small-scale model and mesh, which are used for the postdiction of the experiments with a full depth barrier, are used both in 2D and in 3D with a pipe as a boundary condition of 0 mm depth. These are the same models as used for the comparison of the DgFlow results to the Plaxis results, Appendix C "Comparison DgFlow and Plaxis" of the main report.

Additionally, only for the 2D models with permeability ratios 3 and 100, the Abaqus results are also compared to DgFlow results with different pipe depths. These models have the pipe as a boundary condition, but the depth of the pipe is 2,4,6 or 10 mm as analysed in Appendix Effect of pipe depth in the main report.

### 1.2 Abaqus

The model setup for the Abaqus study is described in the Appendix D Report XI.17.11 in the main report key features are:

- the T shaped pipe has a 'main pipe' transverse to the barrier, and a 'side pipe' parallel to the barrier;

- the depth in the main pipe decreases linearly from the exit hole 10 mm to 5 mm at the side pipe and has vertical sides;
- the side pipe has a bottom width of 20 mm and a depth that varies linearly from 5 mm in the centre to 2.5 mm at the edges. The downstream sides are vertical and the upstream sides slope at 45° into the barrier;
  - because of the linearly decreasing depth of the pipe, the top of the pipe lies within the barrier for 5 mm at the centre and only 2.5 mm at the sides of the setup;
- a pressure difference is applied of 8.99 kPa at the top of the model at the inflow to 4.99 kPa at the outflow (with hydrostatic pressure at the inflow). For comparison to the DgFlow results with boundary conditions 0.4 m head upstream and 0.0 m head downstream these values are scaled to the corresponding hydraulic head values for comparison in the results in this memo;
- the pipe is modelled as a granular material with a high permeability of 20 m/s in the 'main pipe' i.e. the part of the pipe that runs parallel to the flow direction from the outlet hole to the barrier, and 5 m/s in the 'side pipe', i.e. the branches of the T-shaped pipe parallel to the barrier.

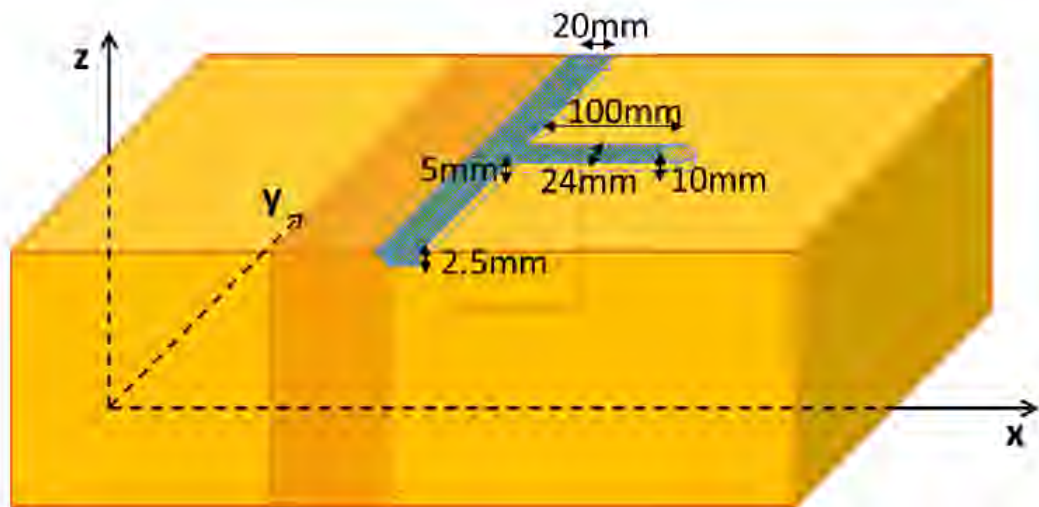


Figure 1.1 Image of the Abaqus model, note the pipe has a sloping edge that goes into the barrier (source Report XI.17.11, appendix D)

## 2 Head profiles

The head profiles through the top centreline of the two 3D models (DgFlow and Abaqus) and through the top of the 2D (DgFlow) models are plotted shown below for the different head contrasts.

Because the pipe in Abaqus has a fixed depth of 5 mm at this point and a slope of 45° the head falls sharply slightly before the end of the barrier in the Abaqus model. Because of this, the head in the barrier is lower in the Abaqus model than in the DgFlow models.

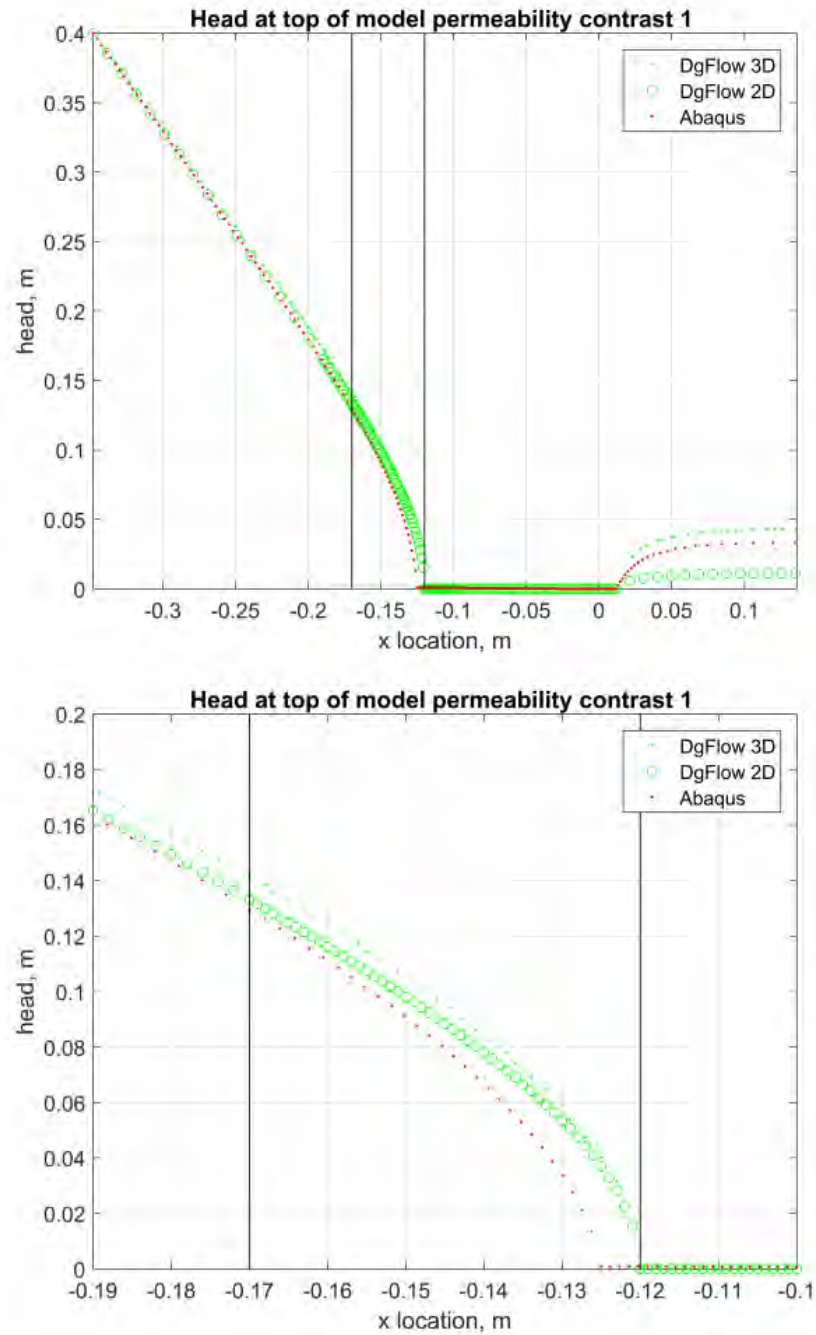


Figure 2.1 Head in the central axis at the top of the model for Abaqus (red) and DgFlow 3D (green dots), also for the top of the 2D model in DgFlow (green circles). Barrier is between -0.12 and -0.17 m

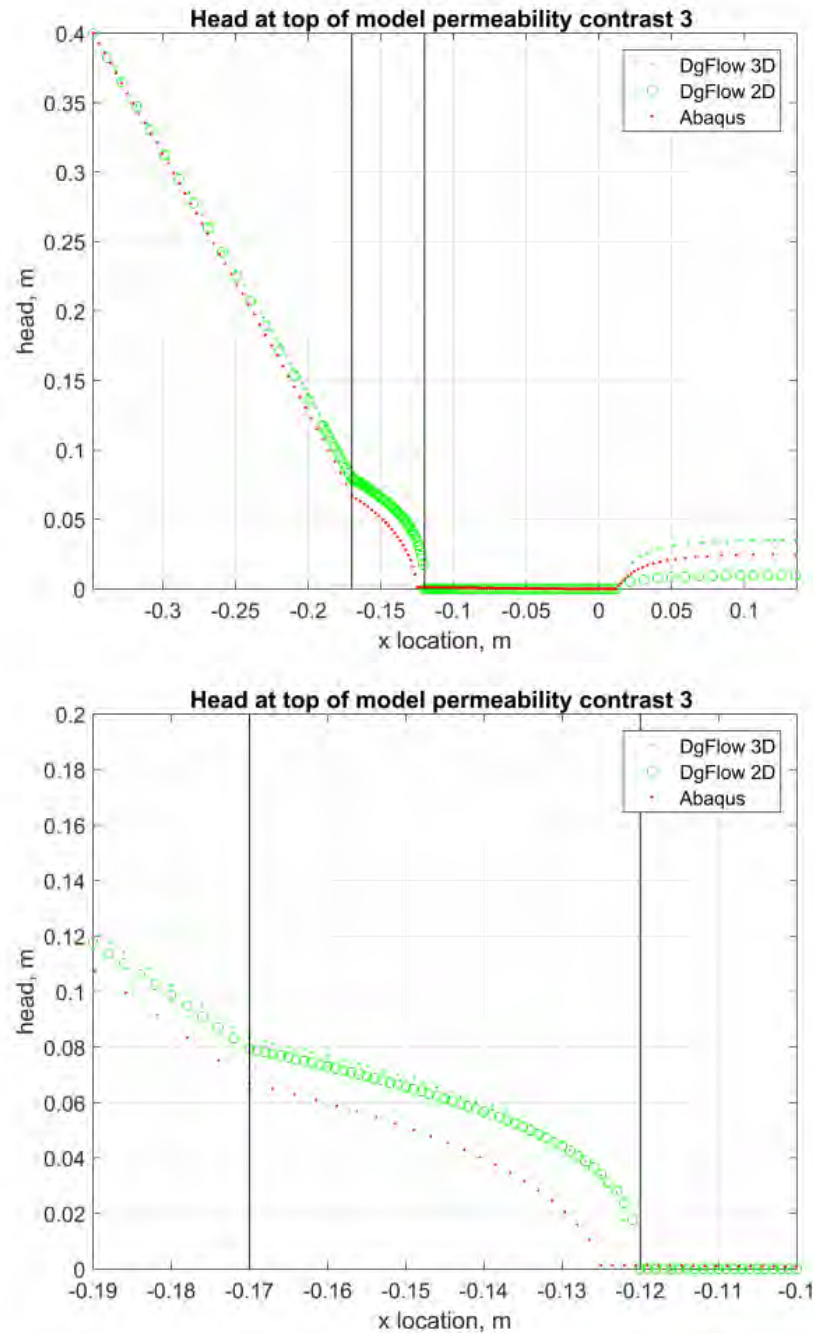


Figure 2.2 Head in the central axis at the top of the model for Abaqus (red) and DgFlow 3D (green dots), also for the top of the 2D model in DgFlow (green circles). Barrier is between -0.12 and -0.17 m

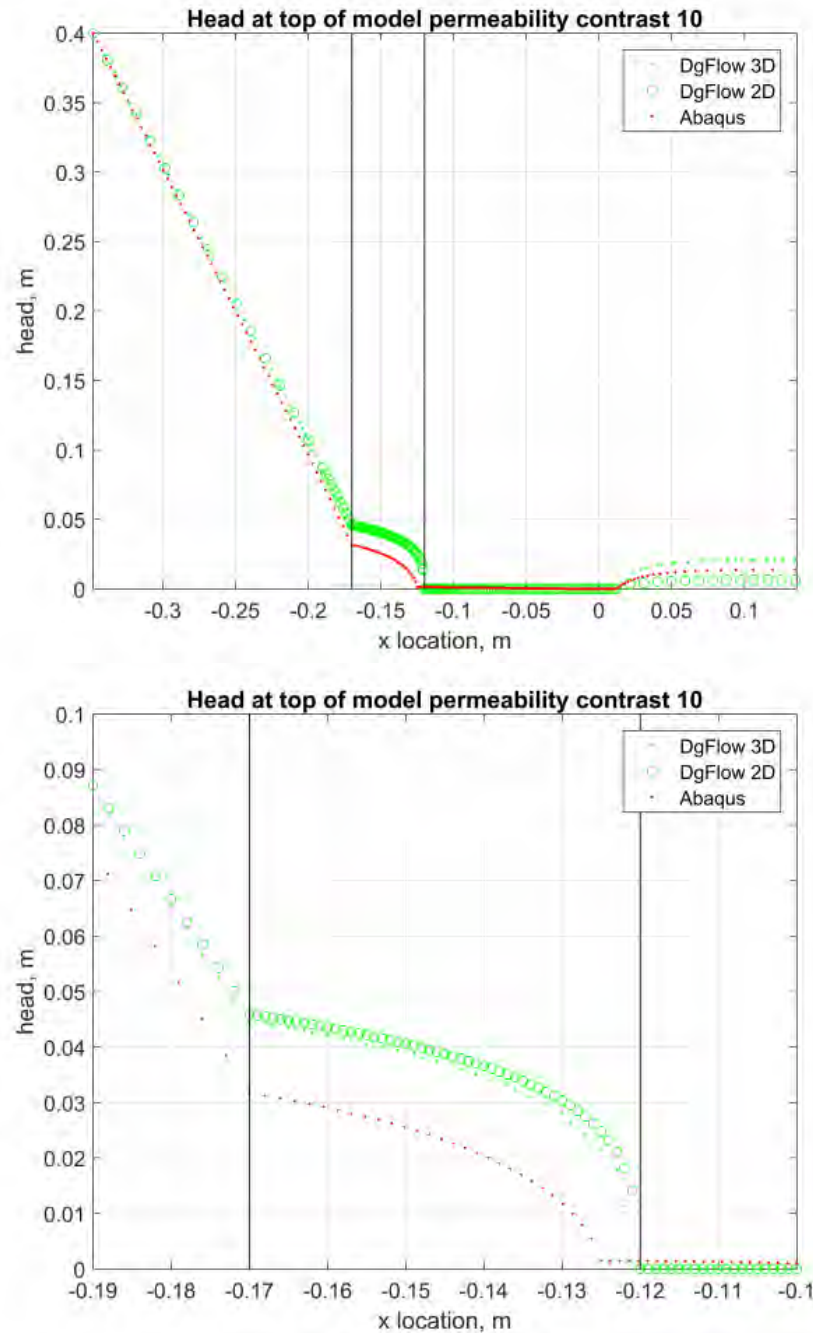


Figure 2.3 Head in the central axis at the top of the model for Abaqus (red) and DgFlow 3D (green dots), also for the top of the 2D model in DgFlow (green circles). Barrier is between -0.12 and -0.17 m

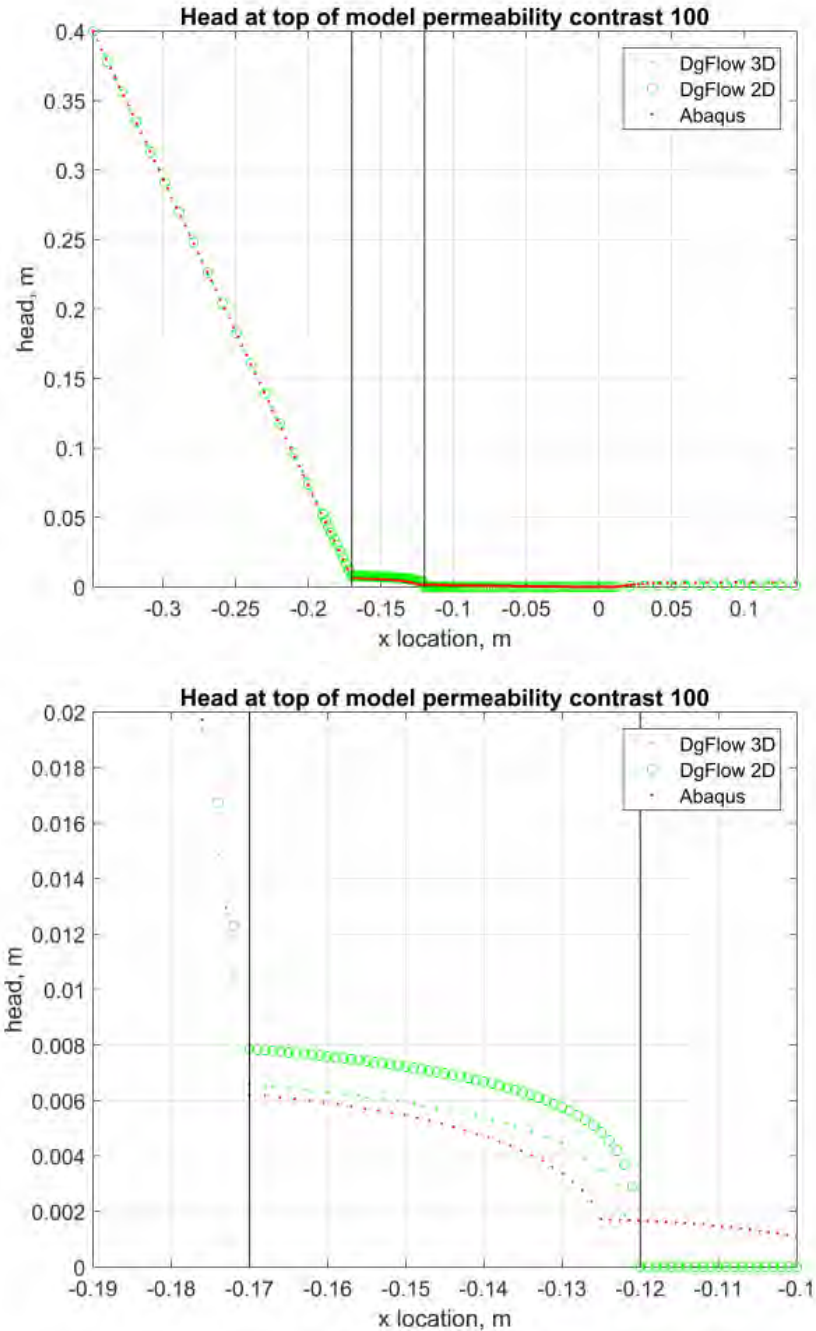


Figure 2.4 Head in the central axis at the top of the model for Abaqus (red) and DgFlow 3D (green dots), also for the top of the 2D model in DgFlow (green circles). Barrier is between -0.12 and -0.17 m

## 2.1 Head profiles for deeper pipe in DgFlow

In Appendix H of the main report, the effect of pipe depth is assessed in DgFlow by lowering the boundary condition that represents the top of the pipe. Thereby there are no elements in the pipe as opposed to the Abaqus model. In those models the pipe has a vertical wall at the interface with the barrier. This is done for 2D models.

The figures below show the head distribution in the 2D models DgFlow with variable pipe depth and in the 3D Abaqus model.

For a permeability contrast of 3 the 2D DgFlow model with a pipe depth of 4 mm corresponds relatively well with the Abaqus results from about 2 cm upstream of the barrier-pipe interface. For the contrast of 100, the Abaqus result lies between the values with 0 mm pipe depth and 2 mm pipe depth in DgFlow.

However, it was noted before that the difference between 2D and 3D models in DgFlow are also dependent on permeability contrast, for the higher contrast the 2D models gives a higher gradient than the 3D model, whilst this is the other way around for the lower permeability contrast. The relative difference between 2D and 3D in DgFlow is also smaller for the lower contrast

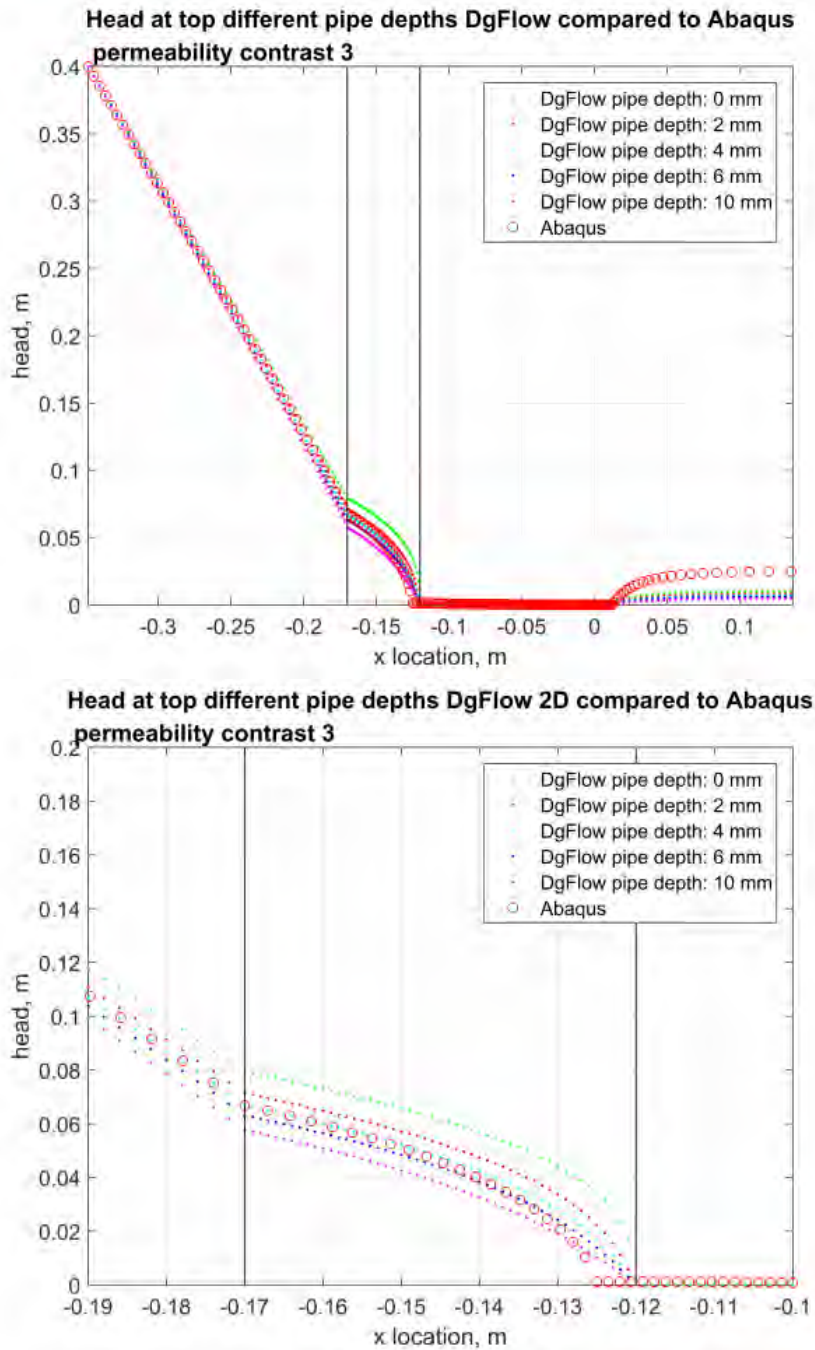


Figure 2.5 Head in the central axis at the top of the model for Abaqus (red circles) and DgFlow 2D (dots) with different pipe depths. Barrier is between -0.12 and -0.17 m

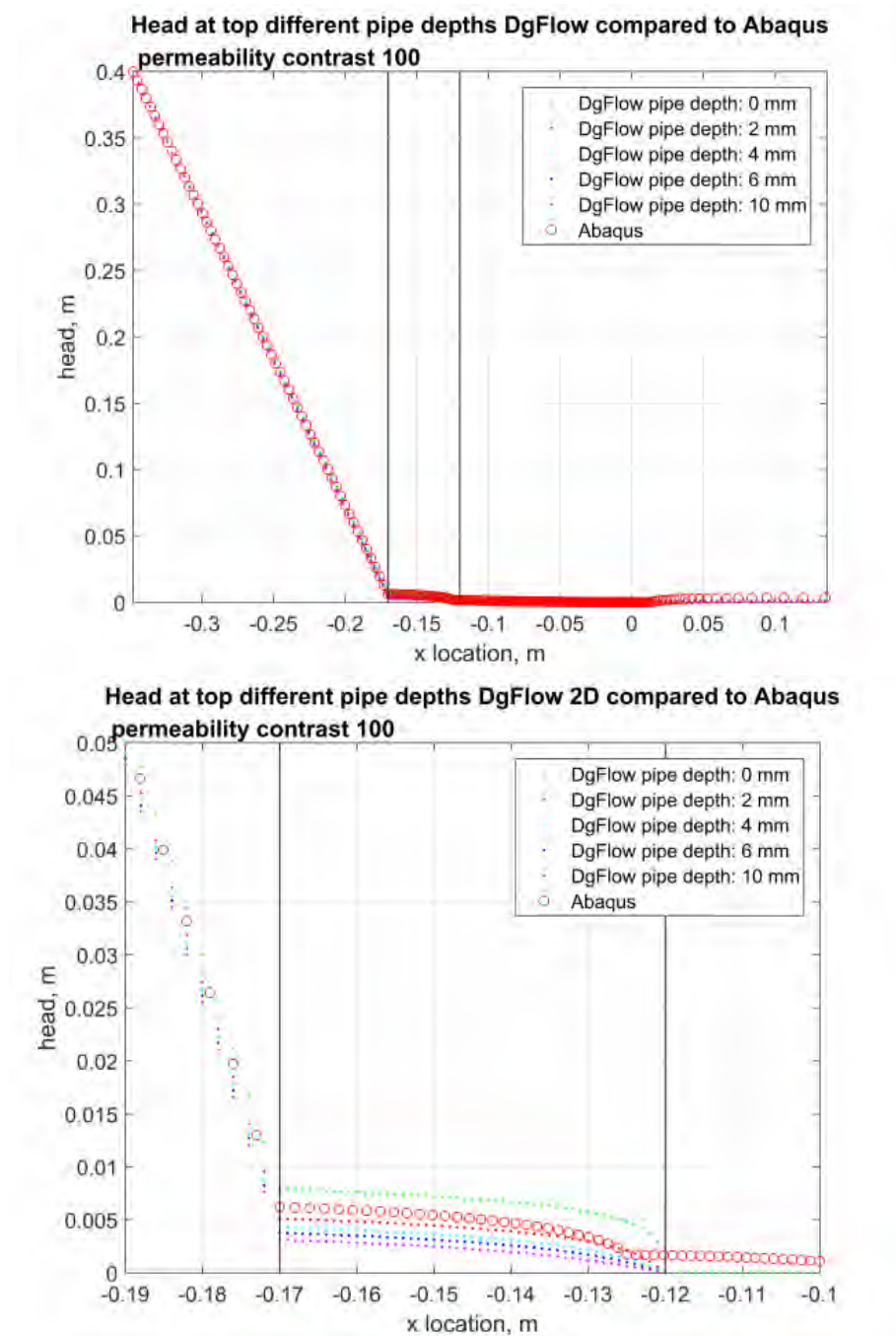


Figure 2.6 Head in the central axis at the top of the model for Abaqus (red circles) and DgFlow 2D (dots) with different pipe depths. Barrier is between -0.12 and -0.17 m.

### 3 Local gradients

The gradient is computed over the entire barrier and also over a 3.5 cm stretch between the interface between the barrier and the pipe and 3.5 cm upstream of this (-0.120 to -0.155 m

from the centre of the outlet hole) and between 1 cm upstream of the interface between the barrier and the pipe and 4.5 cm upstream of this interface (-0.130 to -0.165 m from the centre of the outlet hole).

The tables below show the gradients from the different models and the ratio of the gradient in the DgFlow model, to the gradient found in the Abaqus model.

As expected from the head profiles, difference between the gradients is largest for the models with a high permeability contrast and then it is larger for the 2D DgFlow model than for the 3D model. The DgFlow models give a higher gradient in the downstream part of the barrier, and over the entire barrier, than the Abaqus model. The Abaqus model gives a lower gradient over the upstream part of the barrier.

The damage criterion used in this phase of the project is the gradient between -0.130 and -0.165 m as detailed in the main report. Differences between the gradients over this distance computed using models with 0 mm pipe depth in DgFlow and using a pipe depth of ca. 0.5 mm in Abaqus are in the order of 0.7, which is considered significant.

Table 3.1 Gradients from the models

model name	2D/3D	permeability barrier	permeability fine	permeability ratio	gradient from model at top boundary		
		m/s	m/s		from -0.120 to -0.170 m	from -0.120 to -0.155 m	from -0.130 to -0.165 m
S_2D_k1_w1	2	2.00E-03	6.00E-04	3	1.59	1.99	0.92
S_2D_k2_w1	2	6.00E-02	6.00E-04	100	0.16	0.21	0.06
S_2D_k3_w1	2	6.00E-04	6.00E-04	1	2.66	3.07	2.04
S_2D_k4_w1	2	6.00E-03	6.00E-04	10	0.92	1.20	0.41
S_3D_k1_w1	3	2.00E-03	6.00E-04	3	1.67	2.03	0.95
S_3D_k2_w1	3	6.00E-02	6.00E-04	100	0.13	0.17	0.06
S_3D_k3_w1	3	6.00E-04	6.00E-04	1	2.83	3.18	2.04
S_3D_k4_w1	3	6.00E-03	6.00E-04	10	0.89	1.16	0.44
Abaqus_k1	3	2.00E-03	6.00E-04	3	1.31	1.56	1.21
Abaqus_k2	3	6.00E-02	6.00E-04	100	0.09	0.12	0.08
Abaqus_k3	3	6.00E-04	6.00E-04	1	2.57	2.88	2.44
Abaqus_k4	3	6.00E-03	6.00E-04	10	0.59	0.72	0.53

Table 3.2 Comparison of gradients from DgFlow and Abaqus

permeability contrast/ dimensions	DgFlow/Abaqus		
	from -0.120 to -0.170 m	from -0.120 to -0.155 m	from -0.130 to -0.165 m
Contrast 3: 2D	1.21	1.28	0.76
Contrast 100: 2D	1.73	1.83	0.73
Contrast 1: 2D	1.03	1.06	0.83
Contrast 10: 2D	1.56	1.67	0.78
Contrast 3: 3D	1.27	1.30	0.79
Contrast 100: 3D	1.45	1.47	0.71
Contrast 1: 3D	1.10	1.10	0.84
Contrast 10: 3D	1.51	1.61	0.83

### 3.1 Local gradients for deeper pipe in DgFlow

The local gradients for the models with a variable pipe depth in DgFlow are shown below. For both cases, the models with a pipe depth of 0.4 mm still show a difference with the Abaqus results for the range over which the damage criterion is defined (-130 to -165 mm), however the head profiles in Figure 2.5 and Figure 2.6 are better for the models with a pipe depth of 0.4 mm.

Table 3.3 Gradients from the models

Model name	2D/3D	permeability barrier m/s	permeability fine m/s	permeability ratio	Gradient from model at y=0		
					from -0.120 to -0.170 m	from -0.120 to -0.155 m	from -0.130 to -0.165 m
S_2D_k1_pip0	2	2.00E-03	6.00E-04	3	1.59	1.99	0.92
S_2D_k1_pip1	2	2.00E-03	6.00E-04	3	1.43	1.75	0.99
S_2D_k1_pip2	2	2.00E-03	6.00E-04	3	1.34	1.61	1.01
S_2D_k1_pip3	2	2.00E-03	6.00E-04	3	1.27	1.50	1.02
S_2D_k1_pip4	2	2.00E-03	6.00E-04	3	1.15	1.34	1.01
S_2D_k2_pip0	2	6.00E-02	6.00E-04	100	0.16	0.21	0.06
S_2D_k2_pip1	2	6.00E-02	6.00E-04	100	0.10	0.13	0.06
S_2D_k2_pip2	2	6.00E-02	6.00E-04	100	0.09	0.11	0.06
S_2D_k2_pip3	2	6.00E-02	6.00E-04	100	0.08	0.10	0.06
S_2D_k2_pip4	2	6.00E-02	6.00E-04	100	0.06	0.08	0.05

Table 3.4 Comparison of gradients from DgFlow and Abaqus.

permeability contrast/ dimensions	DgFlow/Abaqus		
	from -0.120 to -0.170 m	from -0.120 to -0.155 m	from -0.130 to -0.165 m
Contrast 3: depth 0 mm	1.21	1.28	0.76
Contrast 3: depth 2 mm	1.09	1.12	0.82
<b>Contrast 3: depth 4 mm</b>	<b>1.02</b>	<b>1.03</b>	<b>0.84</b>
Contrast 3: depth 6 mm	0.96	0.97	0.84
Contrast 3: depth 10 mm	0.88	0.86	0.83
Contrast 100: depth 0 mm	1.73	1.83	0.73
Contrast 100: depth 2 mm	1.13	1.15	0.74
<b>Contrast 100: depth 4 mm</b>	<b>0.94</b>	<b>0.95</b>	<b>0.73</b>
Contrast 100: depth 6 mm	0.83	0.82	0.71
Contrast 100: depth 10 mm	0.69	0.66	0.67

## 4 Conclusions

- By modelling the pipe with a sloping wall into the barrier in the Abaqus model, the head falls upstream of the interface between the pipe and the barrier in the Abaqus model, resulting in lower head profiles than in DgFlow at the centre top axis through the model.
  - The head in the barrier at the location of the pipe in the Abaqus model at the centre top axis is less than 0.2 mm, indicating a negligible head loss in the pipe.
- Relative differences between the local gradients computed with the two models are most significant for higher permeability contrasts.
- Accounting for a pipe depth of 4 mm in the DgFlow models results in the computed gradient over the entire barrier being in the range of 0.9 to 1.1 of the computed gradient in the barrier in the Abaqus models. However, the difference between the computed gradients over the distance over which the damage criterion is defined is larger; in the order of 0.73 for a permeability contrast of 100 and 0.84 for a permeability contrast of 3.
- In Abaqus the pipe is meshed with a finite depth the depth, which affects the head profile and gradients in the model. It can be seen that differences between Abaqus and DgFlow head profiles are relatively large when a 0 mm deep pipe is applied in the DgFlow models, whereas these differences in the head profiles are relatively small for pipes with a depth of 4 mm or 6 mm. The differences between local gradients over the distance of the damage criterion remain large also for a pipe depth of 4 mm in DgFlow, on the other hand the differences between the gradients over the entire barrier are low.

## **F Effect of hydraulic conductivity contrast in 2D and 3D models**

## Memo

**To**  
Vera van Beek, Adam Bezuijen

**Date**  
3 November 2017

**Number of pages**  
6

**From**  
Esther Rosenbrand

**Direct line**  
+31(0)88335 7852

**E-mail**  
esther.rosenbrand@deltares.nl

**Subject**  
Effect of permeability contrast in 2D and 3D models

---

In this analysis, the difference between results from 2D and 3D models is considered. The models used are described in the main report; the pipe has grown along the entire length of the barrier.

5 permeability contrasts are considered:

- 1
- 3
- 10
- 30
- 100

The upstream head is 0.4 for all cases. The permeability of the fine material is  $6e-4$  m/s for all cases.

## 1 Flow profiles

The streamlines indicate the flow paths in the 2D models in the figures below; the background colour is the head distribution. For a higher permeability contrast, the flow converges strongly in the barrier.



Figure 1.1 Head distribution and streamlines permeability contrast 1



Figure 1.2 Head distribution and streamlines permeability contrast 3



Figure 1.3 Head distribution and streamlines permeability contrast 10



Figure 1.4 Head distribution and streamlines permeability contrast 30



Figure 1.5 Head distribution and streamlines permeability contrast 100

## 2 Effect permeability contrast on head distributions in 2D and 3D models

The results from the 2D calculations are very similar to those from the 3D calculations for both a high and a low ratio between the permeability's of the fine and the coarse sand.

The smaller the contrast the higher the head in the barrier and the larger the local gradient over the barrier.

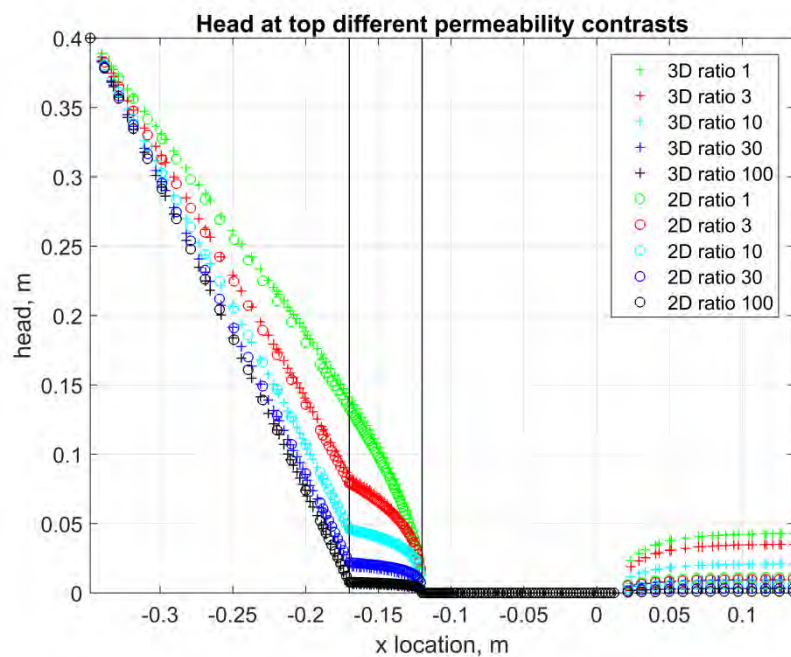


Figure 2.1 Head distribution in the model

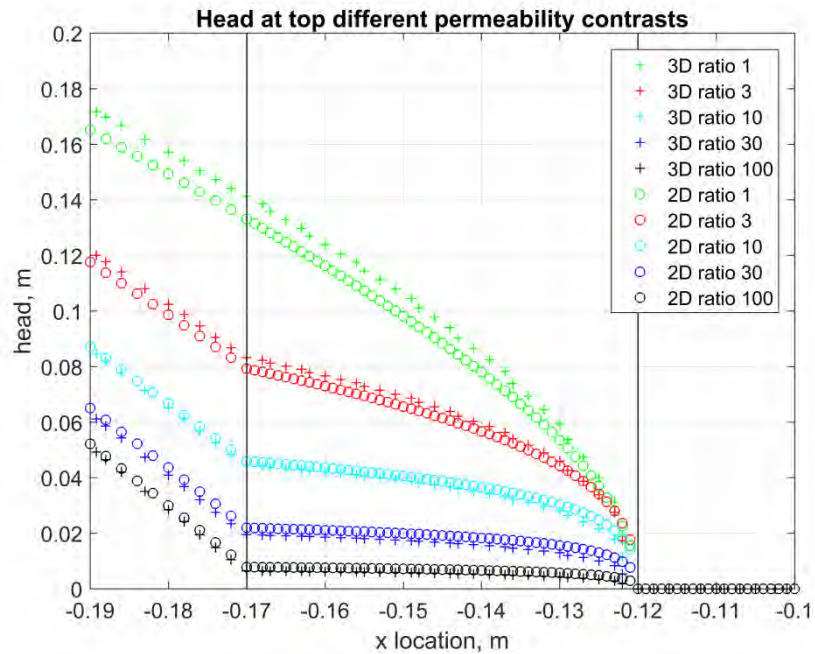


Figure 2.2 Head distribution in the model

### 3 Effect of permeability contrast on local gradients in 2D and 3D models

The effect of permeability contrast on the gradient over the entire barrier is shown below for the 2D and 3D models where the gradient is taken from -120 mm to -170 mm. This shows that the 2D model gives a lower gradient for permeability contrasts below 30, and a higher gradient for contrasts of 30 and 100.

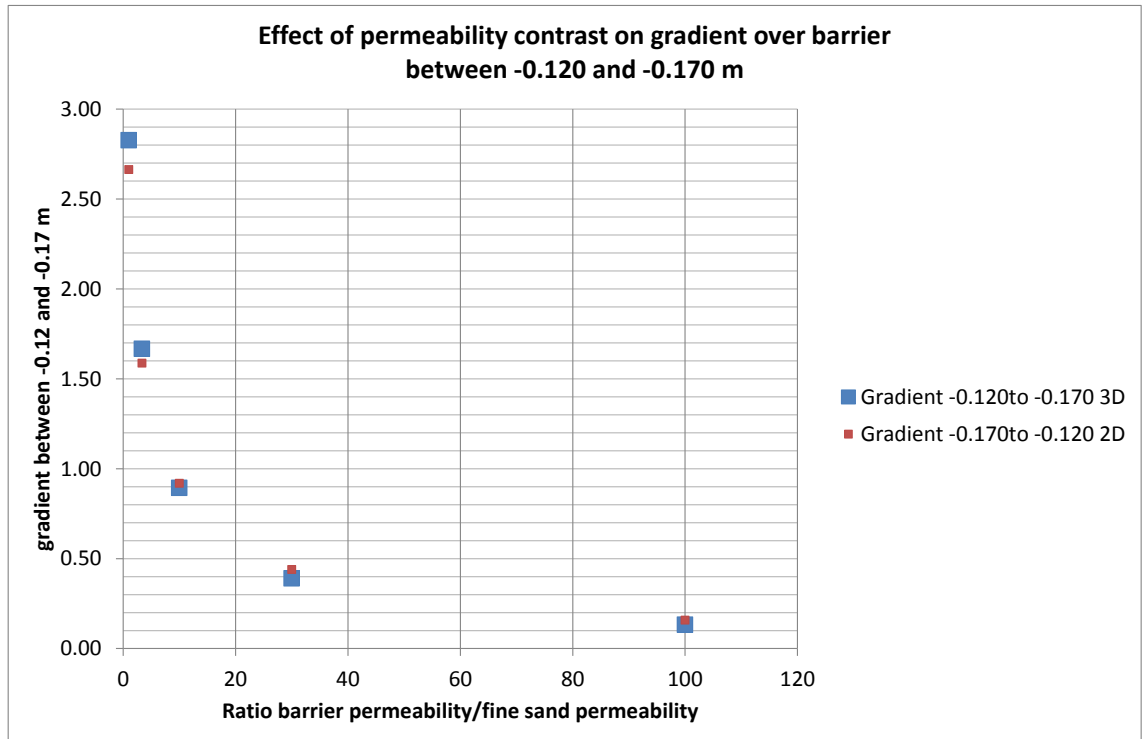


Figure 3.1 Gradients over the barrier show the absolute effect of permeability contrast in 2D and 3D models on the local gradient

The relative effect, i.e. the ratio of the gradient from the 2D and the 3D model as a function of the permeability contrast is shown below. The location within the barrier that is used to compute the gradient affects the difference between 2D and 3D only slightly, this is shown for:

- The gradient over the entire barrier (-0.120 to -0.170 m);
- The gradient between -0.130 and -0.165, the distance of the damage criterion in the current phase of the project (i.e. 1 cm upstream of the interface between the barrier and the pipe and 4.5 cm upstream of this interface).

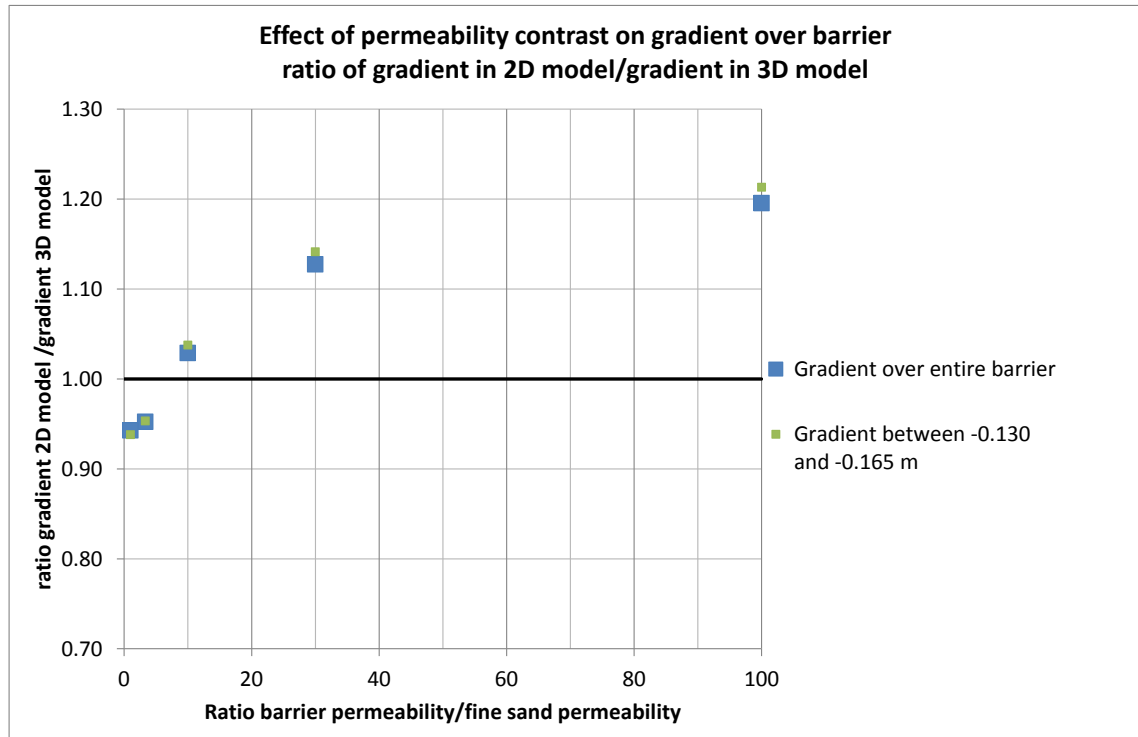


Figure 3.2 The ratio of the gradient over the barrier in 2D over the gradient over the barrier in 3D show the effect of the permeability contrast on the differences between the results in the 2D and the 3D model

## 4 Conclusions

- The larger the permeability contrast the more convergence of flow in the barrier towards the pipe tip.
- The larger the permeability contrast, the lower the head in the barrier and the lower the gradient in the barrier.
- The 2D model and 3D models give quite similar results for the overall head profile. However, the gradient over the barrier (-0.120 to -0.170 m) in the 2D model is lower than in the 3D model for the calculations with the permeability ratios between 1 and 10. For the simulation with a permeability ratio of 30 or 100 the 2D model gives a higher gradient than the 3D model.
- The difference between the 2D and 3D results computed for the gradient inside the barrier is dependent on the location in the barrier over which the gradient is computed. However, the difference between the results for the gradients calculated with the 2D and with the 3D models over the entire barrier, are practically the same as the gradients computed over the distance used for the damage criterion (-0.130 to -0.165 m).
- Although differences between models are larger for a higher permeability contrast, differences between models due to measurement uncertainties are also likely to be larger due to the lower gradient in the barrier. The uncertainty on the measurement accuracy and the fit of the postdiction as analysed in the main report is significantly higher than the differences between the 2D and the 3D models. Thus for the current phase of the project, 2D models are considered adequate.

## **G Sensitivity analysis transverse extension of pipe**

## Memo

**To**  
Vera van Beek, Adam Bezuijen

**Date**  
3 November 2017

**Number of pages**  
14

**From**  
Esther Rosenbrand

**Direct line**  
+31(0)88335 7852

**E-mail**  
esther.rosenbrand@deltares.nl

**Subject**  
Sensitivity analysis transverse extension of pipe

---

In this sensitivity analysis, the effect of a pipe that has not widened parallel to the entire barrier is analysed. Three geometries are analysed in 3D models, with a pipe of width 10 cm, 20 cm and 30 cm (entire model).

Results for the head distribution along the centreline of the model are compared to results from the 2D model. In addition, the heads along lines at 4 cm from the centreline, and 9 cm from the centreline are analysed.

The calculations are performed using 2 permeability contrasts, 3 and 100.

## 1 Head distributions

### 1.1 For pipe of 30 cm width

#### 1.2 Effect of distance from centre of model

With a fully developed pipe (width 30 cm) the head is practically the same at distances 0, 4 and 9 cm from the central axis. The gradients effectively the same with increasing distance from the centre.

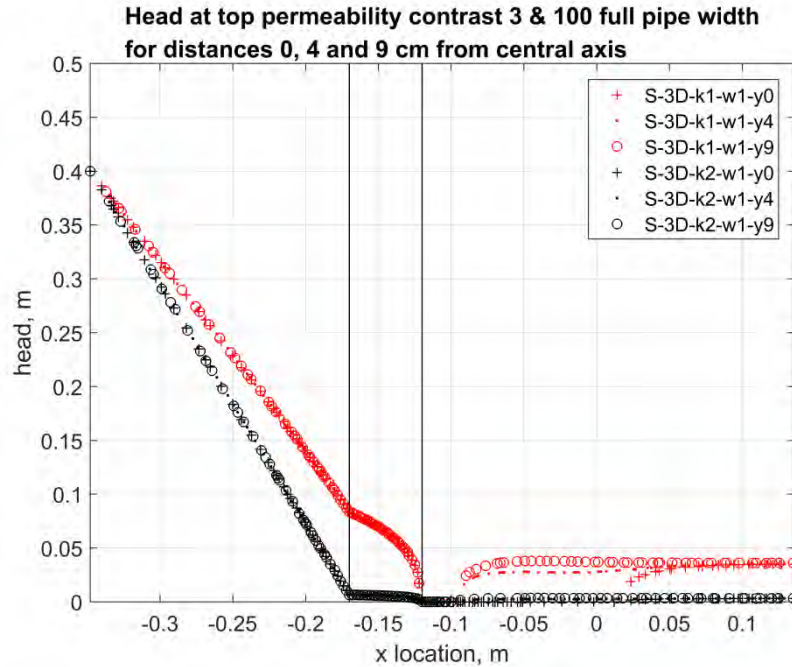


Figure 1.1 Head distribution in the model. k1 (red) is permeability contrast 3, k2 (black) is permeability contrast 100. w1 is width of pipe along barrier of 30 cm, y0, y4, and y9 refer to distance from the central axis in mm in the y direction (i.e. along the width of the model)

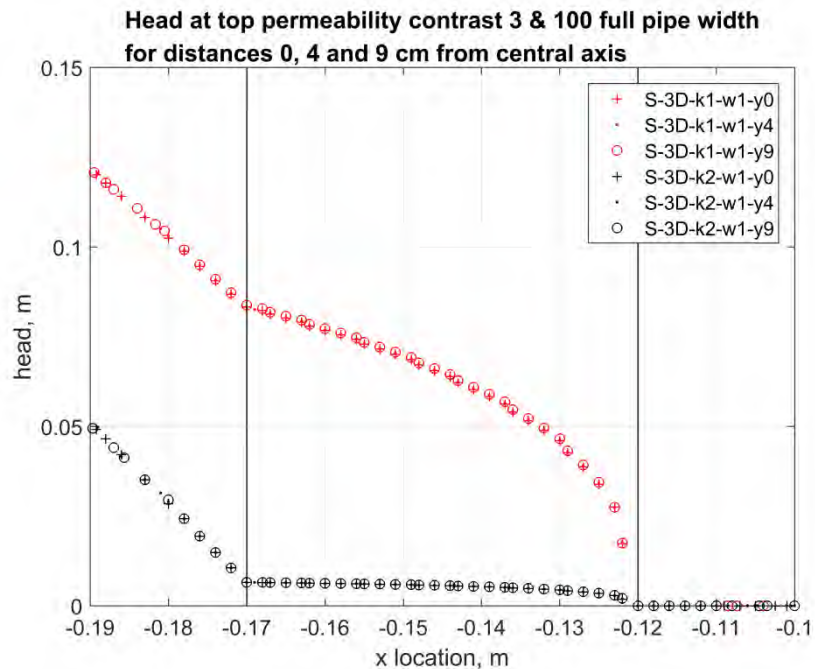


Figure 1.2 Head distribution in the model. k1 (red) is permeability contrast 3, k2 (black) is permeability contrast 100. w1 is width of pipe along barrier of 30 cm, y0, y4, and y9 refer to distance from the central axis in mm in the y direction (i.e. along the width of the model)

### 1.2.1 Difference between 2D and 3D

The results from the 2D calculation are very similar to those from the 3D calculation for both a high and a low ratio between the permeabilities of the fine sand and the coarse sand.

For a low contrast of 1 ( $k_3$ ) or 3 ( $k_1$ ), the 3D model gives a slightly higher head than the 2D model. However, for a large contrast of 100 ( $k_2$ ) the 3D model gives a slightly lower head than the 2D model.

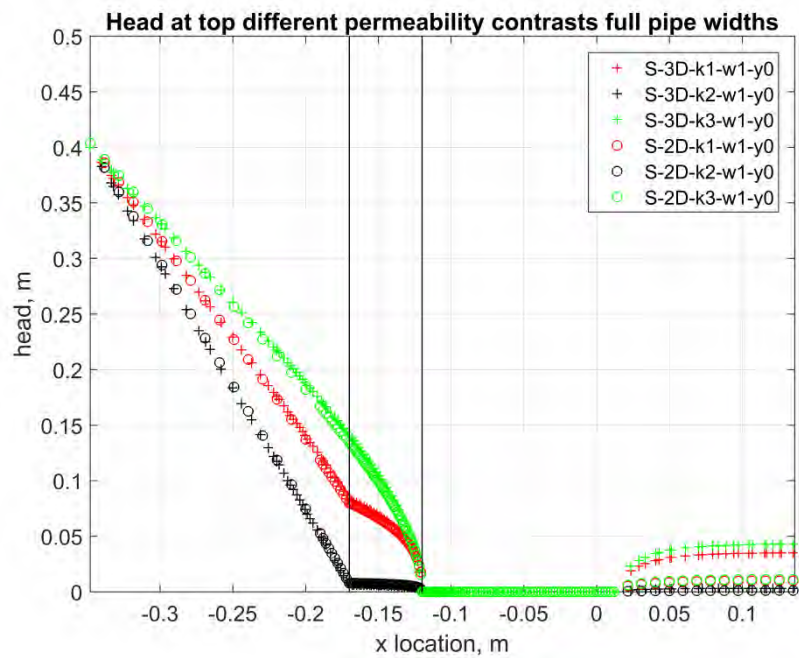


Figure 1.3 Head distribution in the model. Crosses are 3D results circles are 2D results.  $k_1$  (red) is permeability contrast 3,  $k_2$  (black) is permeability contrast 100;  $k_3$  green is permeability contrast 1 (equal permeabilities).  $w_1$  is width of pipe 30 cm along barrier

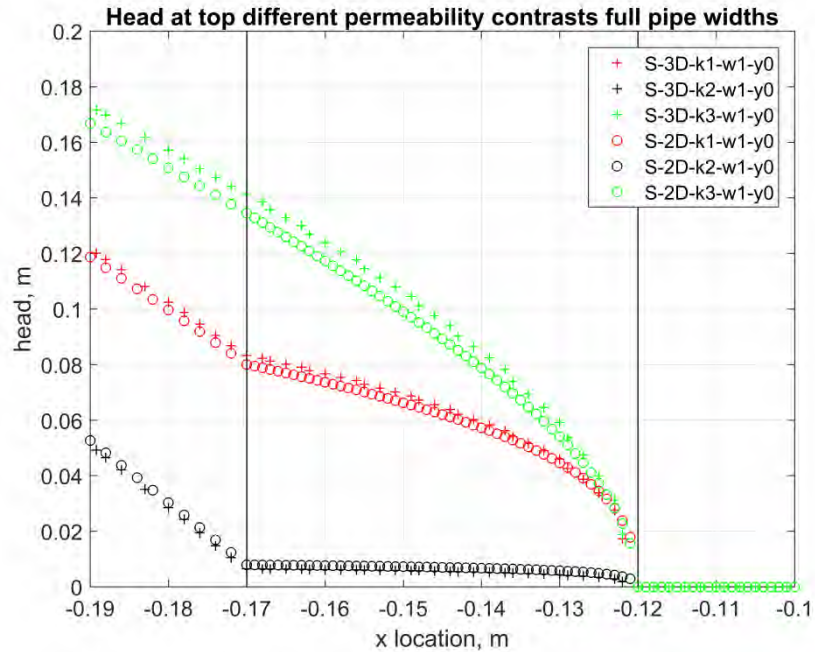


Figure 1.4 Head distribution in the model. Crosses are 3D results circles are 2D results. k1 (red) is permeability contrast 3, k2 (black) is permeability contrast 100; k3 green is permeability contrast 1 (equal permeabilities). w1 is width of pipe 30 cm along barrier

### 1.3 For pipe of 20 cm width

#### 1.4 Effect of distance from centre of model

With a pipe width 20 cm the gradient at 9 cm from the centre of the model, i.e. 1 cm from the edge of the pipe, is higher than in the centre. The absolute difference is strongest in the model with a low permeability contrast; with a high permeability contrast, the gradient in the barrier is negligible. However because of this, the relative difference between the gradient in the 2D and in the 3D models is larger.

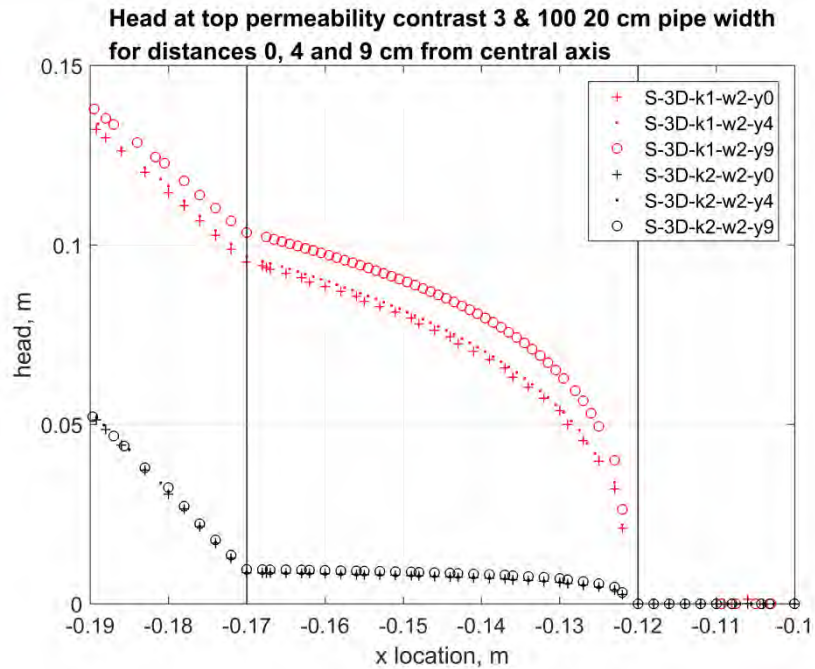


Figure 1.5 Head distribution in the model. k1 (red) is permeability contrast 3, k2 (black) is permeability contrast 100. w1 is width of pipe along barrier of 20 cm, y0, y4, and y 9 refer to distance from the central axis in mm in the y direction (i.e. along the width of the model)

#### 1.4.1 Difference between 2D and 3D at the centre of the model.

With a 20 cm wide barrier the difference between the head from the 2D and 3D model at the centre axis gets larger than in the case of a 30 cm wide pipe. This could be expected, because the pipe will attract water from the sides of the model to the centre, resulting in a larger gradient also in the centre.

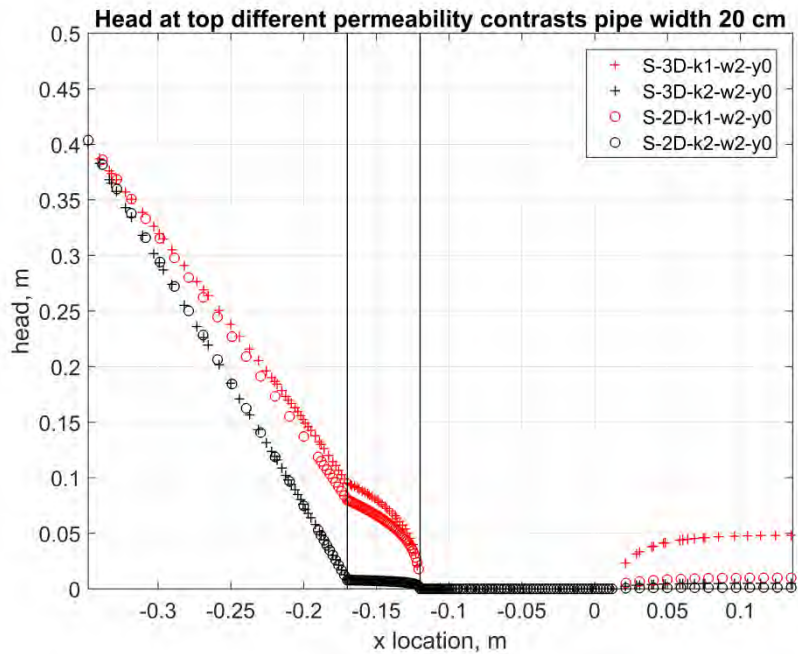


Figure 1.6 Head distribution in the model. Crosses are 3D results circles are 2D results. k1 (red) is permeability contrast 3, k2 (black) is permeability contrast 100. W2 is width of pipe 20 cm along barrier

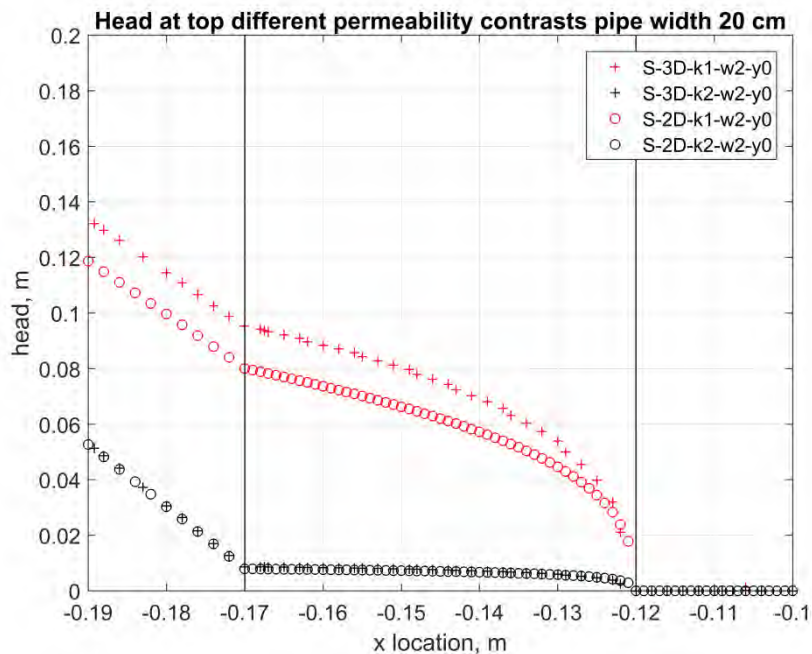


Figure 1.7 Head distribution in the model. Crosses are 3D results circles are 2D results. k1 (red) is permeability contrast 3, k2 (black) is permeability contrast 100. W2 is width of pipe 20 cm along barrier

## 1.5 For pipe of 10 cm width

### 1.6 Effect of distance from centre of model

With a pipe width 10 cm the gradient at 4 cm from the centre of the model, i.e. 1 cm from the edge of the pipe, is higher than in the centre. The difference is strongest in the model with a low permeability contrast; with a high permeability contrast, the gradient in the barrier is negligible. The difference is also larger than the difference between the gradient at 9 cm from the centre and the gradient in the centre in the model with a pipe of 20 cm width.

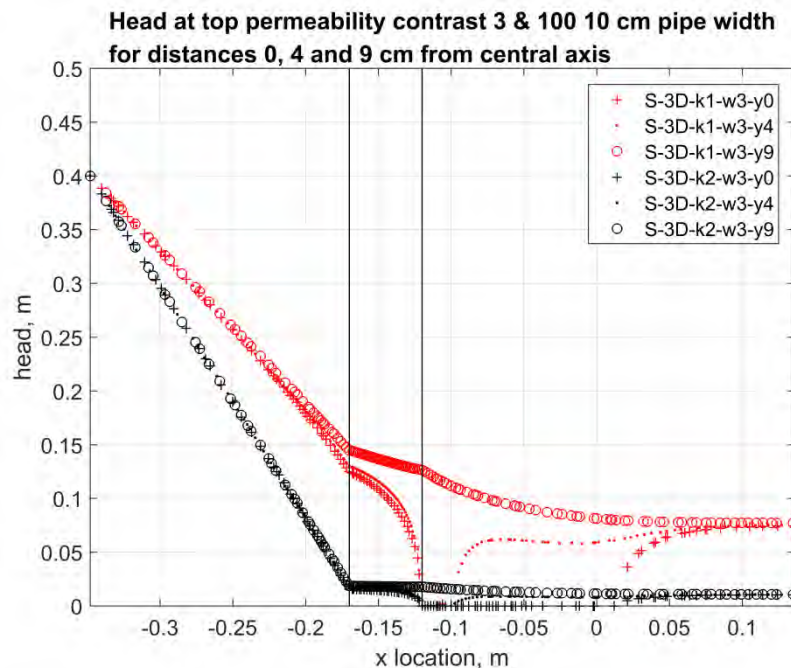


Figure 1.8 Head distribution in the model. k1 (red) is permeability contrast 3, k2 (black) is permeability contrast 100. w1 is width of pipe along barrier of 10 cm, y0, y4, and y9 refer to distance from the central axis in mm in the y direction (i.e. along the width of the model)

#### 1.6.1 Difference between 2D and 3D

With a 10 cm wide barrier the difference between the head from the 2D and 3D model at the centre axis gets larger than it is in the case of a 30 cm wide pipe. Again, this could be expected because the pipe that has not widened as far concentrates the flow to the centre to a greater extent.

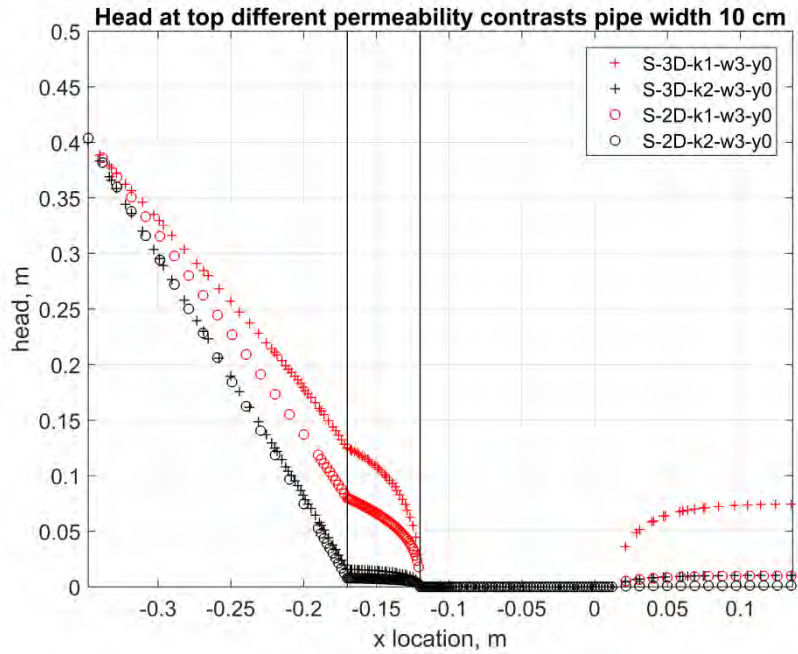


Figure 1.9 Head distribution in the model. Crosses are 3D results circles are 2D results. k1 (red) is permeability contrast 3, k2 (black) is permeability contrast 100. W3 is width of pipe 10 cm along barrier

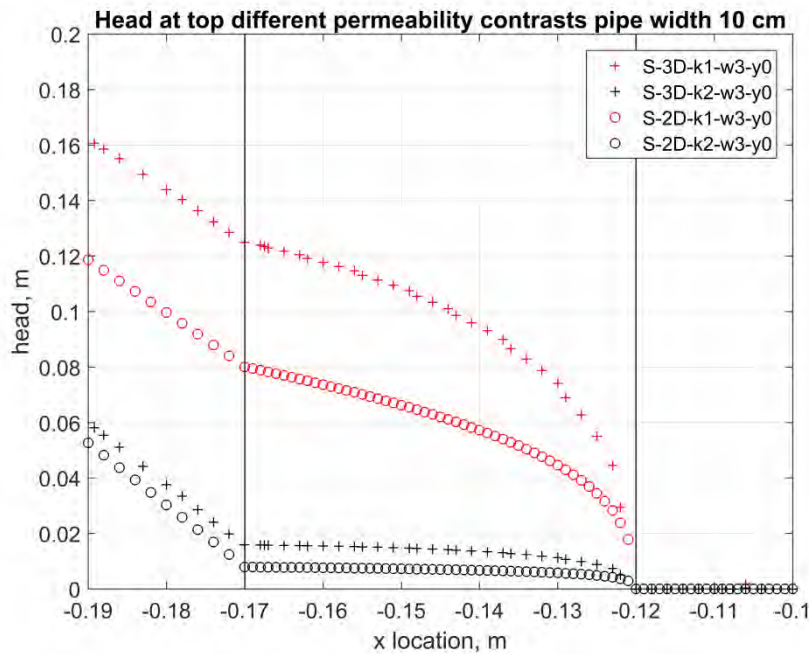


Figure 1.10 Head distribution in the model. Crosses are 3D results circles are 2D results. k1 (red) is permeability contrast 3, k2 (black) is permeability contrast 100. W3 is width of pipe 10 cm along barrier

## 1.7 Effect of pipe width

The figures below summarize the results above, showing the effect of the width of the pipe on the head distribution in the model. The wider the pipe, the lower the hydraulic head in the barrier.

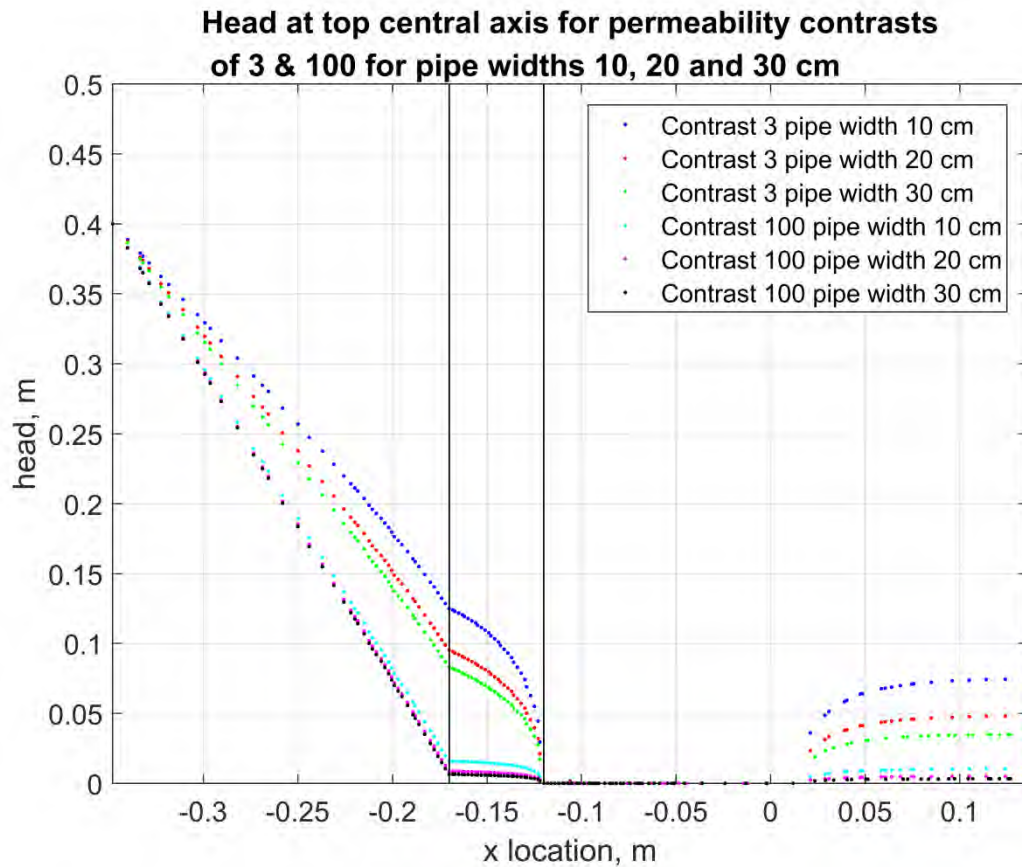


Figure 1.11 Head distribution in the model

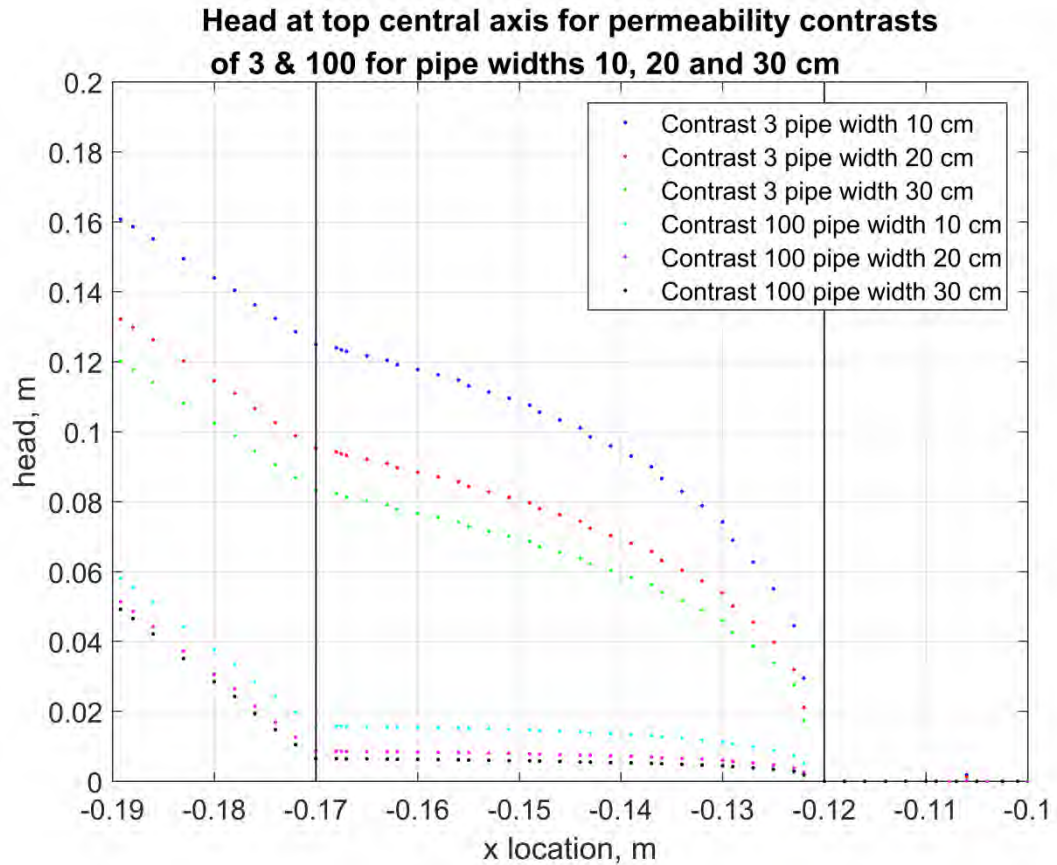


Figure 1.12 Head distribution in the model

## 2 Effect of pipe width on gradient over barrier

The effect of pipe width on the gradient over the entire barrier at different y locations parallel to the central axis is shown below. Note that the low gradients for the location 9 cm when the pipe is 10 cm wide are because the pipe does not extend this far, i.e there is no pipe in front of the barrier at that location (the pipe only extends between y coordinates -5 cm and +5 cm). Also shown for comparison is the gradient computed in the 2D model.

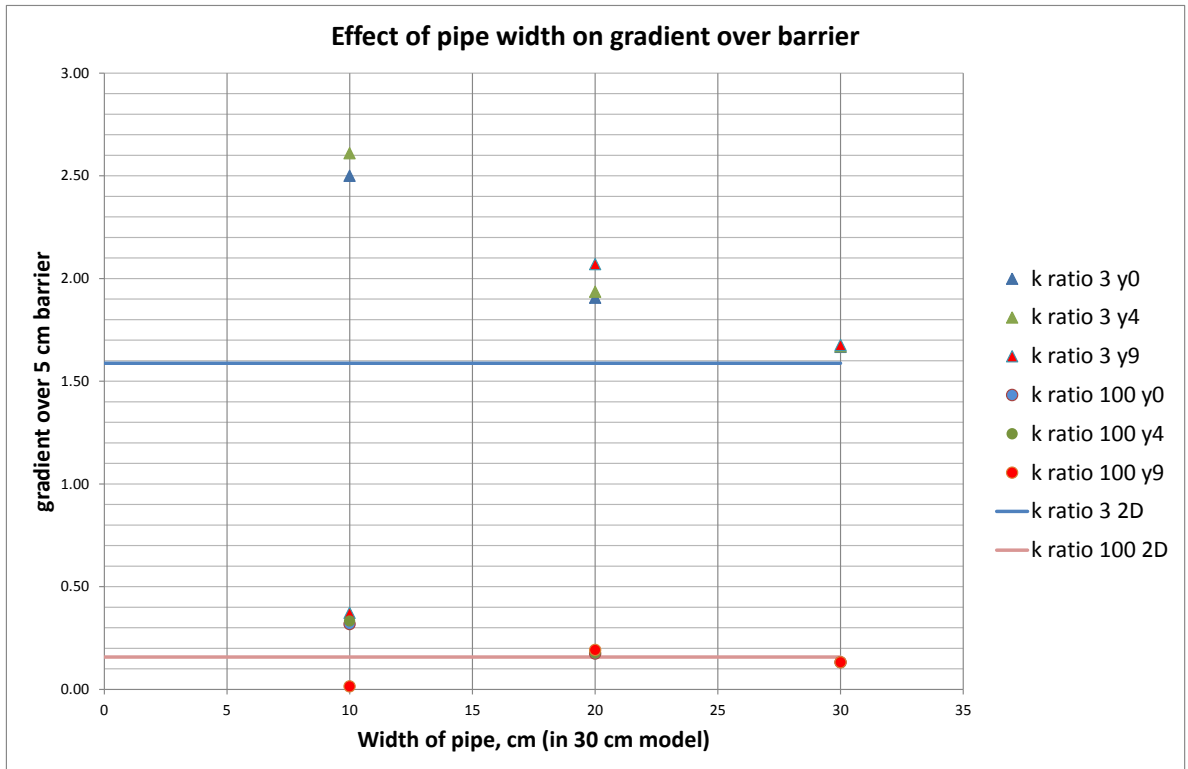


Figure 2.1 Gradients over the entire barrier show the absolute effect of 2D and 3D effects on the gradient over the entire barrier (between -0.120 and -0.170), the model is 30 cm wide

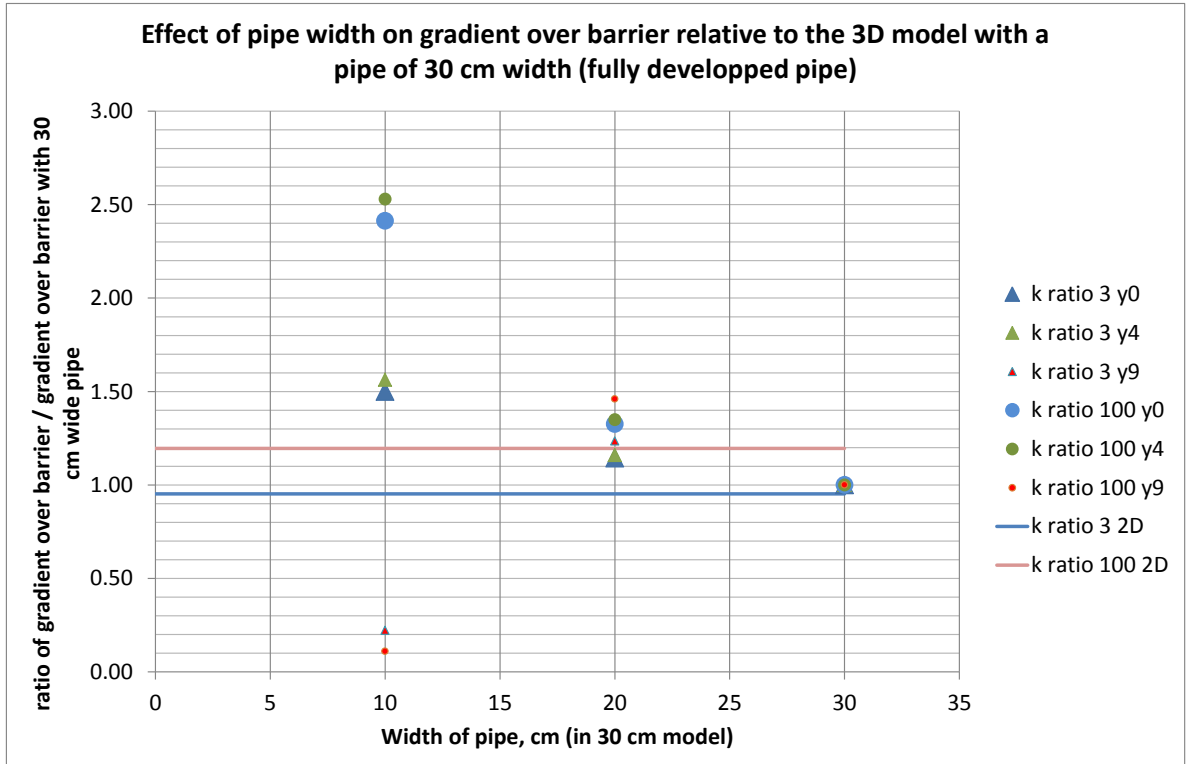


Figure 2.2 The ratio of the gradients over the entire barrier normalised by the gradient computed in the 3D model with a fully developed pipe (i.e. 30 cm wide) show the relative 3D effects on the gradient. Also shown is the ratio of the gradient over the barrier in the 2D model normalised by the gradient computed in the 3D model with the fully developed pipe, the model is 30 cm wide

The effect is similar for the gradient over the distance from -0.130 to -0.165 m in the barrier, which is used as the damage criterion in this phase of the project.

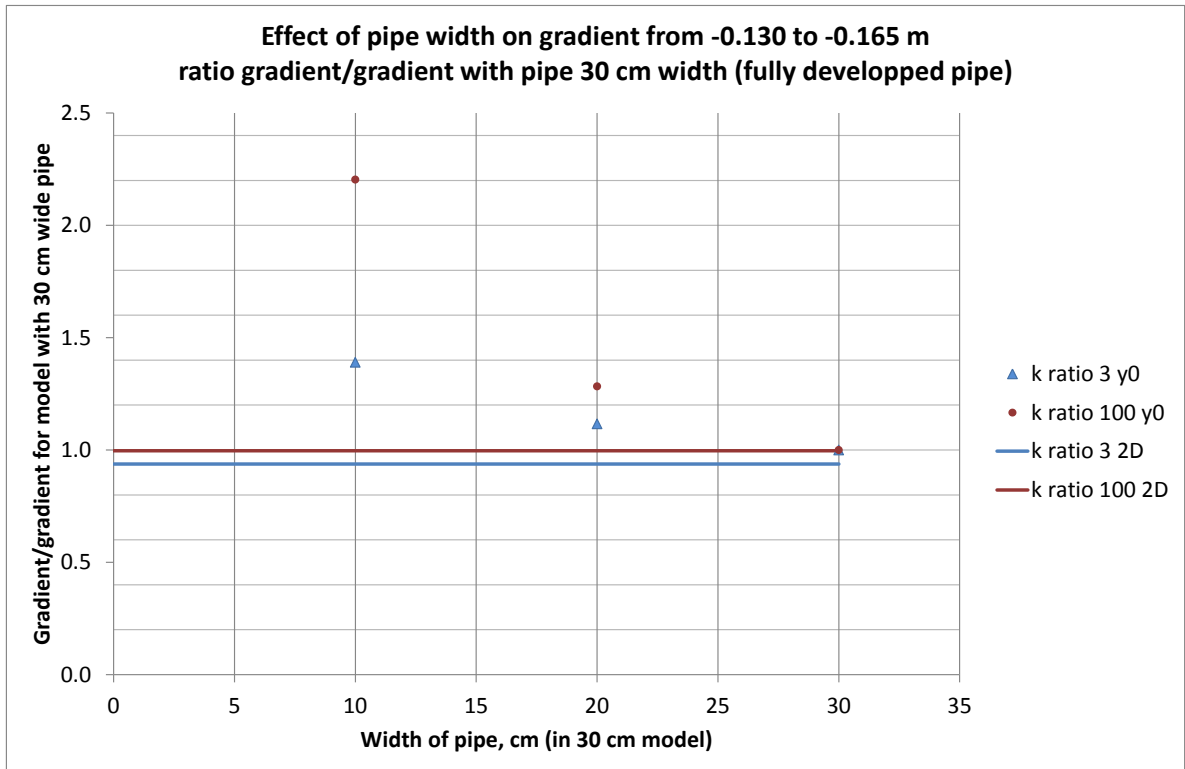


Figure 2.3 Ratio of the gradient over the distance -0.130 to -0.165 m (distance of the damage criterion) for a pipe of different widths normalised by the gradient over this distance for a pipe width 30 cm (the entire width of the model). Results are shown for a permeability contrast of 3 (blue) and 100 (red). The solid lines indicate the ratio of the 2D results over the 3D results with a 30 cm wide pipe, the model is 30 cm wide

### 3 Conclusions

- The gradient in the barrier along the centre line is higher when the pipe is not widened along the barrier. The difference between a pipe width 10 cm and a width 20 cm, is significantly larger than between pipe widths of 20 cm and 30 cm.
- When the pipe is not over the full width, the gradient near the end of the pipe in the barrier is higher than in the centre; this would favour the widening of the pipe in the fine sand when fine grains are significantly easier to erode than the barrier grains
- If the pipe has the full width of the model, the 2D model and 3D models give quite similar results for the overall head profile.
  - For a low contrast of 1 or 3 the 3D model gives a slightly higher head inside the barrier than the 2D model. However, for a large contrast of 100 the 3D model gives a slightly lower head inside the barrier than the 2D model. A detailed analysis of the difference between 2D and 3D results for a 30 cm (full width of the model) width pipe is reported in Appendix F of the main report.
- The difference between 2D and 3D models in the case the pipe has not widened over the full width of the model depends on the permeability contrast; a smaller contrast gives a larger absolute difference, but a smaller relative difference due to the small head drop inside the barrier for the high permeability contrast. A shorter pipe will give a larger difference between the heads in the centre in the 3D models and the 2D models.

- The highest head is not in the centre of the model for the models with a pipe with a limited width; the head is higher near the end of the pipe than in the centre of the model due to convergence of flow from the barrier to the pipe .

## **H Sensitivity analysis of pipe depth**

## Memo

**To**  
Vera van Beek, Adam Bezuijen

<b>Date</b>	<b>Number of pages</b>	
3 November 2017	8	
<b>From</b>	<b>Direct line</b>	<b>E-mail</b>
Esther Rosenbrand	+31(0)88335 7852	esther.rosenbrand@deltares.nl

**Subject**  
Sensitivity analysis of pipe depth

This analysis considers the effect of the depth of the pipe on the head distribution, flow rates and gradients in the models.

The analysis is done in 2D models, flow rates are calculated assuming a width of the model of 30 cm (corresponding to the small scale tests). As the analysis is in 2D the assumption is that the pipe is developed along the entire width of the barrier, and that the pipe also has the same depth along this width.

The effect of the pipe depth is analysed for pipe depths of:

- 0 mm
- 2 mm
- 4 mm
- 6 mm
- 10 mm

In the laboratory experiments, the depth of the pipe was usually greater in the centre of the model than at the edges. The depth also increased throughout the experiment.

For one test (189 Metselzand and barrier 1) there was no failure and the depth of the pipe could be measured, this gave a maximum depth of ca. 1 cm. However, depths estimated during later tests for the depth of the pipe parallel to the barrier at the damage condition (when the pipe enters the barrier) were in the order of a few mm.

When the pipe has a fixed depth, the boundary condition is applied to all sides of the pipe, as shown below

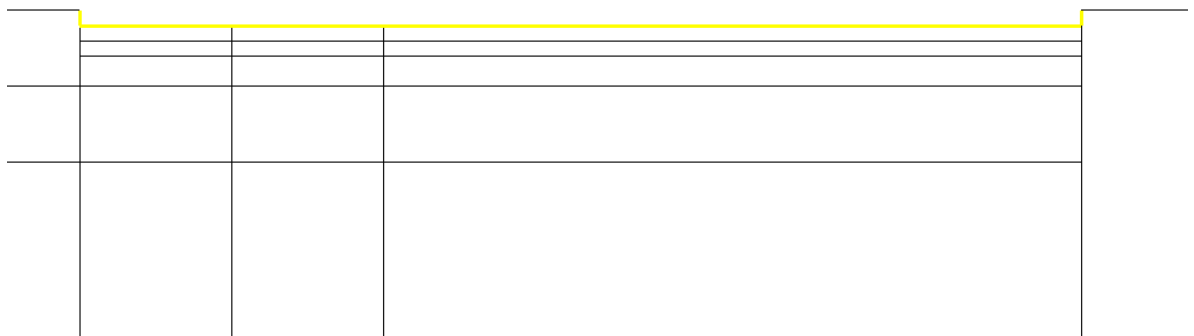


*Figure 1.1 Schematisation of the pipe with a finite depth as a boundary condition. Note the constant head is applied to the bottom and the sides of the pipe*

The effect of pipe depth is analysed for permeability contrasts, 3 (k1) and 100 (k2).

## 1 Main findings

The flow in both models is shown in Figure 1.1. As there is hardly any head drop in the model with a permeability contrast of 100, the contour lines between a head of 0.05 m and 0.0 m are shown in

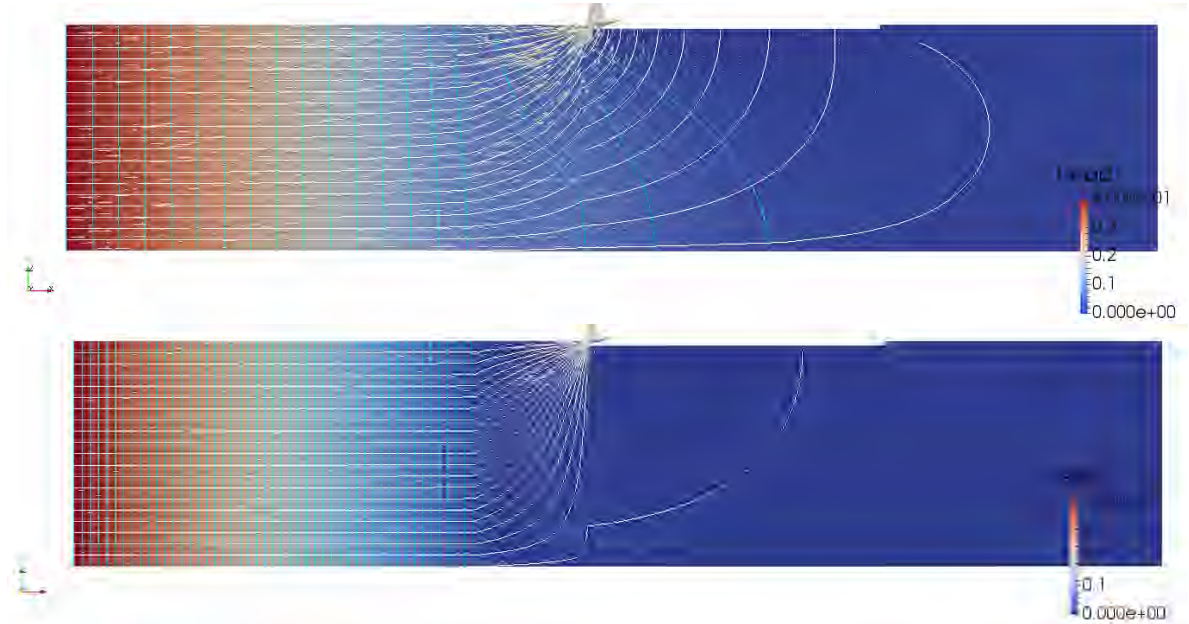


Figure 1.1 Background colour shows the head distribution in both models. Streamlines (white) are shown indicating the flow paths followed from the upstream end of the model. Vectors (size indicates flow velocity, note a different scale is used for the two models) indicate the flow direction and flow velocity, contour lines (cyan) indicate the head distribution. Top model permeability contrast 3, bottom model permeability contrast 100.

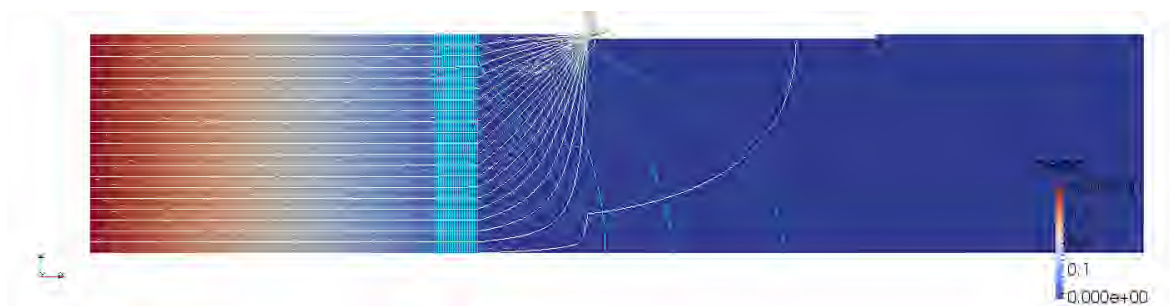


Figure 1.2 Model with permeability contrast 100. Background colour shows the head distribution. Streamlines (white) are shown indicating the flow paths followed from the upstream end of the model. Vectors (size indicates flow velocity, note a different scale is used for the two models) indicate the flow direction and flow velocity, contour lines (cyan) indicate the head distribution, these 20 lines are regularly spaced between 0.0 m and 0.02 m

The streamlines indicate that most flow leaves the barrier at the pipe tip in both models. With a lower permeability contrast there is more flow into the fine sand downstream of the barrier.

## 2 Effect pipe depth on head distributions

### 2.1.1 Effect with permeability ratio 3

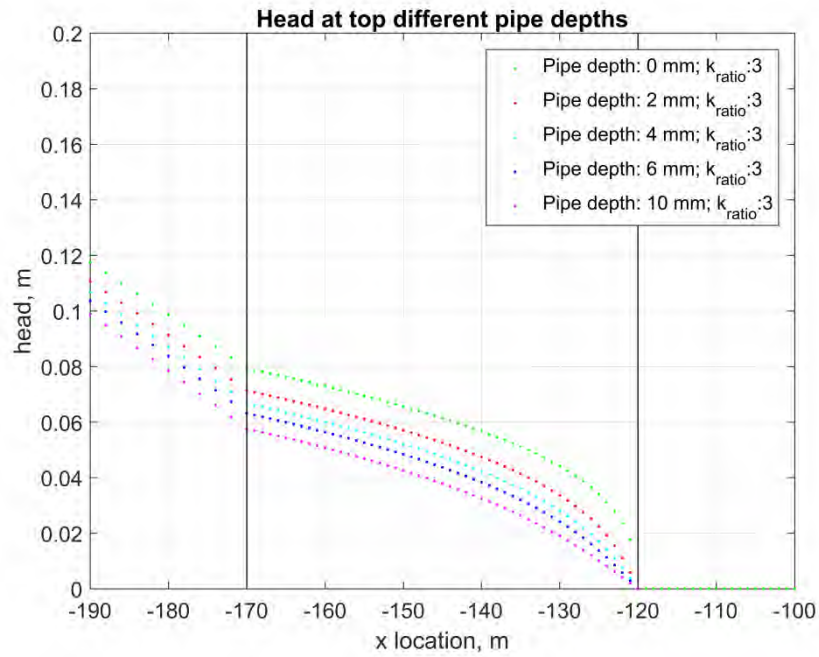


Figure 2.1 Head distribution in the model

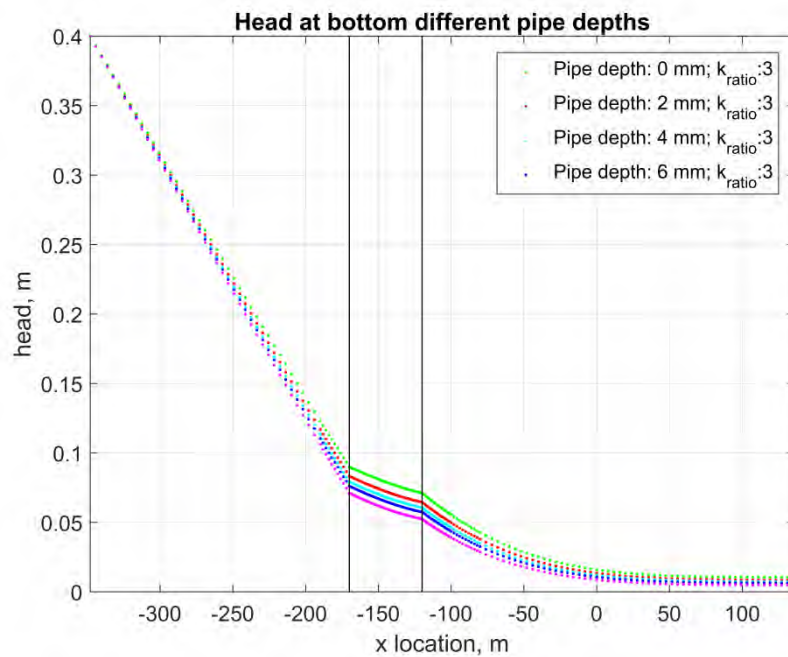


Figure 2.2 Head distribution in the model

## 2.1.2 Effect with permeability ratio 100

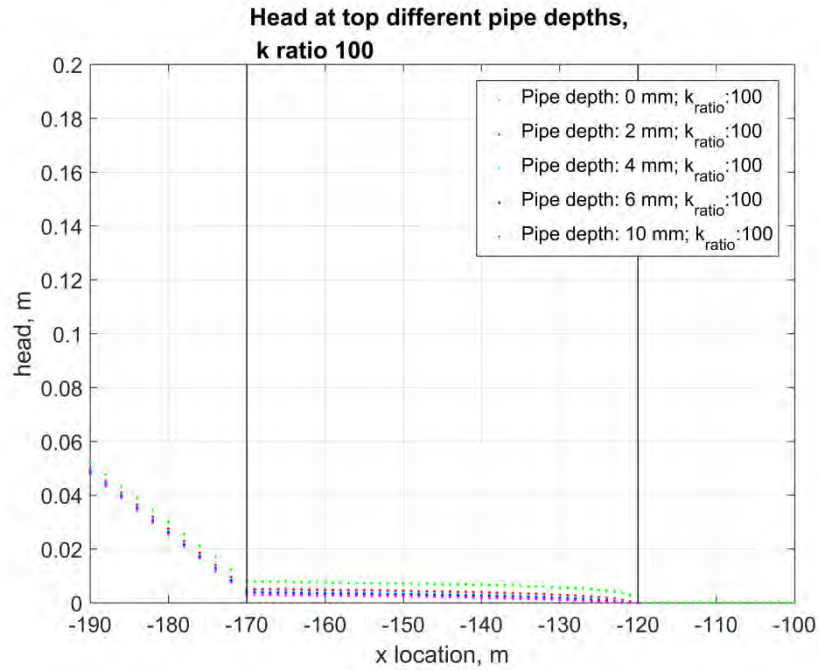


Figure 2.3 Head distribution in the model

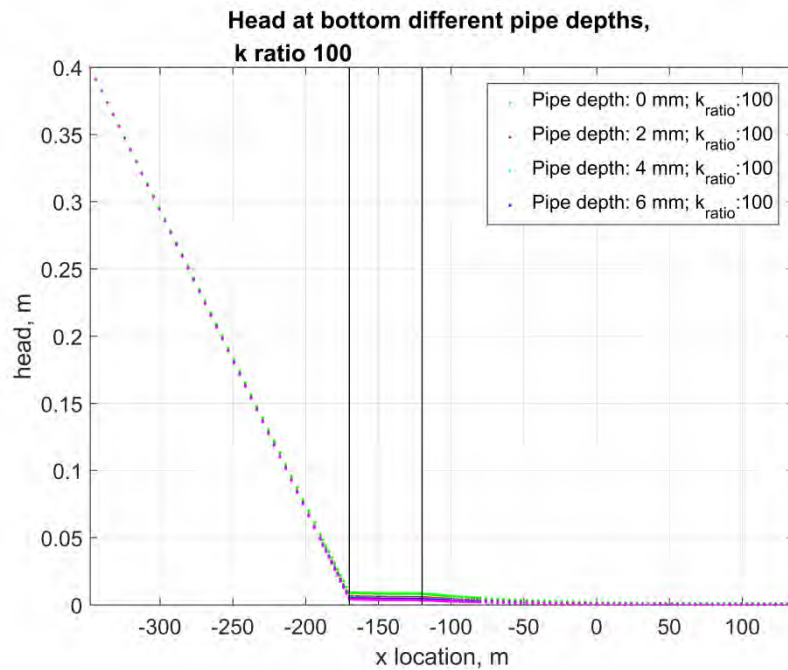


Figure 2.4 Head distribution in the model

### 3 Effect of pipe depth on gradient over barrier

The effect of pipe on the gradient over the barrier for different permeability contrasts is shown below where the gradient is taken from -0.120 to -0.170 m, i.e. the entire barrier.

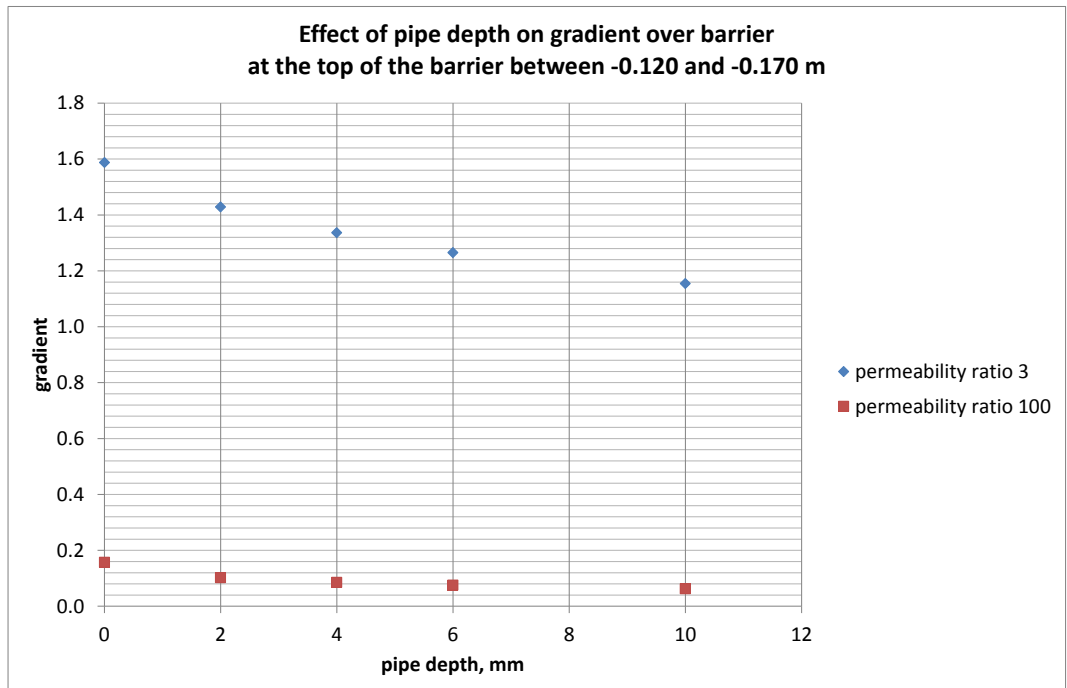


Figure 3.1 Gradients over the barrier show the absolute effect of pipe depth on the gradient

The ratio between the gradient in the models with different pipe depths to the gradient in the model with a pipe depth of 0 mm is shown below. Depending on the location in the barrier the effect is different, results are shown for

- Over the entire barrier (-0.120 to -0.170 m);
- Over the most downstream 3.5 cm of the barrier (-0.120 to -0.155 m) ;
- The distance of the damage criterion (i.e. between -0.130 and -0.165 m).

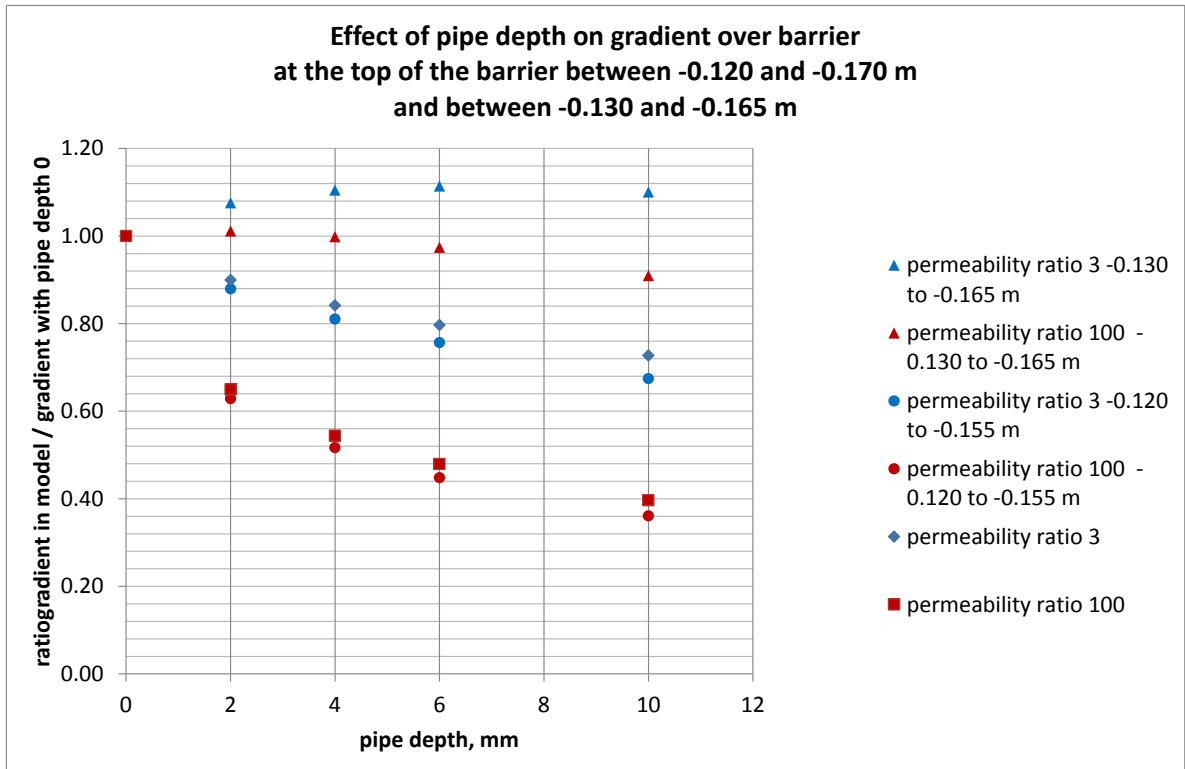


Figure 3.2 The ratio of the gradient over the barrier with 0 mm pipe depth over the gradient over the barrier with a variable pipe depth, for the entire barrier (-0.120 to -0.170 m) and for the downstream part of the barrier (-0.120 to -0.155 m) and distance of the damage criterion (-0.130 to -0.165 m)

Note that the effect on the local gradient over the distance of the damage criterion is much smaller than the effect on the gradient over the entire barrier. The gradient is actually slightly higher with a finite pipe depth as compared to the local gradient with 0 mm pipe depth for a permeability contrast of 3 for the distance of the damage criterion, whereas over the entire barrier the gradient is lower with a deeper pipe. For the permeability contrast of 100 the gradient is slightly higher with a 2 mm pipe depth than with a 0 mm pipe depth over the distance of the damage criterion. But for deeper pipes, the gradient becomes smaller than for a 0 mm deep pipe.

Increasing the depth of the pipe increases the length of interface between the pipe and the barrier, which means that water can flow out of the barrier and into the pipe easier. This reduces the head throughout the barrier and thus the gradient over the entire barrier. However, with a deeper pipe, the gradient in the first centimetre from the interface between the pipe and the barrier also becomes less steep, again as there is a larger outflow area. This can be clearly seen in Figure 2.1. This very local reduction of the gradient offsets the reduction of the gradient in the entire barrier, giving a higher gradient over the area of the failure criterion (-0.130 to -0.165 m) for a permeability contrast of 3.

For a permeability contrast of 100, there is more convergence of flow in the barrier therefore the relative effects in the downstream 1 cm of the barrier and over the entire barrier are different. Thus here for pipe depths greater than 2 mm the local gradient between -0.130 and -0.165 m is less than the local gradient at this location for a pipe depth of 0 cm.

## 4 Effect pipe depth on flow rate

The increase of the pipe depth has a minor effect on the flux through the model.

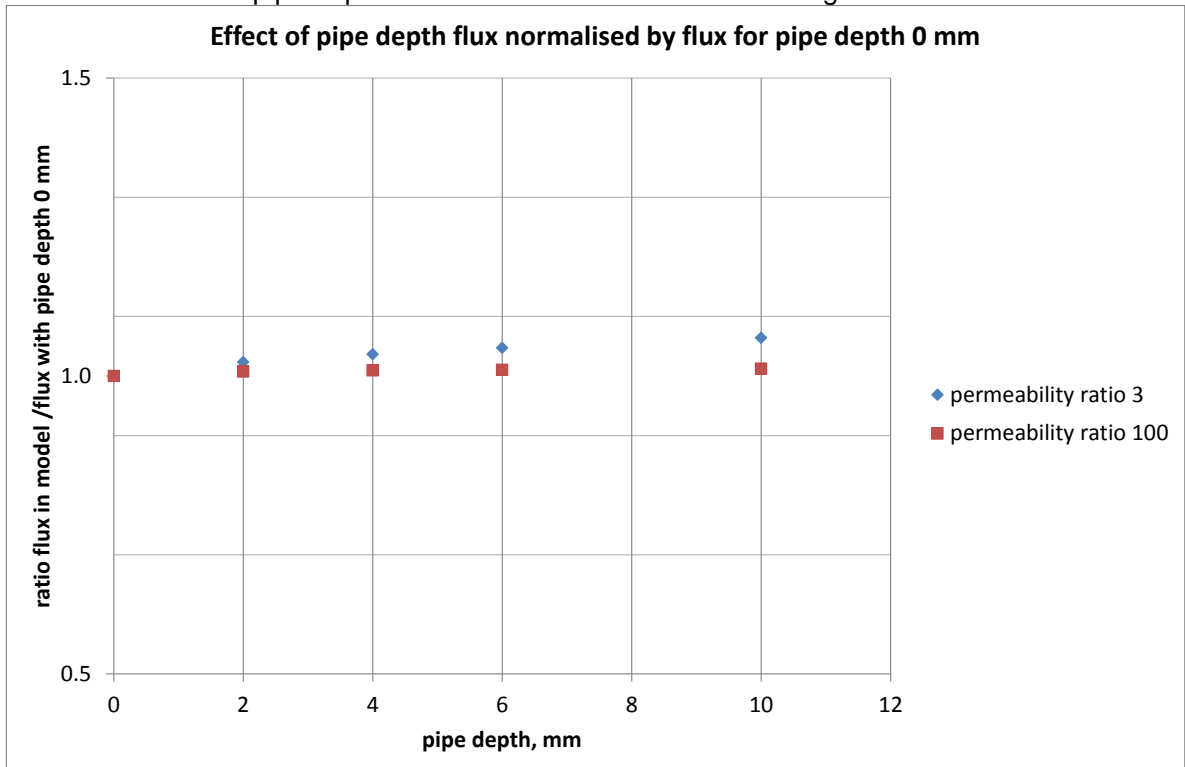


Figure 4.1 The ratio of the flux in the model normalised by the flux in the model with 0 mm pipe depth

## 5 Conclusions

- The effect of the pipe depth on the gradient over the entire barrier, but also the effect on the distance of 3.5 cm just upstream of the interface between the barrier and the pipe is significant; the gradient with a pipe of 2 mm depth is only the order of 64% of the gradient for a model with 0 mm pipe depth, for a model with a permeability contrast of 100. With a smaller permeability contrast, the effect of pipe depth also becomes smaller, this is because there is less concentration towards the interface between the barrier and the pipe.
- The effect of pipe depth is greatest in the barrier closest to the interface between the barrier and the pipe. Further upstream in the barrier, over the range -0.130 to -0.165 m where the failure criterion is, there is actually a slight increase in the gradient for the model with a pipe depth of 2 mm as compared to a model with 0 mm pipe depth, for both permeability contrasts of 3 and 100. For a permeability contrast of 3, the greater pipe depths also give a slightly higher local gradient than the models with a pipe depth of 0 m. But for a contrast of 100, models with greater pipe depths show a lower local gradient than a model with a pipe depth of 0 (or 2 mm).
- The effect of pipe depth on the average gradient over the entire barrier is comparable to the effect of pipe depth on the first 3.5 cm from the downstream end of the barrier.

The gradient over the distance where the damage criterion is computed is less sensitive to differences in pipe depth.

- The effect of the pipe depth on the flux in the model is negligible; the increase in flux is at most 6% for a pipe depth of 1 cm as compared to a model of pipe depth 0 mm.

## **I Sensitivity analysis of barrier depth**

## Memo

**To**  
Vera van Beek, Adam Bezuijen

**Date**  
3 November 2017

**Number of pages**  
17

**From**  
Esther Rosenbrand

**Direct line**  
+31(0)88335 7852

**E-mail**  
esther.rosenbrand@deltares.nl

**Subject**  
Effect of barrier depth

This analysis addresses the effect of the barrier depth in the rotated small scale 2D model with the pipe as a boundary condition with zero pipe depth. Two permeability contrasts are considered, 3 and 30. The upstream head is 0.4 for all cases. The permeability of the fine material is  $6e-4$  m/s for all cases.

The model is shown below for the case with a barrier that is 10 cm deep. The location of the barrier relative to the outflow hole is the same as in the standard model. The location and length of the pipe is also the same as in the standard model. The mesh is uniform with an element size of 1 mm as 1 mm was also found adequate for the standard 2D models, these are shown in the main report.

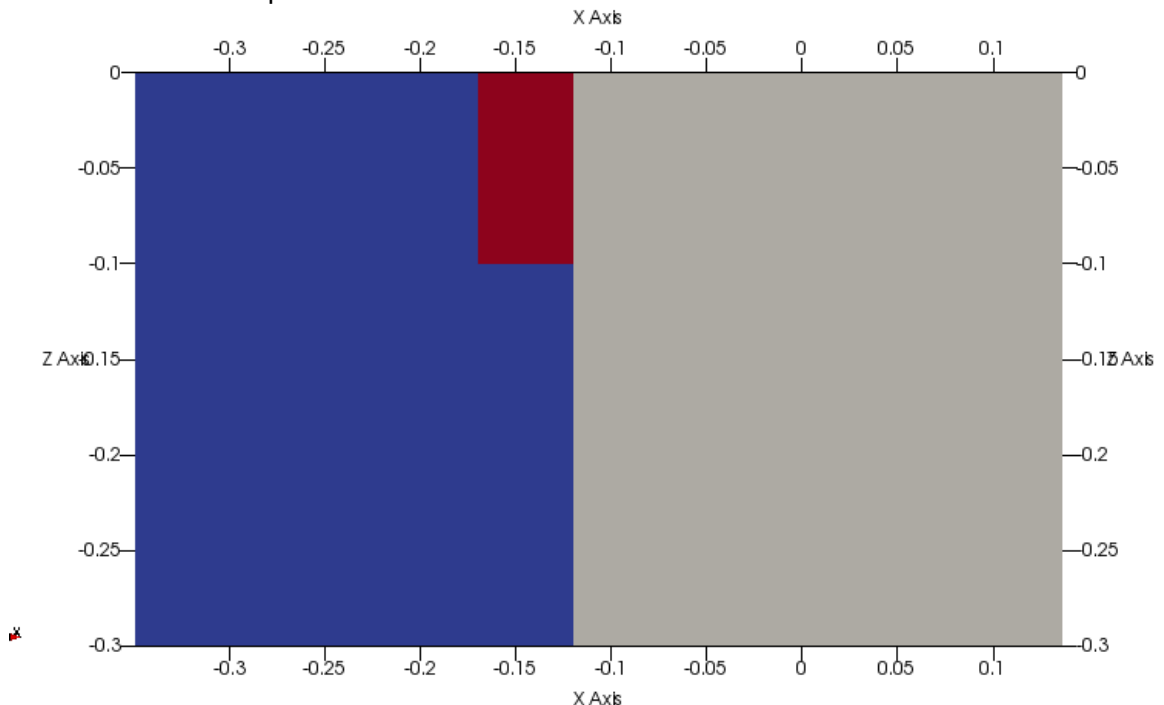


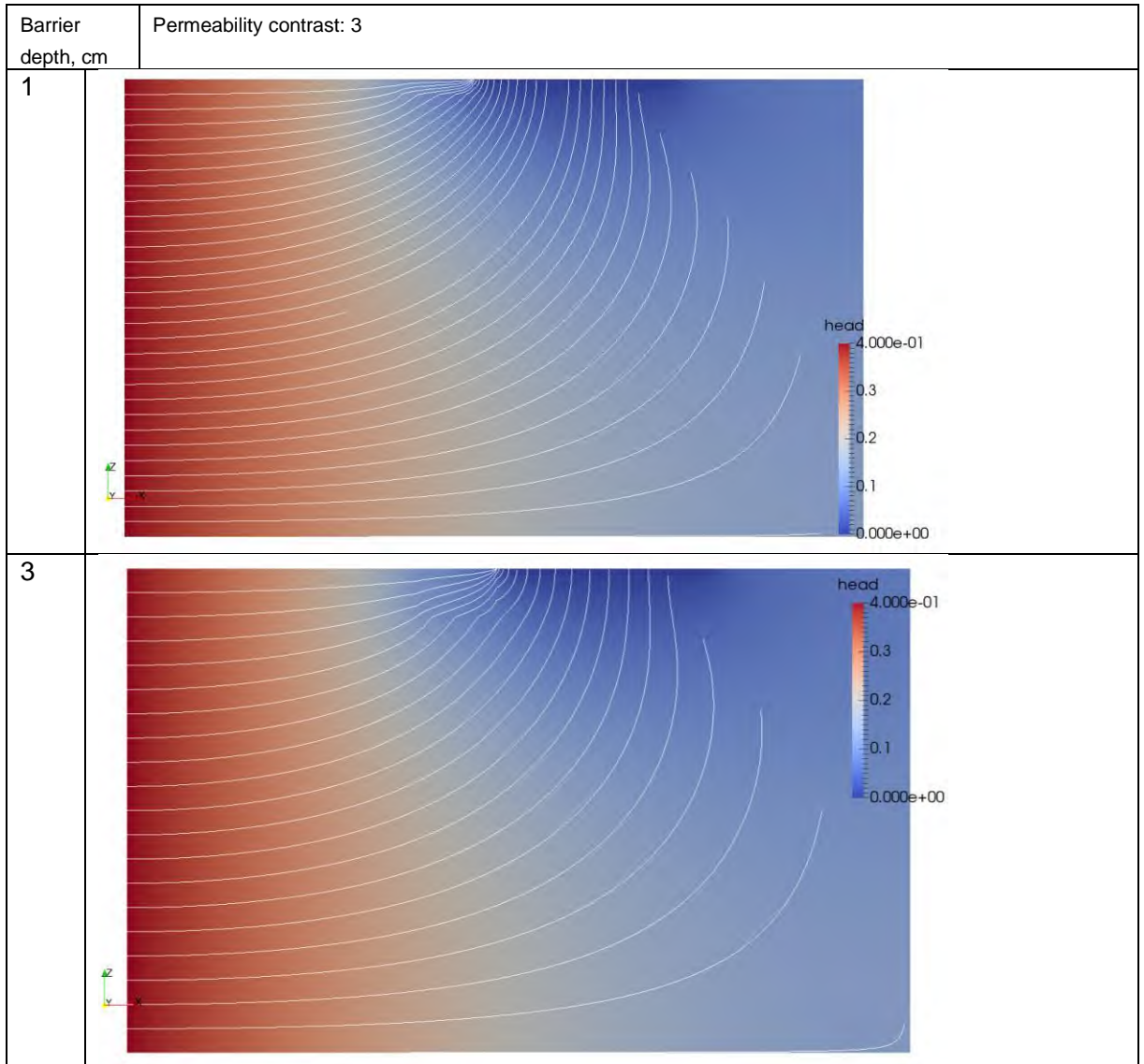
Figure 1.1 Schematisation of the model with a 10 cm deep barrier (red). Blue is upstream fine sand, grey is downstream fine sand

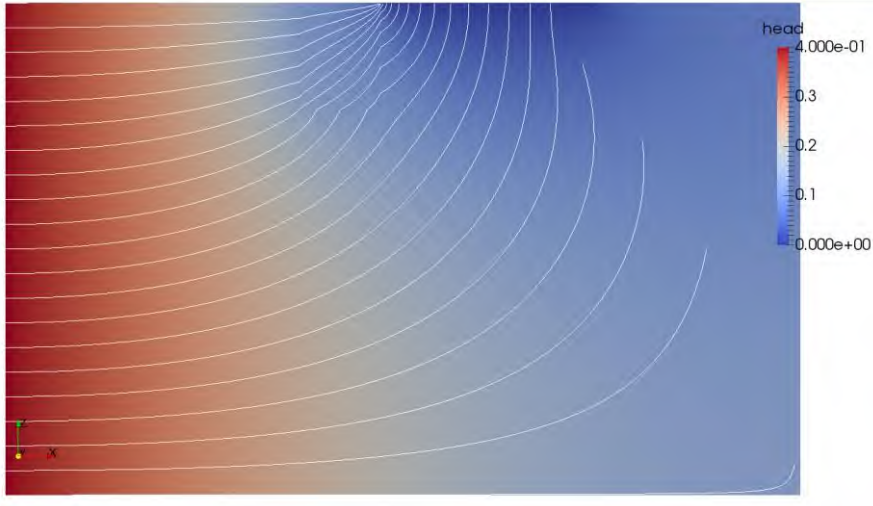
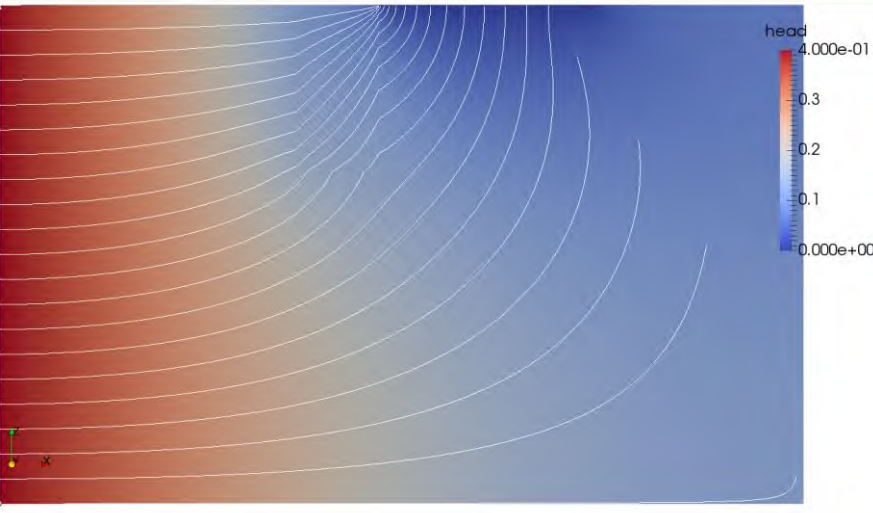
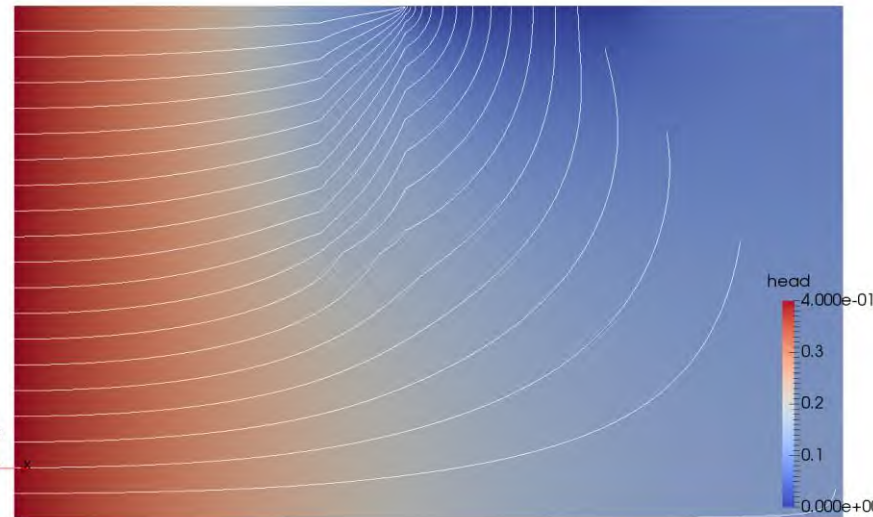
## 1 Head profiles

The flow in both models is shown below with stream lines sourced from the left boundary (inflow) of the model.

There is convergence of flow in the barrier towards the pipe in both cases. However in the case of a permeability contrast of 30 there is near-vertical flow and very little water exits the downstream face of the barrier into the fine sand, most water is concentrated to the pipe. This is less the case with a lower contrast.

Figure 1.1 Background colour shows the head distribution. Streamlines are shown indicating the flow paths followed from the upstream end of the model for the permeability contrast 3



Barrier depth, cm	Permeability contrast: 3
6.5	 <p>Flow head contour plot for a barrier depth of 6.5 cm. The plot shows head values ranging from 0.000e+00 (blue) to 4.000e-01 (red). The head is highest on the left side and decreases towards the right. A coordinate system (x, y, z) is shown in the bottom left corner.</p>
10	 <p>Flow head contour plot for a barrier depth of 10 cm. The plot shows head values ranging from 0.000e+00 (blue) to 4.000e-01 (red). The head is highest on the left side and decreases towards the right. A coordinate system (x, y, z) is shown in the bottom left corner.</p>
14.5	 <p>Flow head contour plot for a barrier depth of 14.5 cm. The plot shows head values ranging from 0.000e+00 (blue) to 4.000e-01 (red). The head is highest on the left side and decreases towards the right. A coordinate system (x, y, z) is shown in the bottom left corner.</p>

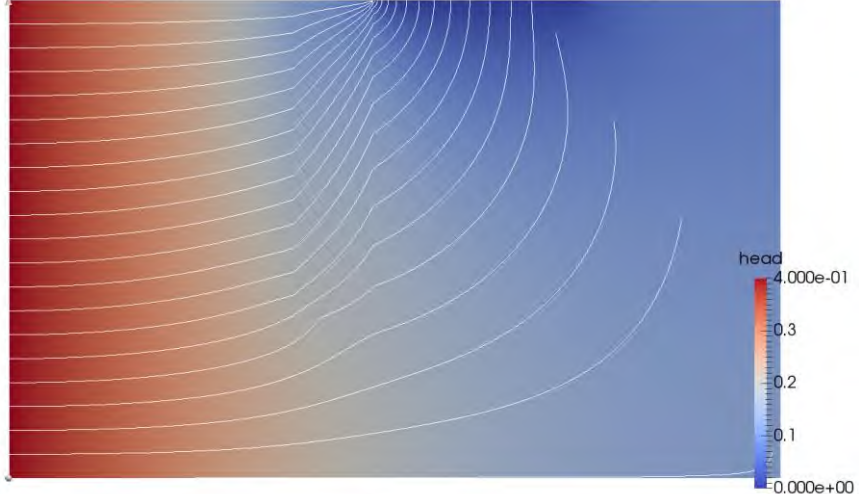
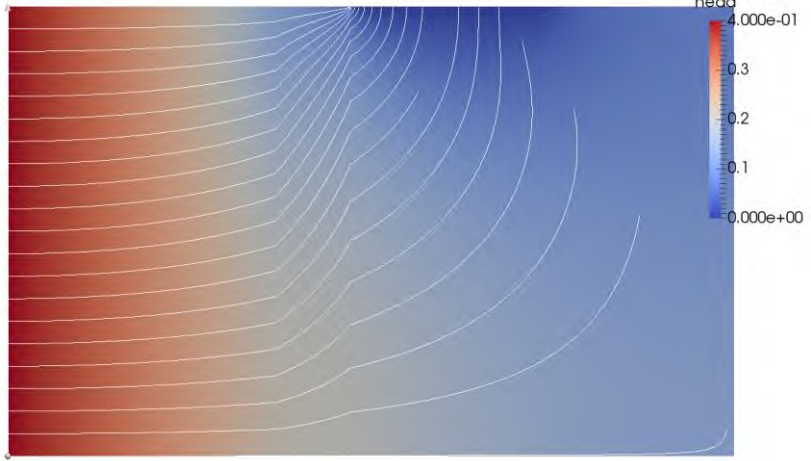
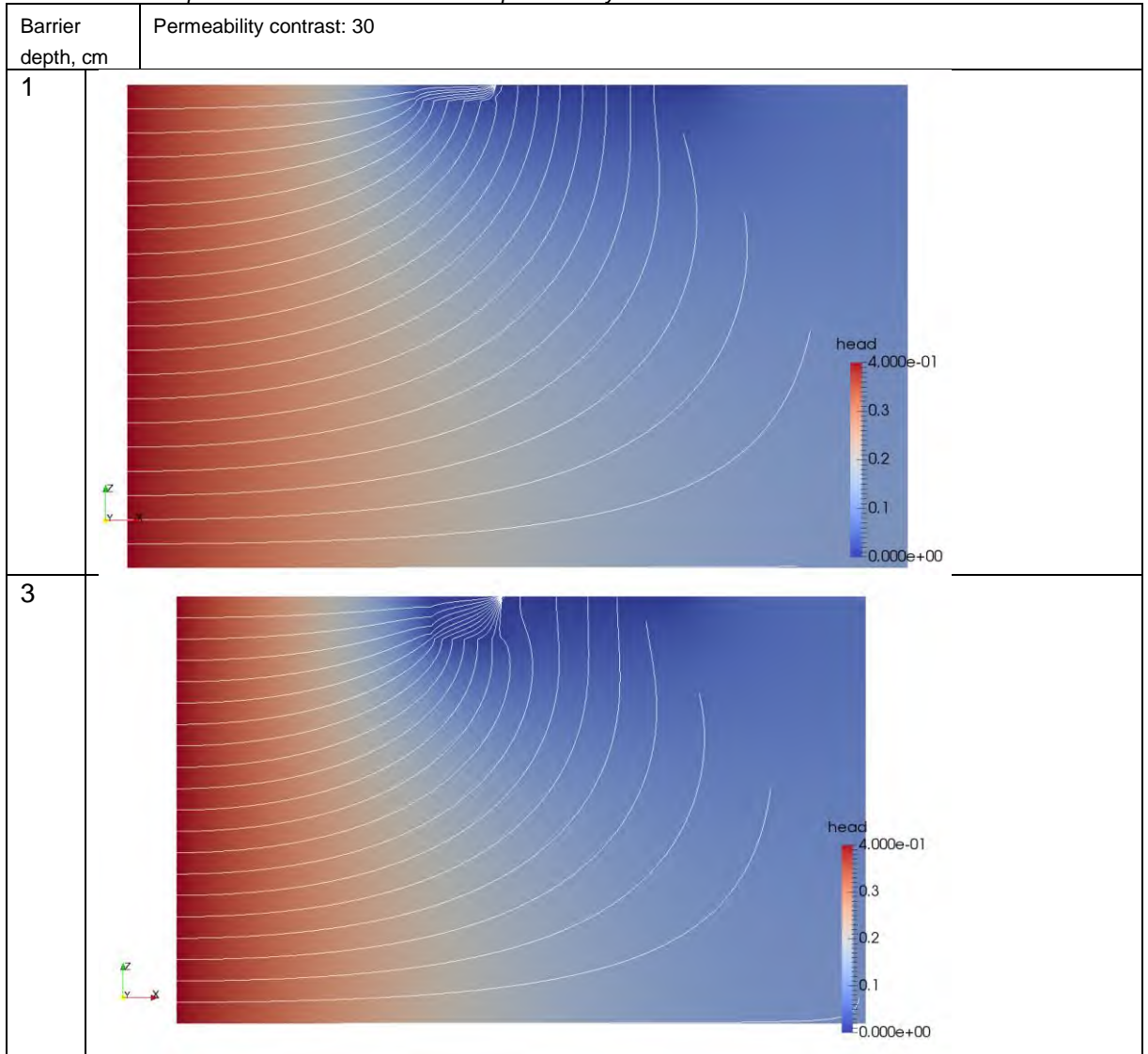
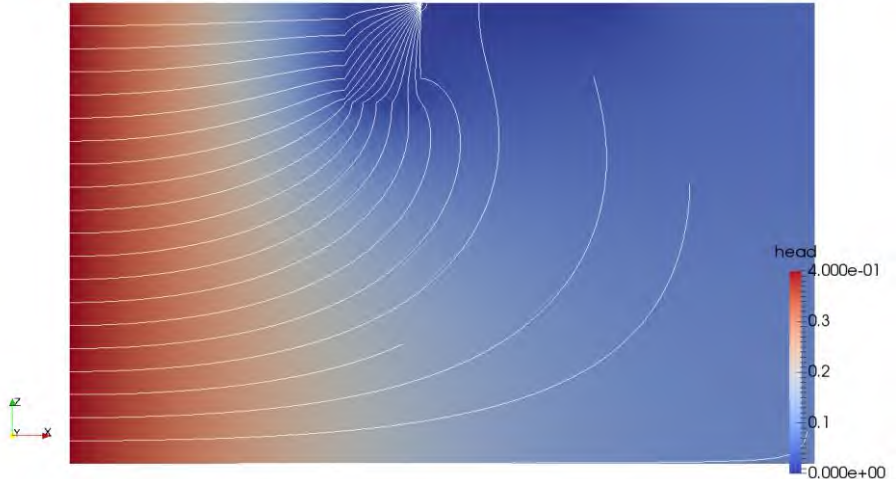
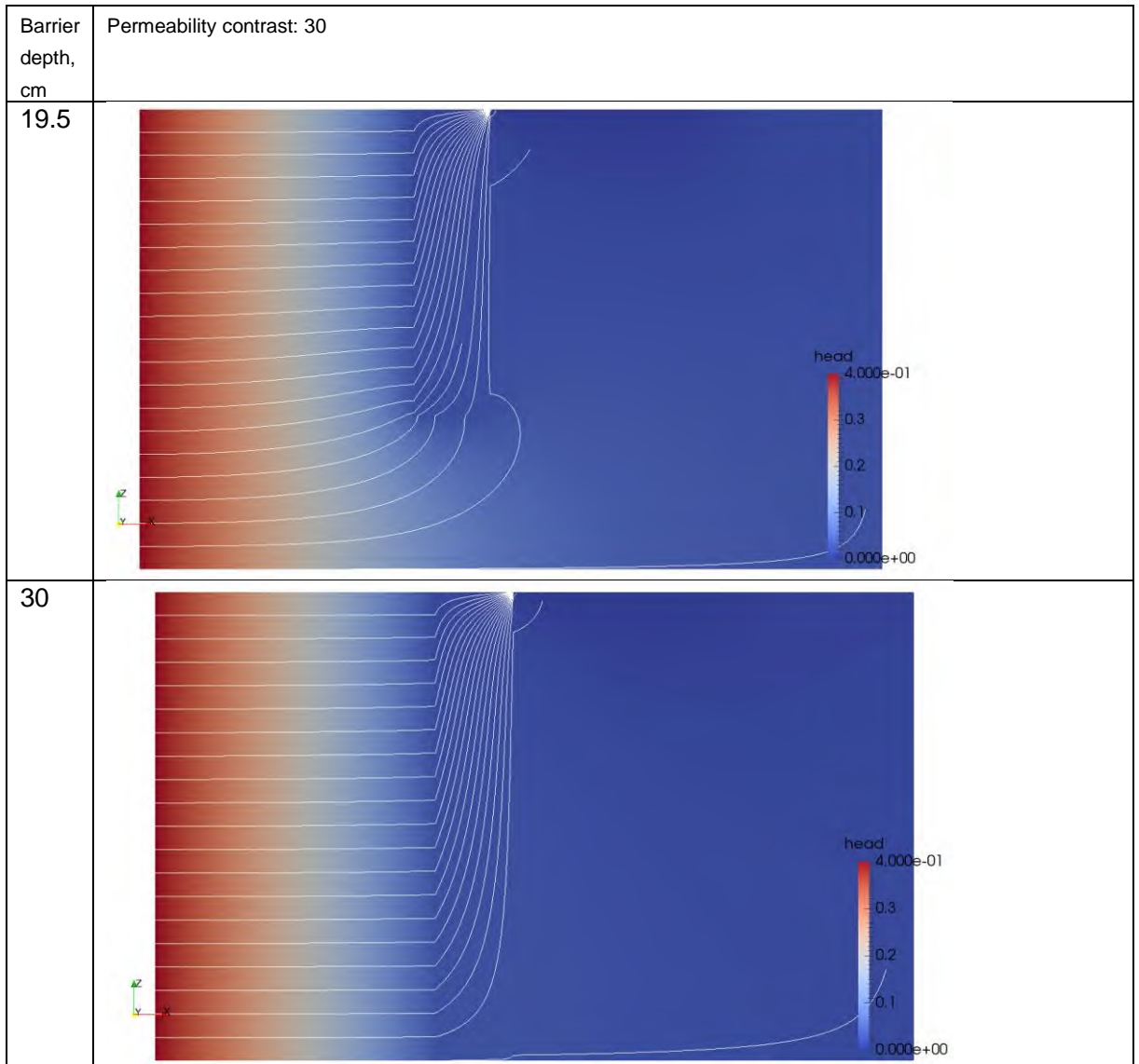
Barrier depth, cm	Permeability contrast: 3
19.5	
30	

Figure 1.2 Background colour shows the head distribution. Streamlines are shown indicating the flow paths followed from the upstream end of the model for the permeability contrast 30



Barrier depth, cm	Permeability contrast: 30
6.5	
10	
14.5	



## 2 Effect barrier depth on head distributions

### 2.1.1 Effect with permeability ratio 3

At -0.200 m, i.e. 3 cm upstream of the upstream interface between the barrier and the fine sand, the head is highest with a barrier depth of 1 cm, the next highest head at this location is found with a barrier depth of 3 cm. But with a barrier depth of 6.5 cm the head at that location is lowest, and from this depth onwards the head increases with increasing barrier depth.

At -0.140 m and downstream of this point, i.e. 2 cm upstream of the interface between the barrier and the pipe, the head is lowest with the shallowest barrier and increases with barrier depth.

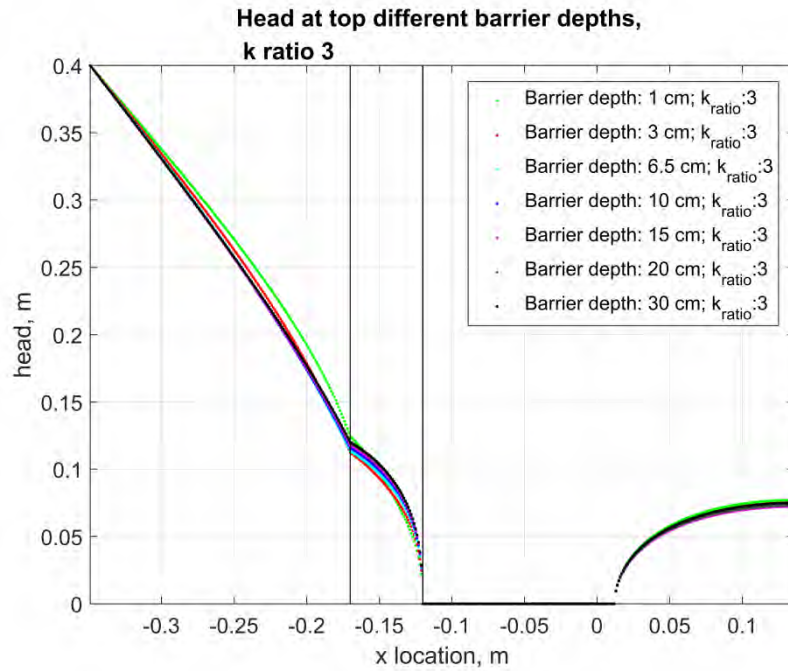


Figure 2.1 Head distribution in the model

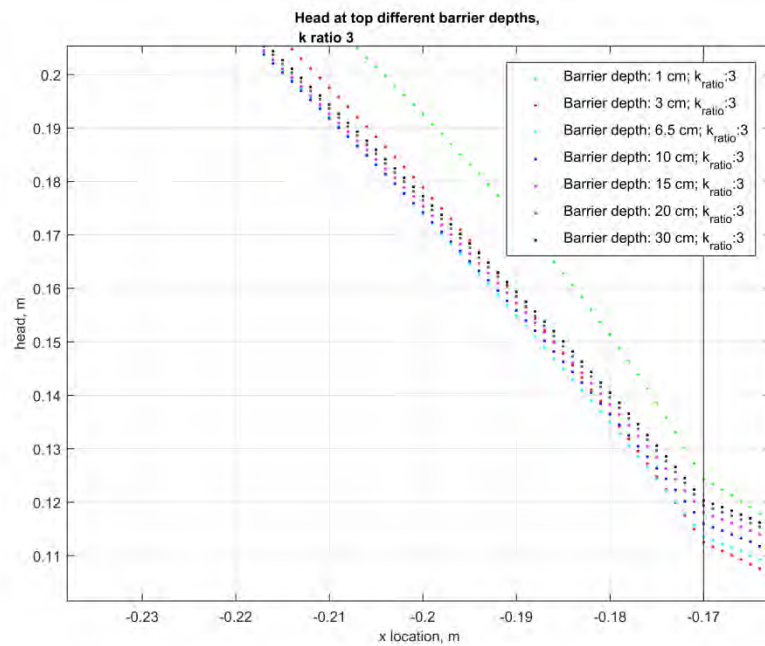


Figure 2.2 Head distribution in the model

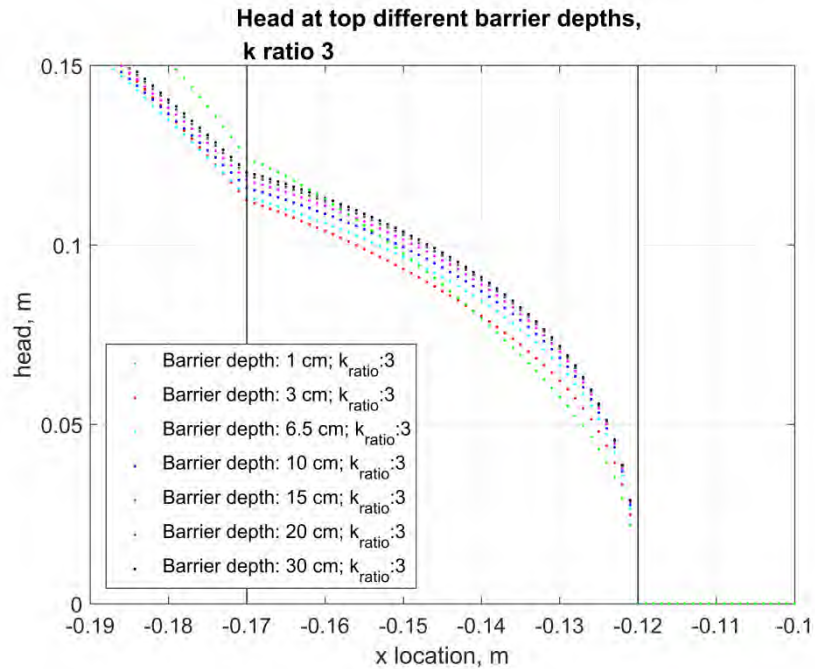


Figure 2.3 Head distribution in the model

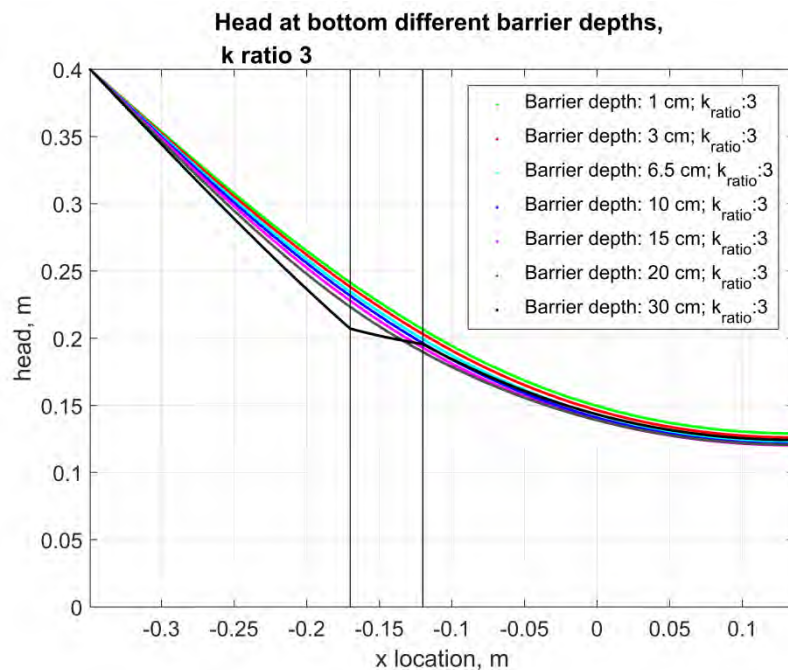


Figure 2.4 Head distribution in the model

### 2.1.2 Effect with permeability ratio 30

The head drop over the upstream sand is higher with a higher permeability ratio, as there is less resistance to flow in the barrier (the upstream permeability is the same in all cases considered here).

Looking at the location -0.200 m, i.e. 3 cm upstream of the upstream interface of the barrier and the fine sand, we see that the head is highest for the shallowest barrier and that the head falls with increasing barrier depth.

Looking at the upstream interface between the barrier and the fine sand, the head is highest with a barrier depth of 1 cm and lowest with a barrier depth of 3 cm. For barrier depths greater than 3 cm the head increases with increasing barrier depth. This order of heads, i.e. with the highest head for a 1 cm barrier, the lowest head for a 3 cm barrier and increasing head with increasing barrier depth remains throughout the barrier. The gradient in the upstream fine sand increases near the upstream interface between the barrier and the fine sand. This effect increases with the depth of the barrier, this causes the head profiles to cross in the first centimetre upstream of the interface between the barrier and the fine sand upstream.

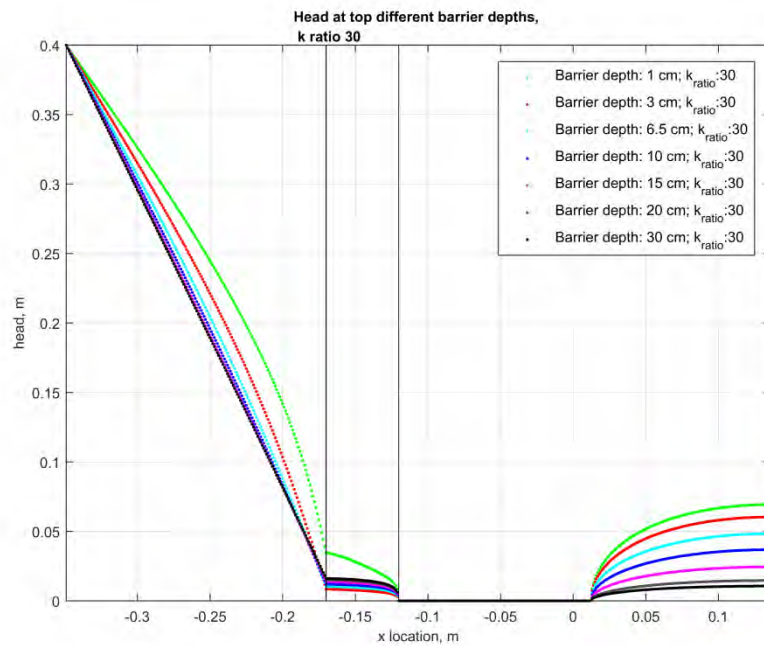


Figure 2.5 Head distribution in the model

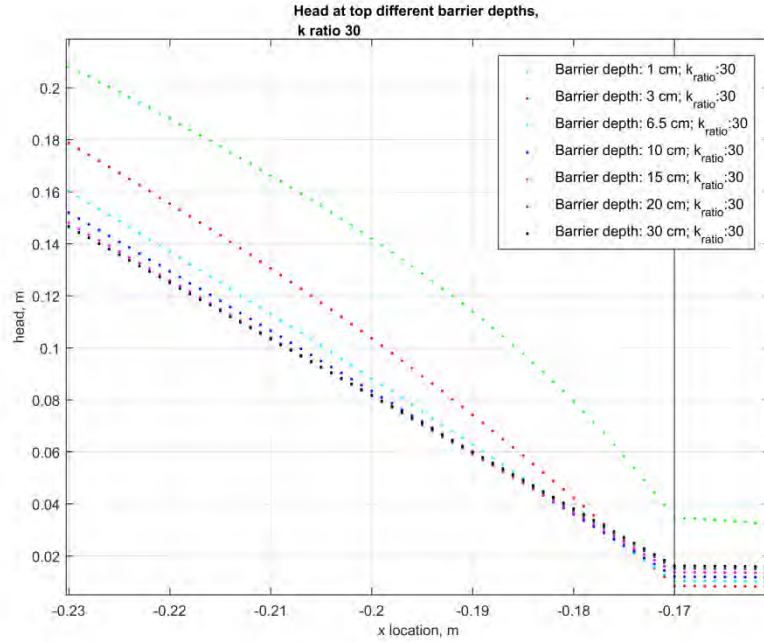


Figure 2.6 Head distribution in the model

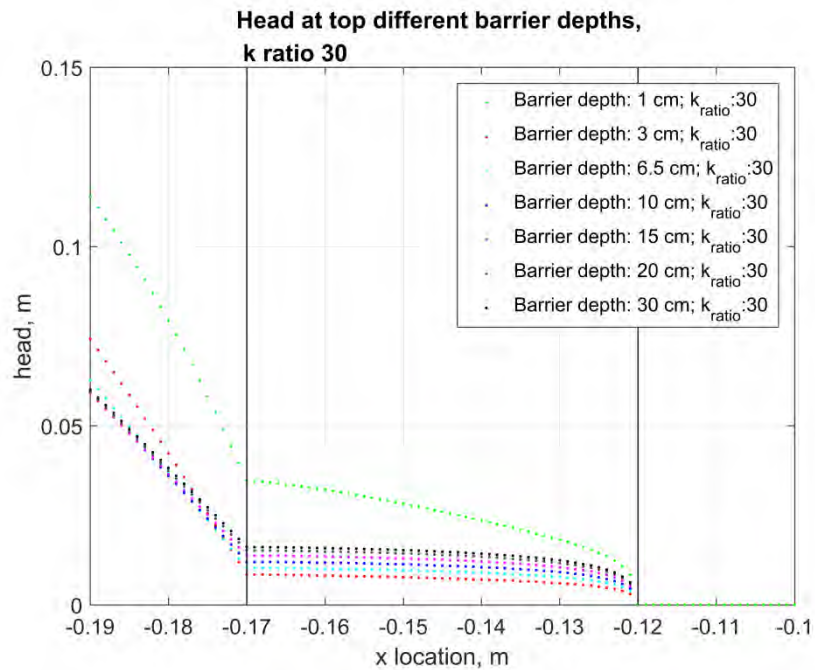


Figure 2.7 Head distribution in the model

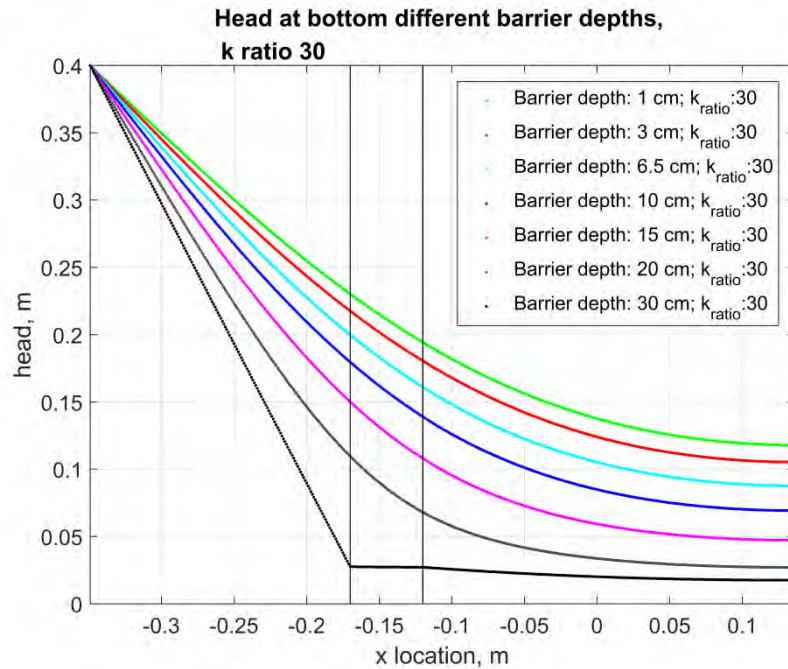


Figure 2.8 Head distribution in the model

### 3 Effect of barrier depth on gradient over barrier

The effect of barrier depth on the gradient over the barrier for different permeability contrasts is shown below where the gradient is computed between  $-0.120$  m and  $-0.170$  m, i.e. over the entire barrier.

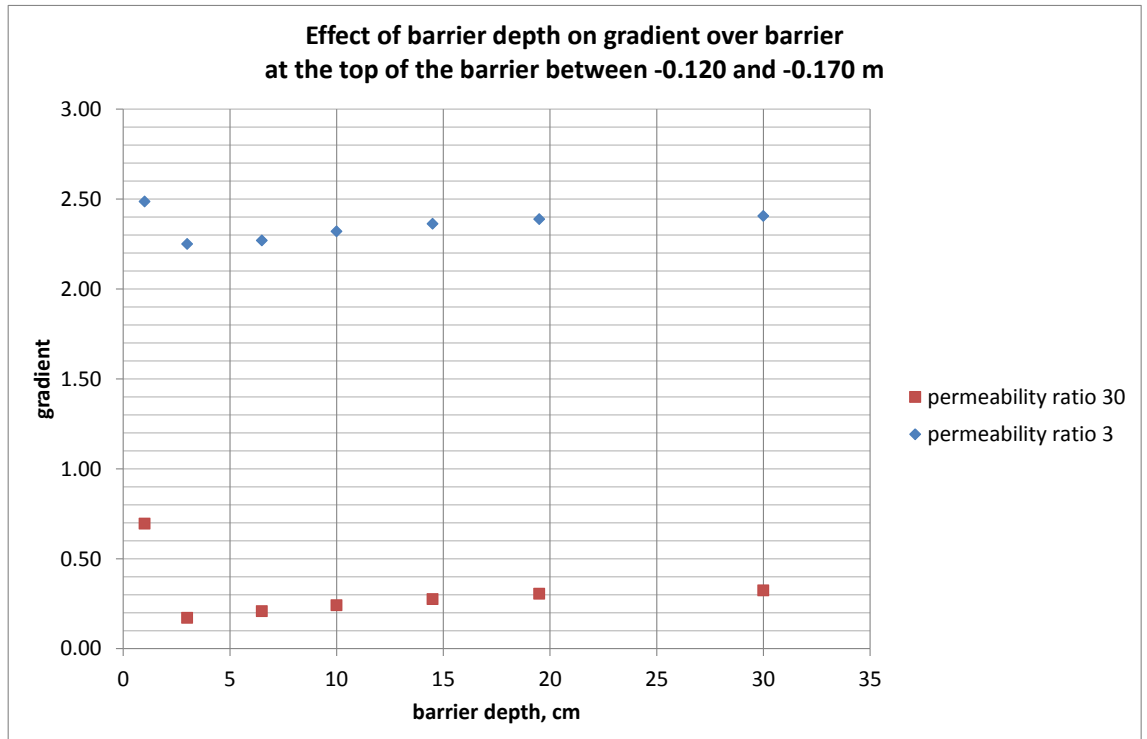


Figure 3.1 Gradients over the barrier show the absolute effect of barrier depth on the gradient

The gradient is highest for a barrier of 1 cm depth, and lowest for a barrier of 3 cm depth. From a 3 cm deep barrier, the gradient increases with increasing barrier depth. This trend is also shown below for the ratio between the gradients in the models with different barrier depths normalised by the gradient in the model with a barrier depth 3 cm, i.e. the relative effect. However, it was observed that depending on the location in the barrier this ratio can differ, results are shown for

- Over the entire barrier (-0.120 to -0.170 m);
- Over the most downstream 3.5 cm of the barrier (-0.120 to -0.155 m);
- Over 3.5 cm between 1 cm upstream of the interface between the barrier and the pipe and 4.5 cm upstream of this interface ( i.e. -0.130 to -0.165 m the damage criterion in this phase of the project).

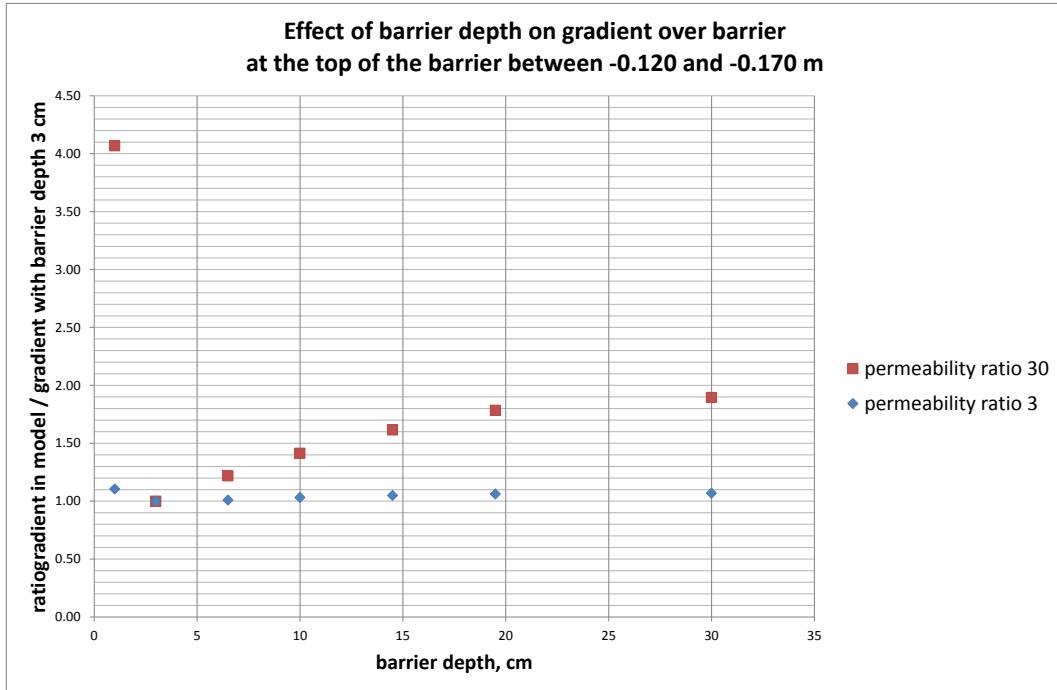


Figure 3.2 The ratio of the gradient over the barrier with 3 cm depth over the gradient over the barrier with a variable barrier depth, here only for distance between -0.120 and 0.170 m

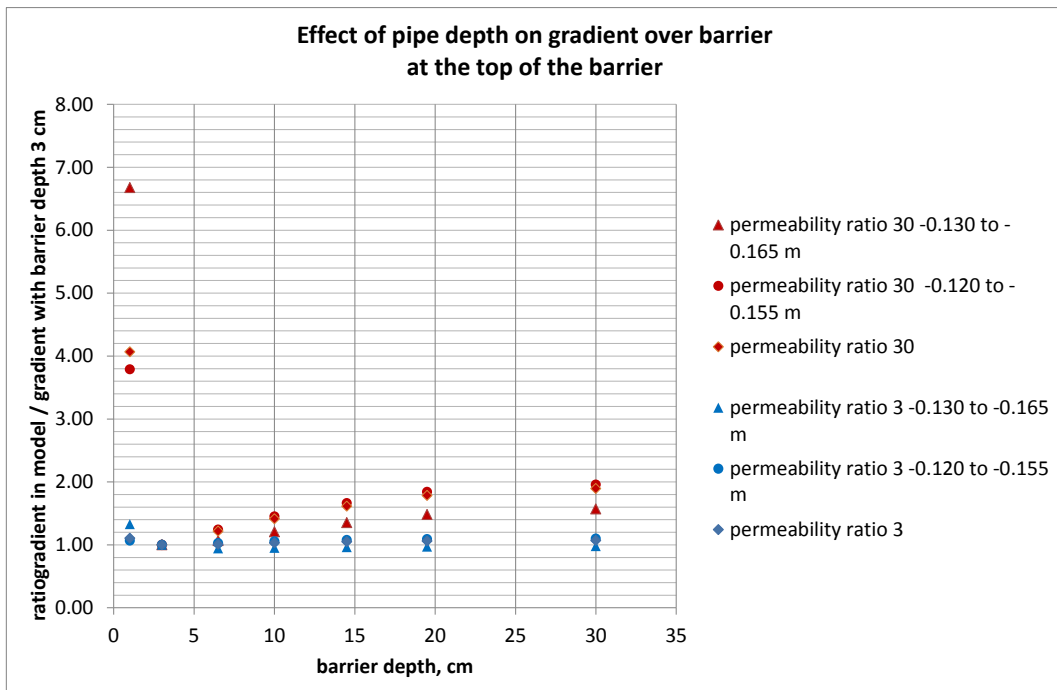


Figure 3.3 The ratio of the gradient over the barrier with 3 cm depth over the gradient over the barrier with a variable barrier depth, for the entire barrier (-0.120 to -0.170 m) and for the downstream part of the barrier (-0.120 to -0.155 m) and for the part corresponding to the damage criterion (-0.130 to -0.165 m)

The gradient is highest for the cases with a lower permeability ratio, as expected due to the lower permeability of the barrier.

It is notable that with a 1 cm deep barrier the gradient over the entire barrier is highest, but with a 3 cm deep barrier this is the lowest and subsequently the gradient increases with barrier depth, not exceeding the gradient in the case with a 1 cm deep barrier. This may be due to the combined effect of flow into the barrier, which is greater with a deeper barrier increasing the heads in the barrier, and flow out of the barrier, which can occur through a larger area with a deeper barrier. The relative significance of these two effects will determine the gradient in the barrier.

The gradient over the distance over which the damage criterion is computed is less than the gradient over the most downstream end of the barrier, as expected.

## 4 Effect of barrier depth on total flow rate

The effect of barrier depth on the flow rate is shown below. For a higher permeability contrast the effect of the depth of the barrier on the total flow rate is larger, as would be expected. Increasing the barrier depth to the full depth of the sample almost doubles the flow rate with a permeability contrast of 30, whereas with a permeability contrast of 3 the increase is only a factor 1.1.

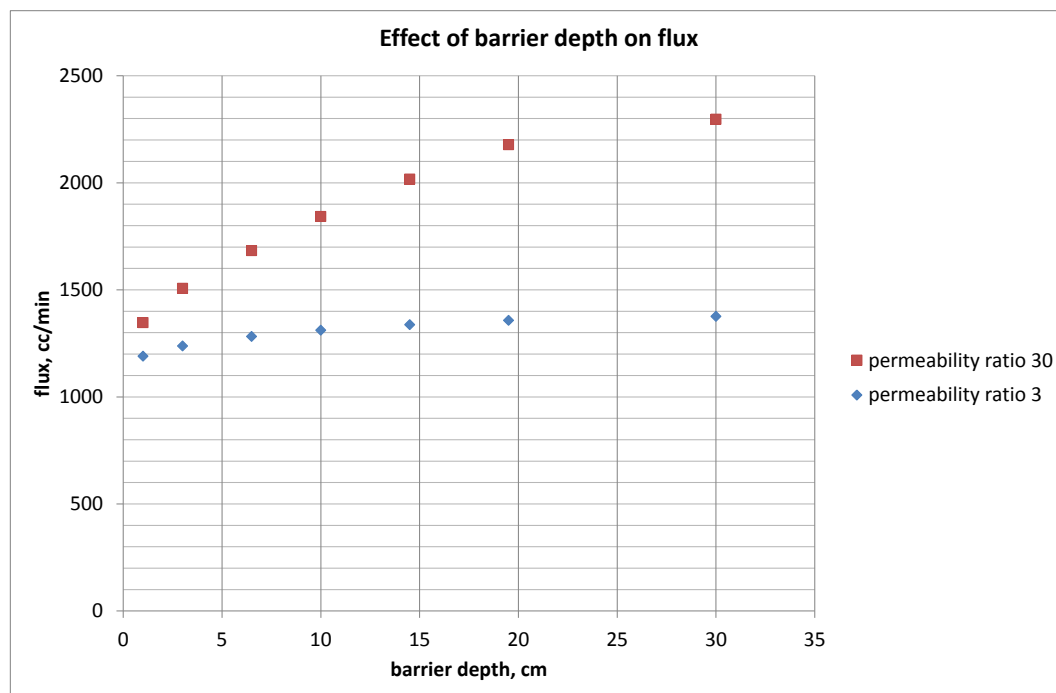


Figure 4.1 The absolute effect of barrier depth on the flux

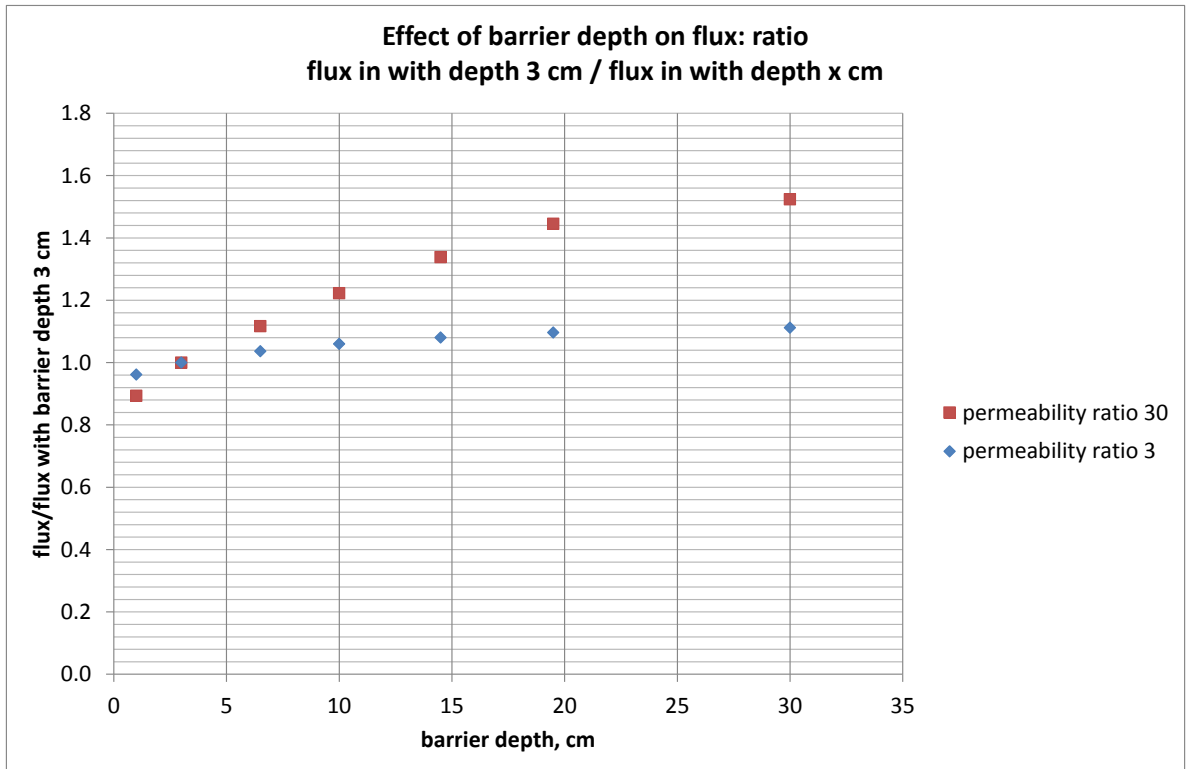


Figure 4.2 The ratio of the flux with the barrier with 3 cm depth over the flux with the barrier with a variable barrier depth

## 5 Conclusions

- The effect of the depth of the barrier on the total flux depends strongly on permeability. For a higher permeability contrast, the flow rate increases more significantly with barrier depth.
- Overall, the gradient over the entire barrier increases with increasing barrier depth, the exception is a very shallow barrier with 1 cm depth, which has a higher gradient. The effect on the gradient is stronger with a higher permeability contrast of 30 than with a contrast of 3, the streamlines show a strong component of vertical flow in the barrier.

## **J Postdictions**

# Memo

**Aan**  
Vera van Beek, Adam Bezuijen

**Datum**  
3 november 2017  
**Van**  
Esther Rosenbrand

**Kenmerk**  
11200952-005-GEO-0003  
**Doorkiesnummer**  
+31(0)88335 7852

**Aantal pagina's**  
4  
**E-mail**  
esther.rosenbrand@deltares.nl

**Onderwerp**  
Postdictie 192

## 1 Model

### Model dimensions

Model width, mm	300
Model depth, mm	101
Model length, mm	483
Barrier width, mm	50
Barrier depth, mm	30

### Input parameters

Hydraulic conductivity fine sand upstream, m/s	3.0E-04
Hydraulic conductivity fine sand downstream, m/s	5.6E-04
Hydraulic conductivity barrier, m/s	2.0E-03
Hydraulic conductivity filter cake, m/s	2.0E-04
Critical head corrected for filter and exit head loss, m	0.408

## 2 Test results

Location barrier in test downstream, mm	117
Location barrier in test upstream, mm	167
Flux in test at critical head, cm/min	987
Critical gradient between H13 and H14 in test, -	0.74

## 3 Model results



Figure 3.1 Head distribution in the model is indicated by the background colour. Vectors represent flow velocity, scaled by velocity. Light blue lines are streamlines and white lines are head contour lines

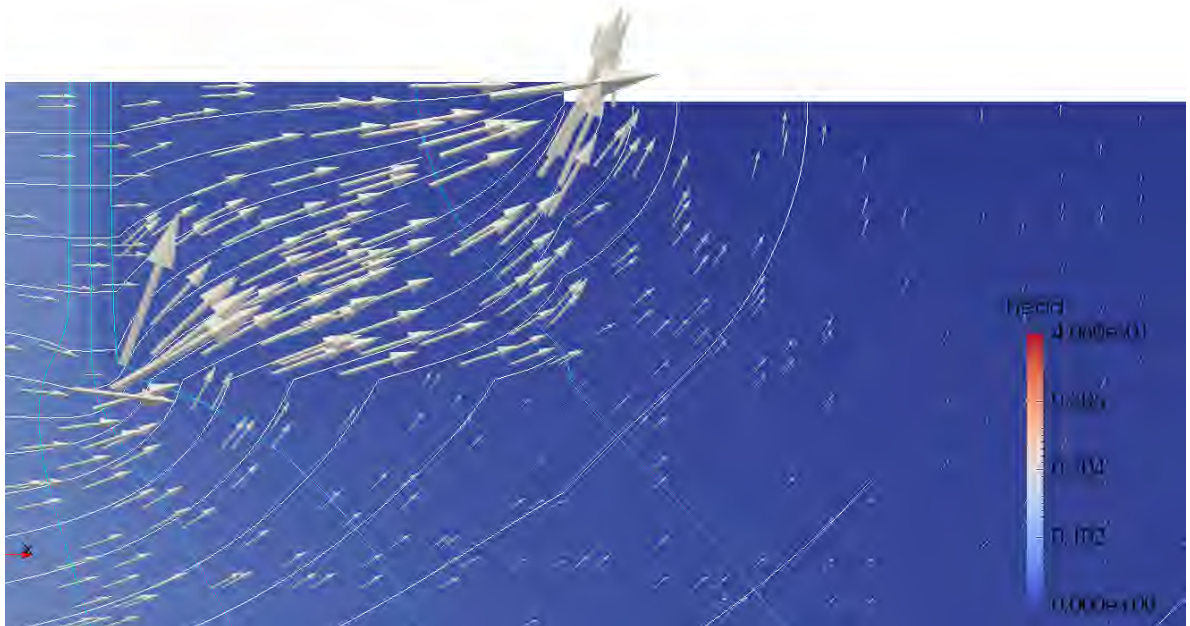


Figure 3.2 Close up inside the barrier. Head distribution in the model is indicated by the background colour. Vectors represent flow velocity, scaled by velocity. Light blue lines are streamlines and white lines are head contour lines

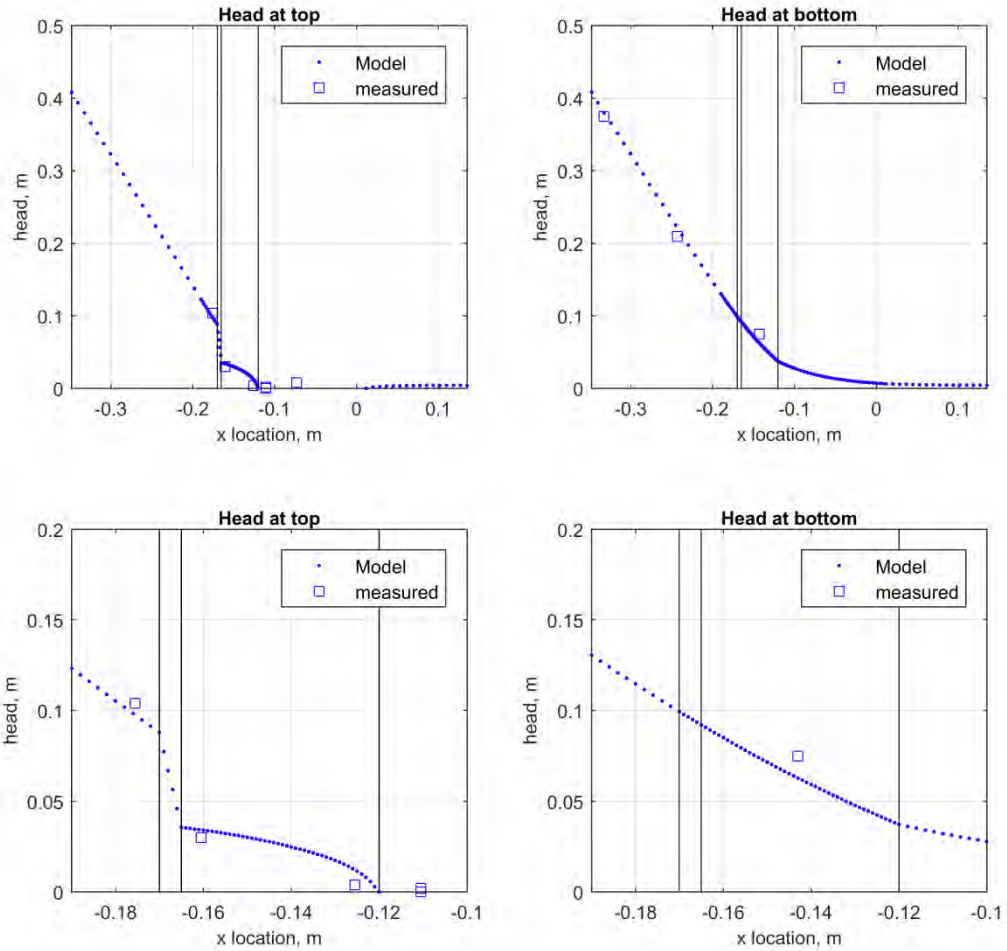


Figure 3.3 Modelled head (blue dots) and measured heads; measured heads are shifted in order to have the same distance from the downstream side of the barrier as was the case in the test

Table 3.1 Model results for gradient between H13 and H14

				uncertainty of modelled gradient due to uncertainty location in barrier*		Critical gradient -0.130 to -0.165 m
				Absolute	Relative	
Flux from model	Gradient H13 to H14 from model	Gradient H13-H14 shifted 2mm closer to barrier	Gradient H13-H14 shifted 2mm further from barrier			
cc/min	-	-	-	-	-	-
962	0.61	0.68	0.56	0.06	10	0.52

\*The location of the barrier is estimated to have an uncertainty of ca. 2 mm (ca.  $2 \cdot D_{50}$ ) along the length of the barrier. Therefore the gradient between H13 and H14 is gradient is calculated for a location shifted 2 mm further upstream from the barrier pipe interface and for a location shifted 2 mm further downstream towards the barrier pipe interface to estimate the uncertainty resulting from this.

*Table 3.2 Model results for damage criteria*

Horizontal gradient between -0.130 and -0.165 m at surface	Vertical Gradient from surface to -0.03 m at -0.130 m from centre of model	Diagonal gradient between (-0.13,0) m and (-0.165,-0.03) m	Average horizontal velocity between -0.130 m and -0.165 m at surface	Average vertical velocity between surface and -0.03 at -0.130 m from centre of model	Average diagonal velocity between (-0.13,0) m and (-0.165,-0.03) m
			cc/min	cc/min	cc/min
0.52	0.24	0.62	6.24	2.91	7.42

*Table 3.3 Comparison test and model*

Ratio flux model/ flux test	Ratio gradient model/ gradient test	Ratio gradient model/ gradient test shifted 2 mm closer	Ratio gradient model/ gradient test shifted 2 mm further
-	-	-	-
0.97	0.83	0.92	0.76

### 3.1 Comments:

The hydraulic conductivity of the fine sand upstream was slightly higher than in test 191 in this test. This may be due to a slightly lower relative density of the fine sand in this test; however, the difference was within the accuracy margin of 5% with which relative density is reported.

The head distribution in the model is matched reasonably well, with the exception of H13 downstream in the barrier. The head measured in H13 is practically zero in this experiment. Possibly, there was some erosion of the barrier or crumbling that led to a locally lower head. Another possibility is that before real erosion the porosity in the sand is increased, leading locally to a higher permeability and consequently a lower head in that area.

Reducing the hydraulic conductivity of the fine sand upstream and below the barrier would give a better fit of H5 (in the fine sand below the barrier) but a worse fit of H3 and H4, and of the flux. Therefore the current model is considered adequate.

The overestimation of the head downstream in the barrier results in an under estimation of the gradient between H13 and H14, the modelled gradient is only 83% of the measured gradient between H13 and H14 (and in the range of 76% to 92%). This is mainly due to the low head in H13.

## Memo

**Aan**  
Vera van Beek, Adam Bezuijen

**Datum**  
3 november 2017

**Kenmerk**  
11200952-005-GEO-0003

**Aantal pagina's**  
4

**Van**  
Esther Rosenbrand

**Doorkiesnummer**  
+31(0)88335 7852

**E-mail**  
esther.rosenbrand@deltares.nl

**Onderwerp**  
Postdictie 191

---

## 1 Model

### Model dimensions

Model width, mm	300
Model depth, mm	101
Model length, mm	483
Barrier width, mm	50
Barrier depth, mm	101

### Input parameters

Hydraulic conductivity fine sand upstream, m/s	2.5E-04
Hydraulic conductivity fine sand downstream, m/s	5.6E-04
Hydraulic conductivity barrier, m/s	1.9E-03
Hydraulic conductivity filter cake, m/s	2.2E-04
Critical head corrected for filter and exit head loss, m	0.4038

## 2 Test results

Location barrier in test downstream, mm	120
Location barrier in test upstream, mm	167
Flux in test at critical head, cm/min	918
Critical gradient between H13 and H14 in test, -	0.74

## 3 Model results

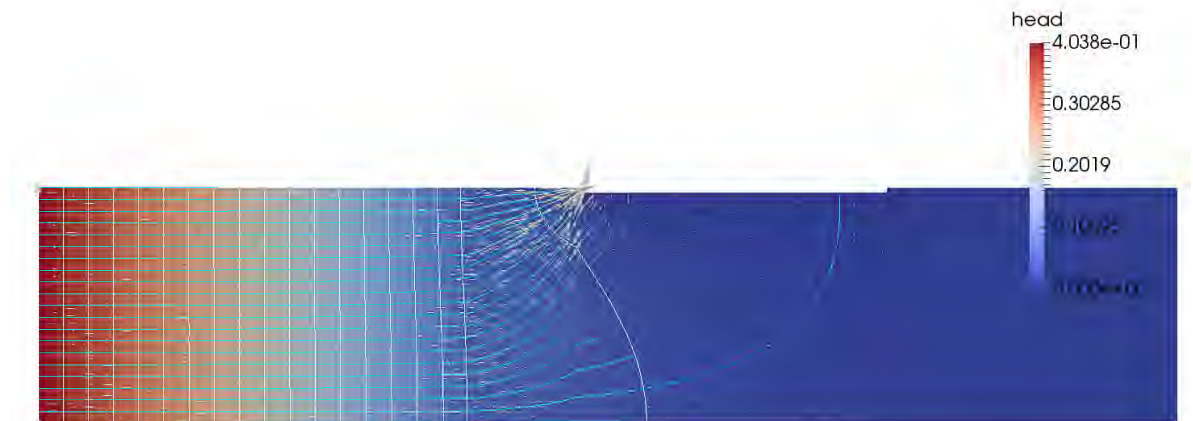


Figure 3.1 Head distribution in the model is indicated by the background colour. Vectors represent flow velocity, scaled by velocity. Light blue lines are streamlines and white lines are head contour lines.

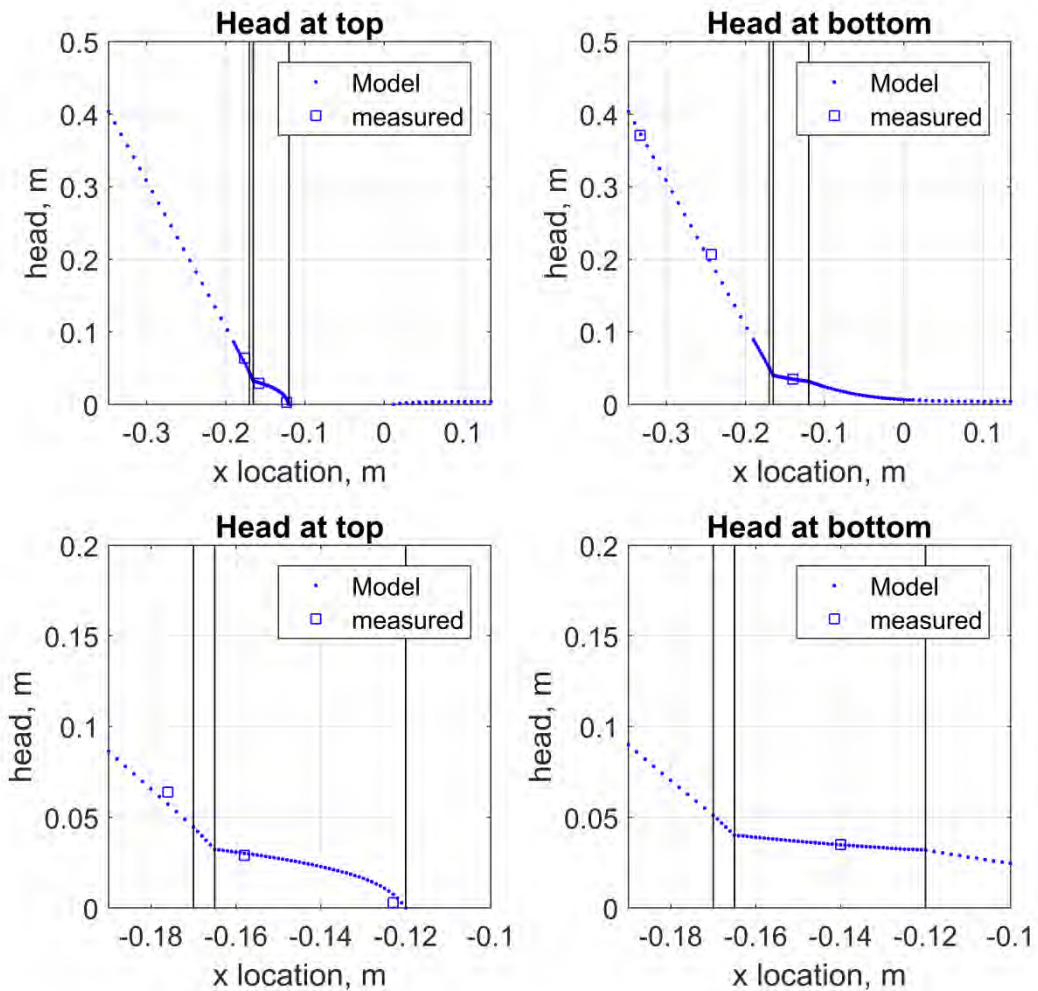


Figure 3.2 Modelled head (blue dots) and measured heads; measured heads are shifted in order to have the same distance from the downstream side of the barrier as was the case in the test

Table 3.1 Model results for gradient between H13 and H14

Flux from model	Gradient H13 to H14 from model	Gradient H13-H14 shifted 2mm closer to barrier	Gradient H13-H14 shifted 2mm further from barrier	uncertainty of modelled gradient due to uncertainty location in barrier*		Critical gradient -0.130 to -0.165 m
				Absolute	Relative	
cc/min	-	-	-	-	%-	-
908	0.65	0.76	0.57	0.10	15	0.46

\*The location of the barrier is estimated to have an uncertainty of ca. 2 mm (ca.  $2 \cdot D_{50}$ ) along the length of the barrier. Therefore the gradient between H13 and H14 is gradient is calculated for a location shifted 2 mm further upstream from the barrier pipe interface and for a location shifted 2 mm further downstream towards the barrier pipe interface to estimate the uncertainty resulting from this.

*Table 3.2 Model results for damage criteria*

Horizontal gradient between -0.130 and -0.165 m at surface	Vertical Gradient from surface to -0.03 m at -0.130 m from centre of model	Diagonal gradient between (-0.13,0) m and (-0.165,-0.03) m	Average horizontal velocity between -0.130 m and -0.165 m at surface	Average vertical velocity between surface and -0.03 at -0.130 m from centre of model	Average diagonal velocity between (-0.13,0) m and (-0.165,-0.03) m
			cc/min	cc/min	cc/min
0.46	0.29	0.40	5.26	3.36	4.56

*Table 3.3 Comparison test and model*

Ratio flux model/ flux test	Ratio gradient model/ gradient test	Ratio gradient model/ gradient test shifted 2 mm closer	Ratio gradient model/ gradient test shifted 2 mm further
0.99	0.87	1.03	0.77

### 3.1 Comments:

The head distribution in the model is matched reasonably well, possibly with the exception of H13 downstream in the barrier closest to the interface between the pipe and the barrier. The head measured in H13 is practically zero in this experiment. Possibly there was some erosion of the barrier or crumbling that led to a locally lower head. This is also indicated by the observations during the test, just prior to the pipe entering the barrier it was observed that there was crumbling of the barrier at the location of H12 and H13.

Increasing the hydraulic conductivity of the barrier would give a lower head in the barrier, giving a better match for H13, but a worse match for both H14 (further upstream in the barrier) and for H5 (in the bottom of the model). Considering that in the case of crumbling of the barrier, the continuum model would not be expected to give reliable results for H13, the current model is considered adequate.

## Memo

**Aan**  
Vera van Beek, Adam Bezuijen

**Datum**  
3 november 2017

**Kenmerk**  
1709-0003

**Aantal pagina's**  
5

**Van**  
Esther Rosenbrand

**Doorkiesnummer**  
+31(0)88335 7852

**E-mail**  
esther.rosenbrand@deltares.nl

**Onderwerp**  
Postdictieon 195

---

## 1 Model

### Model dimensions

Model width, mm	300
Model depth, mm	101
Model length, mm	483
Barrier width, mm	248
Barrier depth, mm	101

### Input parameters

Hydraulic conductivity fine sand upstream, m/s	n.a.
Hydraulic conductivity fine sand downstream, m/s	7.0E-04
Hydraulic conductivity barrier, m/s	1.8E-03
Hydraulic conductivity filter cake, m/s	n.a.
Critical head corrected for filter and exit head loss, m	0.1073

## 2 Test results

Location barrier in test downstream, mm	120
Location barrier in test upstream, mm	n.a.
Flux in test at critical head, cm/min	1085
Critical gradient between H13 and H14 in test, -	0.85

## 3 Model results

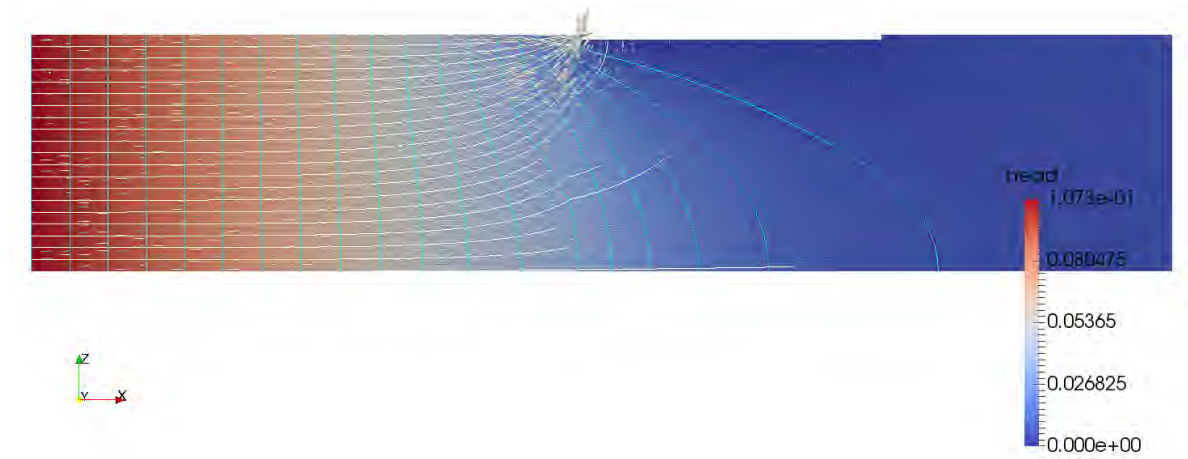


Figure 3.1 Head distribution in the model is indicated by the background colour. Vectors represent flow velocity, scaled by velocity. Light blue lines are streamlines and white lines are head contour lines

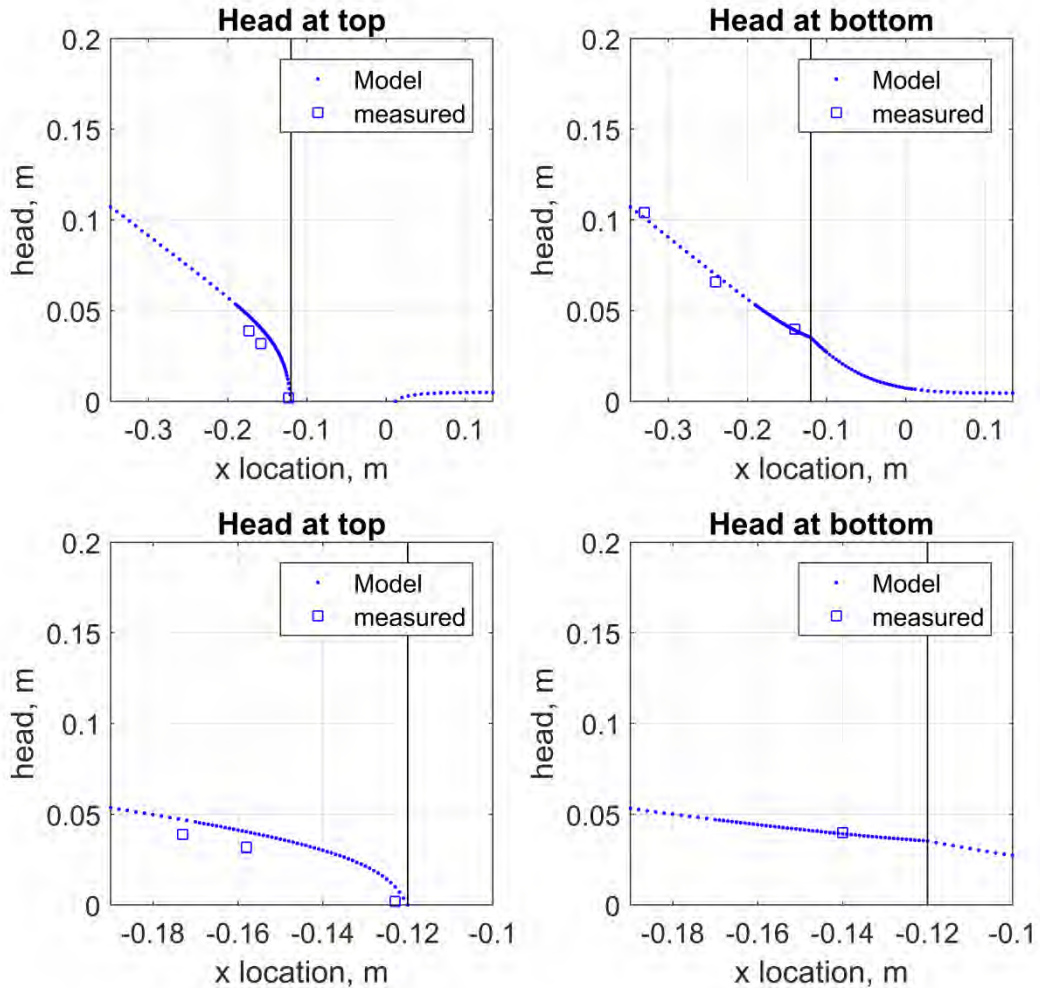


Figure 3.2 Modelled head (blue dots) and measured heads, measured heads are shifted in order to have the same distance from the downstream side of the barrier as was the case in the test

Table 3.1 Model results for gradient between H13 and H14

				uncertainty of modelled gradient due to uncertainty location in barrier*		
Flux from model	Gradient H13 to H14 from model	Gradient H13-H14 shifted 2mm closer to barrier	Gradient H13-H14 shifted 2mm further from barrier	Absolute	Relative	Critical gradient -0.130 to -0.165 m
cc/min	-	-	-	-	-	-
1120	0.87	1.02	0.77	0.12	14	0.63

\*The location of the barrier is estimated to have an uncertainty of ca. 2 mm (ca.  $2 \cdot D_{50}$ ) along the length of the barrier. Therefore the gradient between H13 and H14 is gradient is calculated for a location shifted 2 mm further upstream from the barrier pipe interface and for a location shifted 2 mm further downstream towards the barrier pipe interface to estimate the uncertainty resulting from this.

*Table 3.2 Model results for damage criteria*

Horizontal gradient between -0.130 and -0.165 m at surface	Vertical Gradient from surface to -0.03 m at -0.130 m from centre of model	Diagonal gradient between (-0.13,0) m and (-0.165,-0.03) m	Average horizontal velocity between -0.130 m and -0.165 m at surface	Average vertical velocity between surface and -0.03 at -0.130 m from centre of model	Average diagonal velocity between (-0.13,0) m and (-0.165,-0.03) m
			cc/min	cc/min	cc/min
0.63	0.24	0.45	6.74	2.57	4.75

*Table 3.3 Comparison test and model*

Ratio flux model/ flux test	Ratio gradient model/ gradient test	Ratio gradient model/ gradient test shifted 2 mm closer	Ratio gradient model/ gradient test shifted 2 mm further
-	-	-	-
1.03	1.02	1.20	0.91

### 3.1 Comments:

In this experiment there was no filter cake formation. The hydraulic conductivity of the barrier and of the fine sand were the only fitting parameters. In order to match the head profile and the flux, the hydraulic conductivity of the fine sand downstream had to be increased relative to the hydraulic conductivity that was measured in the column tests. The hydraulic conductivity of the barrier was estimated based on the measurements in the experiments, and as this hydraulic conductivity also has a strong effect on the flux, and the flux was matched relatively well this model is considered adequate.

As the hydraulic conductivity of the Baskarp sand is so much higher than expected, additional attempts were made to model this with a hydraulic conductivity of Baskarp sand of  $2.9e-4$  m/s and for the barrier of  $2.45e-3$  m/s. However this overestimates the flux by a factor 1.2 and gives the head distribution below, which is a worse fit to the results. Reducing the hydraulic conductivity of the barrier, leaving the hydraulic conductivity of the Baskarp sand constant would reduce the flux, but give a worse estimation of the head profile in the barrier. Therefore in the selected postdiction the hydraulic conductivity of the barrier was reduced (to increase the flux) and the hydraulic conductivity of the Baskarp sand was increased (to reduce the head in the barrier).

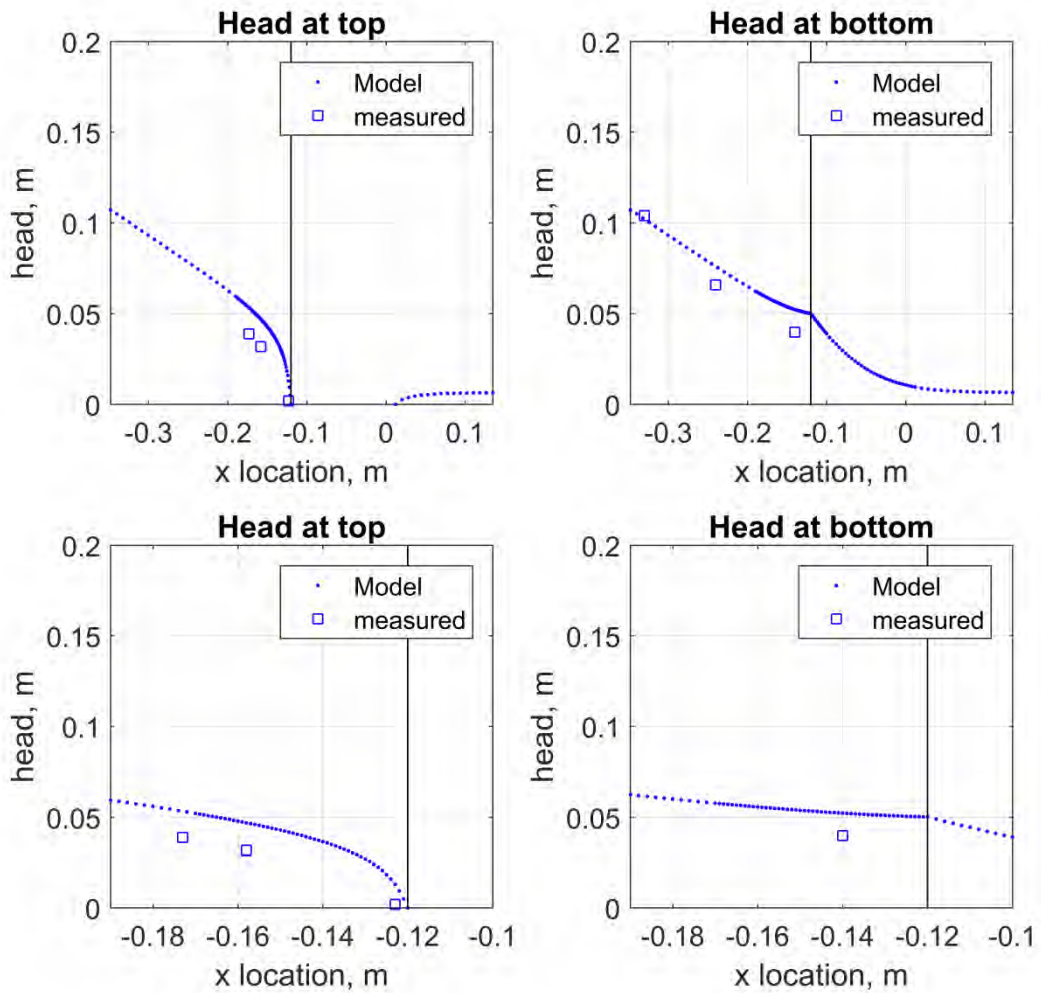


Figure 3.3 Modelled head (blue dots) and measured heads, measured heads are shifted in order to have the same distance from the downstream side of the barrier as was the case in the test. This postdiction uses values of hydraulic conductivity closer to the column test values, but provides a poor fit of the measured results

## Memo

**Aan**  
Vera van Beek, Adam Bezuijen

**Datum**  
3 november 2017

**Kenmerk**  
11200952-005-GEO-0003

**Aantal pagina's**  
5

**Van**  
Esther Rosenbrand

**Doorkiesnummer**  
+31(0)88335 7852

**E-mail**  
esther.rosenbrand@deltares.nl

**Onderwerp**  
Postdictie 193

---

## 1 Model

### Model dimensions

Model width, mm	300
Model depth, mm	101
Model length, mm	483
Barrier width, mm	50
Barrier depth, mm	101

### Input parameters

Hydraulic conductivity fine sand upstream, m/s	3.7E-04
Hydraulic conductivity fine sand downstream, m/s	6.9E-04
Hydraulic conductivity barrier, m/s	4.9E-03
Hydraulic conductivity filter cake, m/s	1.2E-05
Critical head corrected for filter and exit head loss, m	0.5496

## 2 Test results

Location barrier in test downstream, mm	113
Location barrier in test upstream, mm	165
Flux in test at critical head, cm/min	1186
Critical gradient between H13 and H14 in test, -	0.34

## 3 Model results

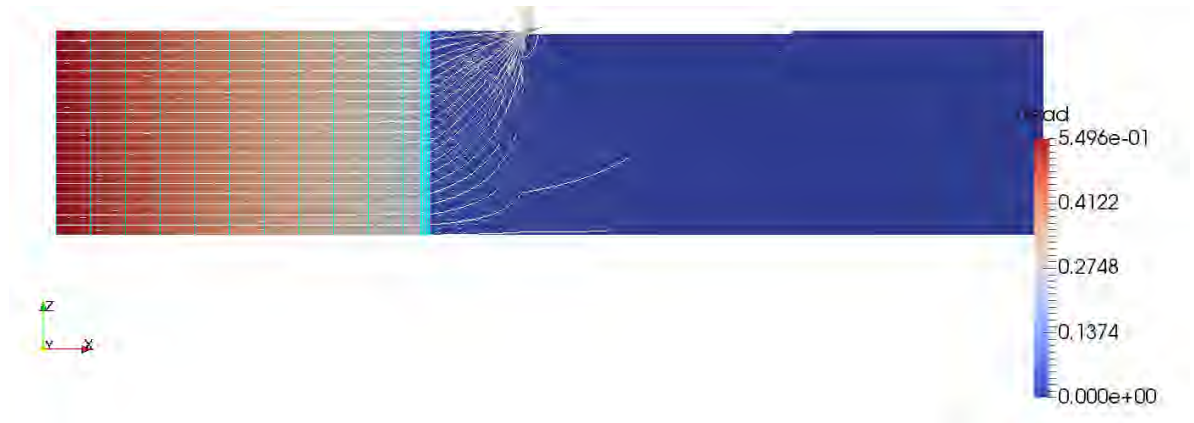


Figure 3.1 Head distribution in the model is indicated by the background colour. Vectors represent flow velocity, scaled by velocity. Light blue lines are streamlines and white lines are head contour lines

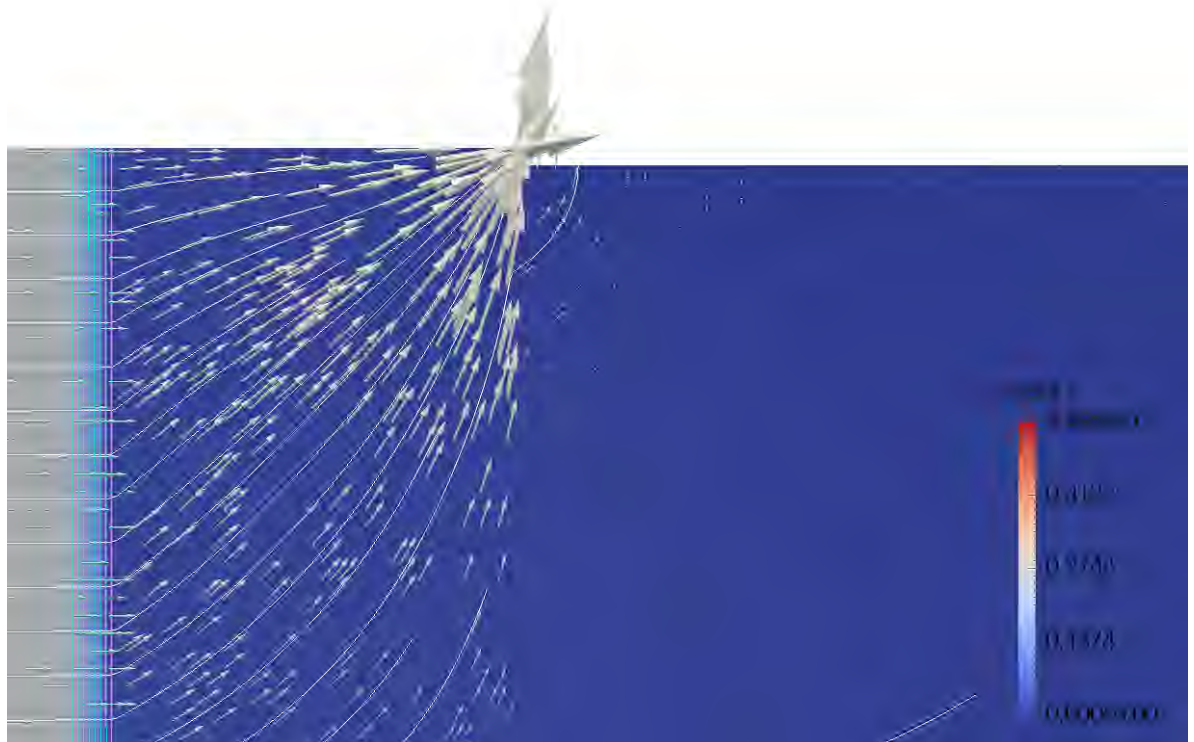


Figure 3.2 Close up inside the barrier. Head distribution in the model is indicated by the background colour. Vectors represent flow velocity, scaled by velocity. Light blue lines are streamlines and white lines are head contour lines

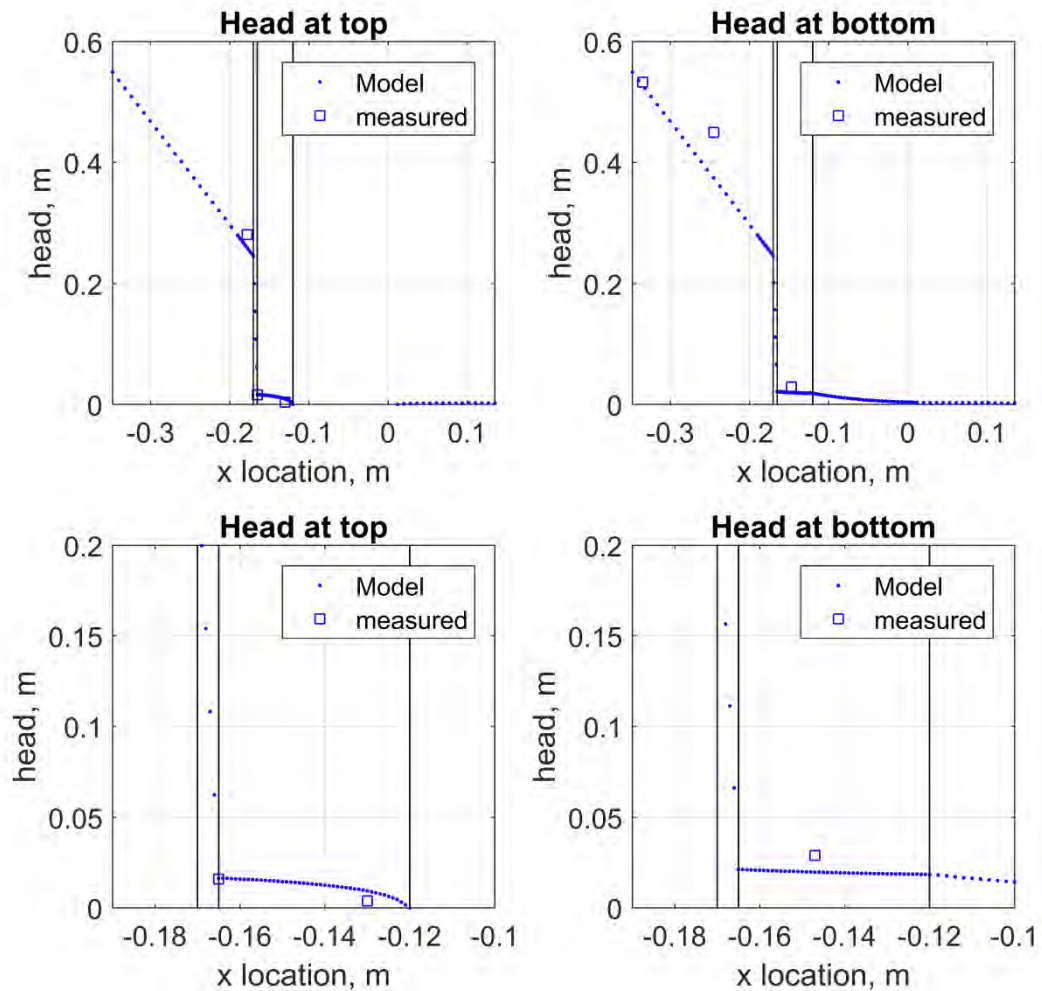


Figure 3.3 Modelled head (blue dots) and measured heads; measured heads are shifted in order to have the same distance from the downstream side of the barrier as was the case in the test

Table 3.1 Model results for gradient between H13 and H14

				uncertainty of modelled gradient due to uncertainty location in barrier*		
Flux from model	Gradient H13 to H14 from model	Gradient H13-H14 shifted 2mm closer to barrier	Gradient H13-H14 shifted 2mm further from barrier	Absolute	Relative	Critical gradient -0.130 to -0.165 m
cc/min	-	-	-	-	-	-
1215	0.20	0.23	2.80*	error of only 2mm closer to the barrier 0.03	relative error for only shift closer to barrier 15	0.20

\*The location of the barrier is estimated to have an uncertainty of ca. 2 mm (ca.  $2 \cdot D_{50}$ ) along the length of the barrier. Therefore the gradient between H13 and H14 is gradient is calculated for a location shifted 2 mm further upstream from the barrier pipe interface and for a location shifted 2 mm further downstream towards the barrier pipe interface to estimate the uncertainty resulting from this.

*Table 3.2 Model results for damage criteria*

Horizontal gradient between -0.130 and -0.165 m at surface	Vertical Gradient from surface to -0.03 m at -0.130 m from centre of model	Diagonal gradient between (-0.13,0) m and (-0.165,-0.03) m	Average horizontal velocity between -0.130 m and -0.165 m at surface	Average vertical velocity between surface and -0.03 at -0.130 m from centre of model	Average diagonal velocity between (-0.13,0) m and (-0.165,-0.03) m
			cc/min	cc/min	cc/min
0.20	0.17	0.19	8.44	6.97	7.66

*Table 3.3 Comparison test and model*

Ratio flux model/ flux test	Ratio gradient model/ gradient test	Ratio gradient model/ gradient test shifted 2 mm closer	Ratio gradient model/ gradient test shifted 2 mm further
-	-	-	-
1.03	0.59	0.66	8.17*

### 3.1 Comments:

Because the downstream interface of the barrier was shifted 7 mm in the model, H14 is in the modelled filter cake. This means that the gradient computed for the point shifted 2 mm upstream is much higher. Therefore this is not a good estimate of the error.

Modelling this experiment required a filter cake with a very low hydraulic conductivity. It was also observed that the fine sand migrated into the barrier over a distance of ca. 0.5 mm to 1 cm at the top of the model which would support the assumption of a filter cake.

The hydraulic conductivity of the fine sand upstream of the barrier is higher than measured in column experiments. This could be due to a slightly lower relative density, but some migration of fines from the Metselzand to the barrier may also contribute to a higher hydraulic conductivity of the upstream sand. The hydraulic conductivity of the barrier is also higher than the hydraulic conductivity determined in the column tests on the barrier material. Again differences may be affected by slight differences in relative density in the column tests and the experiment, and possibly by migration of fines from the barrier to the pipe on the downstream end.

As in tests 191 and 192 the head in the barrier at H13 is overestimated by the model, probably due to some crumbling of the barrier towards the pipe, this results in overestimation of the gradient between H13 and H14.

The head in the top and the bottom of the model is underestimated. This would indicate an even higher hydraulic conductivity of the fine sand upstream of the barrier. However that would result in a higher flow rate as well. Reducing the conductivity of the filter cake would compensate for this. However, in order to match the profile of the heads measured in the bottom upstream requires changes that overestimate the head just upstream of the barrier (as shown below) and the flux is thereby underestimated by a factor 0.6. Therefore the model described above is considered adequate.

In the model, the hydraulic conductivity is assumed to be uniform over the depth, probably the effect of the particle migration is greater in the top of the model, increasing the hydraulic conductivity of the fine sand and reducing the head drop in the than in the bottom. However, it was considered that adding additional zones with different hydraulic conductivity would be over-fitting the model.

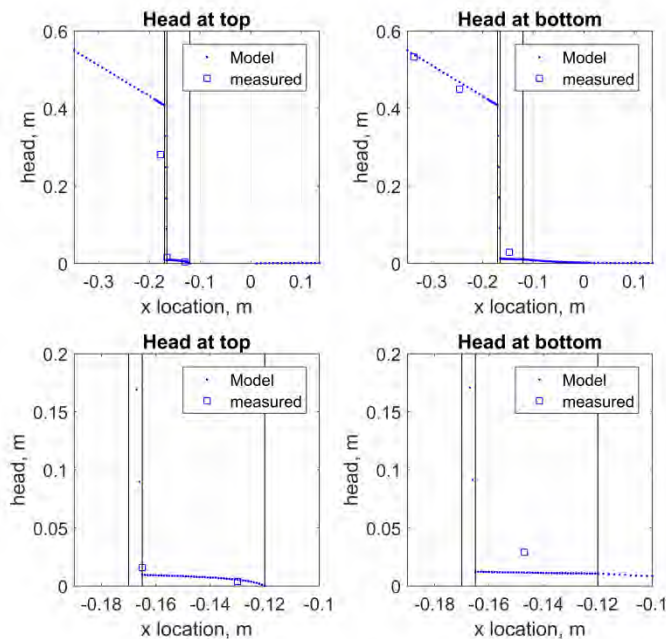


Figure 3.4 Modelled head (blue dots) and measured heads; measured heads are shifted in order to have the same distance from the downstream side of the barrier as was the case in the test. These charts illustrate the model that was not found adequate for postdiction

## Memo

**Aan**  
Vera van Beek, Adam Bezuijen

<b>Datum</b> 3 november 2017	<b>Kenmerk</b> 11200952-005-GEO-0003	<b>Aantal pagina's</b> 4
<b>Van</b> Esther Rosenbrand	<b>Doorkiesnummer</b> +31(0)88335 7852	<b>E-mail</b> esther.rosenbrand@deltares.nl

**Onderwerp**  
Postdictieon 197

---

## 1 Model

### Model dimensions

Model width, mm	300
Model depth, mm	101
Model length, mm	483
Barrier width, mm	248
Barrier depth, mm	101

### Input parameters

Hydraulic conductivity fine sand upstream, m/s	n.a.
Hydraulic conductivity fine sand downstream, m/s	2.9E-04
Hydraulic conductivity barrier, m/s	5.9E-03
Hydraulic conductivity filter cake, m/s	n.a.
Critical head corrected for filter and exit head loss, m	0.032

## 2 Test results

Location barrier in test downstream, mm	121
Location barrier in test upstream, mm	n.a.
Flux in test at critical head, cm/min	844
Critical gradient between H13 and H14 in test, -	0.38

3

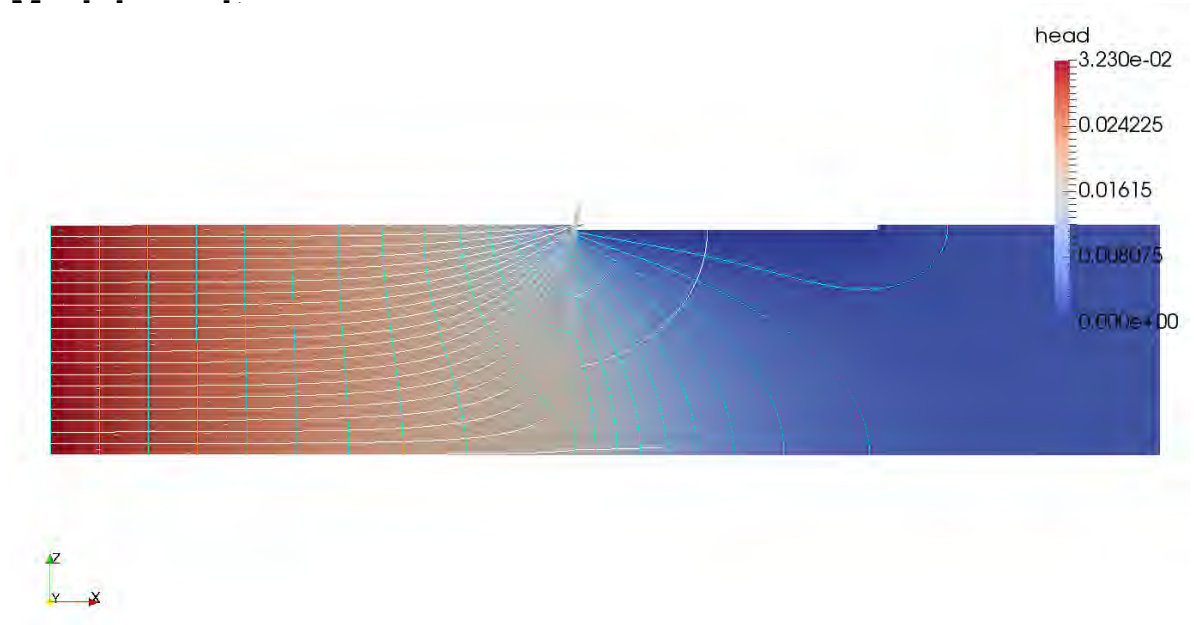


Figure 3.1 Head distribution in the model is indicated by the background colour. Vectors represent flow velocity, scaled by velocity. Light blue lines are streamlines and white lines are head contour lines

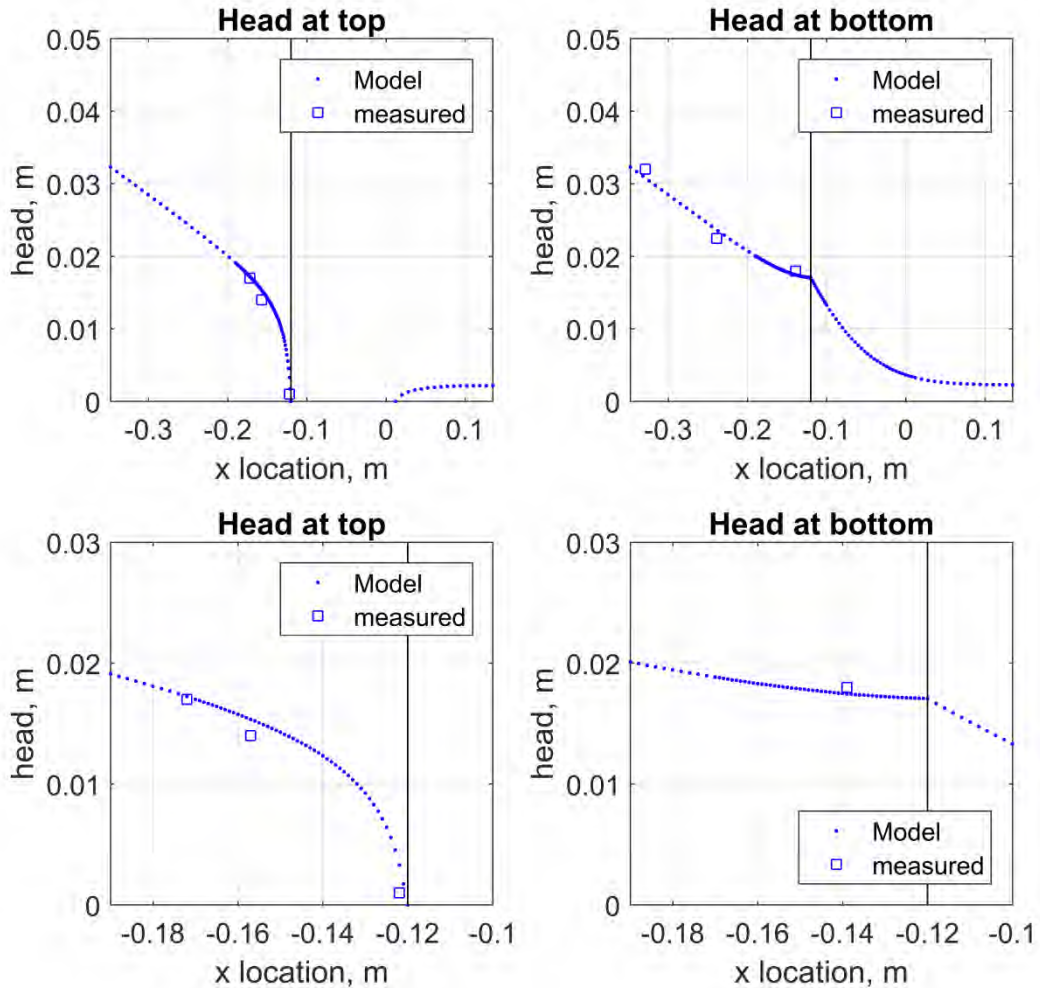


Figure 3.2 Modelled head (blue dots) and measured heads; measured heads are shifted in order to have the same distance from the downstream side of the barrier as was the case in the test

Table 3.1 Model results for gradient between H13 and H14

				uncertainty of modelled gradient due to uncertainty location in barrier*		
Flux from model	Gradient H13 to H14 from model	Gradient H13-H14 shifted 2mm closer to barrier	Gradient H13-H14 shifted 2mm further from barrier	Absolute	Relative	Critical gradient -0.130 to -0.165 m
cc/min	-	-	-	-	-	-
858	0.34	0.43	0.29	0.07	21	0.20

\*The location of the barrier is estimated to have an uncertainty of ca. 2 mm (ca.  $2 \cdot D_{50}$ ) along the length of the barrier. Therefore the gradient between H13 and H14 is gradient is calculated for a location shifted 2 mm further upstream from the barrier pipe interface and for a location shifted 2 mm further downstream towards the barrier pipe interface to estimate the uncertainty resulting from this

*Table 3.2 Model results for damage criteria*

Horizontal gradient between -0.130 and -0.165 m at surface	Vertical Gradient from surface to -0.03 m at -0.130 m from centre of model	Diagonal gradient between (-0.13,0) m and (-0.165,-0.03) m	Average horizontal velocity between -0.130 m and -0.165 m at surface	Average vertical velocity between surface and -0.03 at -0.130 m from centre of model	Average diagonal velocity between (-0.13,0) m and (-0.165,-0.03) m
			cc/min	cc/min	cc/min
0.20	0.27	0.20	7.23	9.40	7.15

*Table 3.3 Comparison test and model*

Ratio flux model/ flux test	Ratio gradient model/ gradient test	Ratio gradient model/ gradient test shifted 2 mm closer	Ratio gradient model/ gradient test shifted 2 mm further
-	-	-	-
1.02	0.91	1.13	0.76

### 3.1 Comments:

In this experiment there was no filter cake formation, as there was no fine sand upstream of the barrier. The hydraulic conductivity of the barrier and of the fine sand were the only fitting parameters. In order to match the head profile and the flux, the hydraulic conductivity of the fine sand downstream had to be increased relative to the hydraulic conductivity that was measured in the column tests but to a much lesser extent than for the postdiction of test 195. The hydraulic conductivity of the barrier is slightly less than measured in the column tests and used in the postdiction of test 196 but the difference is limited. As both flux and head distributions match the measured data quite well, this fit is considered adequate.

## Memo

**Aan**  
Vera van Beek, Adam Bezuijen

**Datum**  
3 november 2017

**Kenmerk**  
1709-0003

**Aantal pagina's**  
3

**Van**  
Esther Rosenbrand

**Doorkiesnummer**  
+31(0)88335 7852

**E-mail**  
esther.rosenbrand@deltares.nl

**Onderwerp**  
Postdictieon 196

---

## 1 Model

### Model dimensions

Model width, mm	300
Model depth, mm	101
Model length, mm	483
Barrier width, mm	50
Barrier depth, mm	101

### Input parameters

Hydraulic conductivity fine sand upstream, m/s	2.9e-4
Hydraulic conductivity fine sand downstream, m/s	5.6e-4
Hydraulic conductivity barrier, m/s	7E-03
Hydraulic conductivity filter cake, m/s	n.a.
Critical head corrected for filter and exit head loss, m	0.5542

## 2 Test results

Location barrier in test downstream, mm	120
Location barrier in test upstream, mm	170
Flux in test at critical head, cm/min	1493
Critical gradient between H13 and H14 in test, -	0.40

## 3 Model results



Figure 3.1 Head distribution in the model is indicated by the background colour. Vectors represent flow velocity, scaled by velocity. Light blue lines are streamlines and white lines are head contour lines

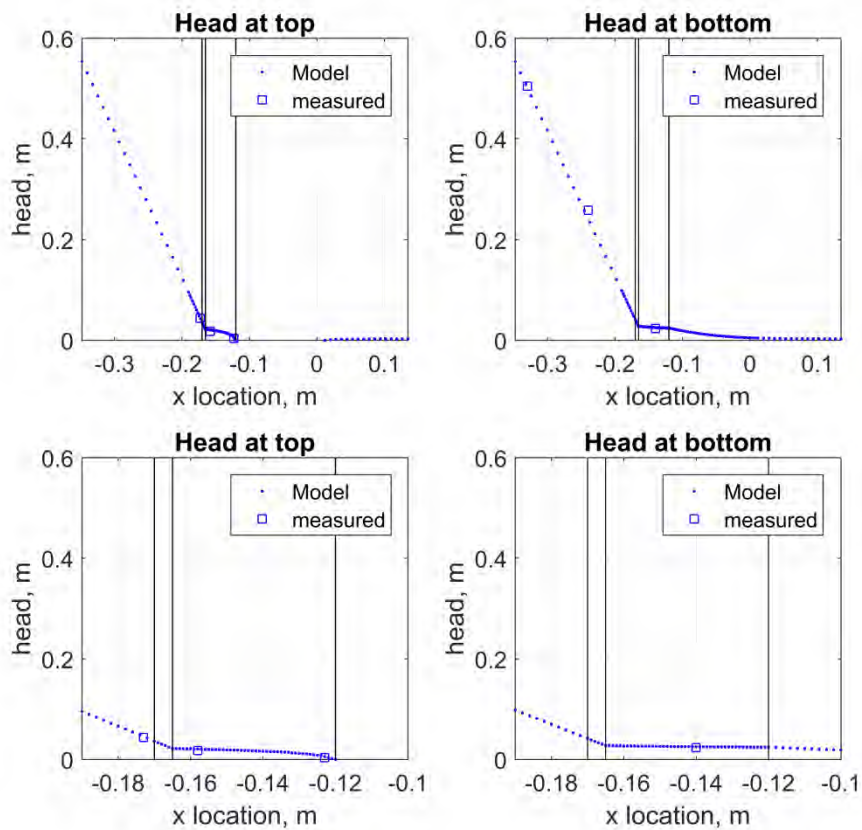


Figure 3.2 Modelled head (blue dots) and measured heads; measured heads are shifted in order to have the same distance from the downstream side of the barrier as was the case in the test

*Table 3.1 Model results for gradient between H13 and H14*

Flux from model	Gradient H13 to H14 from model	Gradient H13-H14 shifted 2mm closer to barrier	Gradient H13-H14 shifted 2mm further from barrier	uncertainty of modelled gradient due to uncertainty location in barrier*		Critical gradient -0.130 to -0.165 m
				Absolute	Relative	
cc/min	-	-	-	-	-	-
1547	0.42	0.52	0.36	0.08	19	0.26

\*The location of the barrier is estimated to have an uncertainty of ca. 2 mm (ca.  $2 \cdot D_{50}$ ) along the length of the barrier. Therefore the gradient between H13 and H14 is calculated for a location shifted 2 mm further upstream from the barrier pipe interface and for a location shifted 2 mm further downstream towards the barrier pipe interface to estimate the uncertainty resulting from this.

*Table 3.2 Model results for damage criteria*

Horizontal gradient between -0.130 and -0.165 m at surface	Vertical Gradient from surface to -0.03 m at -0.130 m from centre of model	Diagonal gradient between (-0.13,0) m and (-0.165,-0.03) m	Average horizontal velocity between -0.130 m and -0.165 m at surface	Average vertical velocity between surface and -0.03 at -0.130 m from centre of model	Average diagonal velocity between (-0.13,0) m and (-0.165,-0.03) m
			cc/min	cc/min	cc/min
0.26	0.22	0.24	11.12	9.38	10.07

*Table 3.3 Comparison test and model*

Ratio flux model/ flux test	Ratio gradient model/ gradient test	Ratio gradient model/ gradient test shifted 2 mm closer	Ratio gradient model/ gradient test shifted 2 mm further
-	-	-	-
1.04	1.05	1.29	0.89

### 3.1 Comments:

The prediction agrees quite well with the measured data, regarding the flow rate, the head distribution and the gradient between H14 and H13. The hydraulic conductivity of the barrier and the fine sand upstream are comparable to the hydraulic conductivity of these materials measured in the filter tests.

## Memo

**Aan**  
Vera van Beek, Adam Bezuijen

**Datum**  
9 november 2017

**Kenmerk**  
11200952-005-GEO-0003

**Aantal pagina's**  
6

**Van**  
Esther Rosenbrand

**Doorkiesnummer**  
+31(0)88335 7852

**E-mail**  
esther.rosenbrand@deltares.nl

**Onderwerp**  
Postdictieion 199

## 1 Model

### Model dimensions

Model width, mm	101
Model depth, mm	300
Model length, mm	488
Barrier width, mm	50
Barrier depth, mm	100

\*model length is slightly longer than in non-rotated test as the inner dimensions of the sample (excluding the filter) are modelled.

### Input parameters

Hydraulic conductivity fine sand upstream, m/s	3.9e-4
Hydraulic conductivity fine sand downstream, m/s	3.4e-4
Hydraulic conductivity fine sand below barrier, m/s	3.4e-4
Hydraulic conductivity barrier, m/s	4.9e-3
Hydraulic conductivity filter cake, m/s	1e-3
Critical head corrected for filter and exit head loss, m	0.2828

## 2 Test results

Location barrier in test downstream, mm	115
Location barrier in test upstream, mm	164
Flux in test at critical head, cm/min	728
Critical gradient between H13 and H14 in test, -	0.63

## 3 Model results

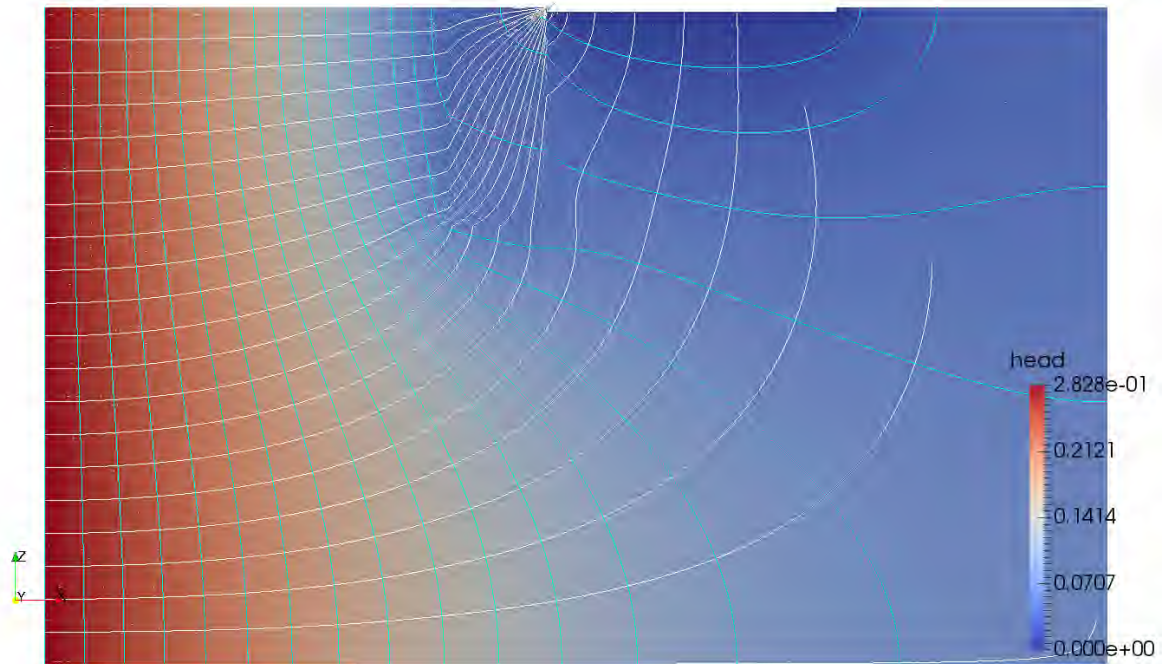


Figure 3.1 Head distribution in the model is indicated by the background colour. Vectors represent flow velocity, scaled by velocity. Light blue lines are streamlines and white lines are head contour lines.

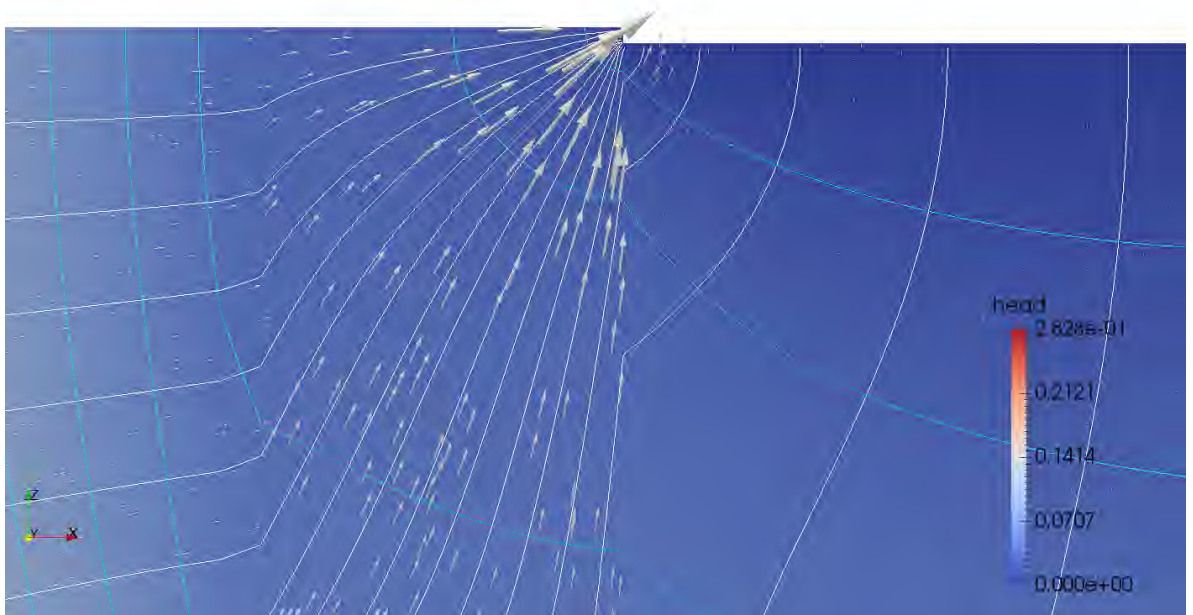


Figure 3.2 Close up. Head distribution in the model is indicated by the background colour. Vectors represent flow velocity, scaled by velocity. Light blue lines are streamlines and white lines are head contour lines.

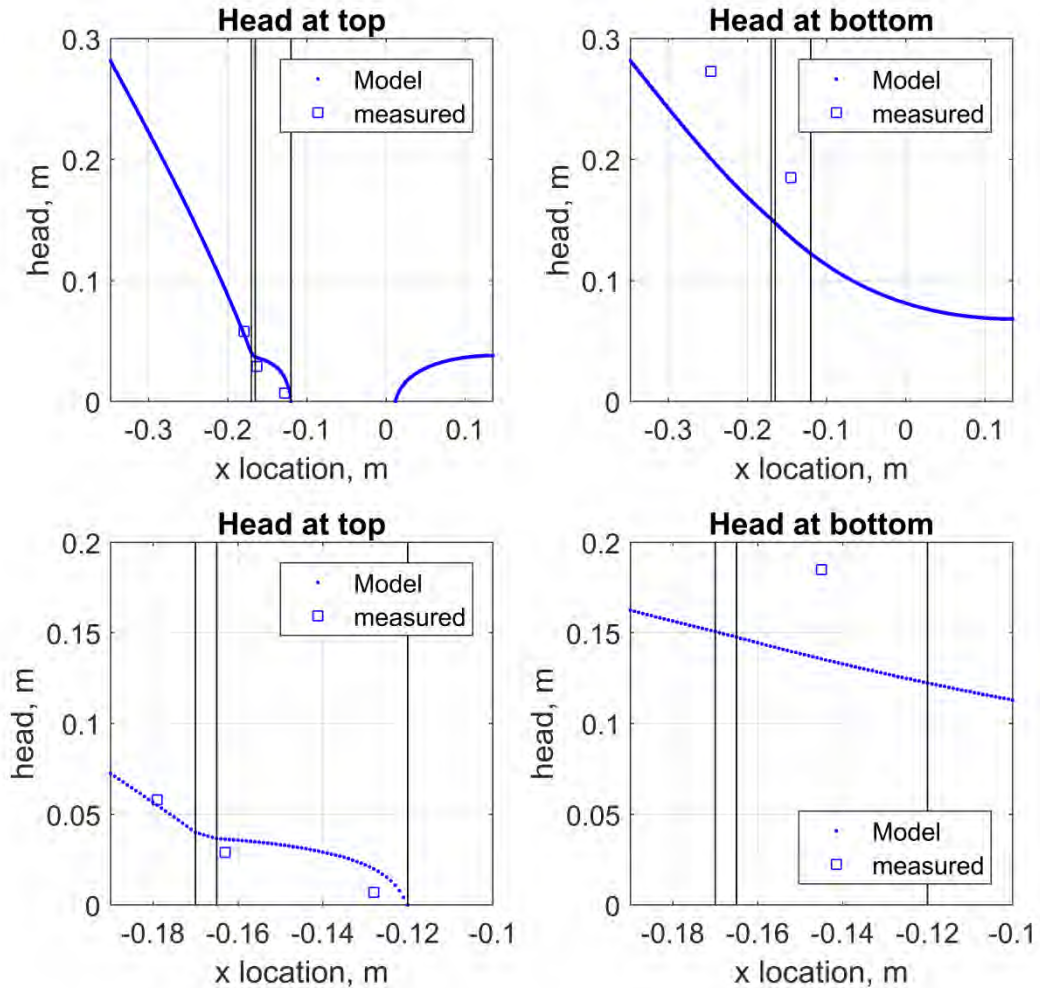


Figure 3.3 Modelled head (blue dots) and measured heads; measured heads are shifted in order to have the same distance from the downstream side of the barrier as was the case in the test.

Table 3.1 Model results for gradient between H13 and H14

				uncertainty of modelled gradient due to uncertainty location in barrier*		
Flux from model	Gradient H13 to H14 from model	Gradient H13-H14 shifted 2mm closer to barrier	Gradient H13-H14 shifted 2mm further from barrier	Absolute	Relative	Critical gradient -0.130 to -0.165
cc/min	-	-	-	-	-	-
722	0.47	0.54	0.41	0.06	13	0.41

\*The location of the barrier is estimated to have an uncertainty of ca. 2 mm (ca.  $2 \cdot D_{50}$ ) along the length of the barrier. Therefore the gradient between H13 and H14 is gradient is calculated for a location shifted 2 mm further upstream from the barrier pipe interface and for a location shifted 2 mm further downstream towards the barrier pipe interface to estimate the uncertainty resulting from this.

Table 3.2 Model results for damage criteria

Horizontal gradient between -0.130 and -0.165 m at surface	Vertical Gradient from surface to -0.03 m at -0.130 m from centre of model	Diagonal gradient between (-0.13,0) m and (-0.165,-0.03) m	Average horizontal velocity between -0.130 m and -0.165 m at surface	Average vertical velocity between surface and -0.03 at -0.130 m from centre of model	Average diagonal velocity between (-0.13,0) m and (-0.165,-0.03) m
			cc/min	cc/min	cc/min
0.41	0.42	0.40	12.18	12.35	11.63

Table 3.3 Comparison test and model

Ratio flux model/ flux test	Ratio gradient model/ gradient test	Ratio gradient model/ gradient test shifted 2 mm closer	Ratio gradient model/ gradient test shifted 2 mm further
-	-	-	-
0.99	0.74	0.86	0.66

## 4 Comments:

As in experiment 198, it was necessary to increase the hydraulic conductivity of all layers relative to the values in the column tests in order to match the measured flow rate; also the downstream hydraulic conductivity was modified. In the finally selected postdiction the downstream hydraulic conductivity was actually lower than the upstream hydraulic conductivity, whereas the relative density of that part of the model was lower when the model was prepared.

The downstream hydraulic conductivity and the conductivity below the barrier affect the head drop in the fine sand upstream of the barrier in the bottom of the model. This is still not matched correctly in the current postdiction, however, it was decided to focus on a correct modelling of the flow rate through the model as well as the head profile, and as the head profile in the top of the model is more relevant to the failure of the barrier.

Several of the iterations in determining this postdiction are shown below in order to account for the selection of this model. Also, the sensitivity to the value of the downstream hydraulic conductivity of the model is checked by doing one computation with the model presented above where the hydraulic conductivity of the downstream fine sand was increased to 5.5 m/s. This resulted in an overestimation of the flow (factor 1.04 instead of current 0.99) and a worse

underestimation of the gradient between H13 and H14 in the test (factor 0.69 instead of current 0.74). The head profile is also slightly worse than in the postdiction presented above, therefore the current model is retained.

Using values similar to those measured in column tests resulted in clear misrepresentation of the measurements as shown below.

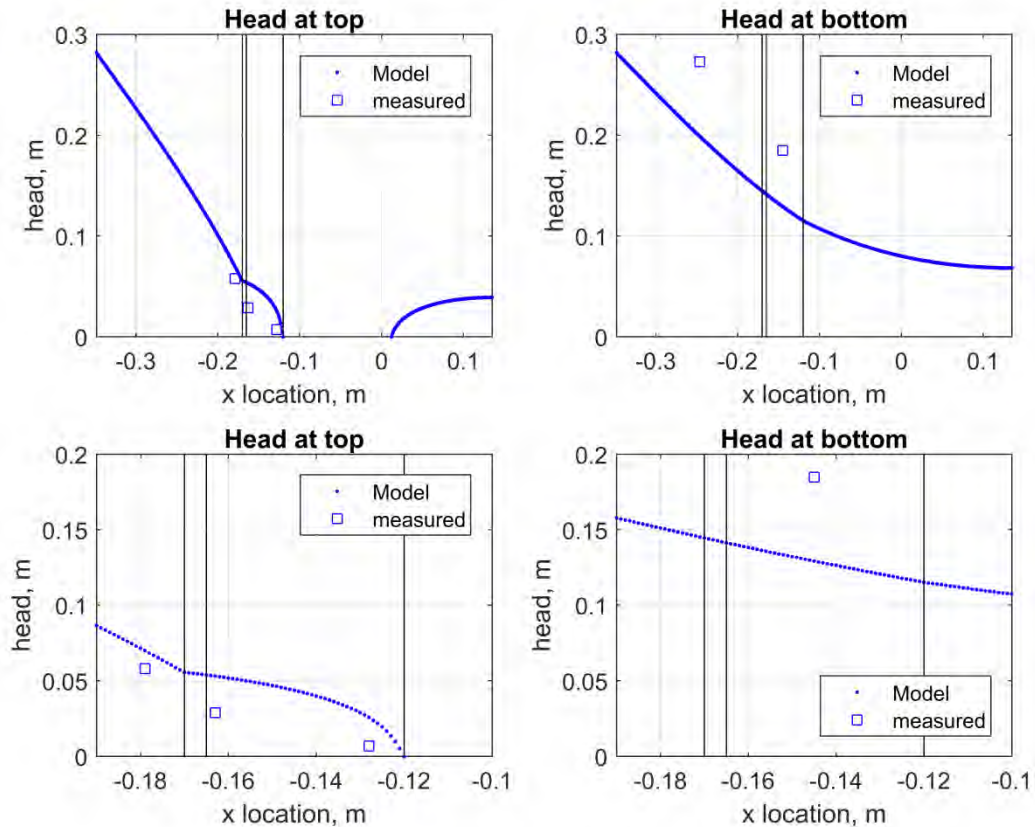


Figure 4.1 Post diction using permeabilities:

- Fine sand upstream:  $3.7e-4$  m/s
- Fine sand below barrier:  $3.7e-4$  m/s
- Fine sand downstream:  $4.9e-4$  m/s
- Barrier:  $2.0e-3$  m/s
- Filter cake  $2.0e-3$  m/s

The flow is 663 cc/min instead of the measured 728 cc/min underestimation of 0.9. The head in the top of the model is overestimated, in the bottom it is underestimated.

Based on this overall hydraulic conductivity is increased, to match flow.

The head profile in the top is improved by increasing contrast between barrier and fine sand upstream (more reduction of head over fine sand).

The head profile in the bottom is improved by increasing head drop over the downstream area of the model, i.e. increasing hydraulic conductivity of the upstream fine sand relative to the downstream fine sand. The downstream sand has a lower relative density than the upstream sand therefore it is counter expectations to give this a lower hydraulic conductivity than upstream.

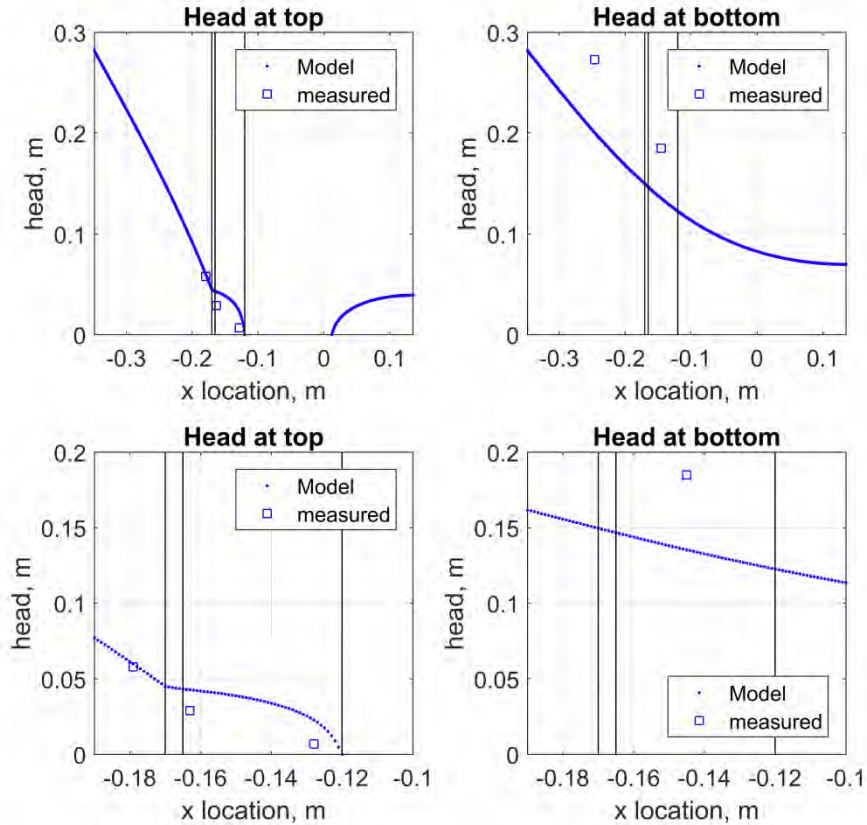


Figure 4.2 Post diction using permeabilities:

- Fine sand upstream:  $3.7e-4$  m/s
- Fine sand below barrier:  $3.7e-4$  m/s
- Fine sand downstream:  $4.9e-4$  m/s
- Barrier:  $2.0e-3$  m/s
- Filter cake  $2.0e-3$  m/s

The flow is 747 cc/min instead of the measured 728 cc/min overestimation of 1.03. The head in the top of the model is overestimated only in the barrier, in the bottom it is still underestimated.

The head profile in the barrier is improved by reducing the hydraulic conductivity of the filter cake and also slightly of the upstream fine sand and increasing the hydraulic conductivity of the barrier.

In the bottom of the model, the head drop upstream would be improved by increasing hydraulic conductivity of upstream relative to below the barrier and downstream further. As noted before, this is contrary to expectations based on the column tests. However, as it was decided to focus on a correct modelling of the flow through the model as well as the head profile, and as the head profile in the top of the model is more relevant to the failure of the barrier this is done resulting the model presented in this postdiction.

# Memo

**Aan**  
Vera van Beek, Adam Bezuijen

<b>Datum</b> 3 november 2017	<b>Kenmerk</b> 11200952-005-GEO-0003	<b>Aantal pagina's</b> 5
<b>Van</b> Esther Rosenbrand	<b>Doorkiesnummer</b> +31(0)88335 7852	<b>E-mail</b> esther.rosenbrand@deltares.nl

**Onderwerp**  
Postdictieion 198

## 1 Model

### Model dimensions

Model width, mm	101
Model depth, mm	300
Model length, mm	488
Barrier width, mm	50
Barrier depth, mm	30

\*model length is slightly longer than in the non-rotated tests as the inner dimensions of the sample (excluding the filter) are modelled.

### Input parameters

Hydraulic conductivity fine sand upstream, m/s	3.5e-4
Hydraulic conductivity fine sand downstream, m/s	7.9e-4
Hydraulic conductivity fine sand below barrier, m/s	3.3e-4
Hydraulic conductivity barrier, m/s	3.9e-3
Hydraulic conductivity filter cake, m/s	3.9e-3
Critical head corrected for filter and exit head loss, m	0.2662

## 2 Test results

Location barrier in test downstream, mm	124
Location barrier in test upstream, mm	159
Flux in test at critical head, cm/min	635
Critical gradient between H13 and H14 in test, -	0.57

## 3 Model results

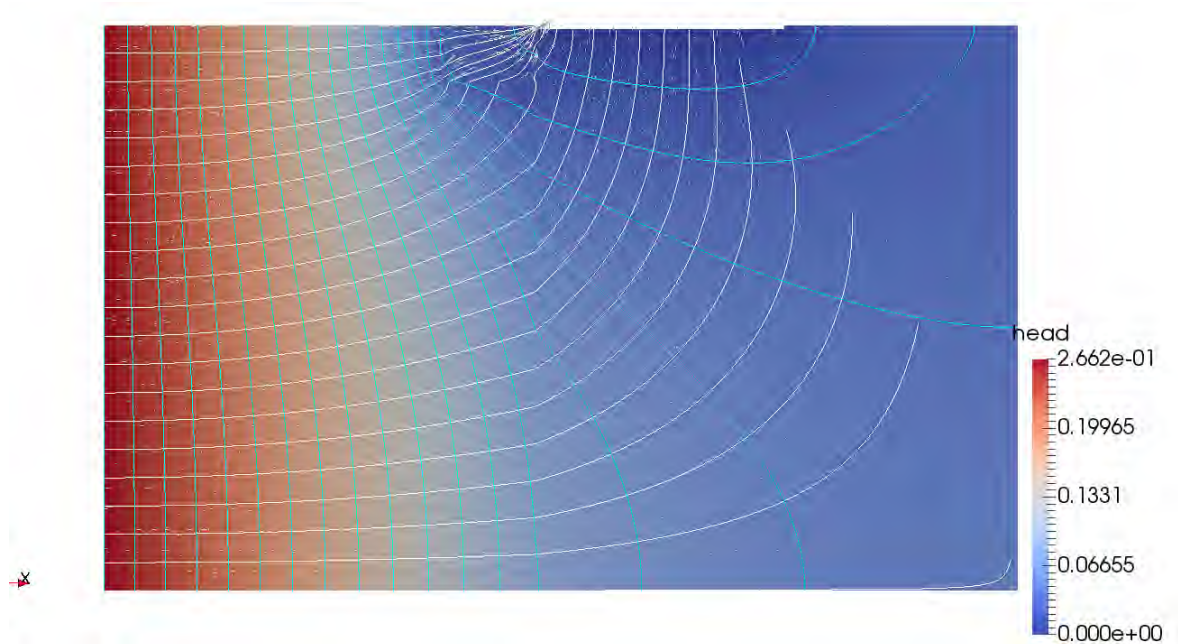


Figure 3.1 Head distribution in the model is indicated by the background colour. Vectors represent flow velocity, scaled by velocity. Light blue lines are streamlines and white lines are head contour lines

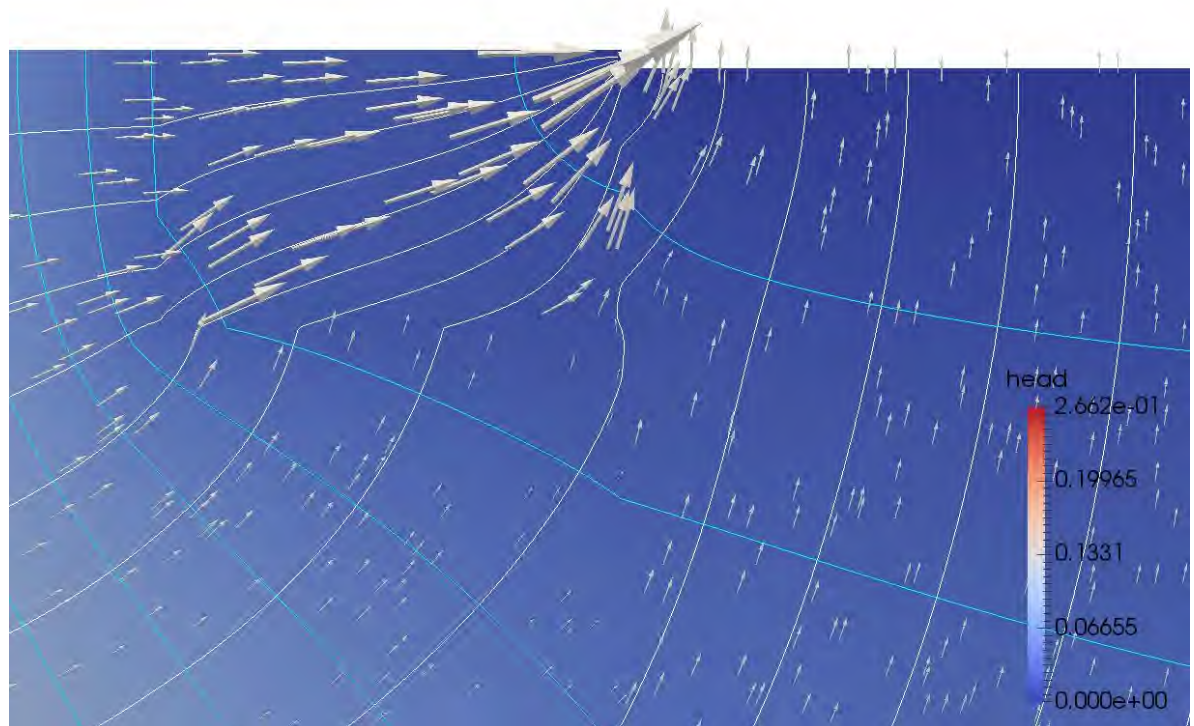


Figure 3.2 Head distribution in the model is indicated by the background colour. Vectors represent flow velocity, scaled by velocity. Light blue lines are streamlines and white lines are head contour lines. Close up, flow velocities in the bottom left hand side of the barrier are high, as well as those at the tip of the pipe

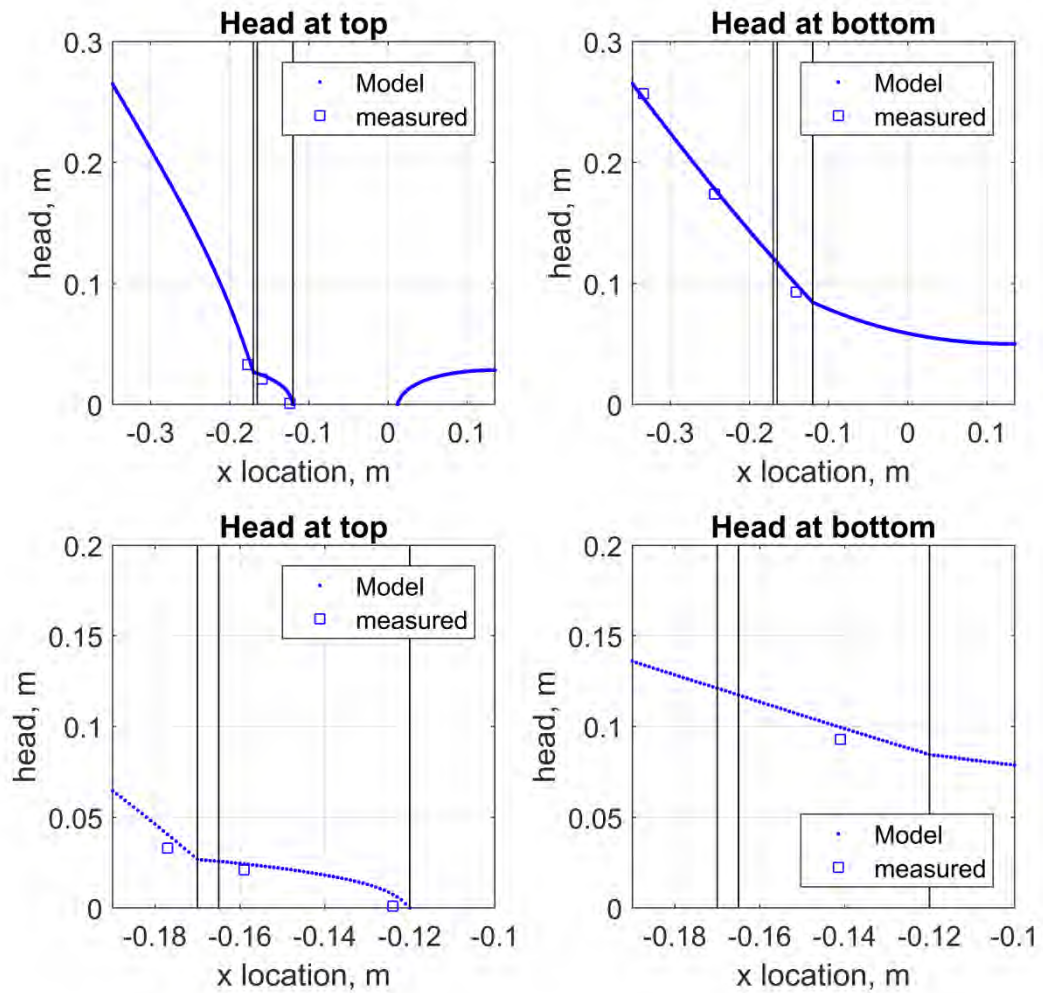


Figure 3.3 Modelled head (blue dots) and measured heads, measured heads are shifted in order to have the same distance from the downstream side of the barrier as was the case in the test

*Table 3.1 Model results for gradient between H13 and H14*

				uncertainty of modelled gradient due to uncertainty location in barrier*		
Flux from model	Gradient H13 to H14 from model	Gradient H13-H14 shifted 2mm closer to barrier	Gradient H13-H14 shifted 2mm further from barrier	Absolute	Relative	Critical gradient -0.130 to -0.165 m
cc/min	-	-	-	-	-	-
620	0.48	0.55	0.43	0.06	13	0.36

\*The location of the barrier is estimated to have an uncertainty of ca. 2 mm (ca.  $2 \cdot D_{50}$ ) along the length of the barrier. Therefore the gradient between H13 and H14 is gradient is calculated for a location shifted 2 mm further upstream from the barrier pipe interface and for a location shifted 2 mm further downstream towards the barrier pipe interface to estimate the uncertainty resulting from this.

*Table 3.2 Model results for damage criteria*

Horizontal gradient between -0.130 and -0.165 m at surface	Vertical Gradient from surface to -0.03 m at -0.130 m from centre of model	Diagonal gradient between (-0.13,0) m and (-0.165,-0.03) m	Average horizontal velocity between -0.130 m and -0.165 m at surface	Average vertical velocity between surface and -0.03 at -0.130 m from centre of model	Average diagonal velocity between (-0.13,0) m and (-0.165,-0.03) m
			cc/min	cc/min	cc/min
0.36	0.18	0.34	8.58	4.34	8.10

*Table 3.3 Comparison test and model*

Ratio flux model/ flux test	Ratio gradient model/ gradient test	Ratio gradient model/ gradient test shifted 2 mm closer	Ratio gradient model/ gradient test shifted 2 mm further
-	-	-	-
0.98	0.84	0.97	0.75

### 3.1 Comments:

In this experiment, it was necessary to increase the hydraulic conductivity of all layers relative to the values in the column tests in order to match the measured flow rate. However, this was also indicated for the fine sand upstream of the barrier by the experimental results. For the

other layers no hydraulic conductivity could be estimated from the measurement data. Indeed the hydraulic conductivity of the fine sand upstream in the postdiction is in between the value indicated by the experimental data and that indicated by the column test. As the hydraulic conductivity based on the measurements in the bottom of the model is generally overestimated due to convergence of flow the value in this postdiction is considered probable.

In previous postdictions, the downstream hydraulic conductivity was not modified relative to the value measured in the column test, as there were no measurements in the bottom of the model to support this, but due to its large influence on the head profile in the current test this value was modified for the postdiction.

To model the results no filter cake with a reduced hydraulic conductivity in the barrier was required.

## **K Analysis of effect pipe depth on postdiction 191**

# Memo

**Aan**  
Vera van Beek, Adam Bezuijen

<b>Datum</b> 3 november 2017	<b>Kenmerk</b> 11200952-005-GEO-0003	<b>Aantal pagina's</b> 5
<b>Van</b> Esther Rosenbrand	<b>Doorkiesnummer</b> +31(0)88335 7852	<b>E-mail</b> esther.rosenbrand@deltares.nl

**Onderwerp**  
Analysis of effect pipe depth on postdiction 191

For this analysis, the hydraulic conductivities that were found for the postdiction of test 191 are used. A pipe depth of 2 mm is used in the postdiction; the results are compared to a model with a pipe depth of 0 mm as is used in the sensitivity analyses.

## 1 Model

### Model dimensions

Model width, mm	300
Model depth, mm	101
Model length, mm	483
Barrier width, mm	50
Barrier depth, mm	101

### Input parameters

Hydraulic conductivity fine sand upstream, m/s	2.5E-04
Hydraulic conductivity fine sand downstream, m/s	5.6E-04
Hydraulic conductivity barrier, m/s	1.9E-03
Hydraulic conductivity filter cake, m/s	2.2E-04
Critical head corrected for filter and exit head loss, m	0.4038

## 2 Test results

Location barrier in test downstream, mm	120
Location barrier in test upstream, mm	167
Flux in test at critical head, cm/min	918
Critical gradient between H13 and H14 in test, -	0.74

## 3 Model results

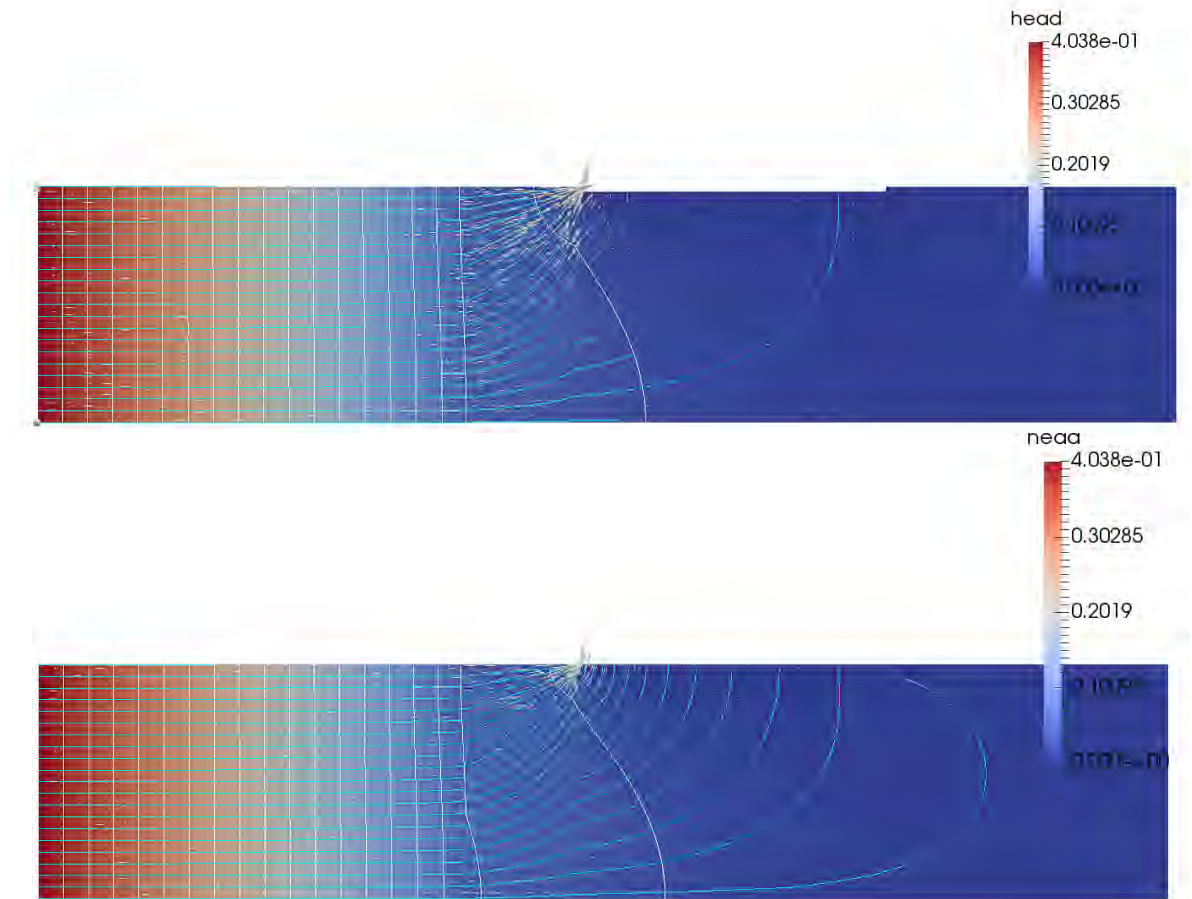


Figure 3.1 Head distribution in the model is indicated by the background colour. Vectors represent flow velocity, scaled by velocity. Light blue lines are streamlines and white lines are head contour lines. Top model with pipe depth 2 mm. Bottom model with pipe depth 0 mm

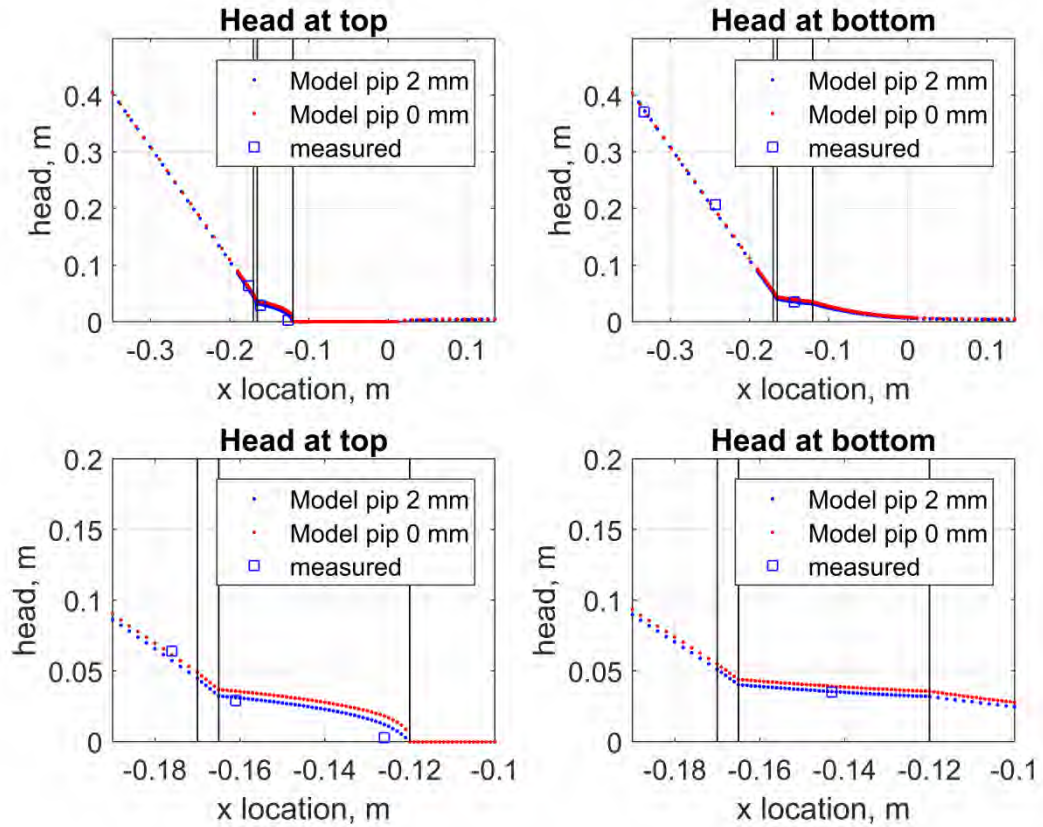


Figure 3.2 Modelled head (blue dots are pipe depth 2 mm, red dots pipe depth 0 mm) and measured heads, measured heads are shifted in order to have the same distance from the downstream side of the barrier as was the case in the test

*Table 3.1 Numerical model results for gradient between H13 and H14*

Model	Flux from model	Gradient H13 to H14 from model	Gradient H13-H14 shifted 2mm closer to barrier	Gradient H13-H14 shifted 2mm further from barrier	uncertainty of modelled gradient due to uncertainty location in barrier*		Critical gradient -0.130 to -0.165 m
					Absolute	Relative,	
	cc/min	-	-	-	-	%-	-
191 pipe depth 2 mm (default postdiction)	907	0.65	0.76	0.57	0.1	15	0.46
191 pipe depth 0 mm	898	0.50	0.56	0.46	0.05	10	0.43
Relative difference between 2 mm pipe depth and 0 mm pipe depth, %	1	5	6	5	12-	--	4

\*The location of the barrier is estimated to have an uncertainty of ca. 2 mm (ca.  $2 \cdot D_{50}$ ) along the length of the barrier.

Therefore the gradient between H13 and H14 is gradient is calculated for a location shifted 2 mm further upstream from the barrier pipe interface and for a location shifted 2 mm further downstream towards the barrier pipe interface to estimate the uncertainty resulting from this.

*Table 3.2 Model results for damage criteria*

Model	Horizontal gradient between -0.130 and -0.165 m at surface	Vertical Gradient from surface to -0.03 m at -0.130 m from centre of model	Diagonal gradient between (-0.13,0) m and (-0.165,-0.03) m	Average horizontal velocity between -0.130 m and -0.165 m at surface	Average vertical velocity between surface and -0.03 at -0.130 m from centre of model	Average diagonal velocity between (-0.13,0) m and (-0.165,-0.03) m
				cc/min	cc/min	cc/min
191 pipe depth 2 mm (default postdiction)	0.46	0.29	0.40	5.26	3.36	4.56
191 pipe depth 0 mm	0.43	0.26	0.37	4.96	2.93	4.27
Relative difference between 2 mm pipe depth and 0 mm pipe depth, %	4%	12%	5%	4%	12%	5%

\*Difference between the results normalised by the result for the basis model with 2 mm pipe depth.

### **3.1 Comments:**

The difference between the flux with a pipe depth of 0 mm and with a pipe depth of 2 mm is negligible. The model with a pipe depth of 2 mm gives a higher gradient in the barrier at the location of H13 and H14 and also at the location for the proposed failure criterion from -0.130 to -0.165 mm. The difference is in the order of 4-6%. The modelled head profile in the barrier fits better with the measured head for 2 mm pipe depth than for 0 mm pipe depth.

## **L Analysis of effect of downstream hydraulic conductivity on postdiction 191**

# Memo

**Aan**  
Vera van Beek

<b>Datum</b> 6 oktober 2017	<b>Kenmerk</b> 11200952-005-GEO-0003	<b>Aantal pagina's</b> 5
<b>Van</b> Esther Rosenbrand	<b>Doorkiesnummer</b> +31(0)88335 7852	<b>E-mail</b> esther.rosenbrand@deltares.nl

**Onderwerp**  
Analysis of effect of downstream hydraulic conductivity on postdiction 191

For this analysis the hydraulic conductivities that were found for the postdiction of test 191 are used. The pipe depth of 2 mm is used in the postdiction, the results are compared to a model with a pipe depth of 0 mm as is used in the sensitivity analyses.

## 1 Model

### Model dimensions

Model width, mm	300
Model depth, mm	101
Model length, mm	483
Barrier width, mm	50
Barrier depth, mm	101

### Input parameters

Hydraulic conductivity fine sand upstream, m/s	2.5E-04
Hydraulic conductivity fine sand downstream, m/s	Basis = 5.6E-04; variant low 0.6 * 5.6 E-04 variant high 1.4*5.6 E-04
Hydraulic conductivity barrier, m/s	1.9E-03
Hydraulic conductivity filter cake, m/s	2.2E-04
Critical head corrected for filter and exit head loss, m	0.4038

## 2 Test results

Location barrier in test downstream, mm	120
Location barrier in test upstream, mm	167
Flux in test at critical head, cm/min	918
Critical gradient between H13 and H14 in test, -	0.74

## 3 Model results

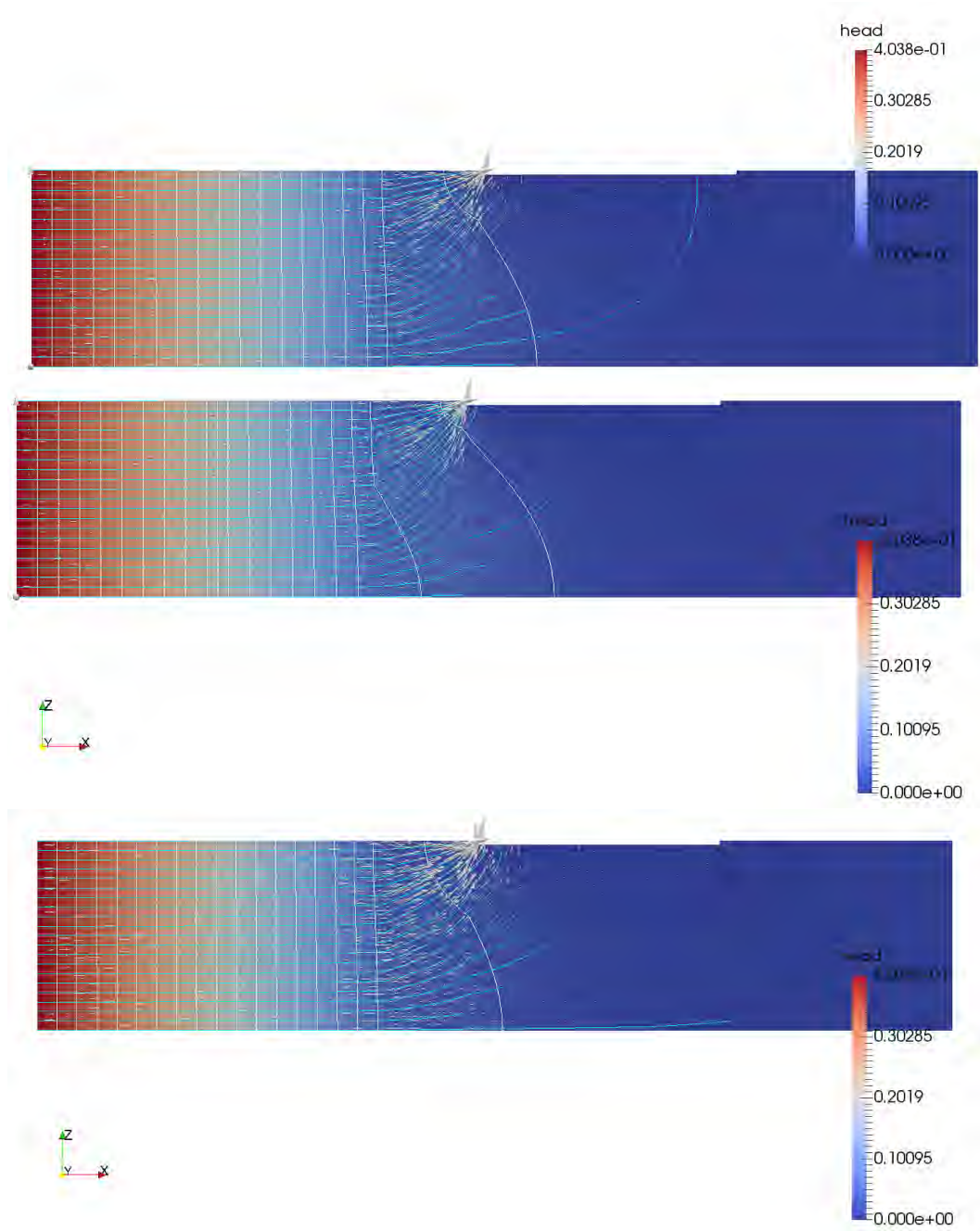


Figure 3.1 Head distribution in the model is indicated by the background colour. Vectors represent flow velocity, scaled by velocity. Light blue lines are streamlines and white lines are head contour lines. The top model has the basis downstream hydraulic conductivity, the middle model is the variant with lower downstream hydraulic conductivity, the bottom model is the variant with higher downstream hydraulic conductivity

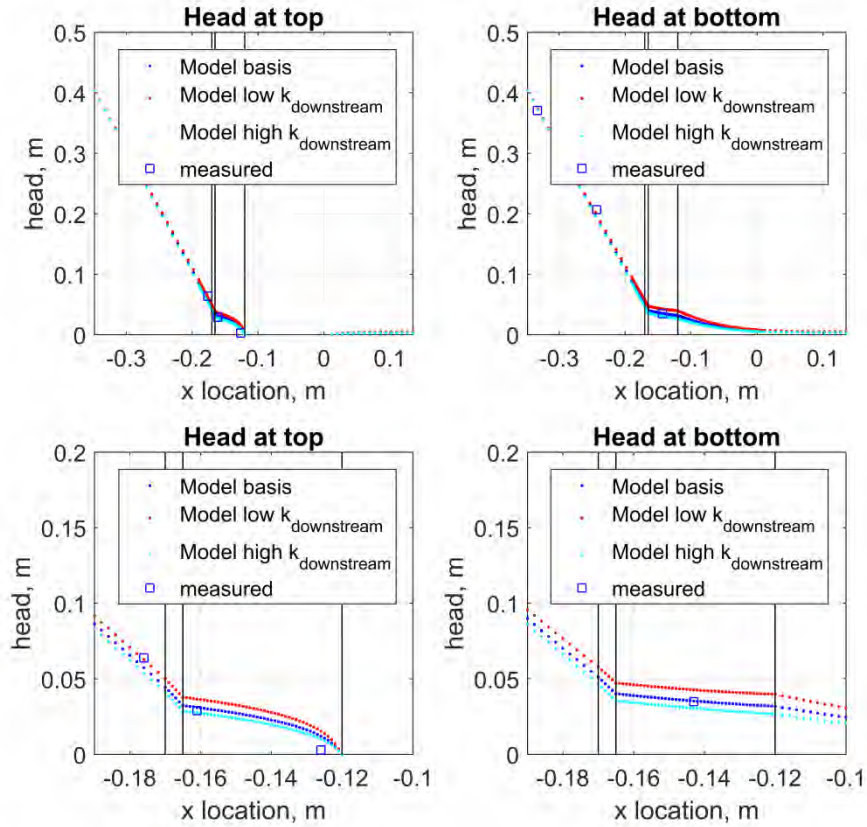


Figure 3.2 Modelled head (dots) and measured heads (squares), (blue dots are basis downstream hydraulic conductivity, red dots show the variant with 0.6 times the downstream hydraulic conductivity, cyan dots show the variant with 1.4 times the downstream hydraulic conductivity). The measured heads are shifted in order to have the same distance from the downstream side of the barrier as was the case in the test

*Table 3.1 Model results for gradient between H13 and H14*

Model	Flux from model	Gradient H13 to H14 from model	Gradient H13-H14 shifted 2mm closer to barrier	Gradient H13-H14 shifted 2mm further from barrier	uncertainty of modelled gradient due to uncertainty location in barrier*		Critical gradient -0.130 to -0.165 m
					Absolute	Relative,	
	cc/min	-	-	-	-	%-	-
191 basis	907	0.65	0.76	0.57	0.1	15	0.46
191 lower downstream hydraulic conductivity	892	0.61	0.69	0.55	0.07	12	0.50
191 higher downstream hydraulic conductivity	919	0.50	0.55	0.46	0.05	9	0.43
Relative difference between low hydraulic conductivity and basis%	2%	14%	16%	13%	29%		11%
Relative difference between high hydraulic conductivity and basis%	1%	6%	7%	5%	17%		4%

\*The location of the barrier is estimated to have an uncertainty of ca. 2 mm (ca.  $2 \cdot D_{50}$ ) along the length of the barrier.

Therefore the gradient between H13 and H14 is gradient is calculated for a location shifted 2 mm further upstream from the barrier pipe interface and for a location shifted 2 mm further downstream towards the barrier pipe interface to estimate the uncertainty resulting from this.

*Table 3.2 Model results for damage criteria*

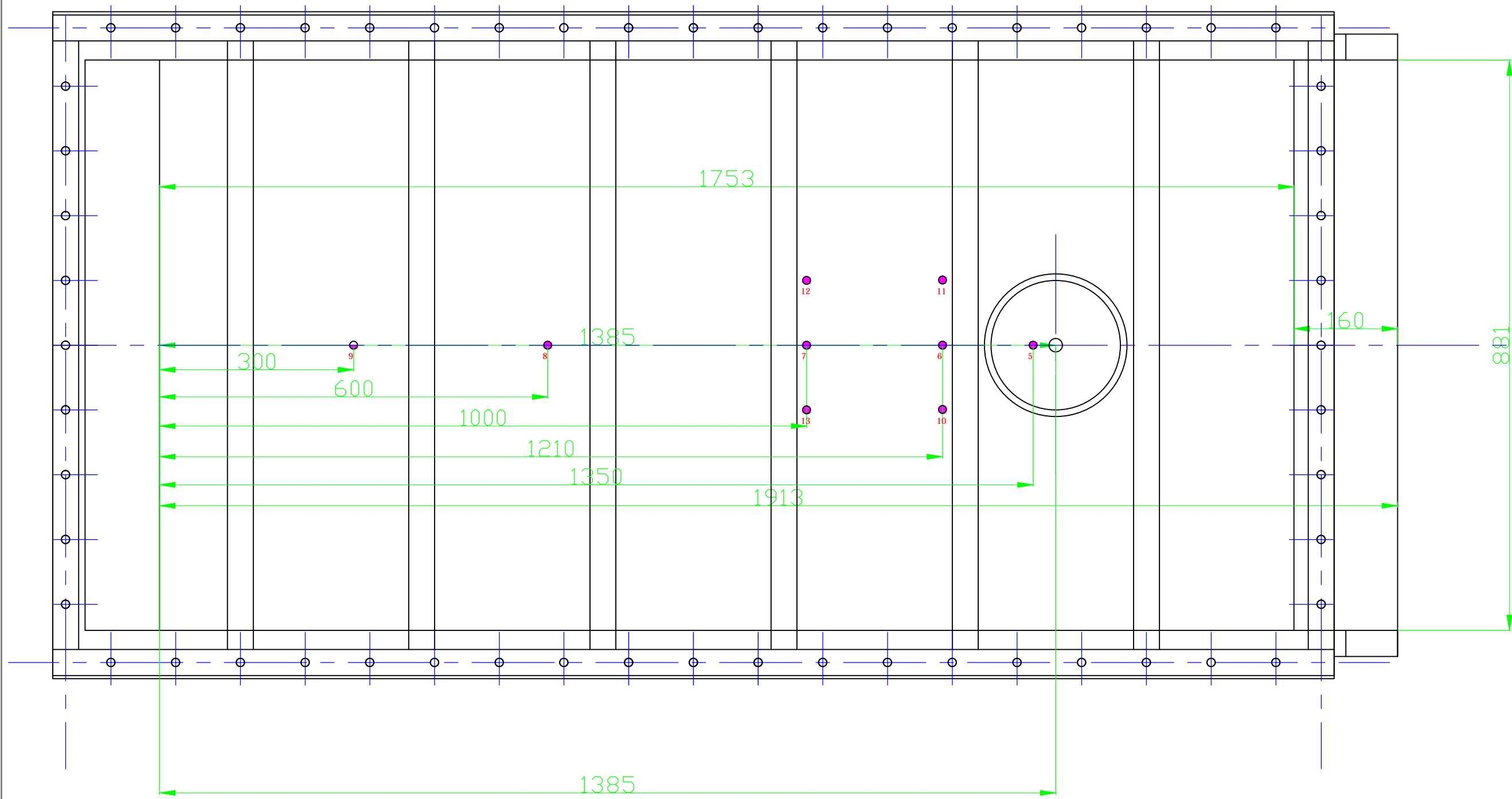
Model	Horizontal gradient between -0.130 and -0.165 m at surface	Vertical Gradient from surface to -0.03 m at -0.130 m from centre of model	Diagonal gradient between (-0.13,0) m and (-0.165,-0.03) m	Average horizontal velocity between -0.130 m and -0.165 m at surface	Average vertical velocity between surface and -0.03 at -0.130 m from centre of model	Average diagonal velocity between (-0.13,0) m and (-0.165,-0.03) m
				cc/min	cc/min	cc/min
191 basis	0.46	0.29	0.40	5.26	3.36	4.56
191 low downstream hydraulic conductivity	0.50	0.36	0.44	5.75	4.18	5.05
191 higher downstream hydraulic conductivity	0.43	0.25	0.37	4.94	2.82	4.24
Relative difference between low hydraulic conductivity and basis%	11%	26%	13%	11%	26%	13%
Relative difference between high hydraulic conductivity and basis%	4%	15%	6%	4%	15%	6%

\*Difference between the results normalised by the result for the basis model with 2 mm pipe depth.

### 3.1 Comments:

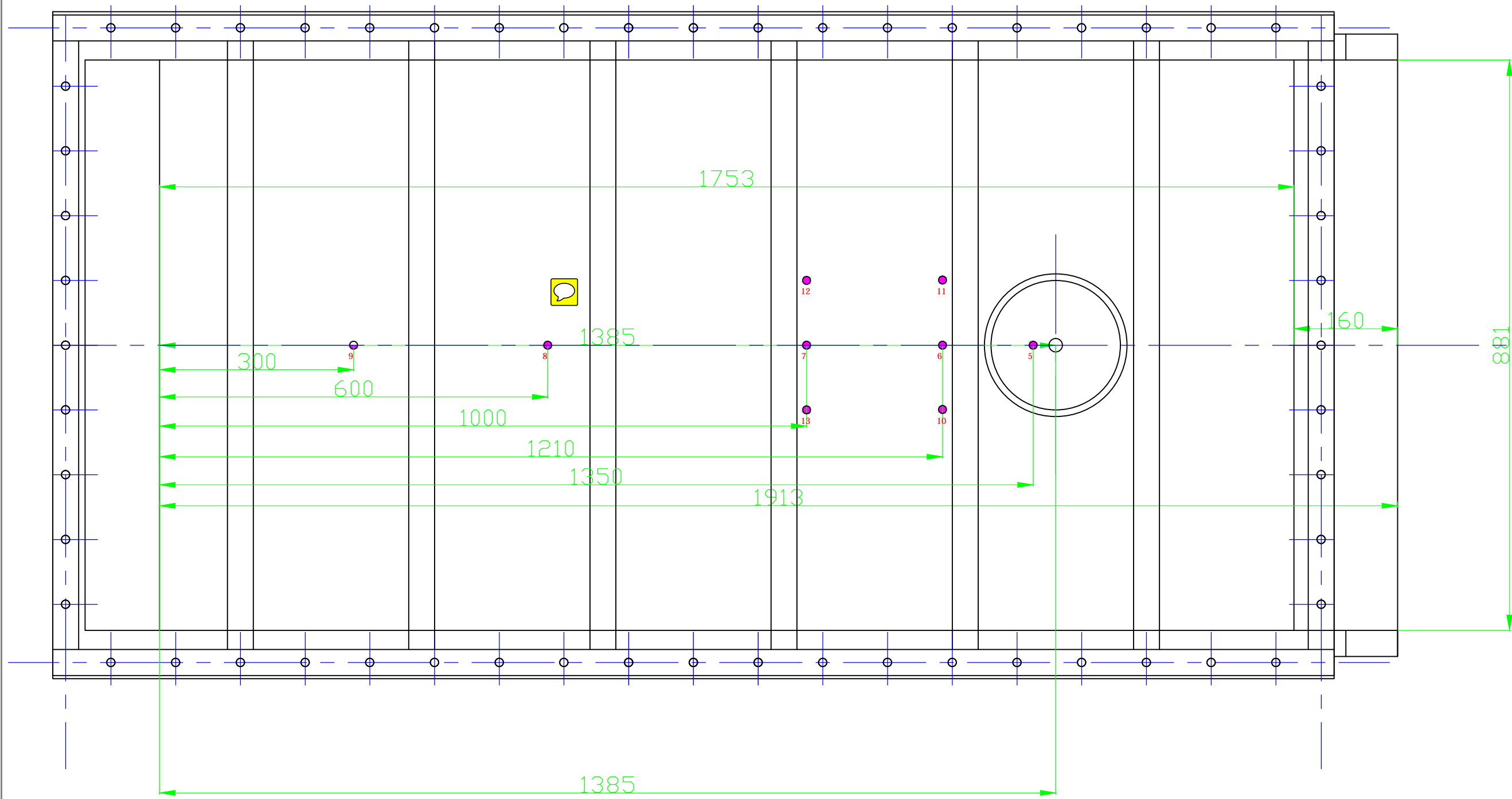
The effect of the downstream hydraulic conductivity on the flow rate is small. This could be expected because the flow rate is mainly determined by the flow resistance upstream of the GZB. The effect on the gradient in the barrier is significant, because more water exits the barrier into the fine sand downstream rather than at the interface between the pipe and the barrier, i.e. there is less convergence of flow at the interface between the pipe and the barrier. For the gradient between H13 and H14, the effect of a lower downstream hydraulic conductivity is in the order of 14-16%, the effect of a higher downstream hydraulic conductivity is smaller. For the gradient between -0.130 and -0.165 mm, the damage criterion, the effect is 11% for the lower downstream hydraulic conductivity and 4% for the higher downstream hydraulic conductivity. The vertical and diagonal failure criteria are more sensitive to differences in the downstream hydraulic conductivity than the horizontal failure criterion. The head profile in the bottom of the model is best modelled using the downstream hydraulic conductivity in the basis model. The hydraulic conductivity in H14 is better modelled using the higher downstream hydraulic conductivity, but this models the head in H15 worst. Additional measurements in the bottom downstream in the model could help to better constrain the postdictions.

## **M Technical drawing of medium-scale set-up**



Filenaam: .dwg      Afdeling:      Gewijzigd:

<b>Deltares</b> PO Box 177, 2600 MH Delft, The Netherlands Stieltjesweg 2, 2628 CK Delft, The Netherlands T +31 (0)15 269 35 00    www.deltares.nl F +31 (0)15 261 08 21    info@deltares.nl	datum	get.
		djk
Medium piping 2013 opnemer positie's Maten Thijs		gez.
		/



Filenaam: **.dwg**    Afdeling:    Gewijzigd:

<b>Deltares</b> PO Box 177, 2600 MH Delft, The Netherlands Stieltjesweg 2, 2628 CK Delft, The Netherlands	T +31 (0)15 269 35 00 F +31 (0)15 261 08 21	www.deltares.nl info@deltares.nl	datum	get. djk
				gez.
Medium piping 2013 opnemer positie's Maten Thijs				

## **N Schematisation of Delta Flume tests**



## **O Small-scale tests with the Sellmeijer model**

# Memo

**To**  
Ulrich Förster

**Date**  
November 7 2017

**Reference**  
11200952-05-GEO-000

**Number of pages**  
25

**From**  
John van Esch

**Direct line**  
+31 (0)6 4655 2906

**E-mail**  
john.vanesch@deltares.nl

**Subject**  
coarse sand barrier

**Copy to**  
Vera van Beek, Esther Rosenbrand

This memo presents the results of DgFlow (Van Esch *et al.* (2013)) computations that simulate small scale laboratory experiments. These experiment were set up in order to investigate the impact of a coarse sand barrier on the development of piping channels. For all simulations the material properties of water are kept constant; the fluid viscosity ( $\mu$ ) is set to  $1.3 \cdot 10^{-3} \text{ Nsm}^{-2}$ , its density ( $\rho$ ) is  $1.0 \cdot 10^3 \text{ kgm}^{-3}$  and its compressibility ( $\alpha$ ) is  $5 \cdot 10^{-10} \text{ m}^2\text{N}^{-1}$ . The compressibility of the soil skeleton is neglected by setting the compressibility parameter of the soil skeleton ( $\beta$ ) to  $0.0 \text{ m}^2\text{N}^{-1}$ . The porosity ( $n$ ) of both the coarse sand barrier and the fine material surrounding the barrier is 0.35. Initial computations set the grain density ( $\rho^s$ ) to  $2.65 \cdot 10^3 \text{ kgm}^{-3}$ , White's constant ( $\nu$ ) equals 0.25 and the bedding ( $\theta$ ) reads 37.0 deg. Additional computations set White's constant ( $\nu$ ) to 0.30 and set the coarse material bedding angle ( $\theta^c$ ) to 18.0 deg. Here the bedding angle ( $\theta^f$ ) is 30.0 deg for test 195 and 197 and for the remaining tests  $\theta^f$  equals 25.0 deg.

Figure 1 presents the layout of the small scale experiments where the position of the barrier is indicated by  $a$ ,  $b$  and  $d$ . Table 1 gives the value of these parameters per experiment and adds the intrinsic permeability ( $\kappa^{fu}$ ) of the fine material upstream, the permeability ( $\kappa^{fd}$ ) of the fine material downstream and the permeability of the coarse material ( $\kappa^c$ ) next to the characteristic grain diameter of the fine material ( $D_{70}^f$ ) and the grain size of the coarse material ( $D_{70}^c$ ) that was used for the construction of the barrier.

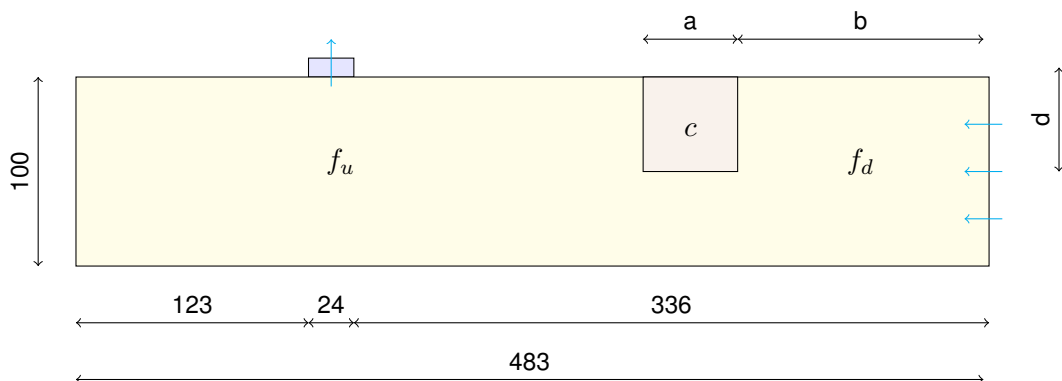


Figure 1: Laboratory setup.

Section 1 presents the results for experiment 191 and Figure 2 shows the finite element mesh that

*Table 1: Material data.*

exp	$a$ (mm)	$b$ (mm)	$d$ (mm)	$\kappa^{fu}$ (m <sup>2</sup> )	$\kappa^{fd}$ (m <sup>2</sup> )	$D_{70}^f$ (mm)	$\kappa^c$ (m <sup>2</sup> )	$D_{70}^c$ (mm)
191	50	178	100	$3.25 \cdot 10^{-11}$	$7.42 \cdot 10^{-11}$	0.52	$2.65 \cdot 10^{-10}$	1.29
192	50	178	100	$3.25 \cdot 10^{-11}$	$7.42 \cdot 10^{-11}$	0.52	$2.65 \cdot 10^{-10}$	1.29
193	50	178	30	$3.25 \cdot 10^{-11}$	$1.04 \cdot 10^{-10}$	0.52	$3.58 \cdot 10^{-10}$	1.29
194	50	178	100	$7.42 \cdot 10^{-11}$	$7.42 \cdot 10^{-11}$	0.52	$7.42 \cdot 10^{-11}$	1.29
195	228	0	100	$2.65 \cdot 10^{-10}$	$9.28 \cdot 10^{-12}$	0.164	$2.65 \cdot 10^{-10}$	1.29
196	50	178	100	$3.25 \cdot 10^{-11}$	$7.42 \cdot 10^{-11}$	0.52	$8.88 \cdot 10^{-10}$	1.85
197	228	0	100	$8.88 \cdot 10^{-10}$	$9.28 \cdot 10^{-12}$	0.164	$8.88 \cdot 10^{-10}$	1.85

was locally refined once (R1) for this experiment. The computational results that were obtained by using this mesh and by imposing the default values for White's constant and the bedding angle ( $\nu = 0.25$ ,  $\theta^f = 37.0$  deg,  $\theta^c = 37.0$  deg) are gathered in Figure 3. The upper left graph shows the development of the pipe by plotting the head drop as a function of pipe length and the upper right graph presents the head as a function of distance. The head in this graph corresponds to the head drop in the previous graph because the head at the inlet boundary at the right side of the model is zero. The pipe develops at the right side of the exit point at a position of 0.15 meters and propagates to the inlet boundary at 0.48 meters. The head along the horizontal line at the top of the model was obtained by a quasi-static analysis and the results are plotted for a number of time steps (20, 40, 60, 80 and 90) that correspond to a head drop of 0.19, 0.39, 0.59, 0.79 and 0.89 meters. The graphs at the bottom present the development of the piping channel height and the fluid velocity in the channel. The product of both gives the flow rate that accumulates in the direction of the outflow point. In the barrier the height of the channel is less than the channel height in the surrounding material at the downstream side. The decrease in height is balanced by an increase of velocity. Table 3 gathers the results for a uniform mesh that is composed out of 2058 nodes (R0), and three locally refined meshes (R1, R2 and R3). The results show that the computation of the critical head  $H_{dg}$  did not converge for a mesh that contains elements of less than a millimeter at the tip of the pipe. Figure 4 shows a detail of the hydraulic head distribution within the barrier along the horizontal boundary where the channel will develop. The graph at the left shows the distribution that was obtained by a flow calculation without the development of the pipe and the graph at the right presents the head if erosion is included within the calculation. Figure 5 illustrates the dependency of the position at which the boundary condition is applied in case of a flow computation. The graph at the left shows the head distribution along the horizontal upper boundary of the barrier for the case in which a pipe did develop towards the barrier with a constant depth of 5 millimeters. The graph at the right shows the distribution for a pipe with constant depth of 1 centimeter for the same periods in time. Additional computational results that set White's constant ( $\nu$ ) to 0.30, the bedding angle in the fine material ( $\theta^f$ ) to 25.0 deg and the bedding angle in the barrier ( $\theta^c$ ) to 18.0 deg are presented by Figure 6 and Table 4. Section 2 until Section 7 present the remaining experiments in the same way.

Table 2 gathers the outcome of DgFlow computations for all experiments. Here  $h_1$  denotes the head drop that was needed to let the pipe propagate up till the barrier and  $a_1$  is the height of the pipe at the tip of the channel for that moment. The critical head drop is given by  $h_2$  and  $a_2$  denotes the height of the channel at the downstream side of the barrier just before failure. The difference between  $a_2$

and  $a_1$  indicates the increase in height at the downstream side of the barrier during the propagation process of the pipe in the barrier.

*Table 2: Computational results.*

experiment	$h_1$ (m)	$a_1$ (mm)	$h_2$ (m)	$a_2$ (mm)
191	0.13	0.41	0.50	1.16
192	0.13	0.41	0.50	1.16
193	0.13	0.52	0.37	1.31
194	0.20	0.16	0.24	0.44
195	0.10	0.26	0.14	1.09
196	0.13	0.52	1.78	2.26
197	0.09	0.48	0.14	2.41

## 1 experiment 191

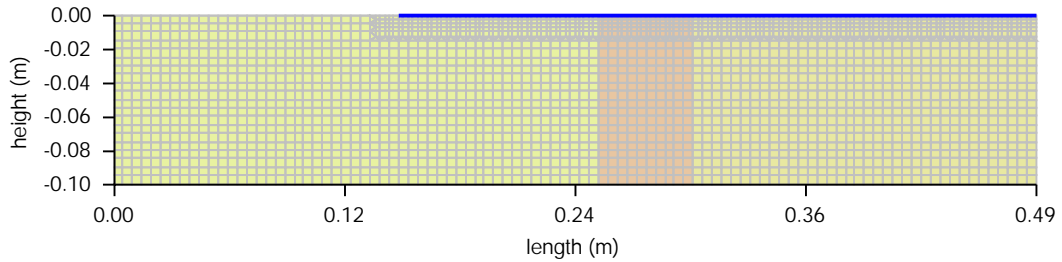


Figure 2: Finite element mesh experiment 191.

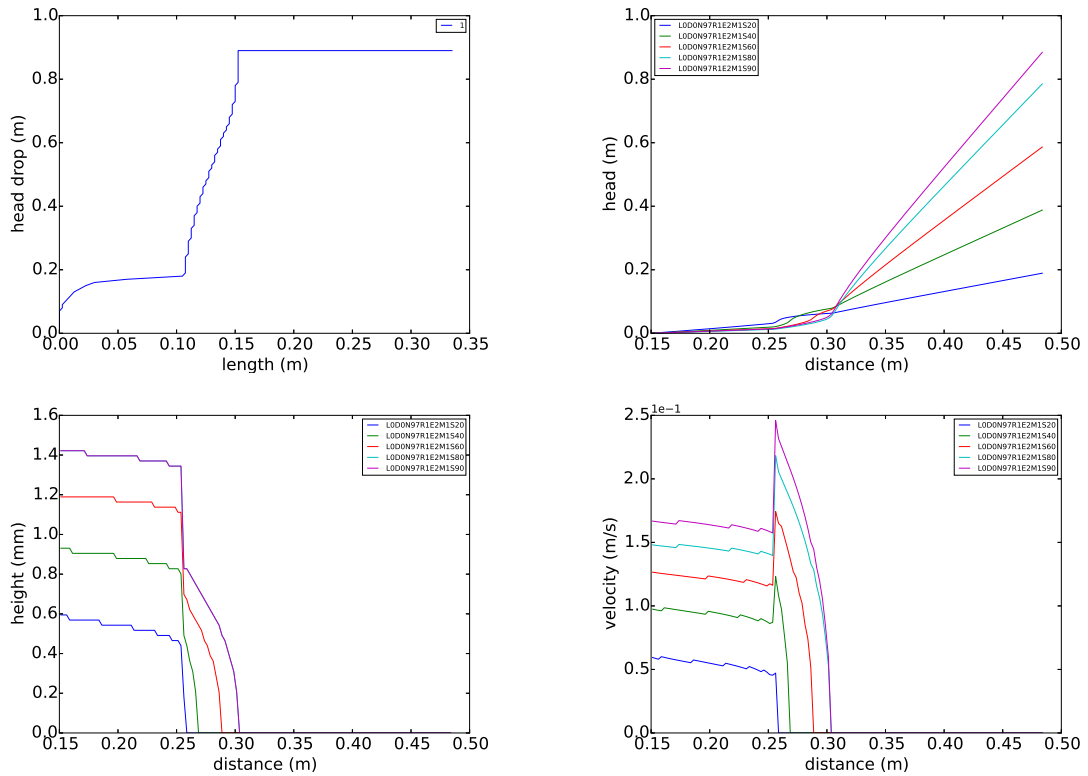


Figure 3: Computational results experiment 191.

Table 3: Computational results experiment 191,  $\nu = 0.25$ ,  $\theta = 37.0$  deg.

$\Delta x$ (mm)	$\Delta y$ (mm)	$\delta x$ (mm)	$\delta y$ (mm)	nodes (-)	steps (-)	$H_{dg}$ (m)	$L_{dg}$ (m)	time (s)
5.00	5.00	5.00	5.00	2058	84	0.83	0.15	132
5.00	5.00	2.50	2.50	2688	90	0.89	0.15	283
5.00	5.00	1.25	1.25	3921	96	0.95	0.15	795
5.00	5.00	0.63	0.63	6360	101	1.00	0.15	622

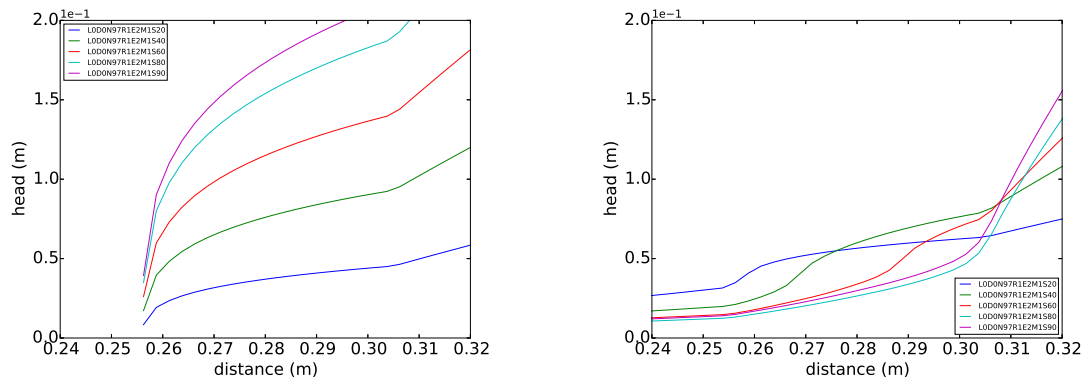


Figure 4: Computational results experiment 191, flow (left) erosion (right).

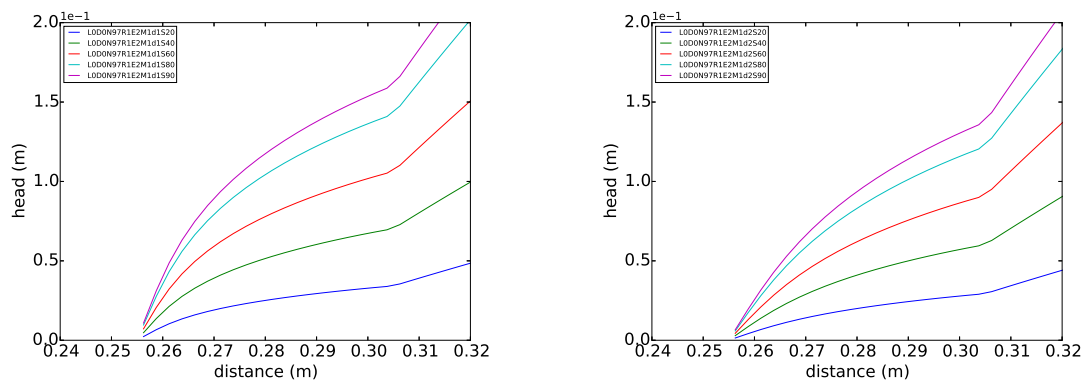


Figure 5: Computational results experiment 191, flow  $d=5\text{mm}$  (left) flow  $d=1\text{cm}$  (right).

Table 4: Computational results experiment 191a,  $\nu = 0.30$ ,  $\theta^f = 25.0$  deg,  $\theta^c = 18.0$  deg.

$\Delta x$ (mm)	$\Delta y$ (mm)	$\delta x$ (mm)	$\delta y$ (mm)	nodes (-)	steps (-)	$H_{dg}$ (m)	$L_{dg}$ (m)	time (s)
5.00	5.00	5.00	5.00	2058	44	0.43	0.15	98
5.00	5.00	2.50	2.50	2688	47	0.46	0.15	247
5.00	5.00	1.25	1.25	3921	51	0.50	0.15	707
5.00	5.00	0.63	0.63	6360	54	0.53	0.15	2350

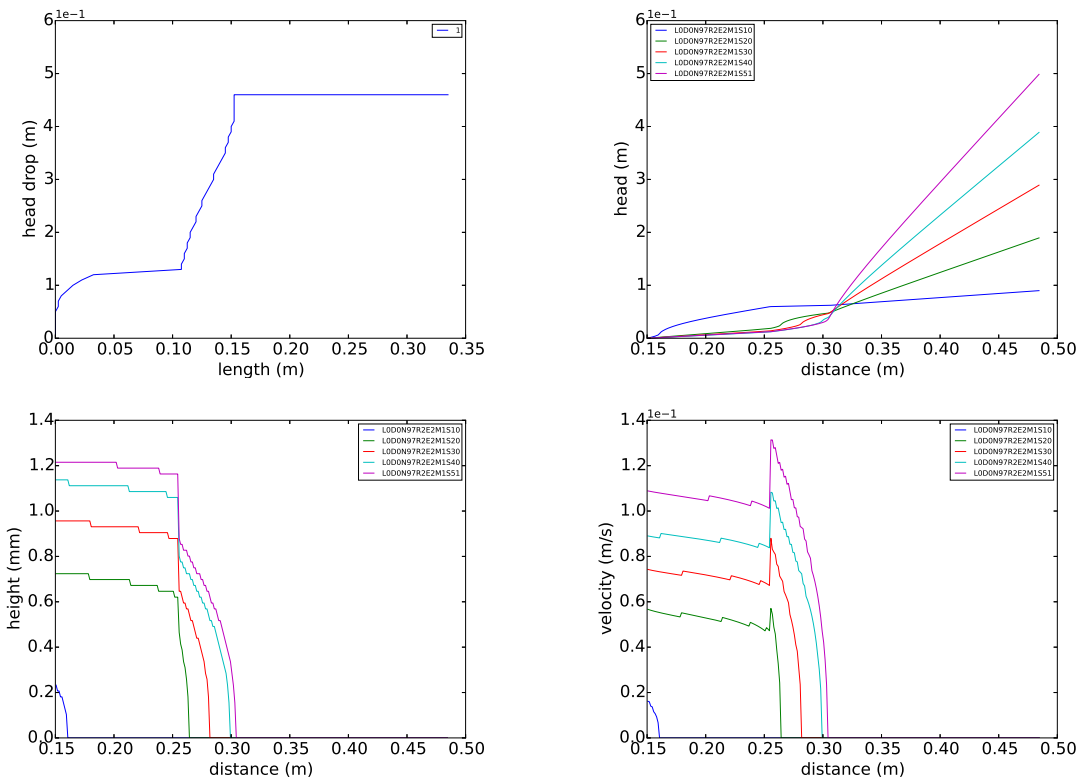


Figure 6: Computational results experiment 191a.

## 2 experiment 192

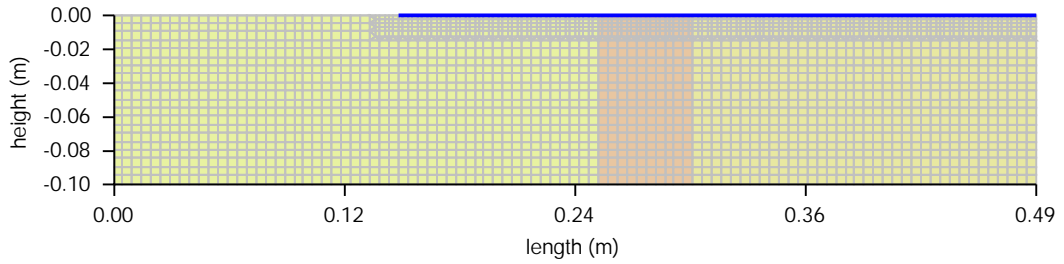


Figure 7: Experiment 192.

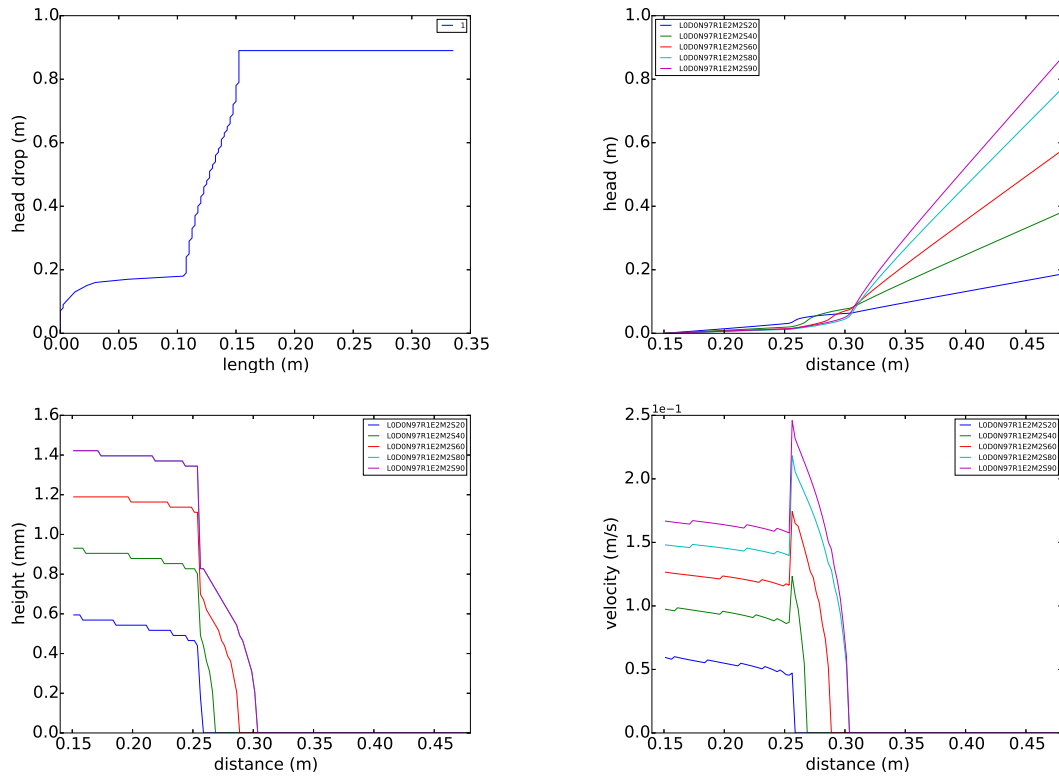


Figure 8: Computational results experiment 192.

Table 5: Computational results experiment 192,  $\nu = 0.25$ ,  $\theta = 37.0$  deg.

$\Delta x$ (mm)	$\Delta y$ (mm)	$\delta x$ (mm)	$\delta y$ (mm)	nodes (-)	steps (-)	$H_{dg}$ (m)	$L_{dg}$ (m)	time (s)
5.00	5.00	5.00	5.00	2058	84	0.83	0.15	130
5.00	5.00	2.50	2.50	2688	90	0.89	0.15	286
5.00	5.00	1.25	1.25	3921	96	0.95	0.15	797
5.00	5.00	0.63	0.63	6360	101	1.00	0.15	623

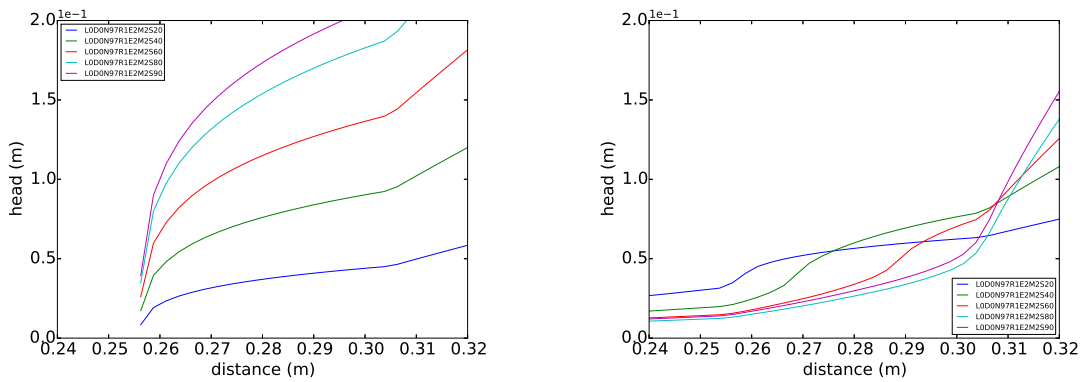


Figure 9: Computational results experiment 192, flow (left) erosion (right).

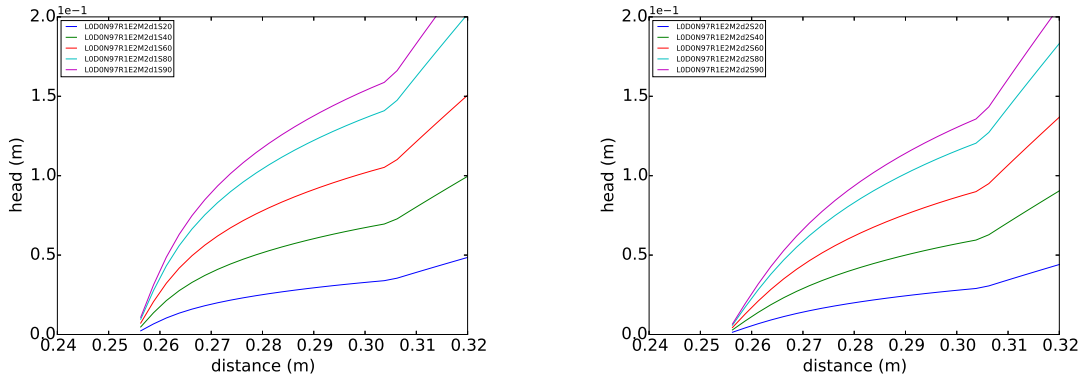


Figure 10: Computational results experiment 192, flow d=5mm (left) flow d=1cm (right).

Table 6: Computational results experiment 192a,  $\nu = 0.30$ ,  $\theta^f = 25.0$  deg,  $\theta^c = 18.0$  deg.

$\Delta x$ (mm)	$\Delta y$ (mm)	$\delta x$ (mm)	$\delta y$ (mm)	nodes (-)	steps (-)	$H_{dg}$ (m)	$L_{dg}$ (m)	time (s)
5.00	5.00	5.00	5.00	2058	44	0.43	0.15	101
5.00	5.00	2.50	2.50	2688	47	0.46	0.15	246
5.00	5.00	1.25	1.25	3921	51	0.50	0.15	704
5.00	5.00	0.63	0.63	6360	54	0.53	0.15	2340

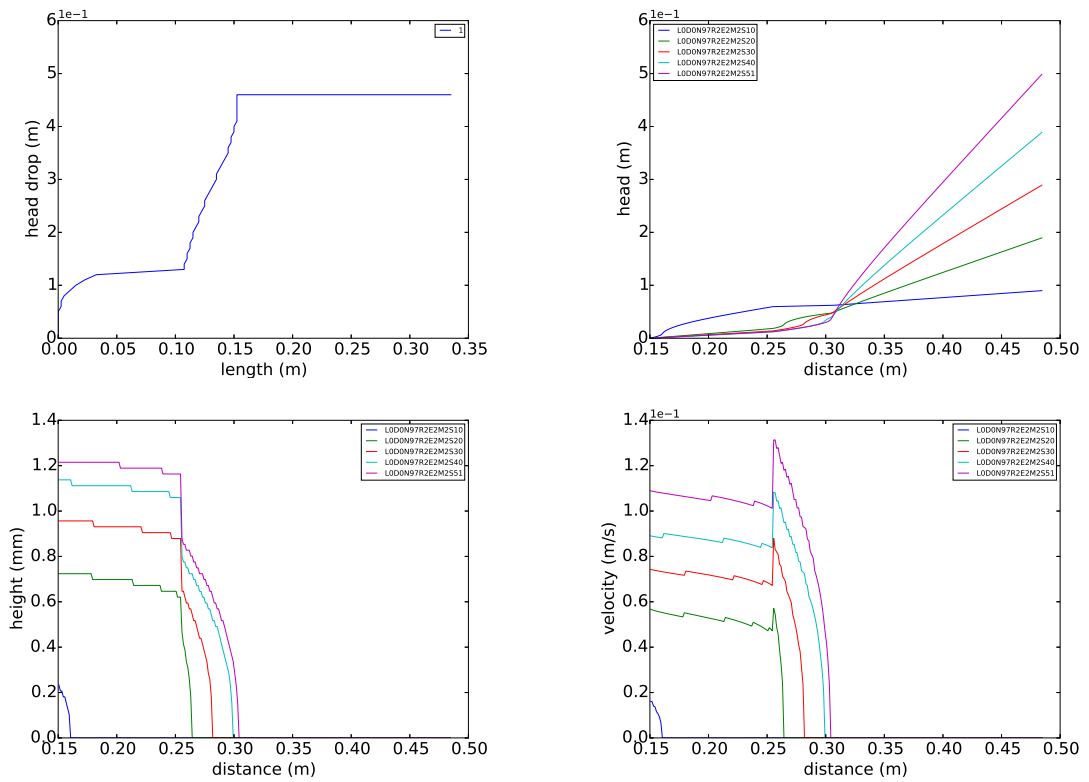


Figure 11: Computational results experiment 192a.

## 3 experiment 193

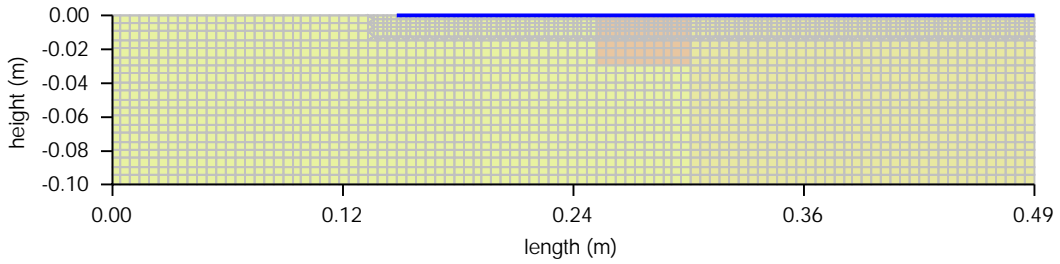


Figure 12: Experiment 193.

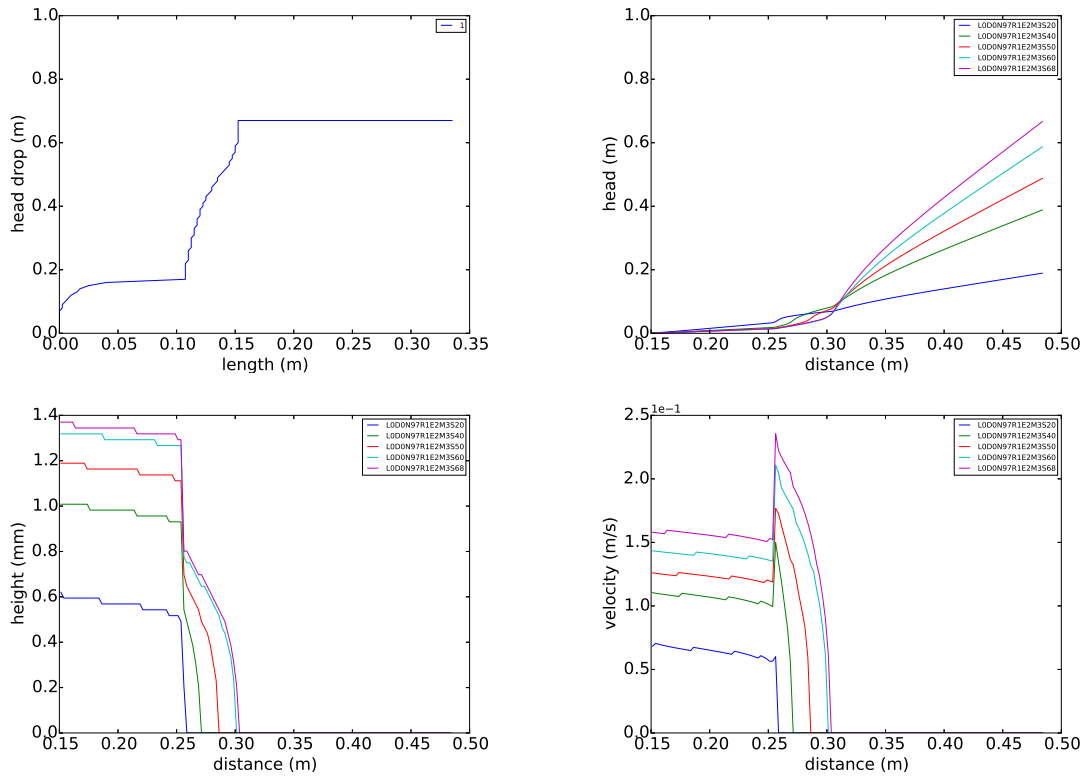


Figure 13: Computational results experiment 193.

Table 7: Computational results experiment 193,  $\nu = 0.25$ ,  $\theta = 37.0$  deg.

$\Delta x$ (mm)	$\Delta y$ (mm)	$\delta x$ (mm)	$\delta y$ (mm)	nodes (-)	steps (-)	$H_{dg}$ (m)	$L_{dg}$ (m)	time (s)
5.00	5.00	5.00	5.00	2058	63	0.62	0.15	124
5.00	5.00	2.50	2.50	2688	68	0.67	0.15	290
5.00	5.00	1.25	1.25	3921	72	0.71	0.15	806
5.00	5.00	0.63	0.63	6360	75	0.74	0.15	2297

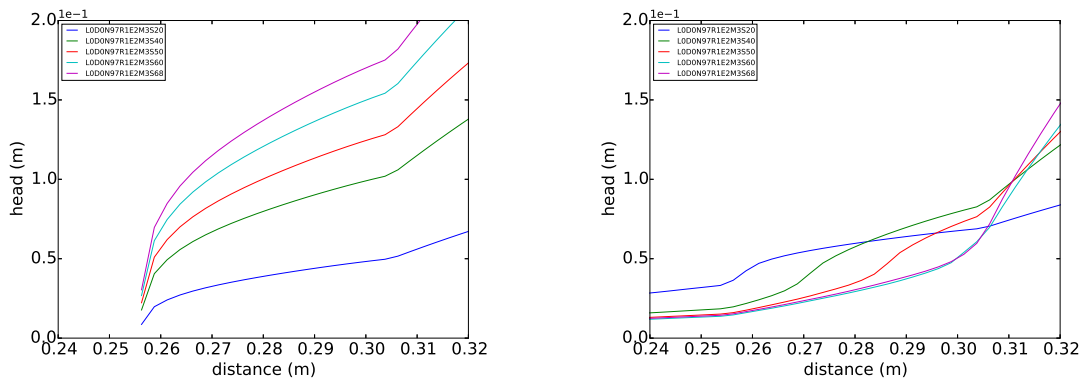


Figure 14: Computational results experiment 193, flow (left) erosion (right).

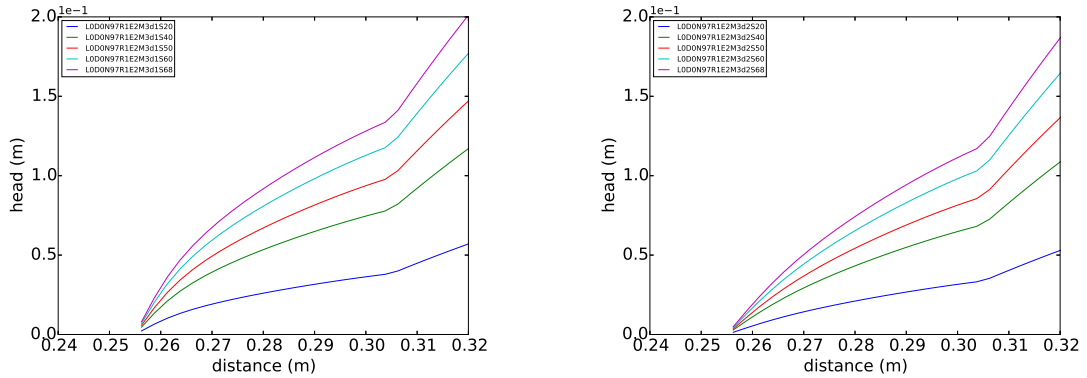


Figure 15: Computational results experiment 193, flow  $d=5$ mm (left) flow  $d=1$ cm (right).

Table 8: Computational results experiment 193a,  $\nu = 0.30$ ,  $\theta^f = 25.0$  deg,  $\theta^c = 18.0$  deg.

$\Delta x$ (mm)	$\Delta y$ (mm)	$\delta x$ (mm)	$\delta y$ (mm)	nodes (-)	steps (-)	$H_{dg}$ (m)	$L_{dg}$ (m)	time (s)
5.00	5.00	5.00	5.00	2058	34	0.33	0.15	104
5.00	5.00	2.50	2.50	2688	36	0.35	0.15	251
5.00	5.00	1.25	1.25	3921	38	0.37	0.15	722
5.00	5.00	0.63	0.63	6360	40	0.39	0.15	2365

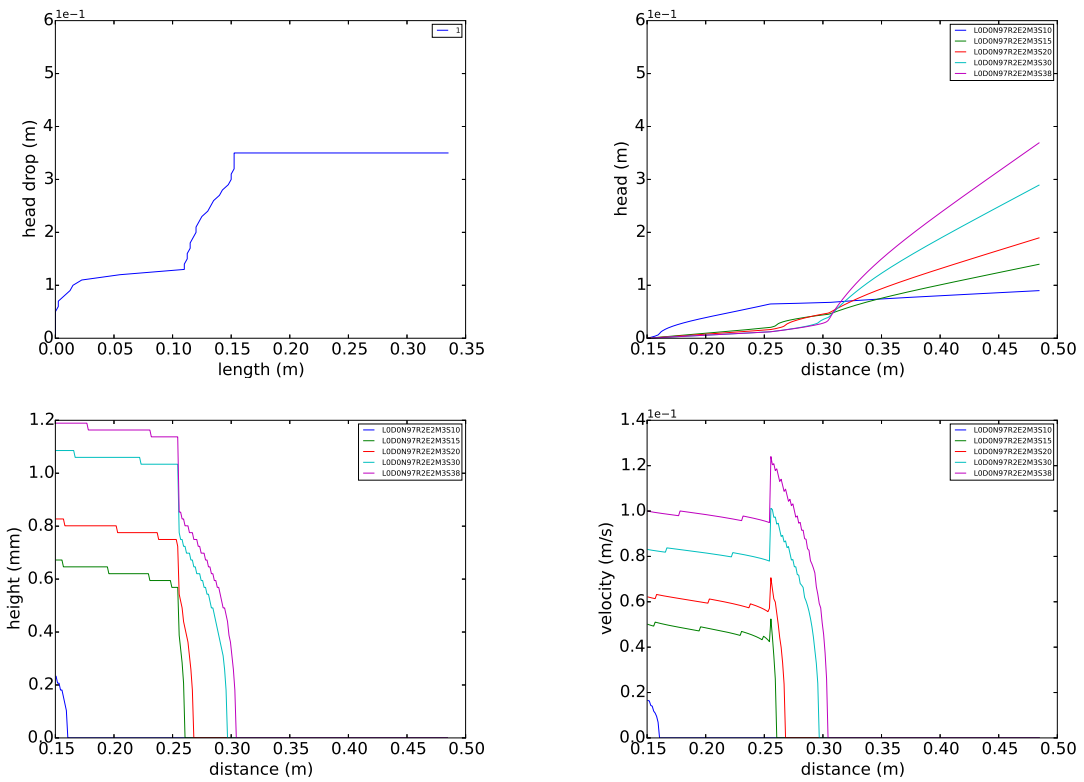


Figure 16: Computational results experiment 193a.

## 4 experiment 194

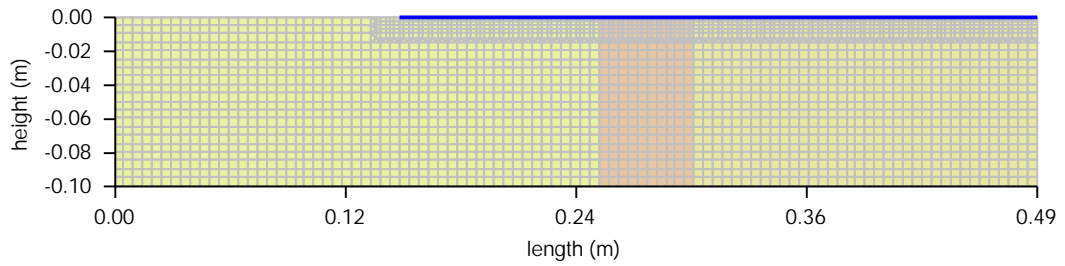


Figure 17: Experiment 194.

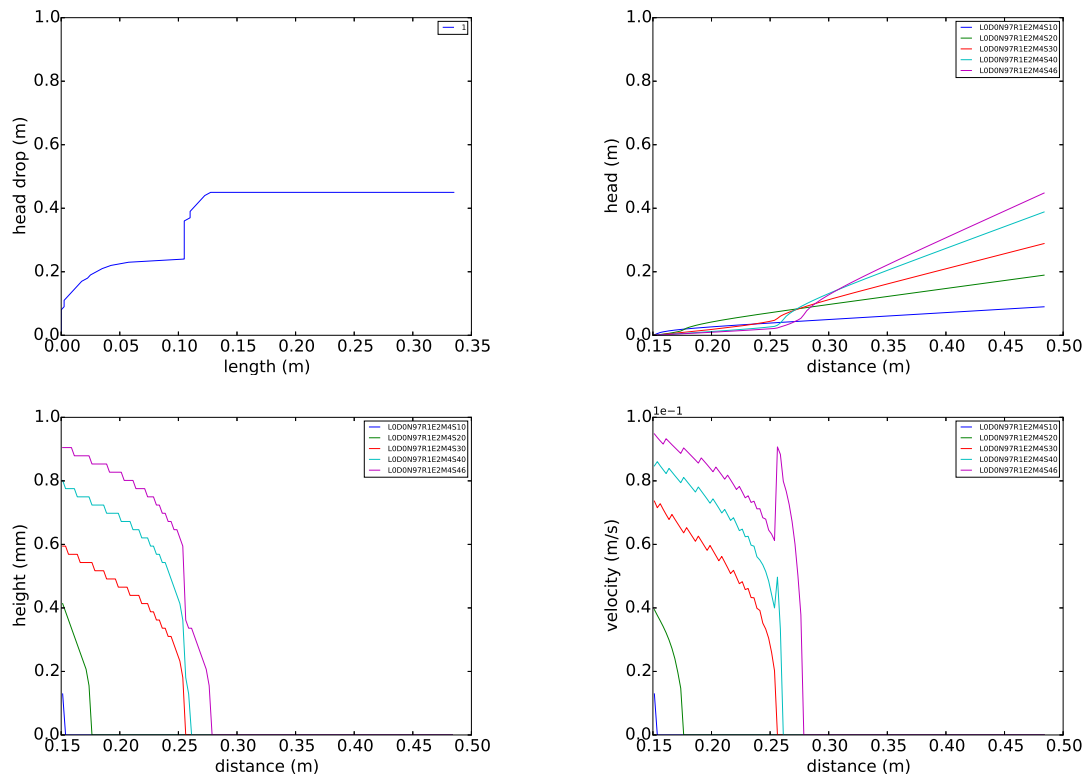


Figure 18: Computational results experiment 194.

Table 9: Computational results experiment 194,  $\nu = 0.25$ ,  $\theta = 37.0$  deg.

$\Delta x$ (mm)	$\Delta y$ (mm)	$\delta x$ (mm)	$\delta y$ (mm)	nodes (-)	steps (-)	$H_{dg}$ (m)	$L_{dg}$ (m)	time (s)
5.00	5.00	5.00	5.00	2058	46	0.45	0.14	95
5.00	5.00	2.50	2.50	2688	46	0.45	0.13	219
5.00	5.00	1.25	1.25	3921	46	0.45	0.13	621
5.00	5.00	0.63	0.63	6360	46	0.45	0.13	1872

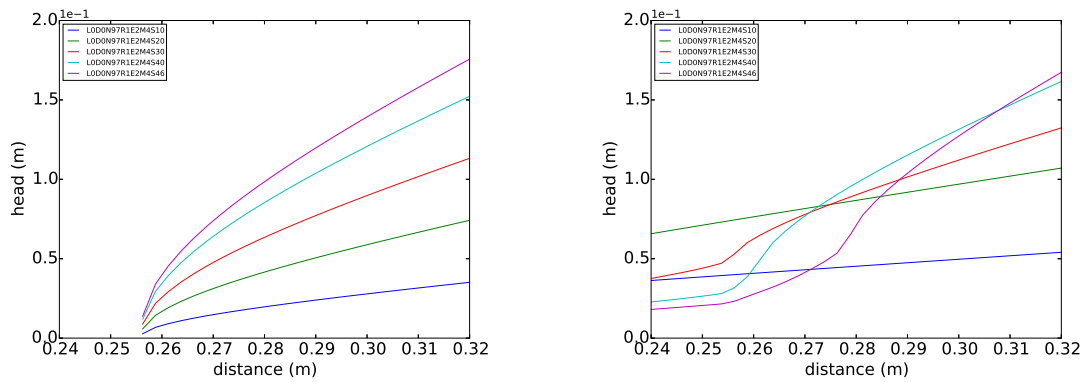


Figure 19: Computational results experiment 194, flow (left) erosion (right).

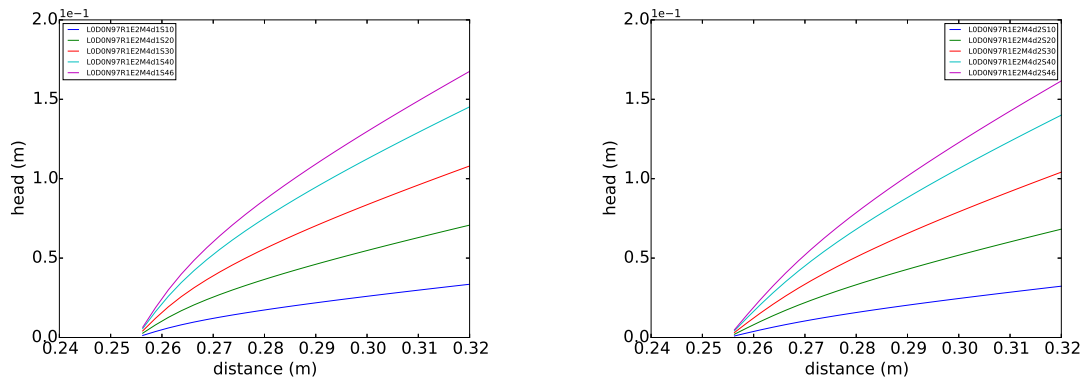


Figure 20: Computational results experiment 194, flow  $d=5\text{mm}$  (left) flow  $d=1\text{cm}$  (right).

Table 10: Computational results experiment 194a,  $\nu = 0.30$ ,  $\theta^f = 25.0$  deg,  $\theta^c = 18.0$  deg.

$\Delta x$ (mm)	$\Delta y$ (mm)	$\delta x$ (mm)	$\delta y$ (mm)	nodes (-)	steps (-)	$H_{dg}$ (m)	$L_{dg}$ (m)	time (s)
5.00	5.00	5.00	5.00	2058	25	0.24	0.13	85
5.00	5.00	2.50	2.50	2688	25	0.24	0.12	197
5.00	5.00	1.25	1.25	3921	25	0.24	0.12	558
5.00	5.00	0.63	0.63	6360	25	0.24	0.12	1977

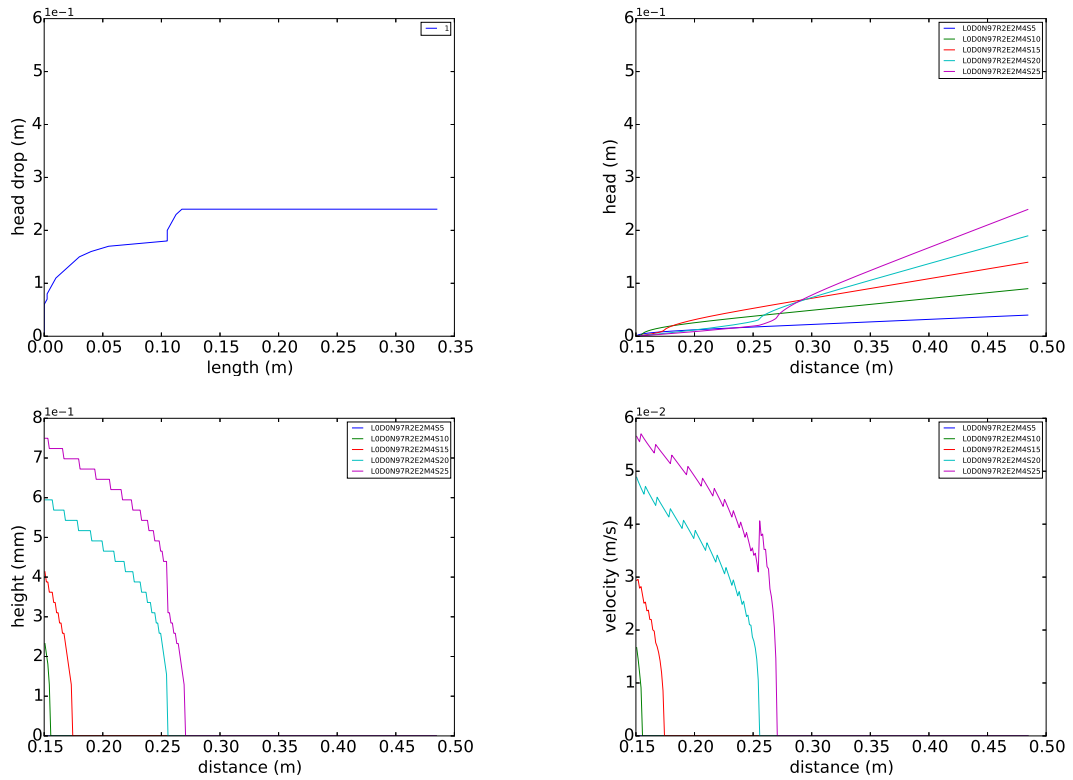


Figure 21: Computational results experiment 194a.

## 5 experiment 195

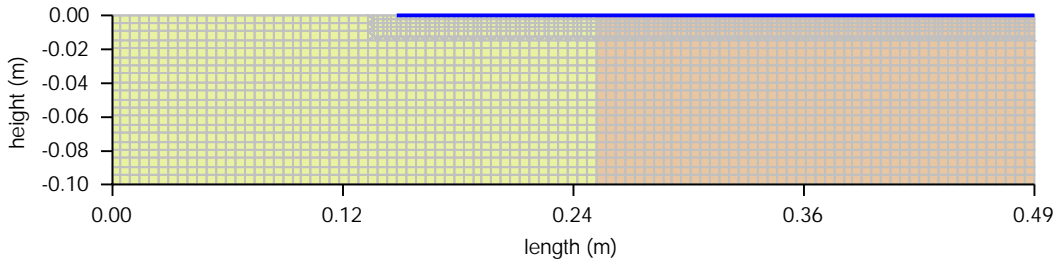


Figure 22: Experiment 195.

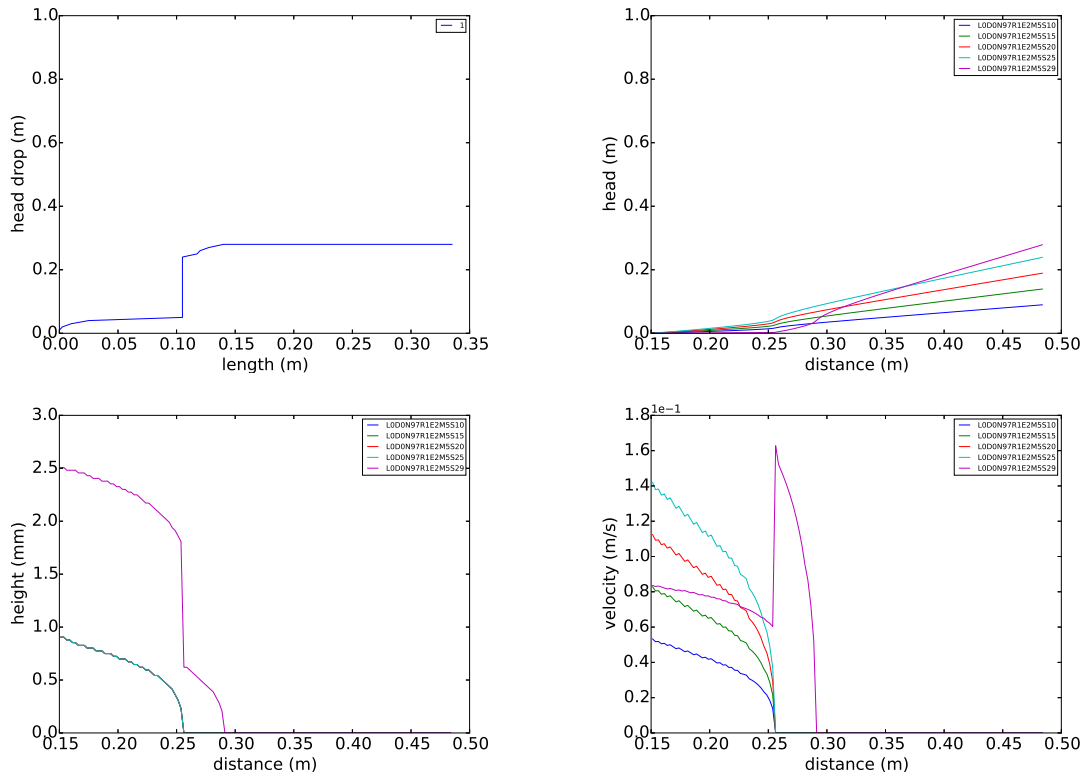


Figure 23: Computational results experiment 195.

Table 11: Computational results experiment 195,  $\nu = 0.25$ ,  $\theta = 37.0$  deg.

$\Delta x$ (mm)	$\Delta y$ (mm)	$\delta x$ (mm)	$\delta y$ (mm)	nodes (-)	steps (-)	$H_{dg}$ (m)	$L_{dg}$ (m)	time (s)
5.00	5.00	5.00	5.00	2058	29	0.28	0.15	97
5.00	5.00	2.50	2.50	2688	29	0.28	0.14	224
5.00	5.00	1.25	1.25	3921	29	0.28	0.14	663
5.00	5.00	0.63	0.63	6360	29	0.28	0.13	1921

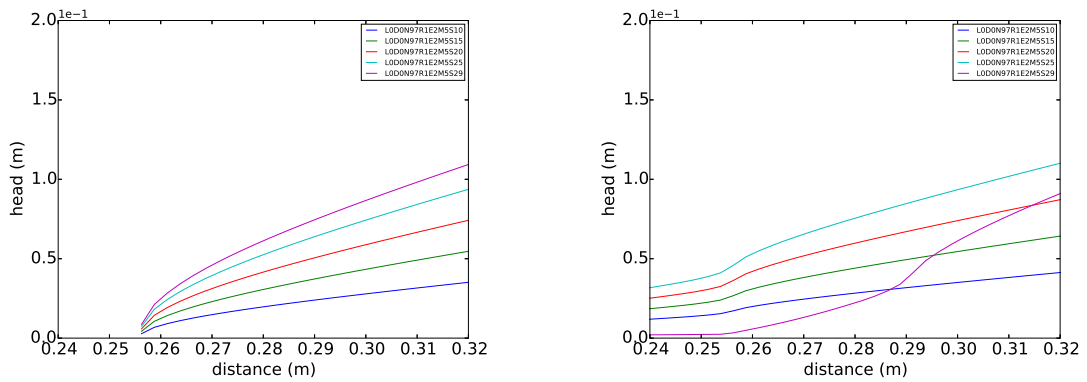


Figure 24: Computational results experiment 195, flow (left) erosion (right).

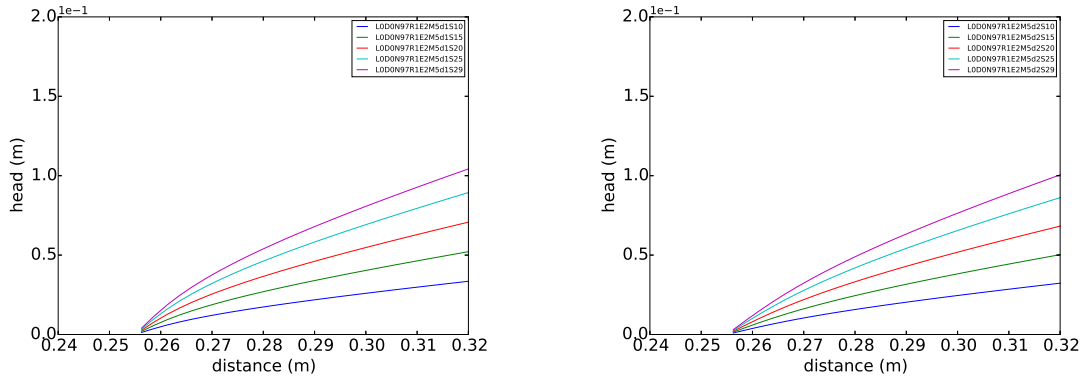


Figure 25: Computational results experiment 195, flow  $d=5\text{mm}$  (left) flow  $d=1\text{cm}$  (right).

Table 12: Computational results experiment 195a,  $\nu = 0.30$ ,  $\theta^f = 30.0$  deg,  $\theta^c = 18.0$  deg.

$\Delta x$ (mm)	$\Delta y$ (mm)	$\delta x$ (mm)	$\delta y$ (mm)	nodes (-)	steps (-)	$H_{dg}$ (m)	$L_{dg}$ (m)	time (s)
5.00	5.00	5.00	5.00	2058	15	0.14	0.13	91
5.00	5.00	2.50	2.50	2688	15	0.14	0.13	216
5.00	5.00	1.25	1.25	3921	15	0.14	0.12	618
5.00	5.00	0.63	0.63	6360	16	0.15	0.14	2191

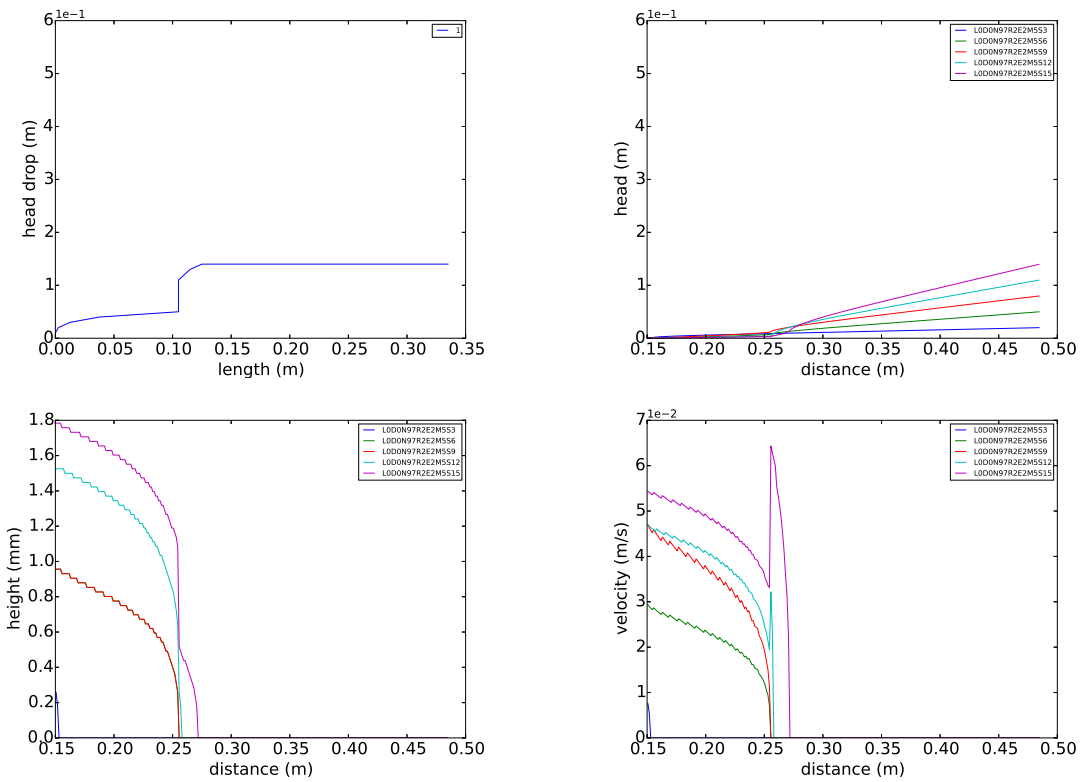


Figure 26: Computational results experiment 195a.

## 6 experiment 196

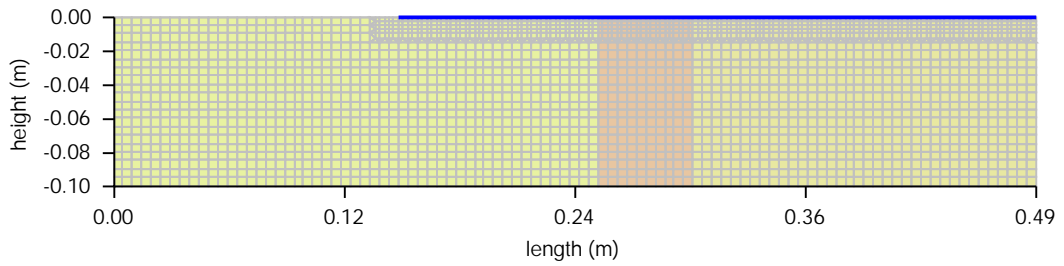


Figure 27: Experiment 196.

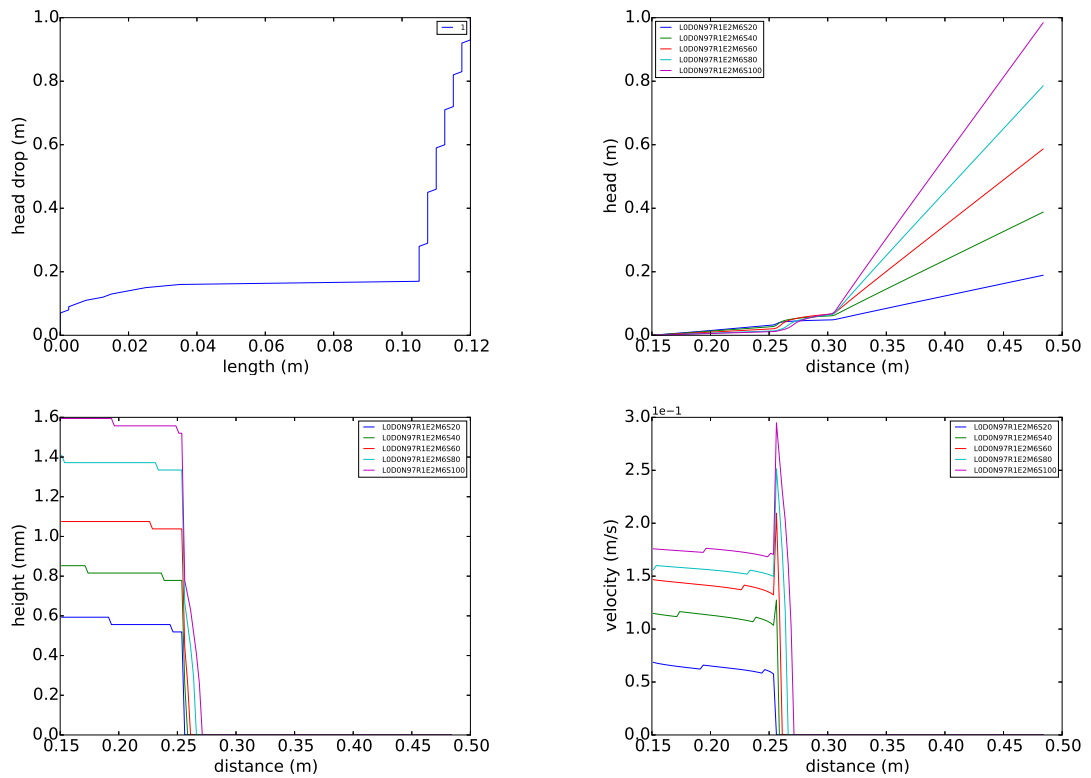


Figure 28: Computational results experiment 196.

Table 13: Computational results experiment 196,  $\nu = 0.25$ ,  $\theta = 37.0$  deg.

$\Delta x$ (mm)	$\Delta y$ (mm)	$\delta x$ (mm)	$\delta y$ (mm)	nodes (-)	steps (-)	$H_{dg}$ (m)	$L_{dg}$ (m)	time (s)
5.00	5.00	5.00	5.00	2688	101	1.00	0.12	77
5.00	5.00	2.50	2.50	2688	101	1.00	0.12	77
5.00	5.00	1.25	1.25	3921	101	1.00	0.12	168
5.00	5.00	0.63	0.63	6360	101	1.00	0.12	503

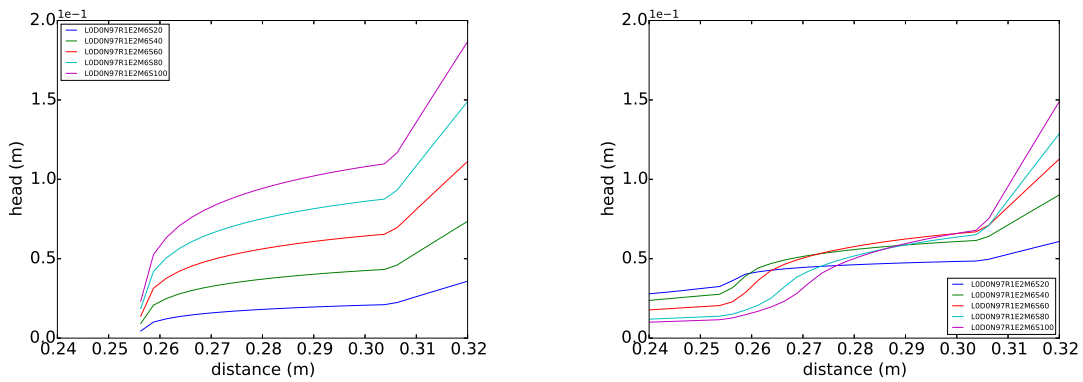


Figure 29: Computational results experiment 196, flow (left) erosion (right).

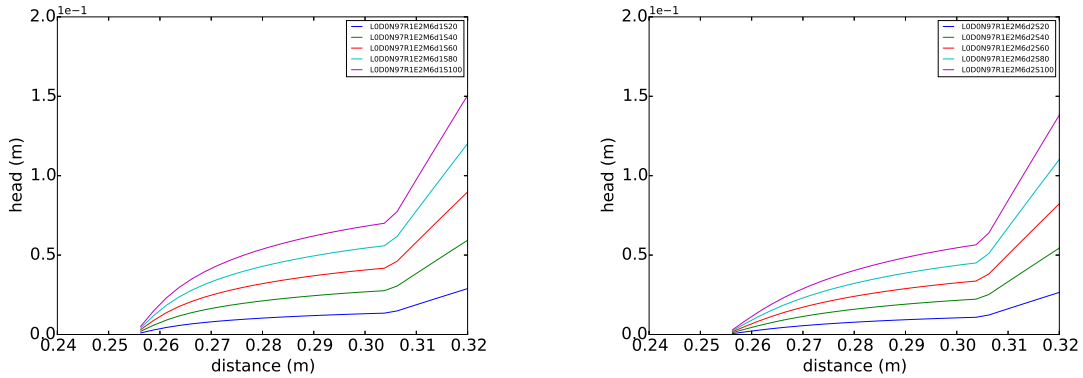


Figure 30: Computational results experiment 196, flow  $d=5\text{mm}$  (left) flow  $d=1\text{cm}$  (right).

Table 14: Computational results experiment 196a,  $\nu = 0.30$ ,  $\theta^f = 25.0$  deg,  $\theta^c = 18.0$  deg.

$\Delta x$ (mm)	$\Delta y$ (mm)	$\delta x$ (mm)	$\delta y$ (mm)	nodes (-)	steps (-)	$H_{dg}$ (m)	$L_{dg}$ (m)	time (s)
5.00	5.00	5.00	5.00	2058	141	1.40	0.15	161
5.00	5.00	2.50	2.50	2688	159	1.58	0.15	343
5.00	5.00	1.25	1.25	3921	179	1.78	0.15	943
5.00	5.00	0.63	0.63	6360	201	2.00	0.15	822

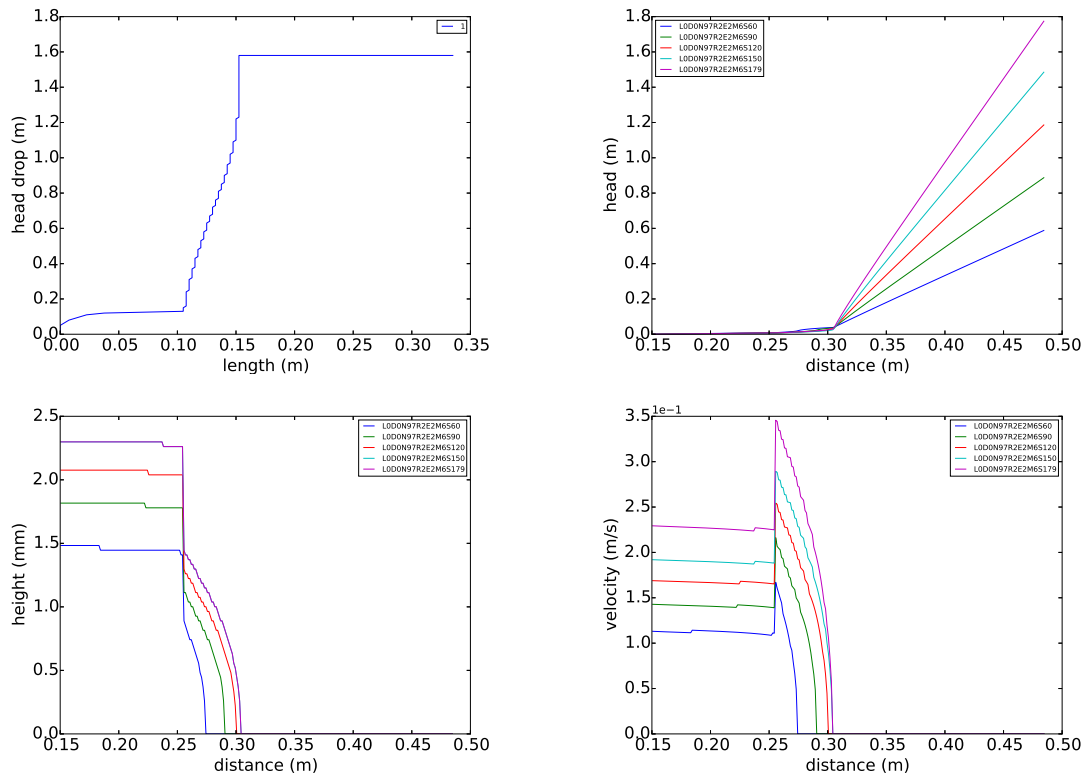


Figure 31: Computational results experiment 196a.

## 7 experiment 197

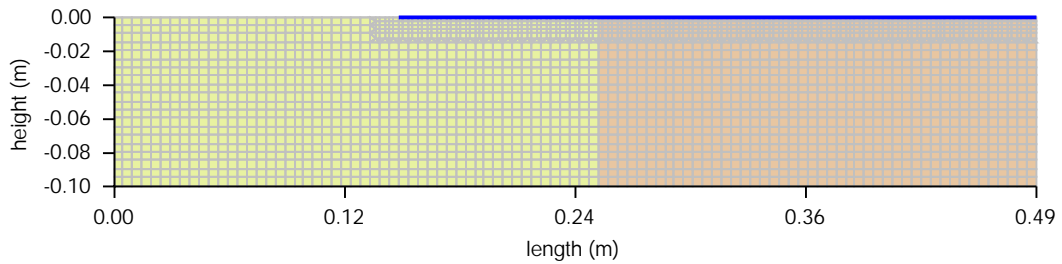


Figure 32: Experiment 197.

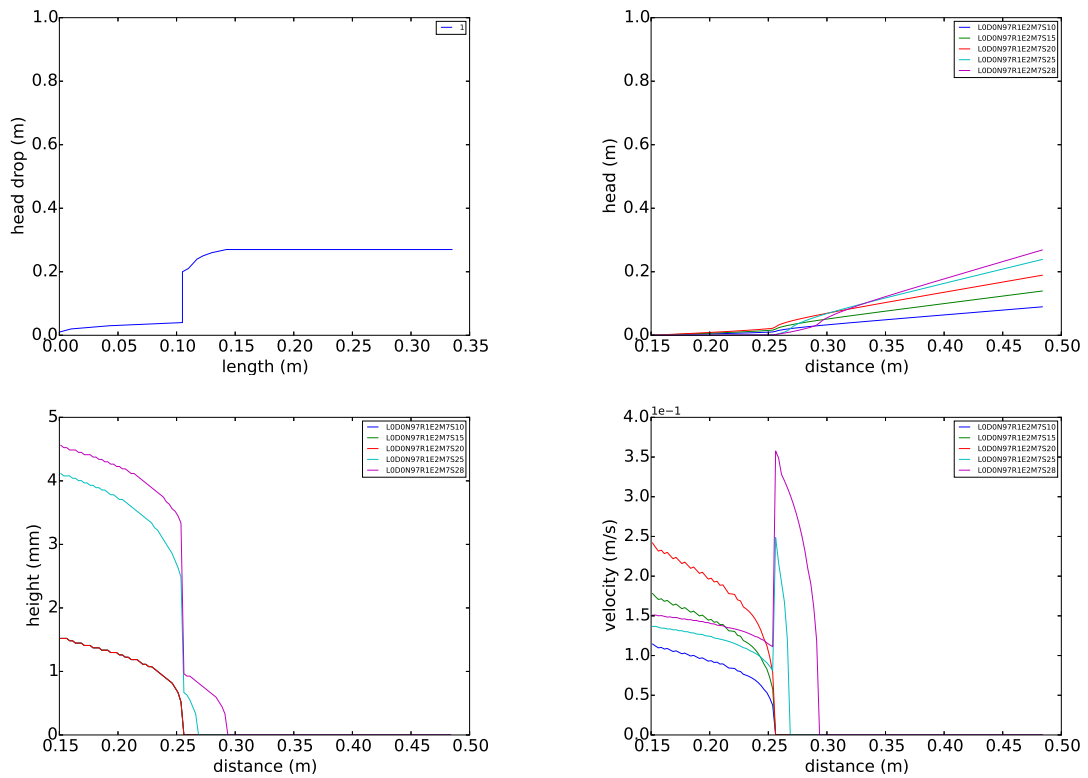


Figure 33: Computational results experiment 197.

Table 15: Computational results experiment 197,  $\nu = 0.25$ ,  $\theta = 37.0$  deg.

$\Delta x$ (mm)	$\Delta y$ (mm)	$\delta x$ (mm)	$\delta y$ (mm)	nodes (-)	steps (-)	$H_{dg}$ (m)	$L_{dg}$ (m)	time (s)
5.00	5.00	5.00	5.00	2058	27	0.26	0.13	91
5.00	5.00	2.50	2.50	2688	28	0.27	0.14	239
5.00	5.00	1.25	1.25	3921	28	0.27	0.14	681
5.00	5.00	0.63	0.63	6360	28	0.27	0.14	2021

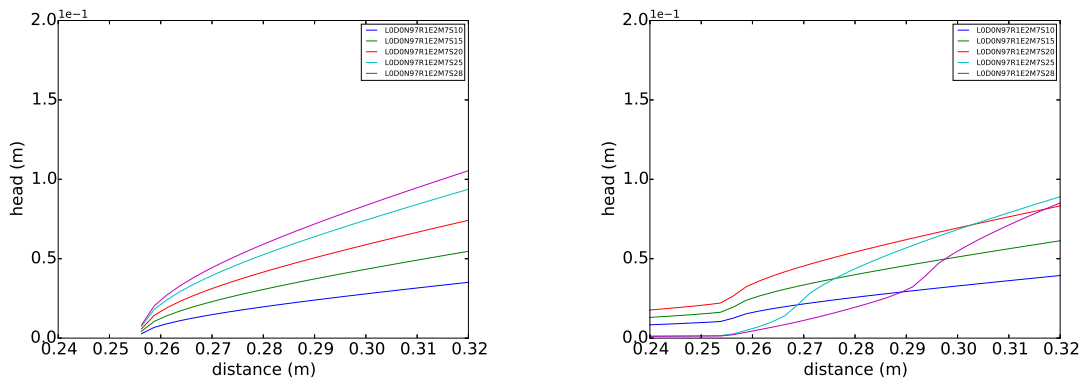


Figure 34: Computational results experiment 197, flow (left) erosion (right).

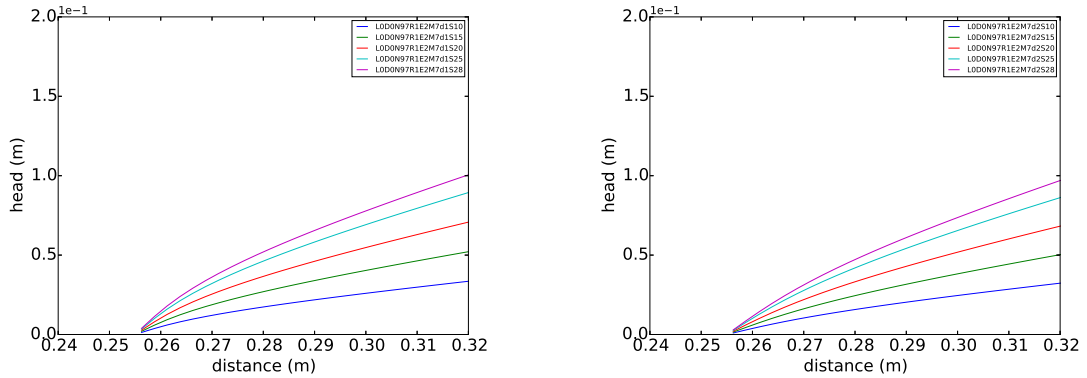


Figure 35: Computational results experiment 197, flow d=5mm (left) flow d=1cm (right).

Table 16: Computational results experiment 197a,  $\nu = 0.30$ ,  $\theta^f = 30.0$  deg,  $\theta^c = 18.0$  deg.

$\Delta x$ (mm)	$\Delta y$ (mm)	$\delta x$ (mm)	$\delta y$ (mm)	nodes (-)	steps (-)	$H_{dg}$ (m)	$L_{dg}$ (m)	time (s)
5.00	5.00	5.00	5.00	2058	14	0.13	0.13	102
5.00	5.00	2.50	2.50	2688	15	0.14	0.14	232
5.00	5.00	1.25	1.25	3921	15	0.14	0.14	671
5.00	5.00	0.63	0.63	6360	15	0.14	0.13	2282

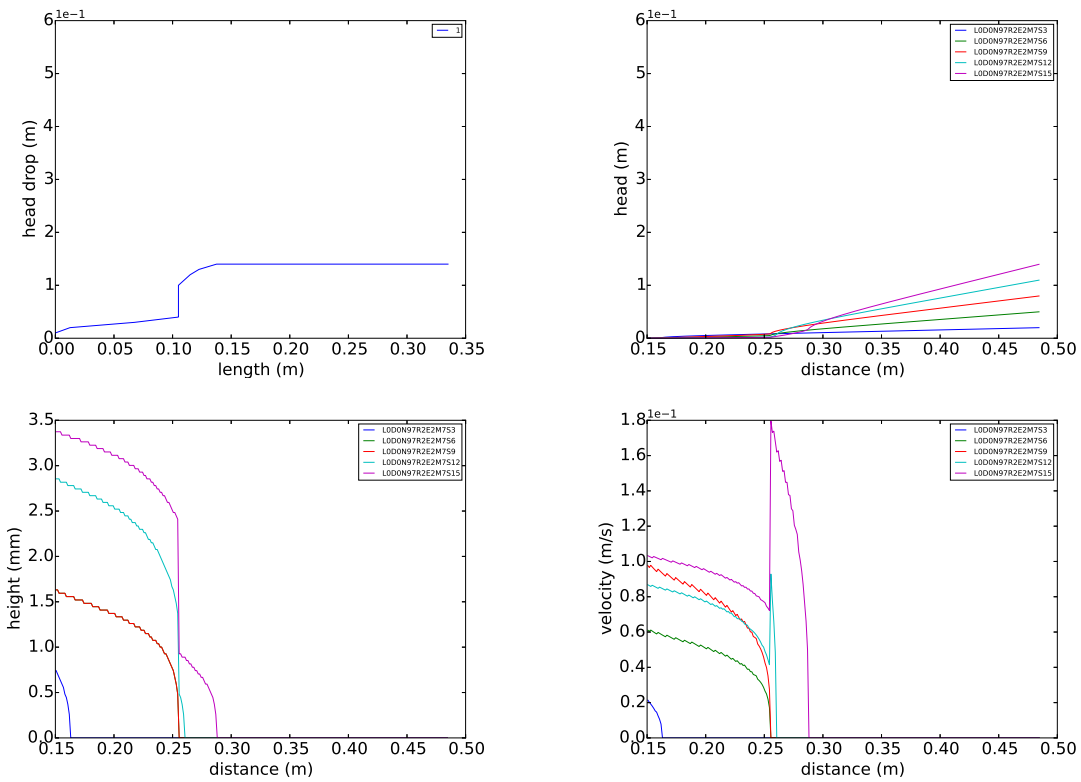


Figure 36: Computational results experiment 197a.

**Date**  
November 7 2017

**Reference**  
11200952-05-GEO-000

**Page**  
25/25

## **Bibliography**

Van Esch, J., J. Sellmeijer and D. Stolle, 2013. "Modeling transient groundwater flow and piping under dikes and dams." *Computational Geomechanics* .